QUATERNARY AEOLIAN SAND MAPPING IN SAUDI ARABIA

USING REMOTELY SENSED IMAGERY

by

KHATTAB GHALIB AL-HINAI
B.Sc., M.Sc.

DEPARTMENT OF GEOLOGY

IMPERIAL COLLEGE OF SCIENCE & TECHNOLOGY

ROYAL SCHOOL OF MINES

LONDON, SW7 2BP

A thesis submitted for the degree of
Doctor of Philosophy of the University of London,
and for the Diploma of Membership of Imperial College

February 1988

Dedicated to the memory of my late uncle Sheikh. Talib Ali Al-Hinai.

To my father, mother, wife, and to my dear sons Omar and Zaid.

Acknowledgements

The author wishes to thank many people and organizations who have provided academic, technical, financial and moral support during the course of this research. The author is very grateful for the King Fahd University of Petroleum and Minerals, Saudi Arabia for their financial and moral support; to Dr. Abdullah Dabbagh, Director of the Research Institute at King Fahd University of Petroleum and Minerals for his moral and academic support and for providing the Landsat MSS images used in this research. The author is very grateful for the Saudi Educational Attache for his continuous support during the course of this research.

In particular, thanks to Mr. John McM. Moore and to Dr. P. R Bush for their supervision, guidance of the research and their encouragement. The author would like to thank Dr. F. Ince and A. Tahir for reading chapters 3 and 4, and Dr. A. Watson for his interesting comments on Chapter 8. Many thanks go to Dr. G. Oakes for providing me with his spatial filtering programs.

The author would like to extend his thanks to all of the following: Mr. D. Wickens at the Photogrammetry Department-University College, London for his technical help in the photogrammetric measurements; Mr. A. Cash for his excellent work in the photograhic production; Miss. C. Kilby for typing the tables; and to all my colleagues at the

Remote Sensing Unit (R. Magee, J. James, and A. Crosta) for their interesting and long lasting discussions.

ABSTRACT

In Saudi Arabia, basic information on sand distribution in desert terrains is limited. The difficulties of direct ground mapping and measurement and the cost of conducting full scale monitoring experiments in remote areas is a major handicap in producing reliable and applicable data. This study is an assessement of air and space photography together with various forms of available scanner imagery as aids to sand dune mapping and movement patterns.

Sand dune types have been identified and mapped at several test site areas. Dune morphology has been investigated together with dune distribution in the Jafurah Sand Sea in the Eastern Province of Saudi Arabia. Comparison of the usefulness in terms of spatial and spectral resolution for sand dune mapping were made between Landsat multi spectral scanner (MSS) and Thematic Mapper (TM) images, Large Format Camera (LFC) photographs, and aerial photographs, together with the Shuttle Imaging Radar (SIR-A) imagery. LFC photographs were also evaluated for dune height measurements in the south eastern Rub'al Khali (Empty Quarter) Sand Sea.

Digital image enhancements including the production of several types of contrast stretched false colour composites, hue saturation intensity images, principal component analysis, and spatial filtering were used as aids to sand type discrimination, delineation and mapping. MSS band 1

(0.5-0.6 μm) and the equivalent TM band 2 images were evaluated for detection and interpretation of possible submerged sand dunes in the shallow waters along the area north of the Gulf of Salwa in the Arabian Gulf.

Estimates of dune movement in the Jafurah Sand Sea were made using the multi-temporal aerial photographs (dated 1949 and 1983) and Landsat MSS images (1972 to 1984) together with field measuremenet (1984 to 1985).

Multi-temporal Landsat MSS images were used for dune movement measurements and showed that individual dunes larger than 100 meters across can be identified but because of slow movement rates of these dunes (3-8m/year) over 12 years period displacement can not be precisely measured. The low spatial resolution of the MSS imagery (pixel size = 80 m) and the lack of precise ground control points in sand sea terrains are two limiting factors in obtaining reliable monitoring of dune movement. Multi-temporal aerial photographs gave better results.

Landsat MSS false colour composites at a scale of 1:250,000 were found to be excellent for producing sand dune morphological maps. TM images and LFC photographs were useful aids in delineating small size dunes (20-50 m across).

Digitally compatible, high resolution data bases acquired over periods of decades will be needed, if systematic sand

movement monitoring is to be made using spaceborne remote sensing images. Some recommendations are made for the formulating of movement monitoring programs in the future.

CONTENTS

PAGE

ACKNOWLEDGEMENTS 3

ABSTRACT 5

CONTENTS 8

LIST OF FIGURES 14

LIST OF TABLES 26

LIST OF APPENDICES 29

LIST OF PLATES (IN POCKET) 29

CHAPTER 1

INTRODUCTION

1.1 Statement of the problem. 30

1.2 Research objectives. 31

1.3 Selection of test site areas. 33

1.4 Structure of the thesis. 34

CHAPTER 2

COMPARISON OF DIFFERENT IMAGE TYPES IN SAUDI ARABIA.

2.1 Introduction. 38

PAGE

2.2 Concept of resolution. 39

2.3 Air photography. 41

2.4 Saudi Arabian aerial photographs. 45

2.5 Space photography. 48

2.6 Large Format Camera (LFC) specifications. 49

2.7 Radar imagery. 55

2.8 Landsat systems. 70

2.9 Discussion and conclusion. 83

CHAPTER 3

DIGITAL IMAGE PROCESSING TECHNIQUES

3.1 Introduction. 87

3.2 Digital images. 87

3.3 Background to digital processing. 88

3.4 Comparison between MSS bands. 90

3.5 Digital image processing procedures. 91

3.6 Image rectification. 92

3.7 Spatial registration. 95

3.8 Image enhancement. 104

3.9 Enhancement of MSS band 1 and TM band 2. 117

3.10 Discussion and conclusion. 120

PAGE

CHAPTER 4

INTERPRETATION OF DIGITALLY PROCESSED IMAGES

4.1 Introduction. 122

4.2 Spectral characteristics of sand. 122

4.3 MSS band investigation results. 124

4.4 False colour compositing results. 129

4.5 Digital colour space transformation results. 134

4.6 Edge enhancement results. 137

4.7 Directional and non-directional filters 140

4.8 Digitization and edge enhancement of LFC phtographs. 173

4.9 Discussion and conclusion. 176

CHAPTER 5

MORPHOLOGY AND DISTRIBUTION OF DUNES IN THE SAND SEAS OF ARABIA

5.1 Introduction. 181

5.2 Previous work on modern sediments in Saudi Arabia. 182

5.3 Formation of sand dunes. 183

5.4 Dune classification. 185

5.5 Sand seas of Arabia. 194

5.6 Dune morphology. 200

PAGE

5.7 Jafurah Sand Sea (case study). 224

5.8 Discussion and conclusion. 247

CHAPTER 6

SAND DUNE MAPPING USING IMAGERY:
CASE HISTORIES

6.1 Introduction. 249

6.2 Literature review. 249

6.3 Materials and methodology. 253

6.4 Dune terminology. 254

6.5 Case History (1) Northern Jafurah Sand Sea (small dunes). 254

6.6 Case History (2) Harad area (large dune forms). 268

6.7 Case History (3) An Nafud Sand Sea (large and small dune forms). 274

6.8 Case History (4) Rub'al Khali (dune height measurement). 278

6.9 Case History (5) Ad Dahna & Wahiba Sand Seas (radar imagery investigation). 284

6.10 Discussion and conclusion. 293

CHAPTER 7 PAGE

MEASUREMENT OF DUNE MOVEMENT

7.1 Introduction. 299

7.2 Sand movement studies. 301

7.3 Selection of the study areas. 303

7.4 Materials used in the investigation. 304

7.5 Ground control points framework. 304

7.6 Ad Dibbiyah area-case history 1. 306

7.7 Landsat MSS investigation. 310

7.8 Aerial photographic investigation. 314

7.9 Field investigation. 324

7.10 Case History (2)-Harad area. 326

7.11 Discussion. 336

CHAPTER 8

LANDSAT MSS AND TM INVESTIGATION OF POSSIBLE SUBMERGED SAND DUNES IN THE ARABIAN GULF.

8.1 Introduction. 343

8.2 Physiography of the Arabian Gulf. 345

8.3 Current action in the Arabian Gulf. 348

8.4 Quaternary history. 348

8.5 Landsat MSS and TM investigation. 351

8.6 Comaparison between on-shore dunes and the off-shore features. 357

PAGE

8.7 Discussion. 365

8.8 Summary. 374

CHAPTER 9

DISCUSSION AND CONCLUSIONS 376

REFERENCES..... 386

GLOSSARY..... 412

LIST OF FIGURES

FIGURE		PAGE
1.1	NOAA Satellite imagery showing major sand seas of Saudi Arabia and the general location of the test sites investigated in this research.	32
1.2	Thesis structure.	35
2.1	Relationship of base-height-ratio to vertical exaggeration for stereo models.	46
2.2	Skylab hand-held photograph over the Rub'al Khali.	50
2.3	Base to height ratio of LFC photographs acquired at a 239 km altitude for different degrees of overlap and vertical exaggerations.	53
2.4	Large Format Camera (LFC) Mission 41-G Flight Path Index over the Arabian Peninsula.	54
2.5	Configuration of the SIR-A system.	58
2.6	Models of surface roughness and radar return.	61
2.7	Models of surface roughness and return intensity for X-band radar.	64

FIGURE		PAGE
2.8	Radar resolution in the range direction.	68
2.9	SIR-A data takes acquired over the Arabian Peninsula.	71
2.10	Primary seasons of dust storms.	79
2.11	NOAA satellite imagery acquired on 1981 over North Eastern Arabia.	80
2.12	Quantitative estimates of the interaction between slope angle aspect and the sun angle.	82
2.13	A panchromatic LFC photograph acquired at a sun angle of 36 degrees over An Nafud Sand Sea.	84
2.14	A panchromatic LFC photgraph acquired at 58 degrees sun angle over the southern Jafurah Sand Sea.	85
3.1	Princple of atmospheric correction.	94
3.2	A diagram illustrating the methodology used for dune movement measurement from multi-temporal Landsat MSS images.	98
3.3	Distribution of selected ground control points in the 1972 and 1984 images.	100

FIGURE		PAGE
3.4	The digitaly registered 1972 and 1984 images.	100
3.5	Landsat MSS false colur composite full resolution subscene (1972) showing the investigated dunes.	102
3.6	A sketch diagram illustrating the method used for dune displacement measurement from Landsat MSS images.	103
3.7	Linear stretch of a single band.	105
3.8	The effect of contrast stretching on Landsat MSS imagery.	106
3.9	Principle of pseudo-colour transformation.	108
3.10	Spectral transmittance for 10 m of various types of water.	109
3.11	Principle of colour space transformation.	112
3.12	A destriped Principal Component 1 (PC1) imagery used as an input image for spatial filtering investigation.	115
3.13	The full log (power) spectrum smoothed with a 5x5 median filter.	115
3.14	A schematic two dimensional cross section through the PDF of an MSS image showing the projections of the first two principal components (PC1 & PC2).	118

FIGURE		PAGE
4.1	Surface reflectance and the wavelength curves for a dry and wet sand.	123
4.2	Contrast stretched MSS band (1-4) images in eastern Rub'al Khali Sand Sea.	125
4.3	Contrast stretched MSS band (1-4) images covering parts of the Jafurah and Ad Dahna Sand Seas.	126
4.4	Visible and near infrared spectra of some iron-bearing materials.	130
4.5	A false colour composite produced from contrast stretched MSS bands.	132
4.6	An HSI imagery showing parts of the Jafurah and Ad Dahna Sand Seas.	136
4.7	Filtered image (17.5 to 72.5 degree filter).	139
4.8	107.5 to 157.5 degrees directional filter.	141
4.9	157.5 to 17.5 degrees directional filtering.	142
4.10	Contrast stretched MSS band 4 & 1 images in	
4.11	Fourier transform (amplitude) for the test site areas.	147
4.12	Frequency response of "tilted Sobel" mask.	150
4.13	NE and NW directional filter images in the Jafurah area.	151

FIGURE PAGE

4.14 NE and NW directional filter images in the Rub'al Khali area. 152

4.15 NE and NW directional filter images in the Ad Dahna area. 153

4.16 Frequency response of "Normal Laplacian", "Sharp Laplacian" and "Laplacian Variant" filters. 155

4.17 "Laplacian Variant" filter images in the test site areas. 159

4.18 "Laplacian Variant" filter applied to MSS band 1 imagery in the Rub'al Khali. 161

4.19 False colour composite imagery of the Rub'al Khali area. 162

4.20 A typical frequency response of DoG filter (3x3 mask). 165

4.21 Contrast stretched DoG filter (0.5-3.0 pixels) imagery in the Jafurah area. 168

4.22 DoG filter (0.3-0.6 and 0.9-1.5 pixels) images in Ad Dahna area. 169

4.23 Contrast stretched DoG filter (0.3-0.6, 0.6-0.9, 0.9-1.5 and 1.5-3.0 pixels) images in the Rub'al Khali area. 170

FIGURE		PAGE
4.24	Large Format Camera (LFC) panchromatic photographs acquired over southern Jafurah illustrating the importance of applying spatial filtering.	174
5.1	A sketch diagram illustrating the principle dune types and the winds responsible for their formation.	187
5.2	Distribution of major dune types in sand seas of Arabia.	195
5.3	A Landsat MSS false colour composite acquired over the western part of An Nafud Sand Sea.	197
5.4	A sketch diagram illustrating the method of measuring on Landsat imagery, space and aerial photographs.	202
5.5	Histogram showing frequency distribution of complex linear dunes.	206
5.6	Histogram showing frequency distribution of simple linear dunes.	207
5.7	Landsat MSS images over the Qa'amiyat area showing the measured linear dunes.	210

FIGURE PAGE

5.8 Histogram showing frequency distribution and morphometry of simple crescentic dunes in the northern Jafurah and the northeastern Rub'al-Khali. 214

5.9 Histogram showing frequency distribution and morphometry of compound crescentic dunes in Rub'al Khali and An Nafud. 216

5.10 Landsat MSS imagery over part of Ad Dahna showing the measured star dunes. 218

5.11 Histogram showing frequency distribution and morphometry of star dunes in Rub'al Khali and Ad Dahna. 220

5.12 Landsat MSS imagery used for measurement of dome dunes in Nafud Ath Thuwayrat. 222

5.13 Histogram showing frequency distribution and morphometry of dome dunes in Nafud Ath-Thuwayrat. 225

5.14 Index map showing the location of Landsat MSS images used for producing plates 1-6. 227

5.15 Legend used for mapping the morphology and distribution of sand dunes in the Jafurah Sand Sea (also given with plates 1-6 at the end of the thesis). 229

FIGURE PAGE

5.16 Typical dune morphology in the Northern Jafurah Sand Sea. 232

5.17 Aeolian landscape associations typical of Southern Jafurah. 232

5.18 Illustration of some dune types as seen in the field. 234

5.19 Sampled area used for measurement of parabolic dunes in the Northern Jafurah. 237

5.20 Sampled area used for measurement of barchanoid ridges in Northern Jafurah. 240

5.21 Sampled area used for measurement of barchanoid ridges in Southern Jafurah. 241

5.22 A sketch diagram illustrating the different phases of dune evolution in Jafurah Sand Sea. 246

6.1 Location map of Case History (1). 256

6.2 Landsat MSS full resolution false colour composite subscene used for spatial resolution assessment. 259

6.3 Landsat TM full resolution false colour composite subscene used for spatial resolution assessment. 260

FIGURE		PAGE
6.4	LFC panchromatic photograph used for spatial resolution assessment.	261
6.5	Panchromatic aerial photograph (1:60,000 scale) used for spatial resolution assessment.	262
6.6	Panchromatic aerial photograph (1:80,000 scale) used for spatial resolution assessment.	263
6.7	Infrared aerial photograph (1:10,000 scale) used for spatial resolution assessment.	264
6.8	Location map of Case History (2).	269
6.9	Landsat MSS false colour composite showing large barchanoid shaped dunes.	270
6.10	Panchromatic aerial photograph (1:60,000 scale) showing a close-up view of the dunes shown in Figure 6.9.	272
6.11	Location map of Case History (3).	275
6.12	Landsat MSS full resolution false colour composite subscene used to investigate large and small barchanoid dunes in An Nafud.	276
6.13	Landsat TM full resolution false colour composite subscene used to investigate the same area shown in Figure 6.12.	277
6.14	LFC panchromatic photograph used for dune height measurement.	280

FIGURE		PAGE
6.15	Location map of Case History (4) in the Wahiba Sands.	285
6.16	SIR-A imagery over the southwestern Wahiba Sands.	287
6.17	Location map of Case History (4) in Ad Dahna Sand Sea.	290
6.18	SIR-A imagery over the western part of Ad Dahna Sand Sea.	297
7.1	Location map of Case History (1).	307
7.2	Aerial photograph acquired in Nov.1949 (1:60,000 scale) showing the dunes used for displacement measurement.	316
7.3	Aerial photograph acquired in Nov.1983 (1:80,000 scale) used for dune displacement measurement of the same area shown in Figure 7.2.	317
7.4	Displacement of dunes between 1949 and 1983 (aerial photogrammetric measurement).	319
7.5	Average annual dune advance versus dune height (measured between 1949 and 1983).	323
7.6	Method used for measuring dune movement in the field.	325

FIGURE PAGE

7.7 Dune advance versus dune height from August 1984 to August 1985 (12 months period). 329

7.8 Location map of Case History (2). 330

7.9 Landsat MSS false colour composite (scene 176/43; Jan.18.1973) over Harad area used for investigating temporal changes of dune patterns. 334

7.10 Landsat MSS false colour composite (scene 164/43; Jan.15.1984) used to investigate the the same area shown in Figure 7.9. 335

7.11 Dune pattern boundaries drawn from the 1973 and 1984 images over Harad area. 337

8.1 Location map of study area. 344

8.2 Bathymetric map showing water depth along the Saudi Coast. 346

8.3 Sediments on floor of the Arabian Gulf. 347

8.4 Landsat TM density sliced imagery showing water depths in the study area. 353

8.5 Landsat MSS band 1 imagery (176/42; 26 January 1973) interactively stretched to show offshore features. 355

8.6 Combined image (false colour composite MSS bands 4 2 1) showing both offshore features and onshore areas. 356

FIGURE PAGE

8.7 A combined Landsat TM band 1 and TM band 2 (164/42; 16 January 1985) displaying the same submarine sand banks shown in Figure 8.6. 358

8.8 Location map of echo sounding profiles. 361

8.9 Sediment echograms of transect A-B & C-D (shown in Figure 8.8) showing mounds interpreted as possible submerged sand dunes. 362

8.10 Onshore dunes prograding into water (Dohat Dhalum) north of the study area. 363

8.11 A comparison between compound crescentic ridges in eastern Rub'al Khali and the submerged sand banks in the Arabian Gulf. 367

8.12 Landsat MSS false colour composite acquired over Qatar showing dunes mainly in southeastern part. 372

LIST OF TABLES

TABLE		PAGE
2.1	Minimum ground separation on typical aerial photographs acquired at different heights.	44
2.2	LFC camera and mission parameters.	52
2.3	Characteristics of the SIR-A and SIR-B systems.	59
2.4	Limiting values of vertical relief for surface roughness categories. Depression and incidence angles are 45 degrees.	65
2.5	Landsat MSS bands.	73
2.6	TM spectral bands and their potential applications.	75
4.1	Test site areas and the DoG filter sizes used.	172
5.1	Terminology of basic dune types and other aeolian deposits.	186
5.2	Basic dune types as seen from different remote sensing images.	188
5.3	Morphometry of linear dunes (width, length and dune spacing) in the Rub'al Khali.	204
5.4	Measurement of linear dune width and dune spacing located in an open area and near a topographic hill.	209

TABLE		PAGE
5.5	Morphometry of crescentic dunes (width, length and dune spacing) in sand seas of Saudi Arabia.	212
5.6	Measurement of star dune diameters and dune spacings in Ad Dahna and Rub'al Khali.	219
5.7	Measurement of dome dune diametres and spacings in An Nafud and Jafurah.	223
5.8	List of Landsat MSS scenes used for producing Plates 1-6.	228
5.9	Percentage of different aeolian deposits in the Jafurah Sand Sea based upon Landsat MSS investigation.	230
5.10	Morphometry of Parabolic dunes (width, length, and dune spacing) in the Jafurah Sand Sea.	238
5.11	Morphometry of barchanoid ridges (width, length and dune spacing) in northern and southern Jafurah.	242
6.1	Investigated test site areas and the image type used for each area.	250
6.2	Dune types investigated in the different test site areas.	251
6.3	Dune morphometry in Case History (1).	257
6.4	Morphometry of representative dunes found in one "chain barchan".	273

TABLE		PAGE
6.5	Large Format Camera accuracies.	282
6.6	Dune height meaurements in the south-eastern Rub'al Khali based on LFC photographs.	283
6.7	Comparison between different sensors for mapping dunes of various sizes.	294
7.1	Residual error of ground control points registration.	311
7.2	Measured values for dune movement obtained from Landsat MSS imagery (between 1972 and 1984).	313
7.3	Dune displacement between 1949 and 1983 based on aerial photographic measurement.	321
7.4	Average annual displacement of 30 barchan and barchanoid ridges according to dune height (aerial photographic measurement).	322
7.5	Dune displacement between August 1984 and August 1985 based on field measurement.	327
7.6	Average displacement of dunes between August 1984 and August 1985 based on field measurement.	328
7.7	Dune movement rates in some sand seas of the world.	340
8.1	Digital number (DN) values of the water depths observed on the Landsat TM band 2 imagery.	354

TABLE PAGE

8.2 Morphometry of the submerged features based on Landsat TM imagery. 359

8.3 Morphometry of the on-shore dunes measured in the field. 364

LIST OF APPENDICES

APPENDIX (1) Satellites and sensors. 420

APPENDIX (2) Fryberger, et al (1984; published paper). 433

APPENDIX (3) Al-Hinai & Moore (1986; published paper). 452

APPENDIX (4) Al-Hinai, et al (1987; published paper). 463

APPENDIX (5) Dune height measurements using LFC photographs in south-eastern Rub'al Khali. 472

LIST OF PLATES (in pocket)

1 - 6 Morphology and distribution of sand dunes in the Jafurah Sand Sea based on Landsat MSS imagery.

CHAPTER 1

INTRODUCTION

1.1 STATEMENT OF THE PROBLEM:

There has been a considerable amount of geological research into desert phenomena but the remoteness of arid regions is a handicap to obtaining data on a regional basis. The problem is more pronounced when dealing with large dispersed sand seas as in Saudi Arabia. The mapping of dune types and forms, measurement of dune height, width, length, wavelength, and the continuous monitoring of dune movement are all laborious and expensive tasks.

Until recently desert travel has been difficult and only the hardy travellers have attempted it. Since there was a little economic justification for desert exploration, relatively few studies were made in the past relative to the size of desert areas.

With the recent expansion in agriculture, urban, and industrial developments in Saudi Arabia it is now a necessity to conduct a long term research in desert terrains. The degradation of soil and the invasion of sand dunes onto arable and agricultural areas creates severe problems which require long term solutions. There is therefore a need to collect basic information in the

different sand seas of Saudi Arabia regarding dune distribution, type, size, and rate and direction of sand movement.

With the launching on July 27,1972 of the unmanned Earth Resources Technology Satellite (ERTS-1) later named Landsat-1 a new and improvement approach of the investigation of sand seas became available. Satellite images and space photographs (Skylab, Apollo, and Shuttle) covering large areas in a single image and with repetative coverage, it is now possiple to study different sand seas and monitor terrain changes.

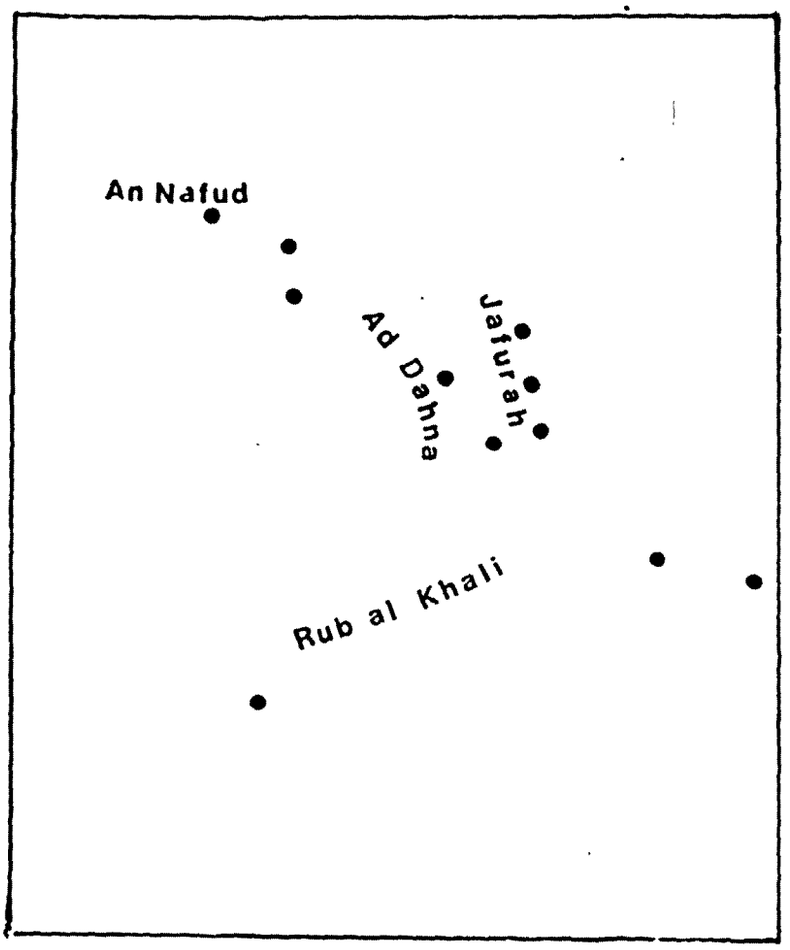
1.2 RESEARCH OBJECTIVES:

Saudi Arabia with its vast area (approximately 3 million square km) contains four major sand seas occuping an area of 795,000 square km (An Nafud, Ad Dahna, Rub'al Khali, and Jafurah; Figure 1.1). These large sand seas with distinctive dune types make excellent sites for study.

The objective of this research can be summarized as follows:

(i) To compare and assess the spatial, spectral, and temporal resolution of space imagery and aerial photography for mapping aeolian features of different types and sizes.

(ii) To evaluate different digital image processing techniques as aids to sand type discrimination and mapping.


An Nafud
Ad Dahna
Jafurah
Rub al Khali

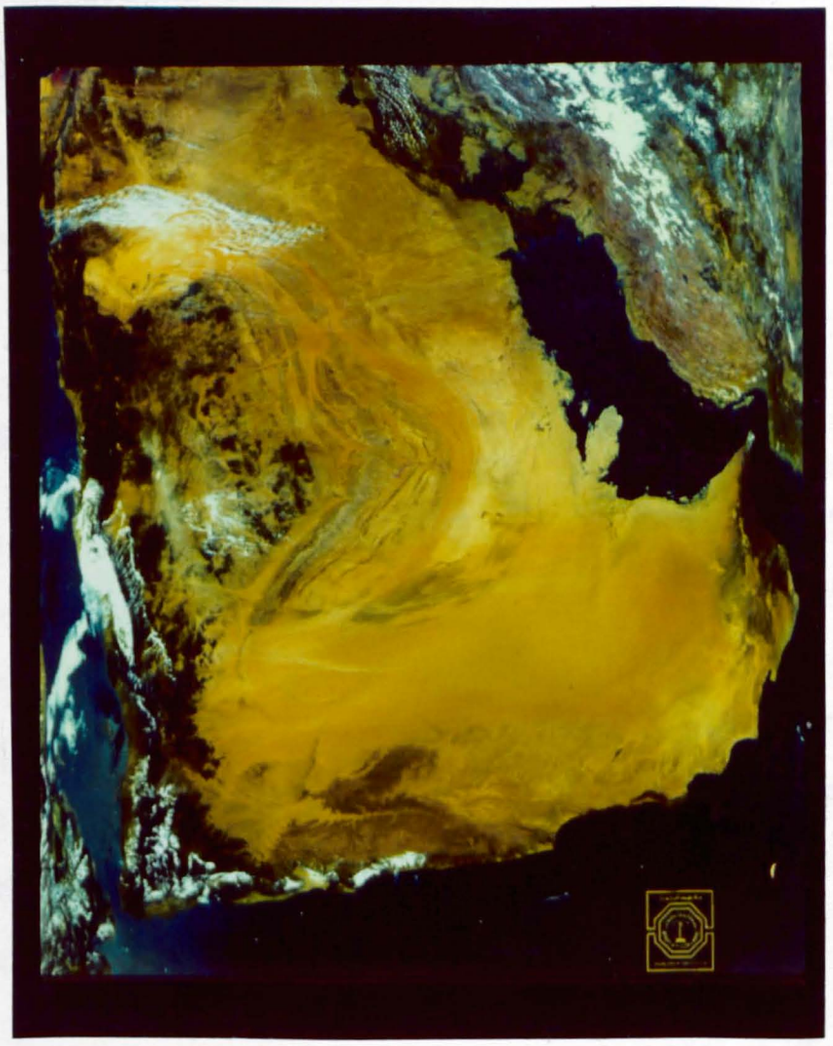


Figure 1.1 NOAA Satellite imagery showing major sand seas of Saudi Arabia and the general location of the test sites investigated in this research. The image is a colour composite produced from the near and thermal infrared bands.

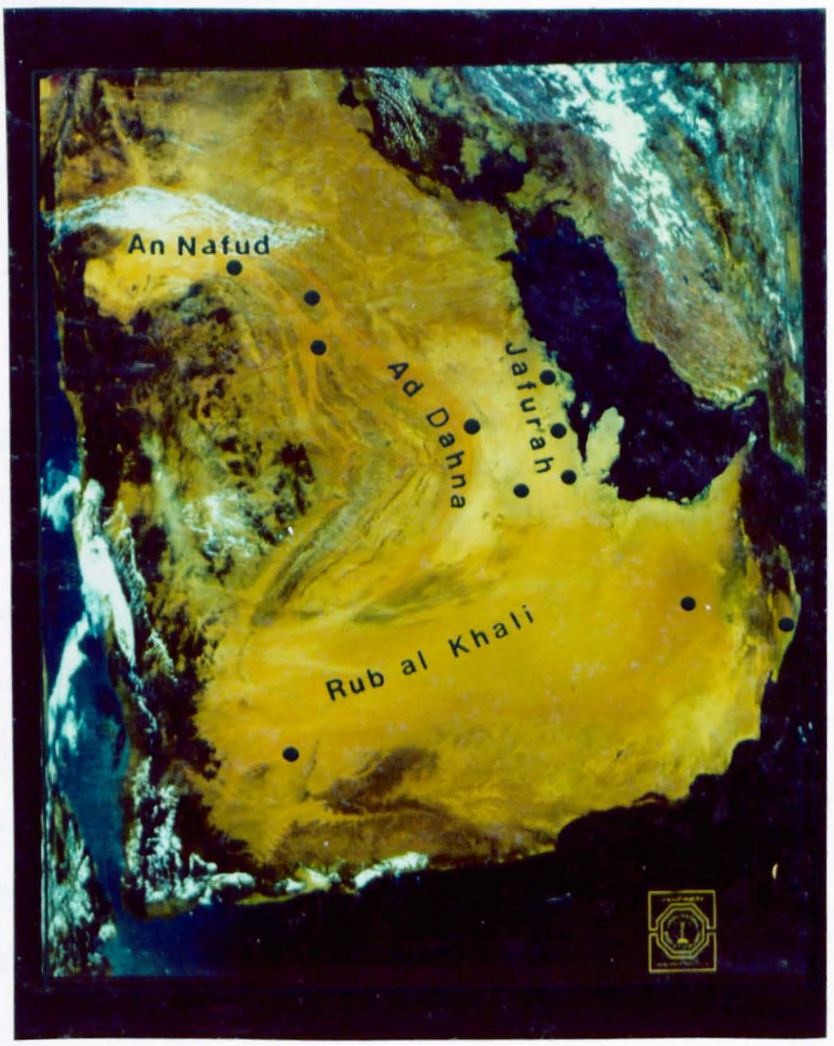


Figure 1.1 NOAA Satellite imagery showing major sand seas of Saudi Arabia and the general location of the test sites investigated in this research. The image is a colour composite produced from the near and thermal infrared bands.

(iii) To evaluate the use of Landsat multi-temporal Multi Spectral Scanner (MSS) images together with multi-temporal aerial photographs and field data for sand dune displacement measurements.

(iv) To investigate the existence of coastal sand features including submarine sand banks in the Arabian Gulf using Landsat MSS and Thematic Mapper (TM) imagery.

1.3 SELECTION OF TEST SITE AREAS:

Because of the diversity of research objectives and wide spread distribution of the investigated sand seas, test site areas were selected in all major sand seas of Arabia. The locations for different test sites selected for a specific investigation are given in the appropriate chapter. Figure 1.1 shows the general distribution of selected site areas. Other reasons for selection of the investigated sites can be summarized as follows:

(i) The availability and the quality of Landsat imagery (MSS and TM).

(ii) The availability of multi-temporal coverage by Landsat imagery as well as aerial photography covering specific sites for sand dune movement investigation.

(iii) The availability of field data to support space imagery and aerial photography interpretations. These data include observations collected during the author's field

investigation studies prior to this research. Logistical problems prohibited field checking in some localities.

(iv) Some test site areas were selected for testing spatial and temporal resolution for identifying dune types of different sizes. Other areas were selected for sand dune movement investigation.

1.4 STRUCTURE OF THE THESIS:

This thesis is structured for readers interested in sand studies without background in remote sensing and digital image processing techniques as well as researchers in image processing. The thesis contains nine chapters each presented to allow separate reading to select the subject of interest.

Chapters 2 and 3 contain an evaluation of imagery and the different digital image processing techniques used in this research. The remainder of the chapters contain assessment results for the different image types and processing techniques for the following:

(i) Morphology and distribution of dunes.

(ii) Sand dune mapping

(iii) Measurement of dune movement.

(iv) Investigation of submarine sand banks in the Arabian Gulf.

Figure 1.2 illustrates the thesis structure.

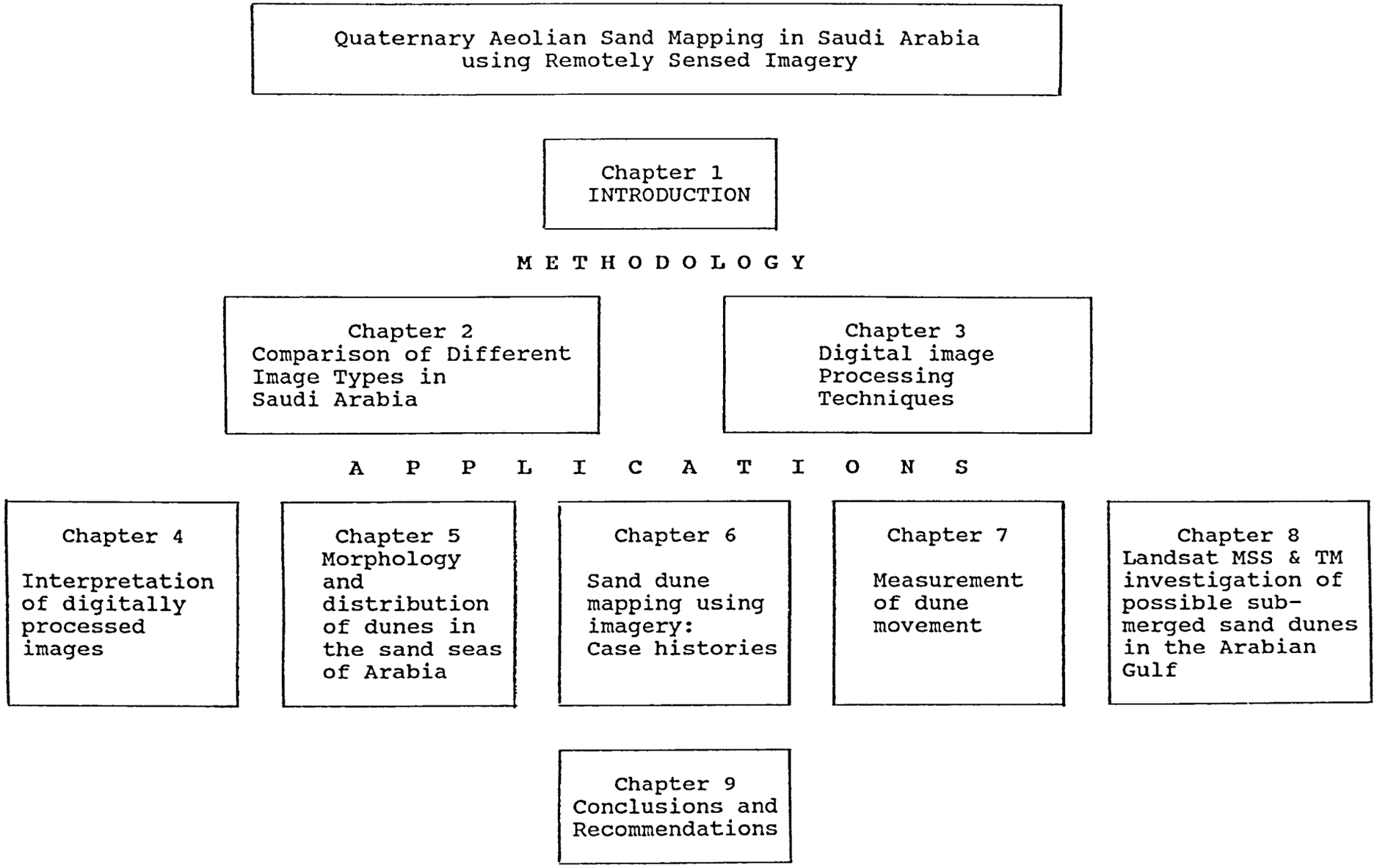


Fig. 1.2: Thesis Structure.

The nine chapters of this thesis are distributed as follows: Introduction (Chapter 1) followed by Chapter 2, which is a comparison between the different spaceborne and airborne images used in this study. The comparison covers the quality and a background information on the theoretical and actual spectral and spatial resolution.

Chapter 3 describes the digital image processing techniques used in this study.

Chapter 4 contains a discussion of the interpretation of digitally processed images and includes interpretation of some images enhanced by the techniques described in Chapter 3.

Chapter 5 is a description of the morphology and distribution of dunes in the sand seas of Saudi Arabia. This chapter serves as an introduction to the major sand seas of Arabia with analysis and comparison of dune morphometric measurements to show distribution of dune sizes and spacings.

Chapter 6 describes sand dune mapping using imagery in the format of case histories. The spatial resolution of the available remote sensing sensors is assessed in relation to detection of dune types of various sizes and types in selected test sites.

Measurement of dune movement is described in Chapter 7. In

this chapter Landsat MSS imagery, aerial photographs, and field data are assessed for monitoring sand distribution patterns and sand dune movement at locations in the Jafurah Sand Sea.

Chapter 8 is a discussion of the submerged sand banks revealed in the Landsat MSS and TM data and their possible origin.

The thesis ends with conclusions and recommendations (Chapter 9).

CHAPTER 2

COMPARISON OF DIFFERENT IMAGE TYPES IN SAUDI ARABIA.

2.1 INTRODUCTION

Parts of the Arabian Peninsula are covered by several types of remotely sensed imagery. The space imagery available for Saudi Arabia includes Landsat Multi Spectral Scanner (MSS) and Thematic Mapper (TM) line scanned images, manned and unmanned space photographs, and Shuttle Imaging Radar (SIR-A and SIR-B). Panchromatic monochrome and false colour infra-red aerial photographs are also available for some areas.

This chapter describes the following:

(i) Background information on the Landsat program, Radar imagery, manned and unmanned space photograhs, and aerial photographs.

(ii) Theoretical resolutions of the available imagery.

(iii) Actual resolutions experienced from the investigated imagery.

2.2 CONCEPT OF RESOLUTION

The amount of data/information contained within an image depends largely on the image resolution. Slater (1980) noted that the different ways in which we can get information can be related to the (dimensional) resolution and that the quality of the information extracted from remotely sensed imagery is strongly influenced by the spatial, spectral, radiometric, and temporal resolution.

SPATIAL RESOLUTION: refers to the finess of detail detected in an image. It describes the minimum size of objects on the ground that can be separately distinguished or measured. In general, spatial resolution is usually described by the instantaneous field of view (IFOV). IFOV is a function of satellite orbital altitude, detector size, and the focal length of the optical system. For the visible and near infrared bands of Landsat MSS, the IFOV is most commonly quoted as being 79 m. However, an IFOV is not in all cases a true indication of the size of the object that can be detected. An object of sufficient contrast with respect to its background, either brighter or darker, can change the overall radiance of a given pixel so that the object becomes detectable (Simonett, 1983). Transport routes which are smaller than 79 m can be detected on Landsat MSS images where the contrast is optimum. On the other hand, objects of the same size or slightly larger than the IFOV might not be detected if they have a low contrast with their surroundings and the IFOV does not cover it or most of it. Moreover, features detected in one band of an image may not

be detected in another band. Thus detectability can vary all over the image and from band to band.

Another factor is atmospheric effects which tend to reduce then contrast of an image or photograph and, hence, its chances of detection. Detectability can also be affected, in the case of Landsat imagery, by sensor caused defects such as variation in the response of detectors resulting in image striping.

These factors become very important when applying different space imagery for sand dune mapping (see Chapter 6). Some of the factors affecting the spatial resolution of an image, such as image striping and atmospheric effects, can be removed by certain digital image processing techniques (see Chapter 3).

RADIOMETRIC RESOLUTION: Is the sensitivity to difference in signal strength. The finer the resolution the greater the opportunity to discriminate between objects within a given spatial resolution. It is the resolving power of an instrument needed for dividing the total range (from black to white) of the signal output (Slater, 1980).

SPECTRAL RESOLUTION: Pertains to the width of the region in the electromagnetic spectrum that are sensed and the number of channels used. Spectral resolution for different line-scanned sensors and optical sensors are discussed in Section 2.8 of this chapter.

TEMPORAL RESOLUTION: Is the length of the time interval between successive environment measurements. Since one of the major objectives of remote sensing is to monitor change through time, temporal resolution is an important consideration when determining the resolution characteristics of any sensor-system. With some applications the time interval at which remotely sensed data are acquired becomes an important factor. To monitor crop growth, for example, images should be obtained at a predetermined time interval, perhaps every 10 days. However, to monitor dune movement imagery acquired at time intervals of 10 years and over may be appropriate. Moreover, for monitoring dune movement, high spatial resolution may be required to identify the investigated dunes. Chapter 7 discusses the aspects of dune movement measurement and the required temporal and spatial resolution of the imagery.

2.3 AIR PHOTOGRAPHY

Photographs are the oldest form of airborne remote sensing. In addition to visible radiation (0.4-0.7 μm) , portions of the UV (0.3-0.4 μm) and infra red (0.7-0.9 μm) spectral regions may be detected by photographic method. The photographic remote sensing spectral region is the wave length range from 0.3 to 0.9 μm.

Aerial photographs record light reflected by a surface, which is determined by the property called "albedo". Albedo is defined as the radiant reflectance of a surface, and is

the ratio of the reflected to the incident energy, so, dark surfaces have a low albedo and light surfaces have a high albedo.

Aerial photographs are acquired with a variety of cameras, films, and filters. Characteristics such as resolution, scale, and relief displacement are common to all aerial photographs. The spatial resoluton of aerial photographs is influenced by several factors:

(i) Atmospheric scattering which results from interactions between light rays and the gases and particles of the atmosphere. Scattered light that enters the camera as 'haze'is a source of illumination but contains no information about the terrain. This illumination reduces the contrast ratio of the scene, thus reducing the spatial resolution of the photograph.

(ii) Vibration and motion of the aircraft which affects the geometry of the photograph.

(iii) Resolving power of the lenses used which is determined by optical parameters (e.g. focal length etc) and size.

(iv) Resolving power of the film wich is determined mostly by the granularity of the film emulsion. Films with high granularity have lower resolving power ('fast' films) than those with low granularity ('slow' films). A widely used black and white film, Kodak Panatomic X aerial film, has a resolving power of 300 line-pairs.\ mm for high-contrast

targets and 80 line-pairs.\ mm for low- contrast targets.

System resolution (Rs) is the result of the resolving power of the lens and film. Ground resolution (Rg) expresses the ability to resolve ground features on aerial photographs and images. Ground resolution can be calculated using the formula:

$$Rg = \frac{Rs \cdot f}{H}$$

where

Rg = ground resolution in line-pairs per meter.

H = camera height above ground in meters.

Rs = system resolution in line-pairs per mm.

f = camera focal length in mm.

" Minimum Ground Separation " which is Rg/2 is another term expressing the minimum distance between two targets on the ground at which they can be resolved on the photograph. Table 2.1 shows the minimum ground separation on typical aerial photographs acquired at different heights (focal length of camera lens = 152 mm).

Air Photography has the disadvantage of radial optical distortion, but this is compensated by parallex which permits stereoscopic viewing and photogrammetric measurement using overlapping photographs. Most aerial photography is acquired with 60 percent forward overlap to allow for stereoscopic viewing. Vertical exaggeration is the ratio of

Camera height, H	Scale of photographs	Minimum ground separation $R_g/2$ for system resolution R_s of:	
		40 line-pairs · mm^{-1}	100 line-pairs · mm^{-1}
6,100 m	1:40,000	0.5 m	0.2 m
4,575 m	1:30,000	0.37 m	0.15 m
3,050 m	1:20,000	0.25 m	0.1 m
1,525 m	1:10,000	0.12 m	0.05 m

Table 2.1: Minimum ground separation on typical aerial photograph acquired at different heights (focal length, f, of camera lens = 152 mm). After Sabins, 1978.

the vertical scale to the horizontal scale of a stereo model and is determined by the geometry of the camera system and of the stereo viewing system. 'Air base' is the ground distance between centres of successive overlaping photographs. The ratio of 'air base' to aircraft height, called 'base-height ratio', determines the vertical exaggeration of the stereo model. The relationship of base - height ratio to vertical exaggeration is shown in Figure 2.1. Aerial photographs of an original scale of 1:60,000 and an ovelap of 60 percent gives an air base of 5,400 m between successive photographs. At the camera height of 9,000 m, the resulting base-height ratio is 0.6. When refering to Figure 2.1 it can be seen that this ratio results in a vertical exaggeration factor of four when these photographs are viewed stereoscopically. This vertical exaggeration becomes very important when viewing dunes of small heights.

Photographs from the air provide some of the most useful aids for sand studies because of their higher resolution and their stereoscopic capability. In Chapter 6 aerial photographs are assessed together with other forms of remote sensing imagery in sand dune type mapping.

2.4 SAUDI ARABIAN AERIAL PHOTOGRAPHS

Saudi Arabia is one of the few countries in the world that was completely covered by aerial photographs which began in 1949 (Powers, et al. 1966). Some areas have been rephotographed for different geological applications,

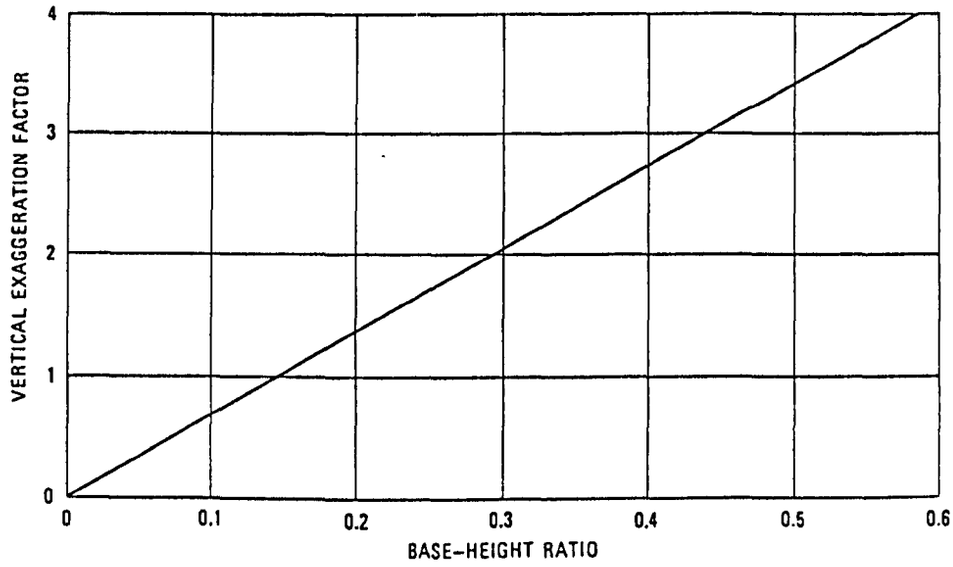


Figure 2.1 Relationship of base-height-ratio to vertical exaggeration for stereo models. From Sabins (1978).

updating of older maps, and civilian projects.

These aerial photographs were taken at different scales. The 1949 panchromatic photographs were acquired at a scale of 1: 60,000. More recently (1983) selected areas were rephotographed at a scale of 1:80,000 in the Eastern Province of Saudi Arabia. Infrared aerial photography was also acquired in 1982 at a scale of 1:10,000 in limited areas of the Eastern Province.

The 1949 panchromatic aerial photographs were taken at normal angle and at 60 percent forward overlap. The photographs were taken about 10.00 a.m LMT at a sun angle of approximately 35 degrees. The film used was Kodak Pan-atomic X aerial film which has a resolving power of 300 line-pairs.\ mm for high contrast targets and 80 line- pairs.\ mm for low contrast targets. The focal length of the camera is 152 mm. Despite the fact that the photographs used for this research are of the third generation, the quality is considered to be good (Figure 7.2).

The Ground Resolution Distance (GRD) of these photographs can be expressed as:

$$\text{GRD (m)} = \frac{\text{Reciprocal of image scale}}{\text{System resolution (lines/mm)} \times 1000 \text{ mm/m}}$$

where the 1000 is a unit conversion factor to yield the grid in metres. At a scale of 1:60,000 and a system resolution of

40 lines/mm, the GRD would be:

$$GRD = \frac{60,000}{(40)1000} = 1.5 \text{ m}$$

The 1983 panchromatic aerial photographs with a scale of 1:80,000 were acquired with a super wide angle camera. The film used was the same as the 1949 photographs. These photographs were acquired on November 1983. The quality of these photographs is comparable with the 1949 photographs (Figure 7.3). The GRD is approximately 2 metres.

Infra-red false colour aerial photographs were acquired on January 1982 using a normal angle camera at a scale of 1:10,000. The infra-red colour film used is Kodak Aerochrome type 2443 which is available only as a positive film. The quality of these photographs is excellent (Figure 6.7). The average ground resolution of these photographs show contrasting objects approximately 0.25 metres across.

2.5 SPACE PHOTOGRAPHY

HAND-HELD CAMERA PHOTOGRAPHY:

Space photographs using hand-held cameras were obtained during manned space missions (Skylab, Apollo, Gemini, Apollo-Soyuz Test Project "ASTP", and the Space Shuttle). Earth orbital photographs produced from early missions were intended to demonstrate the potential value and uses of

images from orbital altitudes. Despite the limited coverage, those photographs provided justification for the unmanned Landsat program.

These photographs were acquired with different types of cameras e.g automatic Mauer 70 mm, 35 mm camera, and 70-80 mm Hasselblad. The quality of photographs ranged from poor to good.

Several coloured photographs were acquired over the Arabian Peninsula during Skylab, Apollo-Soyuz Test Project, and the Space Shuttle missions. The purpose of the majority of these photographs was to illustrate the deserts of Arabia.

The photographs range from high oblique to low oblique. Depending on the altitude of the spacecraft at the time of photography, the scale ranged from 1:800,000 to 1:4,000,000. The average resolution of the photographs is approximately 60 meters (Sabins, 1978). The small scale of orbital photographs permits viewing of a large area on a single frame, but the low resolution prohibits identification of many small and moderate size features. Figure 2.2 is an illustration of space hand-held photography acquired over the Rub'al Khali during Skylab mission.

2.6 LARGE FORMAT CAMERA (LFC) SPECIFICATIONS

The Large Format Camera (LFC) carried on the shuttle mission STS-41G on October, 5, 1984 provided controlled

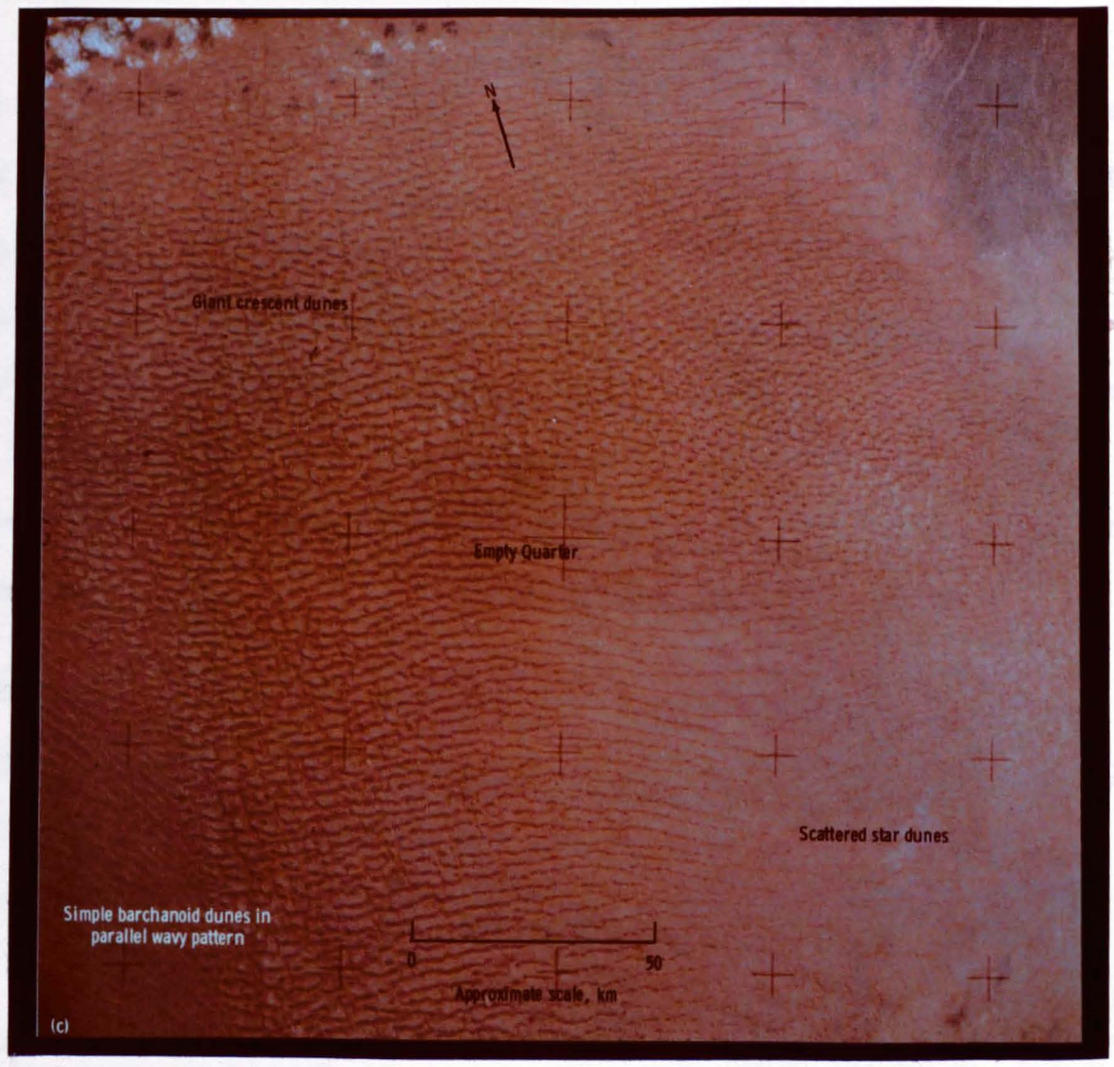


Figure 2.2 Skylab hand-held photograph over the Rub'al Khali. Dunes can easily be identified because of their large sizes. (SL4-141-4255; from McKee, 1977).

vertical photography with 10-15m resolution and 80% overlap. The large format refers to the film size of 23 x 46 cm with the longer dimension in the direction of flight. The area covered in one frame is 178 x 356 km at photo scales ranging between 1: 1,213,000 and 1:788,000. The parameters of the camera system are given in Table 2.2. More details about the different specifications of the LFC are given in Appendix (1) .

A number of LFC photographs were acquired with forward overlap from 20 to 80 percent. (Fig. 2.3) shows base- height ratio, at a 239 km altitude, for the different degrees of overlap and the vertical exaggeration.

QUALITY OF LFC PHOTOGRAPHS IN SAUDI ARABIA:

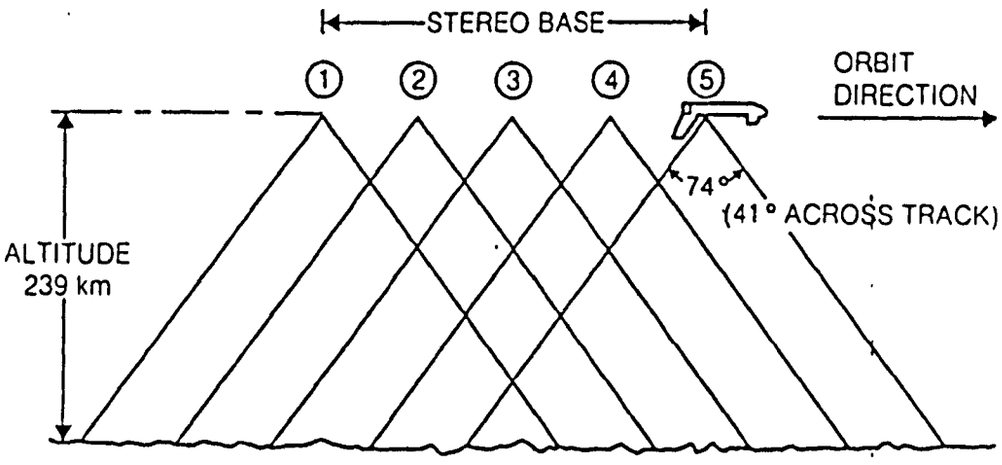
All LFC photographs aquired over the Arabian Peninsula are black and white. They were taken on Oct.5.1984 at altitudes varying between 235 km to 370 km with forward overlap of 80 percent. Figure 2.4 shows the extent of coverage in the Arabian Peninsula.

The scale of the photographs ranged between 1:778,000 to 1:1,213,000. The sun elevation varies between 36 to 61 degrees. The effect of the sun angle on the quality of the photographs is discussed later in this chapter.

Because of the good spatial resolution of the LFC photographs (10 - 12 metres) it is possible to enlarge 15x

Mission	STS 41-G Challenger
Launch	October 5, 1984; Kennedy Space Center, Florida
Landing	October 13, 1984; Kennedy Space Center, Florida
Flying Height	225 to 352 km
Photo Scale	1:740 000 to 1:150 000
Camera Constant	305 mm
Spatial Resolution	80 1 μ/mm AWAR
Radial Distortion	< 20 μ m
Film Format	23 x 46 cm^2
Illuminated Reseau	5 x 5 cm spacing
Illuminated Fiducials	12
Forward Overlap	10,60,70 or 80 percent
Base Height Ratio	1.36, 0.6, 0.45 or 0.3

Table 2.2: LFC camera and mission parameters. From Sabins (1986).



Selected Frames	1 & 2	1 & 3	1 & 4	1 & 5
Forward overlap (%)	80	60	40	20
Stereo base (km)	69	138	207	276
Base/height ratio	0.29	0.58	0.87	1.15
Vertical exaggeration	2.0	4.0	6.0	7.8

Figure 2.3 Base to height ratio of LFC photographs acquired at a 239 km altitude for different degrees of overlap and vertical exaggerations. From Sabins (1986).

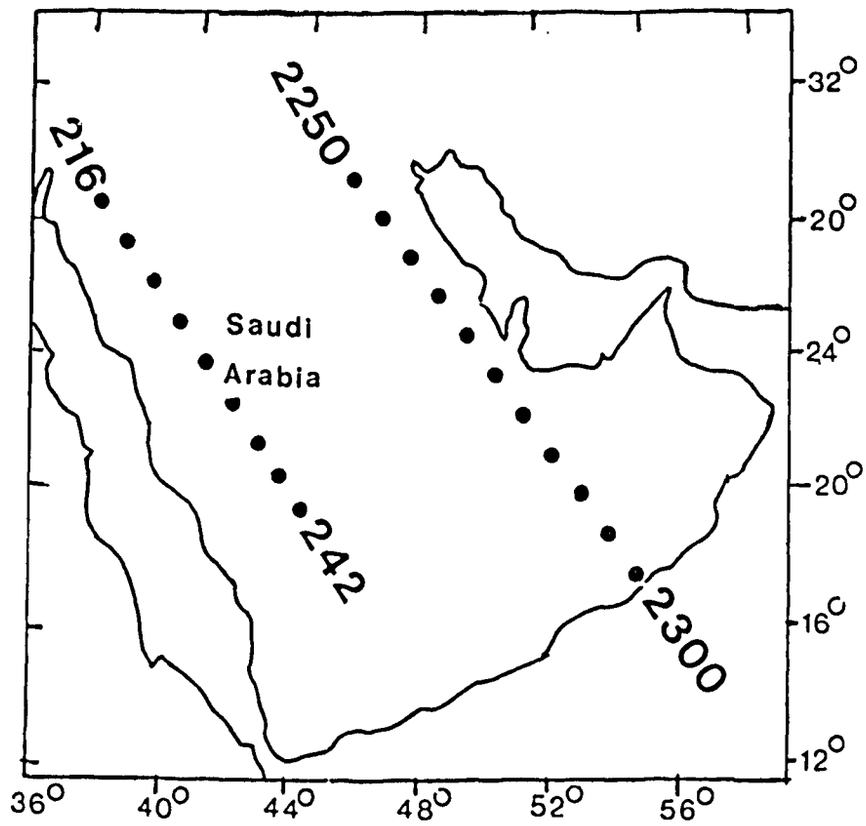


Figure 2.4 Large Format Camera (LFC) Mission 41-G Flight Path Index over the Arabian Peninsula. Numbers at beginning and end of the photo strips are frame numbers.

the original scale without losing detail (Sabins, 1986). The high spatial resolution of LFC photographs make them potential tool for land use and land cover mapping. At a scale of 1:50,000 and 1:100,000 the LFC photographs are comparable with aerial photographs of the same scale (see Chapter 6 for more details)

Because the LFC photographs were aquired with 80 percent forward overlap, it is possible to view them stereoscopically. This helps in the interpretation of dune morphology and in dune height measurements (see Chapter 6).

2.7 RADAR IMAGERY

Radar imagery system provides a source of electromagnetic energy to illuminate the terrain. The basic principle of radar is transmitting short bursts, or pulses of microwave energy in the direction of the required target and recording the strength and origin of echoes or reflections received from objects. Radar systems may be ground based or mounted in aircraft or spacecraft.

Most airborne radar remote sensing is done with systems that use antena fixed below the aircraft and pointed to the side. Such systems are called Side-Looking Radar (SLR) or Side-Looking Airborne Radar (SLAR). SLAR systems produce continuous strips of imagery detecting large ground area located adjacent to the aircraft flight line. The term SLR is widely used now because it includes both spacecraft as

well as aircraft. There are two basic types of SLRs:

(i) Real Aperture Radar (RAR) which is technologically simple and less costly;

(ii) Synthetic Aperture Radar (SAR) which is more expensive to build operating by using complex signal processing techniques and sophisticated aircraft.

One of the outstanding characteristics of SLR is that the resulting synoptic image provides the interpreter an opportunity to differentiate terrain textures and identify regional and geomorphological patterns over a wide area. SLR systems can operate successfully in darkness and poor visibility and can penetrate cloud.

SPACEBORNE RADAR SYSTEMS:

The first spaceborne radar system was the SEASAT satellite which was launched in 1978 and designed by the Jet Propulsion Laboratory (JPL) for studying ocean waves and currents with resolution of about 25 meters (JPL, 1980). Unfortunately, the satellite malfunctioned four months after launch producing limited numbers of images of some parts of the world. The Arabian Peninsula was not included in the coverage of the SEASAT imagery.

The same radar design was then adapted by Jet Propulsion Laboratory for mounting in the NASA space shuttle. This imaging radar is called SIR-A (Shuttle Imaging Radar-A) and

was launched during the second shuttle mission in November 1981 to acquire images of different parts of the world. Figure 2.5 shows the configuration of the SIR-A system and Table 2.3 summarizes its characteristics. More details about the different specifications of the SIR-A are given in Appendix (1). The image data were recorded as holographic film on board the shuttle. The data film was developed and then processed at Jet Probulsion Laboratory to produce the original image film at a scale of 1:500,000.

In October 1984, SIR-B was launched following the success of SIR-A. Wavelength, spatial resolution, and polarization were the same as in the earlier mission. For SIR-B the antenna was modified, however, to permit the depression angle to be changed during the mission within a range of 30 to 75 degrees (Sabins, 1986). Most of the SIR-B images were recorded digitally, while the rest of the images were recorded by on-board tape recorders and returned to earth with the Shuttle vehicle. Table 2.3 summerizes the SIR-B charcteristics.

RADAR TONAL INTERPRETATION GUIDES:

TONE: Is defined as image record of varying microwave backscatter characteristics of targets; strong returns produce light image tones; weak returns produce dark image tones.

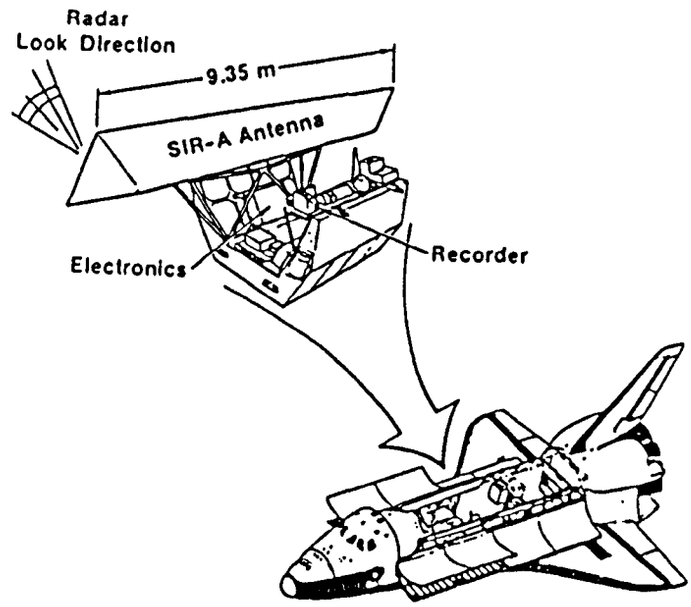


Figure 2.5 Configuration of the SIR-A system. From Sabins (1986).

Characteristics	SIR-A (1981)	SIR-B (1984)
Orbit inclination	38°	57°
Wavelength	L-band (23.5 cm)	L-band (23.5 cm)
Spatial resolution	38 m	25 m
Latitude coverage	50°N to 35°S	58°N to 58°S
Altitude	250 km	225 km
Image-swath width	50 km	40 km
Depression angle, γ	37° to 43°	30° to 75° (variable)
At average γ	40°	52°
Smooth criterion	$h < 1.5$ cm	$h < 1.2$ cm
Rough criterion	$h > 8.3$ cm	$h > 6.8$ cm
Polarization	HH	HH

Table 2.3: Characteristics of the SIR-A and SIR-B systems (Sabins, 1978).

GROUND PARAMETERS:

(i) Topographic expression at the macro-scale; generally, larger feature reflects more than a smaller feature.

(ii) Surface roughness at the micro-scale superimposed on non-normal incidence slopes; wavelength units of roughness.

SCATTERING THEORIES: Figure 2.6 shows 3 types of surface interaction; a. smooth (specular) surface: no return.

b. intermediate rough surface; modern return.

c. Rough surface with diffuse backscatter; strong return.

RAYLEIGH CRITERION: Radar smoothness is described as the Rayleigh Criterion that considers a surface smooth if

$$h < \frac{\lambda}{8 \sin B}$$

where: h = height of surface irregularities

λ = operating radar wavelength

B = depression angle

from Figure 2.6:

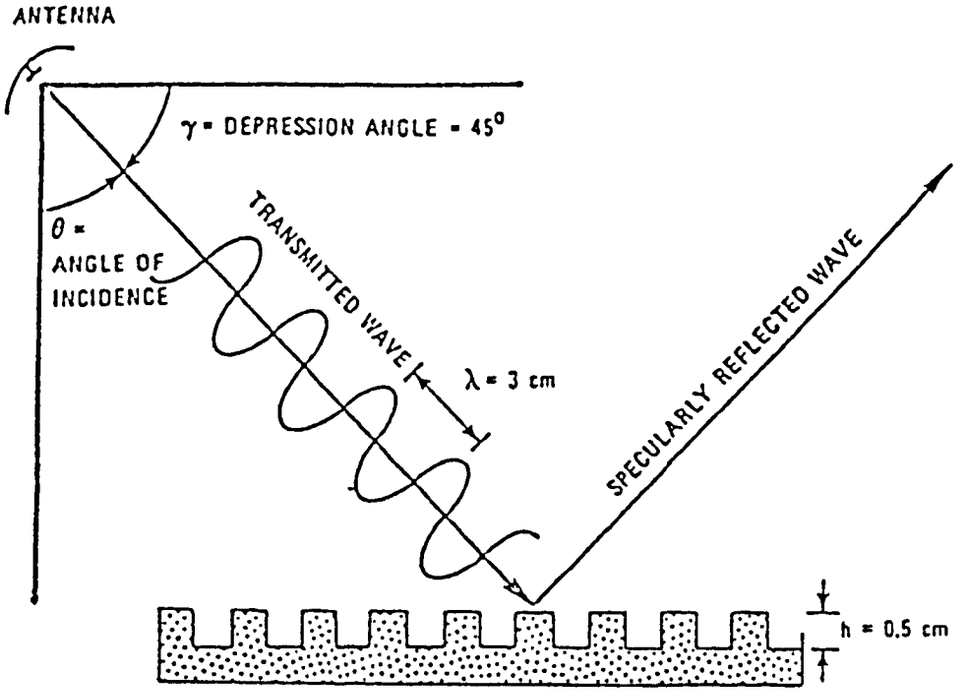
A. = 0.5 cm

B. = 0.8 cm

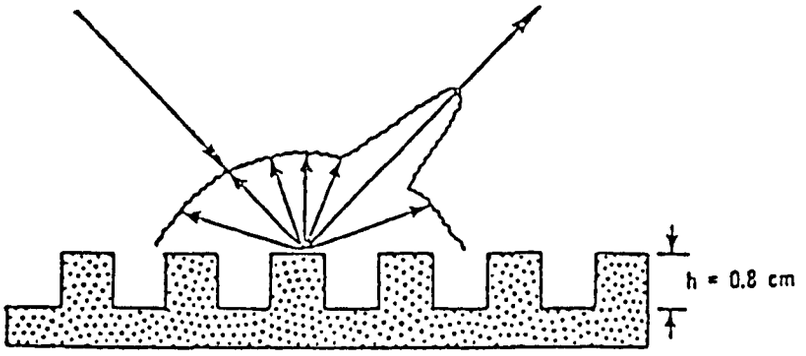
C. = 1.5 cm

= 3.0 cm at 45 dgerees

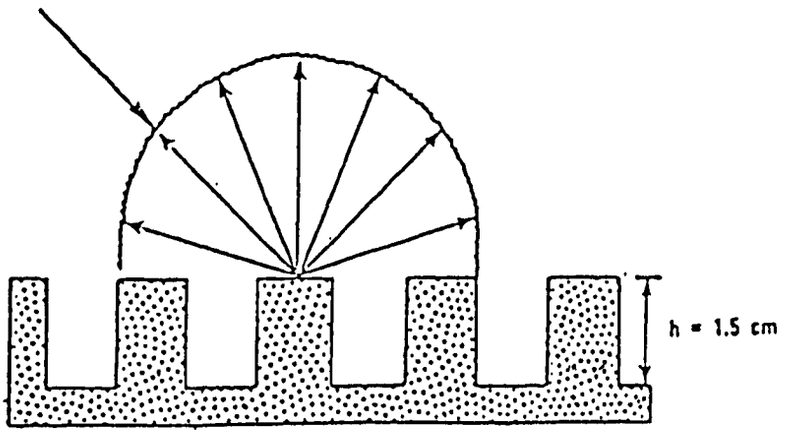
$$h < \frac{3.0 \text{ cm}}{8.\sin 45}$$



A. SMOOTH (SPECULAR) SURFACE; NO RETURN



B. INTERMEDIATE-ROUGH SURFACE; MODERATE RETURN



C. ROUGH SURFACE WITH DIFFUSE BACKSCATTER; STRONG RETURN

Figure 2.6 Models of surface roughness and radar return (not to scale). From Sabins (1986).

$$h < \frac{3.0 \text{ cm}}{8.\ 0.7}$$

$$h < 0.54 \text{ cm}$$

For A. roughness would be specular

For B & C. roughness would be diffuse.

Smooth criterion; a surface is considered smooth if:

$$h < \frac{\lambda}{25.\ \sin B}$$

Rough criterion; a surface is considered rough if:

$$h > \frac{\lambda}{4.4.\ \sin B}$$

if the wavelength of the radar is 3.0 cm and the depression angle is 45 degrees, then:

$$h < \frac{3 \text{ cm}}{25.\ \sin B} \qquad h < \frac{3 \text{ cm}}{4.4 \sin B}$$

$$h < \frac{3 \text{ cm}}{25.\ 0.71} \qquad h < \frac{3 \text{ cm}}{4.4.\ 0.71}$$

$$h < 0.17 \text{ cm} \qquad h < 0.96 \text{ cm}$$

See Figure 2.7 and Table 2.4.

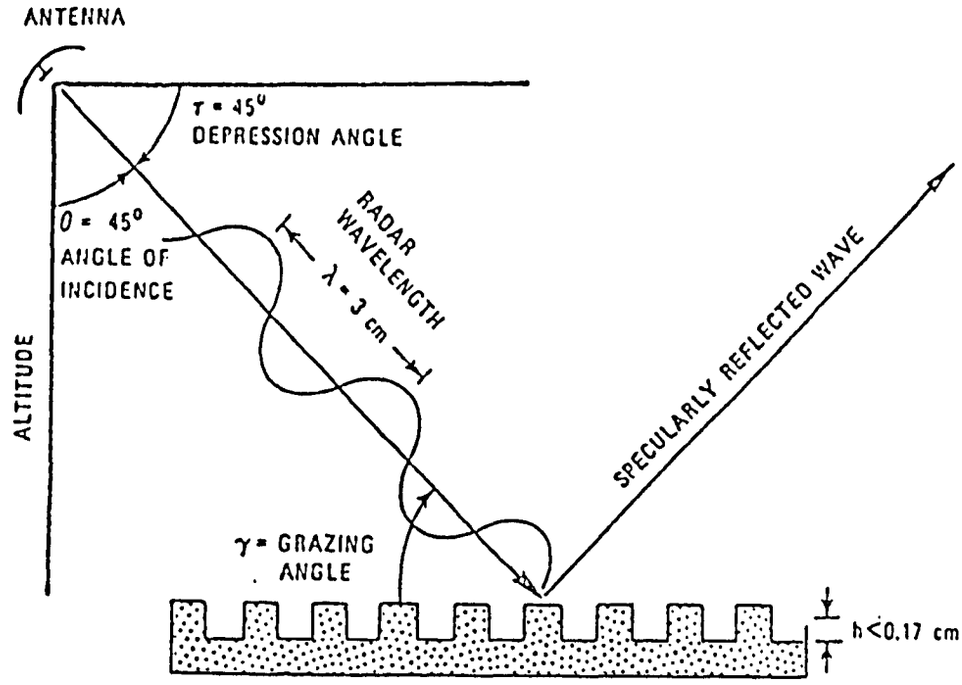
(iii) Complex dielectric properties of the material: Ability to reflect at microwave frequencies. This depends on chemical composition and water content of the material. The dielectric constant of dry sand is equal to 3 while water is 80 (MacDonald & Waite, 1971). Generally, the higher the dielectric constant the greater the reflection. The depth of penetration of radar waves below the surface varies inversely with the dielectric constant of the material and directly with the radar wavelength.

(iv) Orientation of target to antenna (e.g., linear features reflect more strongly when parallel to ground track and may be invisible in the across-track direction).

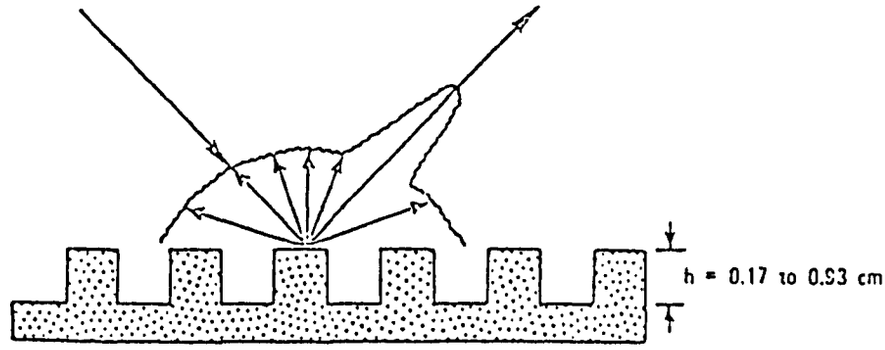
SYSTEM PARAMETERS:

1- Wavelength: Strongly influenced by surface roughness. A surface will appear rougher at shorter wavelengths. Longer wavelenghts have a lower backscatter component because surface appears smoother. The capability to penetrate precipitation and beneath a surface is increased with longer wavelenghts.

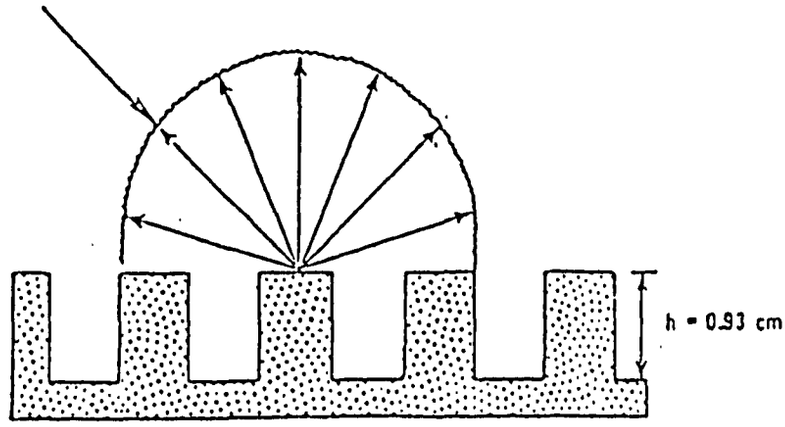
2- Look angle: Backscatter generally increases with increasing B and decreasing θ.



A. SMOOTH SURFACE; SPECULAR REFLECTION



B. INTERMEDIATE SURFACE ROUGHNESS; MODERATE RETURN



C. ROUGH SURFACE WITH DIFFUSE SCATTERING; STRONG RETURN

Figure 2.7 Models of surface roughness and return intensity for X-band radar (λ = 3 cm). (From Sabins, 1986).

Roughness Category	Ka-Band (λ = 0.86cm)	X-Band (λ = 3cm)	L-Band (λ = 25cm)
Smooth	h < 0.05cm	h < 0.17cm	h < 1.39cm
Intermediate	h = 0.05 to 0.27cm	h = 0.17 to 0.93cm	h = 1.39 to 7.85cm
Rough	h > 0.27cm	h > 0.93cm	h > 7.85cm

Table 2.4: Limiting values of vertical relief h for surface roughness categories. Depression angle γ and incidence angle θ are 45^{o}. From Sabins, (1986).

3- Polarization: The electric field vector of the transmitted energy pulse may be polarized or vibrating in either vertical or horizontal plane (Sabins, 1978). When the radar pulse strikes the terrain, most of the energy returned to the antenna has the same polarization as the transmitted pulse. This energy is recorded as parallel-polarized and is designated HH (horizontal transmit and horizontal return) or VV (vertical transmit and vertical return). Some radar systems have a second antenna element that recieves the depolarized energy vibrating at right angles to the polarization direction of the transmitted pulse. The resulting imagery is called cross polarized and could be either HV (horizontal transmit, vertical return) or VH (vertial transmit, horizontal return).

Surfaces rough compared to wavelength result in diffuse reflections and cause depolarization (i.e. plane of polarization is rotated). The rougher the surface the greater the degree of depolarization and hence the stronger will be HV and VH.

Surface irregularities of a size approximately 1/3 to 2x the wavelength (i.e., slightly rough) produce a combination of diffuse and specular reflections and such surfaces (grass, gravel) usually produce more backscatter with vertical than horizontal polarization.

SPATIAL RESOLUTON: Resolution in the range and azimuth directions is determined by separate engineering characteristics of the radar system. The ground resolution cell is defined by combination of range resolution and azimuth resolution.

a- Range resolution: Spatial resolution in the range direction, Rr, is determined by the duration of the pulse of transmitted energy and is theoretically equal to 1/2 the pulse length (Figure 2.8). The pulse length (T) is measured in micro seconds. The depression angle (Y) is the angle between the horizontal plane and the line connecting the target and the antenna.

The equation for range solution is:

$$Rr = \frac{T\ c}{2 \cos Y}$$

For a depression angle of 50 degrees and pulse length of 0.1 microsecond, range resolution is calculated as:

$$Rr = \frac{(0.1.\ 10\ \text{sec})\ (3.\ 10\ \text{m.sec}^{\ })}{2 \cos 50}$$

$$Rr = \frac{0.3.\ 10\ \text{m}}{2.\ 0.64}$$

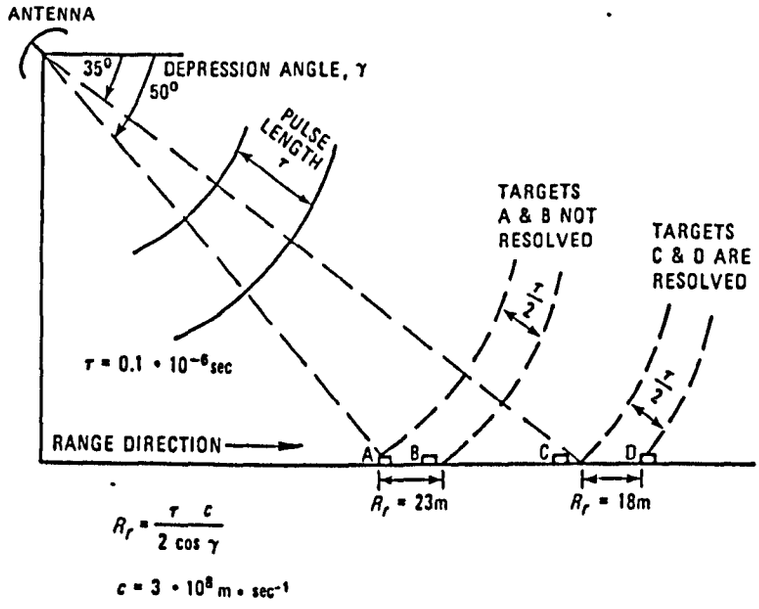


Figure 2.8 Radar resolution in the range direction Rr. From Sabins, (1978).

$$Rr = 23 \text{ m}$$

Thus, at a depression angle of 50 degrees, objects must be separated by more than 23 m in the range direction to be resolved.

b- Azimuth resolution: Azimuth resolution direction, Ra, is determined by the angular width of the terrain strip illuminated by the radar beam (Sabins, 1978). To be resolved, targets must be separated in the azimuth direction by a distance greater than the beam width on the ground. Azimuth resolution is higher for shorter wavelengths. Beam widthis inversely proportional to anttena length (resolution improves with longer anttena length). The equation for Azimuth resolution Ra, is:

$$Ra = \frac{0.7S\lambda}{D}$$

Where, S : the slant range

λ : wavelength of the transmitted energy

D : antenna length

QUALITY AND AVAILABILITY OF RADAR IMAGERY IN SAUDI ARABIA:

Radar imagery acquired over Saudi Arabia is restricted to the synthetic aperture imaging radar system (SIR-A and SIR-B). SIR-B image coverage over Arabia was limited because

of a failure in the transmission and receiving power of the SIR-B system (two-way loss of 12 to 20 dB). Hence, very few images, and these of low quality, were acquired over sandy areas.

SIR-A, on the other hand, produced good images over pre-selected areas of the Arabian Peninsula. Two data take numbers were acquired over the Peninsula (7 & 37A; Fig. 2.9). SIR-imagery is available in the form of photographic prints, negatives, and transparencies. The scale of the image is 1:500,000, with a ground resolution of 40 meters in both range and azimuth. SIR-A was an L-band (23.5 cm wavelength) that incorporated HH polarization and a 47 degrees incidence angle at centre swath. All images were in focus and very clear.

In Chapter 6, SIR-A imagery acquired over parts of the Arabian Peninsula is assessed as an aid in sand dune mapping.

2.8 LANDSAT SYSTEMS

A new dimension to remote sensing of the environment was introduced in the past decade by means of sensing the earth from man-made satellites. This unmanned system was originally called ERTS (Earth Resources Technology Satellite) but later changed to Landsat. Landsat 1 was launched on 23 July 1972 and acquired data until 6 January 1978 when operation ceased. Landsat 2 and 3 were launched on

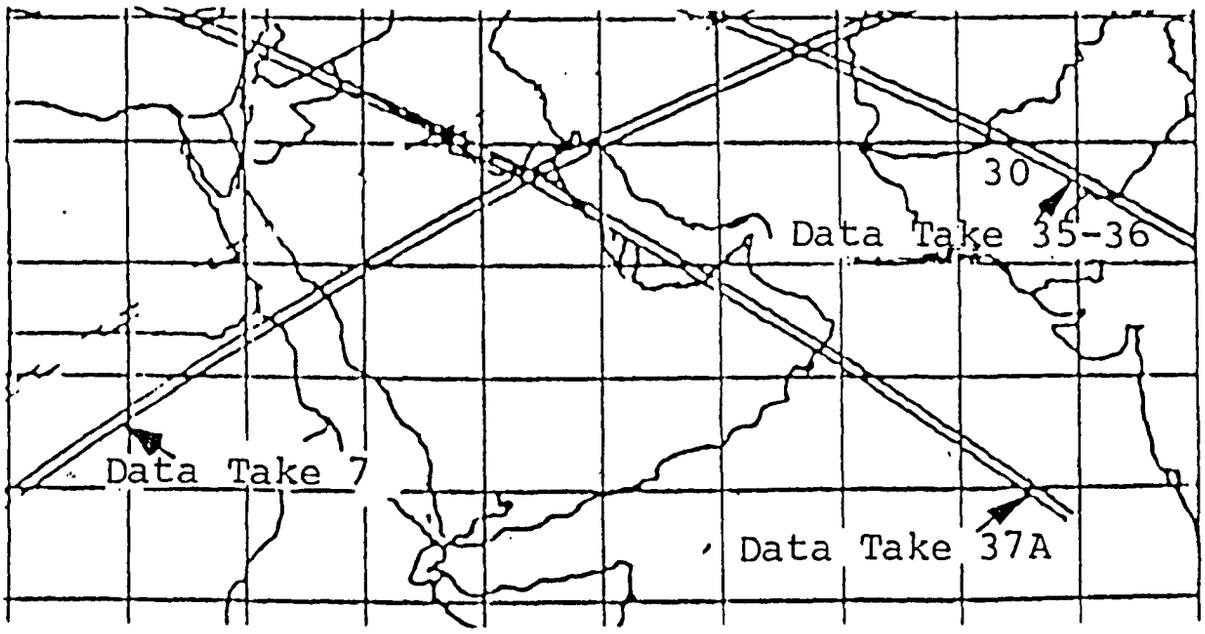


Figure 2.9 SIR-A data takes acquired over the Arabian Peninsula during the Shuttle Columbia Mission in November 1981 (JPL, 1980).

21 January 1975 and 5 March 1978 respectively. Landsat 4 was launched on 16 July 1982 and finally Landsat 5 was launched on 1 March 1984. Landsat has proven to be a highly successful system for imaging the earth. Spatial and spectral resolution were improved in Landsat 4 And 5. The five Landsats belong to two generations of technology with different platforms and orbital characteristics (Appendix 1). Landsats 1,2,3 carried a Multi Spectral Scanner (MSS) imaging system. Landsats 4 and 5 are larger and more complex than their predecessors with major components including a Multi Spectral Scanner (MSS) imaging system and a new system, the Thematic Mapper (TM).

LANDSAT MULTI-SPECTRAL SCANNER (MSS) SYSTEM

This section discusses the spectral and the spatial aspects of the Landsat MSS system. For the orbital and operational characteristics see Appendix (1).

MSS SPECTRAL RESOLUTION:

The MSS on board the Landsat satellites uses an oscillating mirror to scan the earth from west to east. The total field of view scanned is 11.56 degrees, covering an area of 185 x 185 km on the ground.

Table 2.5 lists the MSS band numbers with their corresponding wavelengths.

MSS Band	Wavelength μm	Color	Color normally used for Projection
4	0.5 to 0.6	Green	Blue
5	0.6 to 0.7	Red	Green
6	0.7 to 0.8	Photo. IR	Red
7	0.8 to 1.1	Photo. IR	Red

Table 2.5: Landsat multispectral scanner bands.

MSS SPATIAL RESOLUTION:

As discussed earlier in Section 2.2, the measure of spatial resolution used most widely for the MSS is the instantaneous field of view (IFOV). The MSS nominal IFOV is 79 m square as determined by the nominal altitude of the satellite, the focal length of the optical system and the detector size. Slater (1983) points out that due to cladding around the optical fibers which transfer the radiance to the detectors, the detector size is reduced and this results in an IFOV of 76.2 m square at a nominal altitude of 918.6 km. Since the altitude of the satellite varies between 880 and 940 km (Taranik, 1978) due to noncircularity of the orbit and nonsphericity of the earth, the 79 m IFOV may vary from 76 m to 81 m.

In Chapter 6 , the spatial resolution of Landsat MSS imagery is assessed for sand dune mapping.

LANDSAT THEMATIC MAPPER (TM) SYSTEM

The TM operates in seven spectral bands. The band designations, spectral ranges, spatial resolution, and principal applications are given in Table 2.6. These spectral bands were chosen primarily for vegetation monitoring. The one exception is band 7, which was added for geological applications.

Improved spatial resolution (over that of MSS) is another aspect of TM imagery. A pixel size of 30 m (ground

Band	Range (Micrometres)	Potential Applications
1	0.45 - 0.52	Coastal Water Mapping: Soil/ Vegetation Differentiation; Deciduous/Coniferous Differentiation
2	0.52 - 0.60	Green Reflectance by Healthy Vegetation
3	0.63 - 0.69	Chlorophyll Absorption for Plant Species Differentiation
4	0.76 - 0.90	Biomass Surveys: Water Body Delineation
5	1.55 - 1.75	Vegetation Moisture Measurement; Snow/Cloud Differentiation
6	10.4 - 12.5	Plant Heat Stress Management; Other Thermal Mapping
7	2.08 - 2.35	Hydrothermal Mapping

Table 2.6: TM Spectral Bands and their Potential Applications (NASA, 1982).

resolution) in all but band 6 was achieved. Band 6, a thermal band, has a pixel size of 120 m on the ground (see Appendix 1).

In Chapter 6 the spatial resolution of Landsat TM images is assessed for mapping dunes of different sizes.

SCALE ENLARGEMENT INVESTIGATION OF MSS AND TM IMAGERY:

Because the data comprising the scene are digital, Landsat MSS and TM images can be presented in different scales. An investigation was carried out to test the maximum possible enlargement for Landsat MSS and TM imagery. Two full resolution Landsat (MSS & TM) scenes were produced in negative format. Different enlargements were then made to test the limit of the imagery.

It was found out that the maximum possible representation of an entire Landsat MSS and TM scenes (185 x 185 km) is at scales of 1:250,000 and 1:100,000 respectively. However, for more detailed study an entire Landsat scene can be divided into smaller subscenes with larger scales (see Chapter 6 for interpretation and results).

QUALITY OF LANDSAT MSS IMAGERY IN SAUDI ARABIA:

A survey of available Landsat MSS imagery of Saudi Arabia was completed prior to subsequent processing. The survey was designed to provide the following:

(i) The geographical coverage of the available imagery.

(ii) The percentage of cloud coverage. Only 10-20 % coverage was accepted

(iii) The quality of imagery.

The survey included Landsat MSS imagery acquired between 1972 and 1984 over Saudi Arabia. The survey showed that all Saudi Arabia is covered by Landast MSS imagery (113 scenes). The quality of imagery varied from one location to another. This may be due to the fact the satellite, in some areas, was set at the high gain mode to optimize water quality measurements sacrificing quality of measurement over land. In fact all available Landsat MSS imagery of the eastern coast of Saudi Arabia acquired between 1974 and 1981 were of low quality. Images acquired in this high gain mode have the visible bands (bands 1 and 2) all saturated in the land areas. The remaining two bands (bands 3 and 4) in the infrared, are highly correlated leaving effectively one band to work with. The survey showed a better quality imagery over inland areas.

DUST STORM EFFECTS:

Dust storms in Saudi Arabia contribute to the low quality of some imagery. The Arabian Peninsula has been identified by Idso (1976) as one of five major world regions where dust storm generation is especially intense, and Prospero (1981)

reports that a major zone of dust haze can be observed in the Arabian Sea during June, July and August. Some studies have assessed the aeolian contribution to sediments in the Arabian Gulf, and the Arabian and Red Sea (Emery, 1956; Sugden, 1963; Stewart, Pilkey et al., 1965; Kolla & Biscaye, 1977; Khalaf & Al-Hashash, 1983). However, there is no comprehensive study of dust storm frequency, distribution, and seasonal variation for Saudi Arabia. The best account of dust storm in the Middle East comes from a study carried by Middleton (1986). The area studied included the Arabian Gulf and the south east coast of Arabia. Figure 2.10 shows the primary season of dust storms. The largest part of Saudi Arabia experience dust storm activity through the year but a maximum occurs during the months March, April, and May (Middleton, 1986). In the Eastern Province of Saudi Arabia the principal sandstorm season occurs during the months of May, June, and July locally known as the "Shamal" period (Fryberger, 1984). Dust haze is also experienced throughout the year on the west coast of the Arabian Gulf as far south as Qatar. The most important flow of dust is carried by the prevailing northwesterly "Shamal" wind which raises dust from the alluvial plains of the lower Tigris-Eupherates basin and carries it down the Arabian Gulf (Fig. 2.11). Little dust haze is experienced from October to March, the season of the north-east monsoon, although from mid-December to mid-March the dust "Belat" wind blows off the hot, dry interior of the Rub'al Khali (Middleton, 1986).

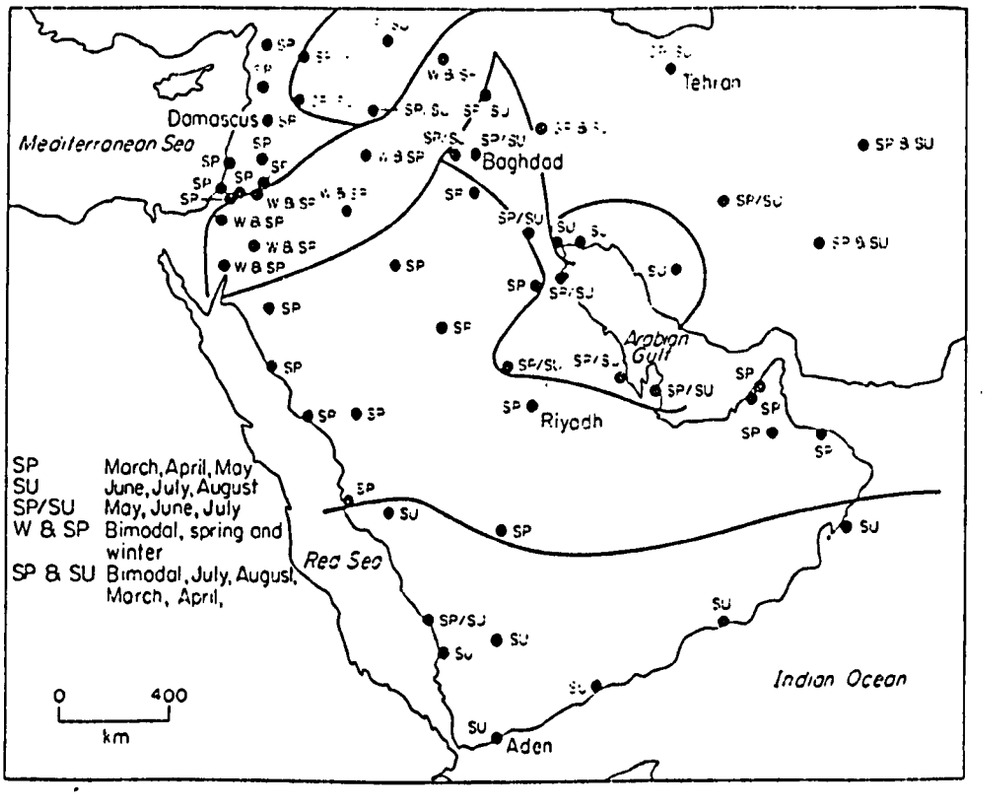


Figure 2.10 Primary seasons of dust storms. From Middleton (1986).

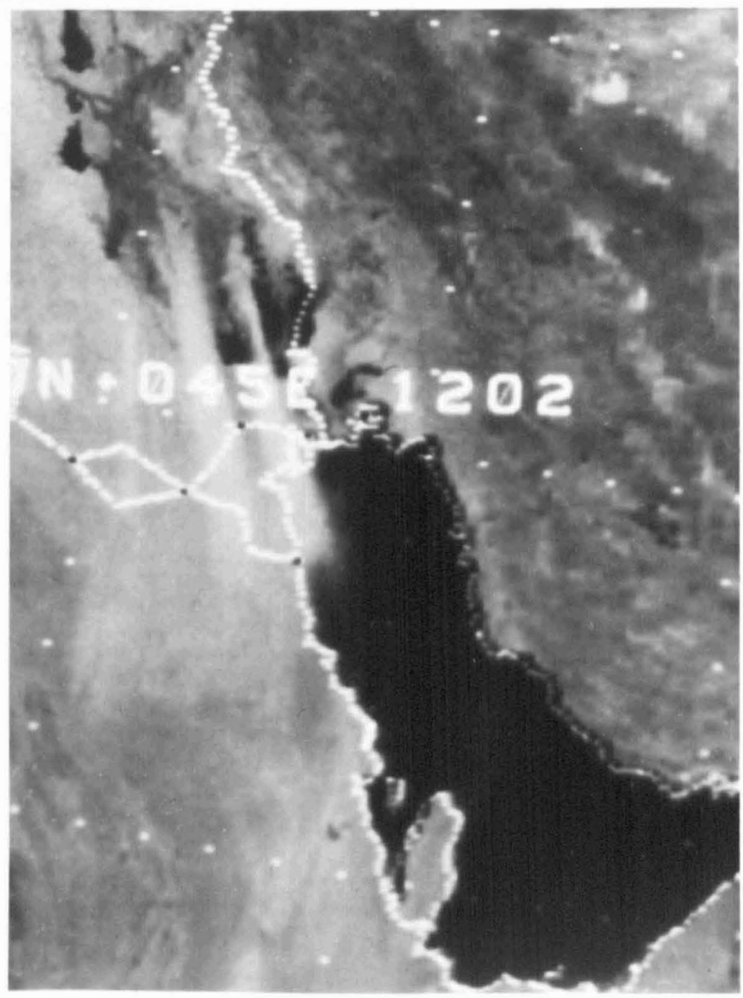


Figure 2.11 NOAA satellite imagery acquired on 1981 over North Eastern Arabia showing a dust plume over Kuwait and part of the eastern coast of Saudi Arabia.

When comparing meteorological observations with the surveyed images acquired over Saudi Arabia it was found that the degradation of some Landsat imagery could be attributed to the dust haze effects.

SUN ANGLE EFFECTS:

Since sun provides most of the electro-magnetic radiation that is incident or reflected from the earth's surface through the atmosphere, the relative position of the sun to the remote objects and the sun angle (from the horizon) play an important role in determining the reflected form of that object on the image. This reflection is a component of many factors such as soil moisture, surface roughness, particle size density (grain size), colour and chemical composition. Figure 2.12 shows a quantitative estimate of the interaction between slope angle, aspect and sun angle for two dates with the maximum difference in sun elevation. The sun angle effect, unlike other atmospheric factors, can not be fully corrected by enhancement techniques.

Since this research deals mainly with mapping aeolian dunes, the sun angle play an important role in such an aspect. Aeolian dunes have an angle of repose of approximately 30 to 32 degrees. Hence, a sun angle of close to 30 degrees would be ideal for enhancing dune relief.

The majority of the images covering Saudi Arabia were acquired during winter season. Winter, Spring and Autumn

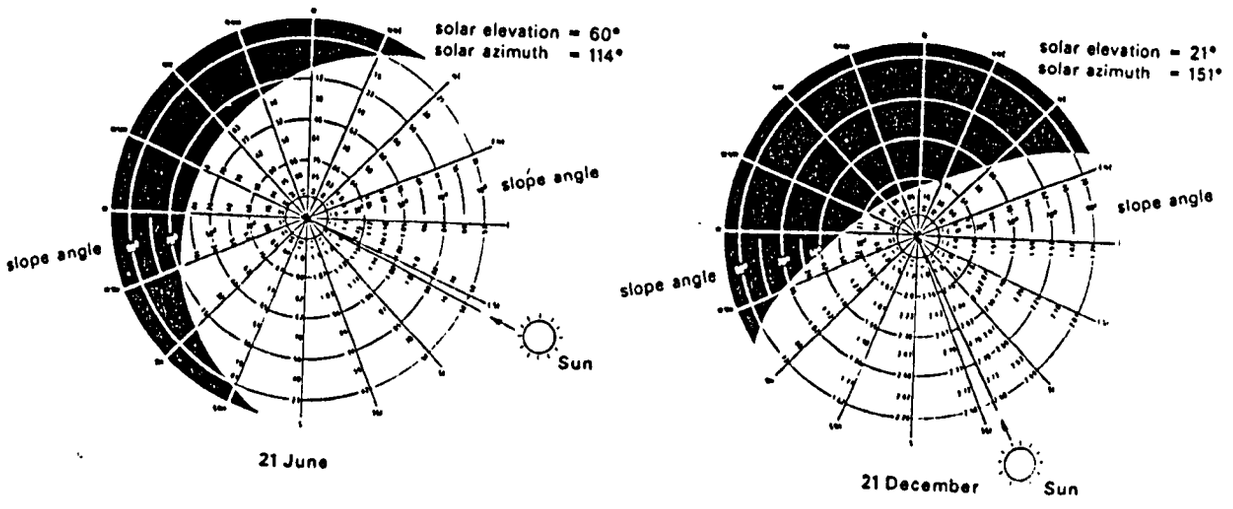


Figure 2.12 Quantitative estimates of the interaction between slope angle aspect and the sun angle for two dates with the maximum difference in sun elevation. The values represent incidence values and the black areas represent slopes in shadow (Justice & Townshend, 1981).

images have relatively low sun angles (34 - 44 degrees) which proved useful in enhacing dune relief. Summer images over Saudi Arabia, on the other hand, are rare. This may be due to the fact that Summer images have a relatively higher sun angle (57 - 64 degrees) which subdued relief leaving topography unshaded. At relatively high sun angles, the sand deposits appear washed out and it is very difficult to distinguish sand dunes from surrounding sediments which appear equally bright. Because of the lack of a summer Landsat MSS imagery over Arabia, LFC photographs acquired at low sun angle (36 degrees) and high sun angle (58 degrees) were selected instead for illustration. Figure 2.13 is a black and white photograph acquired at a sun angle of 36 degrees over An Nafud Sand Sea. Figure 2.14 was acquired at a sun elevation of 58 degrees over the southern Jafurah Sand Sea. At a 58 degree sun angle sand dunes are not recognizable and appear "washed out".

2.9 DISCUSSION AND CONCLUSION

This chapter presented a background information of airborne and spaceborne imagery used in this research. The effect of atmospheric factors on the imagery and the capability and the limitations of each image were discussed.

The survey carried out to investigate the coverage and the quality of airborne and spaceborne imagery over Saudi Arabia shows the follwing:



Figure 2.13: A panchromatic LFC photograph acquired at a sun angle of 36 degrees over An Nafud Sand Sea. Note the high contrast between sand dunes and bedrock and the good definition in dune forms.

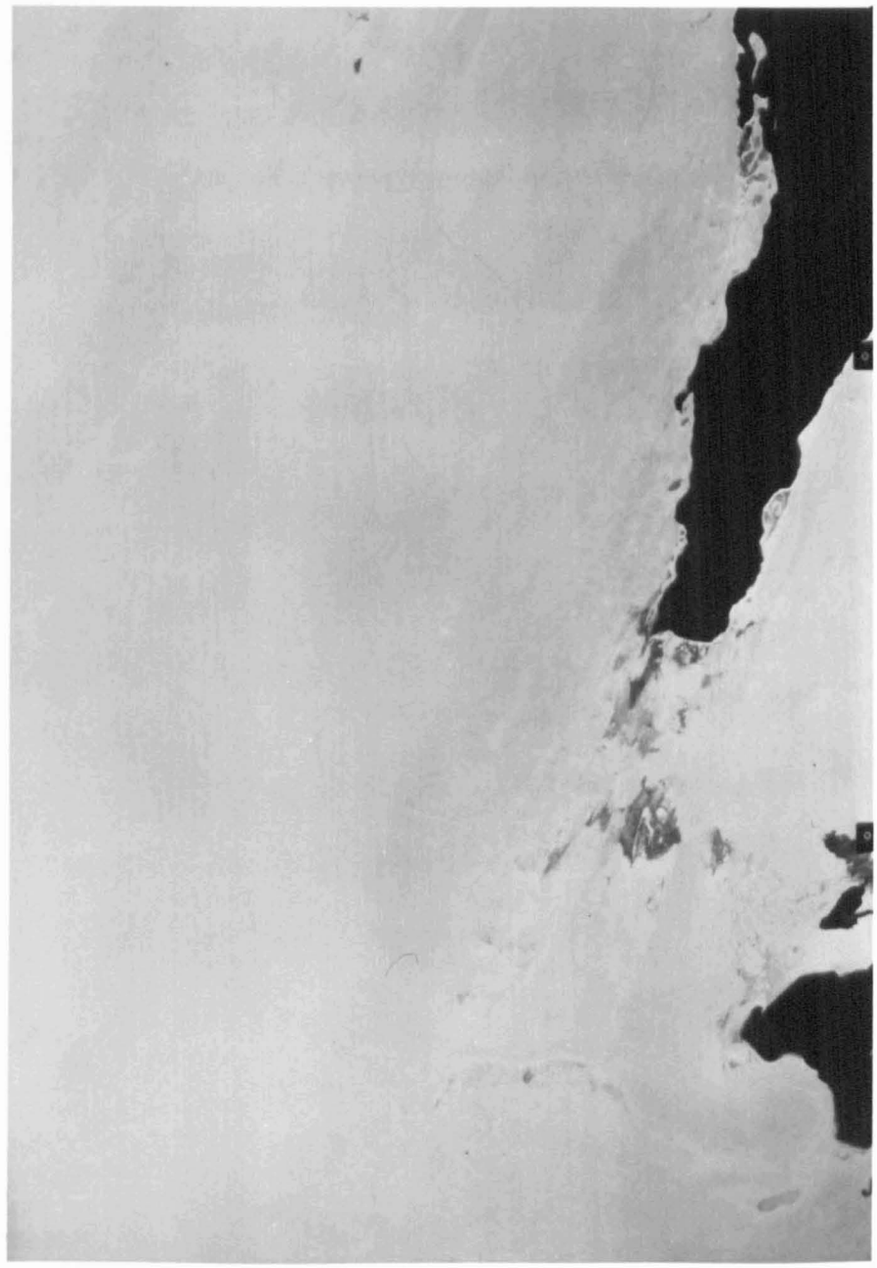


Figure 2.14 A panchromatic LFC photgraph acquired at 58 degrees sun angle over the southern Jafurah Sand Sea. The sand dunes are not recognizable and appear "washed out".

(i) Saudi Arabia is covered partly and fully by different remote sensing data. These include aerial and space photographs, Landsat (MSS & TM) images, and radar imagery (SIR-A & SIR-B).

(ii) The quality of the imagery acquired is dependant upon many factors. The two most important factors were: sun angle variations and dust and haze phenomena. Summer images acquired at sun elevation of about 58 degrees and with the usual sand dust were of low quality. On the other hand, winter images with sun elevation of about 35 degrees and with minimum dust and haze were of superior quality.

(iii) The diversity in the available photography and imagery over the sand seas of Saudi Arabia helps in assessing them for sand dune mapping (see Chapter 6 for this investigation).

(iv) The diversity in the spatial resolution offered by the various remote sensing systems discussed in this chapter allows for a good comparison of these systems in identifying dunes of different sizes. This comparison is presented in Chapter 6 as case histories.

(v) The stereoscopic capability of aerial photographs and the LFC photographs allows for dune height measurement as discussed in chapters 6 & 7. This is an advantage over other forms of remote sensing data which do not have this capability such as Landsat MSS and TM images and radar images.

CHAPTER 3

DIGITAL IMAGE PROCESSING TECHNIQUES

3.1 INTRODUCTION

Image processing techniques can greatly enhance the value of remotely sensed data. These have proven valuable for different geological applications such as mapping, and detection of hydrothermal alteration. However, the value of image processing in mapping sand dunes and other associated aeolian deposits has not been fully investigated.

In this chapter, digital image processing techniques used in this study for sand dune mapping are introduced and reviewed. A discussion of the application results of these techniques to sand dune mapping in Arabia are presented in chapters 4, 5, 6, 7 and 8.

3.2 DIGITAL IMAGES

A digital image is recorded by an array of discrete values, known as digital numbers (DN), at discrete spatial coordinates. Each element of this array is called a pixel, or picture element. Each pixel value relates to the amount of radiance transmitted from an area whose size define the spatial resolution of the scanner system. Each pixel is described by one byte (eight bits) of data with gray levels

ranging from 0 to 255. A multiband digital image consists of several overlapping arrays of pixels, each representing the same scene in a different spectral band.

A Landsat MSS image consists of four bands, for processing purposes conventionally treated as each having a range of 2^8 DN, although the maximum number of grey levels that can be recorded by the sensors is 2 (6 bits) for each band. This represents a compressed DN range of 0-127 for bands 1, 2 and 3 and a linear DN range of 0-63 for band 4.

3.3 BACKGROUND TO DIGITAL PROCESSING

Several authors have reviewed the theory and practice of digital image processing; (Billingsley et al., 1975; Anuta, 1977; Gonzalez & Wintz,1977; Pratt, 1978; Condit & Chavez, 1979; Gillespie, 1980, Schowengerdt, 1983). Digital processing of an image serves two main purposes. These are: (1) enhancement, which improves the quality and appearance of the image as an aid for visual interpretation and (2) extraction of quantitative information from the image by mathematical techniques.

About one tenth of the information contained in an MSS image can be usefully displayed for interpretation at one time (Goetz et al., 1975). Images must therefore be enhanced to enable the interpreter to make full use of them. Photographic methods for contrast enhancement and colour compositing enable the interpreter to extract more

information from the original images but they lack the advantages of digital techniques. The principal advantages of digital processing methods are their versatility, repeatability, and the preservation of the original data precision (Sabins, 1978). Photographic images as well as TV monitors are limited to one band (black & white) or three bands (colour), whereas in a computer there is no such dimensional limitation.

Interactive processing of the MSS images in this study was performed using two systems. The Interactive Digital Image Manipulation System (IDIMS) at the Research Institute - King Fahd Universuty of Petroleum and Minerals, Dhahran-Saudi Arabia and International Imaging System (IIS) at Imperial College were used. These two systems are similar in configuration, having a tape drive to load the image from CCT, a dedicated computer to store and process the image, a terminal at which the operator controls the processing and a colour TV monitor on which the processed image may be displayed. However the two systems use two different computers. The IDIMS is connected to a Hewlett Packard 3000 minicomputer under the Multiprogramming Executive operating system. IIS uses a PDP 11/24 minicomputer together with special IIS image - processing hardware and system 500 software.

The image processing facility at the Research Institute - King Fahd University was found to be more practical, faster

(equipped with an array processor), has more refresh memory channels (8 channels), displays 1024 x 1024 pixels in the TV monitor and is friendly to use. The IIS, on the other hand, was slower, has less fresh memory channels (4 channels), can only display 512 x 512 pixels in the screen. Another advantage of the "IDIMS" system is that it is linked to a drum scanner system capable of reading an image directly from a CCT to a film negative. This process is very important if the full resolution of the image is required. In this research, this process was found to be essential when comparing resolution offered by different image sensors.

3.4 COMPARISON BETWEEN MSS BANDS

An investigation of Landsat MSS imagery was carried out to compare all 4 spectral bands for sand detection. These bands have wavelengths between 0.5 to 1.1 μm. Two test site areas representing different sand seas of Arabia were selected for differentiation of dune sand from other superficial deposits by comparing images in all four spectral bands.

The four bands were displayed on the TV monitor simultaneously. The purpose of displaying the bands is to:

(i) Visually compare the different bands throughout the image.

(ii) From the visual interpretation, selection of specific bands and processing techniques for different applications were then decided on.

The DN values for different sands were also noted and compared. The Results of this investigation are given in Chapter 4.

Landsat MSS band 1 imagery was investigated to show submarine sand banks in the Arabian Gulf. The digital enhancement technique used in this investigation is described separately in section 3.9 and in (Al-Hinai, et al.,1987; Appendix 4).

3.5 DIGITAL IMAGE PROCESSING PROCEDURES

Image processing methods discussed here are restricted to those used in this study. They are grouped into four categories; Cosmetic processing, image rectification, image registration, and image analysis and display. These categories are discussed separately in the following sections.

COSMETIC PROCESSING:

This involves the replacement of defective scan lines by interpolation. The pixels in a defected line were replaced by the mean of the pixels in the preceding and following lines.

The removal of coherent instrument and transmission noise is a pre-requisite for subsequent image enhancement. The main type of coherent noise is periodic striping caused by sensor gain and offset variations (Sabins, 1978). Tape recorder dropouts cause another type of noise.

The first restoration process carried out was the removal of large dropouts. The International Imaging System (IIS) system 500 at the Imperial College was used to perform this task. A function called " Edit" which interactively filters noise in a displayed image via Tukey Median filtering was used. However, the use of Tukey Median Filter may introduce geometric errors and therefore was not used indiscriminately all over the image; only at selected parts, and those parts were not used later in the selection of ground control points nor in the measurement of registration errors. This is because in median filtering a pixel may be replaced by a neighboring pixel and therefore introduces a geometric error. Image striping or sixth line dropouts were removed interactively using the function "Destripe" in the system 500. The "Destripe" function was found to be effective and faster than other non-interactive functions.

3.6 IMAGE RECTIFICATION

Image rectification deals with radiometric and geometric distortions introduced by the scanning and transmission

processes. It aims to compensate for these distortions and to correct for atmospheric effects.

Scattering of light causes the most significant atmospheric effects on MSS images. The atmosphere selectively scatters the shorter wavelengths of light. Landsat MSS band 1 (0.5 - 0.6 μm) has the highest component of scattered light and band 4 (0.8 - 1.1 μm) has the least. There are two main effects of scattering; illumination of the terrain by scattered daylight in addition to direct sunlight, and back scattering of sunlight within the atmosphere. The result of this is to brighten the whole scene, with the loss of contrast. The contrast ratios of images can be digitally improved by correcting for the effects of this differential scattering. Corrections for atmospheric scatter (or haze) are usually performed at the satellite receiving stations. Techniques for determining the correction factor for atmospheric effects are described by Chaves (1975). The technique is basically to offset the DN histogram of each band so that pixels on dark surfaces in deep shadow have a corrected DN of zero (Fig. 3.1).

During the scanning process a number of geometrical distortions are introduced into the image data. The most significant geometric distortion is due to earth rotation during the time required to scan the frame and is called skewing. The amount of skewing is a function of latitude, eg at a latitude of 40 degrees N, the skew angle of the image

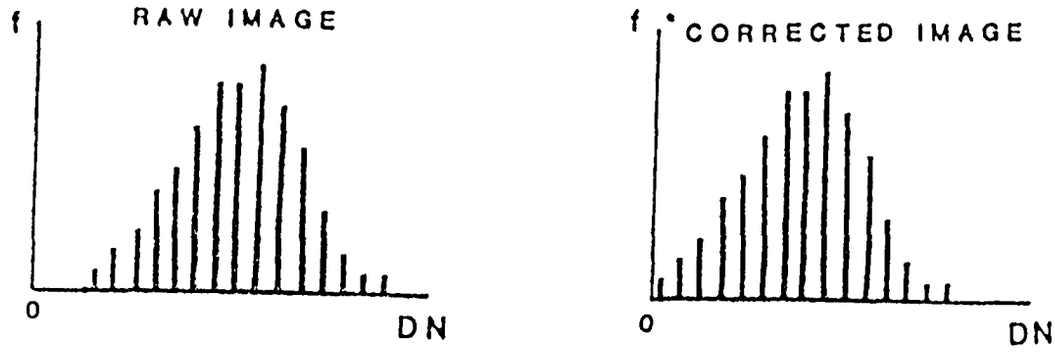


Figure 3.1 Atmospheric correction by offsetting the entire DN histogram so that the darkest pixels in shadow become black (DN = 0).

is 3 degrees, resulting in a shift of 122 pixels between top and bottom line of the image frame (Sabins, 1978).

All Landsat (1-5) images used in this research were geometrically corrected using the function " Deskew" in system 500. This function geometrically corrects a Landsat image to remove the distortion due to the earth's rotation. Geometric distortions caused by the earth's rotation and sensor sampling bias were then removed by using Nearest Neighbor re-sampling method (Siegal & Gillespie, 1980).

3.7 SPATIAL REGISTRATION

Precise image-to-image registration is necessary to form image mosaics, map temporal changes accurately, or compare images from different sensors. Registration accuracy depends on many factors. among these factors is the solar elevation changes which produces different shadow patterns that can produce mis-registration if locations that are heavily shadowed are selected for correlation (Schowengerdt, 1983). Another imoprtant factor is the availibility of ground control points (GCPs) in the area to be registered.

In this investigation, multitemporal images were used to investigate the measurement of dune pattern changes between images. There are two methods for digital spatial registration; Automatic registration; and manual registration.

(i) AUTOMATIC REGISTRATION: Automated digital registration can be accomplished with some measure of similarity or dissimilarity between two images that is calculated as a function of relative shift between them (Schowengerdt, 1983). This is done without generating ground control points. The mathematical calculation and the processing procedure is discussed in Schowengerdt (1983).

An average registration errors of about one-fourth to one-half pixel between two Landsat MSS images from different dates were achieved (Bonrud & Henrikson, 1974). In this investigation, however, automatic registration was not used because of the lack of the software required for such analysis in the IIs image processor (System 500) and in the IDIMS system.

(ii) MANUAL REGISTRATION: This involves the the visual location of ground features in the two images to be registered. This approach is particularly efficient with the aid of CRT image display and a movable cursor that can provide pixel coordinates in the displayed image.

Manual digital image to image registration was performed as an aid to measurement of dune movement rates. Two cloud free Landsat MSS scenes 176/42 (Landsat 1), acquired September 4, 1972 and 164/42 (Landsat 5), acquired January 15, 1984 - were used. These represent a reasonable period of time (12 years) for dune movement measurement. Digital processing was

carried out at Imperial College, using the IIS image processor.

Processing was carried out in three stages:

(i) Selection of ground control points;

(ii) Image to image registration;

(iii) Measurement of sand distribution pattern changes between images. Figure 3.2 illustrates the different stages involved in this process.

(i) SELECTION OF GROUND CONTROL POINTS

Landsat MSS data, although corrected for earth curvature and rotation, satellite altitude variations and sensor non-linearities, still contain geometric distortions with the centre of the scene located only to an accuracy of one kilometer (Davison, 1986). These errors become important when images are to be registered. Hence, geometrically transformed imagery is required in order to locate common ground control points in different scenes of the same area and to perform multi-temporal analysis by registering images acquired at differnt times as "overlays" of the same area.

Ground control points (GCPs) were selected using Landsat MSS band 4 (0.8 - 1.1 um) data as infra-red imagery is least affected by atmospheric haze. An interactive stretch was applied to both Band 4 images (dated 1972 & 1984) to enhance

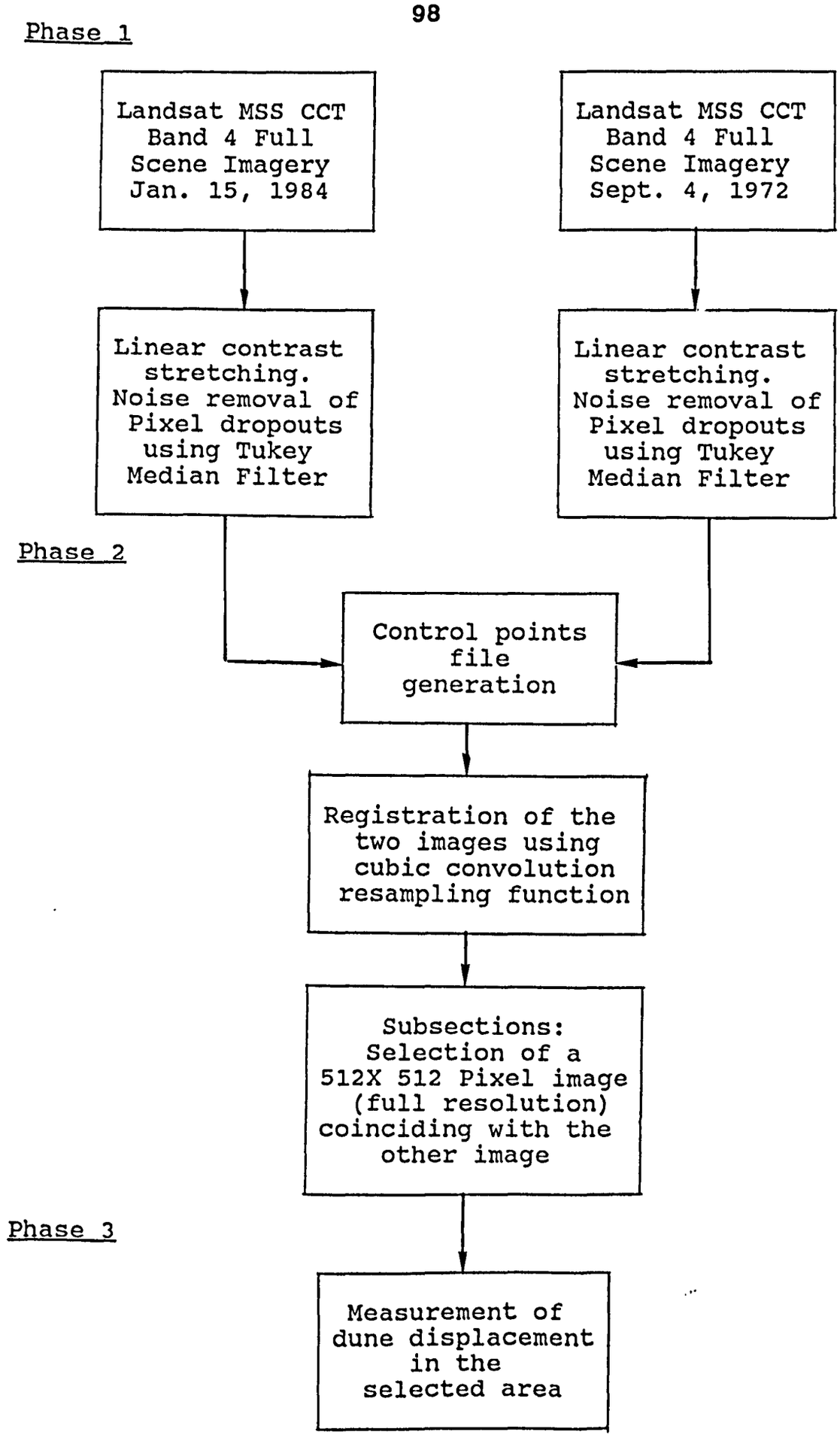


Fig.3.2: A diagram illustrating the methodology used for dune movement measurement from multi-temporal Landsat MSS images.

existing features in both images. Twelve GCPs were then selected using coastline features, road intersections and sabkha-bedrock boundaries. Identification of GCPs proved to be difficult due to the lack of a sufficient number of fixed points in active dune terrains (see chapter 7, for more disussion on the availability of GCPs on sandy terrains). For this reason, the points selected were not distributed evenly throughout the image, but were slightly more numerous along the coastlines and sabkha-bedrock boundary, but less numerous in active dune areas (Fig. 3.3).

(ii) IMAGE TO IMAGE REGISTRATION: Involves correlation of geographical control points and change in image geometry to compensate for variations in satellite attitude and altitude. In this investigation, Landsat MSS imagery of 1972 was taken as a reference frame, and the 1984 imagery was warped to register to it using GCPs identified in each image. A computer generated polynomial fit correlation estimated the average registration error for each GCP file. Average errors of between 0.6 and 0.7 pixels were achieved. A spatial transformation using Nearest Cubic Convolution was then performed to register the 1984 scene to the 1972 scene. The use of spatial transformation functions can introduce some geometric error since the nearest value (DN value) and not the actual value is used. It was therefore very important to select a transformation function which introduces the minimum error. Nearest Neighbour re-sampling was found to introduce a geometric error of about 0.25

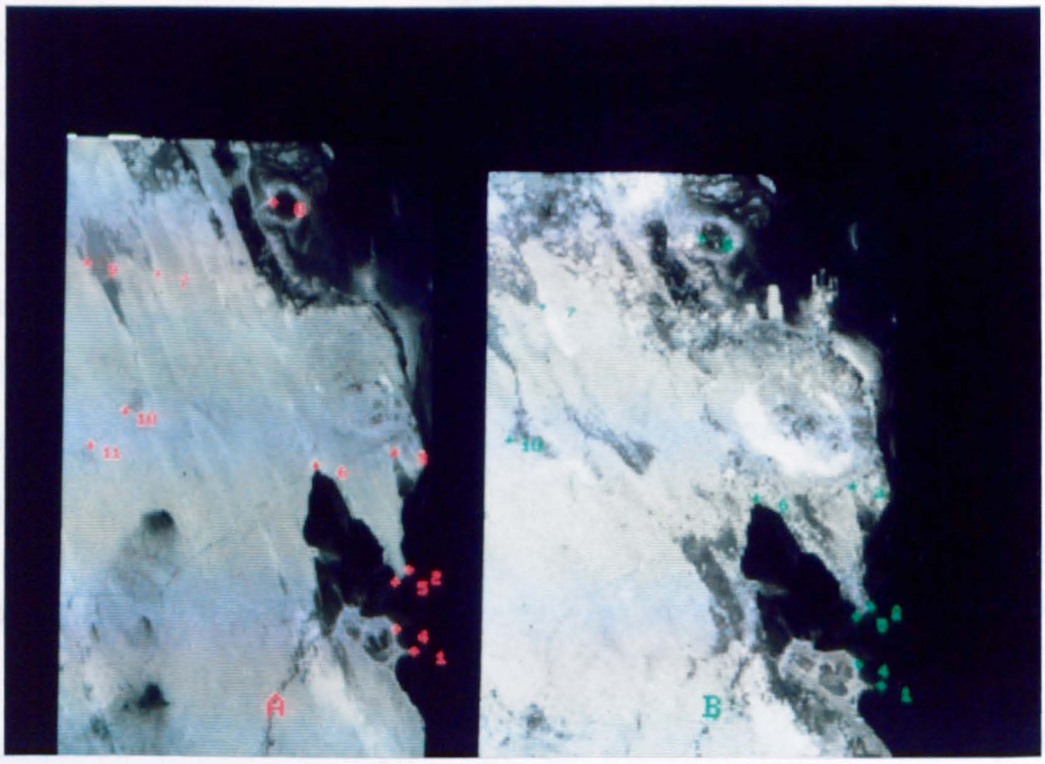


Figure 3.3 Distribution of selected ground control points in the 1972 and 1984 images.

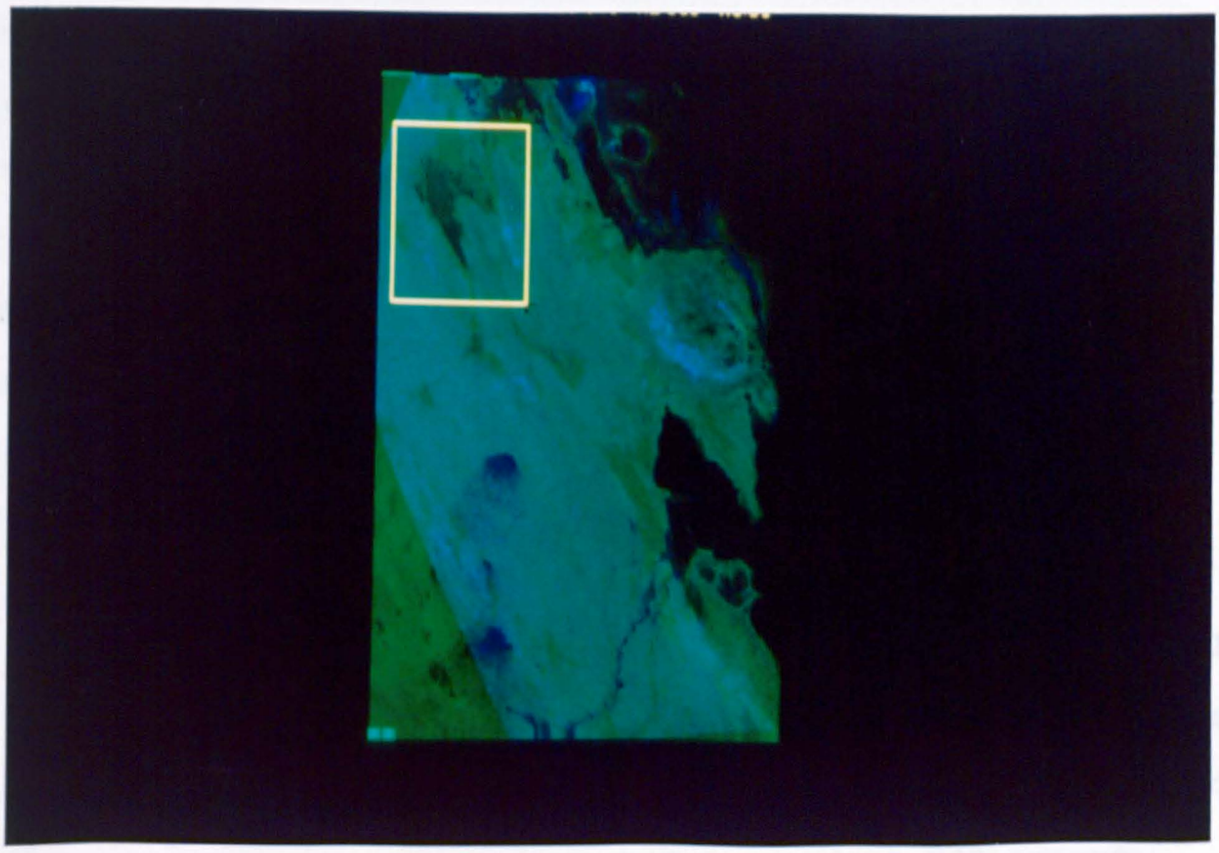


Figure 3.4 The digitally registered 1972 (blue) and 1984 (green) images. The study area is outlined.

pixel. Cubic Convolution re-sampling function introduces a geometric error of less than 0.1 pixel. Therefore, Cubic Convolution re-sampling was selected for the spatial transformation. The overall registration error ranged between 0.7 to 0.8 pixels. Figure 3.4 shows the digitally registered images.

(iii) MEASUREMENT OF SAND DUNE POSITION CHANGES BETWEEN THE IMAGES: After transformation, two registered full resolution 512 x 512 pixels sub-scenes were displayed for dune displacement measurement. Figure 3.5 is a 1972 full resolution subscene showing the investigated dunes. Thirty dunes were defined in each subscene. In order to measure dune displacement, the direction of dune movement had to be established first. Since the dunes investigated are all barchans and barchanoid ridges (slipfaces directed SSE), and the wind is unidirectional (NNW), the dunes are moving from NNW to SSE direction. The distance each dune moved was assertained from the change in position of the crest of the dune. Displacement of these dunes between 1972 and 1984 was recorded by measuring the distance between crests of each dune, using X and Y coordinates (i.e sample & line positions). The difference between the position of the pixel represent movement of the dune expressed in number of pixels (pixel size = 79 m). Figure 3.6 illustrates the method used for measuring dune displacement from Landsat MSS images. Results of this investigation are given in Chapter 7.

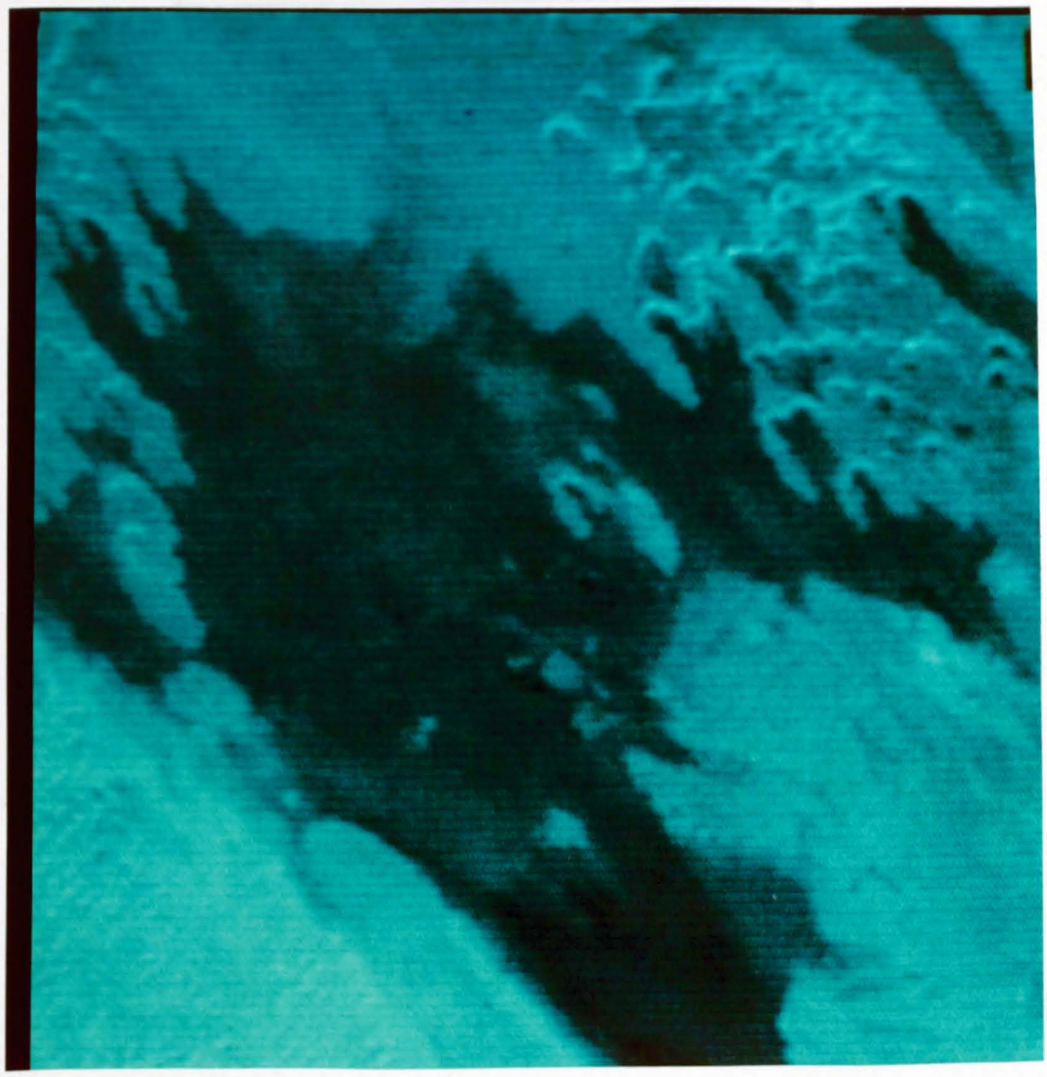


Figure 3.5 Landsat MSS false colur composite full resolution subscene (1972) showing the investigated dunes.

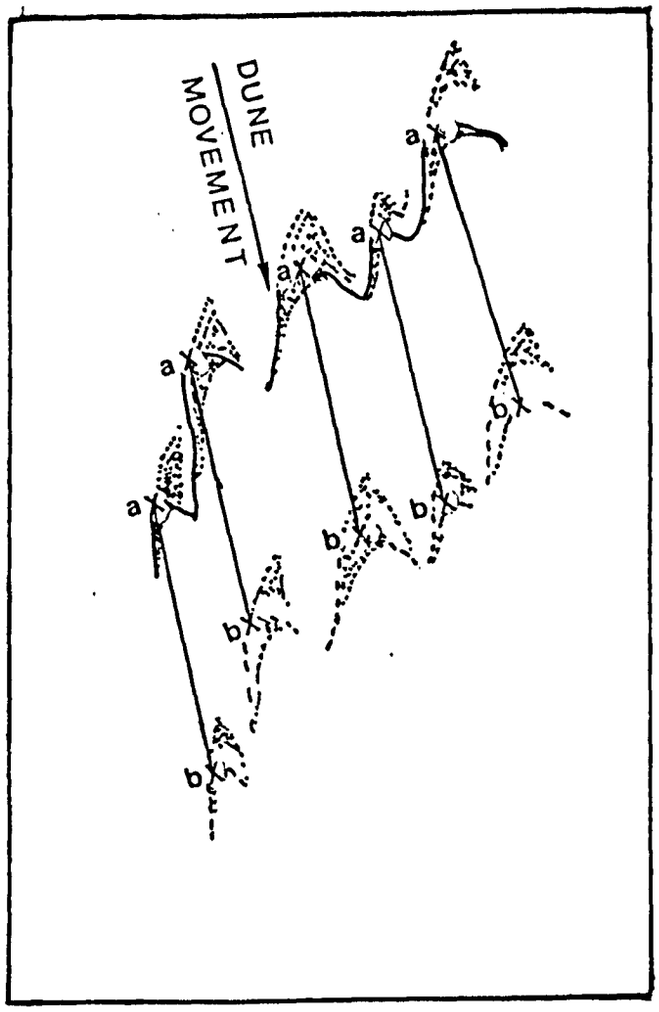


Figure 3.6 A sketch diagram illustrating the method used for dune displacement measurement from Landsat MSS images. Displacement is the change in dune crest positions between 1972 and 1984.

3.8 IMAGE ENHANCEMENT

Image enhancement is the modification of an image to improve its impact on the viewer. Enhancement operations are normally performed on image data prior to visual interpretation. The following sections describe the enhancement techniques used to improve dune sand detectability and to define more sharply the patterns that reveal the geomorphic forms of the various sand bodies.

CONTRAST ENHANCEMENT: Contrast enhancement is a pixel-by-pixel radiometric transformation that is designed to enhance visual discrimination of low contrast image features. The simplest contrast enhancement is called a "linear contrast stretch ". It is a simple point operation that redistributes the pixel values so that a narrow range is expanded to cover the full dynamic range of the display system enabling an important evaluation of radiometric detail. Figure 3.7 illustrates the principle of a linear contrast stretch.

A linear contrast stretch was performed separately for each Landsat MSS band prior to any other enhancement or interpretation. Figure 3.8a is a Landsat MSS band 3 imagery in the Rub'al Khali produced from the CCT data with no contrast enhancement. Figure 3.8b is the same image after applying a linear contrast stretch. The improvement of the image quality is particularly evident in the enhancement of the dunes and the interdune areas.

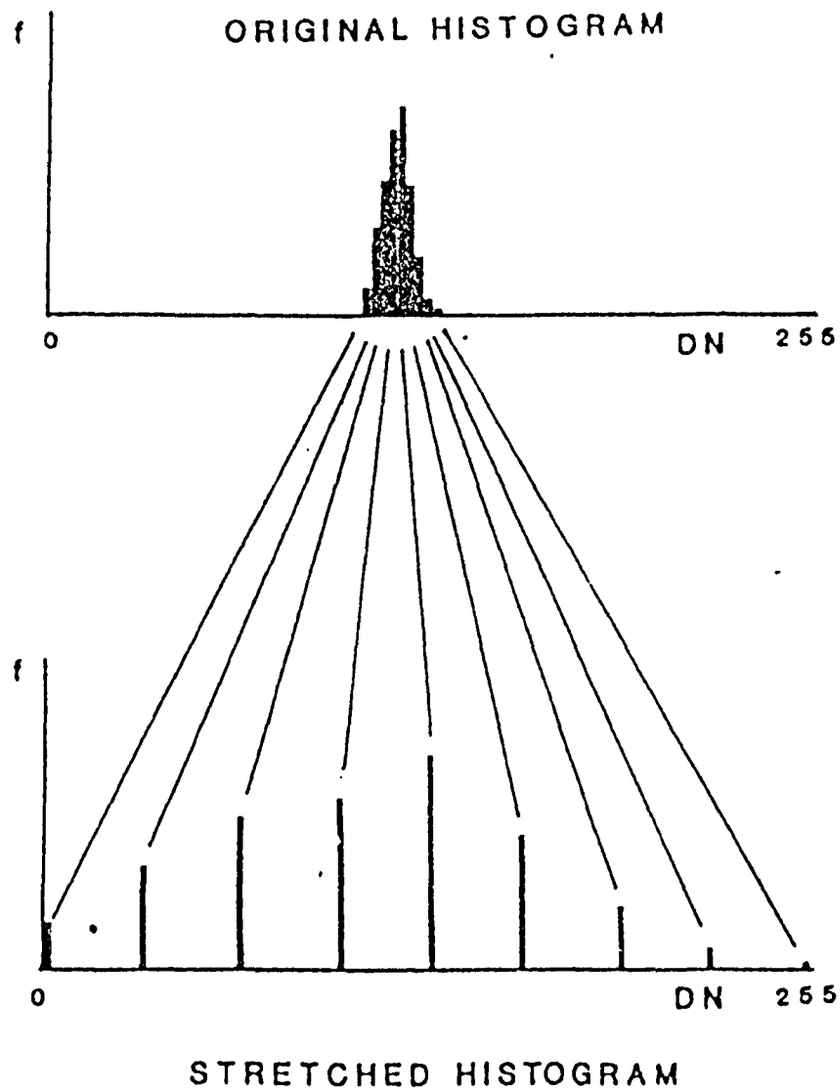


Figure 3.7 Linear stretch of a single band.

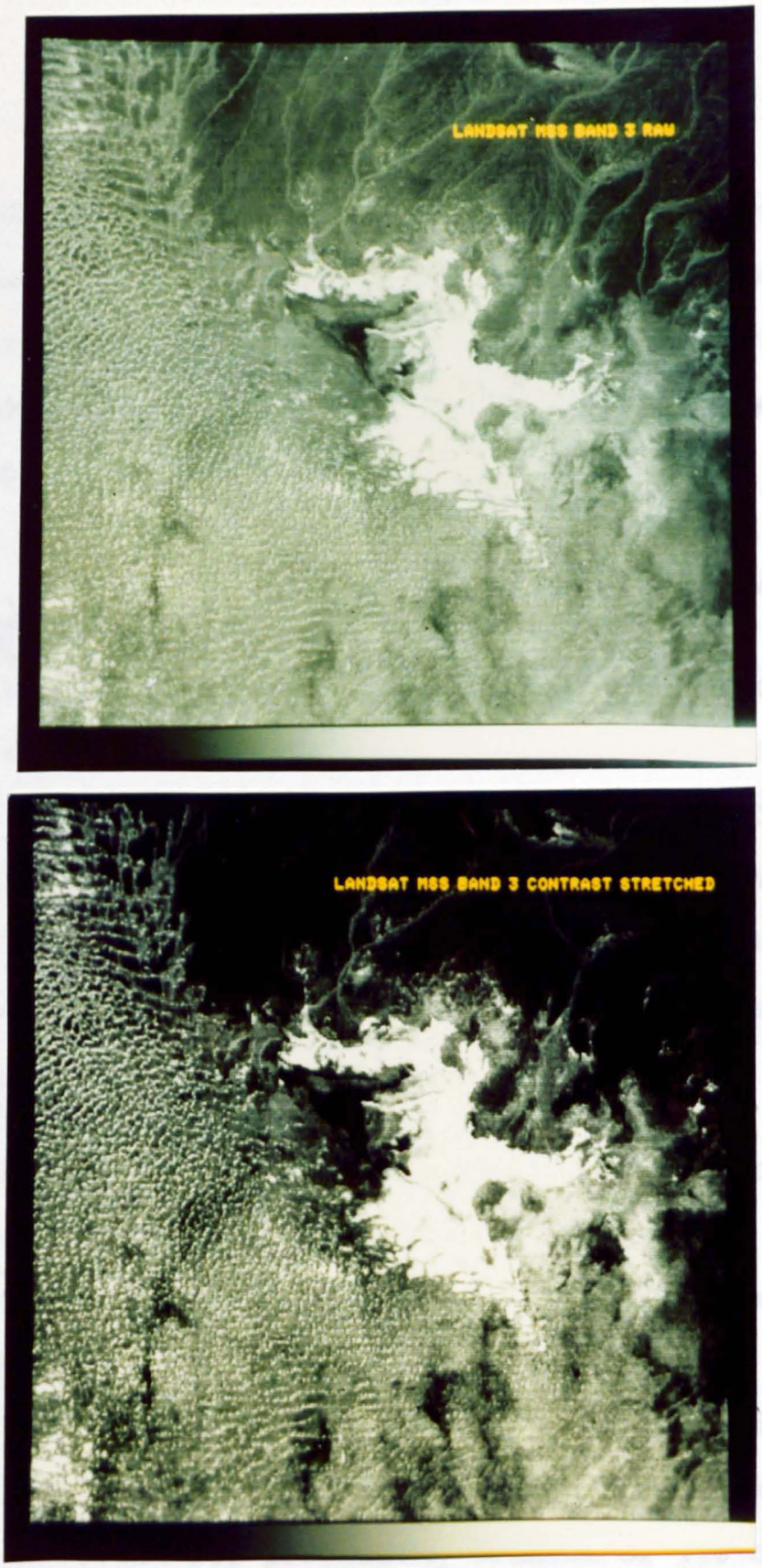


Figure 3.8 The effect of contrast stretching on Landsat MSS imagery. (a) Landsat MSS band 3 imagery in southeastern Rub'al Khali with no contrast stretch. (b) after applying a linear contrast stretch. Dunes and interdunes are more pronounced in (b).

PSEUDOCOLOUR: Colour is sometimes used effectively to enhance small gray level differences in a monochrome image. To create a pseudocoloured (sometimes referred to as colour-sliced or colour-coded) image, each gray level is simply displayed as a unique colour. Figure 3.9 illustrates the principles of pseudo-colour transformation.

Pseudocolouring was applied for bathymetric mapping of the shallow waters of the western coast of the Arabian Gulf. This investigation is part of a general study for evaluating the submerged sand banks in the Arabian Gulf. The processing was done using the IIS image processor at the Imperial College-London using the function "Pseudocolour". This function was found to be useful and requires minimum computer time.

Figure 3.10 shows that transmission of light through water is essentially restricted to the wavelength region from 0.4 to 0.7 um (Sabins, 1978). Since only visible wavelengths penetrate water, MSS band 1 (0.5-0.6 um) or TM band 2 (0.52 - 0.60 um) can be used for differentiating depths in relatively shallow water. For this investigation TM band 2 was selected for processing because of its higher spatial resolution.

TM band 2 imagery was divided into Nine - ten percent DN (digital number) classes with each class assigned a single output colour. The DN values for the different calasses were then given a correspondong image colour and compared

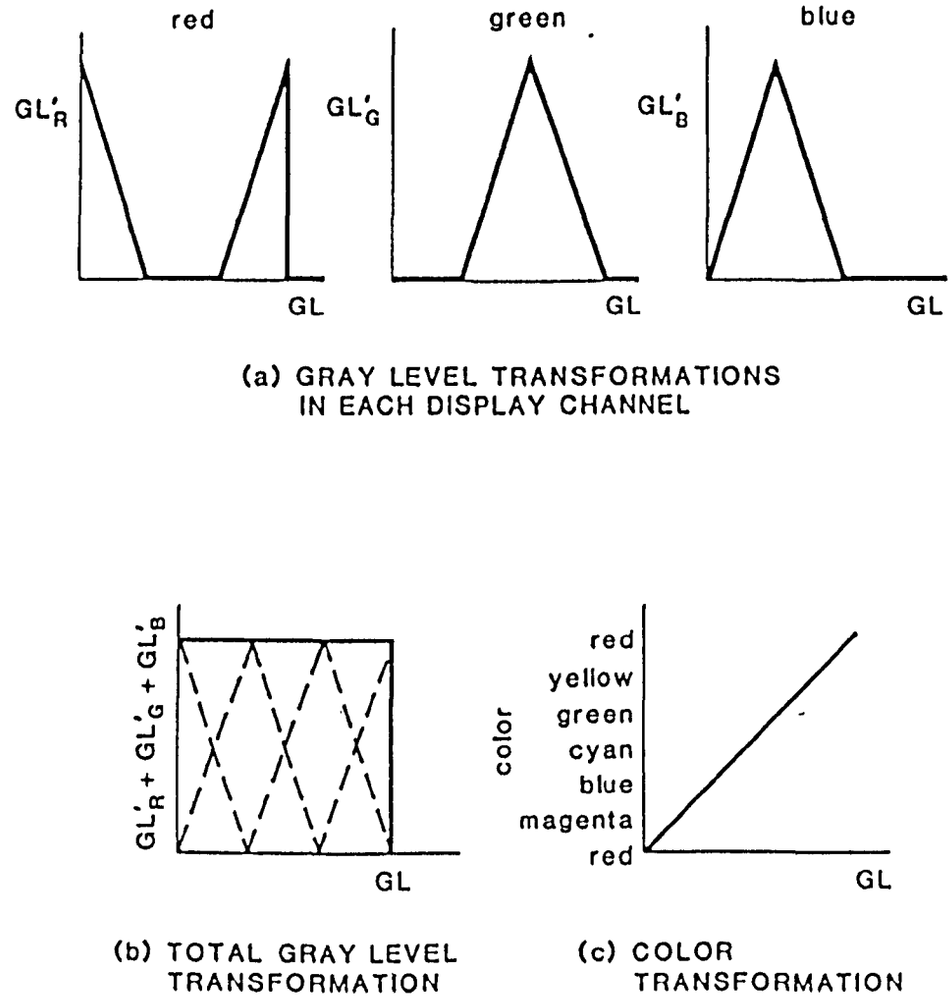


Figure 3.9 Principle of pseudo-colour transformation (Schowengerdt, 1983)

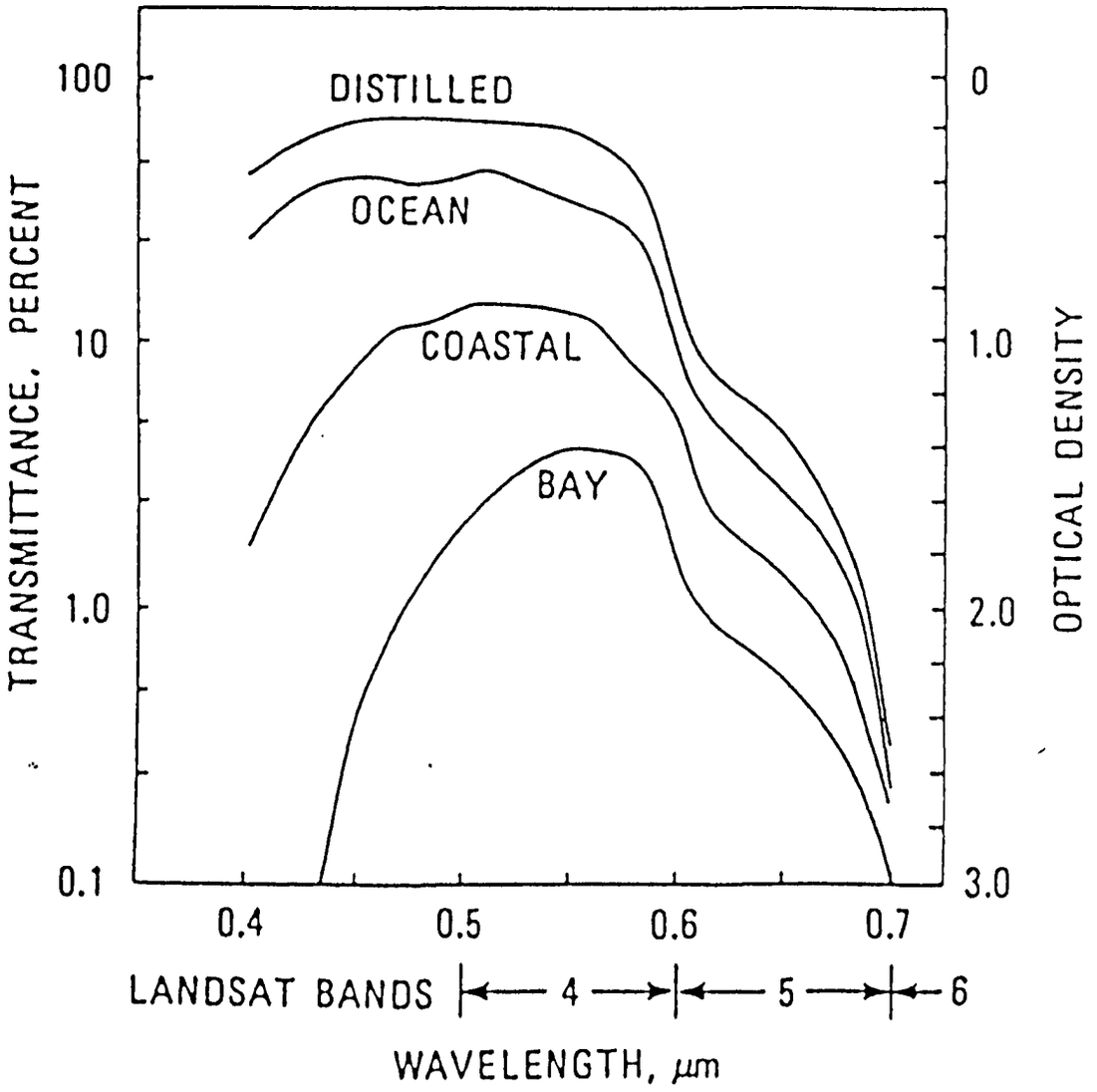


Figure 3.10 Spectral transmittance for 10 m of various types of water. Maximum transmission occurs in the visible part of the spectrum (0.5-0.6 μm) After Sabins, (1978).

with the water depths drawn from existing bathymetric charts. Chapter 8 discusses the results achieved in this investigation.

FALSE COLOUR COMPOSITING: In false colour compositing any three of the MSS bands may be selected and combined by using appropriate primary colours: red, green, and blue. Variations in the spectral response then appear as colour differences in the composite image. Since the eye is more sensitive to coloured images than to monochrome images, visual interpretation of colour differences in a composite image becomes easier.

Producing a good false-colour image requires a careful contrast stretch of each component to obtain a good balance and range of colours in the composite. A linear contrast stretch was applied to individual MSS bands separately. Different band combinations were then tested to find the most useful composite. A false-colour composite of the contrast stretched MSS bands 4, 2, and 1 and TM bands 4, 3, and 2 were found to be the best combination for bringing out the dune sand colour (see Chapter 4 for details).

DIGITAL COLOUR SPACE TRANSFORMATION: The need to define aeolian sand colours accurately has been recognized. Sediment colours are indicative of sources, past geological conditions, maturity and age. Visual observations by different astronauts and early handheld - photographs indicated that the colours of desert surfaces vary

considerably from place to place on both regional and local scales (Elbaz, 1979). False colour composites, as described above, were evaluated as aids for distinguishing the sand colour from other superficial deposits. The purpose of this investigation is to evaluate colour transformation techniques for detection of sand colour variations among and within sand seas.

Colour space can be represented by two different orthogonal coordinate systems:

(i) A red, green and blue (RGB) cartesian system.

(ii) A hue, saturation and intensity (HSI) polar system in which H describes the colour, S the saturation (purity) and I the brightness of the RGB triplet.

A transformation of the RGB components into hue, saturation and intensity (HSI) components before processing provides more control over colour enhancement. The processed images are then converted back to RGB for display (Figure 3.11). The concept of the transformation of the RGB components into hue, saturation, and intensity (HSI) is discussed in (Schowengerdt, 1983). The results of this investigation are discussed in Chapter 4.

SPATIAL FILTERING: The subtle brightness variations that define the edges and texture of objects are important for qualitative interpretation. An enhancement of local contrast may be achieved by suppressing slow brightness variations

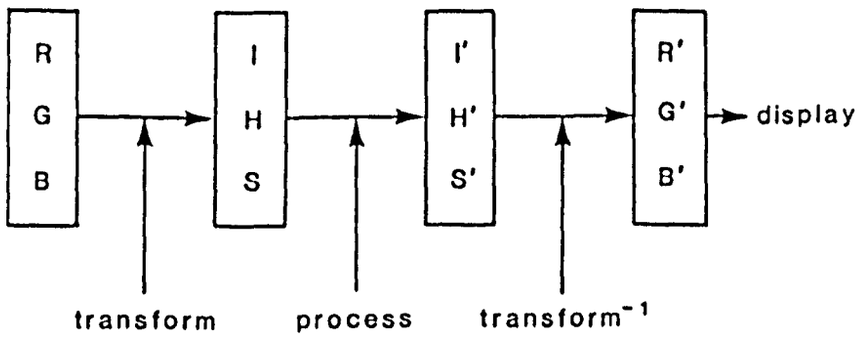


Figure 3.11 Principle of colour space transformation (Schowengerdt, 1983)

that tend to obscure the interesting details of an image. Spatial filtering techniques may be applied to an image either to enhance a particular spatial frequency for visual interpretation, or to pick out such a component automatically (Podwysocki et al., 1975).

A 512 x 512 pixel subscene of Landsat MSS imagery over the Jafurah north (acquired on Sept.4.1973) was processed using the directional filtering system (Oakes, 1987). The main aims were to:

a- enhance NE trending sand dunes, as an aid to identifying their shape.

b- highlight any other linear trends in the image, as an aid to interpreting the underlying geology.

A first principal component image was used as initial input to the system (see discussion on principal component analysis later in this section). This image contains most of the significant intensity information from the four MSS bands (90 % 0f the information), and hence is well suited to lineament analysis techniques, without giving the large processing burden associated with processing four bands separately. The relatively short wavelength of the dunes (approx. 300 metres from crest to crest) dictated that a full-resolution (79 m.pixel) image to be used.

Significant striping was apparent in the original, so the System-500 DESTRIPE filter was applied prior to all other

processing. Figure 3.12 shows the destriped image (principal componenet 1). The Fourier power spectrum of this image was calculated using standard techniques. Figure 3.13 shows the full log (power) spectrum (smoothed with a 5 x 5 median filter). The dynamic range of the linear power spectrum was too great for the spectrum to be adequately displayed on the IIS monitor.

From consideration of the power spectrum, and examination of the original image, three directional windows were selected for further processing:

a- 17.5 to 72.5 degrees (relative to image north): sand dune trend.

b- 107.5 to 157.5 degrees: underlying geology / wind direction trend.

c- 157.5 to 17.5 degrees: cross-cutting linear features.

Three filtered images were produced for each directional window, using standard frequency domain filtering techniques:

(i) window-pass filter: Flat radial frequency response, with Gaussian roll-off at the edge of each window (Mode 3 filter of Oakes, 1987, section 4.4).

(ii) window-emphasis filter: Laplacian radial frequency response within the window, with Gaussian roll-off at the

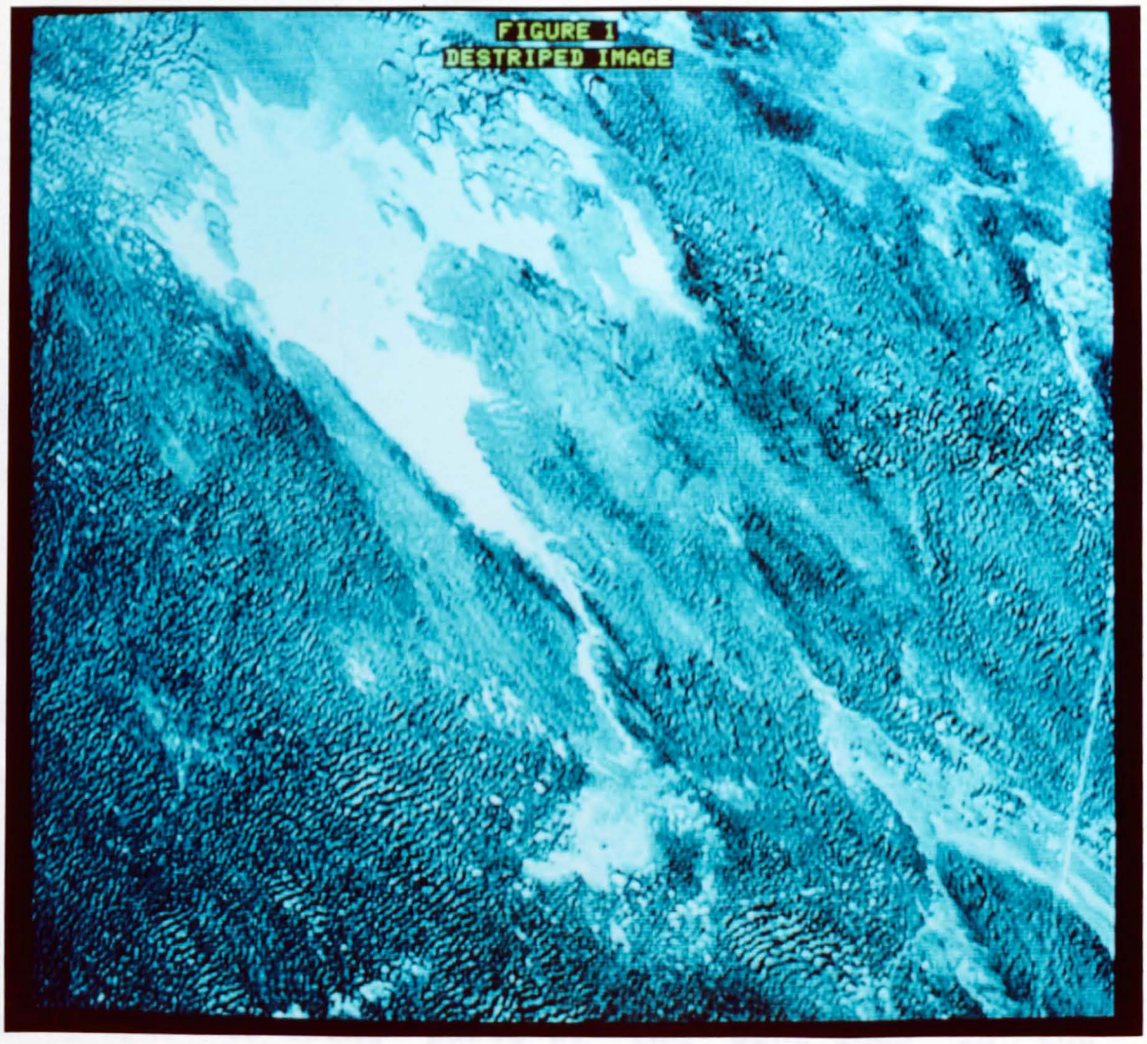


Figure 3.12 A destriped Principal Component 1 (PC1) imagery used as an input image for spatial filtering investigation.

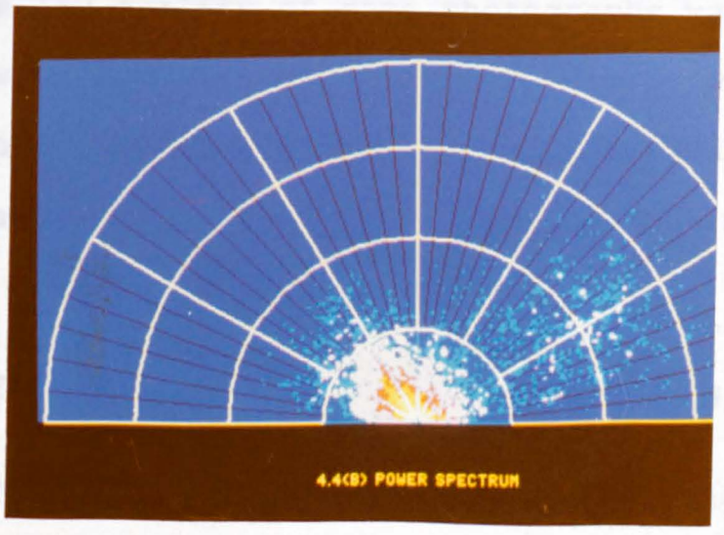


Figure 3.13 The full log (power) spectrum smoothed with a 5x5 median filter.

edges of the window (Mode 1 filter of Oakes, 1987, section 4.4).

(iii) off-window blur filter: Gaussian low-pass filter with superimposed linear enhancement of high frequencies within the window. (Mode 4 filter of Oakes, 1987, section 4.4).

Azimuth whitening and emphasis filters, based on the azimuthal power spectrum, were also applied to the image, but did not yield any significant enhancement. Chapter 4 discusses the results of this investigation.

DIGITIZATION AND EDGE ENHANCEMENT OF LFC PHOTOGRAPHS: The LFC photographs covering parts of the sand seas in the Arabian peninsula were acquired in an analogue format. Digitization was therefore required for the transformation of these photographs from analogue to digital format. Most of the photographs were of excellent quality except for a few areas. The low quality of some photographs was mainly due to the low contrast between the dune sand and other superficial deposits. Such an area is encountered in the northern Rub'al Khali where large size dunes are migrating over a gravel area.

The process of enhancement involved the following steps:

(i) DIGITIZATION: The LFC negative was scanned at a 25 micrometer aperture using the "drum scanner" at the Research Institute, King Fahd University of Petroleum and Minerals,

Saudi Arabia.

(ii) ENHANCEMENT OF THE DIGITIZED LFC PHOTOGRAPHS: The digitized data were then subjected to an edge enhancement (11x11-pixel filter) algorithm and a linear contrast stretch.

Results and interpretations are given in Chapter 4.

PRINCIPAL COMPONENTS ANALYSIS (PCA): A strong correlation in brightness exists between adjacent spectral bands in an MSS image. Figure 3.14 is a schematic two-dimensional cross section through the PDF. It can be seen that it is possible to find a new axis along which data has more spread than on either of the original axes (bands). This new axes (PC1) is a weighted average of the original bands, and is the first principal component of the image. For an n-dimensional PDF, 'n' orthogonal principal components can be found, each containing progressively less of the total variance.

The disadvantages of PCA is that it is scene dependant, but usually over 90% of the image variance is contained within the first principal component of an MSS image. PC1 was used as an initial input image for spatial filtering analysis discussed earlier.

3.9 ENHANCEMENT OF MSS BAND 1 AND TM BAND 2

Landsat MSS band 1 (0.50 - 0.60 μm) has been investigated by many authors to show variations in water depths in shallow

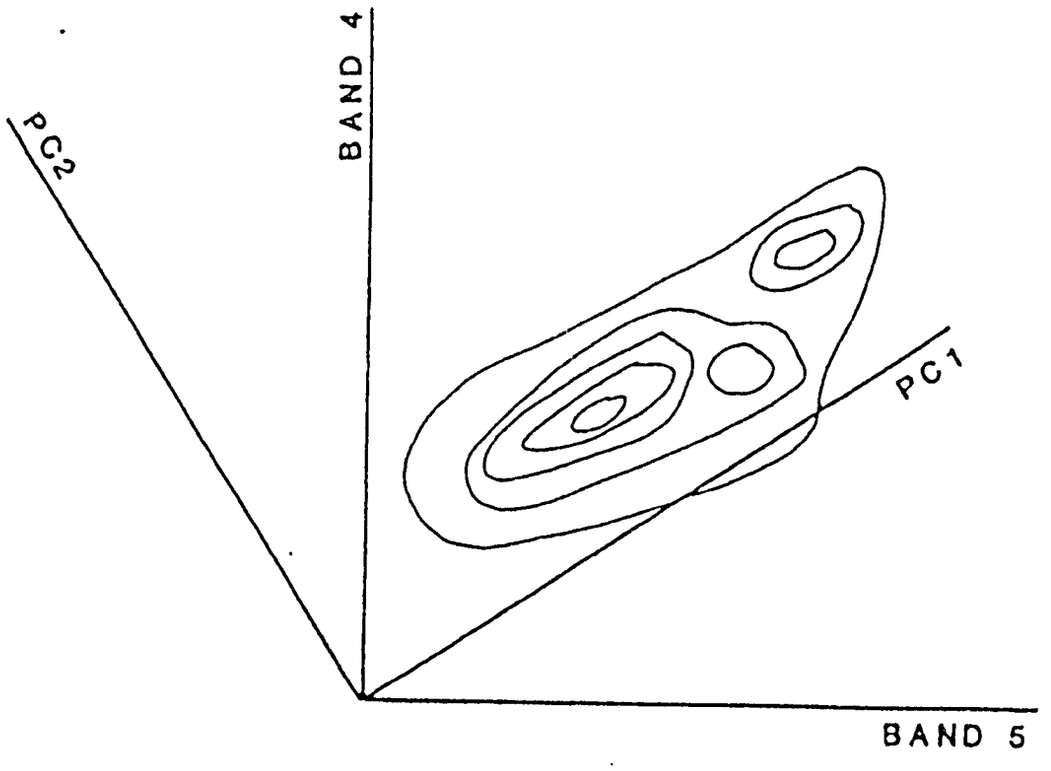


Figure 3.14 A schematic two dimensional cross section through the PDF of an MSS image showing the projections of the first two principal components (PC1 & PC2). Contours represent the density of DN. PC1 is a weighted average of the input bands, and PC2 corresponds approximately to the difference between the bands.

waters. MSS band 1 shows submarine features because of the partial penetration and transmission of the blue-green light by clear water (Polcyn et al., 1970).

This section describes the enhancement techniques used to optimize display of submarine features on the western coast of the Arabian Gulf. Image interpretation and results are given in Chapter 8.

A Landsat MSS band 1 (Landsat 4/5 nomenclature) digital image acquired on 26 January, 1973 (path 176, row 42) was digitally pre-processed for noise removal (sixth-line dropouts, and sixth-line banding) using "Edit" function of the IIs. The image was then displayed and land and sea areas were each separately masked in turn and contrast enhanced independently to display tonal features. This was achieved by applying an interactive contrast stretch which saturated land areas to white, leaving a full range of tone (digital number or DN) for areas of sea.

Data for MSS band 2 (0.6-0.7 μm) and MSS band 4 (0.8-1.1 μm) were then contrast enhanced separately, using a piecewise linear function which clips the histogram tails at the 0.25 and 99.75 percentiles and sets the mean at 128 DN. Using the offshore image (MSS 1) as a digital mask, the stretch parameters were exclusively drawn from the land, thus optimizing the onshore contrast in the band 2 and band 4 images. Each stretched image was then merged with the offshore image to produce a colour composite image

representing the land and sea areas.

Landsat TM band 2 imagery (0.52-0.60 μm) which is equivalent to MSS band 1 spectral wavelength but with higher spatial resolution (pixel size = 30 m) was also investigated for detection of submarine features and for comparison with the MSS inestigation. Landsat TM band 2 subscene image acquired on 16, January, 1985 (path 164, row 42) covering the offshore area north of the Gulf of Salwa was digitally processed for investigation of submarine features using the same technique applied to the MSS band 1. Results and interpretations are given in Chapter 8.

3.10 DISCUSSION AND CONCLUSION

In this chapter, a review of standard digital image processing techniques and their application to aeolian deposit mapping was presented. Although the interpretaion and the results of the different image processing techniques are deferred to later chapters, the following processing techniques were found particularly useful for:

(i) Digital image to image registration proved to be a potential tool for measurement of sand dune pattern changes. However the low registration accuracy result achieved in this investigation is considered to be a drawback in the analysis of dune movement.

(ii) False colour composites of the contrast stretched MSS bands 4, 2, and 1, and TM bands 4, 3, and 2 displayed as red, green, and blue respectively, were found to be the best combination for distinguishing sand from other superficial deposits. To produce a good false colour composite, contrast stretching was applied to each band separately. In this investigation linear contrast stretching gave excellent results.

(iii) Spatial filtering processes were found useful for enhancing dune shapes and dune trends.

(iv) MSS band 1 (0.5-0.6 μm) and TM band 2 (0.52-0.60 μm) were found to be useful in detecting submarine features on the shallow waters of the western coast of the Arabian Gulf.

CHAPTER 4

INTERPRETATION OF DIGITALLY PROCESSED IMAGES

4.1 INTRODUCTION

This chapter is a discussion of some of the different digital image processing techniques described in Chapter 3 which includes the following:

(i) Investigation of Landsat MSS bands for showing spectral characteristics of sand.

(ii) Investigation of false colour composites for mapping aeolian deposits and for sand colour differentiation.

(iii) Investigation of digital colour space transformation for sand colour differentiation.

(iv) Investigation of spatial filtering techniques (directional and non-directional filters) for enhancement of dune textures and dune trends.

4.2 SPECTRAL CHARACTERISTICS OF SAND

Spectral reflectance for different sandy soils have been measured by Condit (1970). Figure 4.1 shows the surface reflectance and the wavelength curves for a dry and wet sand. Such curves help in assessing the spectral bands of different sensors for the selection of optimal

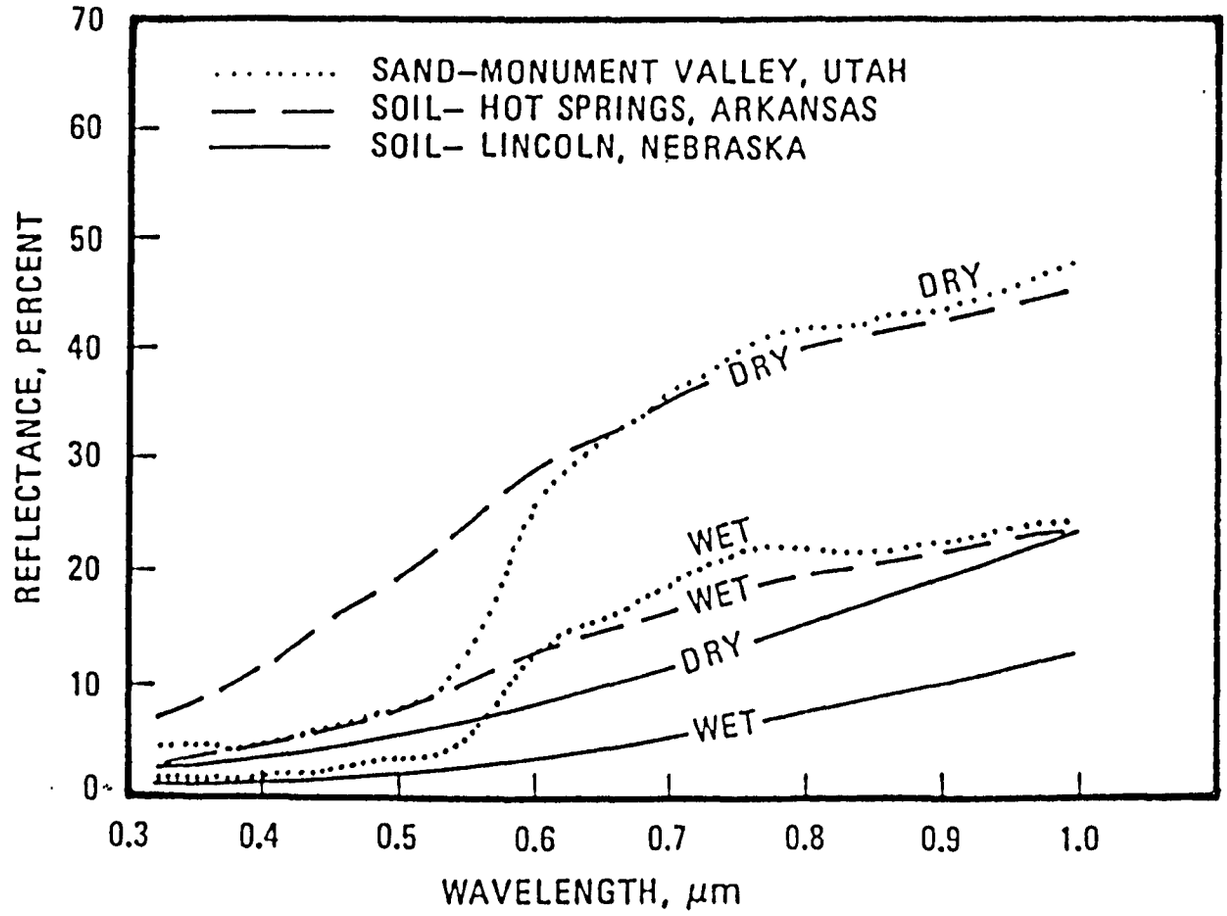


Figure 4.1 Surface reflectance and the wavelength curves for a dry and wet sand. (Condit. 1970)

wavelengths for sand/superficial discrimination. The absorption in the wavelength range between 0.5 and 0.6 μm will be investigated for sand colour discrimination (Section 4.3).

4.3 MSS BAND INVESTIGATION RESULTS

Figures 4.2 and 4.3 are two Landsat MSS scenes of two test sites in Saudi Arabia. Figure 4.2 shows stretched MSS bands (Bands 1 to 4) in eastern Rub'al Khali. The area consists of sand dunes and interdune sabkha. In band 1 imagery the interdune area is light and the dunes are dark (average DN value is 34), whereas in bands 2, 3, and 4, the dunes are light (average DN value is 70) and the interdune area is dark.

Figure 4.3 shows stretched MSS bands (bands 1 to 4) from parts of two different sand seas; the Jafurah and Ad Dahna. The area consists of sand dunes, gravel, and exposed bedrock. In the Jafurah, the dunes are barchans and barchanoid ridges travelling southward on a gravely surface. These dunes appear light in all four bands (average DN value is 70). In Ad Dahna, dune types range from small active barchans to more complex dunes. These dunes appear dark in band 1 (average DN value is 37) and light in bands 2, 3, and 4 (average DN value is 69).

The two figures show that the dunes in the Rub'al Khali and Ad Dahna gave a dark spectral response in band 1. In the

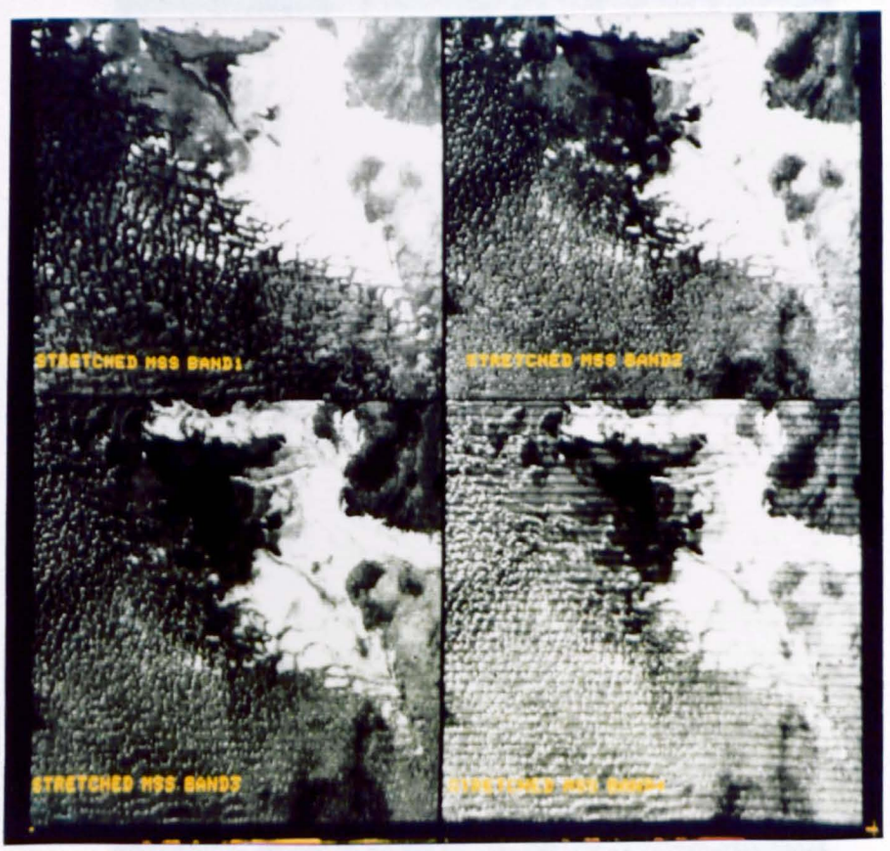


Figure 4.2 Contrast stretched MSS band (1-4) images in eastern Rub'al Khali Sand Sea. In band 1 imagery, the interdune is light and the dunes are dark. In bands 2, 3, and 4, the dunes are light and the interdune area is dark.

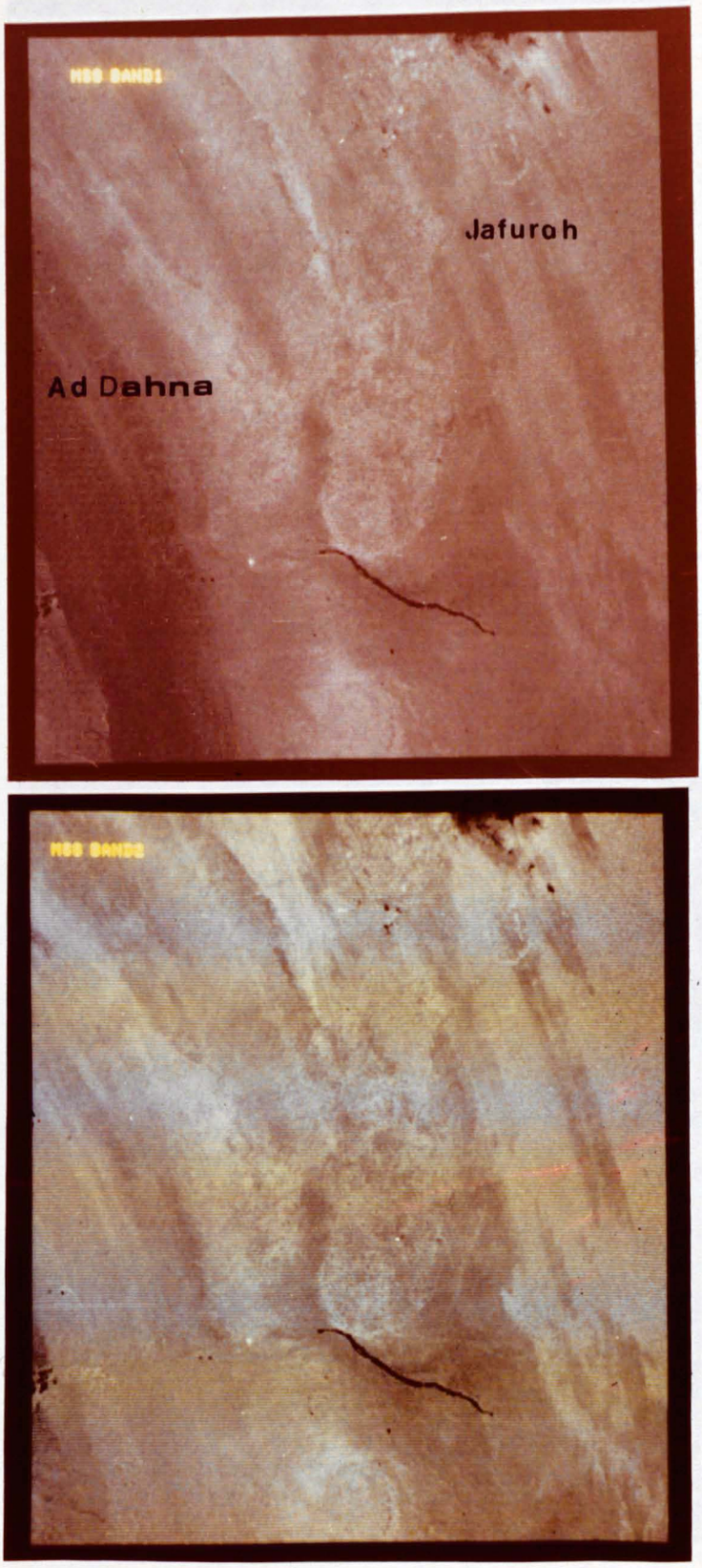


Figure 4.3 Contrast streched MSS band (1-4) images covering parts of the Jafurah and Ad Dahna Sand Seas. In Jafurah the dunes appear light in all bands. In Ad Dahna, the dunes appear dark in band 1 and light in bands 2, 3 and 4.

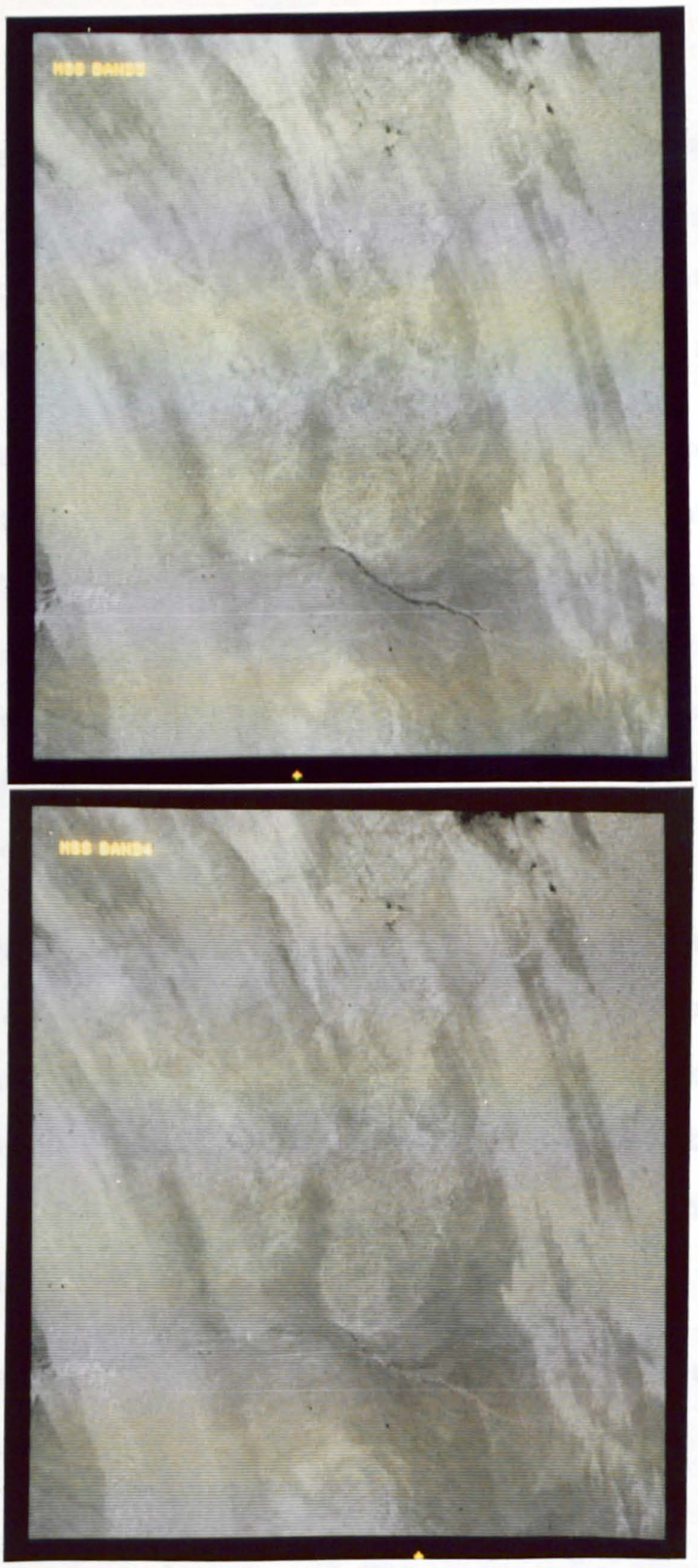


Figure 4.3 (Cont'd).

Jafurah, however, the dunes gave the same reflectance in all bands. In order to explain these variations, samples were collected from the surface of the dunes representing the three sand seas. Laboratory analysis showed the following:

(i) Microscopic analysis of the sand grains collected from the eastern Rub'al Khali showed that they are around 98% quartz. The largest grain size population is formed by coarse grains 0.5 - 0.7 mm with hues from 5 YR to 7 YR (Munsell Colour Chart), values 6 to 7 and chromas around 8. In most of these grains the colour is uniformally distributed on the grain surface.

(ii) The Dahna aeolian sediments are almost as red as the eastern Rub'al Khali sands. The "red" is given by stains in indentations in the large and medium size grains (0.5 - 0.2 mm). About 50% of these grains are reddened by these (iron) stains. The actual colour of the grains is 7.5 YR 7-8/4. The stains are dark and red (2.5 YR 4/8).

(iii) The Jafurah sands are lighter in colour than both the Rub'al Khali and the Ad Dahna sands. The coarse fraction is composed of 10% reddish-yellow individuals (7.5 YR 8/3 in the Munsell colour chart) and 90% very pale brown grains (10 YR 8/3).

The dark response of the dunes in the Rub' al Khali and in Ad-Dahna in MSS band 1 can be explained as follows:

The sun light illuminates the surface, interacts with it,

and is reflected into the Landsat detector, which measures the intensity as a function of wavelength. In reality the radiation arriving at the surface is scattered by the material in all directions. Some penetrates the material, where it is absorbed at wavelengths characteristic of the material. In naturally occuring geological materials most spectral information in the visible and near infrared reflectance spectrum is dominated by the very common presence of iron.

Figure 4.4 shows the spectra of some iron-bearing materials (Hunt, 1979). The rapid fall in reflected intensity toward the visible part of the spectrum is due to the very strong intervalence charge transfer transition between the ferric and oxygen ions. This absorption, caused by the presence of iron bearing minerals, is clearly indicated by the dark response of dune sand in MSS band 1 image (Fig.4.2 & Fig. 4.3). The DN values in band 1 ranged between 37- 47 while in the rest of the bands it ranged between 60-75. Anton and Ince (1986) analysed dune sand samples collected from Ad Dahna and the Rub'al Khali and found that the sand grains are coated with an important amount of hematized iron hydroxides.

4.4 FALSE COLOUR COMPOSITING RESULTS

The yellow colour of sand bodies in general seems to be consistently characteristic of all the deserts of the

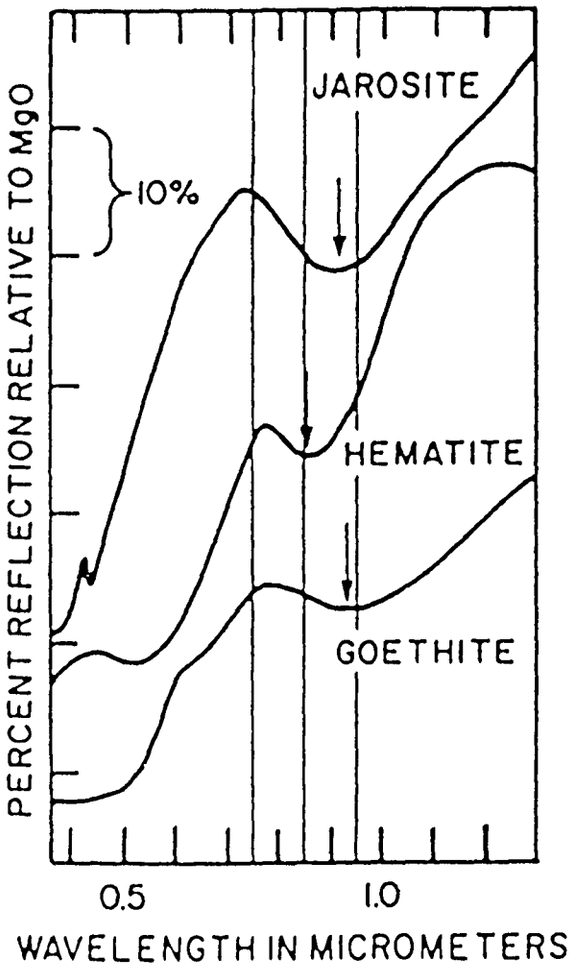


Figure 4.4 Visible and near infrared spectra of some iron-bearing materials. Absorption occurs in the visible spectrum (0.5-0.6 μm). After Hunt, (1979).

world (McKee, 1973). This consistency means that colour composites of some areas can help in the interpretation, where black and white imagery may be ambiguous. Different false colour composits were analysed to select the best band combinations for differentiating dune sand colour from other surficial deposits. The assignement of colours to the different bands was done by trial and error. It was found that a combination of MSS bands 4 or 3 (7, 6), 2 (5) and 1 (4) displayed in red, green and blue respectively gave the best results. For TM images, a combination of bands 4, 3 and 2 produced the same results. This combination (bands and colours) showed the colour of the sand as yellowish orange (close to the natural colour of sand).

Figure 4.5 is a false-colour composite made of contrast stretched MSS bands 4, 2, and 1. A comparison between this figure and Figure 4.2 (black and white images) shows the following:

(i) The nature of the linear and crescentic features is not certain from the black and white prints. The colour print of shows that these features have the characteristic yellow to orange colour of dune sand.

(ii) Salt deposits are sometimes confused with sand bodies, both of which appear similarily bright on the black and white imagery. On the colour composite, sand appears as yellow to orange whereas salt deposits are white.



Figure 4.5 A false colour composite produced from contrast streteched MSS bands 4, 2, and 1 displayed as red, green, and blue respectively. The separation of dune sand colour (yellowish orange) from other superficial deposits is illustrated (compare with Fig.4.2).

Another example which shows the value of producing false colour composites is apparent in Figure 7.10 (Chapter 7). This figure covers parts of two different sand seas; the Jafurah and the Ad-Dahna. In the Jafurah, the area is composed of sand dunes migrating over a gravelly area. Ad Dahna is a narrow corridor of different sand dune complexes surrounded from the east by a Miocene - to Pliocene - age sandstone, marl and limestone strata. In this FCC imagery, colour variations between the two sand seas are clearly detected. The colour of the sand in the Jafurah appears white while in Ad Dahna the colour of the sand is yellowish red. This colour difference is confirmed by analyzing samples of sand collected from both sand seas. Laboratory analysis shows that the sand grains in the Jafurah are reddish yellow. The coarse fraction is composed of 10 % reddish-yellow individuals (7.5 YR 7/8) and 90 % very pale brown grains (10 YR 8/3). The sand grains in Ad Dahna are red (7.5 YR 7-8/4).

The redness of aeolian sand is normally related to the redness of the grains. Some grains acquire their reddish colour from the parent rock (mainly red sandstone, or other sedimentary rocks). Other grains, however, got their reddish colour during recent exposure to surface or near-surface conditions.

In some cases, reddish grains come from eroded/deflated soils (paleo-soils) which are red coloured (including

iron-stained clay or yellow or red coloured iron minerals: limonite, geothite, hematite).

Along the western edge of central Ad Dahna, several reddish alluvial fans are found (reddish brown to light reddish brown). These fans probably acquired their reddish hue during a more humid period (Early Pleistocene) of soil formation (Anton, 1983). These fans may be responsible for the colour of the Ad Dhana Sand Sea.

In the Jafurah Sand Sea, the white sand is probably related to poor soil development during most of the Quaternary. Moreover, because of the proximity of the Jafurah to the Gulf shore, littoral and marine processes have reworked the sands and very few stained grains remained.

False colour composites investigated in Ad Dahna and Jafurah sand seas showed no progressive change in reddening along the direction of sand transport.

Enlarged false-colour composites up to a scale 1: 250,000 were also found to be excellent tools for maping sand dunes and other superficial deposits on a regional basis (see chapter 6 for more details).

4.5 DIGITAL COLOUR SPACE TRANSFORMATION RESULTS

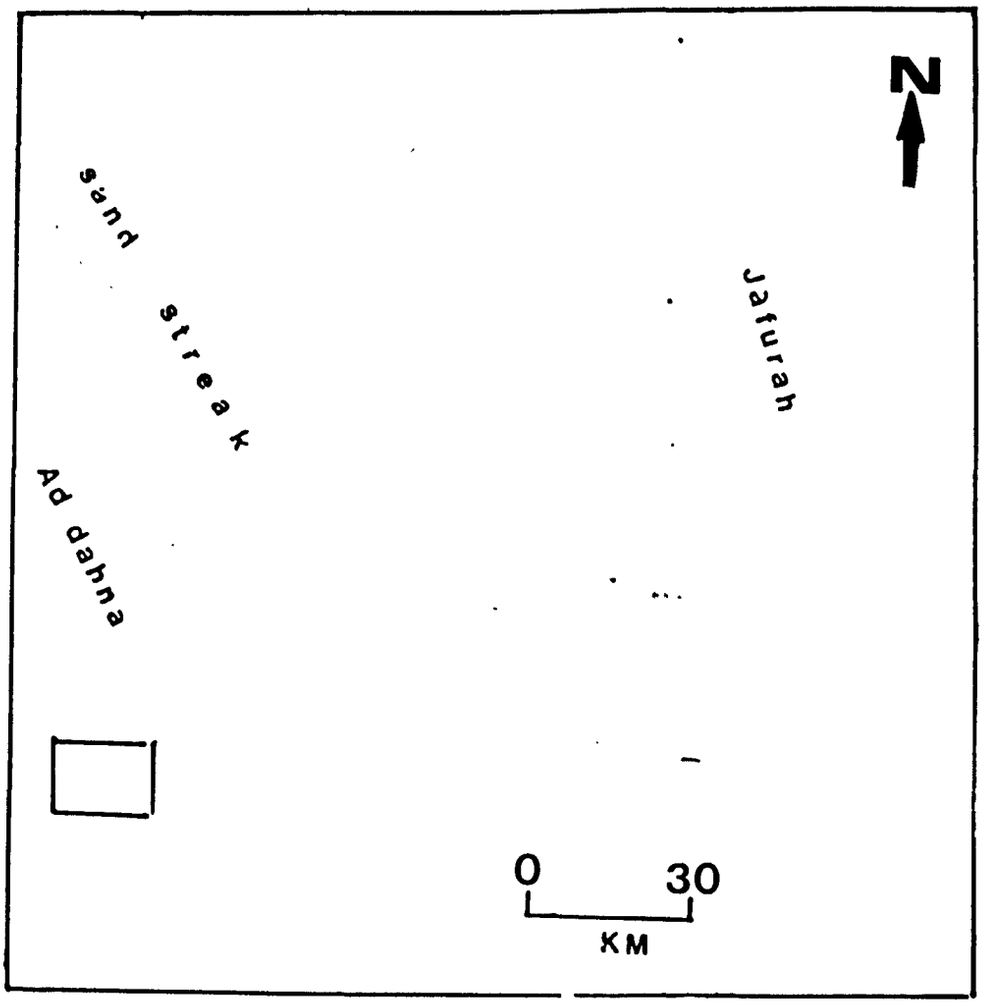
The best representation of sand colour variations between different sand seas are demonstrated in the NOAA satellite imagery covering the entire Arabian Peninsula (Fig. 1.1;

Chapter 1)). In this image, the SE Rub'al Khali and central Ad Dahna sand seas seem to have a more reddish sand colour than neighboring sand seas. On the other hand, the Jafurah Sand Sea shows a rather whitish colour. However, in this type of imagery, these colour changes can only be detected on a regional scale because of low spatial resolution.

The application of the colour transformation technique for sand colour changes is shown in Figure 4.6. This is an HSI image showing parts of two sand seas in Saudi Arabia (the Jafurah and Ad Dahna). In this image Sand colour variations between the two sand seas are apparent. Colour variations within the Ad Dahna are also detected. Thin sand streaks (a few centimeters thick) spreading on the bedrock surface (pale green colour in Figure 4.6) are also detected.

As discussed in section 4.3, false colour composites were found to be useful for detection of sand colour variations between different sand seas. However, colour variations within the sand sea could not be discriminated in the false colour composite imagery (Fig. 7.10 ;Chapter 7). When colour transformation technique was applied to the same image, these variations were detected (Figure 4.6).

Sand colour variations within a sand sea may reflect the thickness of sand cover, or variations in dune morphology. In Ad Dahna, the eastern part contains small active complex dunes. The central part is smoother in texture and appears to have a relatively constant sand thickness.


N
sand streak
Jafurah
Ad dahna
0
30
KM

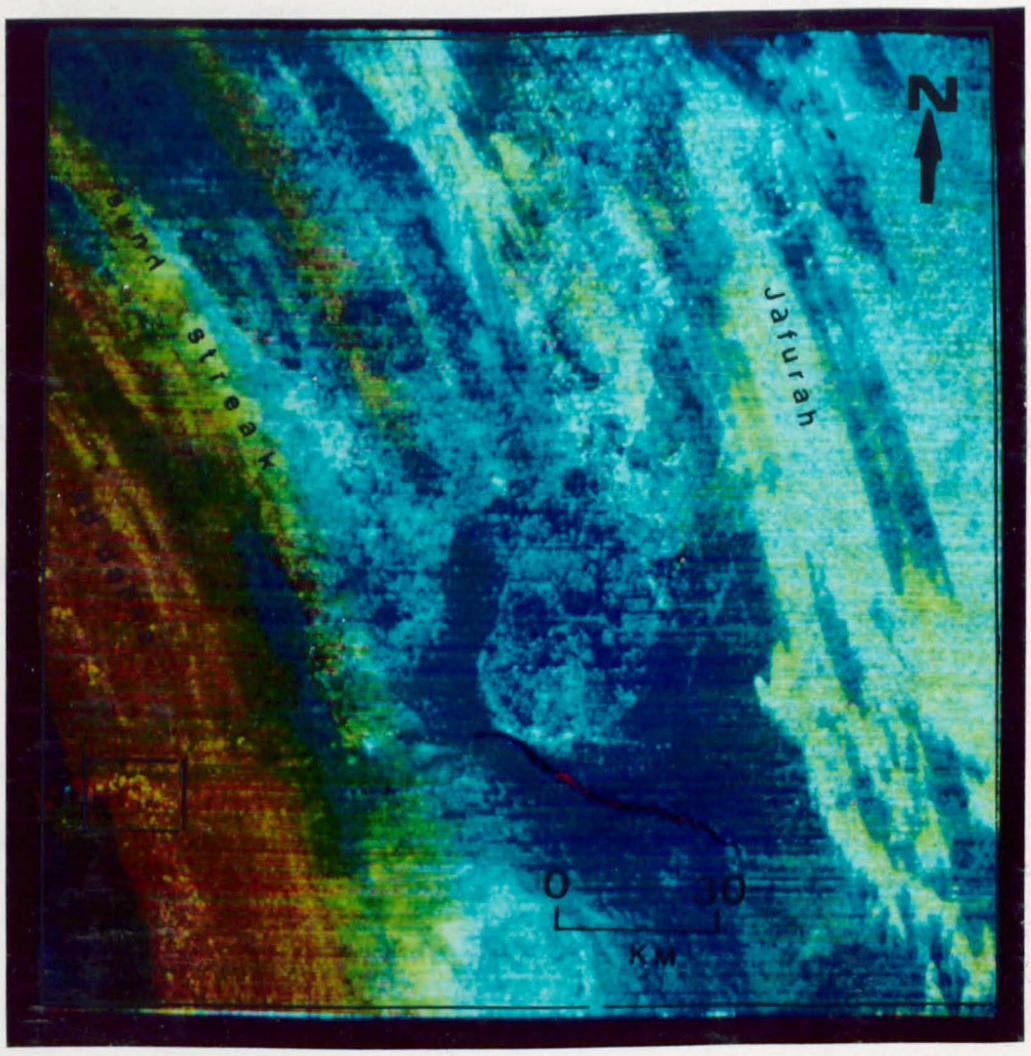


Figure 4.6 An HSI imagery showing parts of the Jafurah and Ad Dahna sand seas. Sand colour variations between the sand seas and within Ad Dahna are clearly visible. The colour of the dune sand (bright yellow) in the outlined area is different from the nearby dunes. The sand streaks are detected as greenish yellow (see text for explanation).

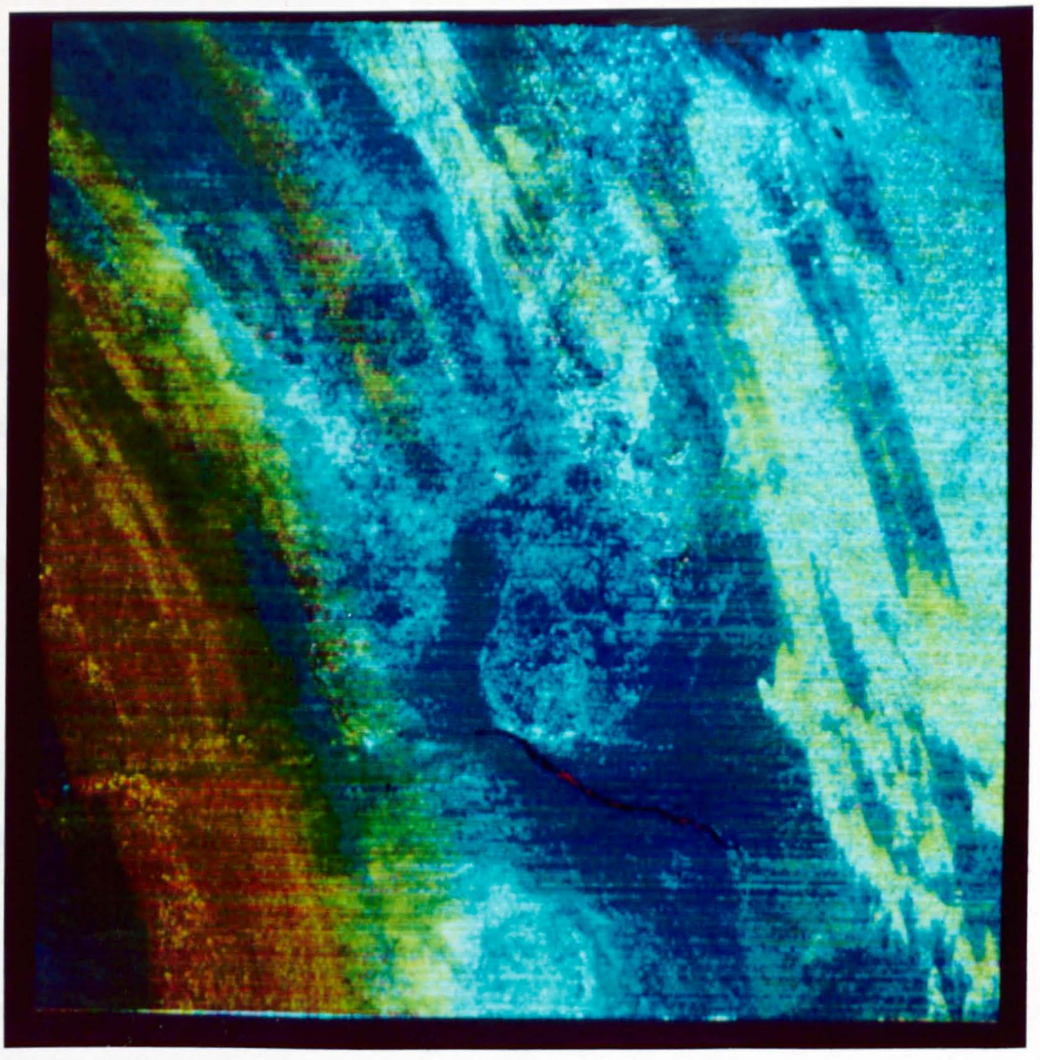


Figure 4.6 An HSI imagery showing parts of the Jafurah and Ad Dahna sand seas. Sand colour variations between the sand seas and within Ad Dahna are clearly visible. The colour of the dune sand (bright yellow) in the outlined area is different from the nearby dunes. The sand streaks are detected as greenish yellow (see text for explanation).

4.6 EDGE ENHANCEMENT RESULTS

Edge enhacement was applied using directional filters to sharpen dune edges as an aid in dune identification and measurement of their wavelength and orientation (see Chapter 3 for procedures). The following is a discussion of the results of this investigation.

POWER SPECTRAL ANALYSIS:

The power spectrum for the image shows four significant trends:

(1) Striping and related system noise is apparent in trends along the frequency axes (azimuths of 0 and 90 degrees relative to image north).

(2) Sand dunes are apparent as a high frequency trend at azimuths between 170 and 070 degrees. This trend may be broken into several peaks, however the significance of these peaks is not known: possibly they reflect dune sets of different orientations, or they may be due to "arms" of parabolic dunes existing in this area. The dominant dune orientation (corresponding to the transverse sand ridges which cover much of the scene) looks to be about 025 degrees. However azimuth 045-050 degrees also appears to be an important dune direction.

The radial frequency of the dune peaks would be consistent with a dune wavelength of approx. 300 m (azimuth 025

degrees) to 450 m (azimuth 050 degrees). There appears to be a consistent trend in dune wavelength: more easterly trending dunes having longer wavelengths. The significance of this trend is not known.

It should be noted that the wavelength of the dunes is not much greater than the Nyquist wavelength for MSS spatial sampling. Although I could see no evidence of undersampling of the dunes, the sampling is close to critical, which makes the extraction of different trends quite difficult. Ideally, data of higher spatial resolution should be used to analyze these dunes.

(3) Underlying geological trends and the effects of wind-blown sand are apparent as a low frequency trend of azimuth 110 to 170 degrees. Peaks at 115, 140-150 and 170 degrees lie within this overall trend, with azimuth 140-150 degrees being by far the dominant feature.

(4) Small, low-frequency trends (best seen in the linear power spectrum) at azimuth about 010 and 060 degrees may reflect geological trends underlying the sand.

FILTERING RESULTS:

Three azimuthal windows were extracted:

a- 17.5 to 72.5 degrees: covers the dominant dune directions. Figure 4.7 shows the filtered image. It is clear that the filtering considerably enhances the continuity of

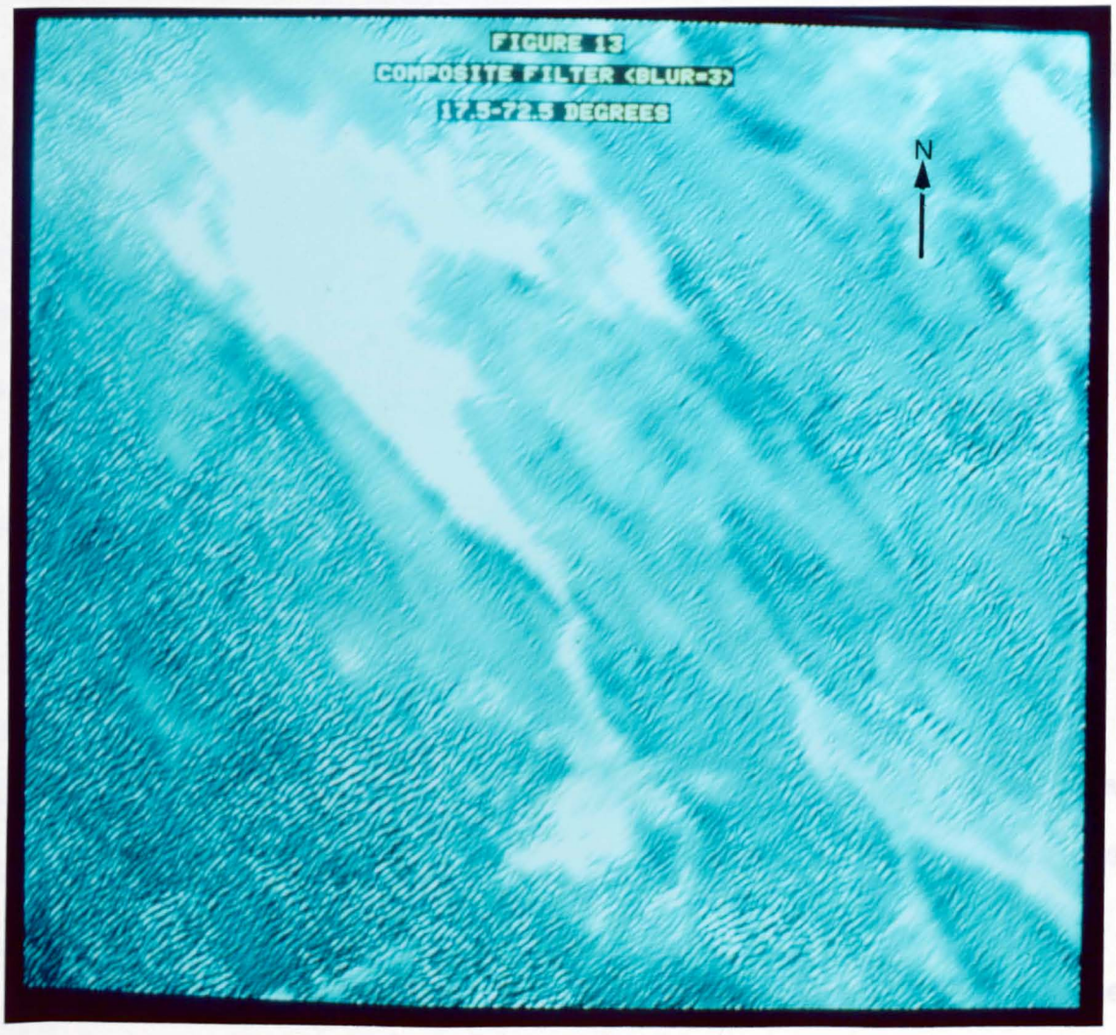


Figure 4.7 Filterd image (17.5 to 72.5 degree filter). The filtering enhances the continuity of the dune trends (NE).

the dunes, making them much easier to map. Close examination of the images reveals that this apparent dune continuity is not a filtering artifact but reflects real trends in the data which were obscured by cross-cutting features.

b- 107.5 to 157.5 degrees: covers the dominant geological/ wind direction trend (Figure 4.8).

c- 157.5 to 17.5 degrees: covers the low frequency peaks of azimuth 170 and 010 degrees. The filtered image highlights a number of features cutting across the dunes and main geological trends. Cursory examination of the image suggests that these features may be of either geological significance (possibly sub-stratum faulting) or an indication of paleo- dune trends (Figure 4.9).
From these images, it can be seen that both original objectives have been achieved: the dunes are easier to map in the enhanced imagery, and an underlying geological trend has been highlighted. In addition, the power spectra can be seen to be of considerable assistance in determining dune parameters (wavelength and orientation).

4.7 Directional and Non-directional Filters

In Section 4.6 specially designed highly directional filters for the enhancement of dune trends in the Jafurah were discussed. In this section more conventional directional filters are investigated for the purposes of quick dune trend assessement, and non-directional filters are applied

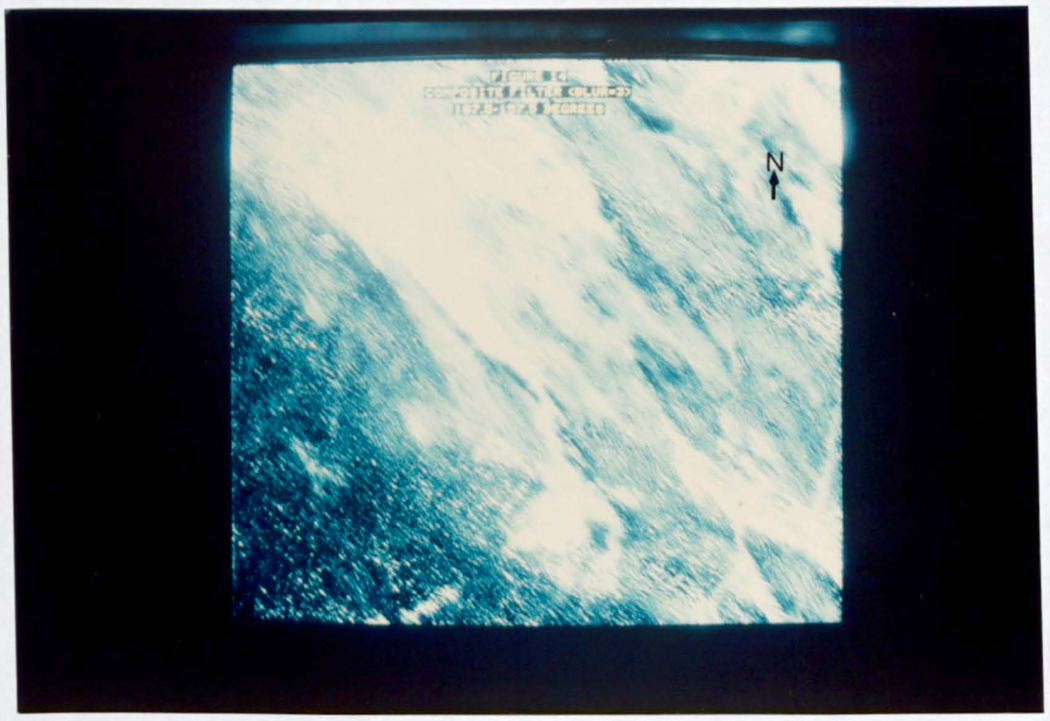


Figure 4.8 107.5 to 157.5 degrees directional filter showing possible geological / wind direction trend (NW-SE).

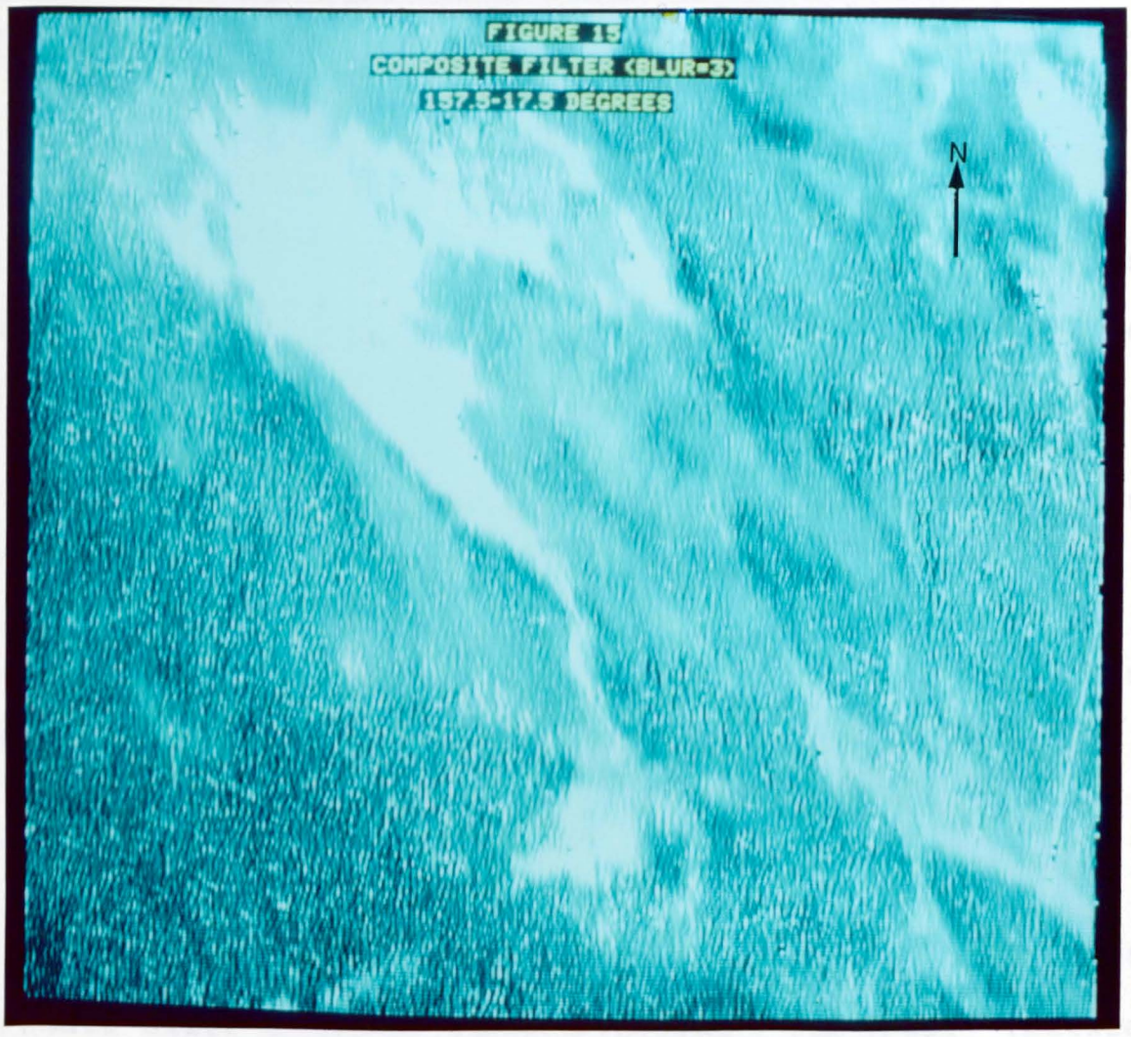


Figure 4.9 157.5 to 17.5 degrees directional filtering. The image highlights features cutting across the dunes indicating possible paleo-dune trends or sub stratum faulting (NE-SW).

for texture analysis. Three subscenes representing major sand seas are used for this study (Rub'al Khali, Ad Dahna, and southern Jafurah).

The purposes of this section are:

(1) To test directional filters for enhancement of different dune trends in comparison with the more advanced filters of the previous section.

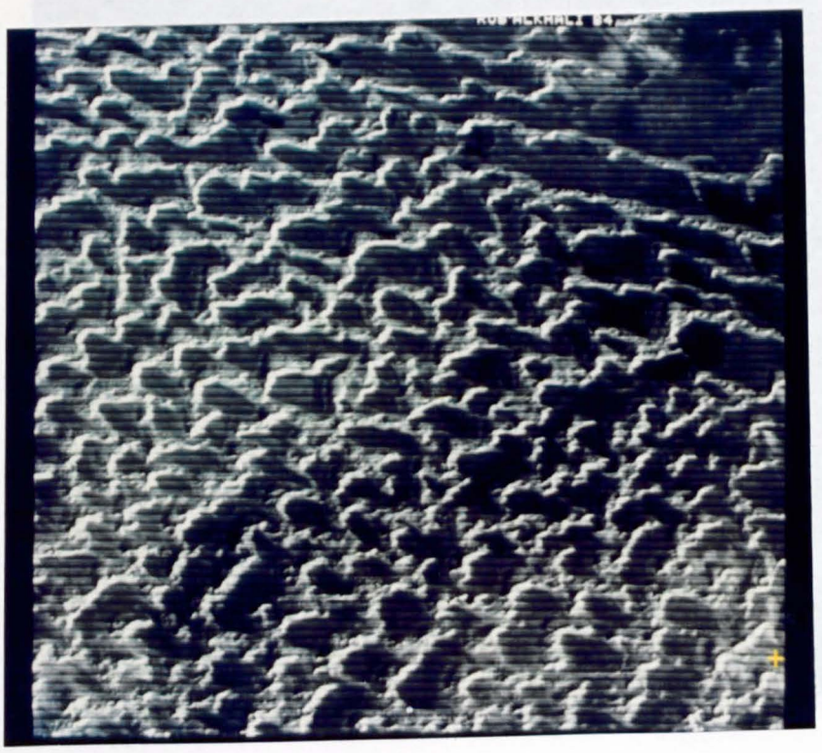
(2) To assess the effectiveness of non-directional filters for enhancing dune texture.

(3) To optimise filter-selection for different scales of dune.

Image Scale and Spectral Band Selection:

All the images used in this investigation are MSS scenes; the small sizes of some dunes relative to a pixel (between 0.6 and 3 pixels across) dictated the use of full resolution subscenes. A careful inspection of the raw bands was carried out in order to assess which one showed dune features most clearly and with as little haze as possible. It was found (Figure 4.10 a,b,c), as expected, that in most cases a well stretched MSS band 4 (7) image gave a good contrast between the dune material and other superficial deposits such as sabkha and gravel. In the Rub'al Khali scene, band 1 (4) was used since the more iron rich dunes appeared with a better contrast than in band 4 (7), even though the shorter

a



b

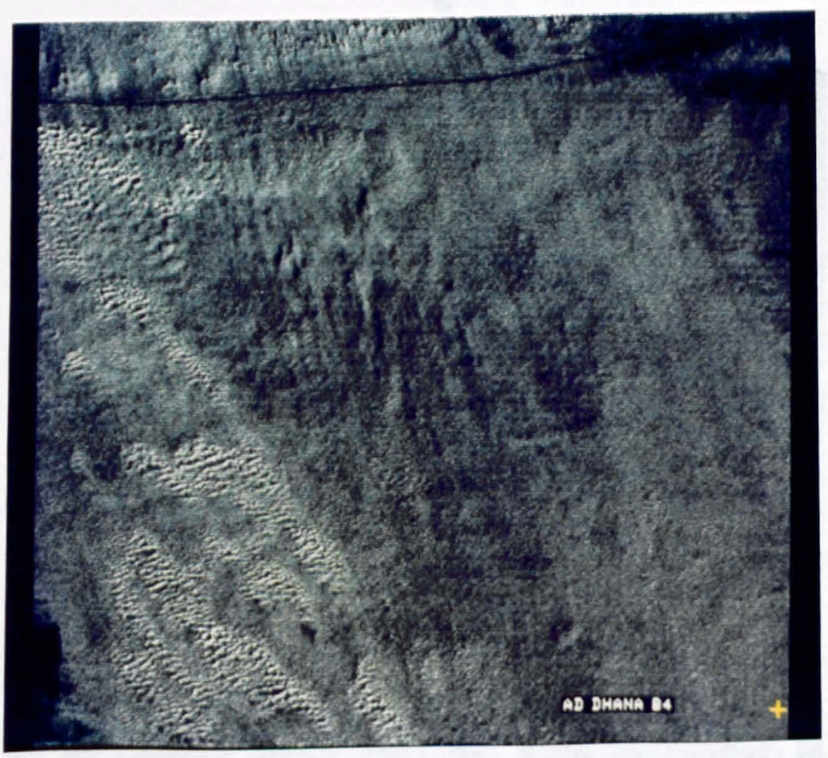
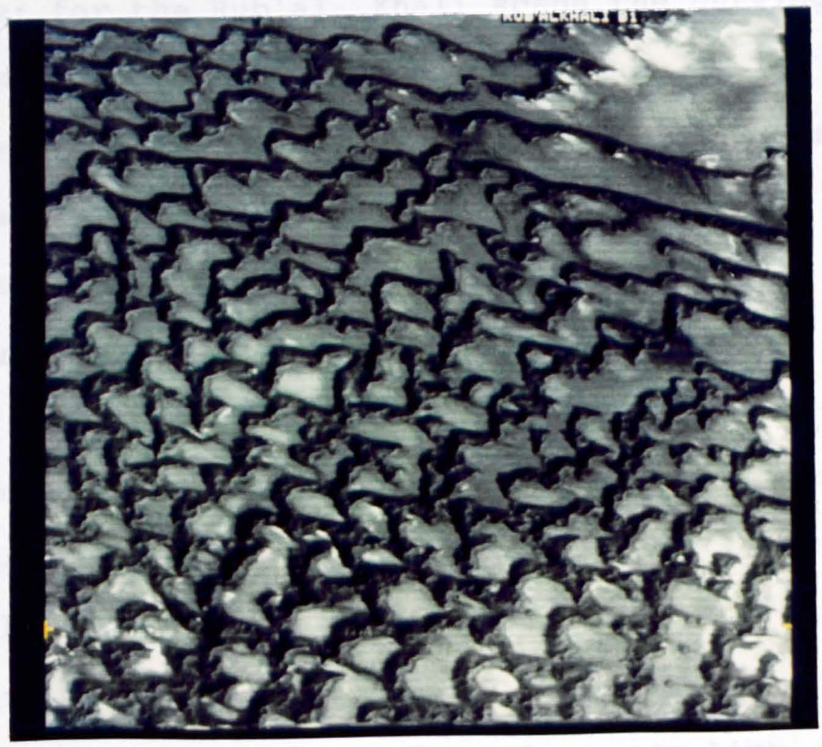


Figure 4.10 a,b,c: Contrast stretched MSS band 4 (7) images in the three test site areas.
d: Contrast stretched MSS band 1 (4) imagery in the Rub'al Khali.



c



d

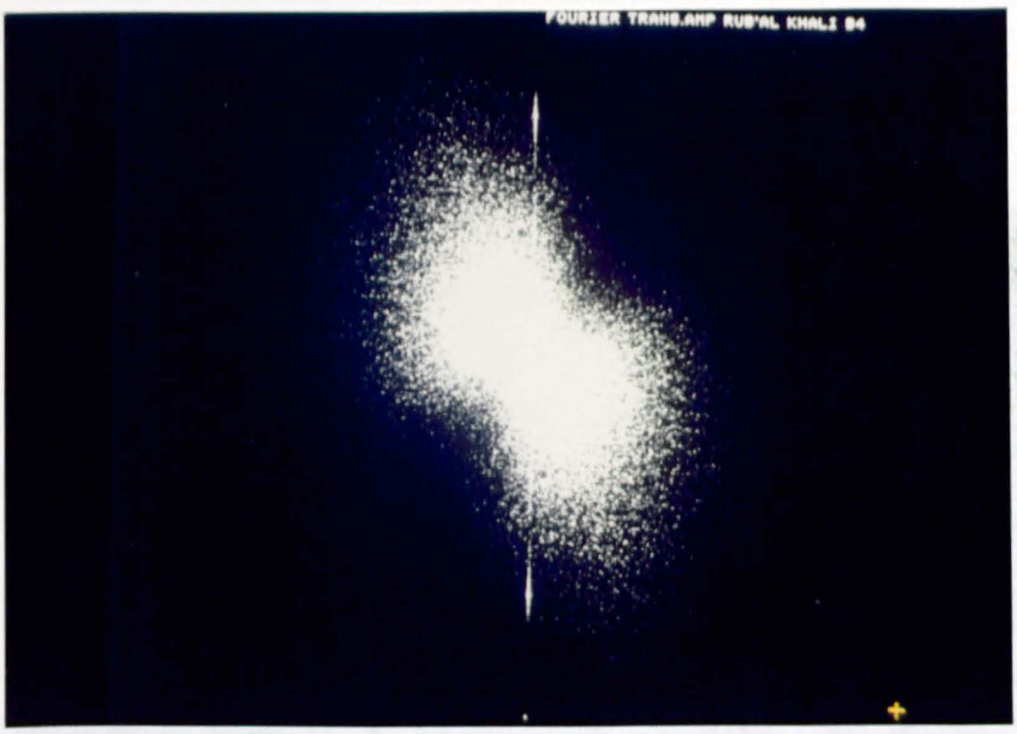
wavelength may give rise to more scattering (Figure 4.10 d). In practice, this was not a problem, and some interesting results were obtained from this scene.

Directional Filters:

Figure 4.11 a,b,c show the Fourier Tranform (amplitude) of each scene, and may be compared with the corresponding raw images in Figure 4.10. These plots are essentialy polar: distance from the origin denotes spatial frequency and the angle of edge features in the scene (with 90 degrees offset). The various dune trends may be seen very clearly in these plots: for the Rub'al Khali scene the curving nature of the dunes and the large range of sizes is obvious, whereas the Ad Dahna scene exhibits a higher proportion of finer dunes and less variation in their direction. On this scene there are also some distinct coarse features running nearly north-south which appear to be related to the underlying rock structures. The Fourier transform of the Jafurah scene reveals less distinct trends but much fine structure (there is lack of fine features trending around north-south). In each case the distinct vertical stripes and sharp spots along the vertical axis are artefacts (caused by geometrical corrections and the six-line banding respectively).

Since diagonal trends are visible from the Fourier transforms, it was decided to enhance these trends using appropriate filters whose convolution masks are shown below:

a



b

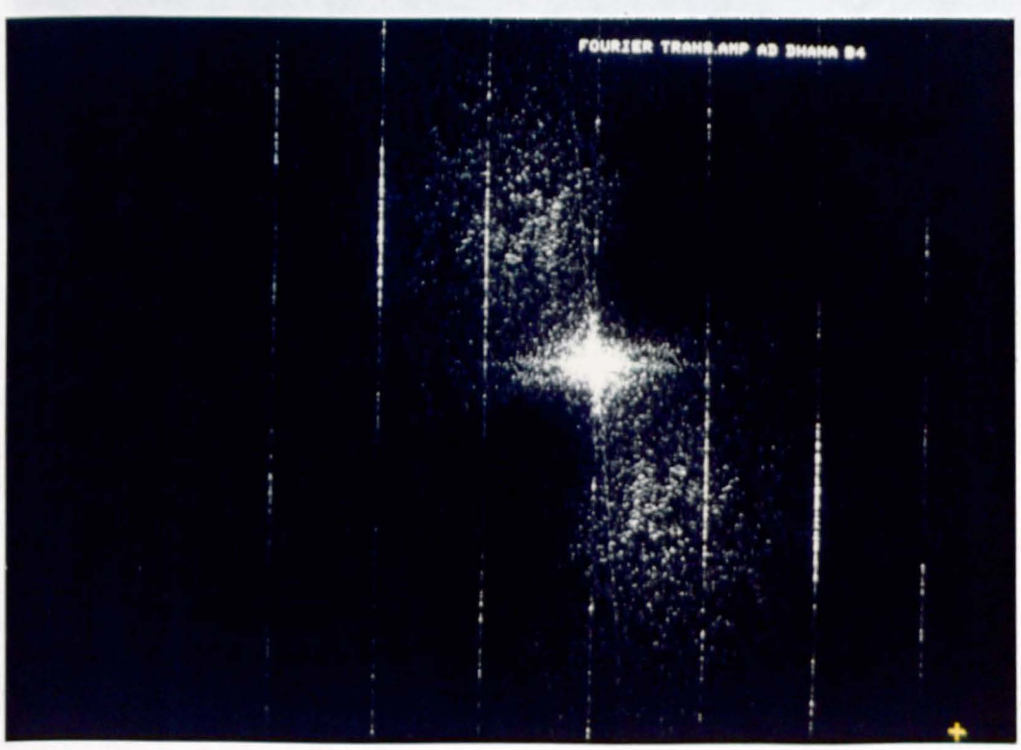
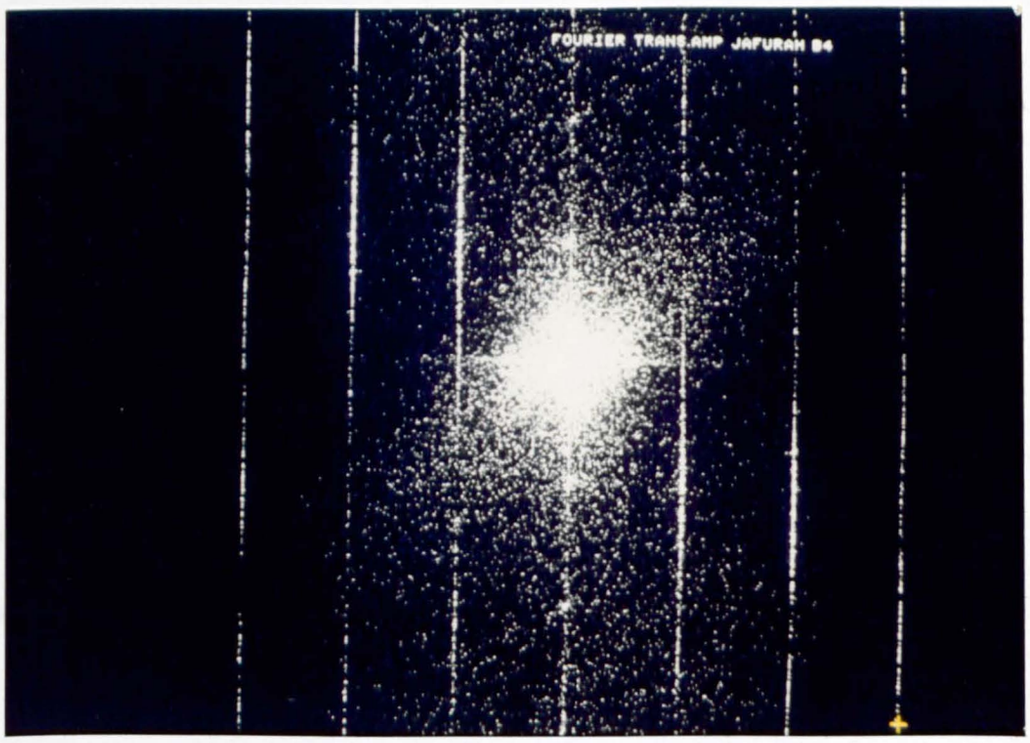


Figure 4.11 a,b,c: Fourier transform (amplitude) for Rub'al Khali (a), Ad Dahna (b) and Jafurah (c).



C

-2	-1	0		0	1	2
-1	0	1		-1	0	1
0	1	2		-2	-1	0
	NE				NW	

These masks are variations on the Sobel operators (see later) and are particularly sharp in their spatial frequency response which is shown in Figure 4.12 (light and dark areas represent high and low responses respectively).

The resulting edge enhancements were then stretched interactively to produce an optimum display in each case, and the results appear in Figures 4.13, 4.14 and 4.15.

Close examination of these images revealed an enhancement of dune trends as expected and this is especially true in the Jafurah scene in which old Wadi drainage systems (running E-W) and the dune edges (running roughly N-S) are much more pronounced in the filtered imagery than on the raw band imagery (Figure 4.13). It was noted however that the small dunes (trending NE) which occur on top of larger dunes in the Rub'al Khali and the transverse dunes in Ad Dahna were not well enhanced (Figures 4.14 and 4.15). This is probably due to the fact that the filters do not have a good response to very fine features (refer to Figure 4.12).



Figure 4.12: Frequency response of "tilted Sobel" mask (3x3). From Canas (personal communication 1988).

a

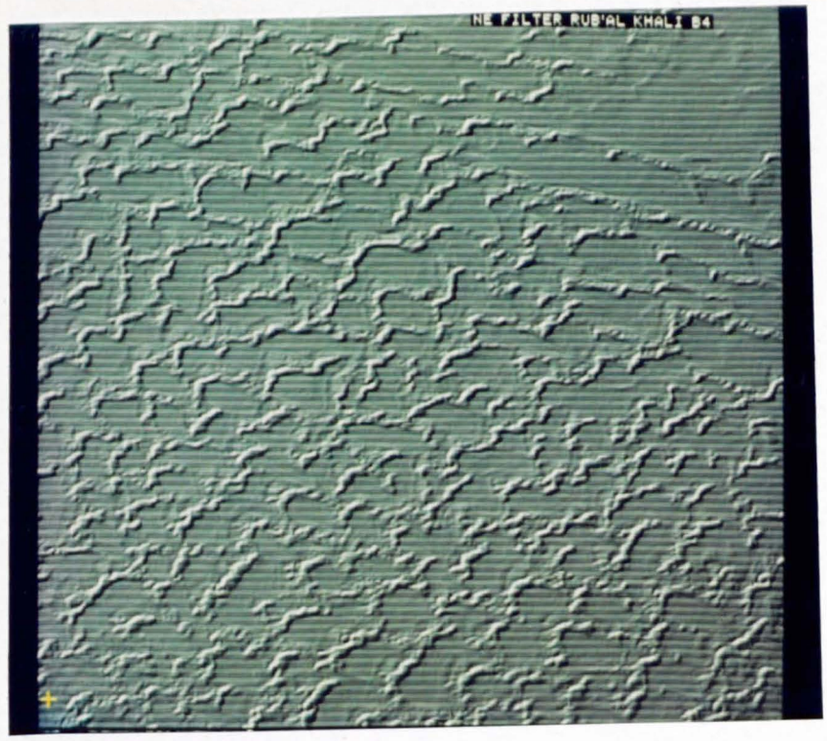


b



Figure 4.13 a,b: NE and NW directional filter images in the Jafurah area.

a



b

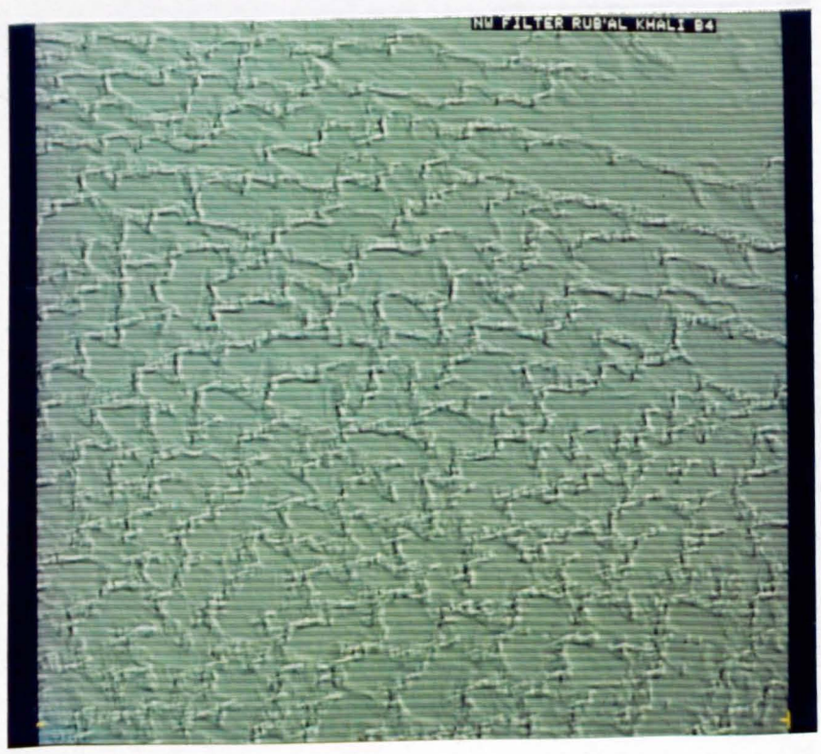
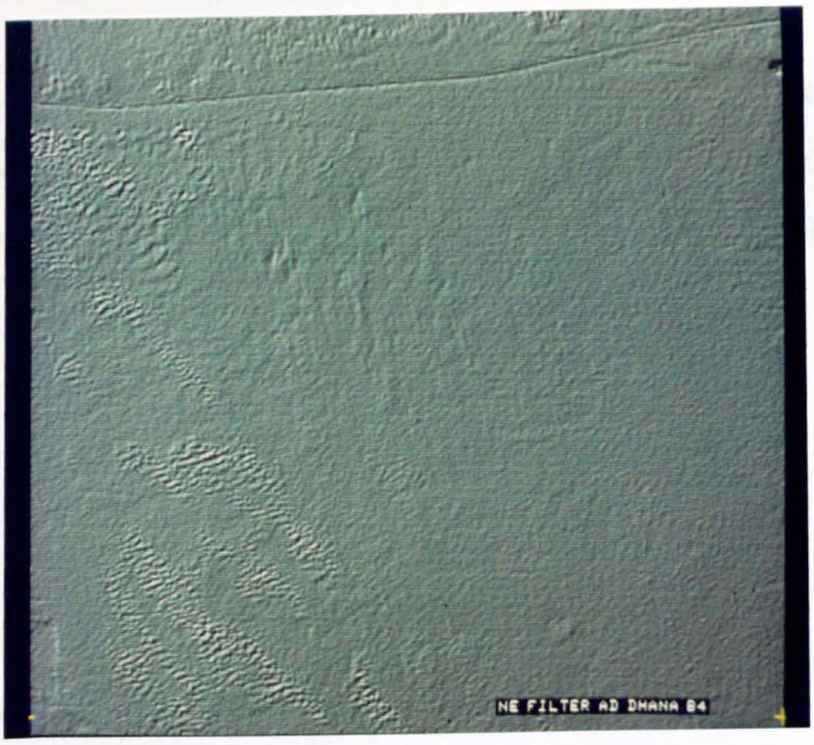


Figure 4.14 a,b: NE and NW directional filter images in the Rub'al Khali area.

a



b



Figure 4.15 a,b: NE and NW directional filter images in the Ad Dahna area.

Non-directional Filters (High-pass):

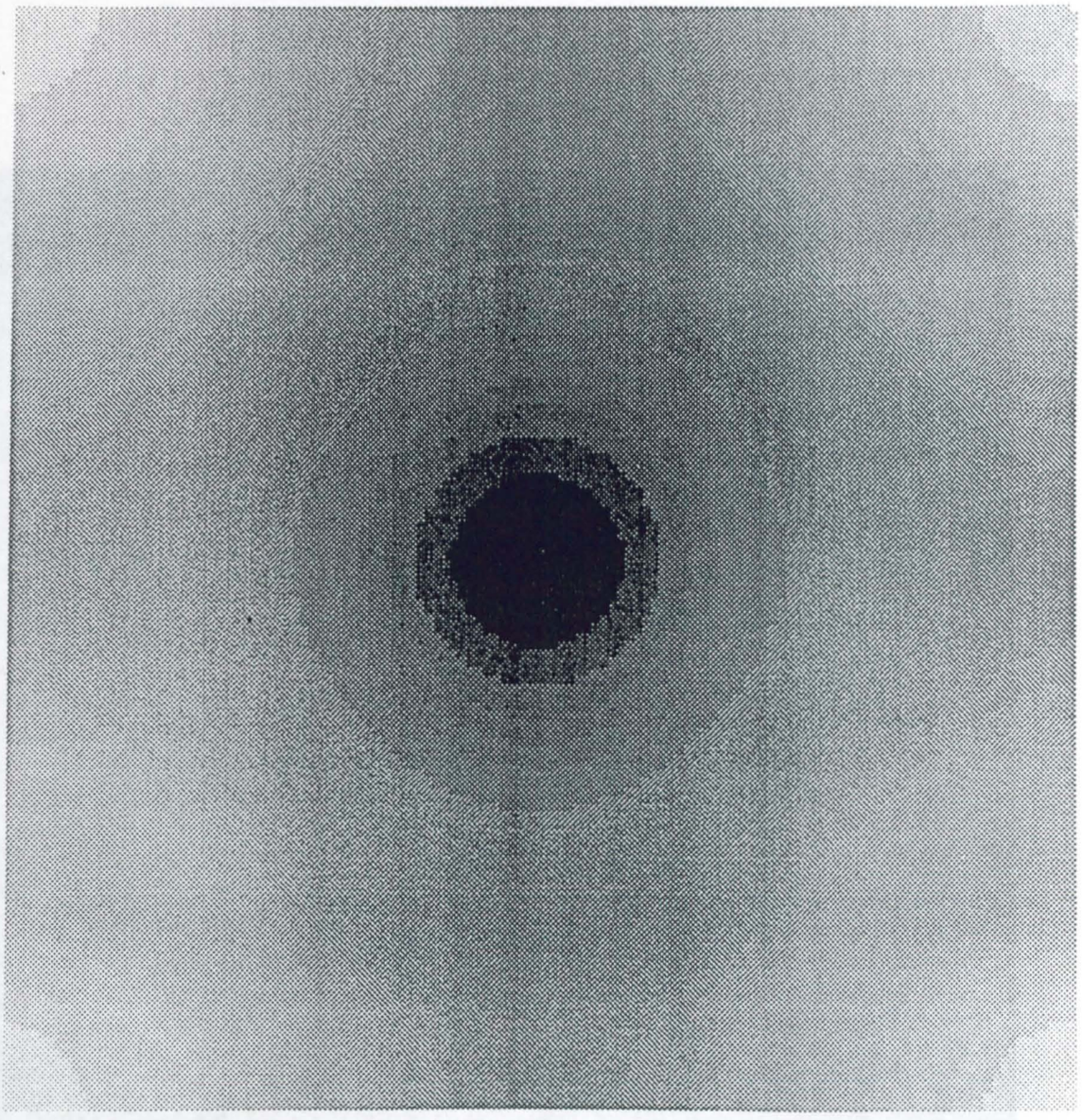
Two coneventional high-pass texture filters were tested for detecting textural differences between different dunes. The "Laplacian" and "Sharp Laplacian" masks (shown below) were applied to all three scenes, as was a "Laplacian Variant" mask.

0	-1	0	-1	-1	-1	-1	-2	-1
-1	4	-1	-1	8	-1	-2	12	-2
0	-1	0	-1	-1	-1	-1	-2	-1

"Normal" Laplacian | "Sharp" Laplacian | "Laplacian Variant"

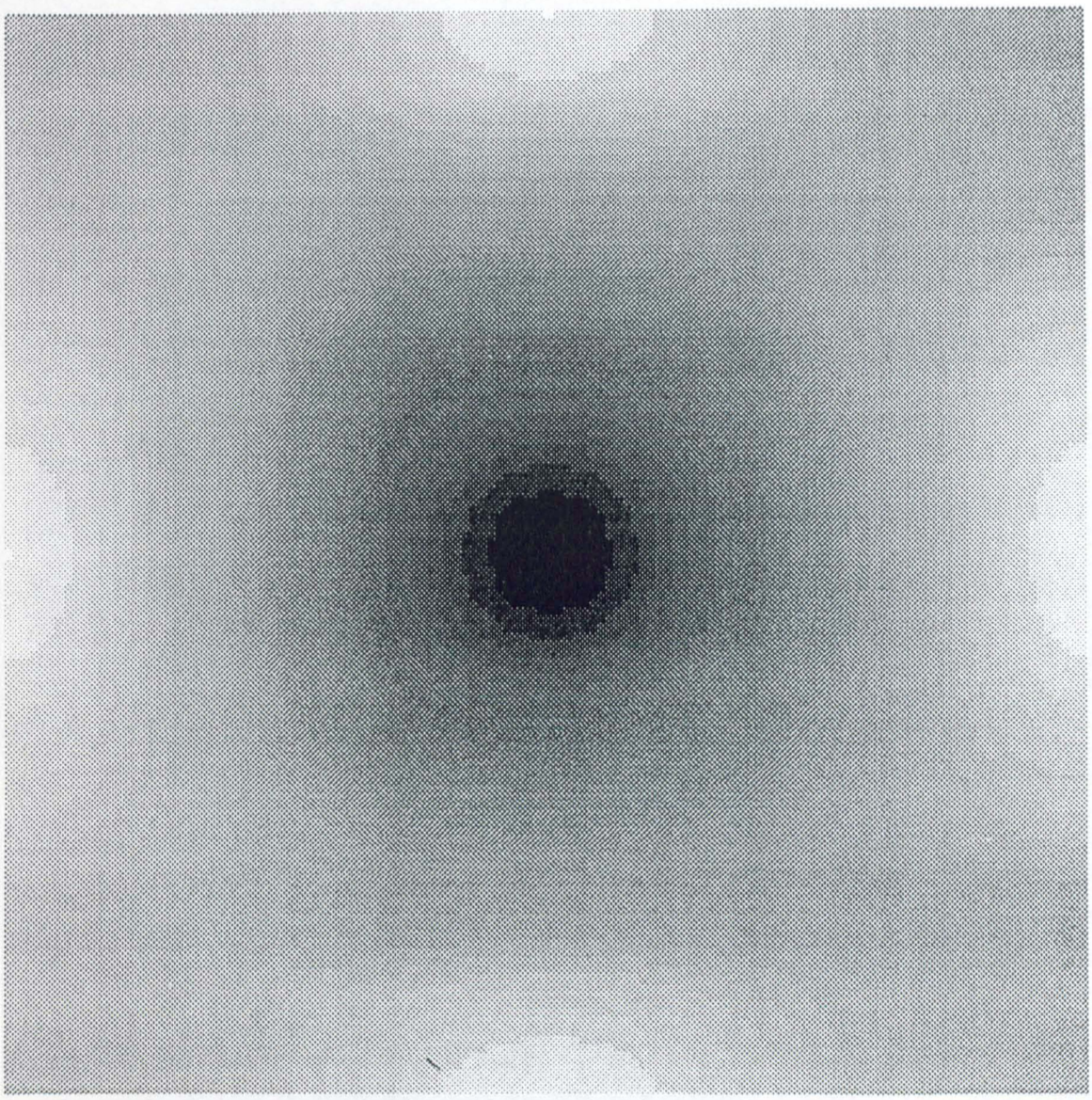
Figures 4.16 a,b shows the spatial frequency responses of the first two masks using the same coding as Figure 4.12, and it is clear that neither filter responds equally to all feature directions. This bias may be significant, but the "Laplacian Variant" mask, whose response is shown in Figure 4.16 c is without bias; this mask is obtained simply by summing the first two.

The results from each filter were contrast stretched interactively as before. The results from the "Laplacian" and "Sharp Laplacian" filters do not provide a useful enhancement of dune texture, and this result might be expected in view of the diagonal trends noted in the Fourier transforms of Figure 4.12. The "Laplacian Variant" filter produced an image in which textural differences were more

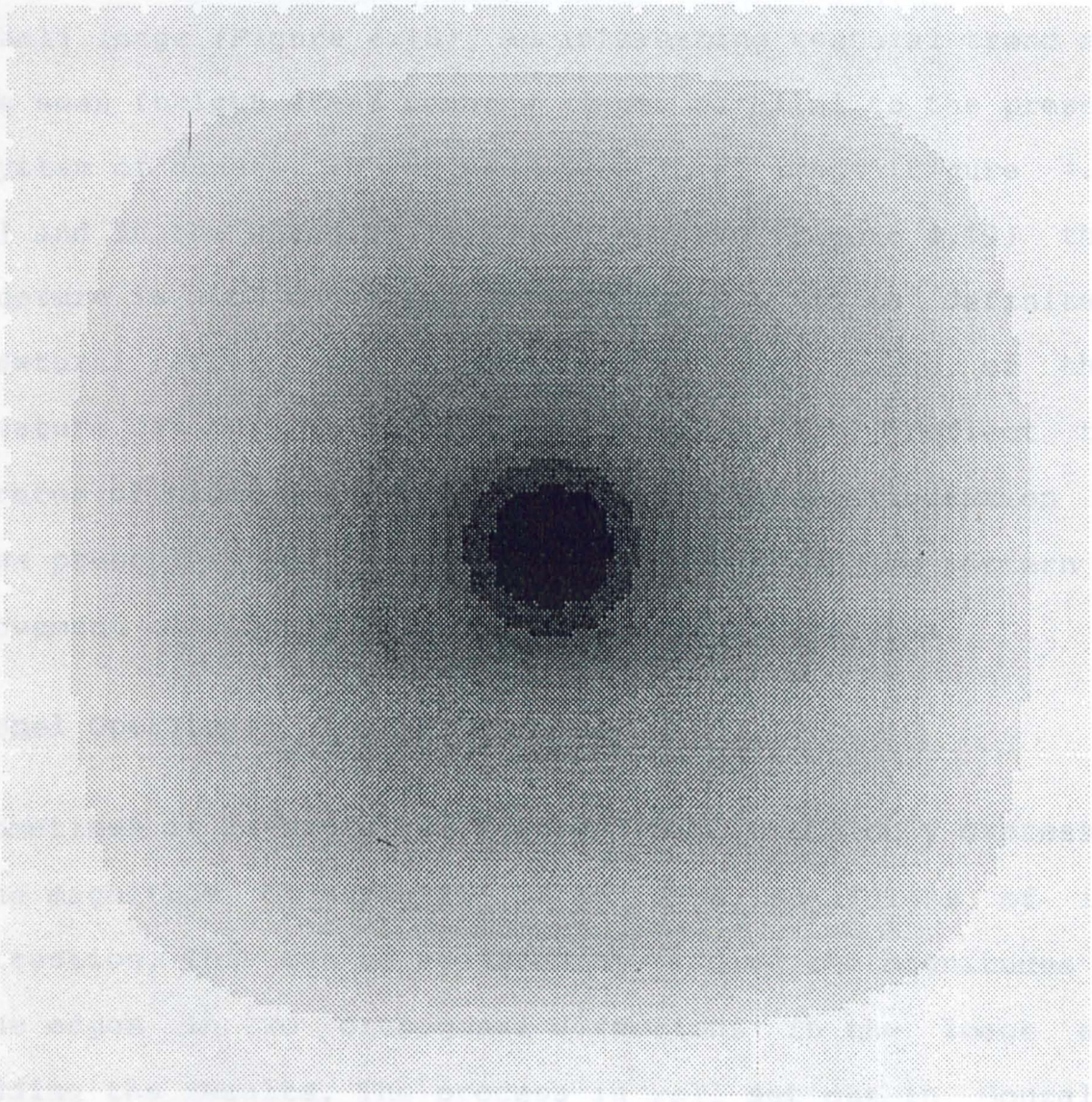


a

Figure 4.16 a,b,c: Frequency response of "normal Laplacian" (a), "Sharp Laplacian (b) and "Laplacian Variant" filters (3x3). From Canas (personal Communication, 1988).



b



c

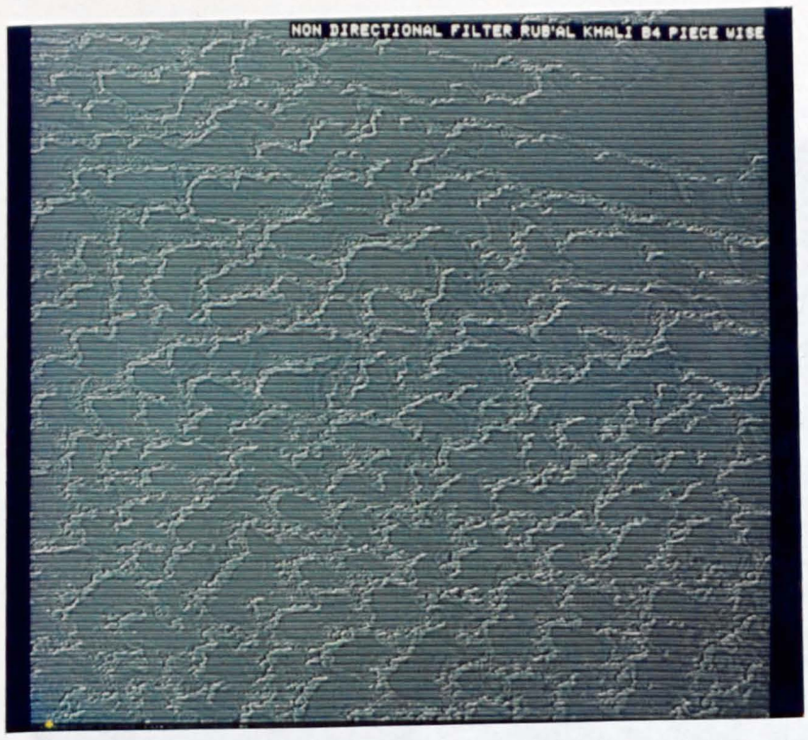
pronounced than on the raw band 4 (7) imagery (Figure 4.17 a,b,c).

When the same mask was applied to MSS band 1 (4) Rub'al Khali image (Figure 4.18), an interesting textural trend may be seen (bright areas running almost parallel to the present system of dunes). In the raw band 1 (4) image (Figure 4.10 d) and in the standard colour composite (Figure 4.19) this feature is not detected, suggesting that it is definitely textural rather than spectral. The significance of this feature can only be guessed at: it may possibly reflect the traces of older dune system with a similar configuration to the present system, or it may be a product of the pattern of movement of lighter sand within the present system.

Sobel Operators:

Sometimes it is useful to have an image which only expresses the magnitude or strength of an edge, regardless of its direction. This can be achieved by finding the magnitudes of the edges in two orthogonal directions in the image and adding the results. The process is well set out in Gonzalez and Wintz (1977), but the results were disappointing, having a confused appearance due to the range of feature sizes present in the scenes. It was therefore concluded that a filter optimised for particular feature sizes would be of greater use.

a



b

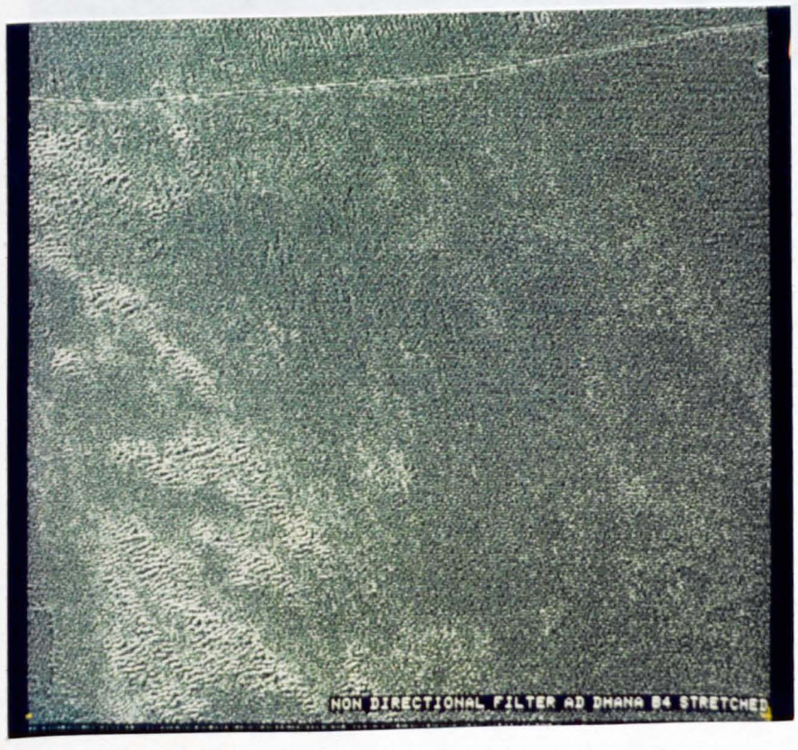


Figure 4.17 a,b,c: "Laplacian Variant" filter images in the test site areas. Textural differences among dunes are more pronounced than on the raw band 4 (7) imagery.



C

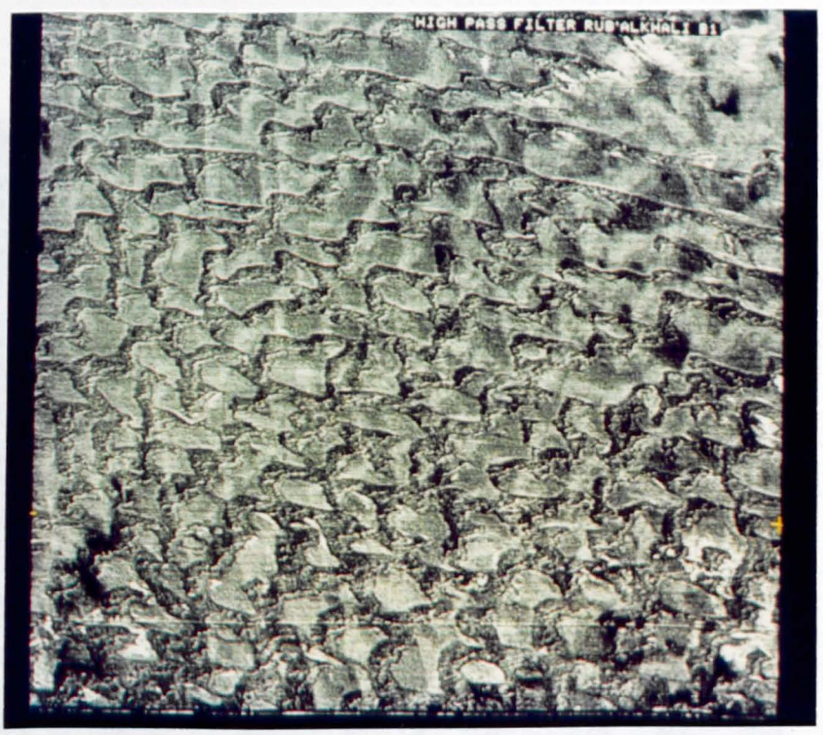


Figure 4.18: "Laplacian Variant" filter applied to MSS band 1 (4) imagery in the Rub'al Khali showing textural features (bright areas) running almost parallel to the present dune system.

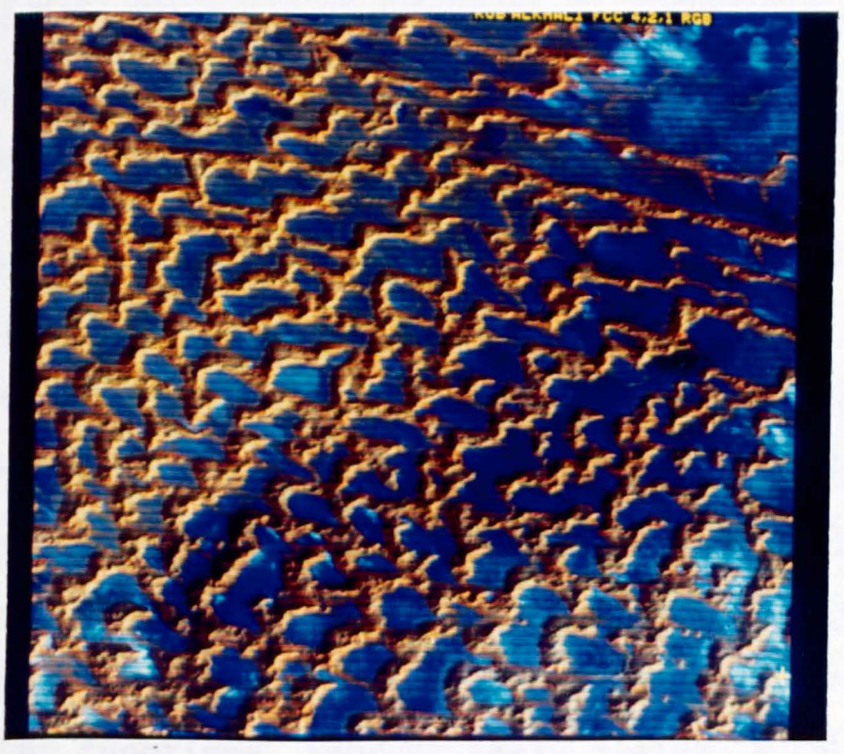


Figure 4.19: False Colour Composite (4,2,1) imagery of the Rub'al Khali area. Textural features detected on Figure (4.18) are not recognized on this imagery.

Difference of Gaussian (DoG) Filters:

The directional and non- directional filters discussed in the above sections gave interesting results with some degree of success. They have, as noted above, highlighted the need for a specific parameter to be included in the design of filters if feature sizes are to be considered. Since in all the scenes presented here we are dealing with dune families of different sizes, a careful filter selection is necessary to achieve optimum results.

DoG filters aim to enhance certain ranges of spatial frequency; in image terms, this corresponds to enhancing textural features of a given range of sizes or scales. If an image consists of low, middle, and high spatial frequencies, one filter might pass low and middle frequencies, whereas another might pass only low frequencies. The convolution mask elements can be calculated from the difference between two Gaussian functions appropriately scaled. Each Gaussian mask is described by the following formula:

$$G(x,y) = \left(\frac{1}{\sigma}\right) \exp \{ - [(x-xo)^2 + (y-yo)^2] / 2\sigma^2 \}$$

The parameter σ is the standard deviation, and it controls the width of the function in the mask. If it is varied (in units of pixels) and the two Gaussian functions corresponding to different values are subtracted, then features whose scale lie approximately between the σ values will be enhanced. In a pure DoG filter, all broad scale features are lost, and this can sometimes cause the

interpreter to become disoriented. The masks used below are designed to leave the broad scale (low spatial frequency) feature in the image intact, and a typical frequency response appears in Figure 4.20; this variation produced clear and interpretable images.

In this investigation the σ value was varied according to the dune sizes present in the image. These sizes were estimated directly from the imagery, and were recorded for each area. Four DoG filters were then designed and appied to each of the three test scenes. These masks, with scale ranges of (0.3-0.6, 0.6-0.9, 0.9-1.5, 1.5-3.0 pixels respectively) are recorded below:

{ 0.3- 0.6 pixel 5x5}

-3	-1	-1	-1	-3
-3.07 10	-1.98 10	-7.94 10	-1.98 10	-3.07 10
-1	+1	+1	+1	-1
-1.98 10	-1.28 10	-5.01 10	-1.28 10	-1.98 10
-1	+1	+1	+1	-1
-7.94 10	-5.01 10	+8.51 10	-5.01 10	-7.94 10
-1	+1	+1	+1	-1
-1.98 10	-1.28 10	-5,01 10	-1.28 10	-1.98 10
-3	-1	-1	-1	-3
-3.07 10	-1.98 10	-7.94 10	-1.98 10	-3.07 10

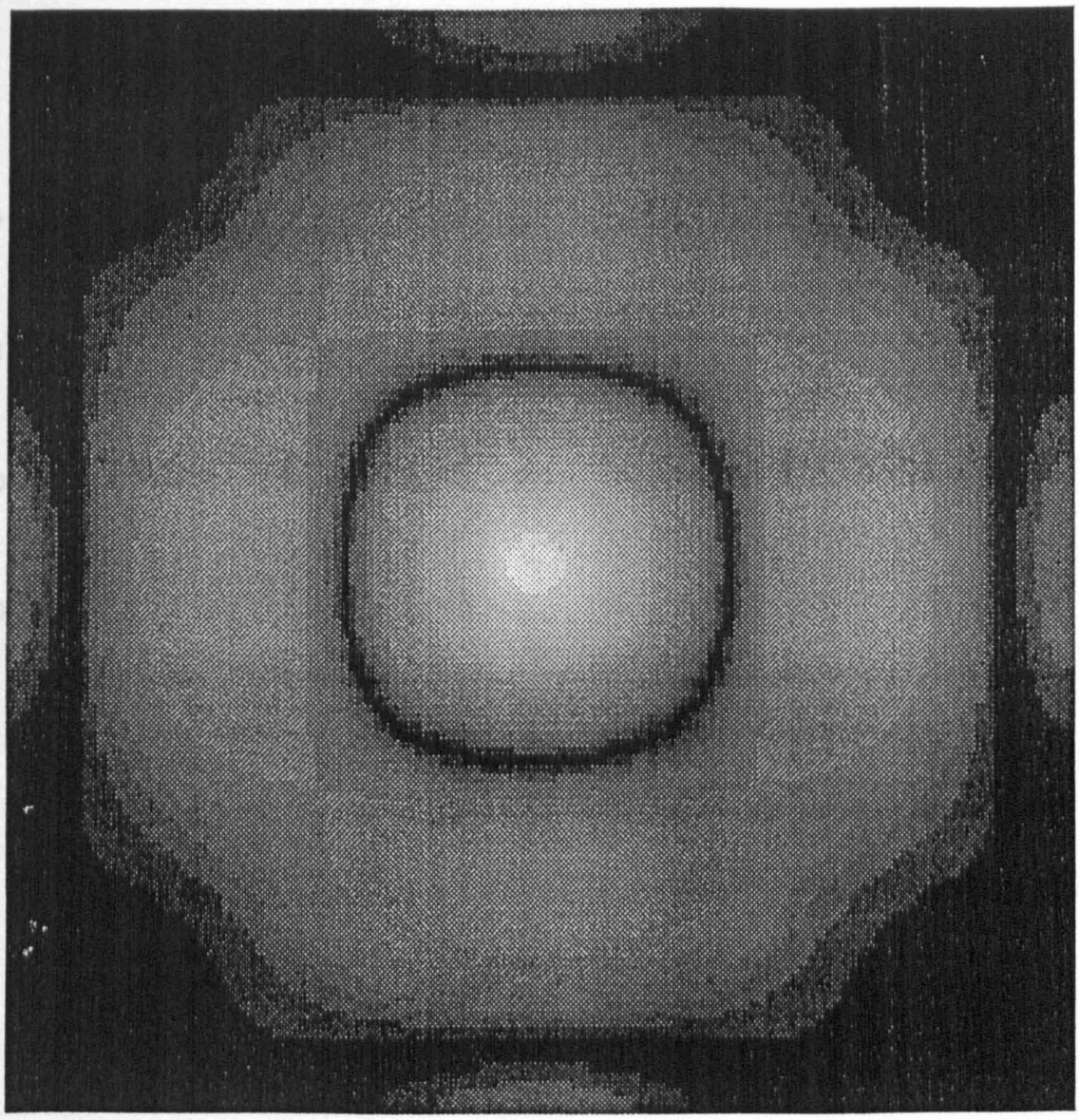


Figure 4.20: A typical frequency response of DoG filter (3x3 mask). The limit of the filter size (0.9-1.5 pixels) is illustrated by the two semi-circles (middle of the figure); bright areas (high response), dark areas (no response).

{ 0.6- 0.9 pixel 5x5}

-3	-3	-2	-3	-3
-1.00 10	-7.00 10	-1.30 10	-7.00 10	-1.00 10
-3	-2	-2	-2	-3
-7.00 10	-3.60 10	-3.90 10	-3.60 10	-7.00 10
-2	-2	-2	-2	-2
-1.30 10	-3.90 10	+3.80 10	-3.90 10	-1.30 10
-3	-2	-2	-2	-3
-7.00 10	-3.60 10	-3.90 10	-3.60 10	-7.00 10
-3	-3	-2	-3	-3
-1.00 10	-7.00 10	-1.30 10	-7.00 10	-1.10 10

{ 0.9- 1.5 pixel 5x5}

-0.021	-0.35	-0.039	-0.035	-0.021
-0.035	-0.035	-0.014	-0.035	-0.035
-0.039	-0.014	+0.038	-0.014	-0.039
-0.035	-0.035	-0.014	-0.035	-0.035
-0.021	-0.035	-0.039	-0.035	-0.021

{ 1.5- 3.0 pixel 5x5}

-0.037	-0.027	-0.020	-0.027	-0.037
-0.027	+0.001	+0.017	+0.001	-0.027
-0.020	+0.017	+0.038	+0.017	-0.020
-0.027	+0.001	+0.017	+0.001	-0.037
-0.037	-0.027	-0.020	-0.027	-0.037

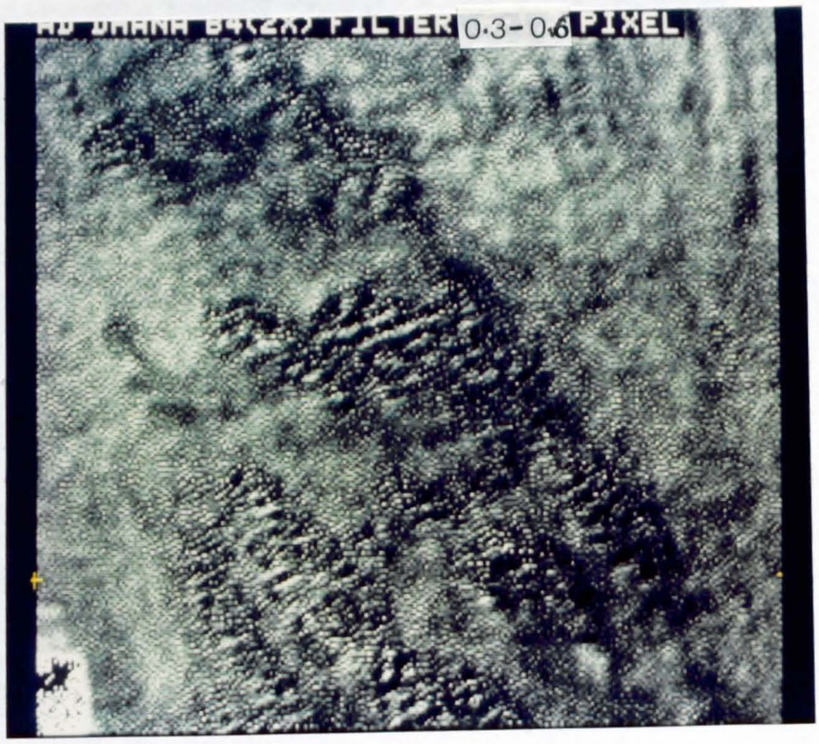
As before the outputs were stretched for optimum display, and the successful results for Ad Dahna and Jafurah images appear in Figures 4.21 and 4.22. Each image was examined closely to assess its quality, and Table 4.1 shows those which performed best for each area. Figure 4.23 shows the result of applying all the masks to the Rub'al Khali scene for comparison purposes.

In the Jafurah, a filter size of 1.5-3.0 pixels (Fig.4.21) gave excellent results (dune textures are much more pronounced than in the raw imagery). In Ad Dahna two filter sizes were successful in enhancing small (0.6-1.2 pixels) and medium (1.8-3.0 pixels) size dunes, indicating that two distinct families are present (Fig.4.22 a,b). In the Rub'al Khali scene only small features could be enhanced (0.6 to 1.2 pixels). and other filters did not give useful results as their scales were inappropriate (Fig.4.23).



Figure 4.21: Contrast stretched DoG filter (1.5-3.0 pixels) imagery in the Jafurah area. At this filter size, textural differences among dunes are more pronounced than on the raw band 4 (7) imagery. Dunes are shown in dark.

a



b

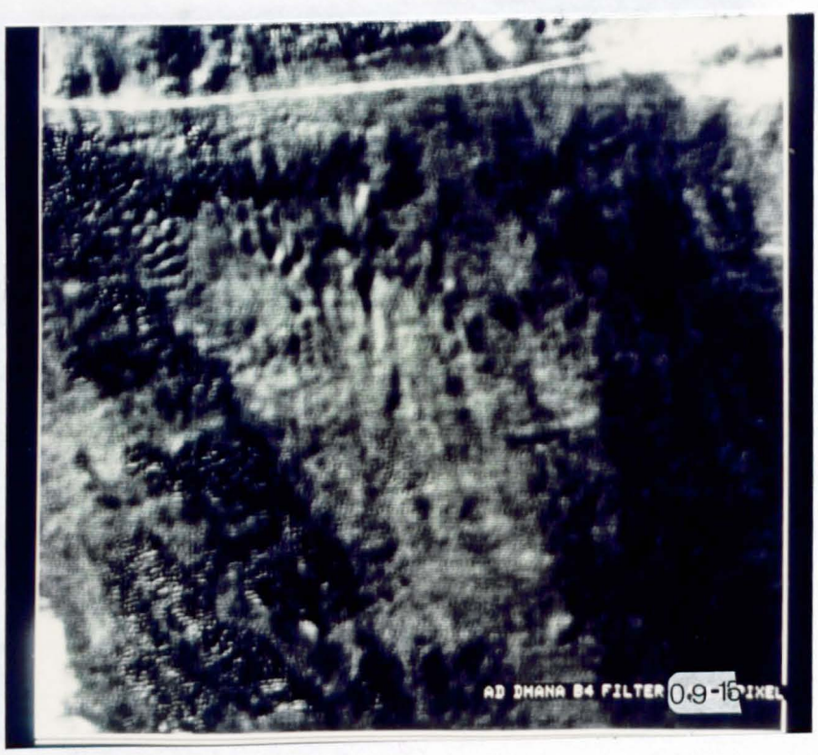


Figure 4.22 a: An enlarged (2x) DoG filter (0.3-0.6 pixels) imagery in Ad Dahna. Textures are clearly detected for dune sizes between (0.6-1.2 pixels).

b: DoG filter (0.9-1.5 pixels) imagery for the same area as in (a). Medium size dunes (1.8-3.0 pixels) are clearly defined (upper left hand side of the imagery).

a



b

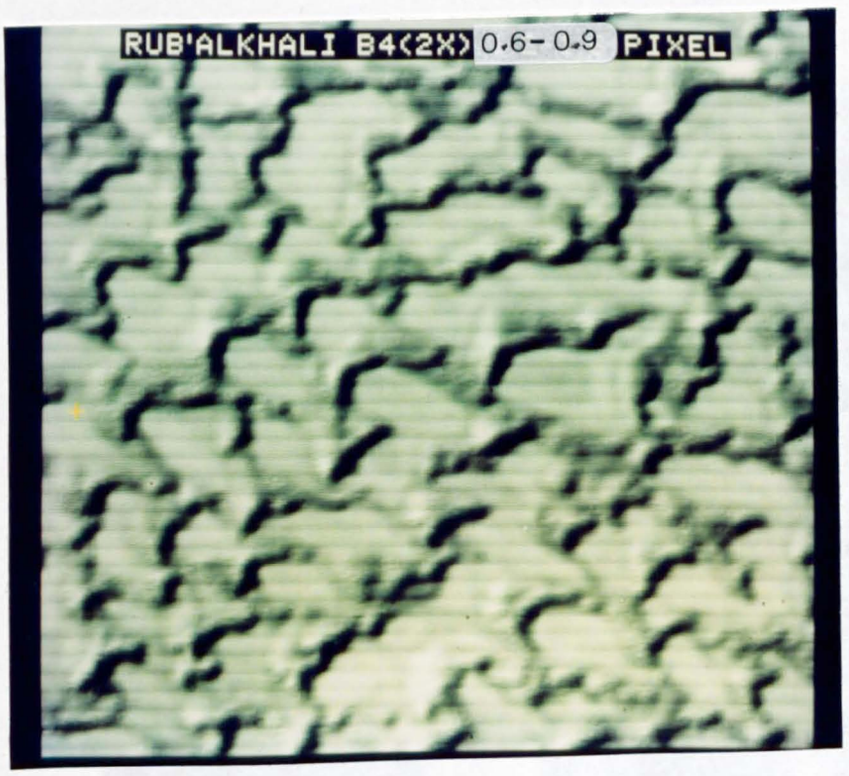
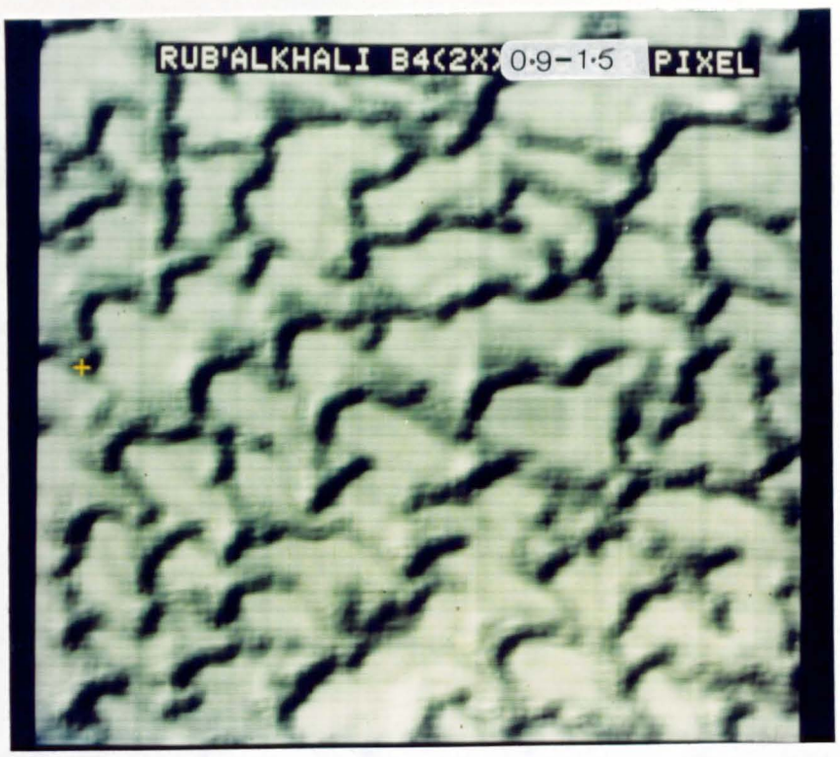
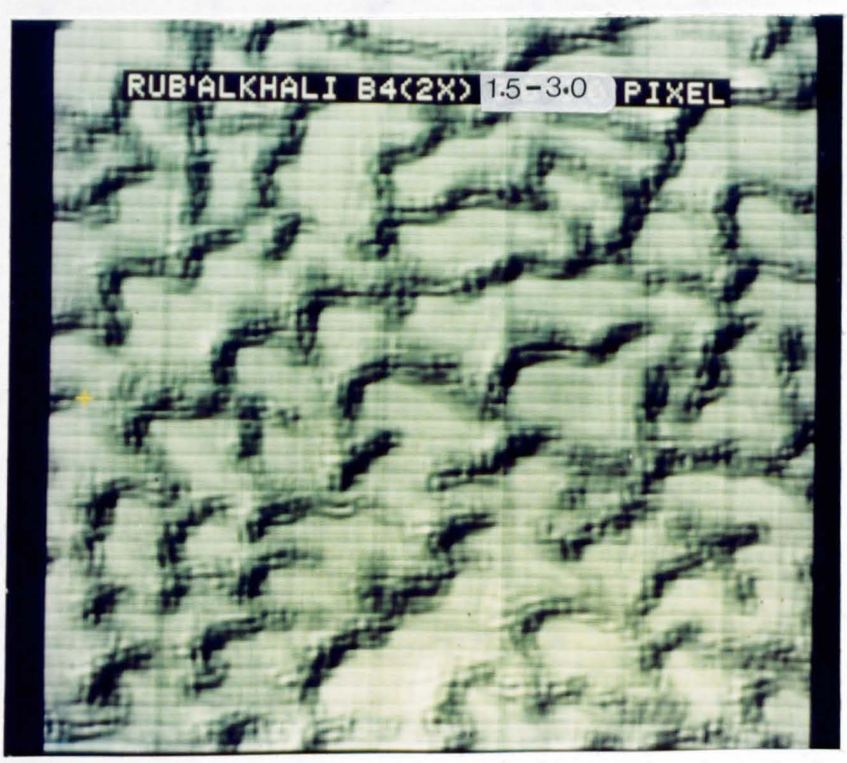


Figure 4.23 a,b,c,d: Contrast stretched DoG filter (0.3-0.6, 0.6-0.9, 0.9-1.5, 1.5-3.0 pixels) images in the Rub'al Khali area. Filter size (0.3-0.6 pixels) clearly shows the textures of the small size dunes found on top of the larger dunes. Other filter sizes were not successful (b,c,d).

c



d



Scene / DoG Filter	Jafurah	Ad Dahna	Rub'al Khali
0.3 - 0.6 pixels	X	✓ Dune size: 0.6 - 1.2 pixels	✓ Dune size: 0.6 - 1.2 pixels
0.6 - 0.9 pixels	X	X	X
0.9 - 1.5 pixels	X	✓ Dune size: 1.8 - 3.0 pixels	X
1.5 - 3.0 pixels	✓ Dune size: 3.0 - 6.0 pixels	X	X

Table 4.1 : Test site areas and the DoG filter sizes used. (✓) successful; (X) unsuccessful.

A false colour composite was tried to combine three different filter sizes on one image for each of the scenes tested. The idea was to test the usefulness of this technique in highlighting successfuly enhanced texture scales as colour difference in one image. In the areas investigated this technique was not found to be successful because of the lack of distinctly different dune sizes in one image. The technique may have potential application when dealing with more than two dune sizes.

This investigation has demonstrated the need for specially designed filters in sand dune studies. Difference of Gaussian filters with careful consideration of the dune sizes have a potential application in enhacing textural differences within dune fields. The use of these filters becomes very important when mapping dune sizes that are close to the spatial resolution of the imagery.

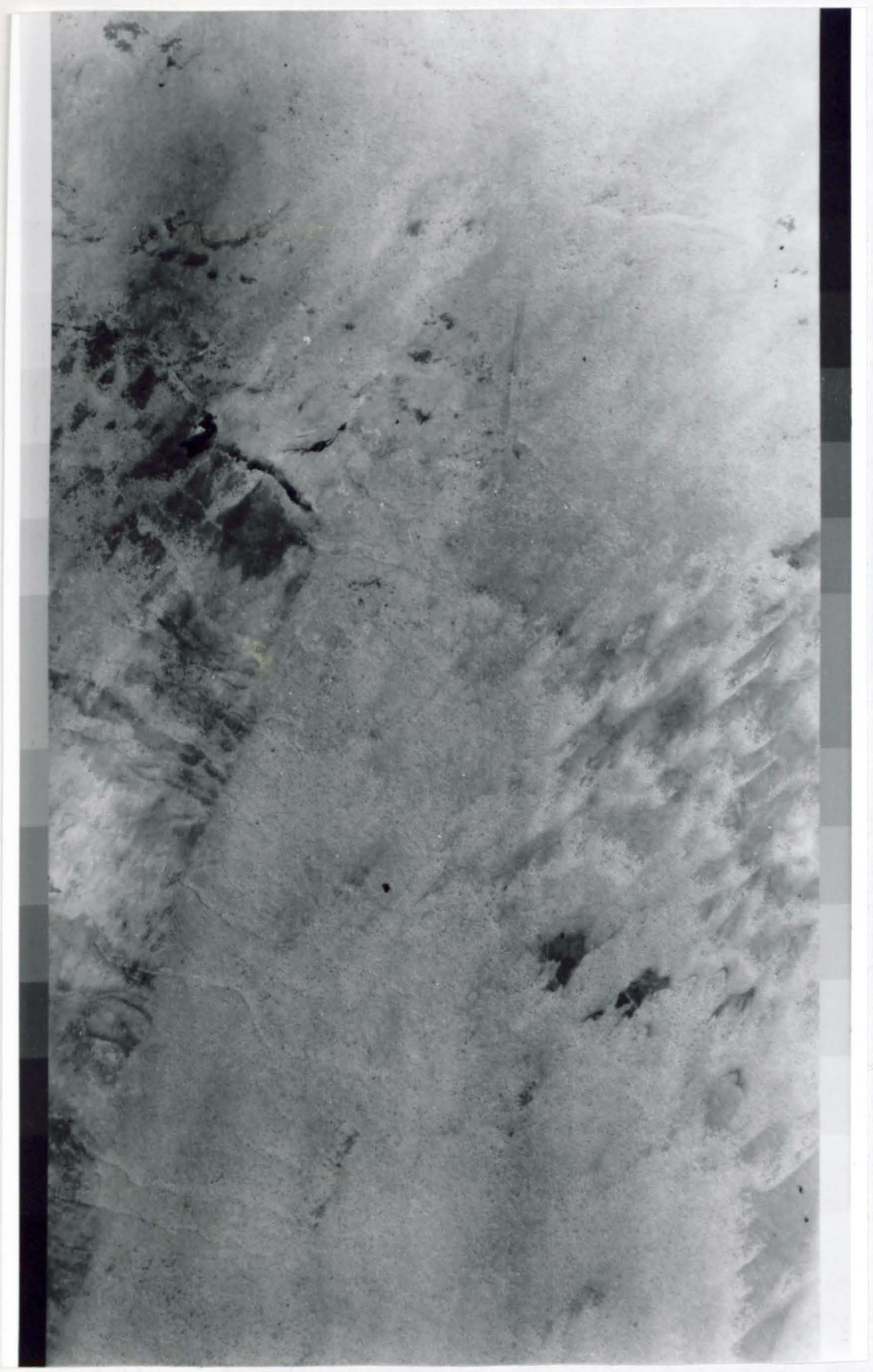
4.8 DIGITIZATION AND EDGE ENHANCEMENT OF LFC PHOTOGRAPHS

The enhanced image shows a great improvement over the original image (Fig.4.24A & 4.24B). In the enhanced image, the dunal details are clearly detected. Moreover, the pattern of paleo-wadi systems which once drained to the Arabian Gulf but now are partly covered by sand, is also highlighted by this imagery.



A

Figure 4.24 Large Format Camera (LFC) panchromatic photograph acquired over southern Jafurah Sand Sea. (A) LFC photograph before applying digitization and spatial filtering. The sand dunes are not recognizable in this photograph. (B) The same photograph after applying digitization and spatial filtering. The patterns of the dunes are clearly defined.



B

Figure 4.24 (Cont'd).

4.9 DISCUSSION AND CONCLUSION

Comparisons between Landsat MSS bands showed that band 1 (green band) is very effective in the detection of iron coating in sand grains. Dune sands appear dark in MSS band 1 imagery. This finding can be used in tracing the origin of the sand source. Samples collected from the south eastern part of the Rub'al Khali showed colour ranges from dark reddish to yellowish red and red in the colour names section of the Munsell chart. These aeolian sands are composed of fine sand (average Md: 0.17mm) and sorting is good (average So: 1.25). The redness of the sands is normally related to the redness of the grains. Some grains may be redder because this was their original colour obtained from the parent rock (mainly red sandstone, or other sedimentary rocks). In other cases, however, the grains got their reddish colour later during relatively recent exposure to surface or near-surface conditions. In the SE Rub' al Khali the red sands are probably related to the soils developed on nearby alluvial fans sloping west and northwest from the Oman range. The red aeolian sands seem to be the result of the deflation of soils formed on these fans during the Pleistocene (Anton, D., 1983). These alluvial surfaces slope west and northwest from the Oman range towards the Rub' al Khali basin. The Oman range is mainly composed of basic rocks and therefore provided iron-rich sediments amplifying the reddening effect of the pedogenetic processes.

Results obtained from three different sand seas in Saudi Arabia show that colour changes within a sand sea is

dependent on location rather than evolution during migration. No progressive sand reddening with increasing maturity along the direction of transport was found in the three investigated sand seas. This finding contradicts Walker's (1979) conclusions that sands become redder with increasing age and distance of transport. Kemp (1985) studied relationships between colours and the amount of extractable-iron or of individual iron oxides of samples from buried and non-buried soils in Eastern England. He found that there was a strong correlation between redness rating and hematite content. Gardner (1981a) investigated the reddening of dune sands in southeastern India. She postulated that the red Teri sands of southeast India were derived from weathering in situe of coastal dune sands. The reddening was due in part to the availability of weatherable minerals and in part to a favorable micro-environment within the coastal dunes. Gardner (1981b) studied reddening of desert sands in three desert areas: southeast India, Sri Lanka and the Natal Province of South Africa. She suggested that reddening of desert sands by mineral breakdown could take place on time-scales that are much shorter than has previously been assumed. She concluded that each area of reddened desert dune sand should be examined on its own merits. Gardner and Pye (1981) suggested that colour is not necessarily a function of age and that temperature, moisture availabilty and dune activity are also important variables. Wasson (1983) has also pointed to the significance of

different source sediments as an influence on dune colour. The results obtained from the three investigated sand seas of Saudi Arabia confirm the conclusions drawn by Gardner and Pye (1981) and Wasson (1983). Obivously further research is requierd to study the causes affecting the colours of desert sands.

Digital image processing techniques such as contrast stretching, false colour compositing, colour transformation and edge enhancement are helpful aids in the final image interpretation as follows:

(i) Production of false colour composites is essential in the identification of sand bodies (yellow) since these can be confused with other superficial deposits which appear similarly bright on black and white images. Sand colour variations between different sand seas can also be detected in false colour composites.

(ii) Colour transformation helped in showing sand colour variations between and within sand seas. Sand colour variations are particularly useful in the interpretation of the dune morphology and the origin of sand sources. The difference in sand colour between the Jafurah and the Ad Dahna, highlighted in the HSI imagery, indicates different sources of sand. Within the Ad Dahna, sand colour variations reflect a change in dune morphology from active small complex dunes in the east to relatively stable large dunes in the west. This result is significantly important in

showing that local variations in sand colours detected in space imagery does not necessarily mean variations in the colour of the sand grains. As seen from the Ad Dahna imagery, colour variations are due to the change in dune patterns rather than changes in the actual colour of the sand.

(iii) Edge enhancement using different directional filters proved to be useful in sharpening dune edges, making them much easier to map. In addition, the power spectra were of considerable assistance in determining dune parameters (wavelength and orientation).

The non-directional filters (textural) highlighted the need for the design of special filter masks with consideration to the sizes of the investigated dunes. Difference Gaussian (DoG) filters with dune size prameters used in the design of the mask elements, gave excellent results. The use of these filters becomes very important when mapping dune sizes that are close to the spatial resolution of the imagery. In order to optimise the use of DoG filters, the following steps are recommended:

i- Select full resolution subscenes.

ii- Select a haze-free band which shows the dunes with good contrast.

iii- Estimate the sizes of the dunes directly from the imagery.

iv- Design the filter to accomodate these dune sizes.

v- If an image contains more than two distinct dune sizes, make a colour composite from three DoG outputs.

CHAPTER 5

MORPHOLOGY AND DISTRIBUTION OF DUNES IN SAND SEAS OF SAUDI ARABIA

5.1 INTRODUCTION

Around one third of the Arabian Peninsula is covered by sand. Sand seas with very large dunes extend over 795,000 square kilometers of the Peninsula (Wilson, 1973). The extent and the distribution of these sand seas make Saudi Arabia an excellent place to study.

This chapter discusses the following:

(i) Review of previous work on modern sediments in Saudi Arabia,

(ii) Dune morohology and distribution in Arabia,

(iii) Measurement of dune parameters such as width, diameter, length, and spacing (wavelength) for different dune types in sand seas of Arabia,

(iv) Analysis and comparison of these measured values to show distribution of dune sizes and spacing of dune types in sand seas of Arabia, and

(v) A detailed investigation (case study) of the Jafurah

Sand Sea.

5.2 PREVIOUS WORK ON MODERN SEDIMENTS IN SAUDI ARABIA

The literature dealing with modern aeolian and related deposits of Saudi Arabia is rather sparse. Distribution of dunes and regional settings of dunes in Arabia have been described by Holm (1953, 1957, 1960) and more recently by Breed et al (1979). Fryberger et al (1983, 1984) studied wind sedimentation and described sedimentary facies of the complex offshore prograding aeolian sand sea in eastern Arabia. Anton (1984, 1985), and Anton and Vincent (1986) studied the general geomorphology and the aeolian deposits in Saudi Arabia. Anton and Ince (1986) studied the sand colour of some Sand Seas of Arabia. Additional descriptions of aeolian deposits of Saudi Arabia are available in Bagnold (1951), Glennie (1970), and Whitney et al (1983); in accounts of early travellers such as, Philby (1933), and Thesiger (1946, 1948, 1949); and in the geologic maps and geographic map series at 1:500,000 scale of the U.S Geological Survey (1966). Other recent contributions include those of Chapman (1971) who discussed the fluvial geomorphology of the Eastern Province, and Patterson and Kinsman (1981) who studied the sabkhas along the Arabian Gulf Coast. McClure (1976, 1978) studied the lakes in the Rub'al Khali and dated some Late Quaternary lakes in Arabia. Johnson et al (1978) also studied the sabkhas in the Eastern Province and made the distiction between " coastal sabkha"

and "inland sabkha". An excellent summary of meteorologic and oceanographic data for the Gulf and Eastern Province is available in Williams (1979).

McKee (1973, 1979a), Mckee and Fryberger (1977), Breed (1979), and Fryberger (1979) all studied the geomorphology and distribution of sand dunes in some sand seas of Arabia using remote sensing images. El-Baz (1979) studied the colour of desert surfaces in Arabia using Earth orbital photographs.

5.3 FORMATION OF SAND DUNES

McKee (1979b) defines a dune as an " accumulation into a mound or ridge of windblown sediment, commonly having a gentle upwind slope and one or more steep lee slopes (slipfaces). Bloom (1978) found that dunes can best be considered as deformable obstructions to air flow that are free to move, divide, grow, and shrink. Bagnold (1941) found that in order for net accumulation of grains to build into a dune, a patch of unorganized sand had to be at least 4-6 m long. The reason for this is that the wind must be sufficiently retarded by the saltation cloud for deposition to occur; for distances less than about 4 m, the wind and its load of sand will simply overshoot the patch. Under conditions of deposition, the patch will continue to grow as a mound of sand until a critical height is reached. When the angle of repose for dry sand is reached downward slipping results and the slipface is formed. Slip face angles

reported in literature vary from 32 to 34 degrees. When a dune has reached its equilibrium shape, it will move forward as a whole conserving its shape.

Several investigators utilized remote sensine imagery for the study of dune patterns in different sand seas of the world. They found close correlations between morphometric parameters (height, width, length and spacing) for all dune types (Breed and Grow, 1979; Lancaster, 1983, Wasson and Hyde, 1983).

Warren (1983, 1985) gave an excellent review of the current research on the shape and behaviour of sand dunes. A critical short discussion on the needs in dune research was presented by Warren and Knott (1983). They noticed that there was slower than usual advance in fundemental studies of moving sand. They argued that the scale of study that would yield the greatest advance is the "graded" scale of the flow around individual dunes. Fryberger (1979), Wasson and Hyde (1982, 1983) and Lancaster (1983) studied the factors determining desert dune types. They argued that both wind regime and sand availability are the two most important determinants of dune type. The influence of sand supply is still contraversial (Rubin, 1984) as is the role of sediment characteristics. Basically, very little is known on the factors which influence the equilibrium size and spacing of desert dunes (Lancaster and Hallward, unknown date).

Other studies of dune dynamics include those of Tsoar (1978, 1982, 1983, 1985), Tsoar and Yaalon (1983), and Tsoar, et al (1985); Lancaster (1982, 1984a, 1984b, 1985), Warren and Kay (1987).

5.4 DUNE CLASSIFICATION

Dune classification is based primarily on the general shape of the sand mass and the number and position of slip faces. The classification adopted for this study is based on McKee (1979a). The reason for adopting this classification is because it combines remote sensing of dunes from orbit with the knowledge of dune formational processes. The dunes in Table 5.1 are mainly; simple dunes (single dunes); compound dunes are composed of two ore more dunes of the same type; complex dunes consist of more than one type of dune. Figure 5.1 is a diagram illustrating the principal dune types. Table 5.2 is an illustration of basic dune types as seen from different remote sensing images.

SIMPLE DUNE TYPES: The most common basic dune forms result from winds having a single dominant direction. The axes of the dunes are oriented at right angles to the wind direction. Such dunes range from the small crescent-shaped type known as barchan, through parallel rows of linked barchans known as barchanoid ridges, to parallel straight ridges known as transverse dunes (Fig.5.1 a, b, c). Most barchan types are too small to be recognized on Landsat imagery and the distinction between tansverse and barchanoid ridges is difficult (see Chapter 6 for more details).

Form	Number of Slipfaces	Name used in Ground Study of Form, Slipface and Internal Structure	Name used in Space-imagery and Air-photo Study of Pattern and Morphology	
Sheetlike with broad flat surface	None	Sheet	Sheet	
Thin, elongate strip	None	Stringer	Streak	
Circular or elliptical mound	None[2]	Dome	Dome	
Crescent in plan view	1	Barchan	Crescentic	Barchan
Row of connected crescents in plan view	1	Barchanoid ridge	Crescentic	Barchan-oid ridge
Asymmetrical ridge	1	Transverse ridge	Crescentic	Barchan-oid ridge
Circular rim of depression	1 or more	Blowout[4]	Not recognised	
"U" shape in plan view	1 or more	Parabolic[4]	Parabolic	
Symmetrical ridge	2	Linear (seif)	Linear	
Asymmetrical ridge	2	Reversing	Reversing	
Central peak with 3 or more arms	3 or more	Star	Star	

Table 5.1: Terminology of basic dune types and other eolian deposits (modified from McKee, 1979).

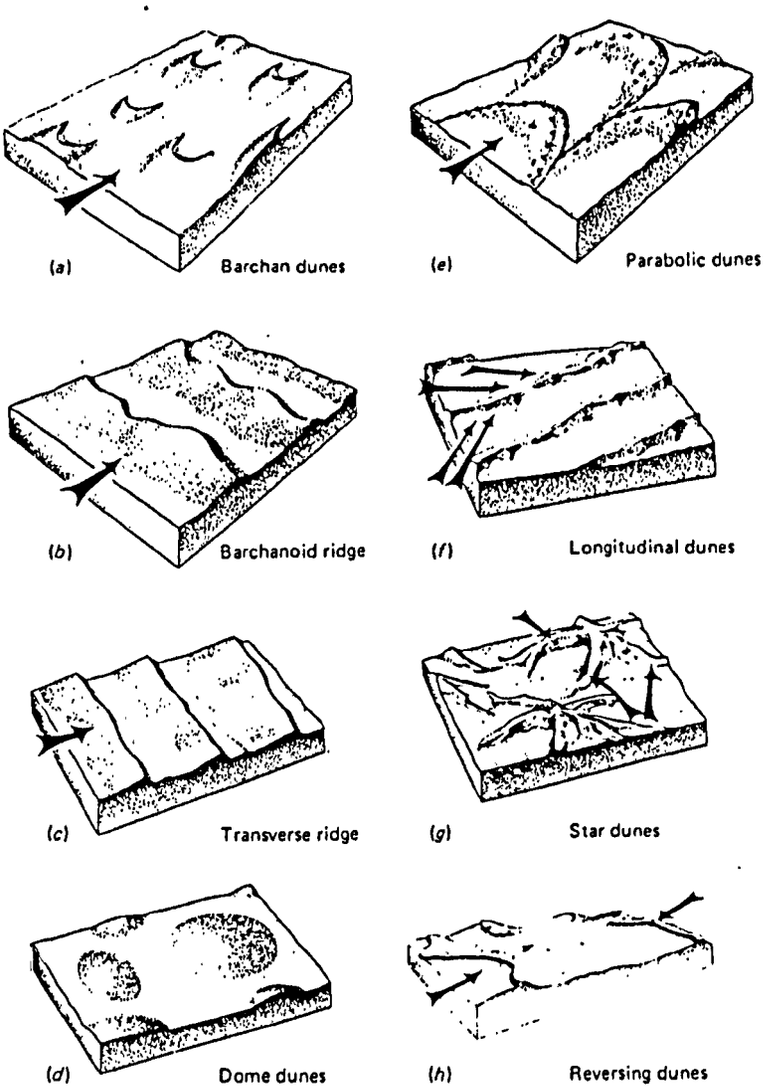


Figure 5.1 A sketch diagram illustrating the principle dune types and the winds responsible for their formation. After McKee, (1979a).

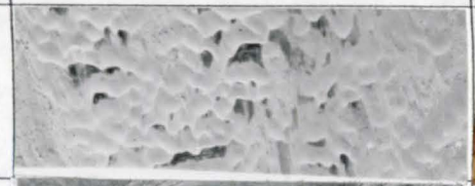
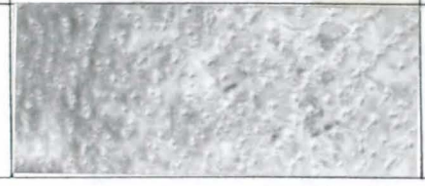
Dune Type	Aerial Photographs	Landsat Images	Space Photographs	Radar Images
Crescentic				See Fig. 6.16
Linear		See Fig. 5.8		
Parabolic	See Fig. 5.20	NR	NA	NA
Dome		See Fig. 5.13	NA	NA
Star		See Fig. 5.11		NA

Table 5.2: Basic dune types as seen from different remote sensing images. NR indicates not recognised; NA indicates not available.

Simple dunes are all characterized by slipfaces in one direction and hence represent unidirectional wind movement (McKee, 1979b). They commonly occur in a sequence downwind as a result of diminishing sand supply. Barchans result from sparse supply of sand and are found scattered over bare rock or, as in Arabia, sabkha surfaces. Transverse dunes, on the other hand, develop where the supply of sand is abundant. The spacing of the transverse and barchanoid ridges is controlled by the strength of the wind and the availbility of sand.

Sand bodies that display no slipfaces are refered to as sheets and stringers. Breed (1979) defined sand sheets as "irregular patches of aeolian sand with external shapes definable on Landsat imagery in terms of the bounding topography, and without discrenible slipfaces ". A stringer, sometimes refered to as a streak, may be considered to be a variety of sand sheet having a stringlike shape, and commonly develops along the margins or at the downwind of a sheet (McKee, 1979b). These sand bodies are not considered to be dunes, because they are flat.

Dome dunes show no external slipfaces and are circular or elliptical in plan view (Fig. 5.1d). Some of the dome dunes began development as barchan dunes but as a result of strong winds the lee slopes of the barchans are truncated and flattened. In Arabia dome dunes are found near coastal areas and always associated with sand sheets and parabolic dunes.

Parabolic dunes are forms of dunes which are controlled more by partial stabilization by vegetation or moisture or both, than by wind strength and direction. They are u-shaped or v-shaped mounds of sand trailed by elongated arms, having slipfaces on the outer convex side and are usually associated with sand sheets (McKee, 1979a; Fig. 5.1e). They are features characteristic of deflation by wind, but as with other dunes, deposition occurs wherever margins are free to migrate (McKee, 1966; Cooper, 1967).

Generally, little is known about parabolic dune sands (Pye, 1982; Ahlbrandt, 1975). Pye studied coastal parabolic dunes in North Queensland, Australia and found dune sands to be poorly sorted and negatively skewed (the most strongly negatively skewed sands having large tails of coarse grains). Ahlbrandt studied parabolic dunes in Killpecker dune field, Wyoming, and found the dune sands to be weel and positively sorted. Mechanical analyses of sand sampled from parabolic dunes in White Sands, New Mexic0, showed medium-sized grains with few coarse grains (McKee, 1971). Anton and Vincent (1986) stdied parabolic dunes of the Jafurah Sand Sea, Saudi Arabia, and found that the coarse grains comprise about 60-70 per cent of the the parabolic dune sand.

Parabolic dunes are forms of dunes which are controlled more by partial stabilization by vegetation or moisture or both, than by wind strength and direction. They are u-shaped or v-shaped mounds of sand trailed by elongated arms, having slipfaces on the outer convex side and are usually associated with sand sheets (McKee, 1979a; Fig. 5.1e). They are features characteristic of deflation by wind, but as with other dunes, deposition occurs wherever margins are free to migrate (McKee, 1971; Cooper, 1967).

Generally, little is known about parabolic dune sands (Pye, 1982; Ahlbrandt, 1975). Pye studied coastal parabolic dunes in North Queensland, Australia and found dune sands to be poorly sorted and negatively skewed (the most strongly negatively skewed sands having large tails of coarse grains). Ahlbrandt studied parabolic dunes in Killpecker dune field, Wyoming, and found the dune sands to be weel and positively sorted. Mechanical analyses of sand sampled from parabolic dunes in White Sands, New Mexic0, showed medium-sized grains with few coarse grains (McKee, 1971). Anton and Vincent (1986) stdied parabolic dunes of the Jafurah Sand Sea, Saudi Arabia, and found that the coarse grains comprise about 60-70 per cent of the the parabolic dune sand.

Parabolic dunes, in Arabia, are usually very small (width 40 to 200 metres) and are not recognizable in either Landsat imagery or Large Format Camera photographs but are detectable in aerial photograophs of 1:10,000 scales (see Chapter 6 for more details).

Linear dunes are straight or slightly sinuous dunes (Fig. 5.1f). Their length is many times greater than their width and have regular spacing. They are commonly known as seif dunes in Saudi Arabia and Africa and as longitudinal dunes or sand ridges in other regions of the world. They occupy about 50% of the area of sand seas. Linear dunes are characterized by their straightness, parallelism and great length. Slip faces may occur on each side of the crest line and may change orientation seasonally. Considerable controversy has surrounded the mechanics of genesis of linear dunes and their relationship to winds (Lancaster, 1982). However, there is a common agreement that they are formed in wind regimes with two main directions of sand moving winds from within a 180 degrees arc (Lancaster, 1982). Groups of these dunes can be seen in space imagery and aerial photography as parallel straight lines.

Dunes with multiple slipfaces are refered to as star dunes and occupy an average of 8% of the area of most sand seas (Fig. 5.1g). Star dunes often form in multidirectional or complex wind regimes and are characterized by their large size and tendancy to grow vertically rather than migrating laterally. They commonly have a high central peak and three or more arms extending radially and can have an infinite variety of shapes.

Intermediate between the star dunes and linear dunes are reversing dunes (Fig. 5.1h). They form where winds from two main directions are opposed in direction and sand moving potential. They may have the general form of transverse ridges with a second slipface developing periodically and in a direction nearly opposite to that of the primary slipface (McKee, 1979b). Reversing dunes are not reported in Arabia.

COMPOUND DUNE TYPES: This group consists of two or more of the same dune type combined by overlaping or by being superimposed on one another. Particularly common are compound cresentic or transverse ridges with superimposed crescentic dunes.

COMPLEX DUNE TYPES: This group results from the combination of two or more of the basic dune types. Thus star dunes may occur on cresentic ridges or on linear dunes as in the southern and southeastrn Rub'al Khali.

5.5 SAND SEAS OF ARABIA

There are four major sand seas in Saudi Arabia; The An Nafud in the northern part of the Peninsula, Ad Dahna in the central part, Rub'al Khali or Empty Quarter in the south, and Al Jafurah in the eastern part. There is another group of small scale sand bodies along the western side of the Tuwayq escarpment but are less significant (Nafud ath Thuwayrat, Nafud as Sirr).

Figure 5.2 shows the major dune types found in the sand seas of Arabia. The following is a discussion of the different sand seas.

AN NAFUD SAND SEA:

This is the least studied sand sea. It covers about 72,000 square kilometers (Wilson, 1973). An Nafud sand fields occupy a relatively depressed area between Lattitude 27 20'N and Longitude 38 20' E and 42 40' E with an approximate length of 300 km and a width of 250 km. In the south, An Nafud links with Ad Dahna sand sea.

An Nafud can be related to the aeolian reworking (under arid conditions) of alluvial deposits brought in by wadis originated in the surrounding watersheds. The presence of sandstones outcropping in the southeast of the region suggests an important source of sand from these sandstones (the Ordovician Saiq Sandstone and equivalent units) (Anton, 1983). The evidence supporting such a hypothesis is

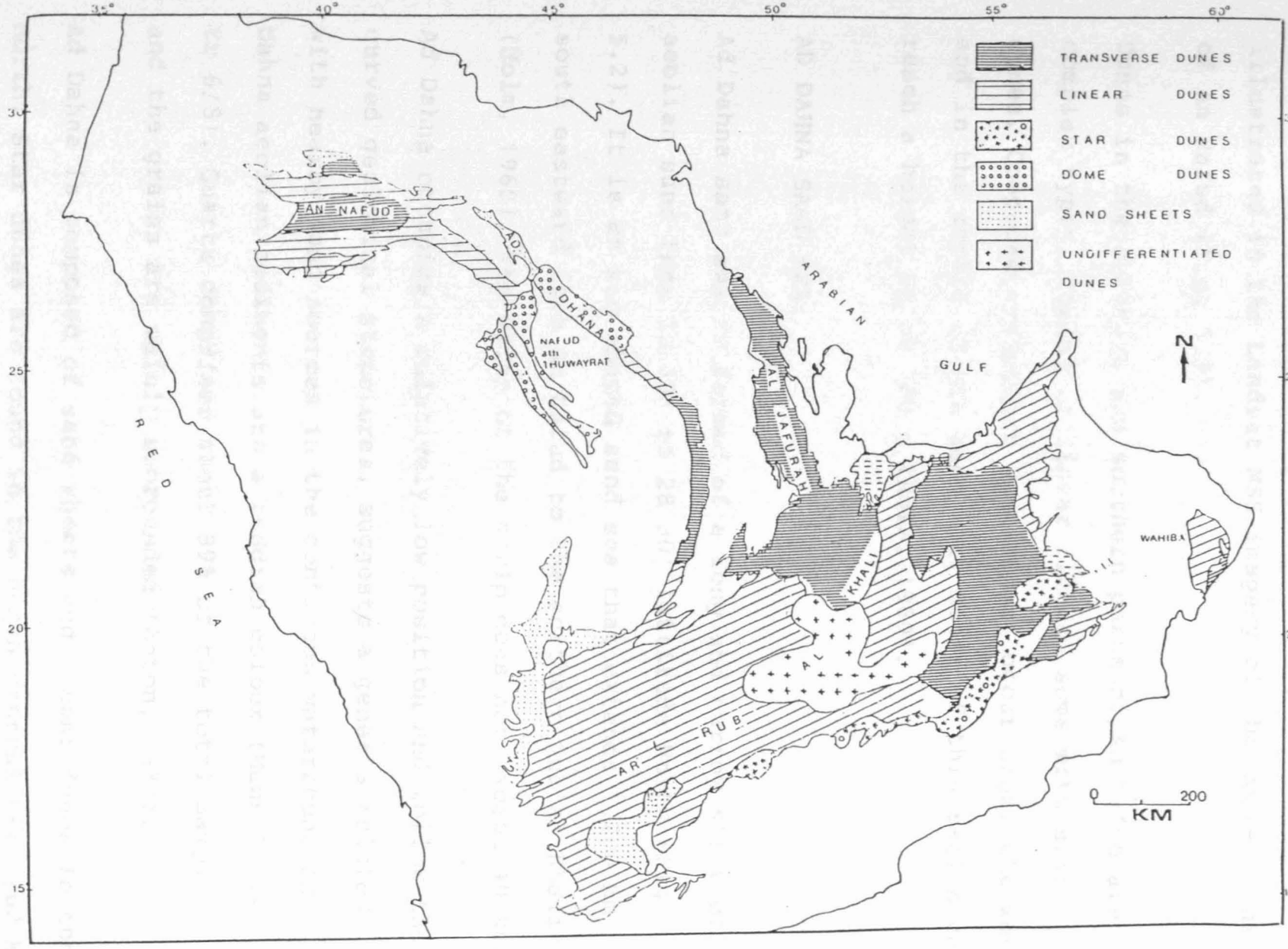


Figure 5.2 Major dune types in sand seas of Arabia.

illustrated in the Landsat MSS imagery of the western part of An Nafud (Fig. 5.3).

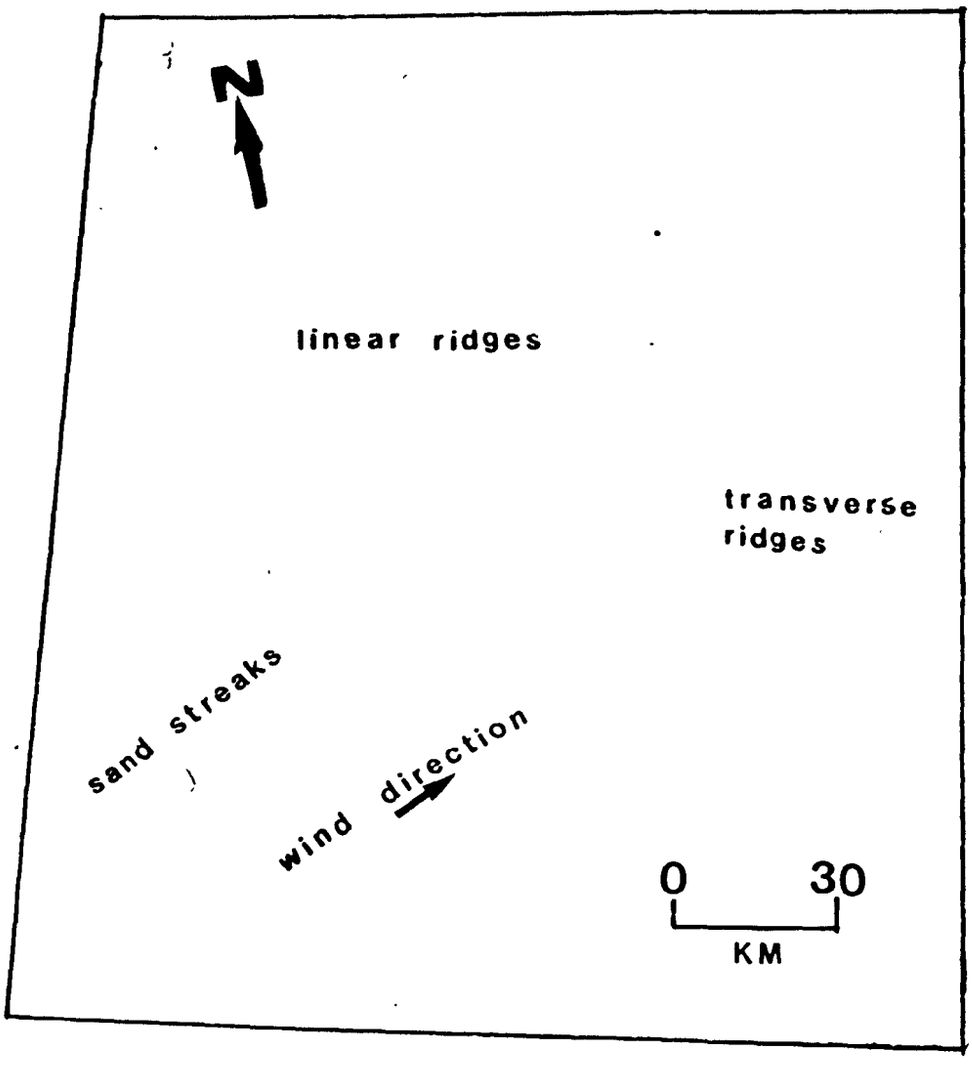
Dunes in the northern and southern parts of An Nafud are complex types, formed of linear ridges, some with star dunes. Compound crescentic dune ridges occur along the west and in the centre of the sand sea. Dunes of this region can reach a height of of 100 m (Holm, 1960).

AD DAHNA SAND SEA:

Ad Dahna sand sea is formed of a long and narrow strip of aeolian sand from 20 30' to 28 30' lattitude North (Fig. 5.2). It is an arc-shaped sand sea that extends 1,200 km south eastward from An Nafud to the northern Rub'al Khali (Holm, 1960). The width of the strip does not exceed 40 km.

Ad Dahna occupies a relatively low position and follow the curved geological structures, suggests a genesis related with nearby sand sources in the continous watershed. Ad-Dahna aeolian sediments are a reddish colour (Munsell 7-5 Yr 6/8). Quartz comprises about 99% of the total samples and the grains are mainly subrounded (Anton, 1983).

Ad Dahna is composed of sand sheets and linear dunes in the north. Star dunes are found in the north central part (60 km south of Zalim village). In the south, linear dunes are dominant.


N
linear ridges
transverse ridges
sand streaks
wind direction
0
30
KM

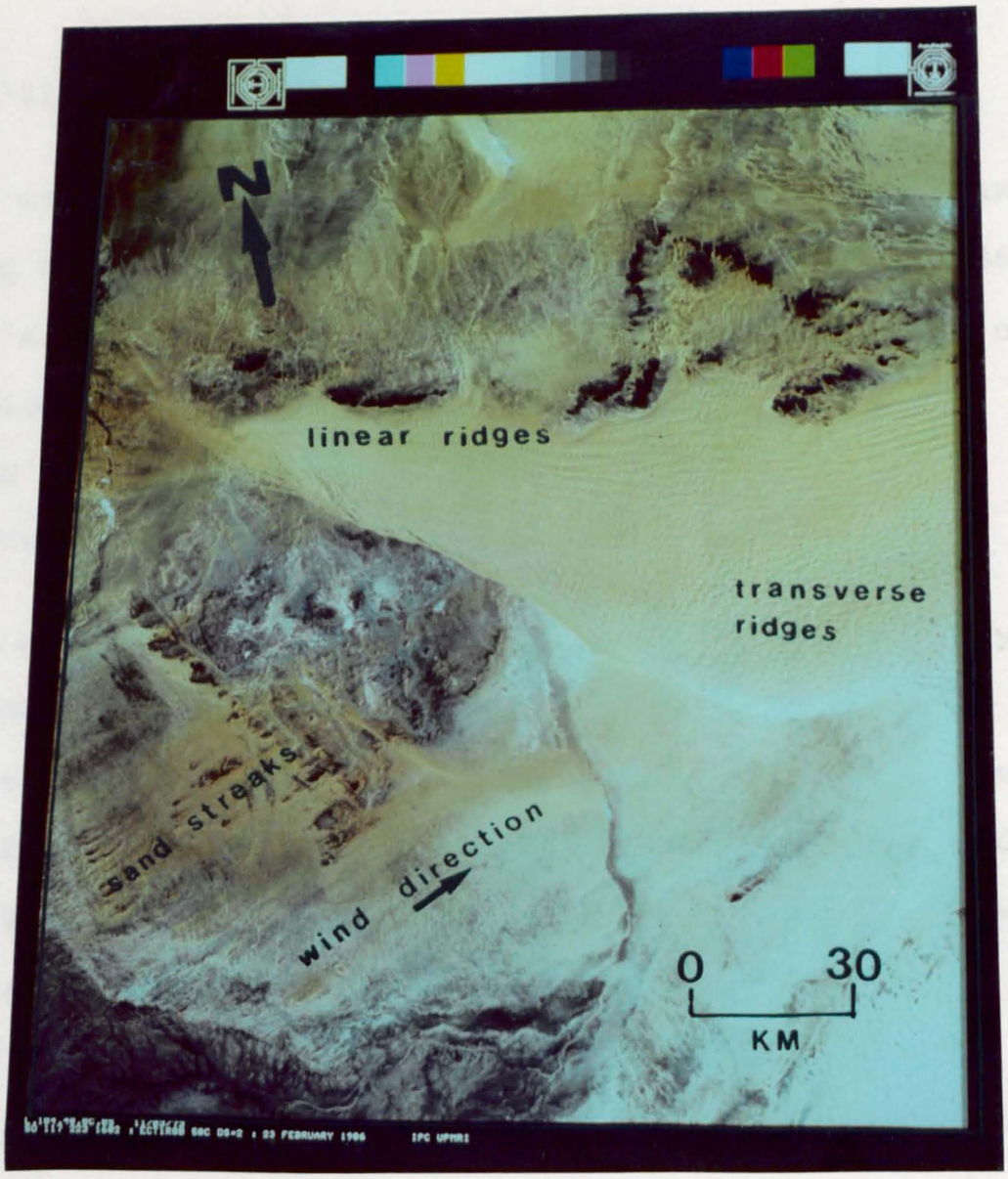


Figure 5.3 A Landsat MSS false colour composite acquired over the western part of An Nafud Sand Sea (184/40; 11.3. 1973). The sand streaks on the left hand side of the image indicate a possible sand source from the surrounding bedrock.

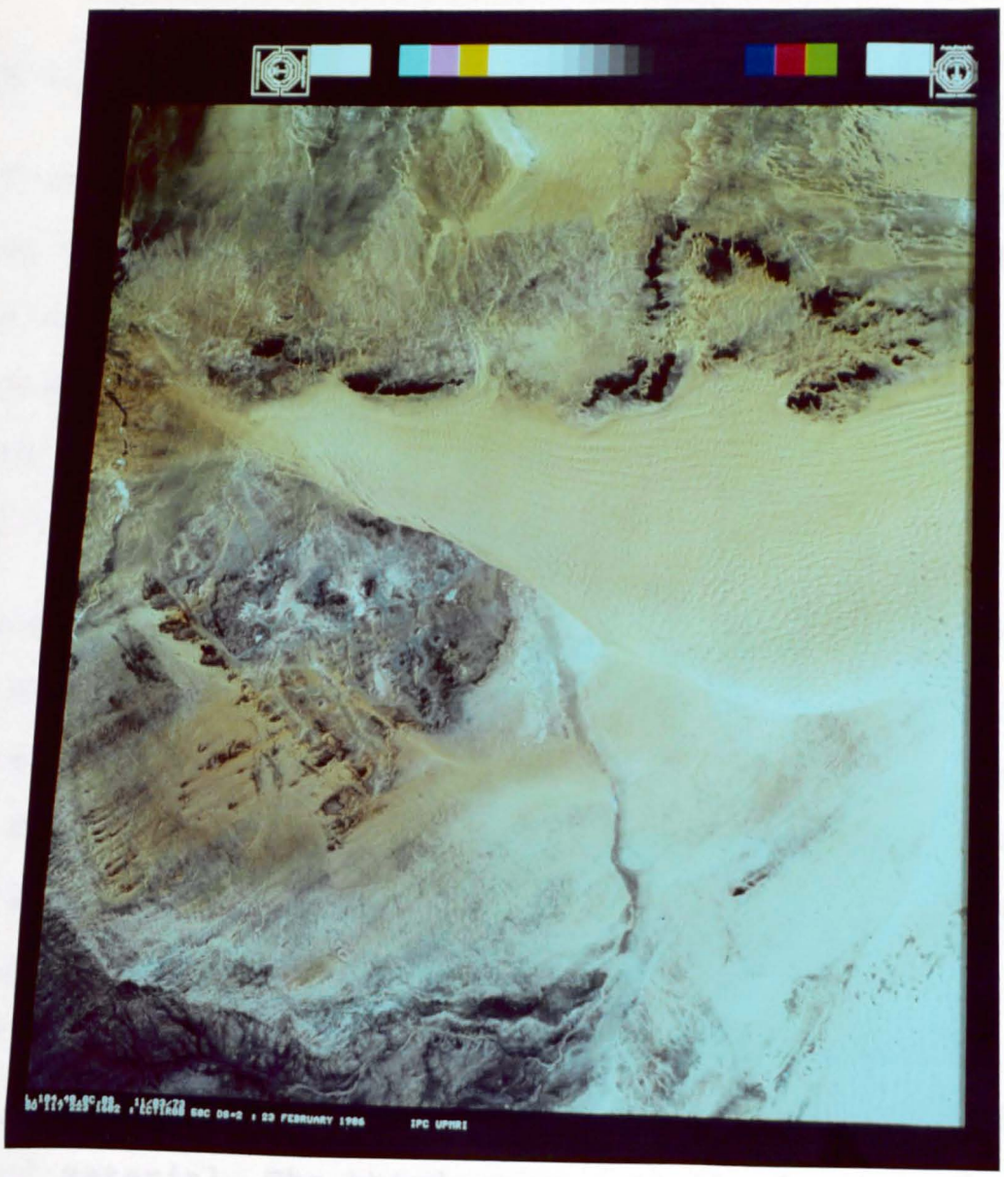


Figure 5.3 A Landsat MSS false colour composite acquired over the western part of An Nafud Sand Sea (184/40; 11.3. 1973). The sand streaks on the left hand side of the image indicate a possible sand source from the surrounding bedrock.

THE RUB'AL KAHALI SAND SEA:

Much of southern Arabia is a structural basin with its axis plunging gently into the Arabian Gulf (Power et al., 1966). The Rub'al Khali covers about 560,000 square kilometers of the region. It extends from the United Arab Emirates westward almost 1,500 km to the foothills of the Yemen mountains (Fig. 5.2).

Sources of aeolian sand in the Rub'al Khali are not fully known. Some authors believe that the sand has been transported by wind from alluvial (wadi) sediments that were eroded from Paleozoic and Mesozoic sandstones (Holm, 1960; Grow, 1960). During pluvial periods Wadi Ad Dawasir and Wadi As Sahba drained the west central shield and sedimentary arc and fed the Rub'al Khali basin. A second source of sand is the Oman mountains in the east which contributed significant amount of material. The third source is the feeding of the Rub'al Khali by the northern sand seas (the Jafurah and Ad Dahna).

Dune heights in the Rub'al Khali reach about 300 metres (Wilson, 1970). Thesiger (1948) reports heights of 153 to 213 metres. Holm (1960) recorded heights of 200 metres. Height Measurements based on the Large Format Camera photographs records heights of 70 to 213 metres in the

southeast of the sand sea (see Chapter 6 for more details). According to Wilson (1971), the growth of dunes to as much as 300 metres may require thousands of years. A Pleistocene age for the large dunes of the Al'Uruq al Mutaridah in the eastern Rub'al Khali is suggested by Glennie (1970).

The changes in wind direction have affected the dune morphology (Anton, 1983). Alternating dune shapes are being built, new complex dunes are being formed, and sand sources are shifting from one place to another. Two forms of crescentic dunes were recognized in the eastern Rub'al Khali; barchan dunes, both single and complex (Glennie, 1970), and "giant sand massifs". Giant sand massifs are in various forms of a barchan like structure with their axes transverse to the dominant wind direction. Holm (1960) called these dunes "giant crescentic massifs". Compound linear dunes of a "hooked " variety are recognized in the north-central Rub'al Khali (Holm, 1960, 1968). In the south western margin, linear or seif dunes separated by flat interdune corridors are present. Star dunes are found along the eastern and southern margins.

AL JAFURAH SAND SEA:

Al Jafurah is an elongate, 30-250 km wide sand sea extending down the western side of the Arabian Gulf, past Qatar and southward, finally merging into the sands of Rub'al Khali (Fig. 5.2).

The dune fields are a product of local phenomenon and the observed aeolian features are barchanoid ridges, transverse ridges, sand sheets, dome and parabolic dunes (Anton, 1983). These aeolian features are due mainly to nearly constant wind direction and very frequent high wind speed. This sand sea has been the main centre of interest for this study. A paper was published as a result of a detailed study on the Jafurah Sand Sea (Fryberger et al, 1984). A copy of this paper is in Appendix (2). A full discussion of the Jafurah Sand Sea is presented in section 5.8 of this chapter.

5.6 DUNE MORPHOLOGY

The advent of satellite and other remote sensing data for desert areas has shown the great variety of dune morphology in sand seas. A potentially valuable area is the study of dune morphometry, particularily the length, height and spacing of dunes, but this has received little attention (Wilson, 1977, Breed & Grow, 1979, Lancaster, 1981a). There have been few studies of the factors which control the morphology and the morphometry of dunes within a sand sea. Such studies may make an important contribution to our understanding of the factors which control the shape and sizes of dunes and the ways in which aeolian sand bodies move and accumulate.

METHODOLOGY: Landsat MSS and TM imagery together with the Large Format Camera (LFC) and aerial photographs were used

for the general description of aeolian bodies in sand seas of Arabia. Supplementary information about dunes of each sand sea was obtained from the studies of other workers (McKee, 1979a; Breed, 1979; Holm, 1960).

Dune lengths, widths or diameters, and dune spacings (crest-to-crest distances) were measured directly from prints or transparencies according to the diagram shown in Figure 5.4 (adopted from Breed, 1979). Landsat imagery was used for measurement of large aeolian sand bodies. Small dunes were measured on LFC and aerial photographs.

Data resulting from measurement were analyzed and compared to show distribution of dune sizes and spacing of dune types in the different sand seas of Arabia.

MORPHOLOGY OF DUNES IN SAND SEAS OF ARABIA:

Breed & Grow, (1979) define a sand sea as "large areas of aeolian sand occupied by dunes which tend to be repeated in orderely sequences rather than occuring as scattered solitary features". Section 5.5 discusses the major sand seas of Saudi Arabia. In the following sections of this chapter, the occurrence of different dune types in sand seas of Arabia and thier morphometry is discussed.

LINEAR DUNES: Simple, compound, and complex linear dunes can all be found in the sand seas of Arabia. Simple linear dunes are found in Ad Dahna, parts of the northern sand seas

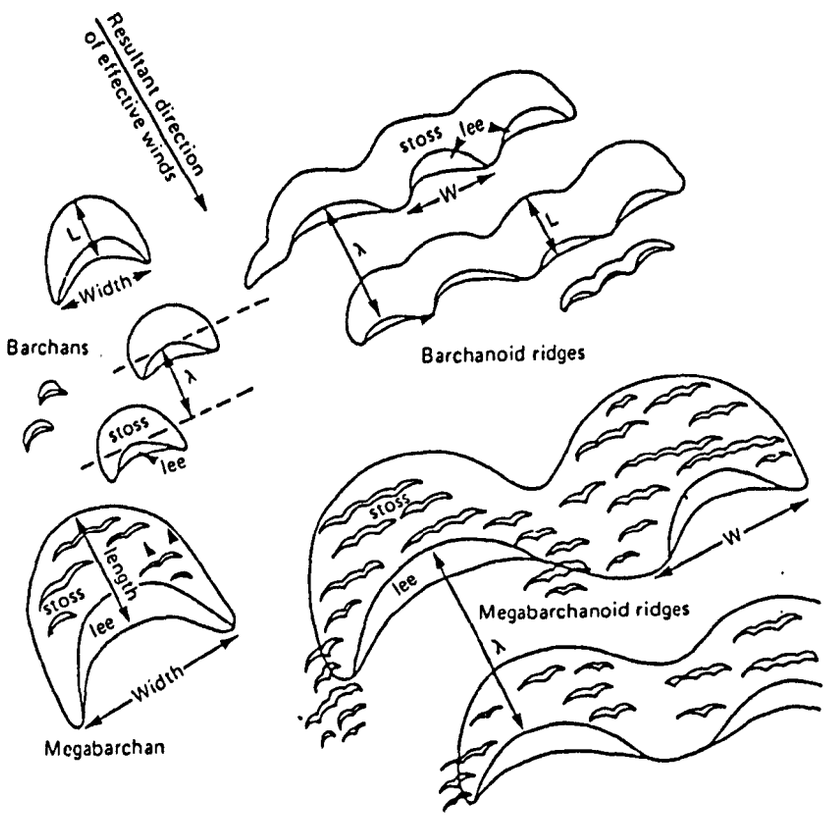


Figure 5.4 A sketch diagram illustrating the method of measuring on Landsat imagery, space and aerial photographs, the length (L), width (W), or (D) diameter, and dune spacing (λ) of the different dune types. From Breed, (1979).

(Nafud thuwayrat, Nafud as Sirr, Nafud Shugayyigah), and in southwestern Rub'al Khali. Compound linear dunes are found in'Uruq al-Qaamiyat' in southeastern Rub'al Khali. Complex linear dunes can be narrow or broad linear ridges superimposed upon other dune types, such as star, dome and barchan dunes. They occur along the west and in the center of An Nafud as closely spaced ridges which obscure interdune areas. Linear dunes with star dunes superimposed upon them are found in Ad Dahna (Remah area) and in southeastern Rub'al Khali.

MORPHOMETRY: Dune width, length, and spacing (wavelength) were measured by Breed (1979) for linear dunes in different parts of the world including parts of the Arabian sand seas. For this investigation, sample areas were selected in the Rub'al Khali sand sea for dune width, length, and dune spacing measurement. These measurements were based on Landsat MSS scenes 176/48, acquired on 10.10.1972 (used for measurement of compound linear dunes); 178/47 acquired on 18.1.1973 (used for measurement of complex linear dunes); LFC photographs acquired on October 1984 (used for measurement of simple linear dunes). Table (5.3) summarizes the results of the measurements.

Dune spacing mean values range from 1400 metres in simple linear forms to 3200 metres for complex forms. Widths vary from 400, 1000, and 1470 metres for simple, compound, and complex forms respectively.

Latitude, longitude	Area Sampled km^2	$\bar{W}$	$\bar{L}$	$\bar{\lambda}$	Fig. No.
Simple Linear Dunes (200 dunes were measured)					
20^{o} 30' - 21^{o} 30'N 52 - 52^{o} 36 E	2400	0.40	15.24	1.42	6.14
Compound Linear Dunes (150 dunes were measured)					
17^{o} - 17^{o} 30' N 45^{o} 30' - 46^{o} E	641	1.0	>31	1.7	5.8b
Complex Linear Dunes (200 dunes were measured)					
18^{o} 45' - 19^{o} 30'N 45^{o} 15' - 46^{o} 00E	2500	1.47	>80	3.2	-

Table 5.3: Morphometry of linear dunes in the Rub al Khali $\bar{W}$, means width; $\bar{L}$, means length (some or all dunes extend beyond edge of image), $\bar{\lambda}$ means dune spacing. All measurements are in km.

Measured values of dune spacing in the sampled area of western Rub'al Khali show approximately unimodal distribution for complex linear dunes (Fig. 5.5). Measured values for widths, lengths and wavelength (dune spacing) also show approximately unimodal distribution for simple linear dunes (Fig. 5.6).

Regression analysis show that wavelengths tend to be about twice the mean widths of linear dunes regardless of their size. This was also confirmed by Breed's measurements (Breed, 1979). Moreover, there seens to be a tendency of a progression of dune form, from simple to compound or complex with increasing size.

TOPOGRAPHIC EFFECT:

The effect of topography and wind regime on dune morphology was investigated by many authors (El-Baz, et al., 1979; Breed and Grow, 1979; Lancaster, 1983; Wasson and Hyde, 1983). Despite the effort, little progress has been made on the effect of topography on dune sizes and spacing. This investigation presents the effect of topography on linear dunes in western Rub'al Khali as seen on Landsat MSS imagery.

The topographic effect was investigated in a group of linear dunes in the Qa'amiyat region of the western Rub'al Khali. These linear dunes are aligned parallel to the resultant direction of effective winds (south western) and extend hundreds of kilometers to the foothills in Yemen.

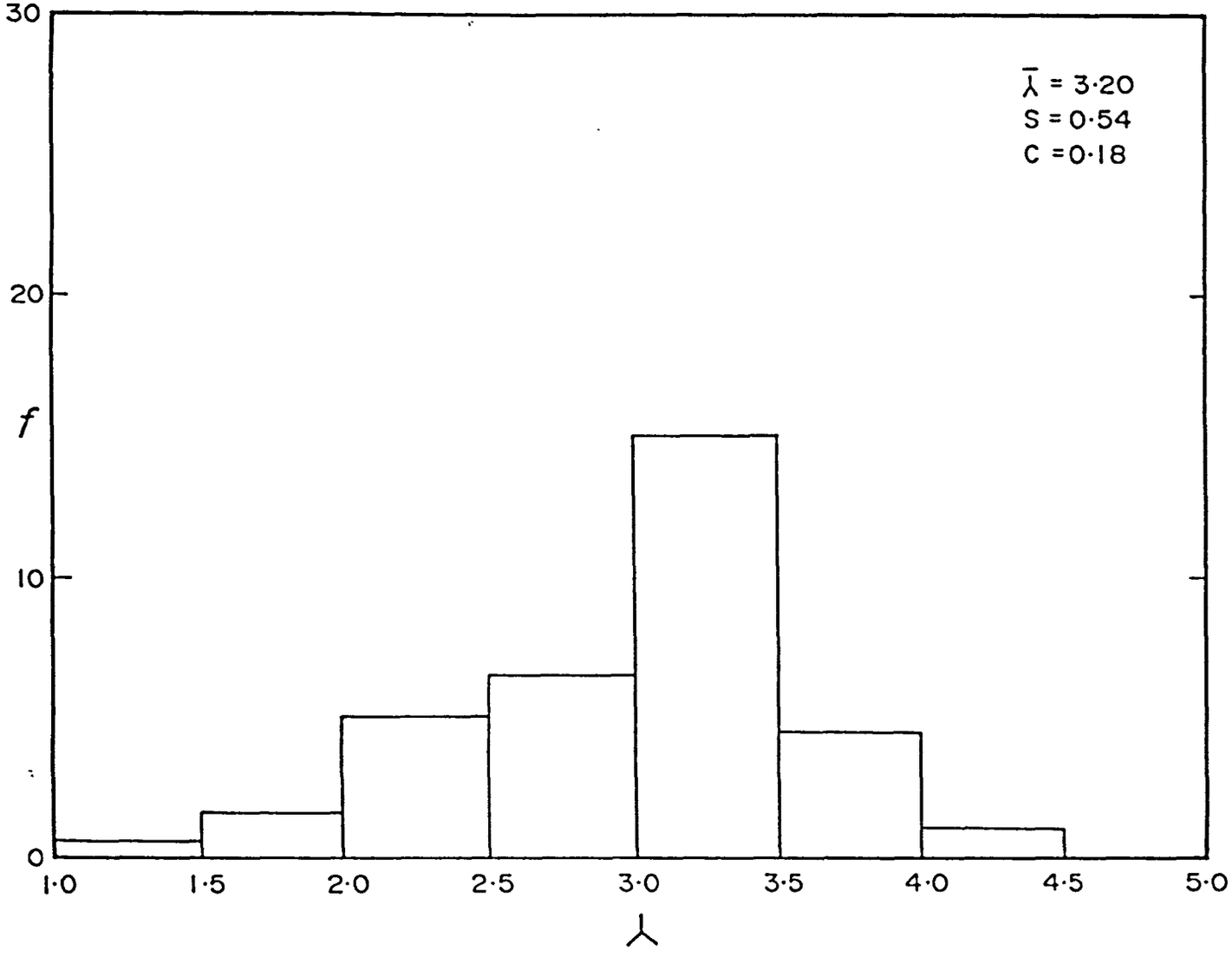


Figure 5.5: Histogram showing frequency distribution (f) of complex linear dune spacing (λ) in km, measured on Landsat MSS imagery (178/47; 18 January 1973); ($\bar{\lambda}$)-mean dune spacing; S, standard deviation; C, coefficient of variation.

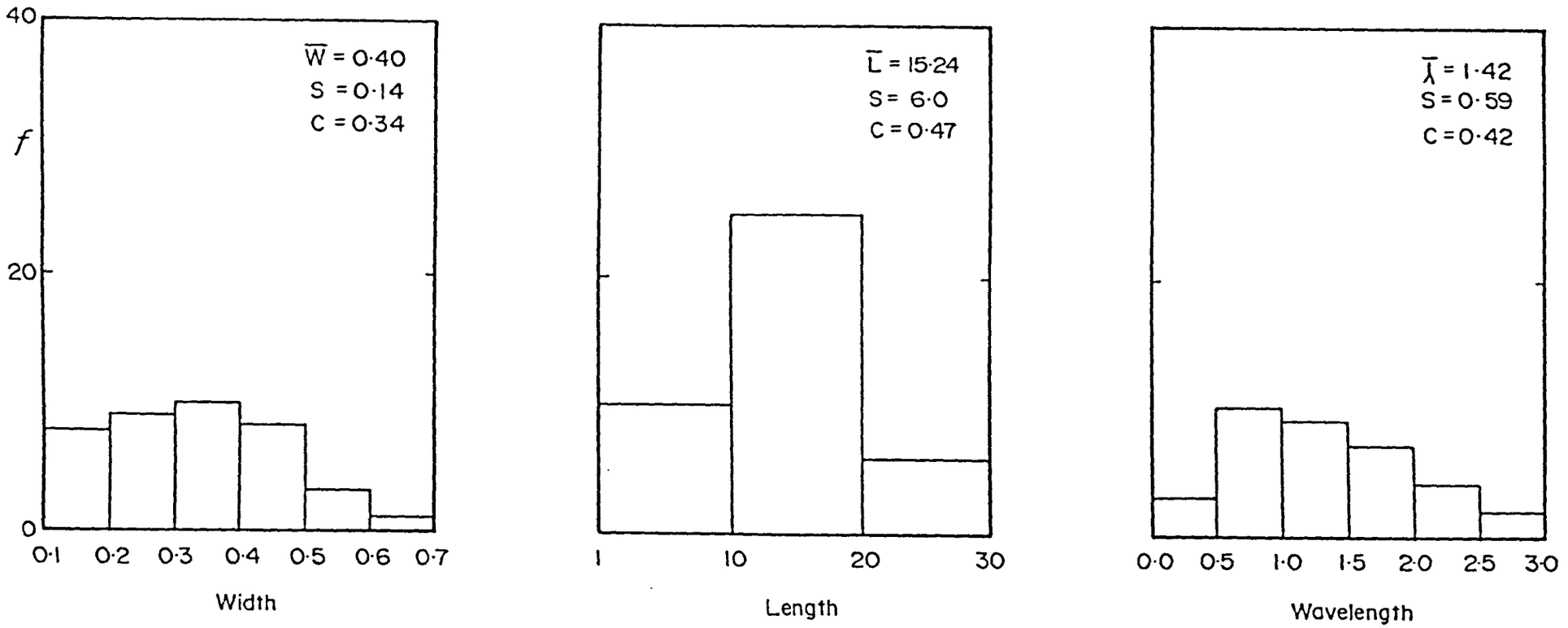


Figure 5.6 Histogram showing frequency distribution (f) of simple linear dune width (W), length (L), and dune spacing (λ) in km. ($\overline{W}$) means average dune width; ($\overline{L}$) means average dune length; ($\overline{\lambda}$) means average dune spacing; S standard deviation; C, coeficient of variation.

Measurements of dune width, and dune spacing were taken in the region between Qa'amiyat and the foothils in Yemen (Table 5.4). Mean wavelength and width of dunes in samples measured in wide open areas were compared with mean wavelengths and width of dunes near topographic barriers (hills). Results show that the spacing of the dunes in these sampled areas increase near the topographic barrier. Dune widths do not vary significantly. It was also observed that as linear dunes approach the topographic barrier, they tend to loose their shape and change to sand sheets. Moreover, on the leeward side of the barrier and at some distance, linear dunes start to form again. Figure 5.7 a & b are Landsat MSS images representing the two sampled areas.

CRESCENTIC DUNES: Four forms of crescentic dunes can be identified in the sand seas of Arabia using remote sensing imagery. This identification is based on the slipface development of these dunes. Three basic forms are discussed in the literature and include; simple crescentic dunes (barchan), crescentic ridges or transverse ridges, and compound crescentic dunes (the "MEGA-BARCHANS" of Norris, 1966). The fourth form called in this study (CHAIN BARCHANS) is a form unique to this area. It comprises a chain of small barchans and barchanoid ridges linked together to form a barchanoid shaped dune (see Chapter 6 for more details).

In the sand seas of Arabia, crescentic ridges or transverse ridges are more common than simple barchans especially in

	Latitude Longitude	Sampled Area km^2	$\overline{W}$	$\overline{\lambda}$	Fig. No.	Comments
A)	16^{o}-$18^{o}30'$N 47^{o}-$50^{o}00$E	5000+	1.3	0.75	5.8a	Dunes located in an open area.
B)	15^{o}-17^{o}N 46^{o}-$48^{o}00$E	5000o	1.2	1.7	5.8b	Dunes located near a topographic hill.

Table 5.4: Measurement of linear dune widths and dune spacings located in an open area and near a topographic hill. The sampled area is between Qa'amiyat and the foothills of Yemen. $\overline{W}$, means dune width, $\overline{\lambda}$, means dune spacing. All measurements are in km.

\+ 250 dunes were measured.
o 250 dunes were measured.



a



b

Figure 5.7 (a): Landsat MSS imagery (177/48) over the Qa'amiyat area showing the measured linear dunes (open area). (b): Landsat MSS imagery (176/48) near the foothills of Yemen showing the measured linear dunes (near a hill).

the Jafurah Sand Sea. Compound crescentic dunes are found on the eastern part of the Rub'al Khali. Groups of isolated relatively small crescentic dunes occur in southeastern Rub'al Khali (Lat. 20 N, Long. 55 E). These dunes have slipfaces facing north opposite to those of the southward-facing slipface of the barchanoid ridges found in the north.

In Arabia barchans and barchanoid ridges are more common in areas bordering the sea, such as in the Jafurah Sand Sea. (eastern coast of Saudi Arabia). In the Jafurah, the majority of the dunes are found either as small crescentic mounds (barchans) or small transverse ridges. Because of their small sizes and their narrow spacing these dunes can not be measured on Landsat MSS imagery except in areas of high contrast (dunes found in sabkhas; see Chapter 6 for more details).

MORPHOMETRY:

Dune width, length, and wavelength were measured on five sample areas representing three sand seas (Rub'al Khali, An Nafud, and Jafurah). Simple and compound crescentic dunes were measured on Landsat MSS imagery, LFC and aerial photographs. Some of the sampled areas were previously measured by Breed (1979) but upon Breed's advice these measurements were repeated (personal communication, 1985).

Measurements in each sampled sand sea are summarized in Table 5.5. The frequency distributions of measured values

Latitude, Longitude	Sand Sea	Area Sampled km^2	Range of Dune Length	$\bar{L}$	Range of Dune Width	$\bar{W}$	Range of Dune Spacing	$\bar{\lambda}$	Fig. No.
Simple crescentic dune ridges (barchans and barchanoid ridges). 150 dunes were measured in Jafurah (N) and Rub'al Khali.									
A) $26^{o}30'-26^{o}20'N$, $49^{o}30'-50^{o}E$	Jafurah (N)	200	0.36-0.84	.50	0.1-0.4	0.3	0.4-0.90	0.70	5.21
B) $22^{o}15'-23^{o}30'N$ $58^{o}-54^{o}30'E$	Rub'al Khali (Al Jiwa area)	5000	0.1 - 0.9	.60	0.3-1.4	.85	0.3-1.3	.67	-
Compound crescentic ridges. (150 dunes were measured for Rub'al Khali and An Nafud)									
A) $21^{o}N$, $56^{o}-57^{o}E$	Rub al Khali (SE)	2500	1.4 - 3.4	2.1	1.7-4.1	2.80	1.4-4.0	2.60	6.14
B) $27^{o}-29^{o}N$, $37^{o}-38^{o}E$	An Nafud	900	0.6 - 2.2	1.2	0.7-2.6	1.47	0.9-3.4	1.87	6.13

Table 5.5: Morphometry of crescentic dunes in sand seas of Saudi Arabia. $\bar{L}$, means length; $\bar{W}$, means width; $\bar{\lambda}$, means dune spacing. All measurements in km.

are shown in Figures 5.8 a & b, for simple crescentic dunes and in Figure 5.9 a & b for compound crescentic dunes. Measurements in each sampled area are fairly uniform. However, each sand sea shows different values.

STAR DUNES: Star dunes occupy far smaller areas within the sand seas of the world than do either linear or crescentic dunes. In Saudi Arabia, they occupy part of the southeastern and the southern end of the Rub'al Khali and central Ad Dahna. They are found near the mouths of dry washes along the southeastern edge of the Rub'al Khali as simple star dunes, then they grade northward and westward into complex star dunes (Breed, 1979).

MORPHOMETRY:

Star dune diameters and wavelengths were measured in two sampled areas representing Ad Dahna and Rub'al Khali sand seas. Measurements were based on Landsat MSS imagery for Ad Dahna (Fig. 5.10) and LFC photographs for the Rub' al Khali (Fig. 6.14). Table 5.6 summerizes the results of the measurements. Figure 5.11 is a histogram showing frequency distributions of dune diameters and wavelengths.

Among sampled areas star dunes tend to be uniformally distributed, indicating the regular pattern for each sand sea. Breed (1979) investigated star dunes of different sand seas of the world and found that the spacing of star dunes, unlike that of linear and crescentic dunes does not vary

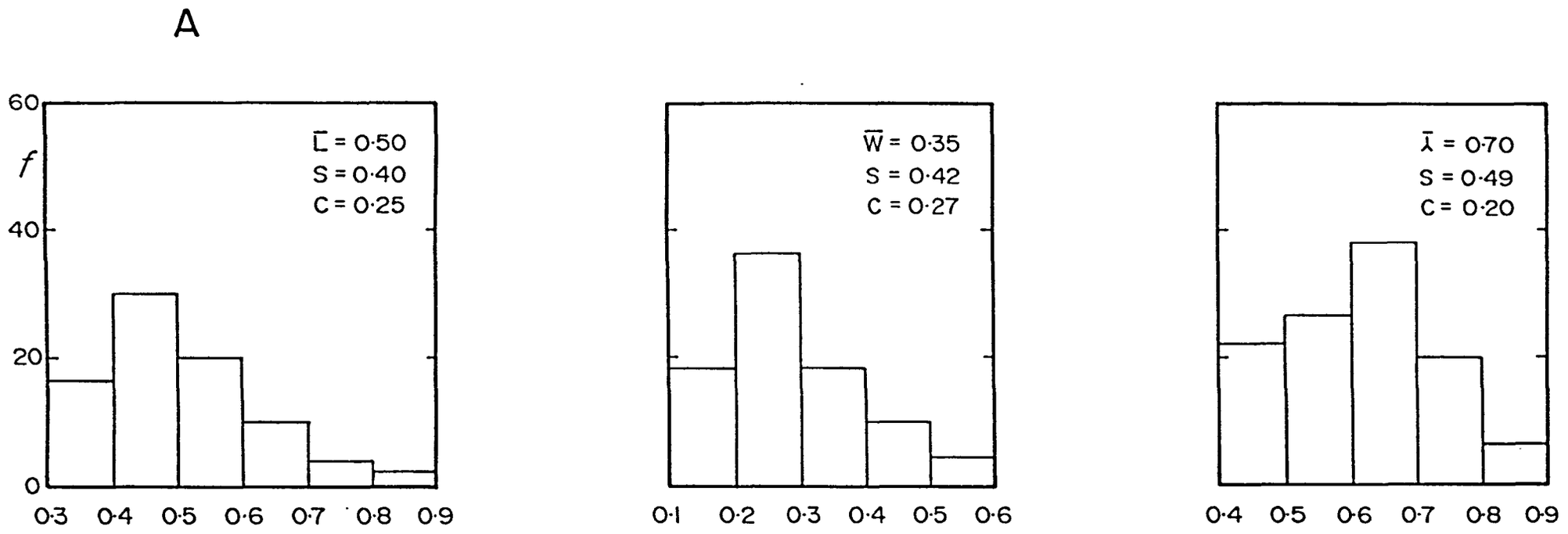
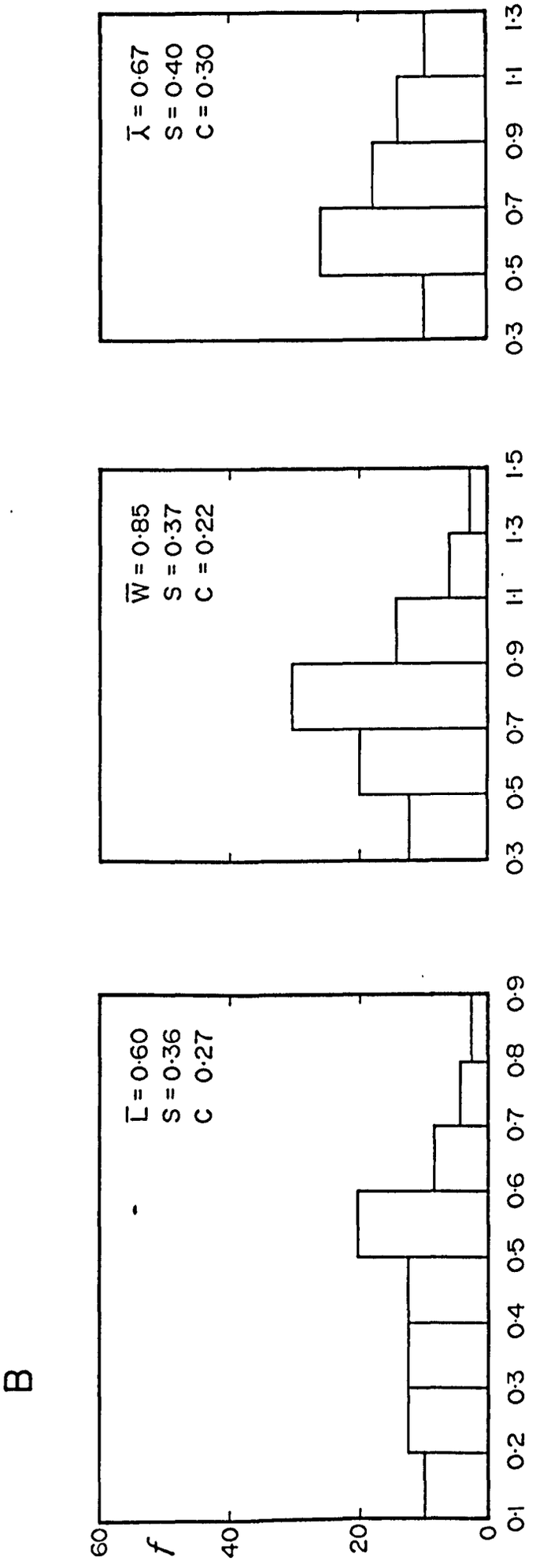


Figure 5.8 Histogram showing frequency distribution (f) of simple crescentic dune width (W), length (L), and dune spacing (λ) in: (A) Jafurah North; (B) Al-Jiwa (Rub'al Khali). All measurements are in km.


B
f
60
40
20
0
$\bar{L}$ = 0·60
S = 0·36
C 0·27
0·1 0·2 0·3 0·4 0·5 0·6 0·7 0·8 0·9
$\bar{W}$ = 0·85
S = 0·37
C = 0·22
0·3 0·5 0·7 0·9 1·1 1·3 1·5
$\bar{\lambda}$ = 0·67
S = 0·40
C = 0·30
0·3 0·5 0·7 0·9 1·1 1·3

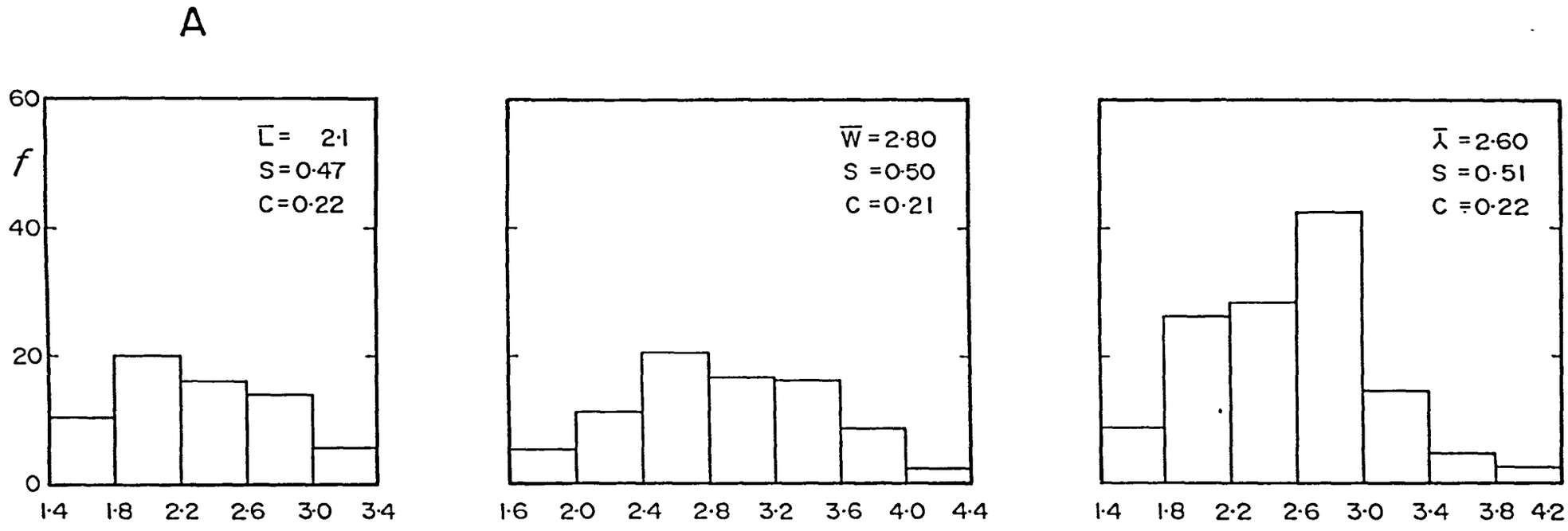


Figure 5.9 Histogram showing frequency distribution (f) of compound crescentic dune width (W), length (L), and dune spacing (ƛ) in: (A) Rub'al Khali; (B) An Nafud.

B

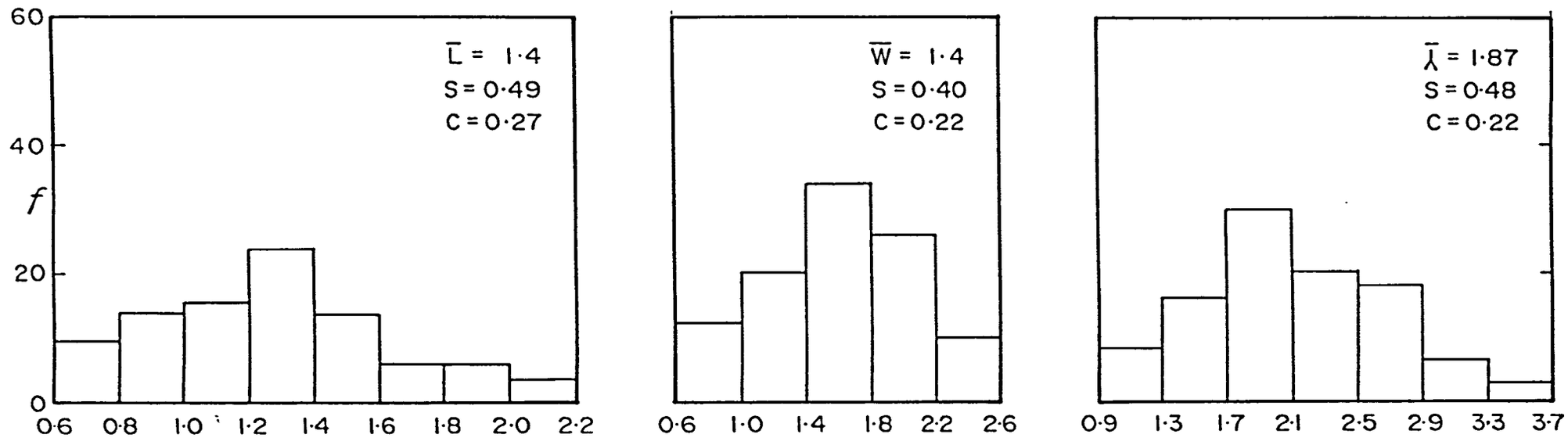

60
40
f
20
0
L̄ = 1·4
S = 0·49
C = 0·27
0·6 0·8 1·0 1·2 1·4 1·6 1·8 2·0 2·2
W̄ = 1·4
S = 0·40
C = 0·22
0·6 1·0 1·4 1·8 2·2 2·6
λ̄ = 1·87
S = 0·48
C = 0·22
0·9 1·3 1·7 2·1 2·5 2·9 3·3 3·7



Figure 5.10 Landsat MSS imagery (181 / 40) over part of Ad Dahna Sand Sea showing the measured star dunes.

Latitude, Longitude	Sand Sea Area	Area Sampled km^2	Range of Dune Diameter	$\bar{D}$	Range of Dune Spacing	$\bar{\lambda}$	Fig. No.	Comments
A) 19^{o}-$20^{o}30'$N $53^{o}30'$-$54^{o}30'$E	SE Rub'al Khali	3,500*	0.5 - 1.4	.87	0.97 - 2.86	2.10	6.14	Measurement from LFC photographs
B) $25^{o}30'$-$26^{o}00$N	Ad Dahna	3,000*	0.8 - 1.8	1.2	1.3 - 3.3	2.7	5.11	Measurement from Landsat MSS imagery

Table 5.6: Morphometry of star dunes.
$\bar{D}$, means dune diameter; $\bar{\lambda}$, means dune spacing.
All measurements in km.
* 200 dunes were measured.

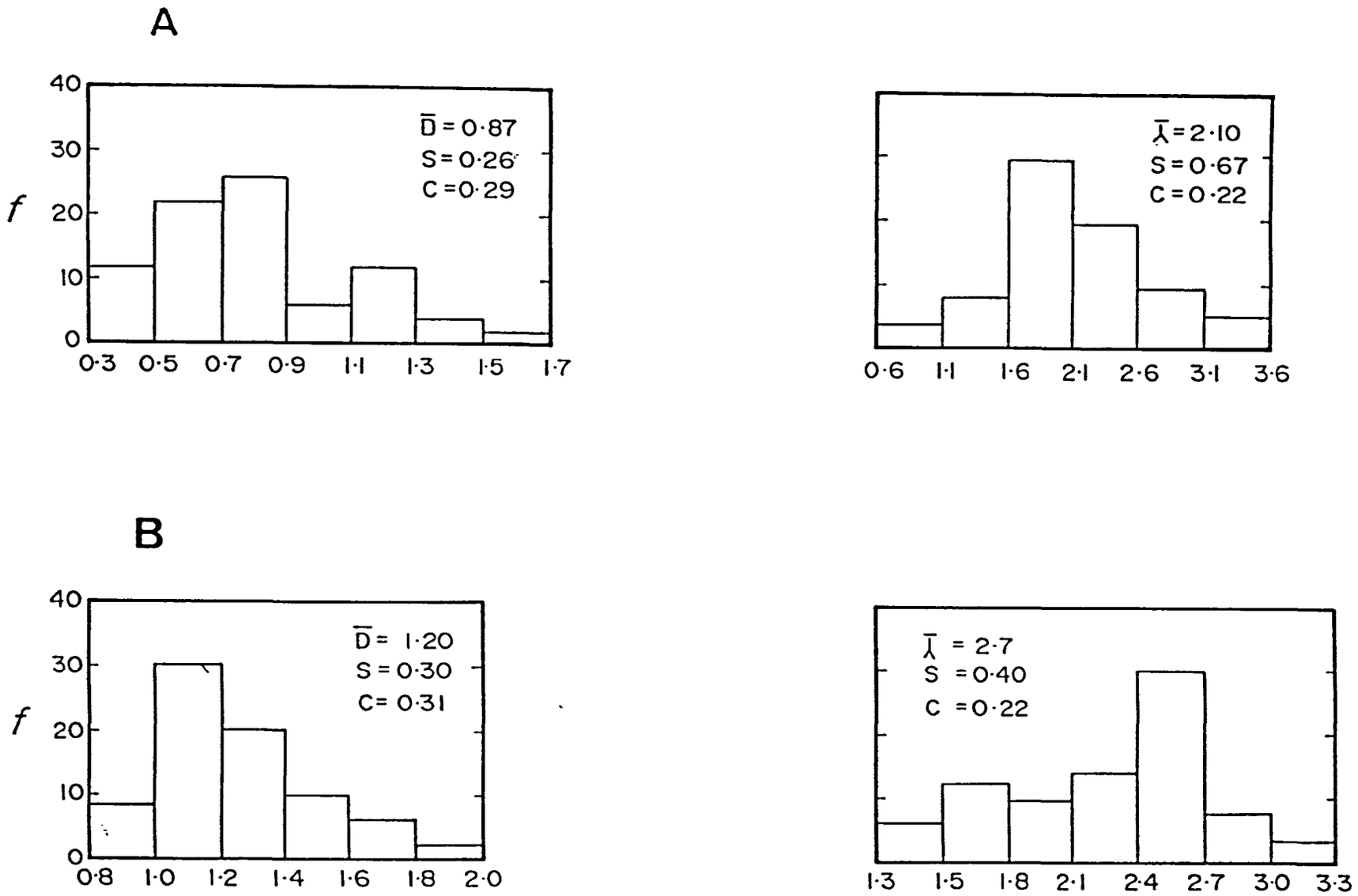


Figure 5.1 Histogram showing frequency distribution (f) of star dune diameter (D) and spacing (λ) in: (A) Rub'al Khali; (B) AD Dahna.

directly with their size. Samples are too few, however, to test any relationship.

PARABOLIC DUNES: Parabolic dunes of a size visible on Landsat imagery (Spatial resolution = 79 m) are not recognized in Saudi Arabia. However, aerial photographs reveal the existence of simple small-size (average width 70 metres) parabolic dunes in the Jafurah Sand Sea. These dunes are V-shaped and consist of a convex mound with two long trailing arms. In Jafurah they are found associated with sand sheets (Dikakhs). Section 5.8 of this chapter gives a detailed account of the origin and the morphometry of parabolic dunes found in the Jafurah Sand Sea.

DOME DUNES: Dome dunes in Arabia show a variety of sizes. Large size domes are observed in Nafud Ath Thuwayrat in northern Arabia. According to Breed (1979) these dunes , based on aerial photographic investigation, are interpreted as complex because their rounded crests are covered by rows of crescentic dune ridges. Simple small-size domes are found mostly in the coastal areas of the Jafurah.

MORPHOMETRY:

Measurements of dome dunes were made for two sample areas in Nafud Ath Thuwayrat and the Jafurah Sand Sea. These measurements were based on Landsat MSS imagery and aerial photographs (Figure 5.12). Table 5.7 summarizes the diameters and wavelengths of dome dunes. Histogram (Fig.

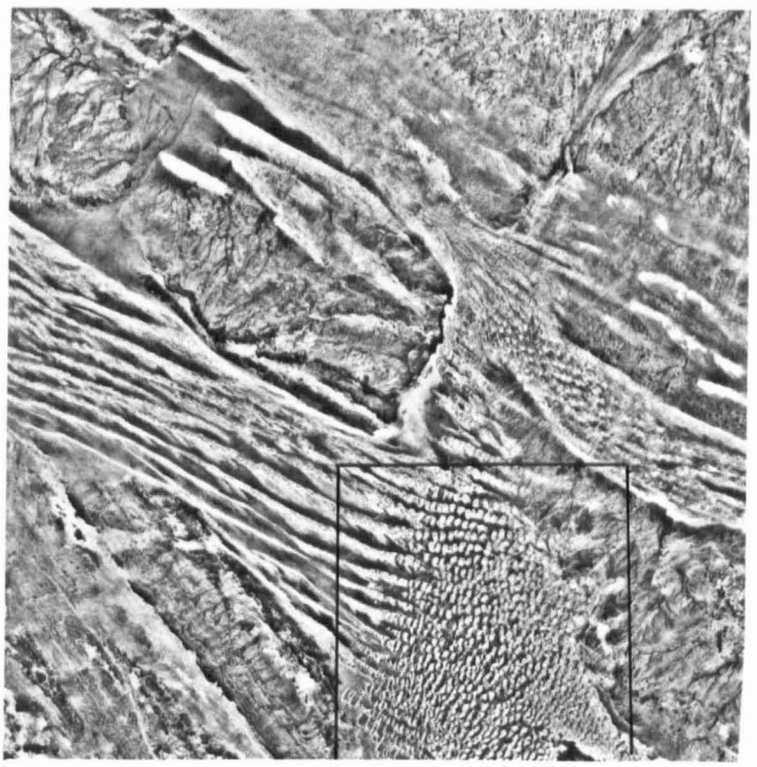


Figure 5.12 Landsat MSS imagery (180 / 40) of sampled area in AN Nafud Ath Thuwayrat used for measurement of dome dunes.

	Latitude, Longitude	Sand Sea Area	Area Sampled km^2	Range of Dune Diameter	$\bar{D}$	Range of Dune Spacing	$\bar{\lambda}$	Fig. No.	Comments
A)	$25^{o}20'-27^{o}00'N$, $44^{o}-45^{o}E$	An Nafud	3000*	1.0 - 2.1	1.61	1.4 - 4.4	2.4	5.13	Measurement from Landsat MSS imagery.
B)	$26^{o}30'-26^{o}90'N$, $49^{o}50'-49^{o}55'E$	Jafurah	207*	0.18-0.42	.300	.300 -.900	0.6	-	Aerial photographic measurement.

Table 5.7: Morphometry of dome dunes. $\bar{D}$, means diameter, $\bar{\lambda}$, means dune spacing. All measurements in km.
* 150 dunes were measured.

5.13) indicates that the dune diameters and wavelengths are relatively constant throughout the sampled area.

SAND SHEETS AND STREAKS: Sand sheets are found nearly in all sand seas of Arabia. In the Jafurah, sand sheets are flat, or gently rolling tabular bodies of sand up to several metres thick which may extend many meters or even kilometres horizontally (Fryberger et al, 1984; Appendix 2). The direction of the elongation of sand sheets is usually parallel to the long-term effective wind direction.

Streaks (termed stringers by many authors) are defined by Breed (1979) as " elongate patches of sand with sharply defined edges". Sand streaks are uncommon in Arabia. They are found mostly in the northern sand seas and are usually associated with linear dunes.

5.7 JAFURAH SAND SEA (CASE STUDY)

The Jafurah Sand Sea is located between 27 and 24 Latitude South, East of the Meridian 49 30. It is a narrow strip in the north which widens southwards merging in with the Rub'al Khali.

The purpose of this investigation is to:

(i) Map the general distribution of the dune types in the Jafurah Sand Sea.

(ii) Measure dune parameters (width, length, diameter, and

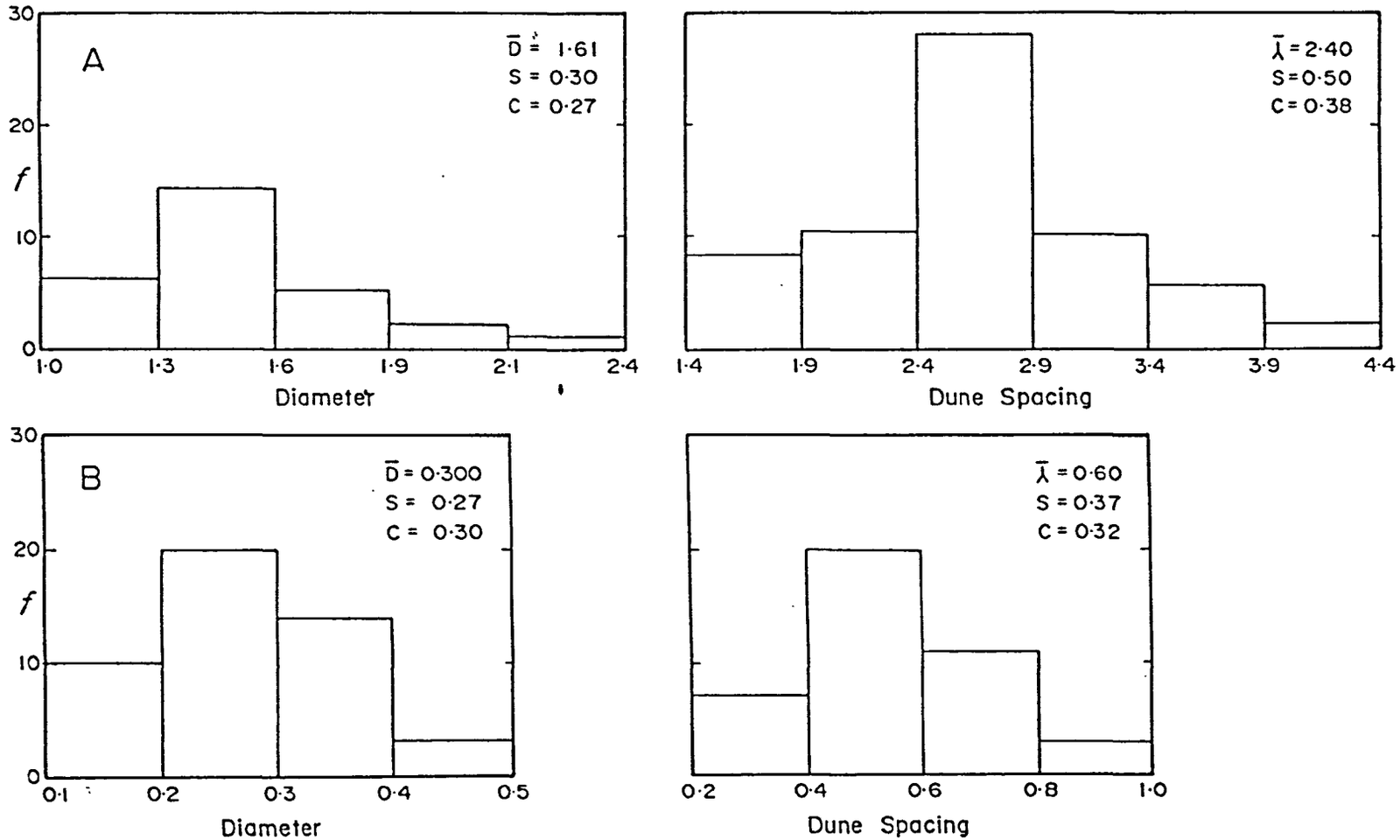


Figure 5.13 Histogram showing frequency distribution (f) of dome dune diameter (D) and spacing ( ) in Nafud Ath Thuwayrat. All measurements are in KM.

dune spacings).

(iii) Investigate the evolution of dune types in the Jafurah.

METHODOLOGY: Landsat MSS false colour composite prints (six scenes) at scales 1:250,000 covering the entire Jafurah were used to map the distribution of dunes (Fig. 5.14). The Landsat MSS scenes used in this investigation are given in Table 5.8.

Dune types that were clearly detected on the false colour composites were mapped on a 1:250,000 scale map. For mapping small size dunes (less than the MSS spatial resolution i.e <80 m), aerial photographs, Large Format Camera photographs, and minimum ground checking were utilized. Six maps were produced at a scale of 1:250,000 covering the entire Jafurah. These maps were then reduced to a scale of 1: 750,000 and presented as Plates 1-6 at the end of the thesis. The legend used for mapping dune morphology is given in Figure 5.15 (also given with the Plates at the end of the thesis).

GENERAL DISTRIBUTION OF DUNES: Plates 1 ,2 ,3 ,4 ,5 , and 6 show the distribution of the dunes in the entire Jafurah. Table 5.9 summerizes the percentage of each dune type in the Jafurah.

The dominant aeolian features is the sand sheets which are

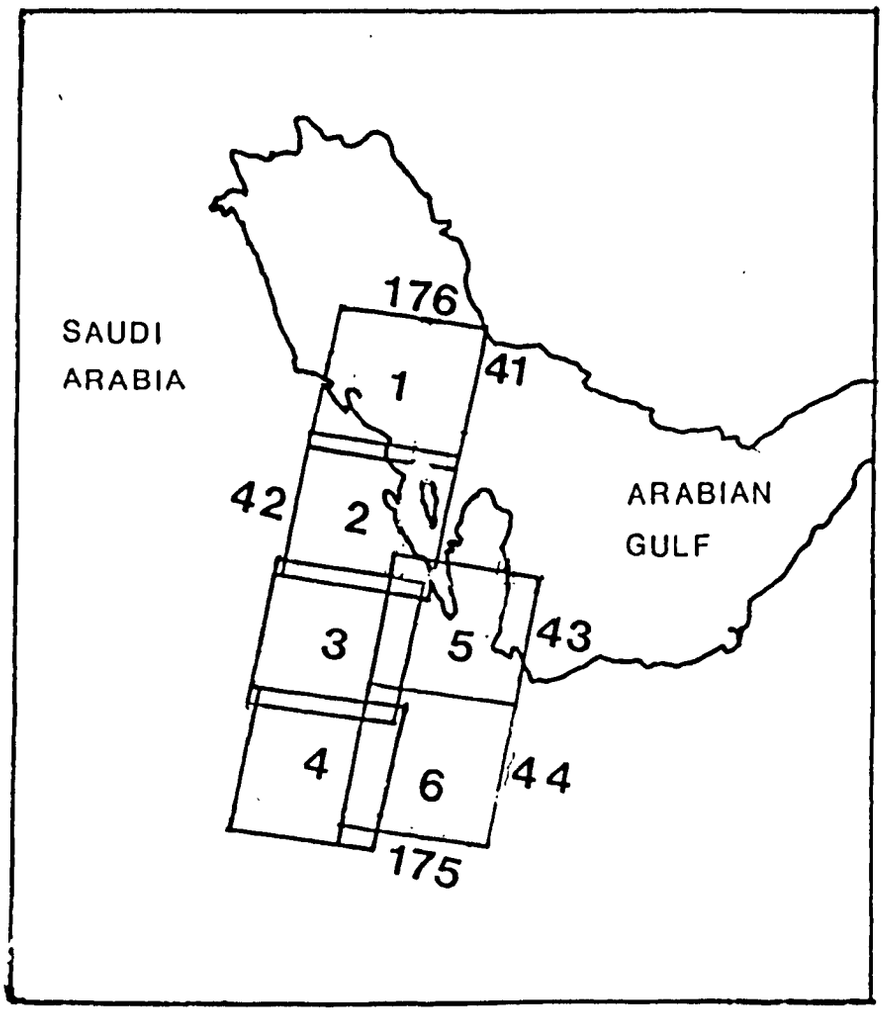


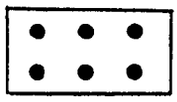
Figure 5.14 Index map showing the location of Landsat MSS images used for producing plates 1-6.

Plate No.	MSS Scene Path/Row	Acquired Date	Scene ID No.
1	176/41	8 Jan 1973	1169-06405
2	176/42	8 Jan 1973	1169-06411
3	176/43	26 Jan 1973	10187-06415
4	176/44	8 Jan 1973	1169-06420
5	175/44	4 Oct 1973	1438-06344
6	175/43	25 Jan 1973	1186-06360

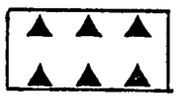
Table 5.8: List of Landsat MSS scenes used for producing Plate 1 - 6.

Figure 5.15 MORPHOLOGY AND DISTRIBUTION OF SAND DUNES IN THE JAFURAH SAND SEA.

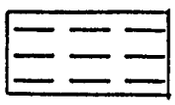
EXPLANATION:



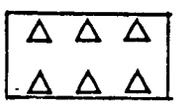
Quaternary Sabkha: with barchans & barchanoid ridges.



Transverse Dunes: Barchans & barchanoid ridges.



Sand Sheets: with parabolic and dome dunes.



Complex dunes: Transverse dunes & sand sheets.



Chain barchans.



Substratum (gravel and/ or bedrock).



Old wadi channels.

Dune Type	Percentage of Aerial Coverage
Transverse ridges	
- Barchans	14
- Barchanoid ridges	28
Sand sheets	46
Parabolic dunes	8
Dome dunes	2
Sabkhas	2

Table 5.9:
Percentage of different aeolian deposits in the Jafurah Sand Sea based upon Landsat MSS investigation.

mostly associated with parabolic and dome dunes (46 %). Transverse dunes (barchans and barchanoid ridges) are the second most abundant dunes (42 %). Sabkhas constitute about 2 % of the area in the Jafurah.

The Jafurah can be divided into two zones:

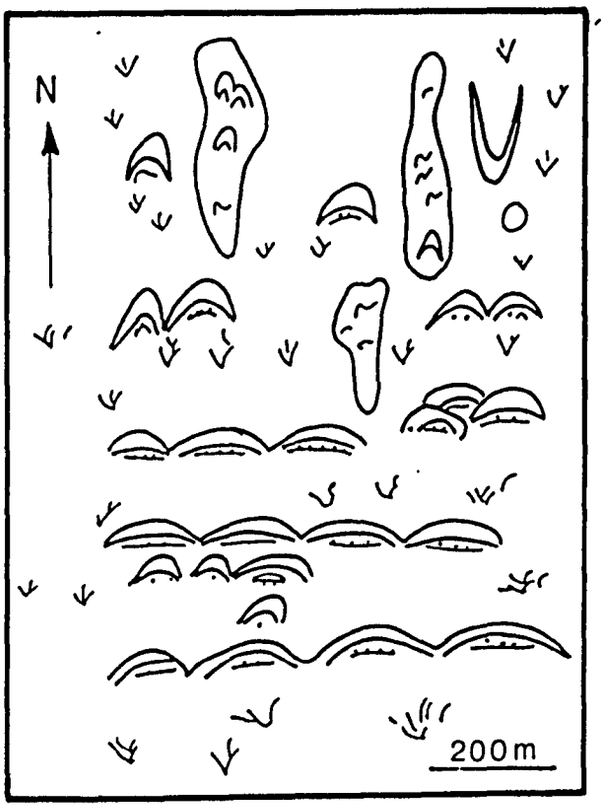
(i) The northern Jafurah which lies between 26-27 degrees N and 49-50 degrees E. The majority of the aeolian features characteristic of this zone are vegetated sand sheets, parabolic dunes, dome dunes, barchans, barchanoid ridges and sabkhas. The typical morphology of the dunes is illustrated in Figure (5.16).

(ii) The southern Jafurah which extends between 25-24 degrees N and 49-50 degrees E. Figure 5.17 is a schematic diagram showing aeolian landscape associations typical of this zone. The dunes are mostly barhans, barchaoid ridges, and dune complexes. The "Chain barchans" defined in Section 5.7 are found at the dune field edges (Plates 3, 4, 5 and 6).

DUNE TYPES:

SAND SHEETS: In the Jafurah, sand sheets are flat bodies of sand up to several metres thick, which may extend horizontally tens of metres or sometimes kilometers. Sand sheets are commonly vegetated and consist of sand more poorly sorted than in the surrounding dunes (Fig. 5.18a).

Figure 5.16 Typical dune morphology in the Northern Jafuarh Sand Sea.



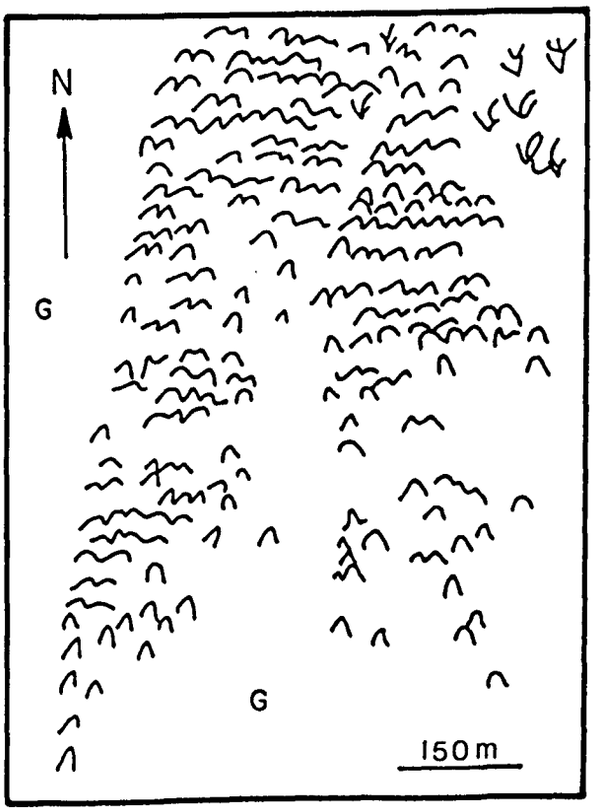


Figure 5.17 Aeloian landscape associations typical of Southern Jafurah.

Figure 5.18 Illustration of some dune types as seen in the field. (a) sand sheet; (b) parabolic dune; (c) barchan dune.

a



b



c



The amount and kind of vegetation differs from one place to another.

PARABOLIC DUNES: Parabolic dunes are found associated with vegetated sand sheets (Plates 1, 2 and 5). They are found mostly in the northern Jafurah especially near Dammam and Al Qatif areas. In the central Jafurah extensive parabolic dune fields are found along the Al Hofuf-Salwa highway. In the southern Jafurah, parabolic dunes are less common especially towards the southern margin with the Rub'al Khali. Anton and Vincent (1986) gave a good account of the morphology and distribution of parabolic dunes in the Jafurah.

Parabolic dunes in the Jafurah are too small to be resolved by the Landsat MSS imagery. Hence the morphometry of the dunes was measured using aerial photographs.

Parabolic dune widths and lengths were measured using infrared aerial photographs at a scale of 1:10,000. Infrared aerial photographs were used because of their ability to show the definition of the parabolic dunes. Field measurements are not easy as parabolic dunes are only 1 to 3 m above the surface and hence can be overlooked in the field (Fig. 5.18b).

On aerial photographs, parabolic dunes can look very similar in plan view to barchans; but can be differentiated from them by the long, vegetated trailing arms which extend upwind, and by the absence of a slip-face. In plan,

parabolic dunes have a v-shape pointing windward (Fig. 5.19).

Table (5.10) gives the morphometry of the parabolic dunes (width, length, and dune spacings). Measured dunes are shown partly in Figure 5.19. The area sampled is 100 square km, and 200 dunes were measured. Dune width ranged between 40 to 200 m with an average of about 70 m. Arm length of the dunes ranged between 100 and 400 m with an average of 250 m. The eastern arms are longer than western arms. The spacings between dunes ranged between 200 to 300 m with an average of 150 m.

DOME DUNES: Like parabolic dunes, dome dunes are associated with vegetated sand sheets. They are also found along the coastal areas especially near Ras al Qurayah. However, their abundance is too small to make any usefull measurements.

TRANSVERSE DUNES: The term 'transverse dunes' is used here to include barchan and barchanoid ridges. In the Jafurah, transverse dunes exist in isolation or in dune complexes. Barchan dunes found on sabkhas are usually found in isolation. Barchanoid ridges, on the other hand are found in complexes. A typical Jafurah barchan dune is shown in Figure 5.18c.

Barchanoid ridge widths, lengths and spacing between dunes were measured using aerial photographs at 1:60,000 scale.

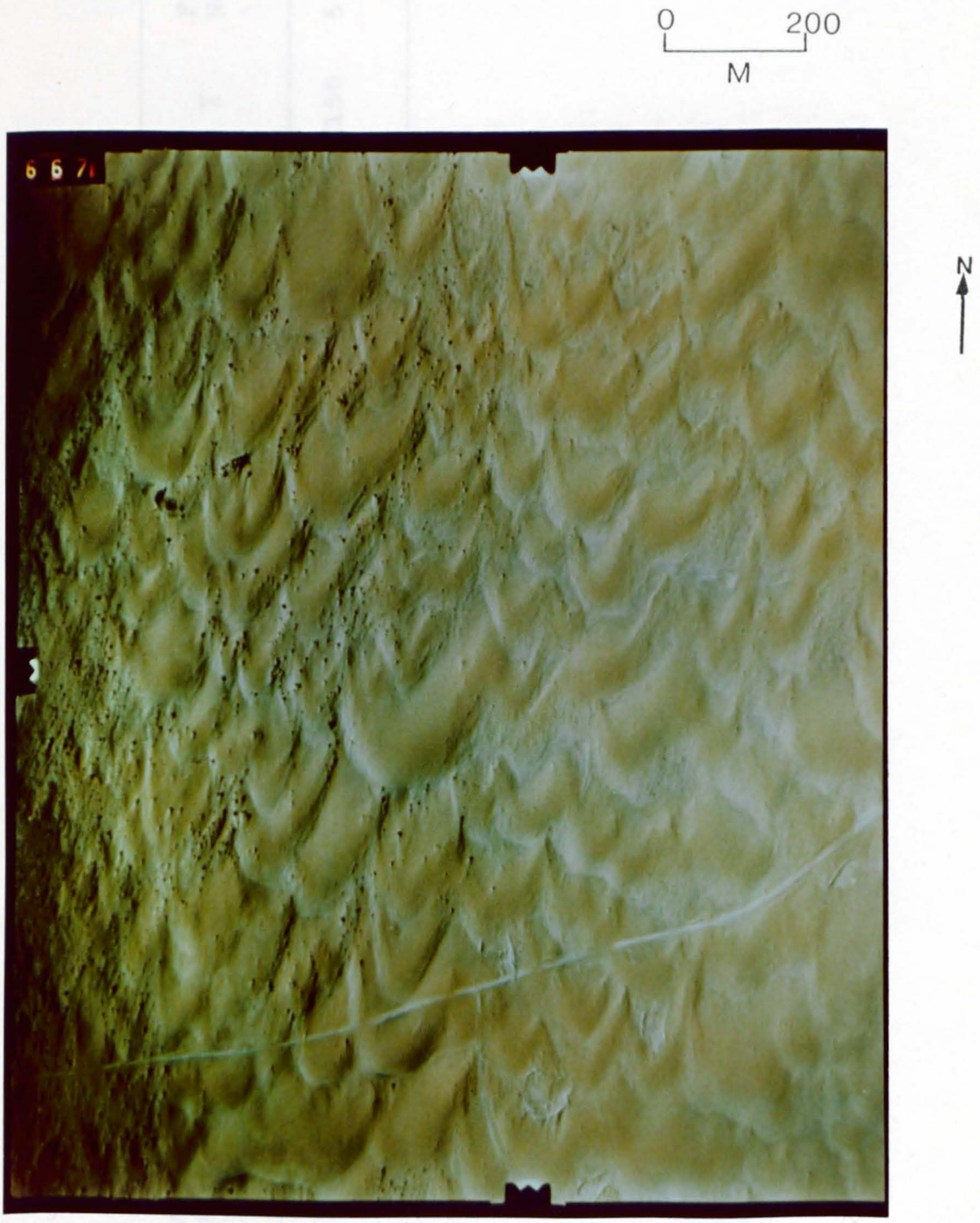


Figure 5.19 Sampled area used for measurement of parabolic dunes in the Northern Jafurah Sand Sea. (Infrared aerial photograph).

Latitude, Longitude	Area Sampled km^2	Range of Dune Width	$\overline{W}$	Range of Dune Arm Length	$\overline{L}$	Range of Dune Spacing	$\overline{\lambda}$	Fig. No.
$26^{o}30'-26^{o}40'N$, $49^{o}45'-49^{o}50'E$	100	.40-.200	.70	.100-.400	.250	.200-.300	.150	5.20

Table 5.10: Morphometry of parabolic dunes in the Jafurah Sand Sea. $\overline{W}$, mean dune width; $\overline{L}$, mean arm length; $\overline{\lambda}$, mean dune spacing. All measurements in km.

Two areas representing Northern (Fig. 5.20) and Southern (Fig. 5.21) Jafurah were selected for comparing dune morphometry. Table 5.11 summarizes the results.

The results of measurements indicate that barchanoid ridges in the north are larger than those on the south. This could be attributed to the following reasons:

(i) The sand supply in northern Jafurah is more abundant than in the south which helps in the vertical growth and the horizontal extension of the dunes.

(ii) Dunes in the south are located in an open gravely area. This allows more mobility for the dunes. Hence, dunes are in the process of transportation rather than accumulation.

SABKHAS: In the Jafurah, sabkhas are broad, flat, salt encrusted sandy plains whose topographic expression is controlled by ground-water table. Sabkhas are very stable terrains, usually experiencing little erosion or deposition during the course of the year (Fryberger, et al., 1984). However, sabkhas are relatively exposed due to their flat topography and lack of vegetation. In such circumstances, high sand drift rates might be expected.

Sabkhas are concentrated mostly in the northern Jafurah, with Sabkhat Ar Riyas and Sabkhat Ad Dabbiyah forming the two largest sabkhas. Other smaller sabkhas are mainly located near the coast (Al Qurayah and Al Urayo areas) and

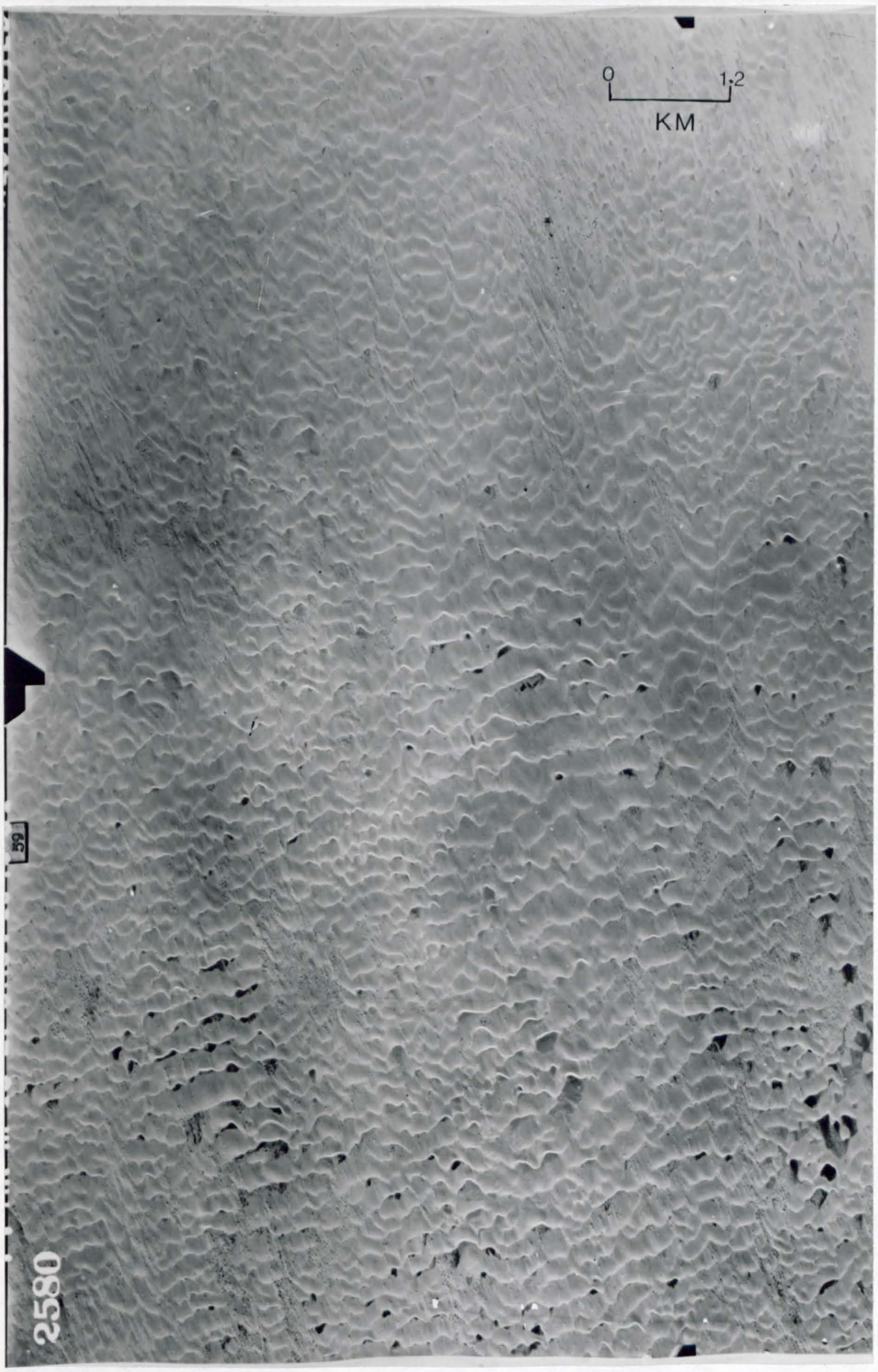


Figure 5.20 Sampled area used for measurement of barchanoid ridges in Northern Jafurah (panchromatic aerial photograph).

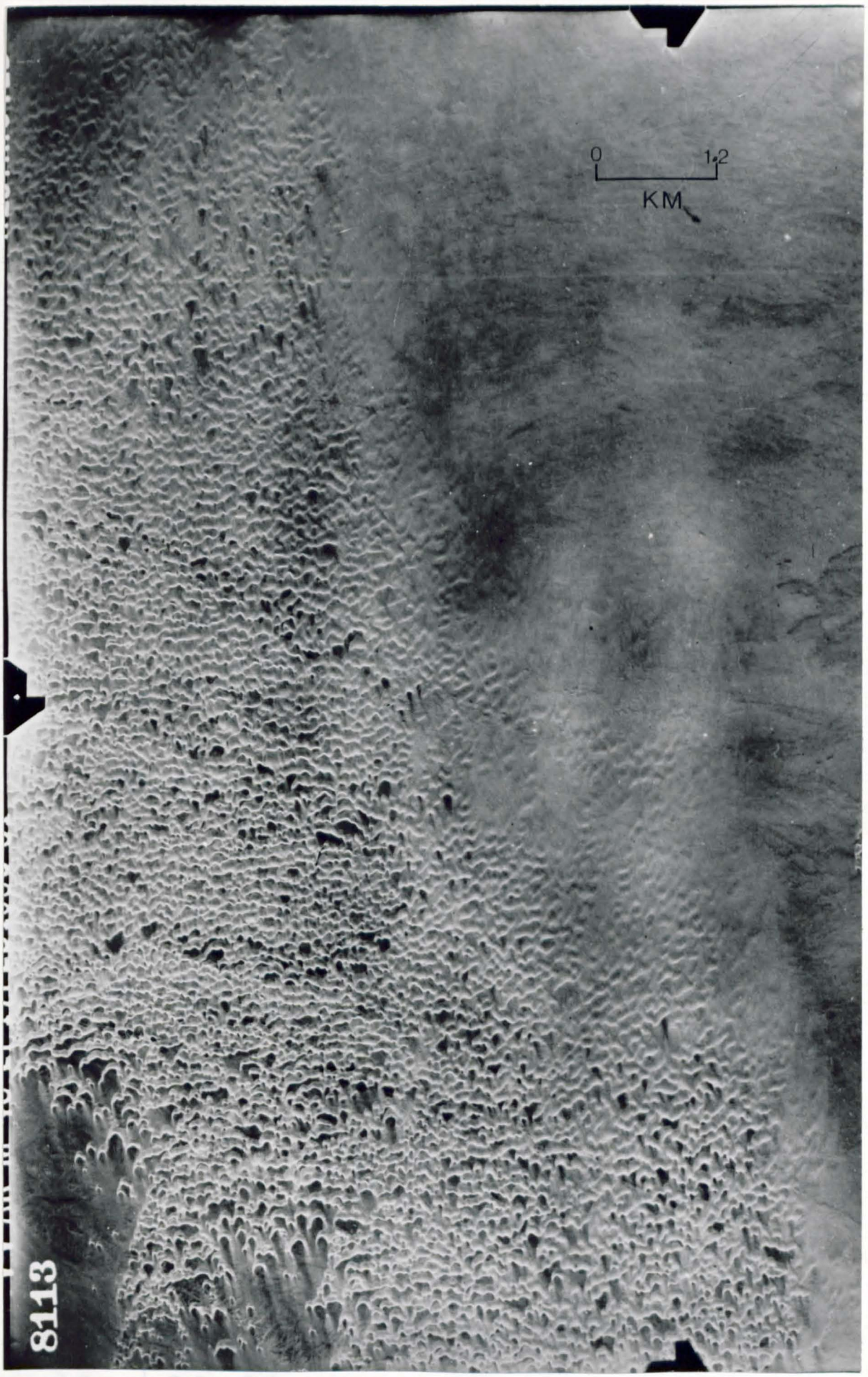


Figure 5.21 Sampled area used for measurement of barchanoid ridges in Southern Jafurah (panchromatic aerial photograph).

Latitude, Longitude	Sand Sea	Area Sampled km^2	Range of Dune Length	$\overline{L}$	Range of Dune Width	$\overline{W}$	Range of Dune Spacing	$\overline{\lambda}$	Fig. No.
$26^{o}30'-26^{o}40'N$, $49^{o}45'-49^{o}50'E$	Jafurah (N)	200*	0.36-0.84	0.50	0.1 - 0.4	0.3	0.4 - 0.90	0.70	5.21
$24^{o}00'-24^{o}10'N$, $49^{o}30'-49^{o}40'E$	Jafurah (S)	200*	0.01-0.35	0.20	0.06-0.24	0.12	0.3 - 0.7	0.50	5.22

Table 5.11: Morphometry of barchanoid ridges in Northern and Southern Jafurah. $\overline{L}$, mean dune length; $\overline{W}$, mean dune width; $\overline{\lambda}$, mean dune spacing. Measurements based on aerial photograph (1:60,000). All measurements are in km. * 100 dunes were measured.

around Al Hofouf area. Barchan and barchanoid ridges are found in all sabkhas observed.

GEOMORPHOLOGICAL BACKGROUND:

The Jafurah sand sea is relatively young compared to its westernly neighbour (Ad Dahna) and the southernly neighbour (Rub'al Khali). This age difference is reflected by the sand colour and the size of the dunes. Jafurah sand is very pale brown (Munsell dry 10 yr 7/3) while Ad Dahna is strongly reddish (Munsell 7.5 yr 6/8) and the Rub'al Khali reddish (Munsell dry 6 yr 6/7). Moreover the size of the dunes in the Rub' al Khali and Ad Dahna are larger than those in the Jafurah reflecting a longer period of deposition. Anton (1983) estimated the age of Jafurah to be around 3000 to 4000 years B.P.

The primary sources of sand feeding the Jafurah can be grouped as follows:

(i) The primary source of sand was the Quaternary gravel fans distributed between the Arabian shield in the east and the Arabian Gulf in the west. Deflation of fans such as the Wadi Al Batin system, north of Jafurah, and Wadi Sahba, in the south, were two important suppliers of sand for the Jafurah.

(ii) The present shore line may contribute sediments to the Jafurah. This could occur by depositing sand in the littoral zone by longshore drift and subsequent removal by wind

deflation (Fryberger, et al., 1983).

(iii) The Jafurah Sand Sea as detected on Landsat MSS images terminates in the north near Al Jubayl city (Plate 1). This upwind cutoff of the Jafurah, indicates that distal sources available during Pleistocene owing to lowered sea levels and active wadi systems are now not available (Fryberger, et al., 1983). Thus only local sources such as older aeolian deposits or bedrocks are now contibuting sand to the Jafurah system.

EVOLUTION OF DUNES IN JAFURAH:

The evolution of dunes in some sand seas of the world has been disscussed by many authors. McKee (1966) presented a good account of the sequence of dune evolution in the White Sands of New Mexico based on field observations.

There is very little literature on dune formation in the Jafurah. Anton (1983) described briefly the change of dune types from sand sheets (upwind) to transverse dunes (downwind). This section presents a possible model for dune evolution in the Jafurah based on aerial photographic investigation and field observations. The process of evolution can be described as follows:

(i) Vegetated sand sheets in the Jafurah are found with varying vegetation densities. Some sand sheets have high vegetation density while others are highly degraded. In Jafurah, vegetation cover is composed of Xerophytic

and/or halophytic plants, including grasses, shrubs, bushes, and plant trees.

On sand sheets with high vegetation density, sand drift is small, and any sand transported from outside is trapped. On the other hand, on degraded sand sheets (low vegetation density) sand trapping is reduced and deflation starts to develop.

(ii) When vegetation density reaches the lower threshhold, wind action starts to scour the sand and depressions starts to form. A mound of sand starts to form downwind of the depression covering more vegetation and increasing gradually in size. The shape of these mounds, in the Jafurah, assume a parabolic shape. Parabolic dunes are hence formed through degradation of sand sheets.

(iii) As parabolic dunes grow in size their sand trapping efficiency is increased, and the mound (now a dune) starts to move. Usually, at the early stages, this dune assumes a dome shape, but later changes into crescentic shape with a slipface developing in the downwind.

(iv) The final stage of this process is the formation of barchans and/or barchanoid ridges.

The gradual downwind transition from parabolic dunes, usually associated with sand sheets, to transverse dunes is typical throughout the Jafurah. Figure 5.22 is a sketch illustrating the stages of dune evolution in Jafurah. Figure

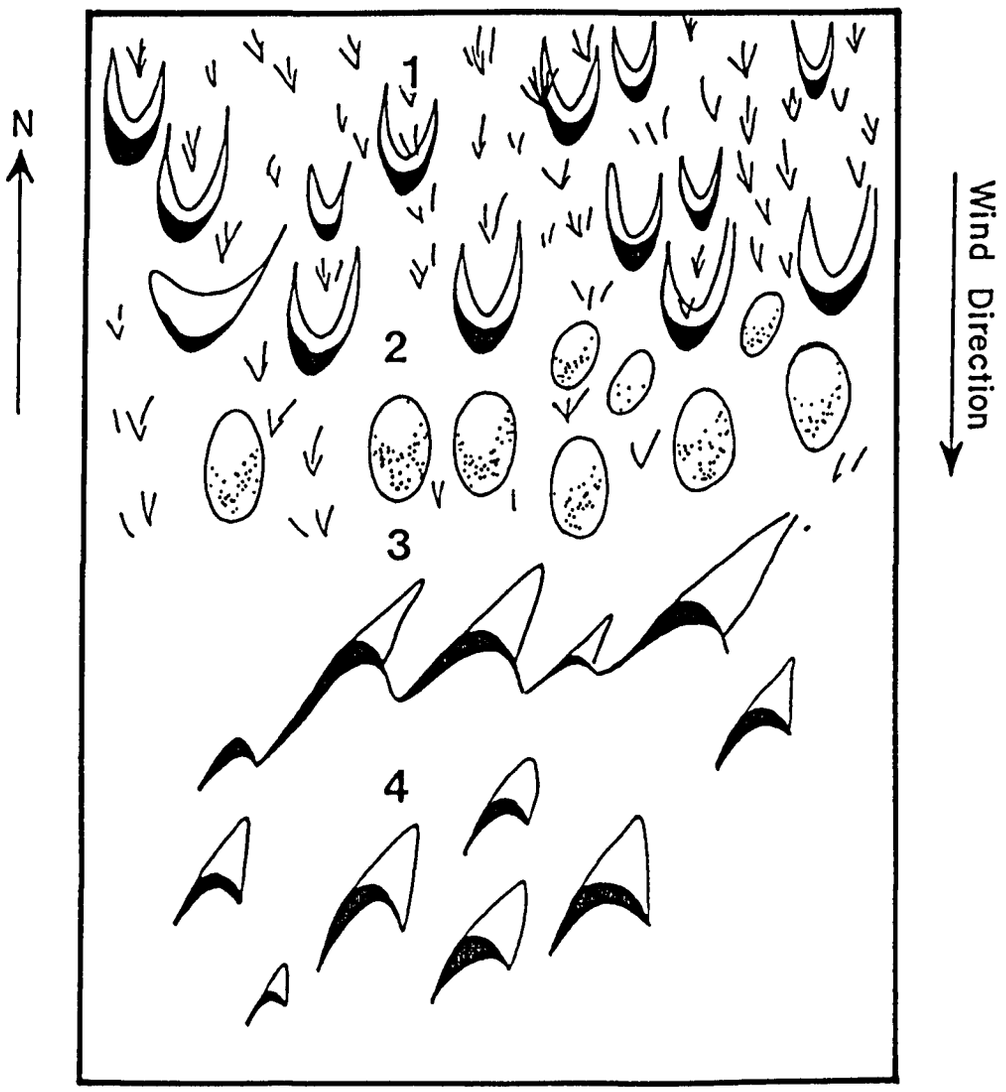


Figure 5.22 A sketch diagram illustrating the different phases of dune evolution in Jafurah Sand Sea. (1): Parabolic dunes; (2): Dome dunes; (3): Barchanoid and barchan dunes(4)

6.7; Chapter 6) is an infrared aerial photograph showing dune evolution in the northern Jafurah (near sabkhat Ad Dibbiyah).

5.8 DISCUSSION AND CONCLUSION

In this chapter, morphology and regional distribution of dunes in sand seas of Arabia as observed by different remote sensing images was discussed. Dune types observed (according to relative abundance) in the major sand seas are linear, crescentic, star, parabolic, and dome-shaped dune.

Measurement of dune length, width (or diameter), and wavelength were made on Landsat MSS imagery, space photography (LFC, and handheld cameras), and aerial photography. The following is a summary of the results of this investigation:

(i) Within each sand sea in Arabia there is a uniformity in the measured values of dune width, length, and wavelength. This is in agreement with Breed's investigation for other sand seas of the world (Breed, 1979).

(ii) The morphological change of dune form from simple to compound or complex was observed in sand seas of Arabia. This is well illustrated in the linear dunes of southwestern Rub'al Khali which progresses from simple to complex form. This progression is commonly associated with growth to larger sizes.

(iii) The wind regime and topography are partly responsible for the morphology and the distribution of the dunes. In sand seas where there is a dominant wind direction, such as in Jafurah, dunes are mostly of crescentic type. Multi-directional wind produces dunes of star type such as in southeastern and southern Rub'al Khali. The effect of topography is well illustrated in western Rub'al Khali. In this area, the wavelength (dune spacing) of the linear dunes increases as they approach an elevated area.

(iv) Landsat MSS false colour composites at a scale of 1: 250,000 complimented by aerial photographs and minimum field work proved to be effective tools for mapping regional distribution of most aeolian dunes.

CHAPTER 6

SAND DUNE MAPPING USING IMAGERY: CASE HISTORIES

6.1 INTRODUCTION

Chapter 5, contains background information on the different types of space images and aerial photographs used for this study. In this chapter the value of these images for sand dune type mapping is assessed for test sites in selected parts of the Arabian Peninsula.

Five areas from different sand seas in the Arabian Peninsula containing different sizes and types of dunes were selected for investigation. The test sites were selected to illustrate different dune types in areas displayed a variety of image types (Table 6.1 & Table 6.2). They include barchans and barchanoid ridges, Parabolic dunes, and linear dunes.

6.2 LITERATURE REVIEW

Aerial photographs and Landsat imagery were used by many geologists and geomorphologists in the study of arid and semi-arid areas. Smith, et al (1970) studied desert basins in North Africa using aerial photography. McKee investigated sand seas of the world largely by using Landsat MSS imagery

	Test Site				
Imagery	1	2	3	4	5
LFC	✓				
MSS	✓	✓	✓		
TM	✓		✓		
SIR-A					✓
Aerial Photograph	✓	✓		✓	

Table 6.1: Investigated test site areas and the image type used for each area.

Dune Type	Test Sites 1	2	3	4	5
Barchan	✓	✓	✓	✓	✓
Barchan-oid ridges	✓	✓	✓	✓	
Parabolic	✓				
Linear					✓

Table 6.2: Dune types investigated in the different test site areas.

and Skylab photographs (McKee, et al 1973; McKee & Breed 1974a, 1974b, 1974c, 1976; McKee, et al 1977, McKee, 1979a, 1979b). El-Baz used Apollo-Soyuz photographs to map types, establish the degree of reddening and to explain patterns of shifting sands in Austalia and Egypt (El-Baz, 1976, 1978, 1979a, 1979b, 1984, El-Baz, et al., 1979). Breed studied the morphology and distribution of dunes in sand seas using remote sensing imagery (Breed, et al., 1978; Breed & Grow, 1979; Breed & Breed, 1979; Breed, et al., 1979; Breed, et al., 1982). Marrsand Kolm (1982) edited a special paper on the interpretation of wind flow characteristics from aeolian landforms with emphasis on remote sensing techniques. Elachi and Blom investigated the use of spaceborne imaging radar in the study of sand dune fields (Elachi, 1980; Elachi, et al, 1980; Elachi., et al, 1982a; Elachi., et al, 1982b; Blom & Daily, 1981; Blom & Elachi, 1981; Blom, et al, 1982a; Blom, et al 1982b). Berlin investigated SIR-A and SIR-B imagery for subsurface imaging of a sand - buried landscape in Saudi Arabia (Berlin, 1984; Berlin et al, 1985; Berlin et al, 1986).

The literature review showed the need for the following:

(i) Comparison of spatial resolution between space imagery and aerial photographs for mapping dunes of different sizes and types.

(ii) Evaluation of scale requirements for mapping sand dunes.

6.3 MATERIALS AND METHODOLOGY

The investigated remote sensing data included the following:

(i) Aerial photographs representing scales of 1:60,000 and 1:80,000 (panchromatic), and 1:10,000 (false colour infrared).

(ii) Landsat MSS images (176/42, 182/41; acquired on 21.11.1972).

(iii) Landsat TM images (164/42, 169/41; acquired on 30.3.1985).

(iv) SIR-A images.

(v) LFC photographs.

The space images and the aerial photographs are compared in four different test sites distributed in major sand seas of Arabia.

Landsat MSS and TM images were compared for spatial resolution assessment in mapping dunes of different sizes. Two test site areas covered by both MSS and TM images were selected for this comparison (Jafurah and An Nafud).

Aerial photographs were used as a complementary tool to Landsat MSS and TM images in mapping small dunes in the Jafurah Sand Sea. Aerial photographs were also compared with the LFC photographs in the Jafurah Sand Sea.

LFC photographic prints were investigated for dune height measurement in the south eastern part of the Rub' al Khali .

Shuttle Imaging Radar (SIR-A) imagery was tested for identifying different aeolian features and how the imaging system might be constrained by the need to image these features. Two test site areas were selected for this investigation; the Wahiba sand sea in Oman and An Nafud in northern Saudi Arabia.

6.4 DUNE TERMINOLOGY

Aeolian sand features recognized on Landsat imagery, aerial and space photography include dunes, irregularly shaped sand sheets, and elongate sand streaks. The term "dune" is used here for all well defined aeolian sand mounds or ridges that exist independently of surrounding topography whether slipfaces are visible or not (Bagnold, 1951). Classification of aeolian sand features based on remote sensing was first introduced by McKee, et al (1977). Dune terminology used in this investigation is based on McKee's classification (1979) which was discussed in Chapter 5 (Section 5.5).

6.5 CASE HISTORY (1) NORTHERN JAFURAH SAND SEA (SMALL DUNES)

An area near Sabkhat Ad Dibbiyah in the northern Jafurah Sand Sea was selected to map dune types of different sizes

using aerial photographs, Landsat MSS and TM imagery, and LFC photographs.

Fig. 6.1 shows the location of the test site. This area is part of the Jafurah Sand Sea which lies within the Arabian Gulf coastal region. The bedrock underlying the aeolian deposits consists of Tertiary sandstone, sandy limestone, and marls of primary continental origin (Powers et al, 1966). These strata are in places poorly consolidated, and thus may supply some of the sediments carried by the wind (Fryberger et al, 1983).

The area consists of five major types of Quaternary sand bodies; barchans, barchanoid ridges, sand sheets, parabolic dunes, and sabkhas. Table 6.3 gives the average widths, lengths, dune spacings, and heights of the dunes as measured from aerial photographs and from the field.

Figures (6.2, 6.3, 6.4, 6.5, 6.6, and 6.7) represent Landsat MSS and TM images, LFC photograph, and aerial photographs taken over the same area.

Fig. 6.2 and 6.3 are Landsat MSS and TM false colour composite full resolution subscenes. Figure 6.4 is an enlarged LFC panchromatic photograph. All images were printed at an approximate scale of 1:100,000 scale.

Figures 6.5, and 6.6 are panchromatic aerial photographs

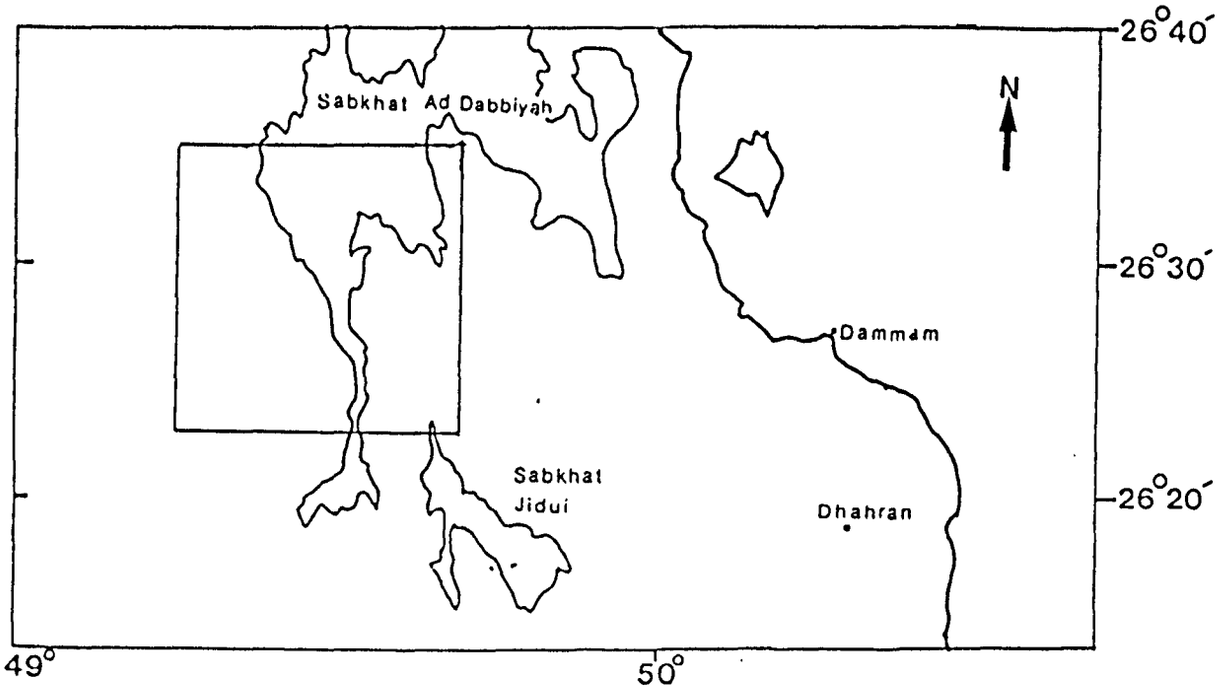


Figure 6.1 Location map of Case History (1).

Dune Morphometry

Dune Type	Average Width ($\bar{W}$)	Average Length ($\bar{L}$)	Average Dune Spacings ($\bar{\lambda}$)	Average Dune Height ($\bar{H}$)
Transverse	100*	500	350	15
Parabolic	70*	150	150	3

Table 6.3: Dune morphometry in Case History (1).
Measurements are in metres.
* 100 dunes were measured.

Captions for figures (6.2, 6.3, 6.4, 6.5, 6.6 and 6.7) used to illustrate case history (1). W means average dune width. See text for more discussion.

Figure 6.2 Landsat MSS (176/42) full resolution false colour composite (bands 4, 2, 1) subscene. Barchans and barchanoid ridges located on sabkha are clearly detected. Parabolic dunes are not recognized.

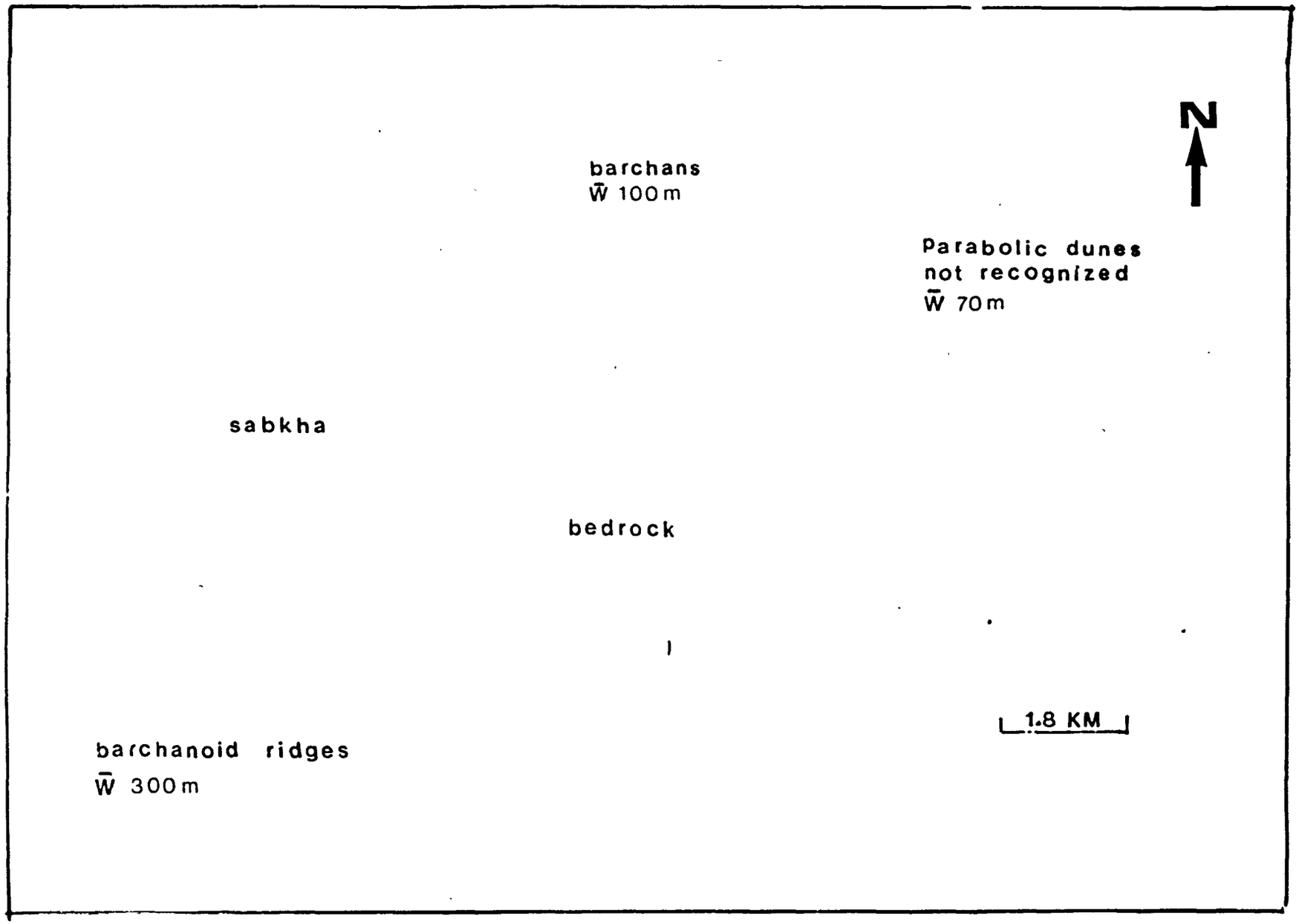
Figure 6.3 Landsat TM (164/42) full resolution false colour composite (bands 4, 3, 2) subscene. See text for explanation.

Figure 6.4 LFC panchromatic photograph enlarged from an original scale of 1:778,000 and printed at 1:100,000. Barchans and barchanoid ridges on sabkha are clearly defined. Parabolic dunes are not covered by the photograph.

Figure 6.5 Panchromatic aerial photograph printed at the original scale (1:60,000). Barchans and barchanoid ridges on sabkha are clearly defined. Parabolic dunes can be detected but with difficulty.

Figure 6.6 Panchromatic aerial photograph printed at the original scale (1:80,000). At this scale parabolic dunes are not clearly recognized.

Figure 6.7 Infrared aerial photograph (1:10,000 scale) covering the eastern part of the test site. Parabolic dunes and small size barchans are clearly defined.


N
barchans
$\bar{W}$ 100 m
Parabolic dunes
not recognized
$\bar{W}$ 70 m
sabkha
bedrock
1.8 KM
barchanoid ridges
$\bar{W}$ 300 m

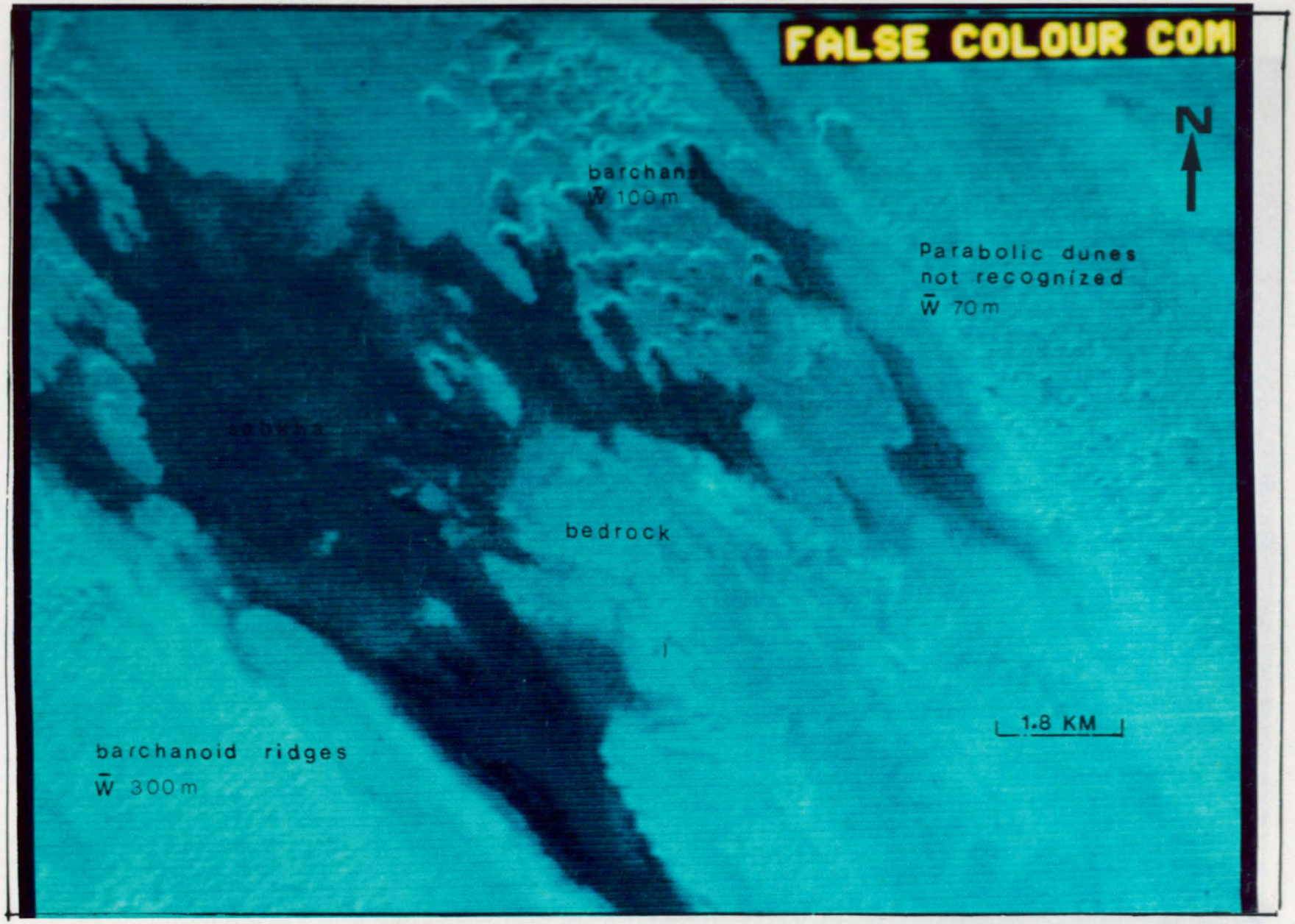

FALSE COLOUR COM
N
barchan
W̄ 100 m
Parabolic dunes
not recognized
W̄ 70 m
sebkha
bedrock
1.8 KM
barchanoid ridges
W̄ 300 m

Figure 6.2

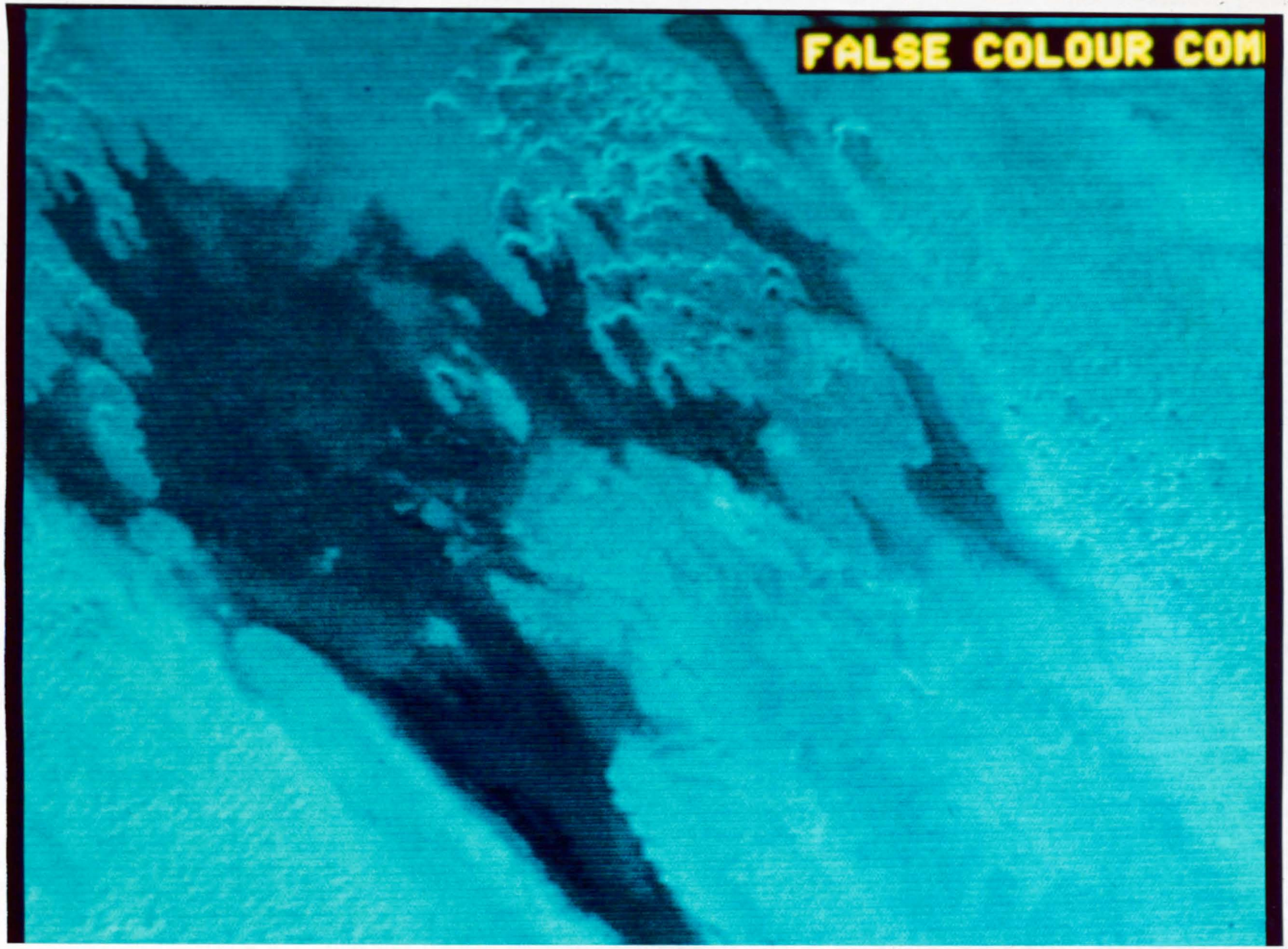
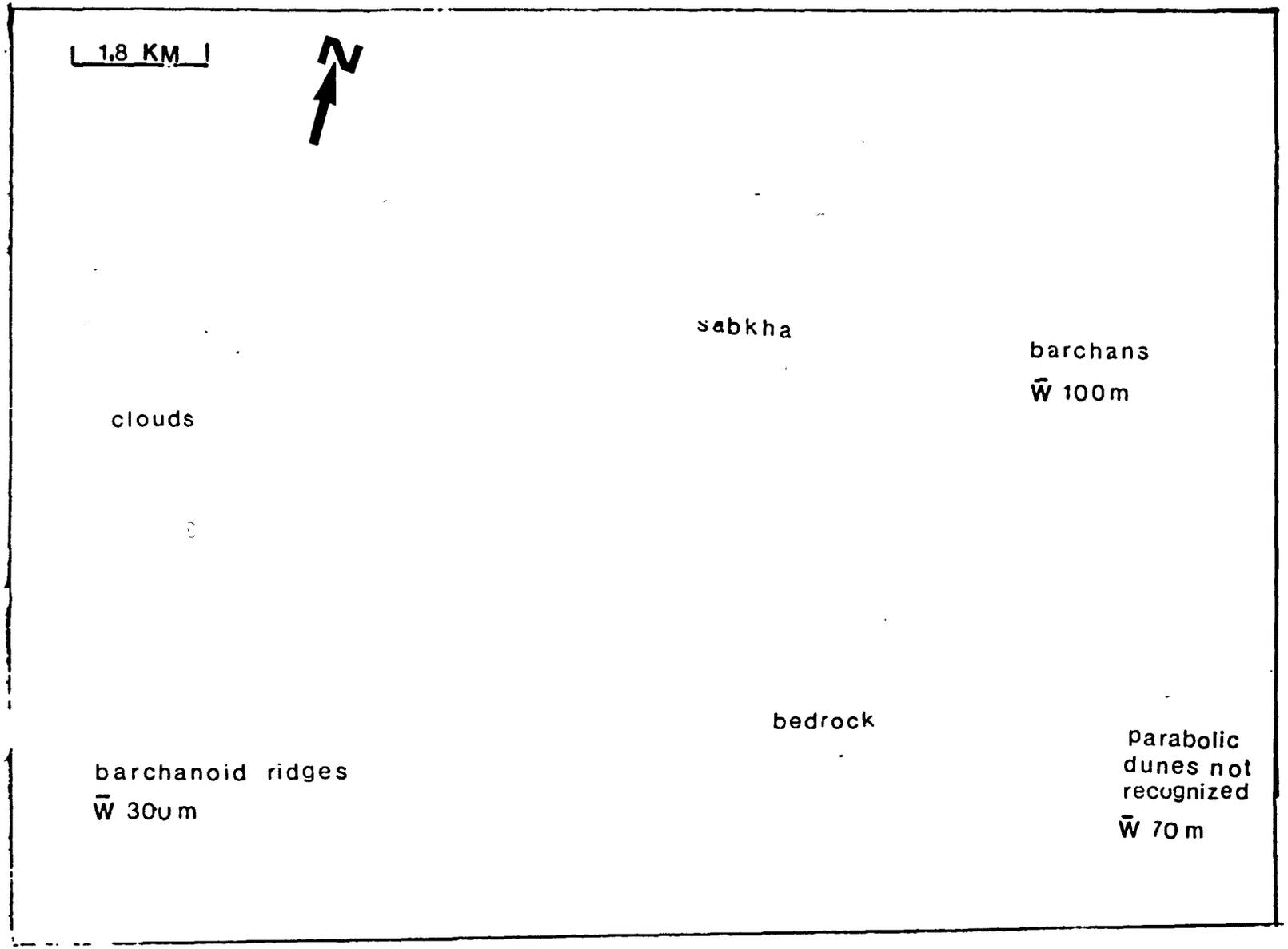


Figure 6.2


1.8 KM
N
sabkha
barchans
$\bar{W}$ 100m
clouds
bedrock
barchanoid ridges
$\bar{W}$ 300m
Parabolic dunes not recognized
$\bar{W}$ 70m

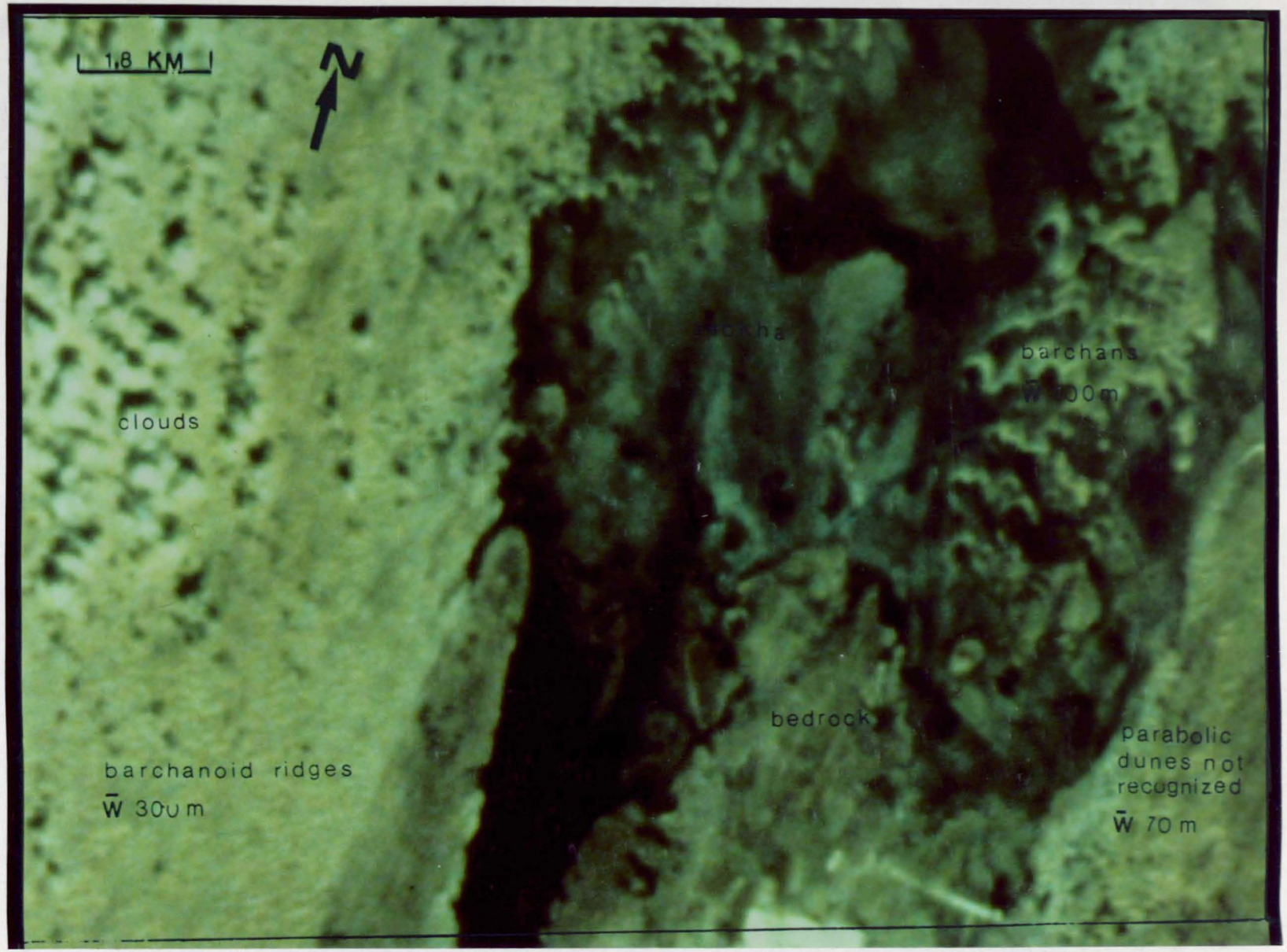

1,8 KM
N
clouds
barchans
W 100m
bedrock
barchanoid ridges
W 300 m
parabolic
dunes not
recognized
W 70 m

Figure 6.3

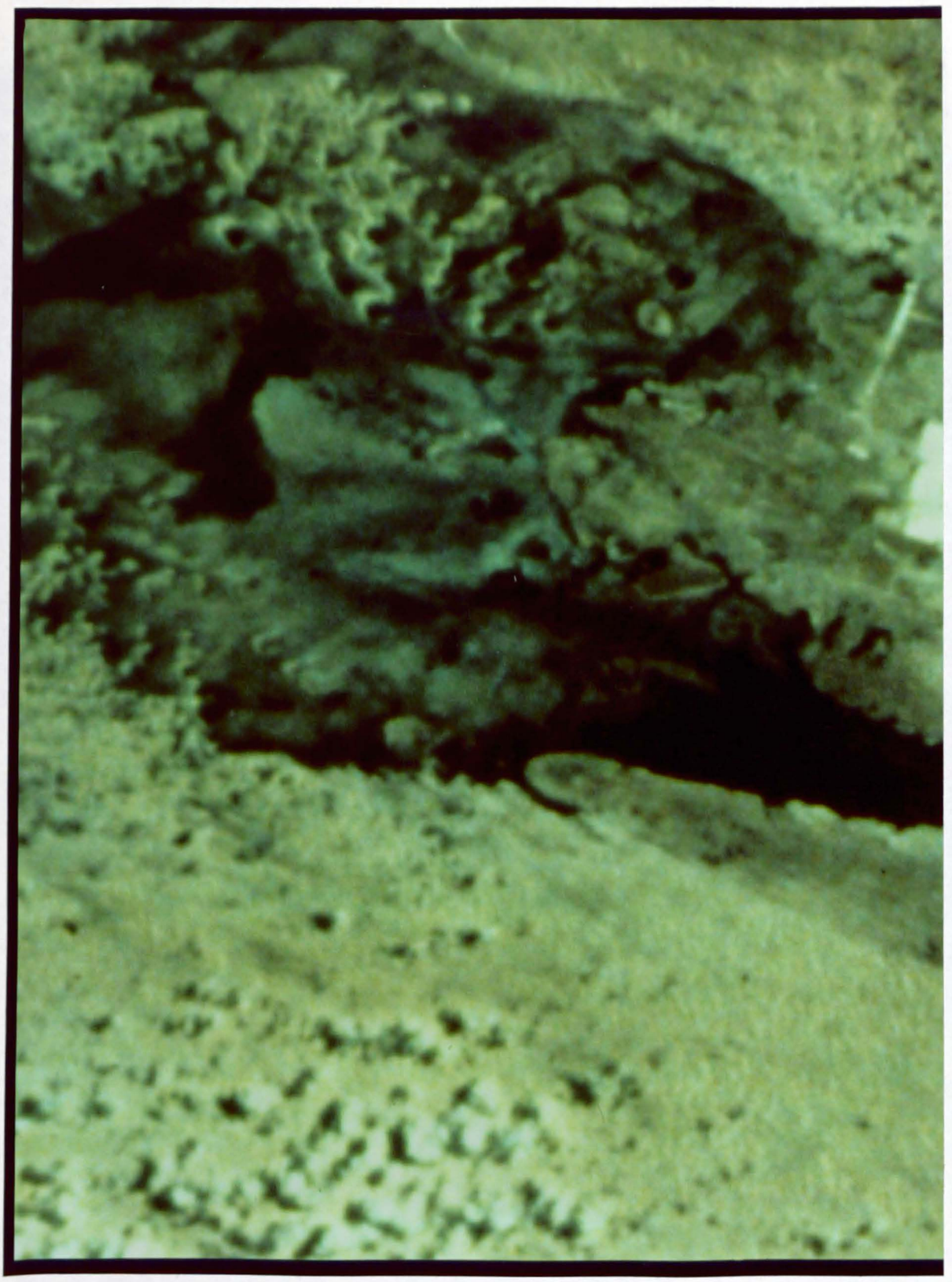


Figure 6.3

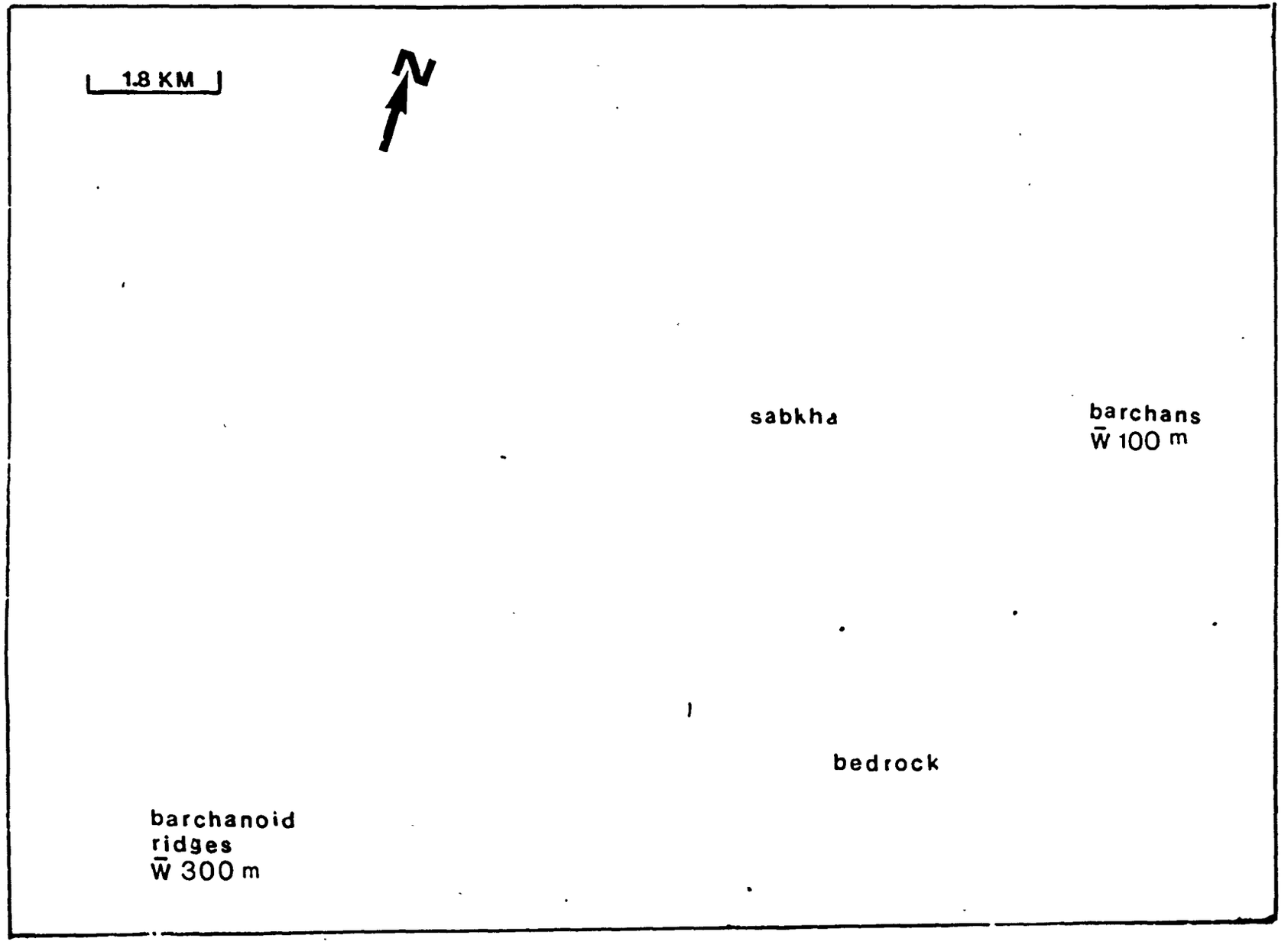

1.8 KM
N
sabkha
barchans
$\bar{W}$ 100 m
bedrock
barchanoid
ridges
$\bar{W}$ 300 m



Figure 6.4



Figure 6.4

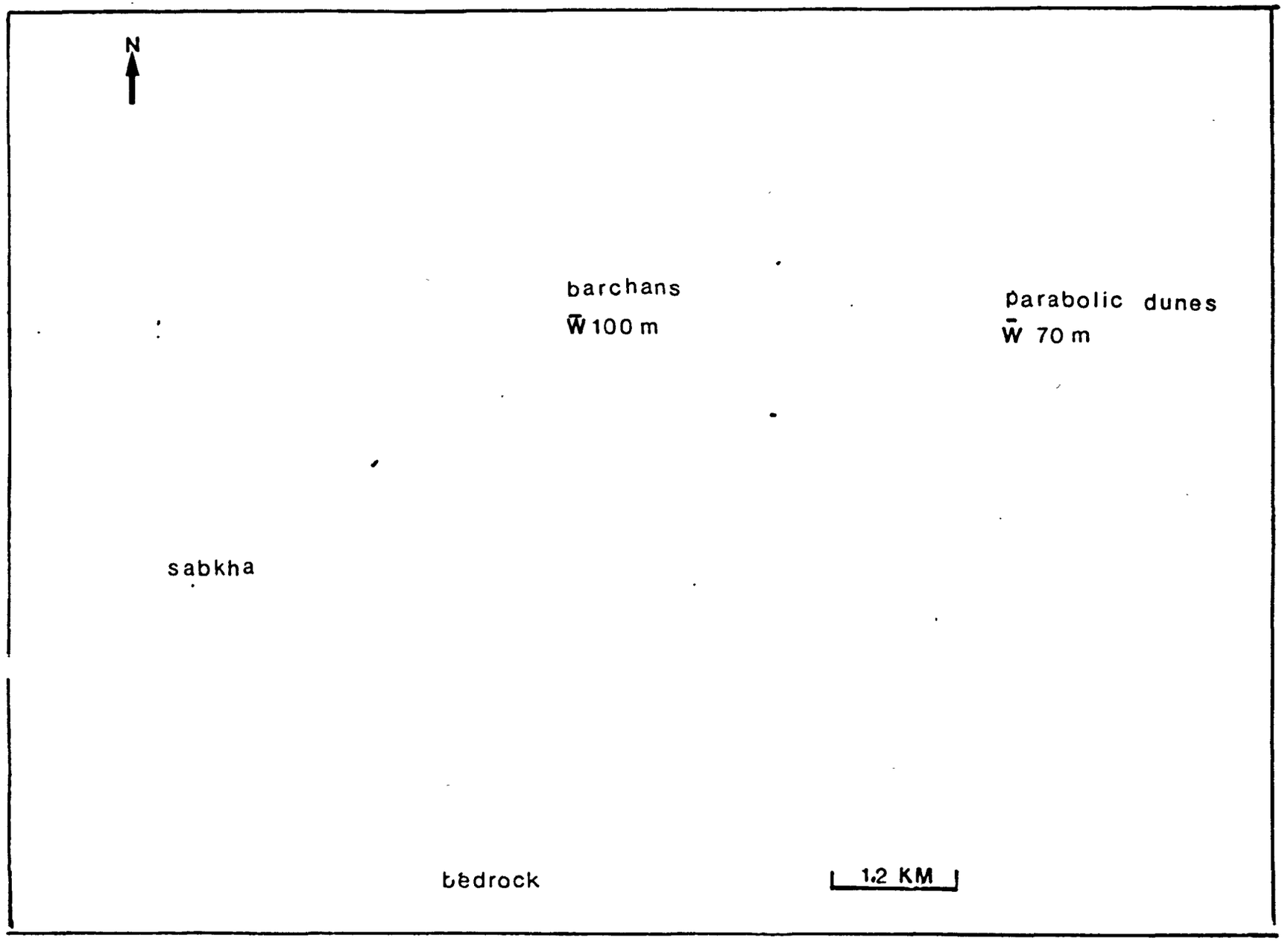

N
barchans
$\bar{W}$ 100 m
parabolic dunes
$\bar{W}$ 70 m
sabkha
bedrock
1.2 KM

Figure 6.5

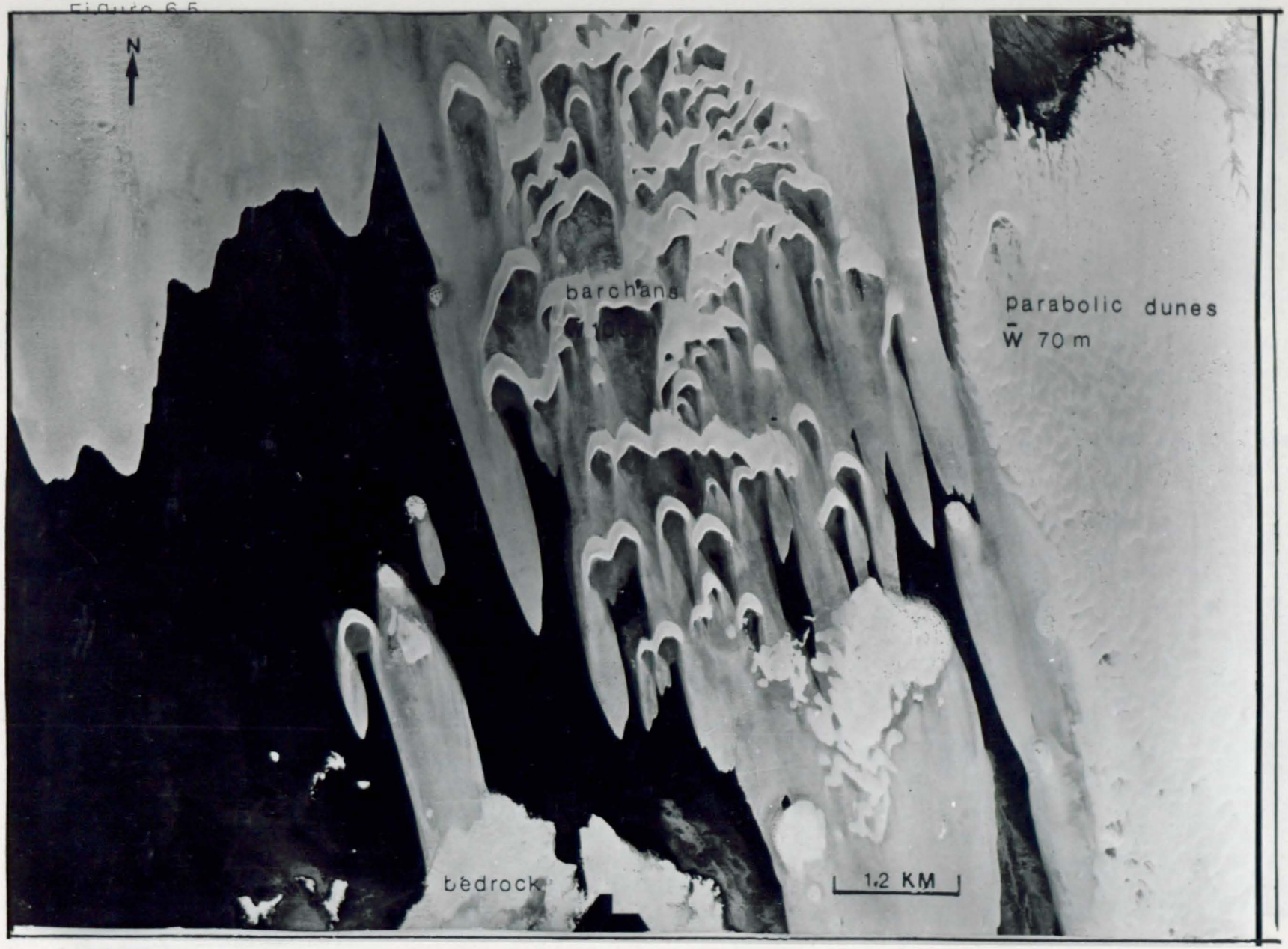
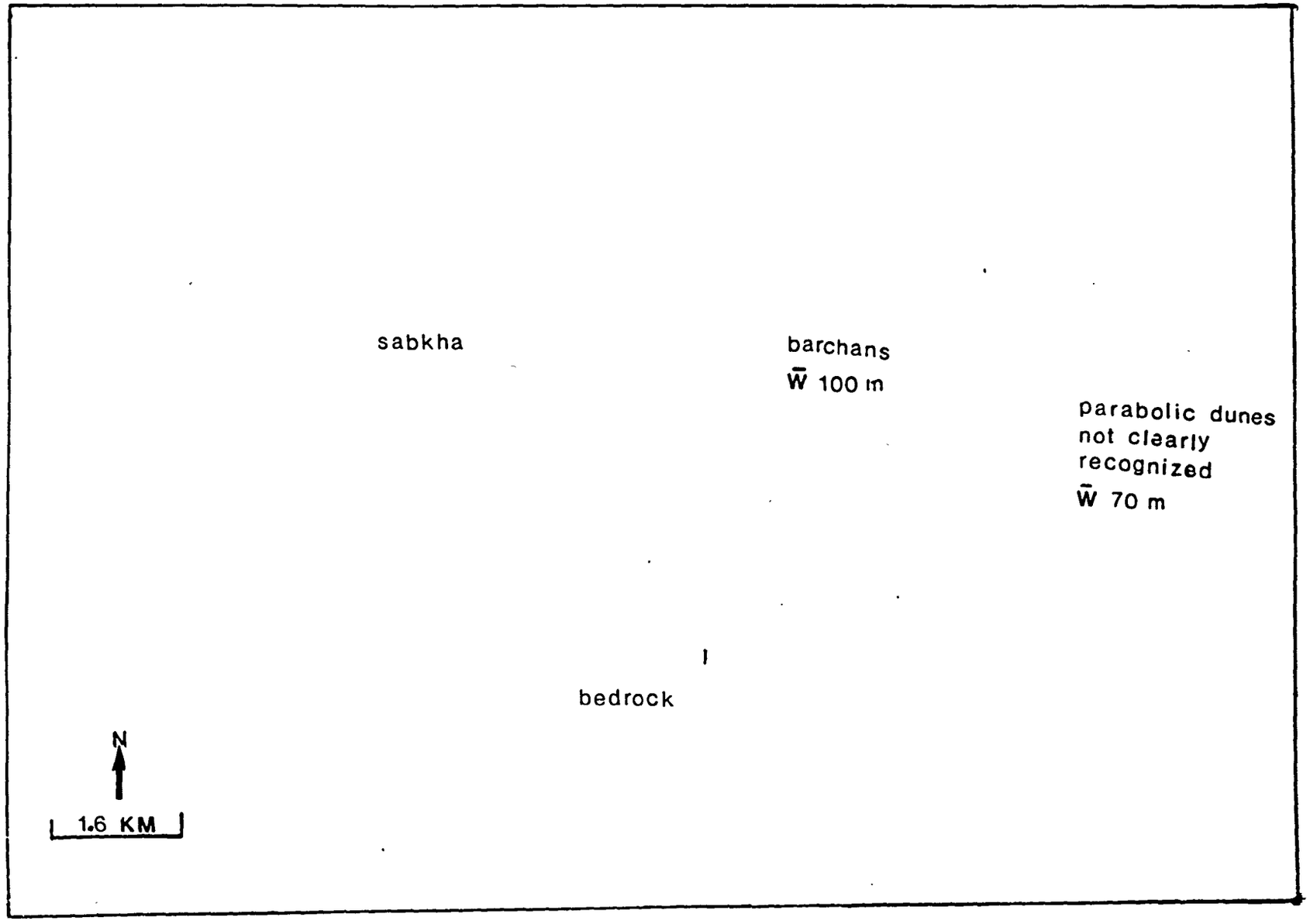




Figure 6.5

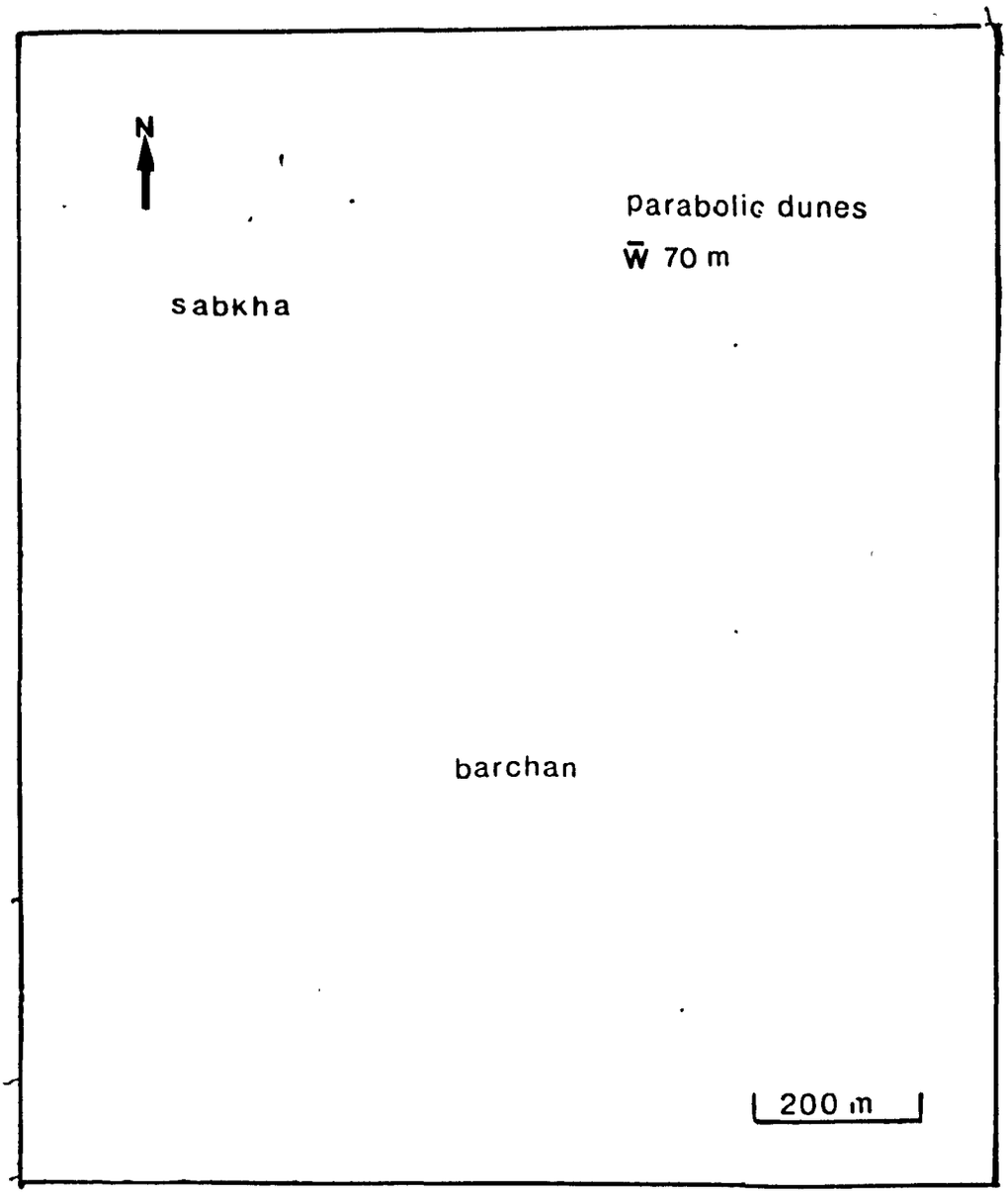

sabkha
barchans
$\bar{W}$ 100 m
parabolic dunes
not clearly
recognized
$\bar{W}$ 70 m
bedrock
N
1.6 KM


sabkha
barchans
$\bar{W}$ 70 m
parabolic dunes
not clearly
recognized
$\bar{W}$ 70 m
bedrock
N
1.6 KM

Figure 6.6



Figure 6.6


N
Parabolic dunes
W̄ 70 m
sabkha
barchan
200 m

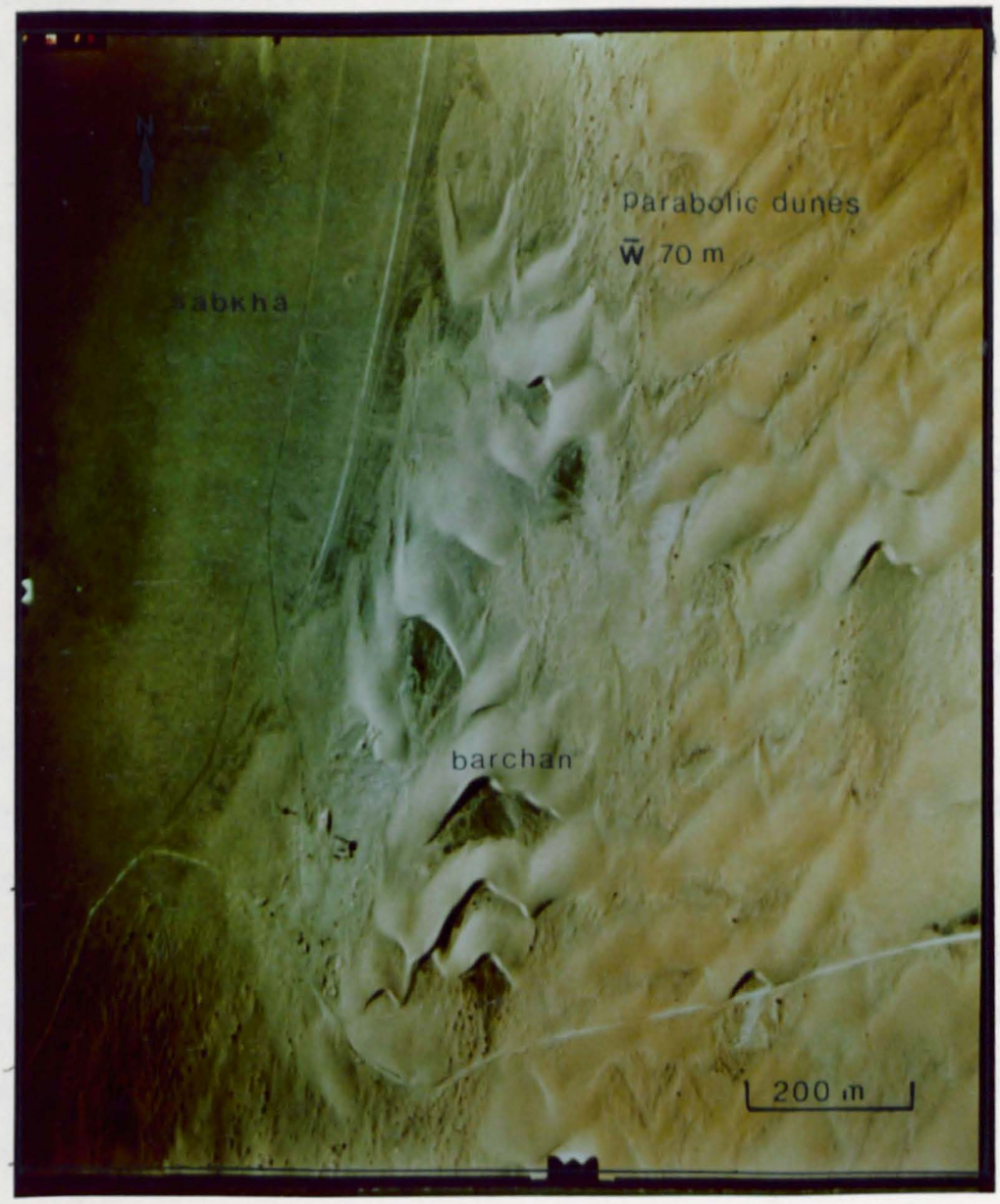


Figure 6.7



Figure 6.7

acquired at 1:60,000 and 1:80,000 scale. Figure 6.7 is a false colour infrared aerial photograph acquired at 1:10,000 scale.

A comparison among these images and photographs indicates the following:

Landsat MSS imagery shows clearly the individual barchans and the barchanoid ridges located on the sabkha down to a size of 100 m. This is because of the high albedo contrast between sabkha and sand. However, in areas of low contrast such as those located east and west of the sabkha dunes of 100 m size are not as clearly defined as those on sabkha. This may be also due to the fact that the majority of these dunes are narrowly spaced, which inhibits detection of the dune shape. Landsat MSS imagery failed to detect parabolic dunes widths (20 - 70 metres) which are below the resolving power of the Landsat MSS imagery (nominal resolution = 79 metres).

Landsat TM imagery (nominal resolution = 30 meters) showed a general improvement over the MSS imagery. The individual barchans and the barchanoid ridges located on the sabkha are clearly more pronounced in the TM imagery than on the MSS imagery (Figure 6.2). Dunes located east and west of the sabkha show a better definition than on the MSS imagery. However, TM imagery failed to detect the 20-70 m parabolic dunes. Unfortunately, due to the poor photographic product, the presented imagery lacks the sharpness to illustrate the

drawn interpretations. The results presented here are based on an interactive interpretation of a full resolution (512 x 512 pixels) imagery displayed on the TV monitor.

Landsat MSS and TM imagery failed to detect dunes smaller than 100 metres and 40 meters in width respectively on sabkha substratum (high contrast). On low contrast sandy terrains, dunes of widths greater than 200 m could only be detected on Landsat MSS imagery. Dunes with widths between 40-200 metres were detected on Landsat TM imagery.

The LFC panchromatic photograph shows a more prounouced configuration of dunes located on the sabkha. At an enlarged scale of 1:100,000 (a nominal resolution of 10- 12 metres, the features visible in the LFC photograph are comparable with those shown in aerial photography of 1:80,000 scale. Although the dunes located east and west of the sabkha show a better definition than on the MSS and TM imagery, there is still some difficulty in recognising all the individual dunes. This LFC photograph is illuminated by a sun angle of about 56 degrees. At such a relatively high sun angle, the configuration of the photographed dunes will be obscured even if the dunes are aligned transversely to the illumination azimuth. A lower sun angle illumination would provide shadows which could enhance dune shapes. There are no parabolic dunes in the area covered by the LFC photographs.

Panchromatic aerial photographs at scales of 1:60,000

and 1:80,000 and a resolution of 1-2 metres offers an improvement in detecting the majority of the dunes in this area. Vegetated sand sheets consisting of small bushes (10 x 10 m in dimension) can also be identified. However, only at a scale of 1:60,000 and larger, can parabolic dunes be distinguished.

At a scale of 1:10,000, infrared aerial photgraphs could only cover part of the investigated area. For this reason, the area located east of the sabkha was investigated since it consists of both parabolic and barchan dunes. Because of the high spatial resolution (0.25 m across) and the high sensitivity of the false colour infrared film, parabolic dunes are clearly defined. These parabolic dunes (average width is 70 metres) are forming in a vegetated sand sheet and are v- shaped with arms drown out on the sides and pointing north. The dark spots in the photographs are the bushes covering parts of the parabolic dunes. Barchan dunes, at the edge of the sabkha, with widths of 30 m are clearly detected on these photographs.

This case history demonstrated the importance of spatial resolution and scale as two important factors in mapping small size dunes. This case history also investigated the different aspects of spatial resolutions (detection of dunes located in high contrast areas compared with dunes located in low contrast areas).

6.6 CASE HISTORY (2) HARAD AREA: LARGE DUNE FORMS

This area located south of the Jafurah Sand Sea is selected to emphasize the importance of spatial resolution in sand dune mapping in terrain with apparently larger dunes. The comparison is made between black and white aerial photographs and Landsat MSS imagery.

Figure 6.8 shows the location of the test site area. This area consists of large barchanoid dune forms, gravel, and bedrock. It lies in the transition zone between the Jafurah and the Rub'al Khali. The terrain is flat and is dissected from west to east by an old valley (Wadi Sahba) which was partially or totally filled with sediments and later covered with aeolian sand. Under the arid conditions that have persisted for the last 5000 years (Anton, 1983), this gravel terrain has been covered with aeolian sand supplied from the north and from the surrounding bedrock outcrops.

Figure 6.9 is a Landsat MSS false colour composite (bands 4 2 1) showing large barchanoid shaped dune forms. Fig. 6.10 is a detailed aerial photograph of these dunes at a scale of 1:60,000. Comparison between these two figures show that Landsat MSS imagery with 79x79 meters resolution can only detect large barchan form bodies. An aerial photograph, on the other hand, reveals small barchan dunes and ridges linked together to form a large barchanoid shaped dune. This Large barchan complex has a width of 3.6 km and will be

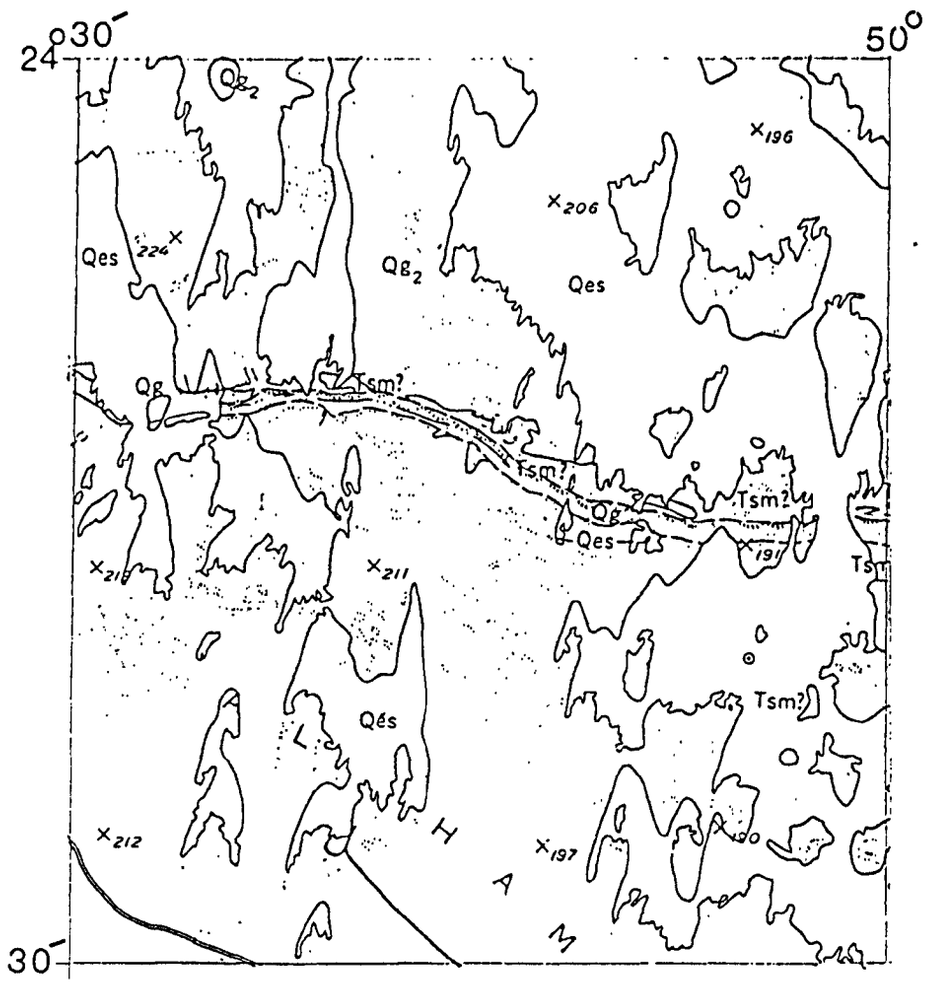


Figure 6.8 Location map of Case History (2).

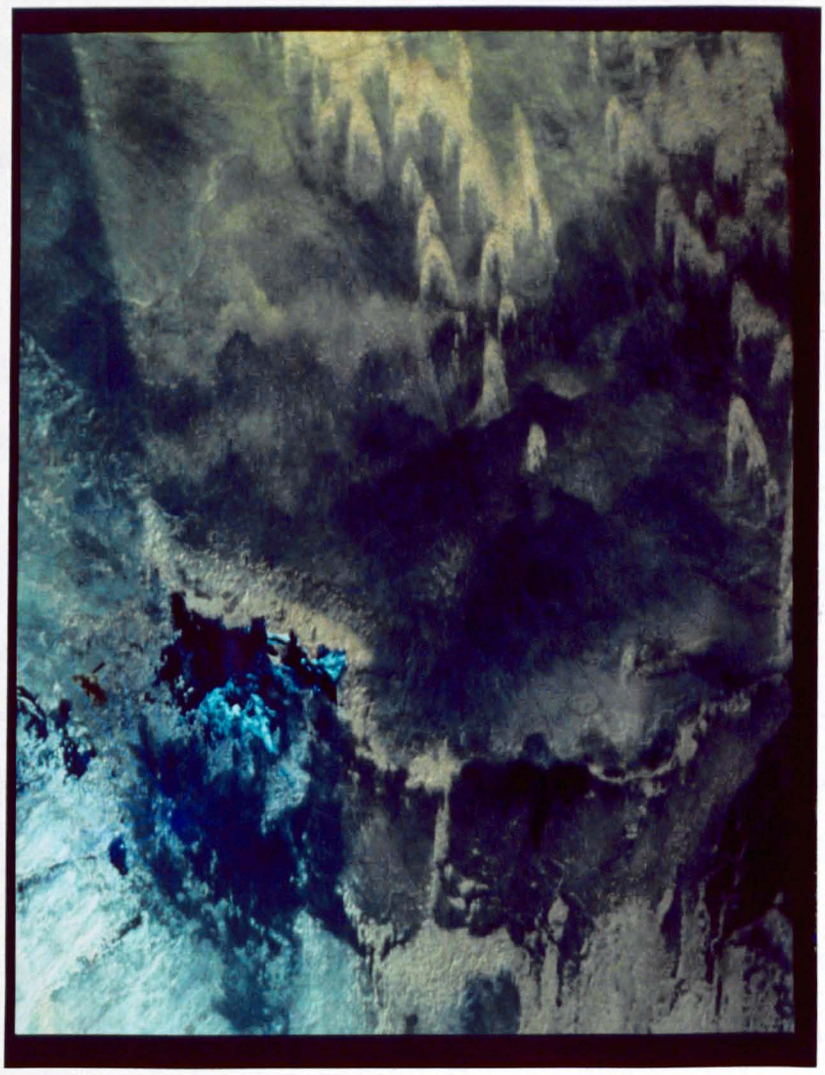


Figure 6.9 Landsat MSS (176/44) false colour composite (bands 4, 2, 1) full scene showing large barchanoid shaped dunes.

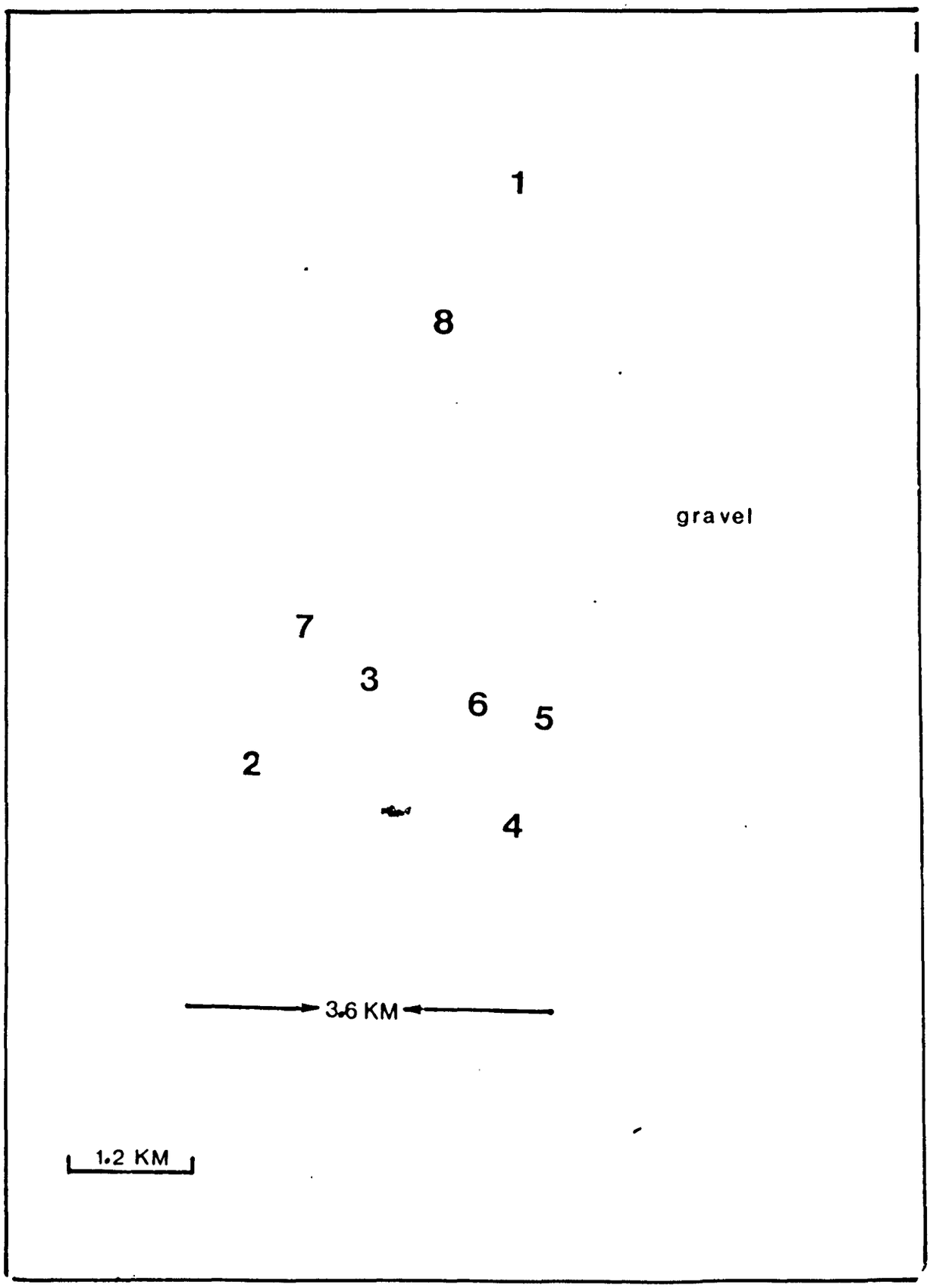
called "chain barchan " to differentiate it from the mega-barchans described by (Norris, 1966).

The " chain barchan" dunes are found at the edges of the dune field. One typical " chain barchan " dune was measured in the field. Figure 6.10 indicates the locations of the measured individual barchans. Table 6.4 is a summary of the measurements of heights and widths of these dunes.

There is no published explanation of the origin and development of these dunes. It is possible that in an open gravel area with no topographic barriers, such as the area illustrated, small barchans may travel fast enough to catch up with larger dunes and then link together to form chains.

This is in contrast to the mega-barchan dunes sometimes referred to as compound crescentic dunes which are generally much larger than simple crescentic dunes. They are also characterised by the presence of smaller crescentic dunes with slipfaces oriented the same as the main slipfaces but developed secondarily on the gentle slope of each major dune mound or ridge. Such dunes are found in Al 'Uruq al Mu' taridah in the northeastern Rub'al Khali (Fig.8.11a). These dunes are composed of curved segements with slipfaces having a mean width (horn to horn) of 2.8 km and a mean length of 2.1 km (McKee, 1979).

This case history illustrates the danger of drawing oversimplified conclusions about the form of large sand bodies based on only Landsat MSS data. Clearly many sand


1
8
gravel
7
3
6
5
2
4
3.6 KM
1.2 KM

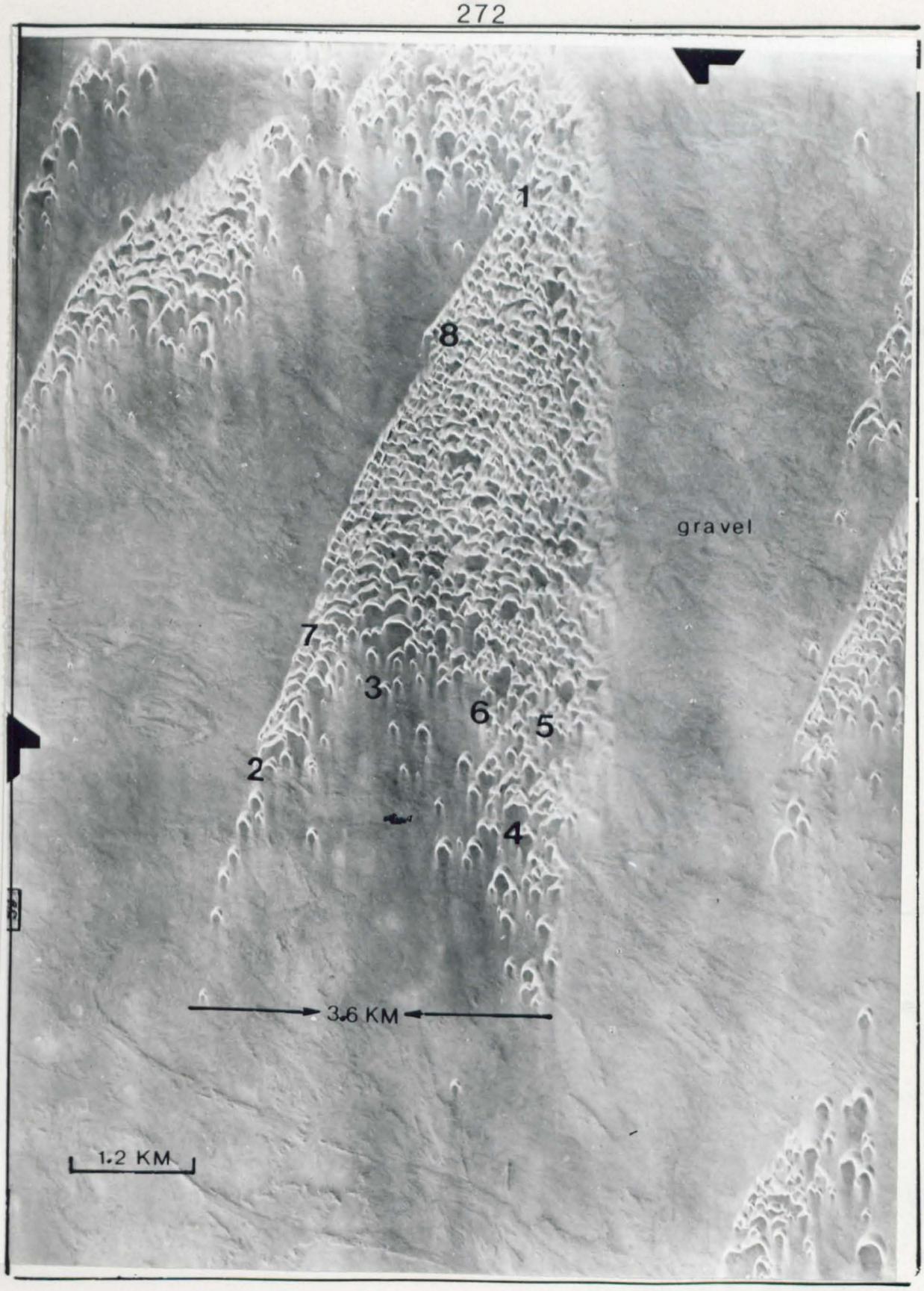


Figure 6.10 Panchromatic aerial photograph (1:60,000 scale) showing a close-up view of the dunes shown in Figure 6.9. Small barchans and/ barchanoid riges linked togther to form a large barchanoid form (chain barchan). Width of the dune is 3.6 km. Numbers refer to the dunes measured in the field (see Table 6.4).



Figure 6.10 Panchromatic aerial photograph (1:60,000 scale) showing a close-up view of the dunes shown in Figure 6.9. Small barchans and barchanoid riges linked togther to form a large barchanoid form (chain barchan). Width of the dune is 3.6 km. Numbers refer to the dunes measured in the field (see Table 6.4).

Dune No.	Dune Height (m)	Dune Width (m)	Comments
1	2	48	Barchanoid ridge.
2	6	150	Individual barchan.
3	7	125	Individual barchan surrounded by barchans, but not nearly as high. More sand is available in the inside, so more barchans are found in this part.
4	6	150	Poorly developed barchan compared to the West Wing. Coarser grains to the Eastern Wing than Western Wing.
5	7	155	Barchanoid ridge.
6	6	145	Individual barchan found among a group of barchans.
7	7	125	Barchanoid ridge.
8	8	160	Barchanoid ridge; east tip is like a snake.

Table 6.4: Morphometry of representative dunes found in one "chain barchan". The width of the measured chain barchan is 2.8 km (see Figure 6.10).

bodies which appear simple in MSS imagery may be revealed as complex structures when examined in higher resolution imagery.

6.7 CASE HISTORY (3) AN NAFUD AREA: (LARGE AND SMALL DUNE FORMS)

This area northwest of Hail located in An Nafud sand sea was selected to compare Landsat MSS and TM images for identifying large and small barchanoid dunes.

The area is part of the Nafud Sand Sea located in northern Arabia (Fig. 6.11). Stablized linear and crescentic ridges with a north eastern to eastern orientation are common in this area. From the south the area is bordered by the Precambrian shield complex of igneous, metavolcanic, and metasedimentary rocks.

Figures (6.12 & 6.13) are two full resolution false colour composite subscenes representing Landsat MSS and TM respectively. The area consists of closely spaced large compound crescentic dune ridges with smaller barchans and barchanoid ridges confined to the crests of the larger dunes. On the Landsat MSS imagery the large compound crescentic dune ridges can be detected. However, smaller crescentic dunes found on top of these dunes are not clearly recognized on the Landsat MSS imagery because of resolution limitation. On the other hand, Landsat TM imagery can easily detect both large and small dunes. Small dunes are less than

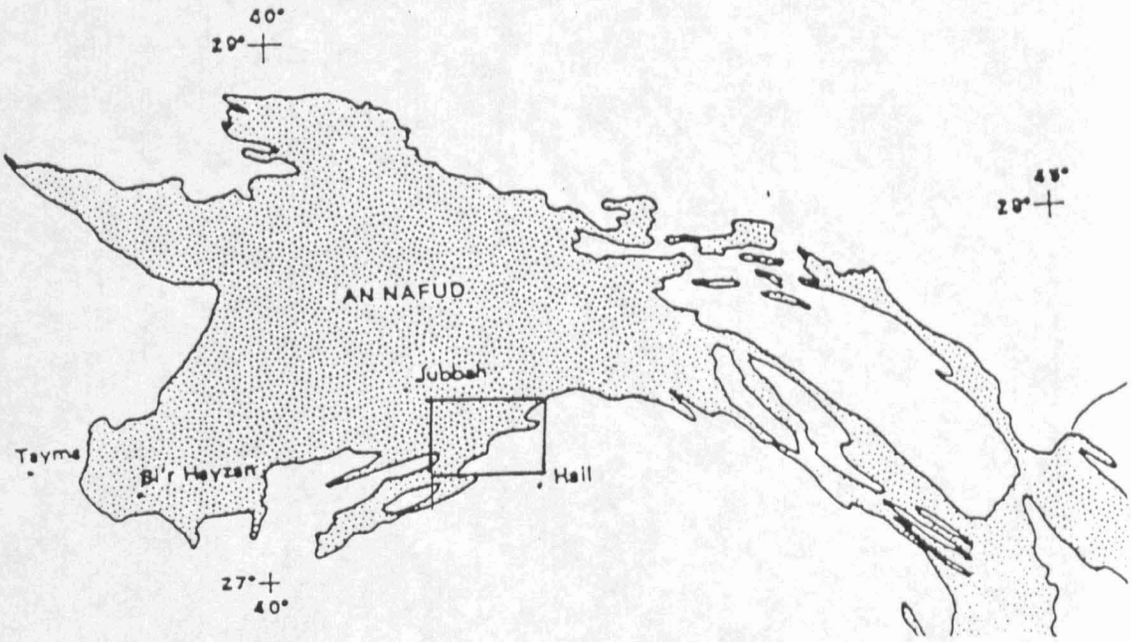
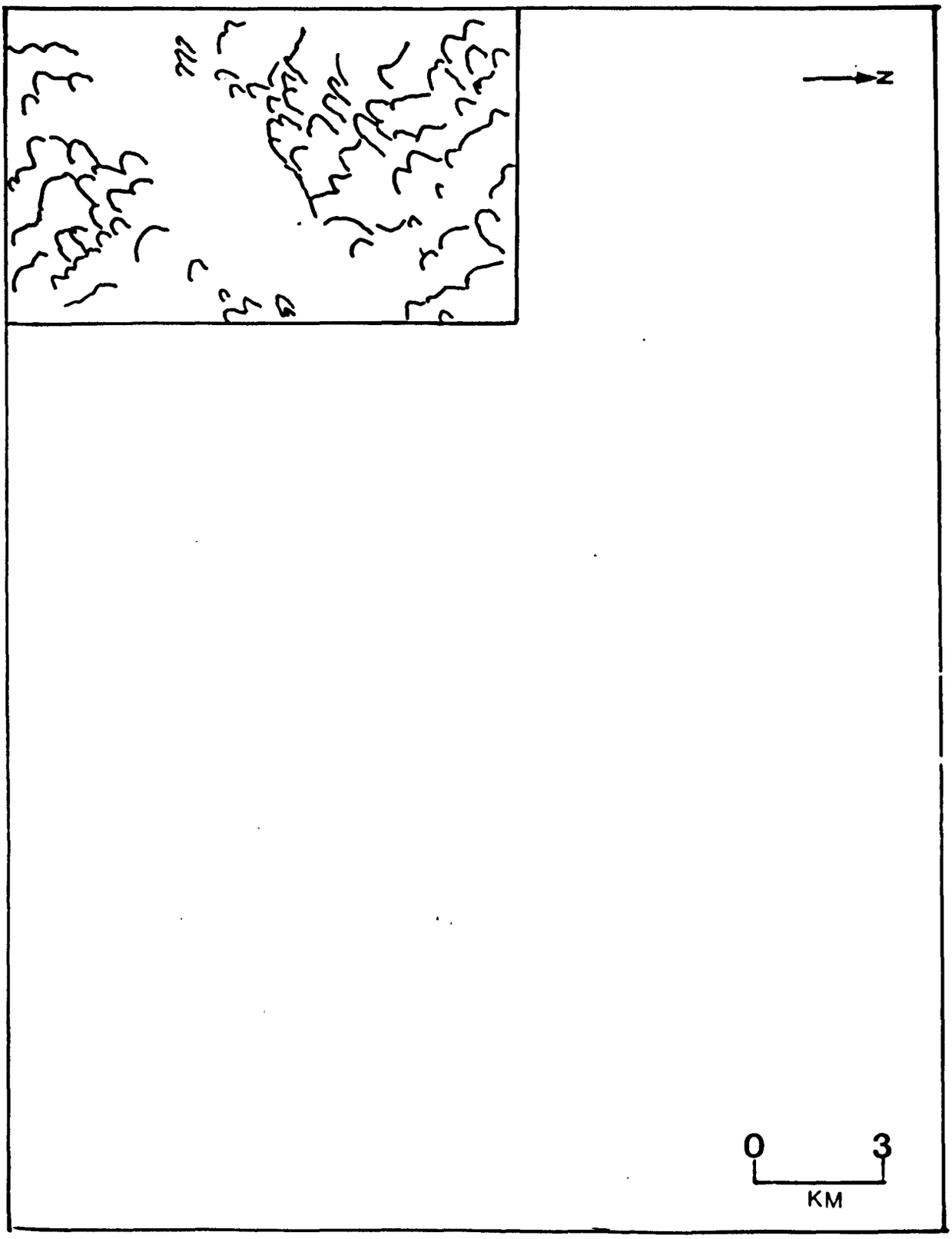


Figure 6.11 Location map of Case History (3).


N
0
3
KM

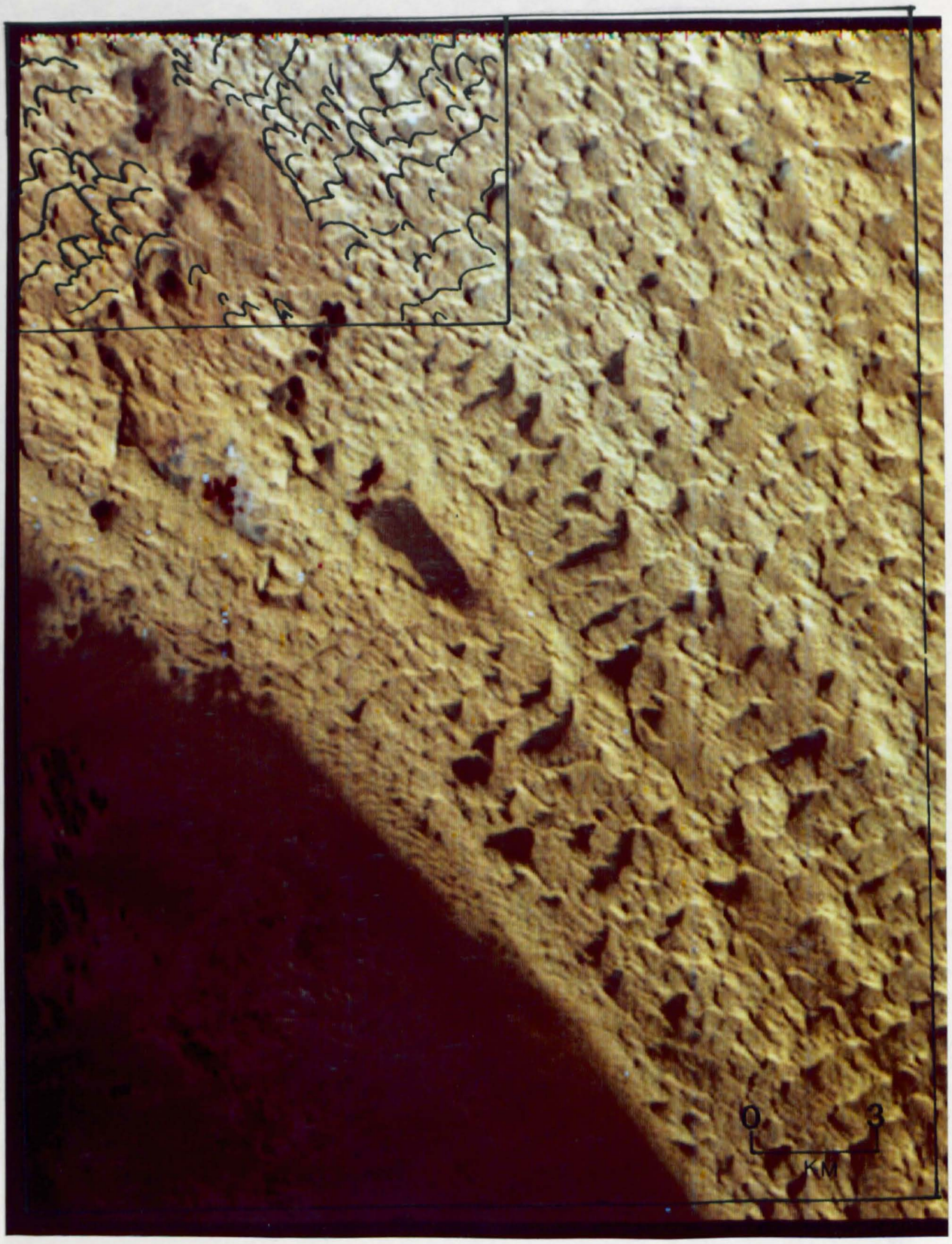


Figure 6.12 Landsat MSS (182/41) full resolution false colour composite subscene showing large barchanoid dunes. Small size barchans are not clearly detected.

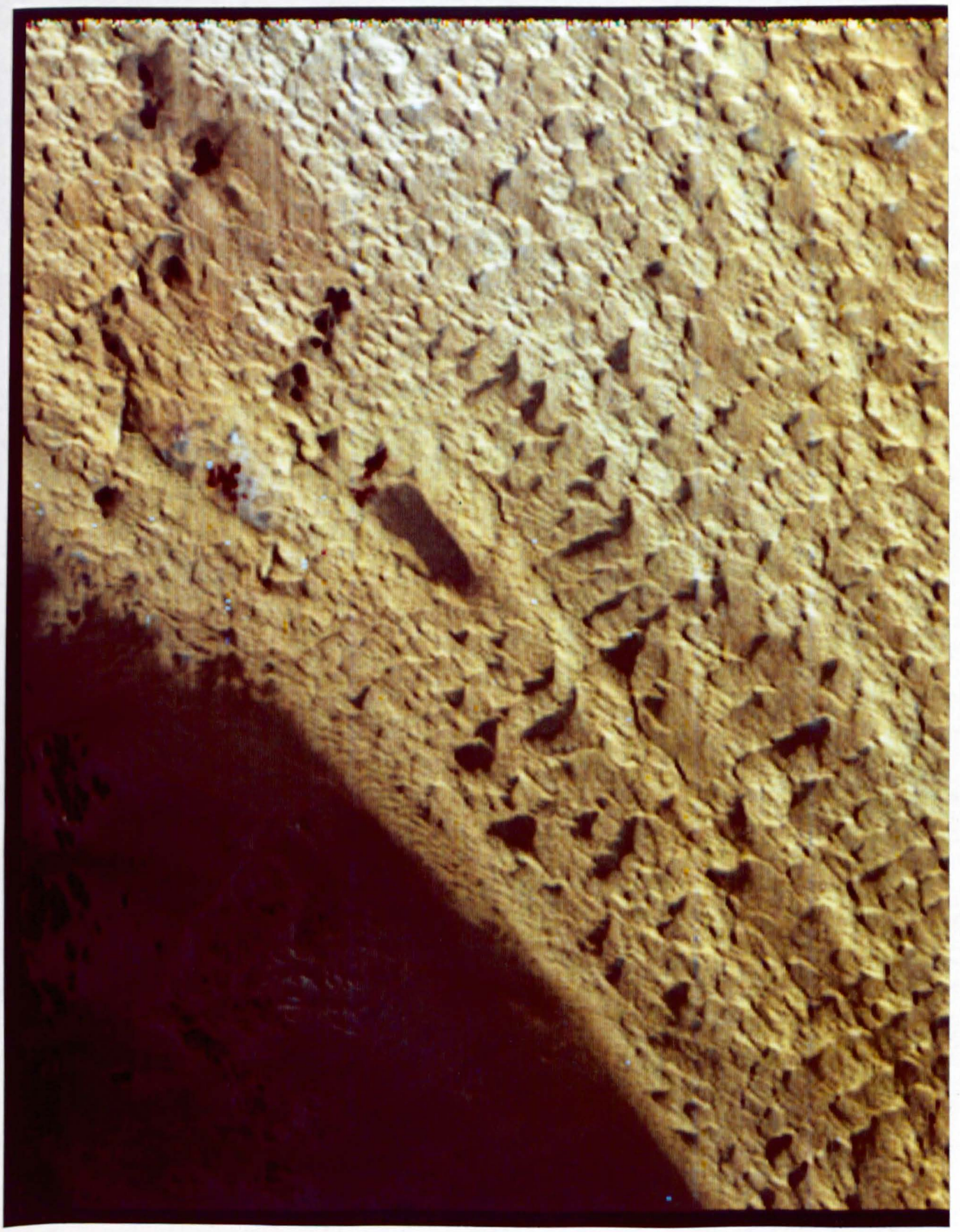
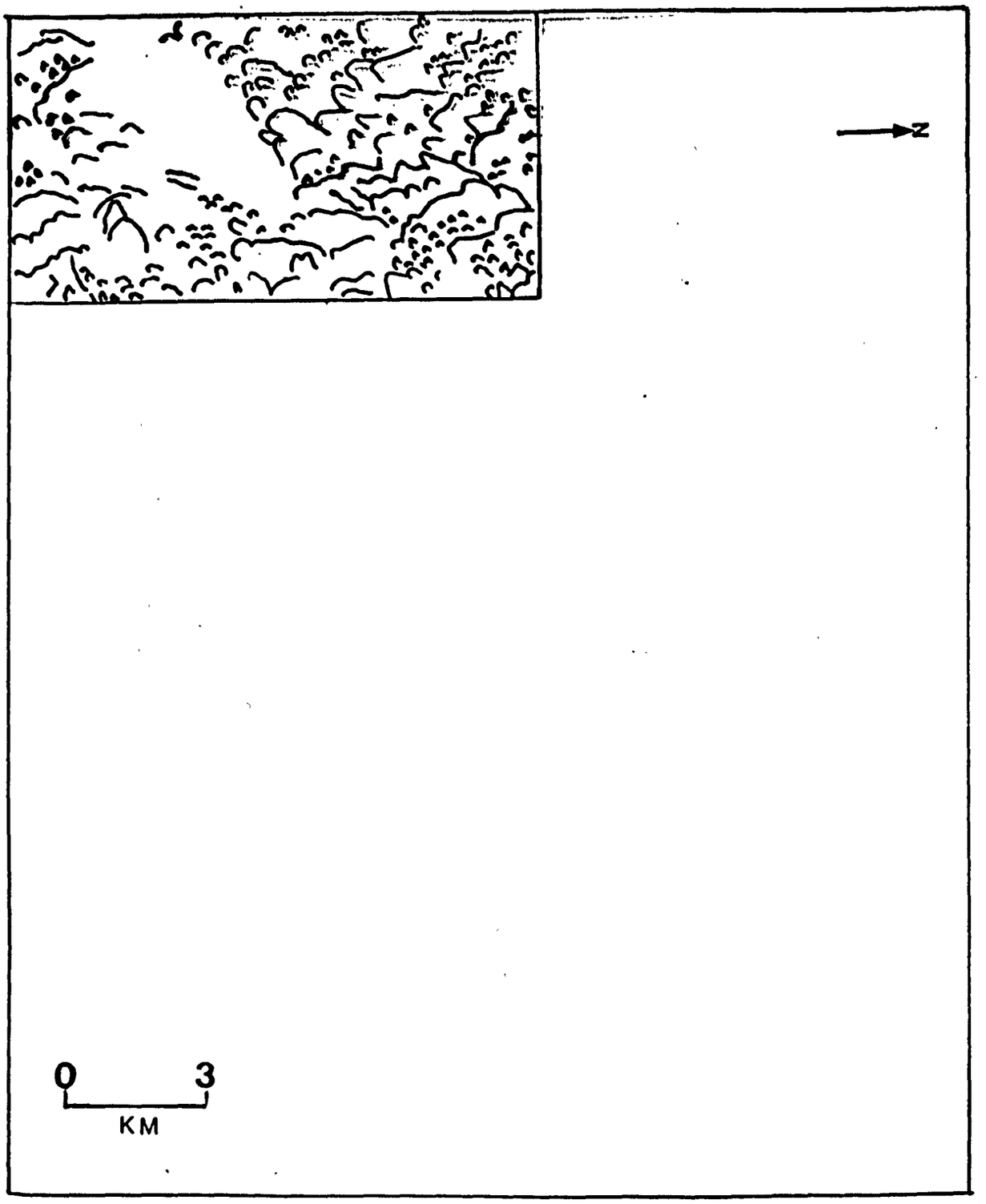


Figure 6.12 Landsat MSS (182/41) full resolution false colour composite subscene showing large barchanoid dunes. Small size barchans are not clearly detected.


N
0
3
KM

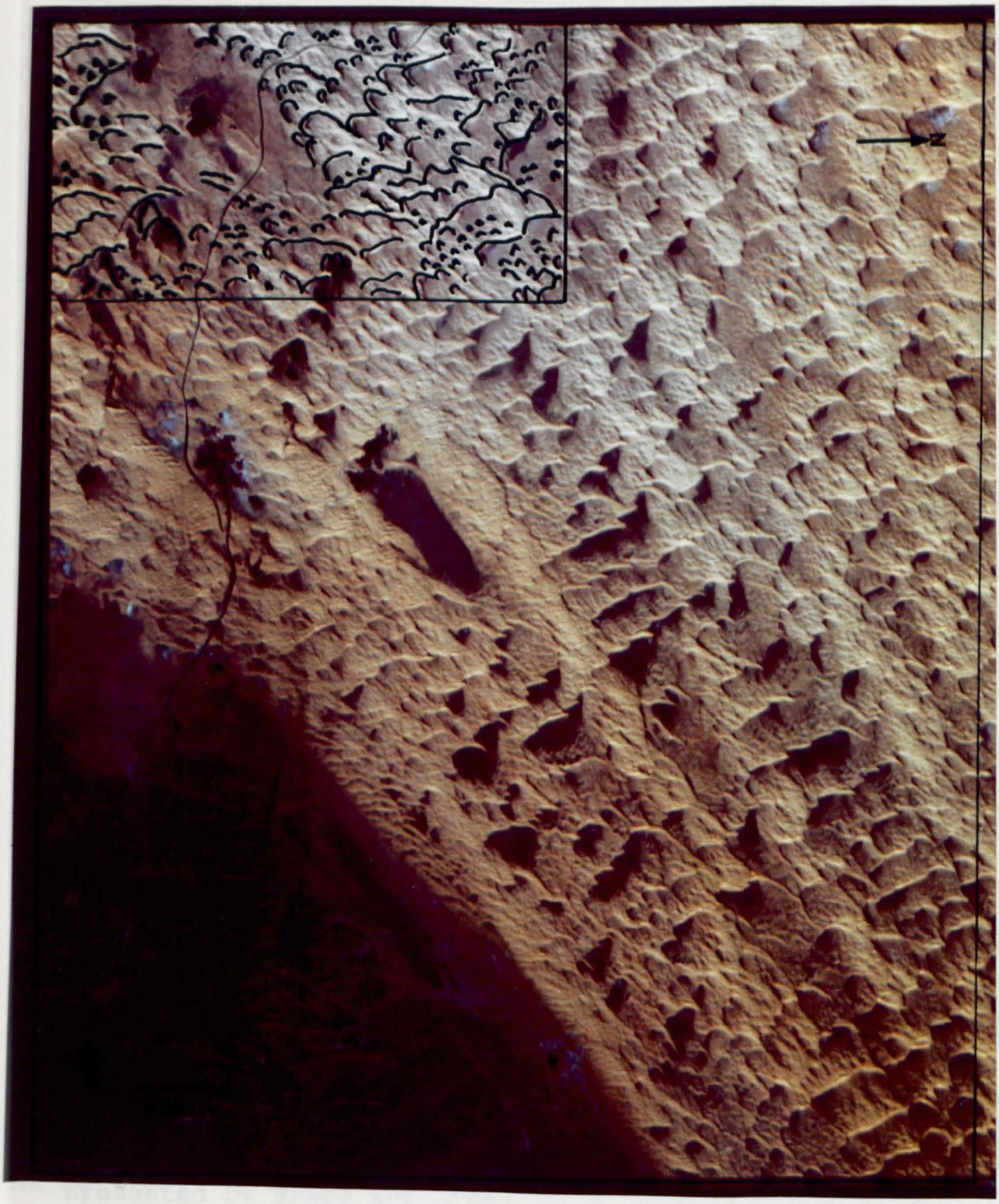


Figure 6.13 Landsat TM (169/41) full resolution false colour composite subscene showing the same area and printed at the same scale as in Figure 6.12. The small barchan dunes are clearly defined.

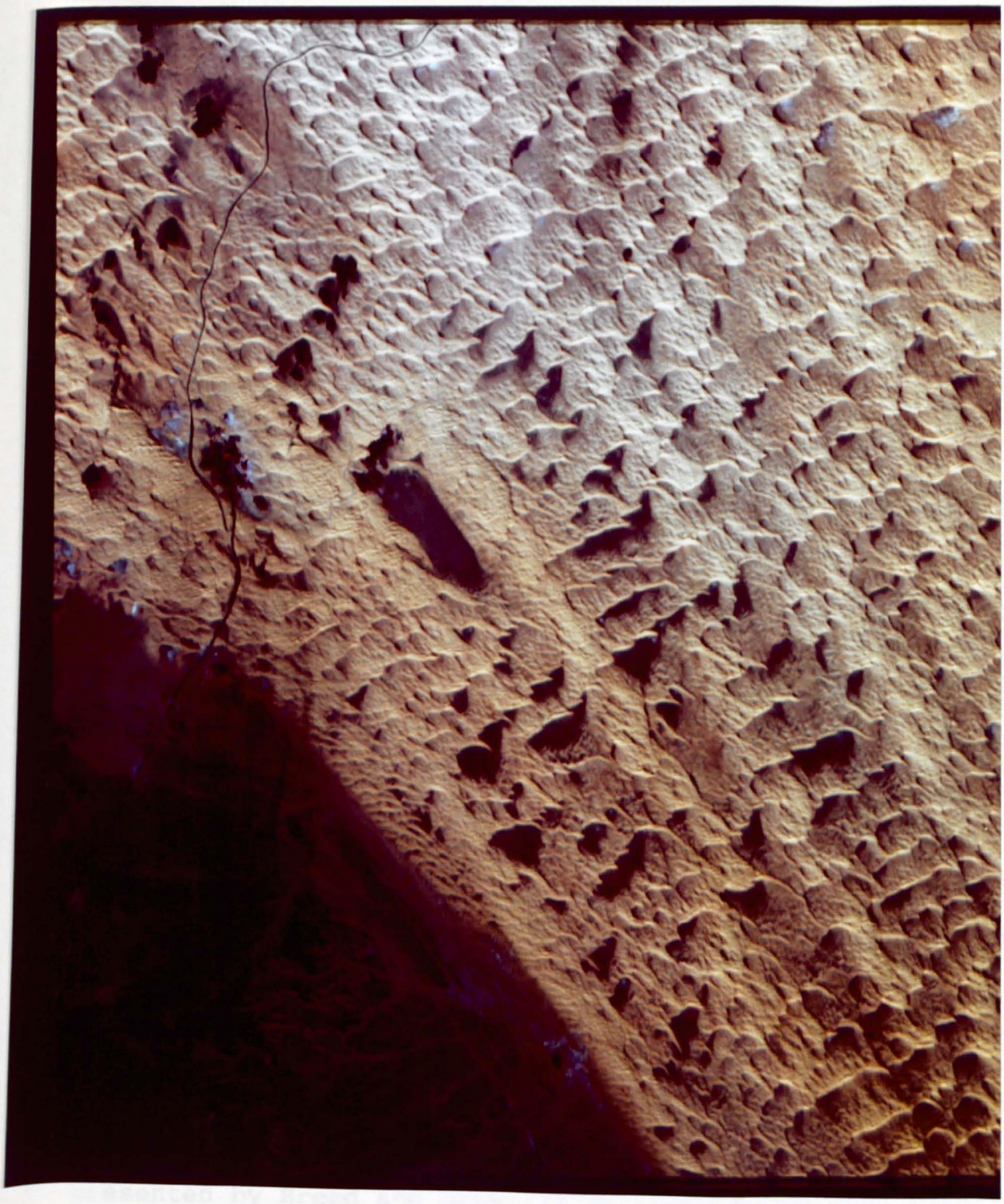


Figure 6.13 Landsat TM (169/41) full resolution false colour composite subscene showing the same area and printed at the same scale as in Figure 6.12. The small barchan dunes are clearly defined.

10 metres high, whereas the large dunes are commonly more than 100 metres high (Whitney, et al 1984). No data is available for the dune widths in this area.

This case history demonstrated the advantages of high spatial resolution imagery in mapping small size dunes. The identification of small active dunes superimposed upon much larger (possibly stable) dunes, as illustrated in this area, helps in the comparison between paleo-wind and present wind regimes.

6.8 CASE HISTORY (4) RUB'AL KHALI: (DUNE HEIGHT MEASUREMENT)

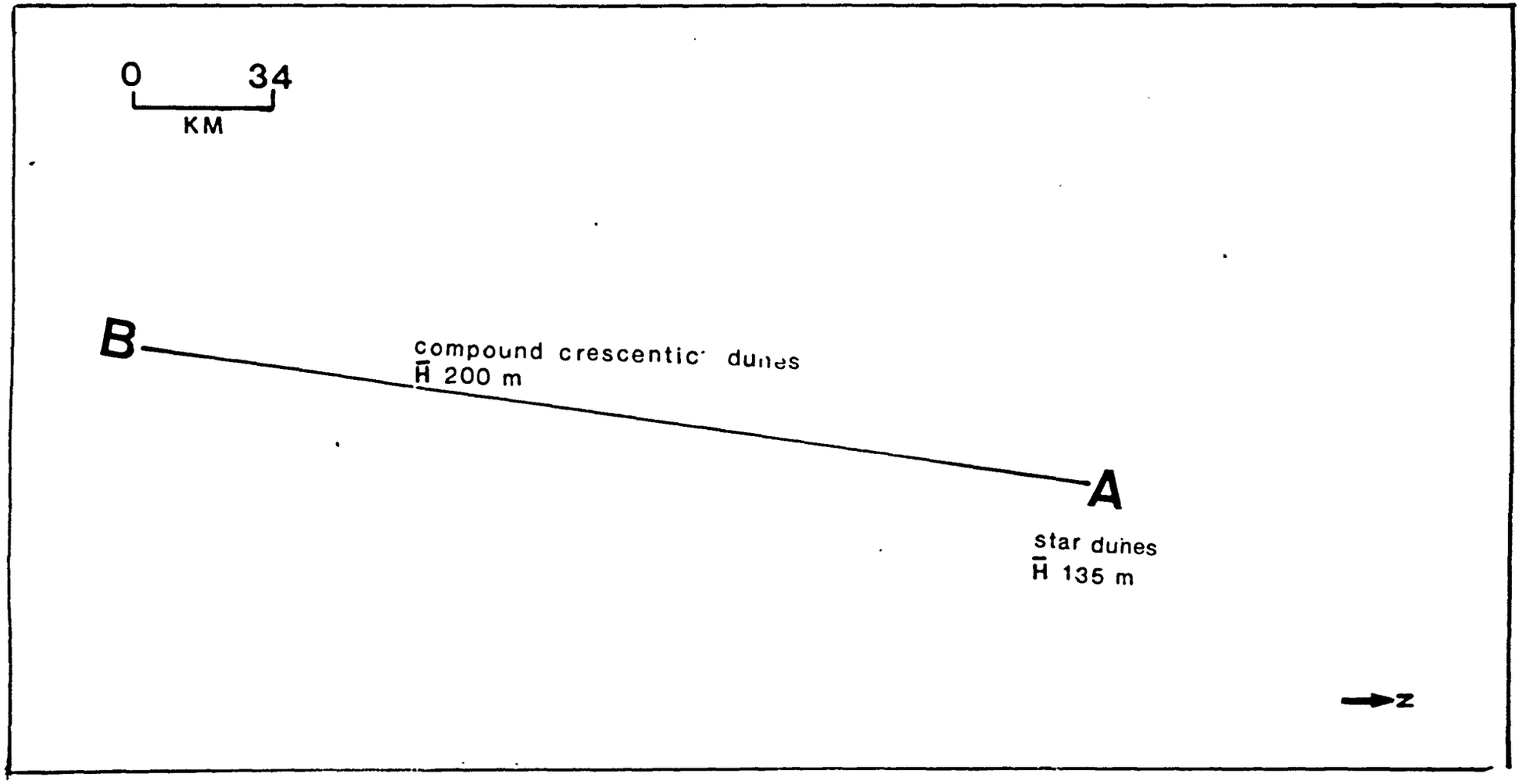
An area south east of the Rub Al khali (near Erq Al Mu taridah) between 23-21 degrees North and 54-55 degrees East was selected for dune height measurement using the LFC photographs. This area was described by Holm (1960) as consisting of giant crescentic massifs and star dunes. The giant crescentic massifs are refered to as compound crescentic dunes (Breed, 1979). Using the classification presented by Breed and Grow (1979) these dunes were referred to as compound crescentic dunes.

The area is coverd by a panchromatic LFC photograph with 80 % forward overlap, 2.0x vertical exaggeration, and a scale of 1: 778,000.

A subscene was selected to evaluate the stereo capability of

the LFC in measuring dune heights using the photgrammetric equipments at the University College-London (photogrammetry Department).

METHOD: One profile runing N-S as indicated on the photograph (Fig. 6.14) was selected for dune height measurement. Since no proper control was available, the scale was determined from the mean scale of the photographs. Four widely separated points were then allocated the same heights in order to define an arbitrary datum plane. Two models were set up on the Kern DSR11 to make the necessary measurements. On each model two widely separated points were pricked on one photograph. The distance between these points was measured using a ruler and the ground distance was calculated according to the given photo scale. These prick marks were used as plan control for the absolute orientation. The profile was measured using the Maps 200 data recording programs. The XYZ co-ordinates together with the distance along the profile were recorded on file. A graphical representation was produced by plotting the Z against the profile distance on the GP1 plotting table. Each profile was measured twice with the graphical records superimposed in different colours. Points were positioned on the crests of the dunes and the dune floors for height measurements. The height of the dunes was measured by subtracting dune floor points from dune crest points.


0 34
KM
B
compound crescentic dunes
H̄ 200 m
A
star dunes
H̄ 135 m
N

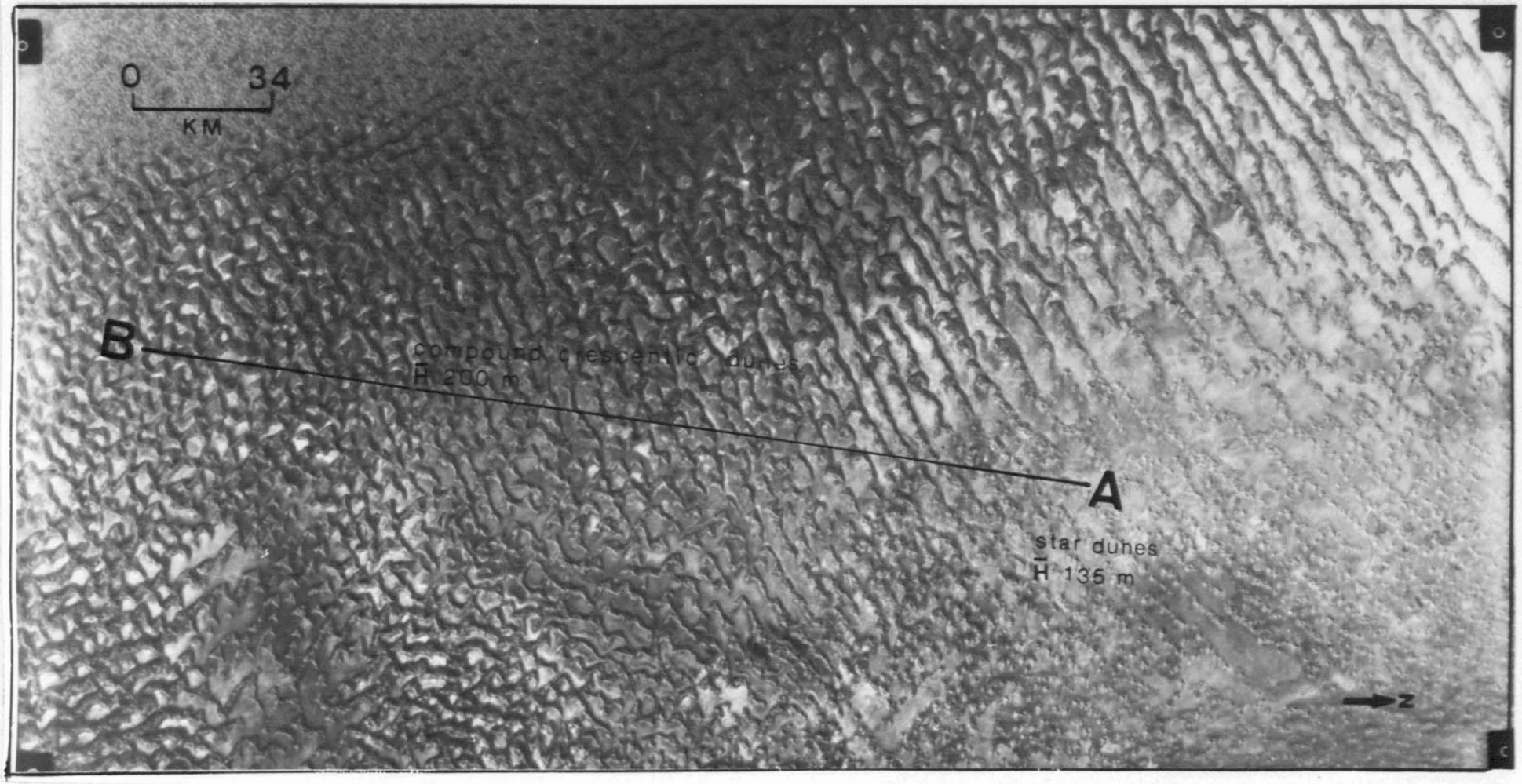


Figure 6.14: LFC panchromatic photograph used for dune height measurement. A-B is the measurement profile H̄ is average dune height.

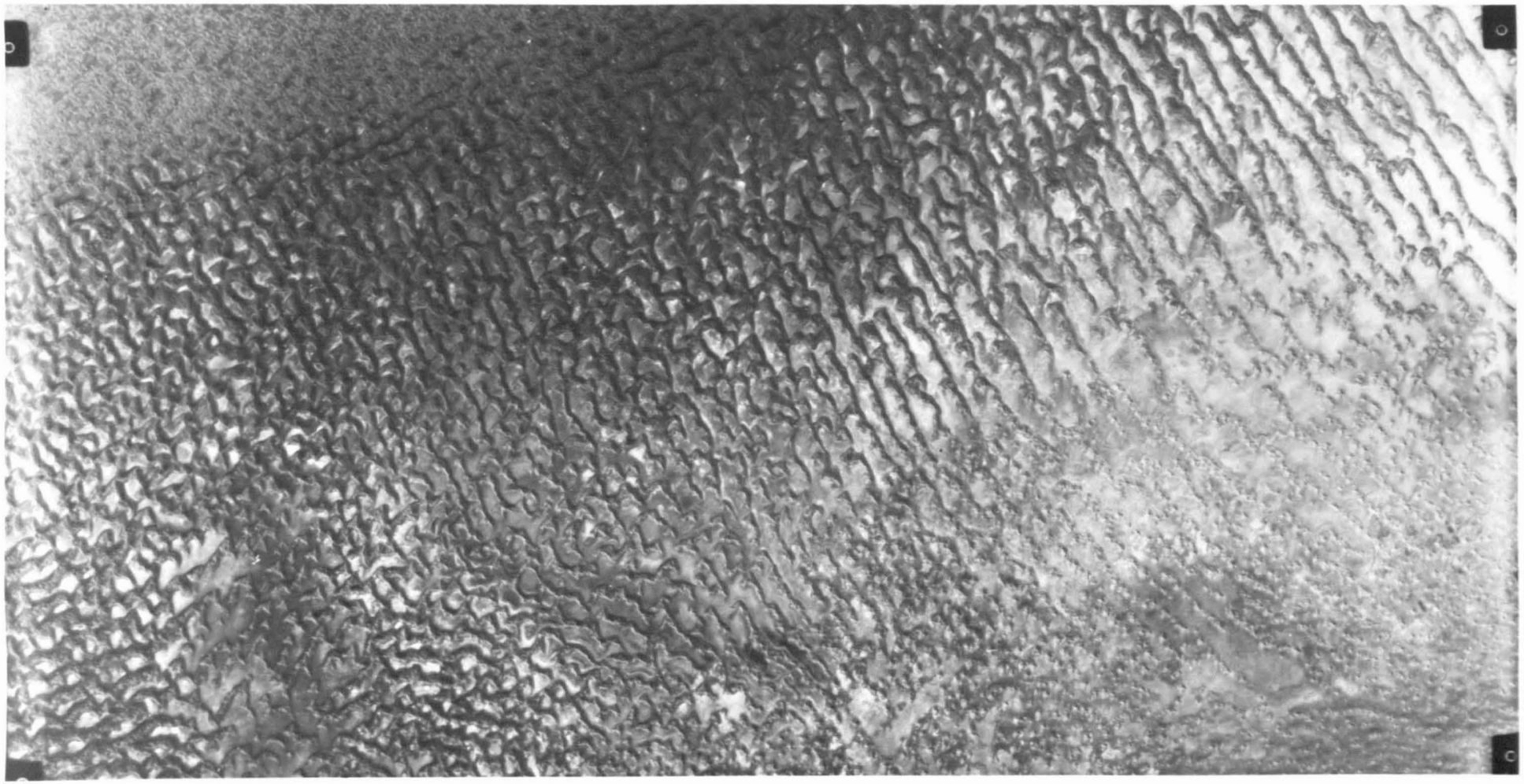


Figure 6.14: LFC panchromatic photograph used for dune height measurement. A-B is the measurement profile $\bar{H}$ is average dune height.

RESULTS: The heights of forty dunes were measured. Heights varied between 70 to 213 metres with an average of 130 metres. Repeated height observations showed a height precision of 15 metres. Accuracy of height measurements achieved in this investigation are comparable with those reported by other workers assessing LFC photographs for topographic mapping in other parts of the world (Newton, et al., 1986; Table 6.5).

Star dune heights ranged between 68 and 176 metres with an average height of 175 metres. Compound crescentic dune heights ranged between 145 and 213 metres with an average height of 200 metres. Appendix (5) contains all measurement results. Table 6.6 is a summary of these results.

There are few publications which report dune height measurements in this area. Thesiger (1948) reported heights of 153 to 213 metres for some compound cresentic dunes. Holm (1960) surveyed some dunes and found that no dune height exceeded 200 metres. He reported that star dune are seldom less than 50 metres in height and range up to 150 metres in Arabia. However, star dune heights in the southeastern Rub' al Khali have not been surveyed. The measured heights of the dunes from the LFC photographs seem to agree reasonably with Holm's and Thesiger's measurements.

This case history illustrated the value of obtaining space photography with stereoscopic capability for measuring dune

	Height (m)
Theoretical	21.08
Reported (Newton et al, 1986)	14.9
Actual	15.0

Table 6.5: Large format camera accuracies.

Dune Type	Range of Dune Height (m)	Average Dune Height (m)
Star dunes*	68 - 176	135
Compound crescentic dunes*	145 - 213	200

Table 6.6: Dune height measurements in the south-eastern Rub' al Khali based on LFC photographs.
* 40 dunes were measured.

heights especially in remote and hostile areas such as the Rub'al Khali.

6.9 CASE HISTORY (5): AD DAHNA & WAHIBA SAND SEAS: (RADAR IMAGERY INVESTIGATION)

Two test sites were selected for SIR-A image interpretation; an area south west of the Wahiba Sand Sea in Oman and the northern Ad Dahna.

The investigated area in the Wahiba Sand Sea is shown in Figure 6.15. The most prominent features of the sand sea are the large linear dunes which trend about N-S and the smaller crescentic dunes trending about NW-SE. Cresentic dunes occur along the coast and linear dunes are farther inland. Linear dunes have a mean width of 1.1 km, and an average length of 31.3 km, and are spaced at an average of 1.6 km apart (Breed, et al, 1979). According to Glennie (1970) these dunes are Pleistocene features and do not correspond with the trends of present - day winds. In contrast, the cresentic dunes are active with average heights of 30 metres and a spacing of 500-1000 metres (Brunsden & Cook, 1986).

SIR-A imagery shows two different dune types; linear dunes at the centre of the image and cresentic dunes near the coast (Fig. 6.16). Linear dunes are fairly bright parallel ridges while the crescentic dunes are slightly less bright than the ridges. The look direction of this imagery is from the North and the look angle (incidence angle) at the centre is approximately 47 degrees.

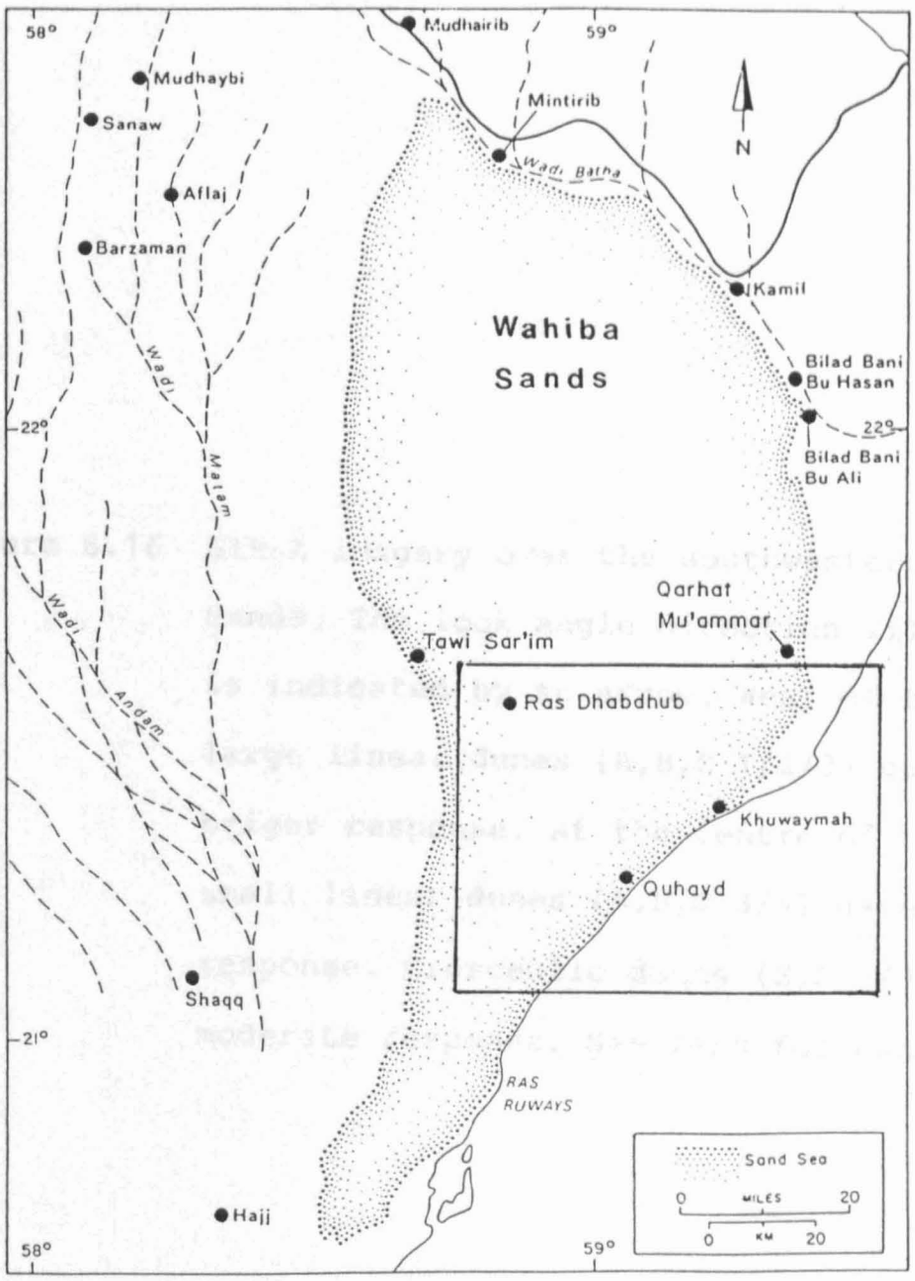
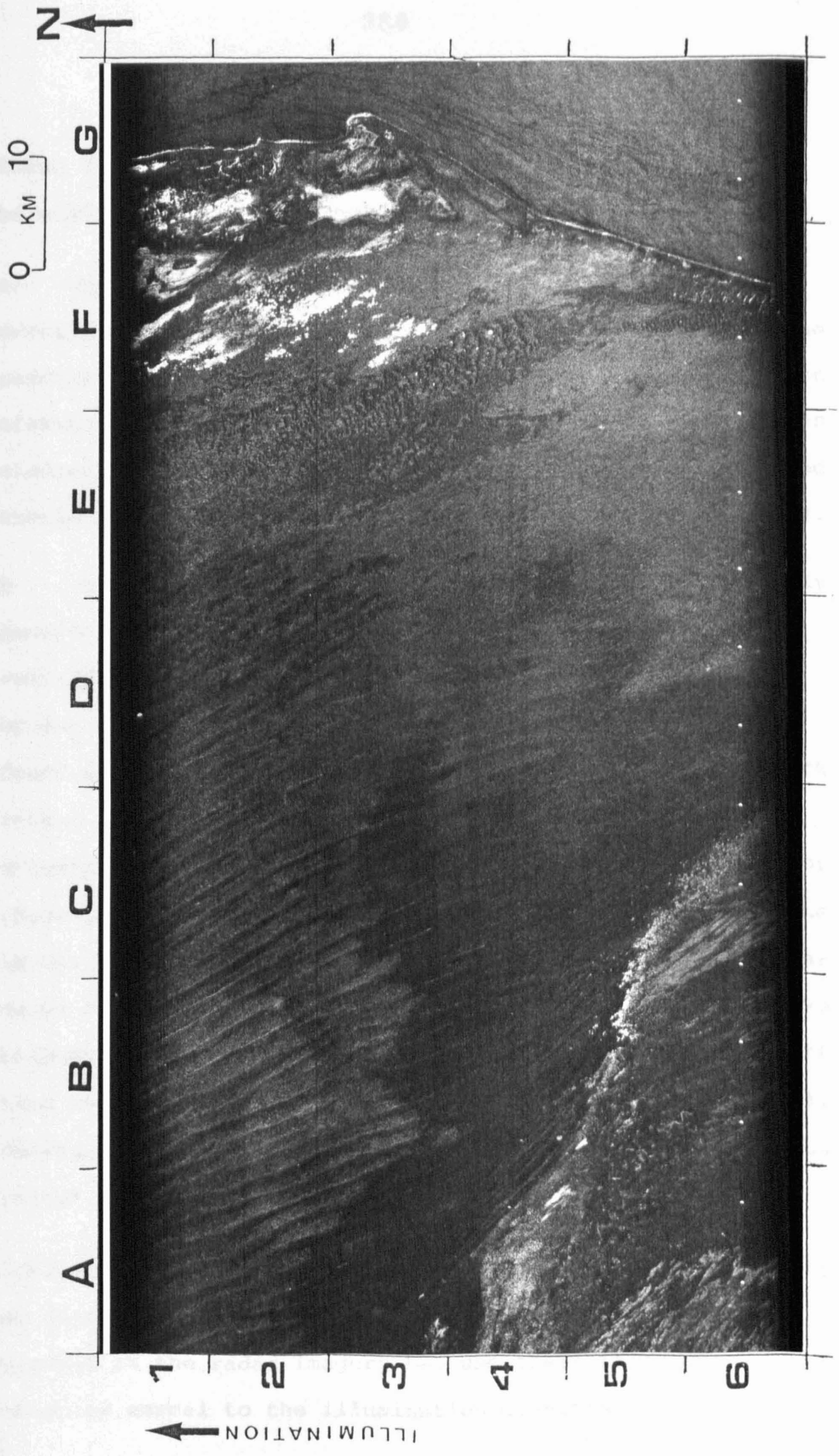


Figure 6.15 Location map of Case History (5) in the Wahiba Sands.

Figure 6.16 SIR-A imagery over the southwestern Wahiba Sands. The look angle direction (illumination) is indicated by an arrow. West of the image, large linear dunes (A,B,C 1/2/3) gave a fairly bright response. At the centre of the image, small linear dunes (A,B,C 3/4) gave a dark response. Crescentic dunes (E,F 2/3/4) show a moderate response. See text for explanation.


N
A
B
C
D
E
F
G
0 KM 10
1
2
3
4
5
6
ILLUMINATION

These linear dunes were detected on the SIR-A imagery because of the following reasons :

a- The spacing between these dunes is about 1.6 km which exceeds the limit set by Blom and Elachi (1981) for the recognition of such features (about 3 or 4 resolution elements). In this area the spacing is about 40 resolution elements (Spatial resolution of SIR-A is 40 metres) and should therefore be easily discernible on the SIR-A imagery.

b- Although the main trend of these dunes is roughly parallel to the SIR-A look direction, the size and the vertical relief of the crests and the troughs gave the bright returns from the dunes. On the other hand, linear dunes on the lower left hand side of the imagery gave a dark return despite the fact that both dunes have the same orientation. There is a difference in the radar return for these dune types. The reason may be due to the marked dune height difference between the two similar dunes. Linear dunes seen on the right hand side of the imagery have heights between 60 to 100 metres while those on the left hand side are only 10 metres high (Brunsden & Cooke, 1986). Because of this topographic variation, linear dunes of low relief produced a dark return on this imagery.

Crescentic dunes on the lower right hand side of the imagery produced a moderate to bright return. These dunes are visible on the radar imagery because their faces are oriented normal to the illumination direction.

The investigated area in Ad Dahna Sand Sea area is shown in Figure 6.17. Broad sheets of sand and linear dunes trending N-S are characteristic of this area. These dunes form parallel ridges separated by rocky interdune corridors and extend for tens of kilometres southward.

In Ad Dahna area, SIR-A imagery clearly shows linear dunes, sand sheets, and exposed bedrock (Fig. 6.18). These deposits are depicted in different image tones. These tones reflect the actual surface roughness of the different aeolian deposits.

Normally, the relationship of wavelength and incidence angle to micro-scale roughness is described by the Rayleigh criterion, which considers a surface to be smooth if:

$$h < \frac{\lambda}{8 \cos 0}$$

where h = average vertical height of micro-relief

λ = operating radar wavelength

0 = incidence angle of the radar beam

By solving for h, the theoretical breakpoint or boundary between radar-smooth and radar-rough is defined for a given wavelength and incidence angle. Hence, surfaces with a value of h less than the calculated value should produce dark image tones (radar-smooth surface), and surfaces with a value of h greater than calculated value should be

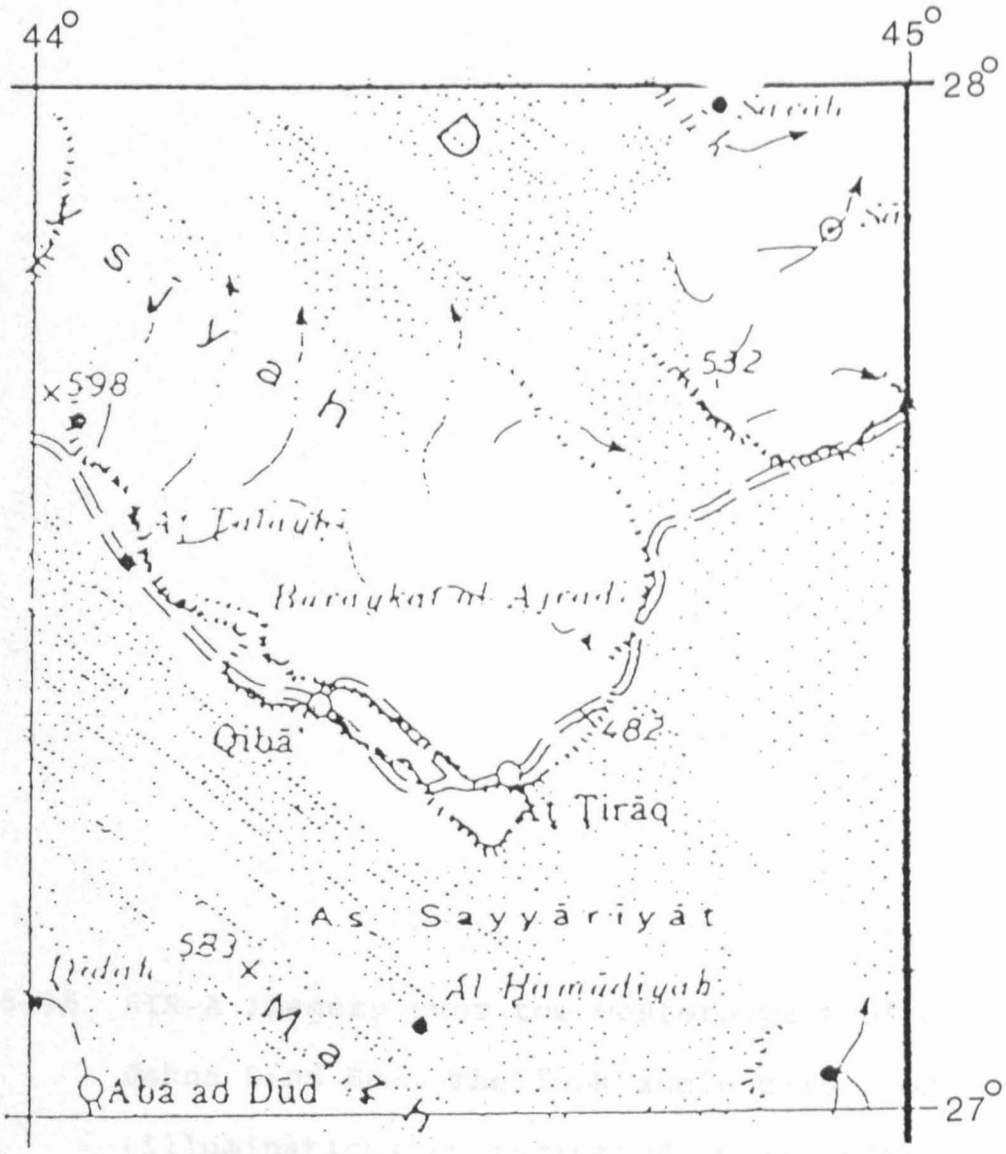


Figure 6.17 Location map of Case History (4) in Ad Dahna Sand Sea.

Figure 6.18 SIR-A imagery over the western part of Ad Dahna Sand Sea. The look angle direction (illumination) is indicated by an arrow. Linear dunes (A,B,C 1/2/3/4/5/6) and sand sheets (E,F 2/3/4) gave a dark image tone. Areas with bright response are bedrock outcrops.

N
A
B
C
D
E
F
G
1
2
3
4
5
6
ILLUMINATION
0 KM 10

responsible for light image tones (radar-rough surface). For SIR-A system, h equals 4.3 cm (Berlin, et.al., 1985).

Linear ridges and sand sheets are depicted in very dark image tones (h < 4.3 cm, i.e. radar-smooth surfaces) because there were no steep slopes oriented normal to the incident radar beam or an adequate vegetation density that would produce a strong return to the antenna (Blom & Elachi, 1981). The interdune areas that are floored with pebbles and cobbles are depicted as gray tones in the imagery (intermediate rough-surface). The exposed bedrock with little or no drift sand is detected as very light tone (radar-rough surface).

A factor which might influence the image tone is variation in the sand moisture. The area investigated is assumed to have been dry at the time of the Shuttle overpass in November 1981 because only about 25 mm of rainfall were recorded in the region between November 1980 and March 1981 (Berlin, et.al., 1985). In addition, no precipitation was recorded between April and November. The measured moisture content of sand in this region was less than one percent (Berlin, et al., 1985). This would have resulted in a low complex dilectric constant of value 2.5 to 3.5. This factor is probably too small to alter the radar signal and hence the image tone.

6.10 DISCUSSION AND CONCLUSION

Table 6.7 summarizes the spatial resolution limitations of

Type of Sensor	Sizes of Dunes Located in Low Contrast Areas in Metres				Sizes of Dunes Located in High Contrast Areas in Metres			
	5-10	10-70	70-200	>200	5-10	10-40	40-100	>100
Landsat MSS	NR	NR	NR	✓	NR	NR	NR	✓
Landsat TM	NR	NR	✓	✓	NR	NR	✓	✓
LFC	NR	✓	✓	✓	NR	✓	✓	✓
SIR-A	NR	NR	✓	✓	NR	NR	✓	✓
B&W Aerial Photograph 1:60,000-1:80,000	NR	✓	✓	✓	✓	✓	✓	✓
Infra-red Aerial Photograph 1:10,000	✓	✓	✓	✓	✓	✓	✓	✓

Table 6.7: Comparison between different sensors for mapping dunes of various sizes. NR = not recognisable.

the investigated airborne and spaceborne images for sand dune mapping.

Broad lineation, regional trends, and dune field boundaries in sand seas are best recognized from Landsat imagery. The consistent scale and the area coverage in a Landsat scene (185 x 185 km) provides a good basis for aeolian sand type mapping and other associated superficial deposits (Sabkhas, bedrock, etc). The major problem encountered in using Landsat imagery for mapping aeolian features is the low spatial resolution of the images. Although Landsat TM imagery offers a higher resolution (30 m) than MSS imagery (80 m), small parabolic dunes found in low contrast areas (average width is 70 m) cannot be detected in TM images.

The LFC photographs provided an improvement in resolution and in the extent of the area covered in one photograph (306 x 260 km). Additional advantage of the LFC photographs is the stereo capability which permits measurement of dune heights to an accuracy of about 15 metres. The high spatial resolution of the LFC photographs helped in mapping small size dunes (10 metres and above) which are beyond the resolution offered by Landsat MSS and TM imagery. However, there are some restrictions in using LFC photographs in sand dune mapping and height measurement which can be summarized as follows:

(i) In Saudi Arabia, the LFC photographs were taken in

black and white. This restricted the separation of sand from the associated superficial deposits surrounding it. If natural colour or false colour infrared photographs were available, the discrimination of sand through its yellow colour would make the interpretation of sand bodies in the LFC photographs easier.

(ii) The sun angle was about 55 degrees when the photographs were taken. This relatively high angle accounts for the low definition of sand dunes. In some photographs, sand deposits appear washed out and it was very difficult to distinguish sand dunes from surrounding sediments. This problem may be due to the difference between the angle of repose of sand dunes (about 32 degrees) and the sun angle at which the photographs were taken. Low sun angle illumination provides shadows that clearly delineate the dunes. A sun angle close to the angle of repose of sand dunes will be ideal for enhancing dune relief provided the dunes are aligned transversely to the illumination azimuth.

(iii) Although the LFC was designed to have the capability for stereo viewing, dunes with heights less than 20 m could not be measured because of limited vertical exaggeration of the LFC photographs caused by spacecraft altitude.

Radar imagery provided a good basis for mapping dune types. For sand dune type mapping the SIR-A imagery showed no

advantages over other forms of remotely sensed images. In fact, Landsat MSS imagery with lower spatial resolution than the SIR-A imagery shows a better dune defintion. The limitations of the SIR-A imagery in sand dune mapping arises from restrictions in the radar look direction (one look direction). When imaging an area consisting of different dune shapes (e.g star and barchan dunes) more than one look direction is required to detect both dune types. The availability of more than one illumination direction will help in recognizing different dune types and in the understanding of dune structures. This information is required for inference of wind regimes responsible for the dune structures especially in unexplored regions. Another restricting factor in sand dune mapping is that imaging radar resolution must be adequate to detect the changing distribution of dune faces as a function of of dune morphology.

Aerial photographs were examined to complement or substantiate interpretations drawn from other forms of remote sensing data. Infrared aerial photographs of 1:10,000 scale were found to be extremely helpful in detecting small size dunes, and to delineate parabolic dunes. At scales of 1:60,000 and 1:80,000 panchromatic aerial photographs were useful in identifying narrowly spaced medium size barchanoid ridges and barchan dunes which were not recognizable in Landsat MSS or TM imagery. A scale of 1:25,000 will be extemely useful in sand dune mapping and in morphometric measurements such as dune height, width, length, and the

spacing between different dunes. At this scale, aerial photographs can be used as a ground truth for other remote sensing data.

CHAPTER 7

MEASUREMENT OF DUNE MOVEMENT

7.1 INTRODUCTION

Encroachment by wind blown sand is a major economic problem for industrial installations, road and airport maintainance, urban development and agriculture in eastern Arabia. Acquiring basic information on sand dune migration in desert areas is difficult and expensive.

The continuing expansion of towns, agriculture, industry, and transport infra-structure within arid lands has increased the awareness of the problems caused by blowing sand. Petroleum installations, industrial complexes, residential developments, transport and communication facilities, and agricultural projects require protection and maintainance.

The action of wind upon unconsolidated surficial sediments can cause severe engineering problems in areas of scarce vegetation. Dune movement can cause burial of roads and agricultural areas, and abrasion of natural and man-made structures. One such area, where such problems were encountered on a large scale, is the Jafurah sand sea located in the Eastern Province of Saudi Arabia. The Jafurah is a region of strong unidirectional winds, and abundant

sand dunes.

The difficulties of direct dune measurement on the ground and the cost of conducting full scale sand monitoring experiments in remote areas is a major handicap in producing reliable and applicable data on sand movement direction and rates.

In this chapter Landsat MSS imagery, aerial photographs and field data are assessed for monitoring sand distribution patterns and sand dune movement in the Jafurah Sand Sea, eastern Arabia.

Two test site areas were selected for this investigation. In the first test site, refered to as "Ad Dibbiyah", dune movement is examined using MSS imagery, aerial photography, and field observations. In the second test site, referred to as "Harad area", multi-temporal Landsat MSS imagery has been assessed for monitoring sand dune distribution patterns.

Estimates of dune movement have been made for a thirty four year period (1949-1983), by registration and comparison of individual barchan and barchanoid ridge positions on several sets of aerial photographs at 1:60,000 and 1:80,000 scales. Digital registration of Landsat MSS imagery dated 1972 and 1984 has also been investigated as an aid to measurement of dune movement rates. Field measurement of dune movement during a one year period was used as a ground check for the aerial photographic and Landsat MSS imagery investigation.

7.2 SAND MOVEMENT STUDIES

Bagnold (1941), and Wilson (1971) promulgated theories on the mobility of wind-blown sand in deserts. Lettau & Lettau (1969), and Fryberger & Ahlbrandt (1979) developed equations representing sand drift rates. The movement of sand has never been measured directly on a regional basis except for a study by Fryberger, et al (1984; Appendix 2) who monitored sand drift rates and Jafurah dune movement directly in the field. The author of this thesis participated in that study.

Aerial photographs and Landsat MSS imagery have been used by many workers in the study of arid and semi-arid areas. Finkel (1961) studied the movement of barchan dunes using aerial photogrammetry on the southern coast of Peru. Brera (1979) utilized multi-temporal Landsat MSS imagery to investigate dune movement between 1972 and 1976 in the Sahara desert of Libya. He concluded that Landast MSS imagery can be used to measure sand dune movement of greater than 1 km if proper image analysis and registration techniques are used. His Landsat image based measurement lacks the necessary supporting field data. Moreover, the claim that some dunes in the Sahara desert, according to his measurement, travel annually about 5 km is doubtful for the following reasons:

First, there was no clear definition in his study of what exactly was measured (dune movement rate or sand pattern shifts). If individual dune movement was measured then the

results achieved in his study are different from those reported by others in other deserts of the world. Maximum annual dune movement reported in Mauretania by Sarnthein and Walger (1974) was 63 metres. On the other hand, if sand pattern changes were investigated then results achieved are more plausible.

Secondly, the image to image registration accuracy achieved in this study was not reported. Hence measurements reported become meaningless.

Kerr & Nigra (1952) measured dune movement from aerial photographs between 1934 and 1949 in Al-Hofuf area of Saudi Arabia. They found that small crescentic dunes (5-7 meters high) move approximately at the rate of 20 metres per year. The larger barchans (averaging 12 metres in height) move approximately 6-10 metres per year. They concluded that dune movement is inversely proportional to the height of the slipface. However, Watson (1985) measured the movement of 68 barchan dunes north of Al-Hofuf in the Jafurah using aerial photographs (between July 1979 and June 1980) and found no significant correlation between dune height and dune movement. Abolkhair (1981) studied sand movement in Al-Hasa, Saudi Arabia and found that dune movement ranged between 3 to 12 metres per year. Hunting Surveys LTD (1977) measured dune movement using aerial photographs in Qatar and reported an average movement of 8 metres per year. Jones, et al (1986) studied blowing sand and dust hazard in Northern Arabia using remote sensing imagery, meteorological data, geomorphological mapping and process monitoring. Bofah and Al-Hinai (1985) monitored different designs of fences used for sand control in the Jafurah Sand Sea.

The movement of sand dunes has never been measured using co-ordinated Landsat MSS imagery, aerial photographs, and actual field measurement. This chapter reports an integrated study of dune movement in the Jafurah Sand Sea, based on field measurement, multi-temporal MSS images and aerial photographic investigation.

7.3 SELECTION OF THE STUDY AREAS

Two test site areas, located in the Jafurah Sand Sea, were selected for this investigation; Ad Dibbiya area and Harad area. Two approaches to investigating dune movement were applied in the two test site areas. The first approach emphasises the quantitative measurement of dune movement using Landsat MSS imagery, aerial photographs, and field data. This methodology was employed in the Ad Dibbiyah area (sabkha substrate) because of the clear defintion of the dunes seen in the Landsat images and the aerial photographs.

The second approach emphasises the qualitative investigation of temporal dune pattern changes (if any) using Multi-temporal Landsat MSS images. This methodology was applied in Harad area because of the clear distinction between the investigated dune field boundaries and the underlying and interdune surficial deposits (gravel).

7.4 MATERIALS USED IN THE INVESTIGATION:

MAPS: Topographic and geologic maps (USGS) at a scale of 1:500,000 were used at the first stages of the research for selection of test site areas and for locating ground control points. However, as the research progressed it was found that ground control points identified in the maps could not necessarily be seen on Landast images. Hence, These maps were not used for selection of control points.

AERIAL PHOTOGRAPHS: Multi-temporal black and white aerial photographs (1949 & 1983) at scales of 1:60,000 and 1:80,000 were used for sand dune movement measurement. These photographs were used for selecting test site areas and as ground truth for Landsat investigations.

LANDSAT MSS IMAGES: Multi-temporal Landsat MSS images used for dune movement measurement included: Landsat (1) scene 176/42 acquired Sept.4.1972 and Landsat (5) scene 164/42 acquired Jan.15.1984.

7.5 GROUND CONTROL POINTS FRAMEWORK

Because tracking and spacecraft attitude data are not known precisely, ground control points (GCP) are used to obtain external refernce information. A GCP is a physical feature detectable in a scene whose location can be located to a certain degree of accuracy.

Ground control points are required in any analytical or

digital image to image registration. Two types of points are available for any investigation: (a) natural points which show distinct ground details such as airports, highway intersections, land-water interfaces, geological and field patterns, etc; and (b) artificial points which are marked in topographic maps and then transferred to the imagery with the help of a transferring device. Only natural points were used in this study due to its simplicity and the lack of accurate topographic maps.

Figures 3.3 (Chapter 3) & 7.13 show the distribution and location of ground control points selected for Ad Dibbiyah and Harad test sites.The process used in this investigation for generating ground control points in the investigated images can be described as follows:

(i) Selection of cloud-free Landsat MSS scenes. This helps in identifying the maximum available GCPs in each Landsat scene.

(ii) Landsat MSS band 1 (0.4-0.5 μm) was used to inspect for haze in the scene. To avoid haze detected in some images, Landsat MSS band 4 (0.8-1.1 μm) image was used for locating GCPs since this infrared imagery is least affected by haze. However, in haze-free scenes other MSS bands can be used for locating GCPs.

(iii) The search for GCPs was concentrated in areas of high-contrast features. Such areas exist on land-water

and sand-sabkha boundaries. This is well illustrated in case history (1) - Ad Dibbiyah.

(iv) Selection of GCPs was based on features which can be easily identified on other imagery of the same area and must not change with time.

(v) In Ad Dibbiyah area 12 GCPs were identified in Landsat scenes (Figure 3.3). The points identified are motorway intersections, coastal areas such as headlands and the tips of shorelines, and the bedrock-sabkha boundary. In Harad area, 6 control points were located (Figure 7.13).

(vi) After selection of GCPs, a digital image to image registration then followed. The procedure for digital registration is discussed in Chapter 3.

The search for ground control points in images of Saudi Arabia was not an easy task especially in sandy areas. This was mainly due to the difficulty of finding fixed points among mobile sand dunes. In this investigation it was possible to identify 12 GCPs in Ad Dibbiyah only because it is located near a residential area. In very remote sand seas, such as the Rub'al Khali, with no artificial land marks, the search for GCPs becomes more difficult.

7.6 AD DIBBIYAH AREA: CASE HISTORY (1)

Ad Dibbiyah area selected for this investigation lies in north central Jafurah (Fig.7.1). The reasons for the

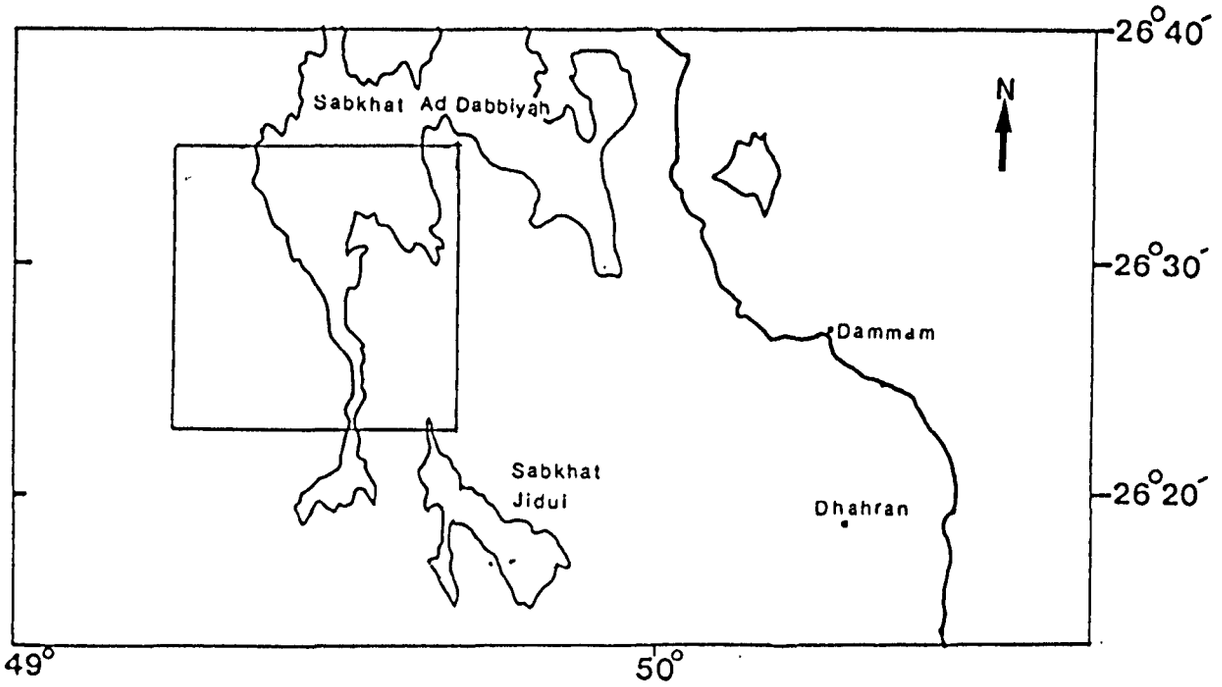


Figure 7.1 Location map of Case History (1).

selection of this area were based on the following:

(i) Investigated dunes in the area are all active dunes thus creating a good case for determining their behaviour (rate and direction of movement if any).

(ii) Investigated dunes are all located on a sabkha substrate. Thus dunes can be distinguished easily in aerial photographs and Landsat MSS imagery because of the high contrast between sand (bright) and sabkha (dark).

(iii) Investigated dunes can be identified easily in successive images because they are either found in isolation or the spacing between them is wide. The average dune spacing in this area is 500 m. Compacted dunes (dune spacing less than 200 m) cannot be distinguished in Landsat MSS imagery because of spatial resolution limitations (see Chapter 6 on the discussion of resolution).

(iv) The area was represented in both Landsat MSS imagery and aerial photographs.

(v) The area was accessible for field studies.

The study area is located in the Jafurah Sand Sea, an elongate, 30-250 km wide sand sea, extending down the western side of the Arabian Gulf, merging southward into the sands of the Rub'al Khali. Tertiary gravels, sandstones, and lime marls form the sub-stratum and exposed locally within the sand sea and on the western boundary of the Jafurah.

Wind deposits consist of dunes, interdunes, sandsheets, and aeolian silica sand sabkhas. Most of the dunes are of the barchanoid type which includes barchans, barchanoid ridges, transverse ridges, and dome dunes. Two other common types of vegetationally controlled dunes found in the study area are the parabolic dunes and the obstacle or "coppice" dunes. Dune heights average 5 to 12 metres. Crests of dunes are usually very active and unvegetated; however, some vegetation commonly grows on the windward slope of some dunes.

Dunes in the study area exist in isolation, or in dune complexes, oriented with long axes transverse to the wind. Dune complexes are efficent subregional traps for sand, and thus tend to starve areas of sand downwind. A result is that sabkhas in many areas exist downwind of dune complexes (or large individual dunes).

Sand dunes in the region constitute the least stable aeolian terrain. Although the dunes are relatively stable in size and shape, the rapid advance of the barchans, barchanoid ridges, transverse ridges, domes, and parabolic dunes of the area creates a principal cause of sand control problem.

Sabkha deposits are most common along the coast and along the western margin of the Jafurah. Distribution of sabkhas in the study area is controlled by topography, with sabkhas occupying low areas along the coast.

CLIMATE: The study area is typical desert with average annual rainfall of 65 mm. The wind direction is primarily from the north or northwest blowing southward towards the Rub'al khali (Empty Quarter). Wind reversals occur mainly during winter, causing reversed slipfaces on the crests of dunes, but having little effect on overall sediment transport (Fryberger. et al, 1984). The magnitude of wind velocity is varies seasonally with maximum occurring between May and July (locally termed the "Shamal").

7.7 LANDSAT MSS INVESTIGATION

Two Landsat MSS images, representing cloud free scenes 176/42 (Landsat 1), acquired (Sept.4 1972) and 164/42 (Landast 5), acquired (Jan.15 1984) were used to represent a reasonable period of time (12 years) for investigating dune movement. Details on the methodology and the image processing technique used in this investigation are given in Chapter 3 and in Al-Hinai & Moore (1986; Appendix 3). In this section only the results of the investigation are discussed.

DIGITAL REGISTRATION ACCURACY: Table 7.1 lists the residual errors of the pixel co-ordinates (column and line number) for each selected GCP. The results showed temporal registration error (residual error) of 0.7 to 0.8 picture elements (pixels) or 56 to 64 metres. The low accuracy in the registration of this investigation is mainly due to the

Control Point	Residual Error (Pixel)	Residual Error in Metres
1	0.70	56
2	0.80	64
3	0.75	57
4	0.90	72
5	0.70	56
6	0.80	64
7	0.90	72
8	0.70	56
9	0.90	72
10	0.80	64
11	0.75	60
12	0.80	64

Table 7.1: Residual error of Ground Central Points (GCPs) Registration. Numbers represent the difference between Pixel Co-ordinates (column and line numbers) for each GCP.

following:

First, the lack of sufficient number of fixed points in active dune fields. There is no specific number reported in the literature for achieving high accuracy because of variations between different geographic locations. Bernstein, (1983) used 69 ground features per scene in an experiment for digital registration of multitemporal imagery in Washington D.C. He reported a residual error of less than 0.24 picture element (19.2 m) and less than 0.11 picture element in line location (8.8 m) for 90% of the features. This proves that higher accuracy can be achieved if sufficient GCPs can be located.

Secondly, the relatively low resolution of the Landsat MSS imagery proved to be a handicap for detecting small size features usually found in deserts. Such features include small size oases (dimension less than 80 x 80 m) or small size dry ponds could be used as control points in desert regions. In the Ad Dibbiyah area several small oases exist but they could only be distinguished in aerial photographs of scale 1:10,000 and up to 1:60,000. It was not possible to transfer such features to Landsat MSS imagery because of geometric and scale variations between aerial photographs and Landsat MSS imagery.

DUNE MOVEMENT MEASUREMENT RESULTS:

Table 7.2 lists the results obtained from Landsat MSS

Dune No.	ΔX (Pixel)	ΔY (Pixel)	Dune Displacement (Pixel)	Dune Displacement (m)	Direction of Dune Movement	Comments
1	0	1	1	80	SE	
2	-	-	-	--	--	Dune not recognised
3	1	0	1	80	SE	
4	0	0	-	--	--	
5	1	1	1.4	112	--	
6	-	-	-	--	--	Dune not recognised
7	-	-	-	--	--	Dune not recognised
8	0	1	1	80	SE	
9	0	0	0	--	--	
10	0	0	0	0	--	
11	0	0	0	0	--	
12	0	0	0	0	--	
13	0	0	0	--	--	
14	0	0	0	0	--	
15	-	-	-	--	--	Displacement not recognised
16	0	1	1	80	SE	
17	0	1	1	80	SE	
18	0	0	0	0	--	
19	0	0	0	0	--	
20	-	-	-	--	--	Dune cannot be identified
21	1	1	1	112	SE	
22	0	0	0	0	--	
23	-	-	-	--	--	Displacement not recognised
24	-	-	-	--	--	" " "
25	-	-	-	--	--	" " "
26	-	-	-	--	--	Dune not recognised
27	0	1	1	80	SE	
28	0	1	1	80	SE	
29	-	-	-	--	--	Displacement not recognised
30	0	1	1	80	SE	

Table 7.2: Measured values for dune movement obtained from Landsat MSS imagery (between 1972 and 1984). Location of dunes is given in Fig.3.5 . X and Y are Pixel co-ordinates of the crest of the dune.

imagery (between 1972 and 1984). Dune advance between 1972 and 1984 ranged between 0 to 1 pixel (0-80 metres). Field data in this area suggest a maximum dune movement of 8 meters per year. Hence, during the period between 1972 and 1984 (12 years) the dunes would have migrated about 96 meters, or approximately 1.2 of a pixel. Given the registration accuracy of 0.7 to 0.8 pixels, no reliable measurement could be achieved over this time period. Comparison of the results from Landsat investigation and field data suggest dune movements of 2-8 metres per year has occurred over the last 12 years.

7.8 AERIAL PHTOGRAPHIC INVESTIGATION

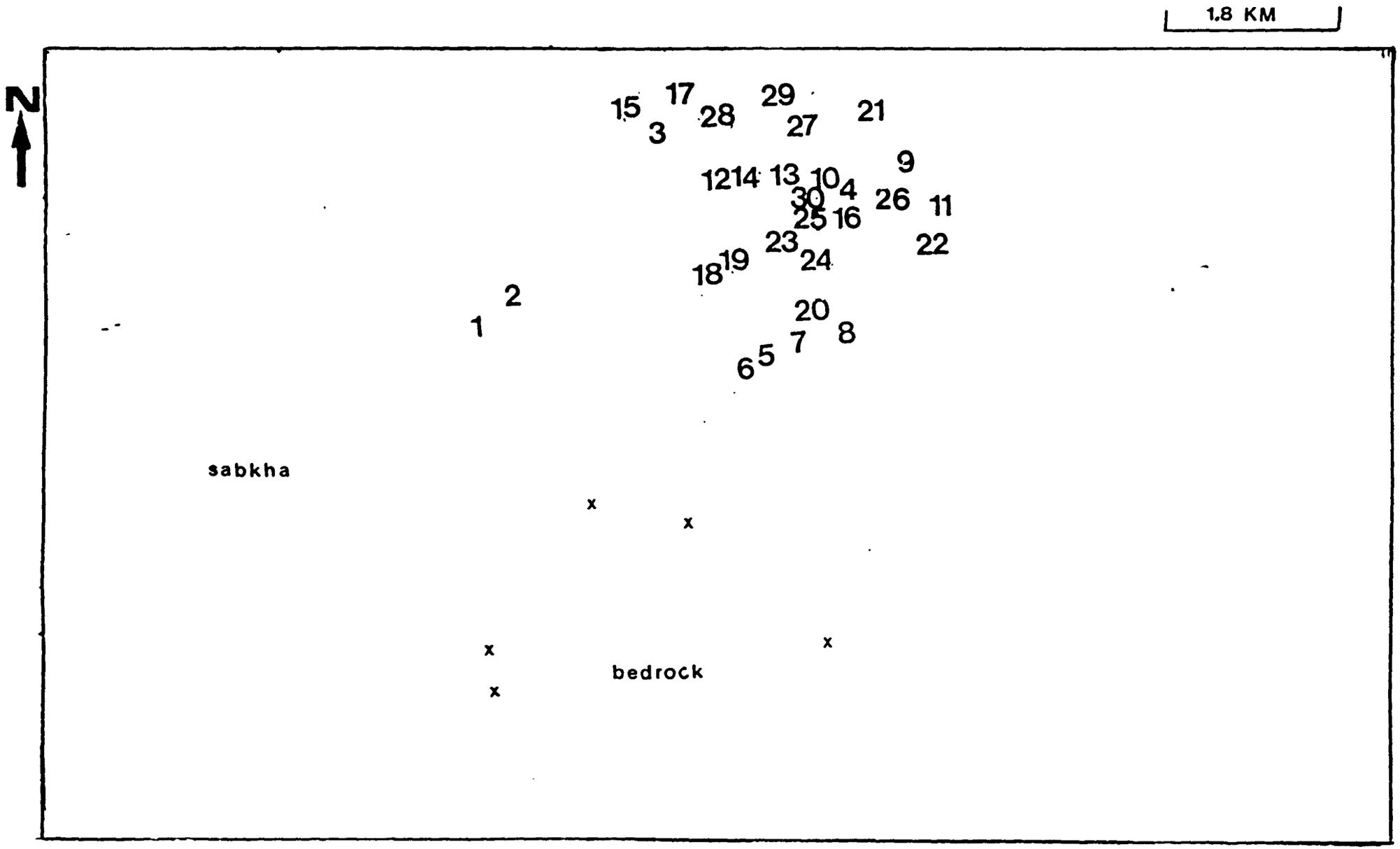
Aerial photos were used to determine the rate and direction of movement of sand dunes in northern Jafurah by photogrammetric measurements using prints of two different dates (1949 & 1983).

The entire area of eastern Arabia was flown in 1949 by Hunting Ltd. The scale of the photographs is approximately 1:60,000, (Fig. 7.2). Due to the clear desert atmosphere, there is good definition in the photographs and each dune is sharply outlined. Part of the area was re-photographed in 1983 to a scale of 1:80,000 (Fig. 7.3). These photographs were used for the photogrammetric measurements.

The purpose of this investigation is to measure the planimetric movement of identified sand dunes over the 34

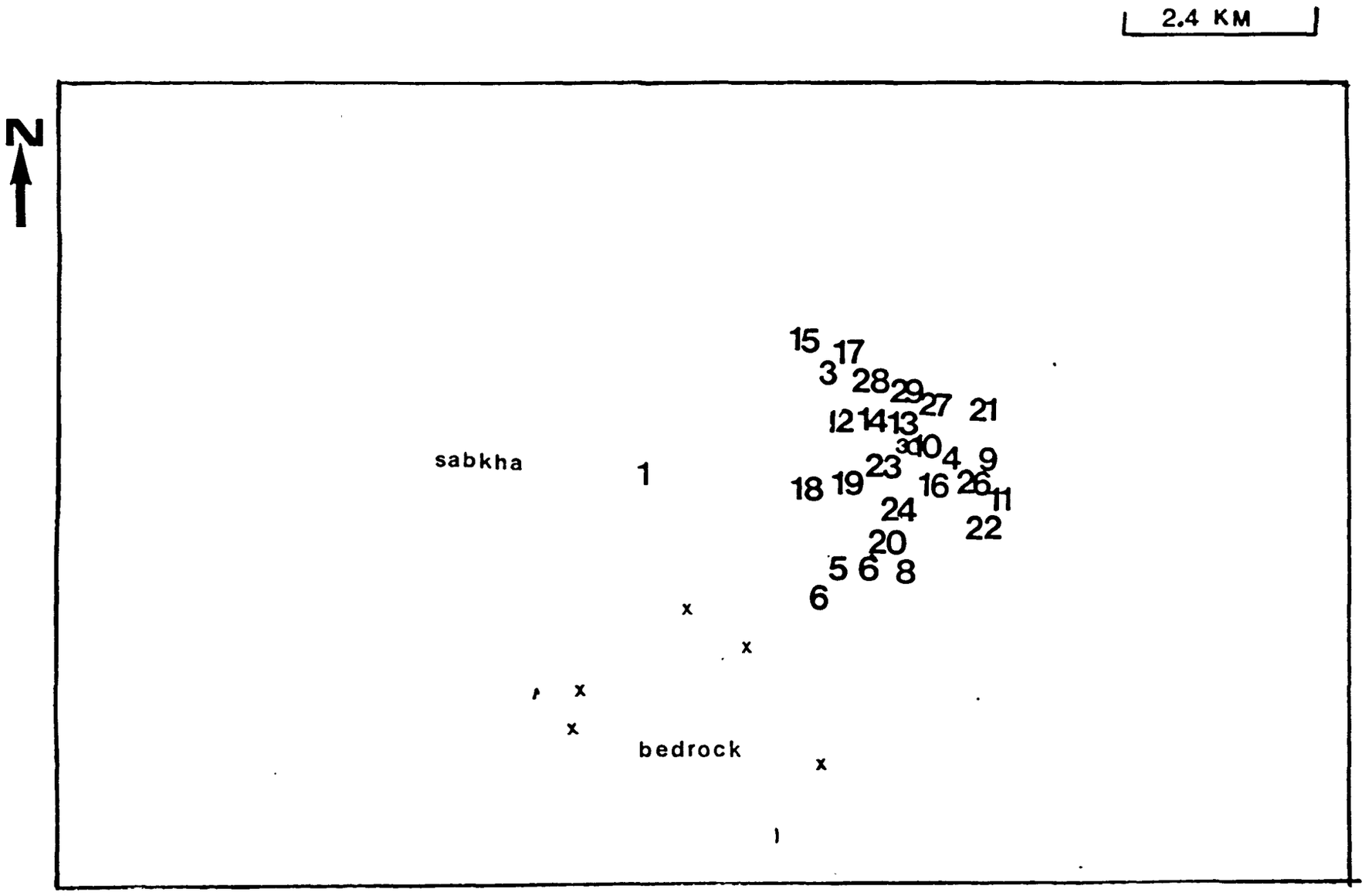
Figure 7.2 Aerial photograph acquired in Nov.1949 (1:60,000 scale) showing barchans and barchanoid ridges in the area studied. Numbers indicate the investigated dunes for movement measurement. Ground control points locations are shown as (X).

Figure 7.3 Aerial photograph acquired in Nov.1983 (1:80,000 scale) covering the same area as Figure 7.2. Numbers on the dunes correspond to the same dunes shown in Figure 7.2. Ground control points locations are shown as (x).


1.8 KM
N
15
17
28
29
27
21
3
9
12
14
13
10
4
26
11
30
25
16
22
23
24
18
19
2
1
20
7
8
6
5
sabkha
bedrock

1.8 KM
bedrock
N




2.4 KM
N
sabkha
bedrock
15
17
3
28
29
27
21
12
14
13
30
10
4
9
23
1
18
19
16
26
11
24
22
20
5
6
8
6


2.4 KM
N
sabkha
bedrock
15
17
3
28
29
27
21
12
14
13
10
4
9
18
19
16
26
24
22
20
5
6
8
6

Figure 7.3

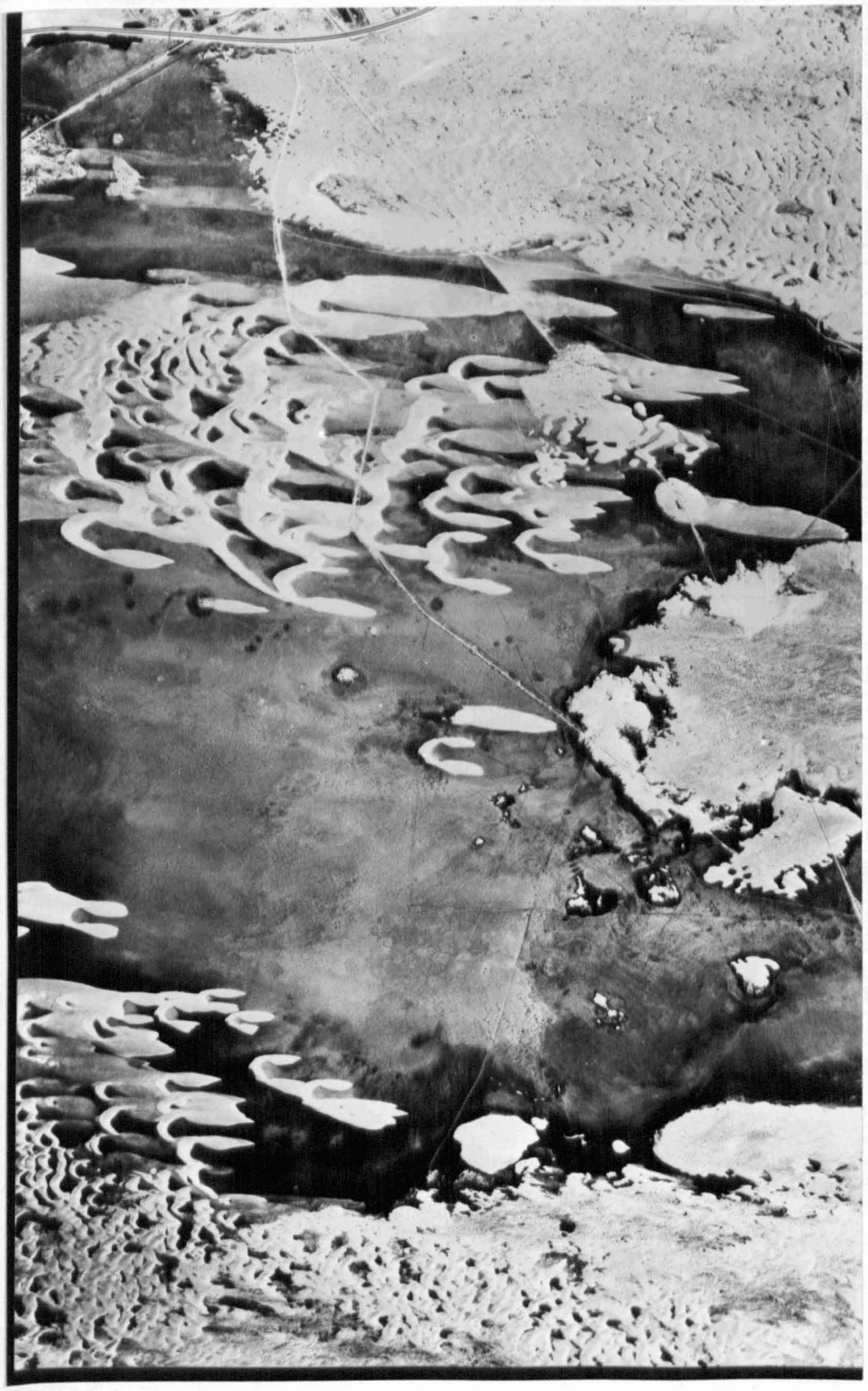


Figure 7.3

years period. The dune outline in each picture was reduced to a common scale of 1:25,000 using the CP1 plotting instrument at the Photogrammetric Department, University College- London.

The photographs used were without sufficient ground control. Hence, ground control points had to be established and selected from ground features detected on the 1949 and 1983 photograps. Four ground control points from the bedrock-sabkha boundary and were identified and marked in the photographs (Figures 7.2 & 7.3).

The sand dunes within the specified area were plotted with their crest heights recorded beside them. The positions of the dunes were drawn on a sheet of transparent paper to a scale of 1:25,000. The entire planimetric outline of each dune was drawn for both flights and each dune was numbered. Different colours were used to distinguish between the 1949 and the 1983 positions (Fig. 7.4).

Two techniques were used for crest height measurements. The first technique used was to measuring crest heights by stereoscopic methods. This technique was not adopted, however, because the 1:60,000 and the 1:80,000 scales used in this investigation gave an accuracy of 3 to 4 metres at best. Instead, crest heights were measured in the field using a Hewlett Packard 3810-a Total station as described in section 7.7 (field measurements). The disadvantage of using

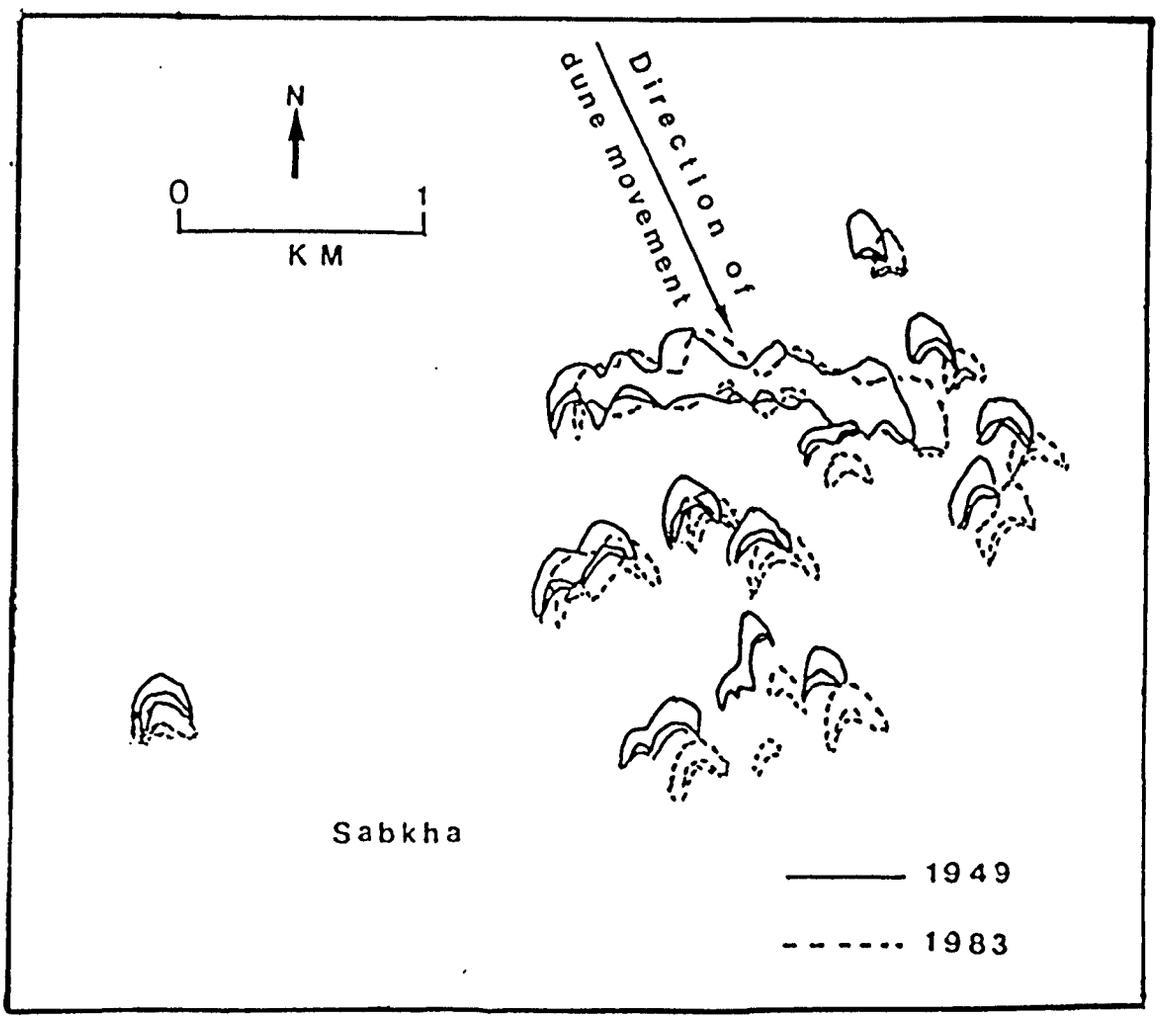


Figure 7.4 Displacement of dunes between 1949 and 1983 (aerial photogrammetric measurement).

this technique is that the heights of the dune crests in 1949 were not measured. Hence, a comparison of crest heights between 1949 and 1983 was not possible.

The horizontal displacement of 30 barchans and barchanoid ridges were measured from crest to crest using a caliper. Planimetric measurement of dune displacement on 1:25,000 scale photo enlargements using a limited number of control points (4) gave a planimetric accuracy of 2 metres.

Dune position changes plotted from the 1949 and 1983 photographs are readily apparent on Figure.(7.4). These changes indicate variation in the migration rates of individual dunes due to differences in dune heights. Table 7.3 shows measurement of annual displacement of 30 barchan and barchanoid ridges according to height of the crest of these dunes. Table 7.4 gives a summary of these measurements. Figure 7.5 is a graphic presentation of dune movement versus dune height. Results obtained from aerial photographic interpretation show the following:

(i) Dune movement measurement for 30 barchans and barchanoid ridges ranged between 2.2 and 8 metres annually with an average of 4.6 metres (Table 7.3).

(ii) Small dunes travelled faster than large dunes with few exceptions (Table 7.3).

(iii) Indvidual barchans move faster than barchanoid ridges (Table 7.3 & Figures 7.2 and 7.3).

Dune Numbers	Dune Movement (m)	Dune Height (m)	Direction of Dune Movement
1	204.74	14.74	SE
2	-	-	-
3	282.82	10.54	SE
4	290.17	10.24	SE
5	295.60	9.95	SE
6	300.00	6.00	SE
7	305.00	7.65	SE
8	280.00	10.65	SE
9	200.15	13.00	SE
10	125.40	18.00	SE
11	140.00	16.00	SE
12	135.00	16.12	SE
13	100.11	17.42	SE
14	90.76	18.62	SE
15	80.00	20.17	SE
16	220.12	12.0	SE
17	190.14	14.07	SE
18	180.24	16.00	SE
19	117.00	17.00	SE
20	250.00	8.00	SE
21	270.00	10.00	SE
22	180.14	12.00	SE
23	65.28	18.14	SE
24	67.28	19.76	SE
25	-	-	-
26	240.00	8.20	SE
27	180.29	14.17	SE
28	240.28	10.15	SE
29	150.00	16.00	SE
30	183.25	12.00	SE

Table 7.3: Dune displacement between 1949 and 1983 (34 years period) based on aerial photographic measurement. Location of dunes is given in Fig.7.2 .

Dune Height (m)	10	12-13	14	16	17-18	18-20
Average annual displacement (metres)	8	6	5.8	2.9	2.2	2.9

Table 7.4: Average annual displacement of 30 barchans and barchanoid ridges according to dune height (aerial photographic measurement).

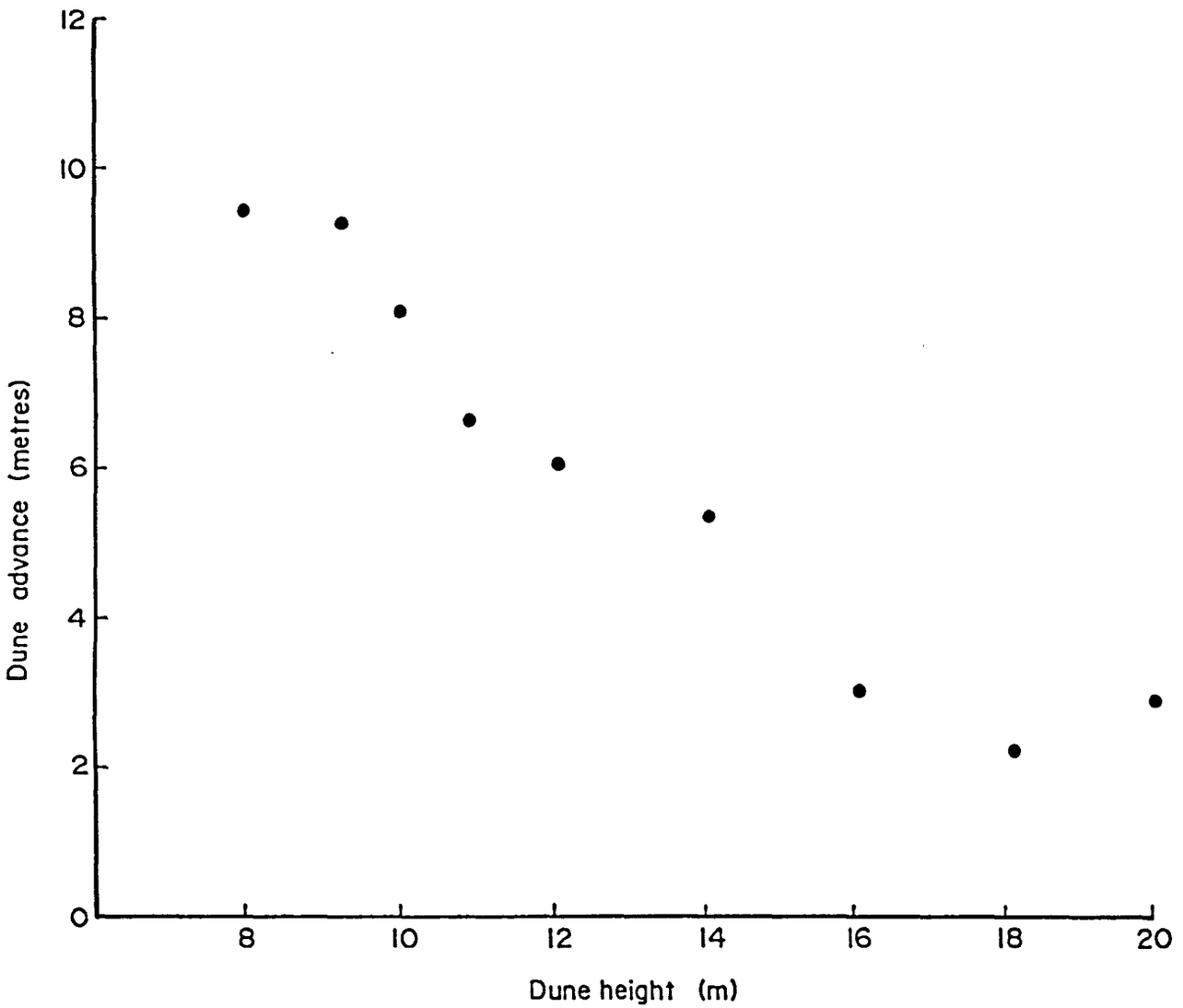


Figure 7.5 Average annual dune advance versus dune height (measured between 1949 and 1983).

(iv) Some small dunes diminished in size as they get separated from the larger dunes. Two small dunes present in the 1949 photograph disappeared completely in the 1983 photograph (dune no.2 & 25, Figures 7.2 & 7.3).

(v) The direction of dune advance in the Jafurah area is S to SE. This is generally parallel to the long-term wind direction for the Dhahran area (Williams, 1979). The general north east orientation of long axes of dunes studied did not vary during the 34 years period.

(vi) There is a shift of some dune positions to the east (Figure 7.4). This change in position is partly due to the shift in seasonal wind direction and partly to the error in the superposition of the photographs.

7.9 FIELD MEASUREMENT

Dune advance was measured during twelve months from October 1979 to October 1980 for 20 dunes in selected areas of the Jafurah Sand Sea (Fryberger,et al, 1984). The method used for measuring dune advance was to tape the distance to a number of places along the base of the slipface from a stake hammered into the ground about 15 metres downwind of the dune (Figure 7.6). Dune advance was then evaluated by plotting successive slipface positions on a graph paper at the appropriate scale and graphically measuring average slipface displacement in a direction parallel to the dominant wind direction (NNW). The same approach was applied

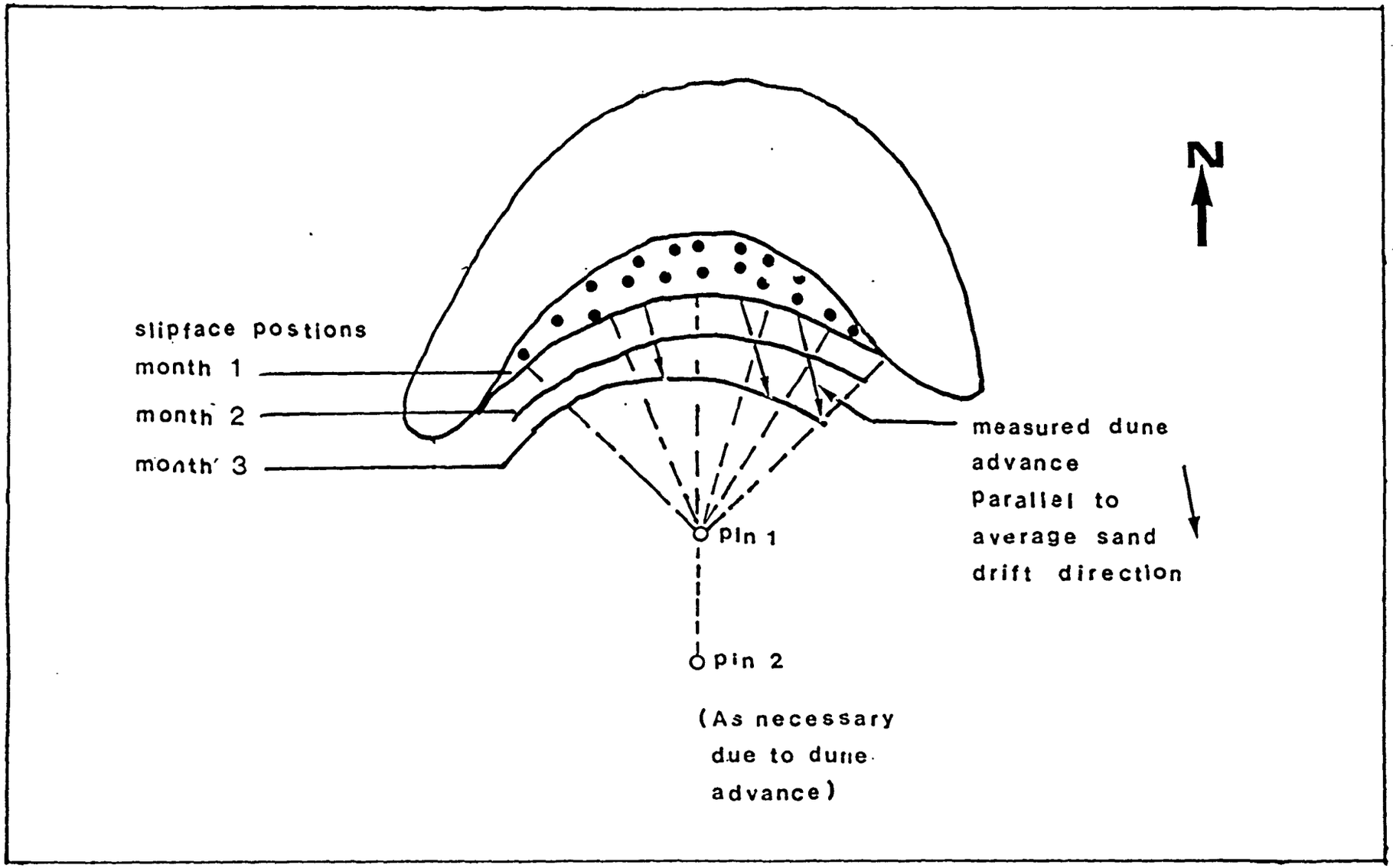


Figure 7.6 Method used for measuring dune movement in the field.

to this study with emphasis on the area covered by both Landsat MSS imagery and aerial photographs.

Movement of 30 dunes were measured during twelve months period from August 1984 to August 1985. Dune heights were surveyed in August 1984 and August 1985 using a Hewlett Packard 3810-A Total Station to an accuracy of 0.1 metre. The measured dunes correspond to those dunes selected in the Landsat MSS and Aerial photographic investigation (as shown in Figures 7.2 & 7.3).

Table 7.5 shows the dune movement between August 1984 and August 1985. Table 7.6 is a summary of the average annual displacement. These field results correlate with aerial photographic measurements (Table 7.4) and are consistent with the crude measurements otained from Landsat MSS investigation.

Dune advance varied between 8 metres for small dunes (10 meters high) and 4 metres for larger dunes (18 metres high). When the annual displacement of 30 dunes is plotted against dune height, it becomes clear that there is a significant correlation (Fig. 7.7).

Dune height, did not undergo any appreciable change during the 12 months period.

7.10 CASE HISTORY (2) - HARAD AREA

Figure 7.8 shows the location of the test site area. This

Dune Number	Dune Movement (m)	Dune Height (m)	Direction of Dune Movement
1	6.2	14.74	SE
2	-	-	-
3	8.70	10.54	SE
4	8.20	10.24	SE
5	9.40	9.95	SE
6	10.00	6.00	SE
7	10.40	7.65	SE
8	8.10	10.65	SE
9	7.40	13.00	SE
10	3.40	18.00	SE
11	5.70	16.00	SE
12	5.00	16.12	SE
13	4.75	17.42	SE
14	3.76	18.62	SE
15	3.00	20.12	SE
16	7.20	12.00	SE
17	6.40	14.07	SE
18	5.10	16.00	SE
19	4.00	17.00	SE
20	10.17	18.00	SE
21	8.00	10.00	SE
22	7.20	12.00	SE
23	4.25	18.14	SE
24	3.15	19.76	SE
25	-	-	-
26	9.27	8.20	SE
27	6.10	14.12	SE
28	8.40	10.15	SE
29	5.00	16.00	SE
30	6.75	12.00	SE

Table 7.5: Dune displacement between August 1984 and August 1985 (12 months' period) based on field measurements.

Dune Height (metres)	10	12-13	14	16	17-18	18-20
Dune Displacement (metres)	8	7	6	5	4	3

Table 7.6: Average displacement of dunes between August 1984 and August 1985 (12 months' period) based on field measurements.

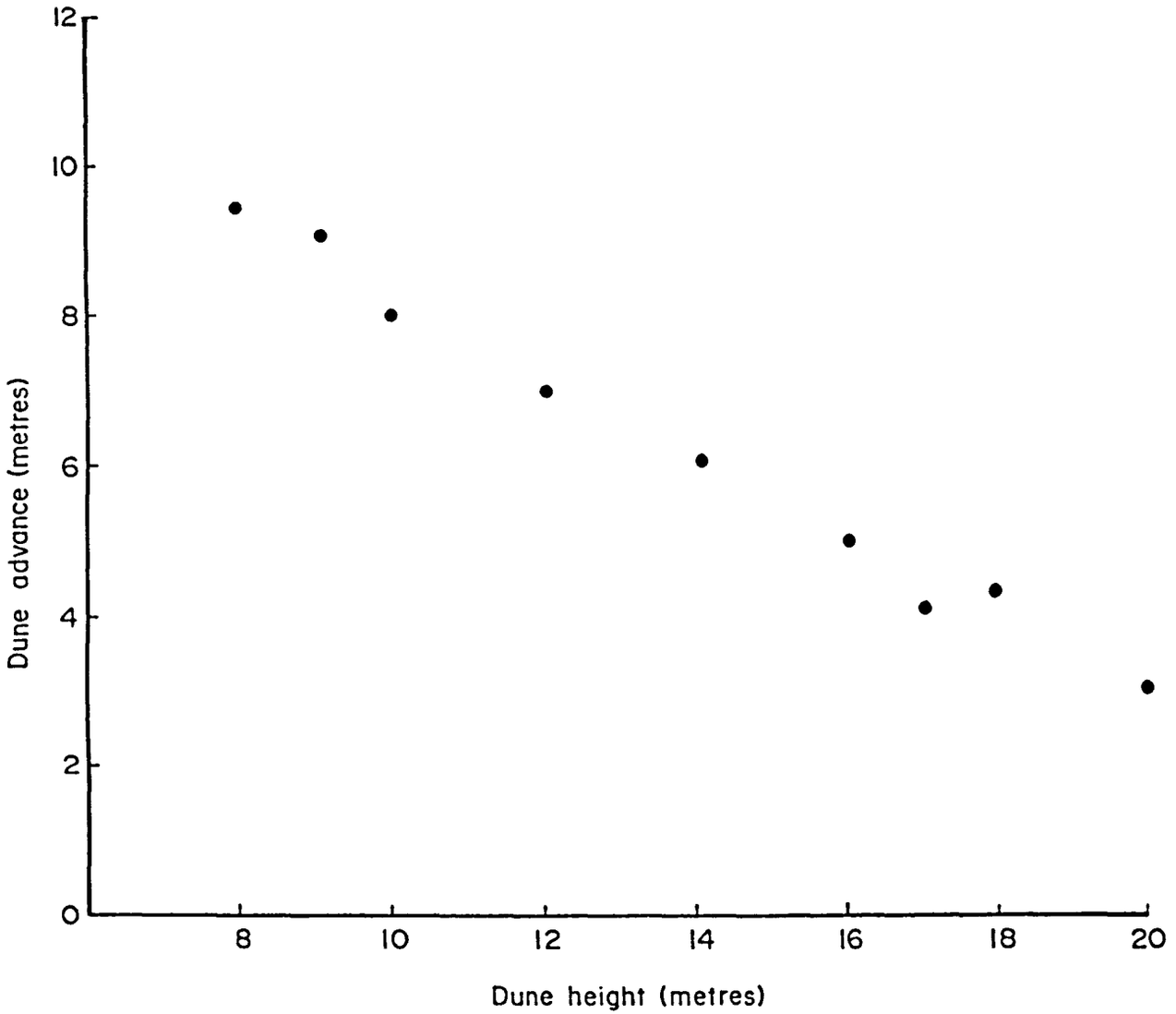


Figure 7.7 Dune advance versus dune height from August 1984 to August 1985 (12 months period).

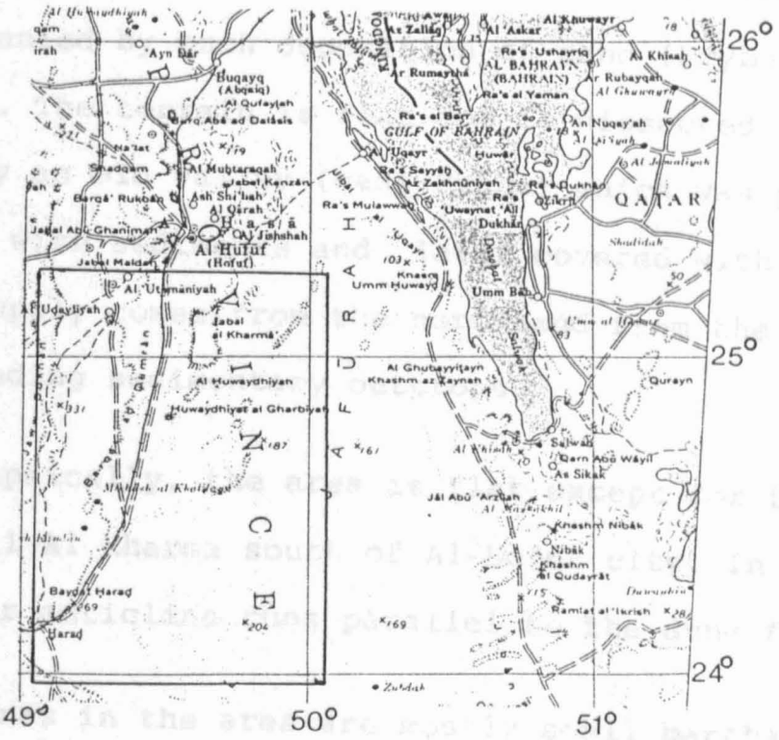


Figure 7.8 Location map of Case History (2).

area is part of the Jafurah south and consists of sand dunes, gravel, and bedrock. The area lies in the transition zone between the Jafurah North and the Rub'al Khali. This zone is considered to be partly a zone of transport accompanied by much deposition of sand (Fryberger, et al (1984). The terrain is flat and is dissected from west to east by an old valley (Wadi Sahba) which was partially filled with sediments and later covered with aeolian sand. Sand supply comes from the north and from the surrounding sedimentary outcrops.

Topographically, the area is flat except for the existence of Jabal Al Kharma south of Al-Hofuf city. In the west, the Al.Gawar anticline runs parallel to the dune field.

Sand dunes in the area are mostly small barchans and barchanoid ridges migrating southwards in a gravel surface (section 6.6 in Chapter 6 gives more details on the dune morphology in this area).

LANDSAT MSS INVESTIGATION:

Landsat MSS imagery acquired at two different dates was investigated to detect any changes in sand patterns over an 11 year period. The emphasis of this investigation is on the detection of changes, if any, in dune patterns rather than the measurement of individual dune movement.

Two Landsat MSS images, representing cloud-free scens 176/43

(Landsat 1), acquired Jan, 18, 1973 and 164/43 (Landsat 5) acquired Jan, 15, 1984 were used to represent a reasonable period of time (11 years) for investigating dune patterns.

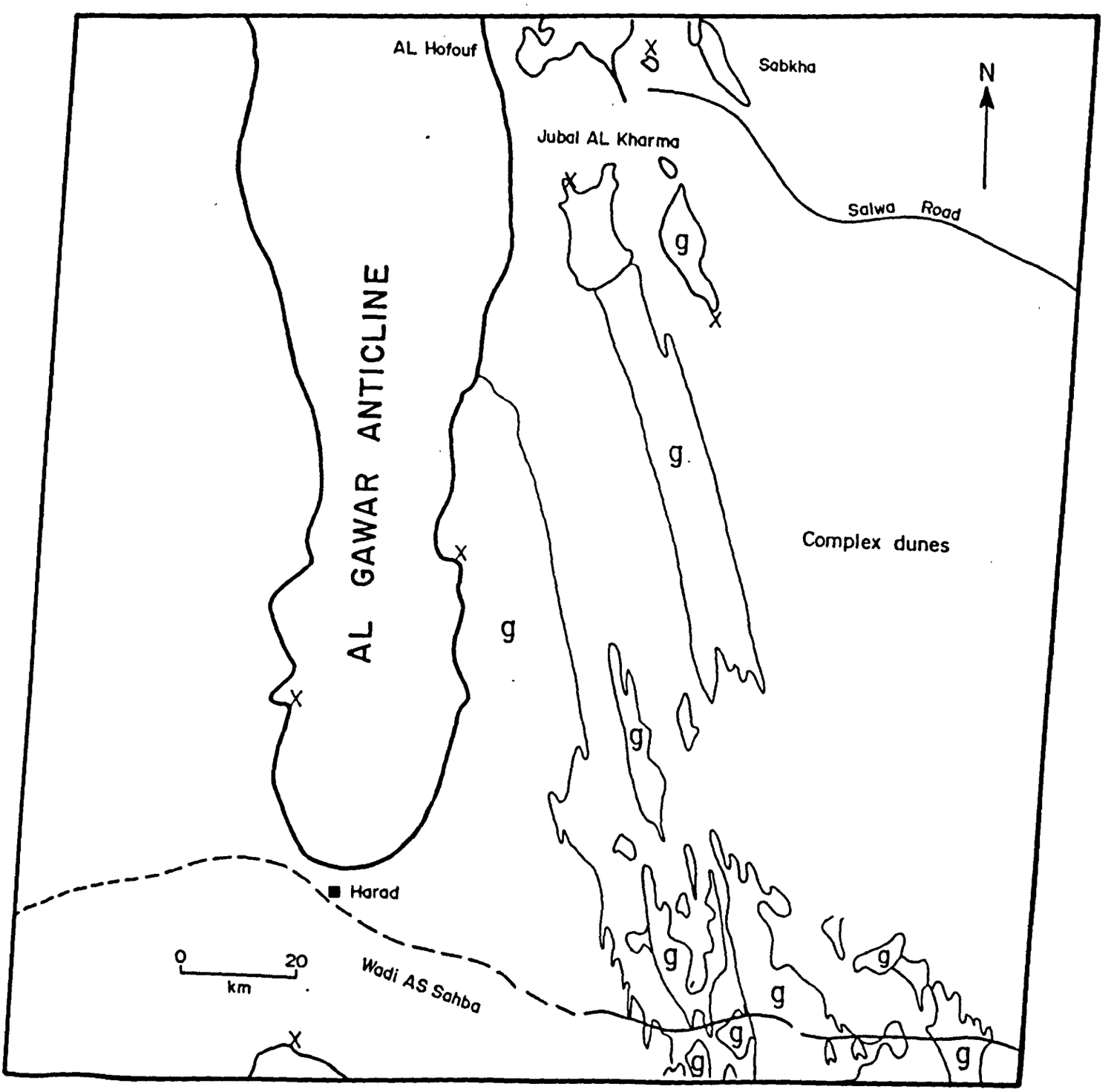
Digitally enhanced false-colour composites (MSS bands 4, 2, and 1 shown as red, green, and blue respectively) were produced for each Landsat scene (figures 7.9 & 7.10). Two transparencies representing scenes 176/43 and 164/43 were then produced. The scale used for mapping the dune patterns was 1: 250,000. A scale larger than 1:250,000 was found to lack the sharpness and the good defintion of features seen in the imagery. False colour composites were used in this invetigation because they reveal the distinctive yellow colour of sand from other superficial deposits. In black and white imagery the distinction is ambiguous.

The analysis consisted of superimposing the two scenes and tracing the boundaries of dune patterns of 1973 and 1984. The mountains and other fixed features were used as ground control points for proper analogue registration of the two scenes. Six ground control points were identified in each scene (Fig. 7.9). The registration error was calculated to be between 200 and 250 m. Since this investigation emphasises qualitative comparison of dune patterns rather than measurement of dune movement, the marginal error did not have a significant effect on the results.

When comparing the two images, it is clear that no significant shifting in dune patterns occurred between

Figure 7.9 Landsat MSS false colour composite (scene 176/43; Jan.18.1973) over Harad area.The overlay is a map of the dune patterns. (x) indicates ground control points locations; (g) refers to sand free corridors (gravel).

Figure 7.10 Landsat MSS false colour composite (scene 164/43; Jan.15.1984) over the same area as in Figure 7.9. The overlay is a map of the dune patterns. (g) indicates sand free corridors (gravel).


AL Hofouf
Sabkha
N
Jubal AL Kharma
Salwa Road
AL GAWAR ANTICLINE
Complex dunes
Harad
0
20
km
Wadi AS Sahba

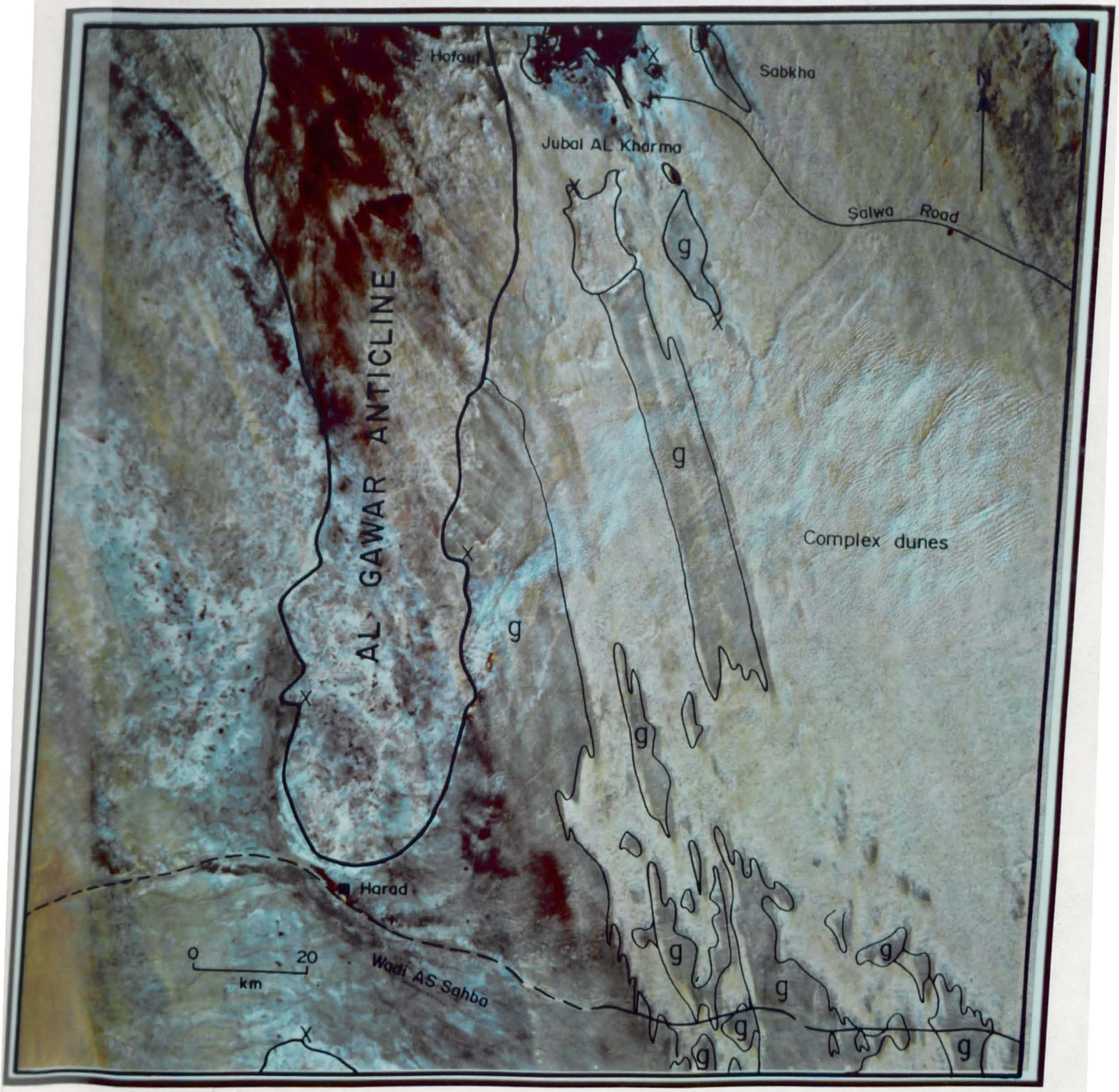
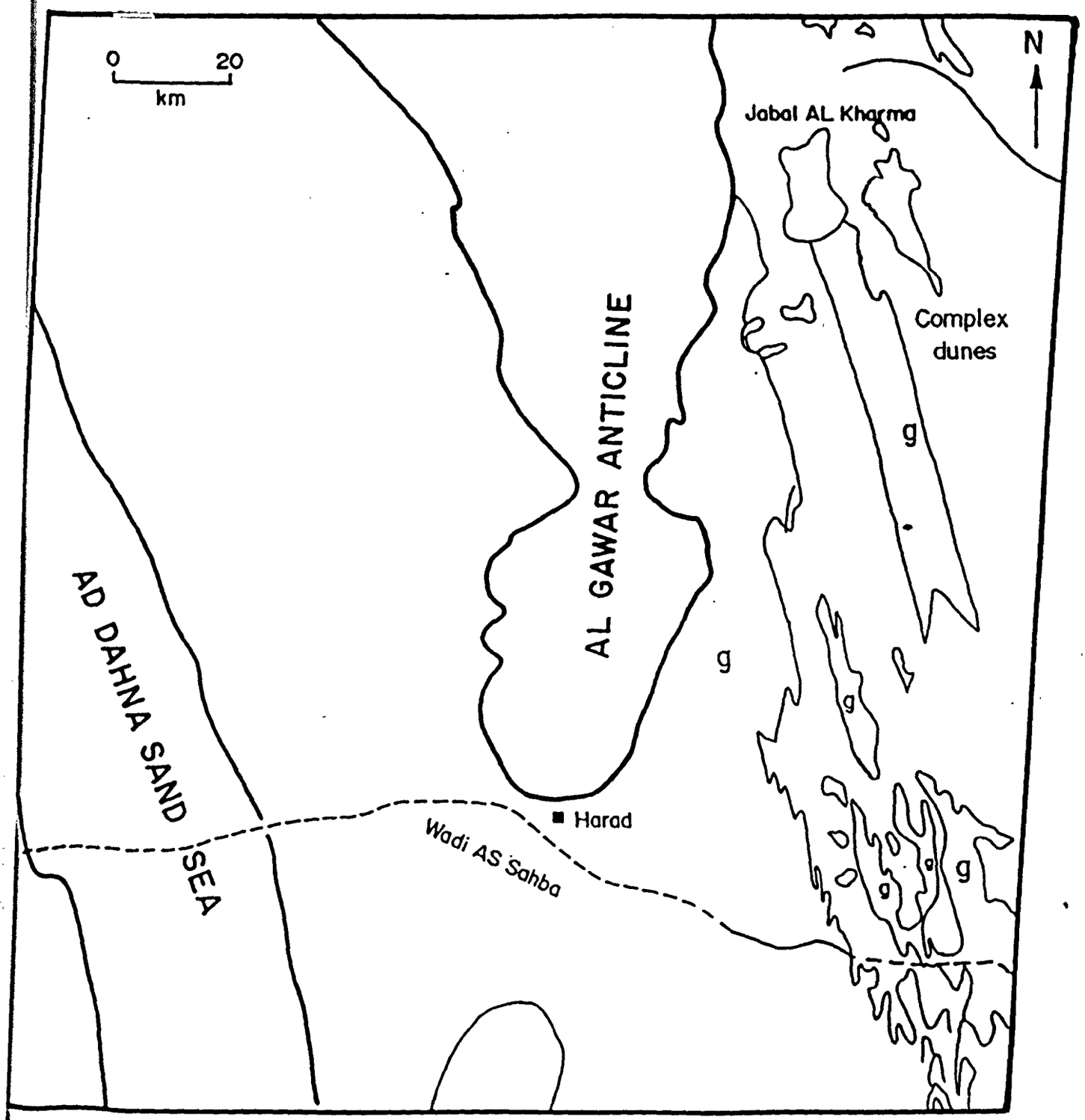

Hofouf
Sabkha
N
Jubal AL Kharma
Salwa Road
AL GAWAR ANTICLINE
Complex dunes
Harad
0
20
km
Wadi AS Sahba

Figure 7.9



Figure 7.9


0
20
km
N
Jabal AL Kharma
Complex
dunes
AL GAWAR ANTICLINE
AD DAHNA SAND SEA
Harad
Wadi AS Sahba
g

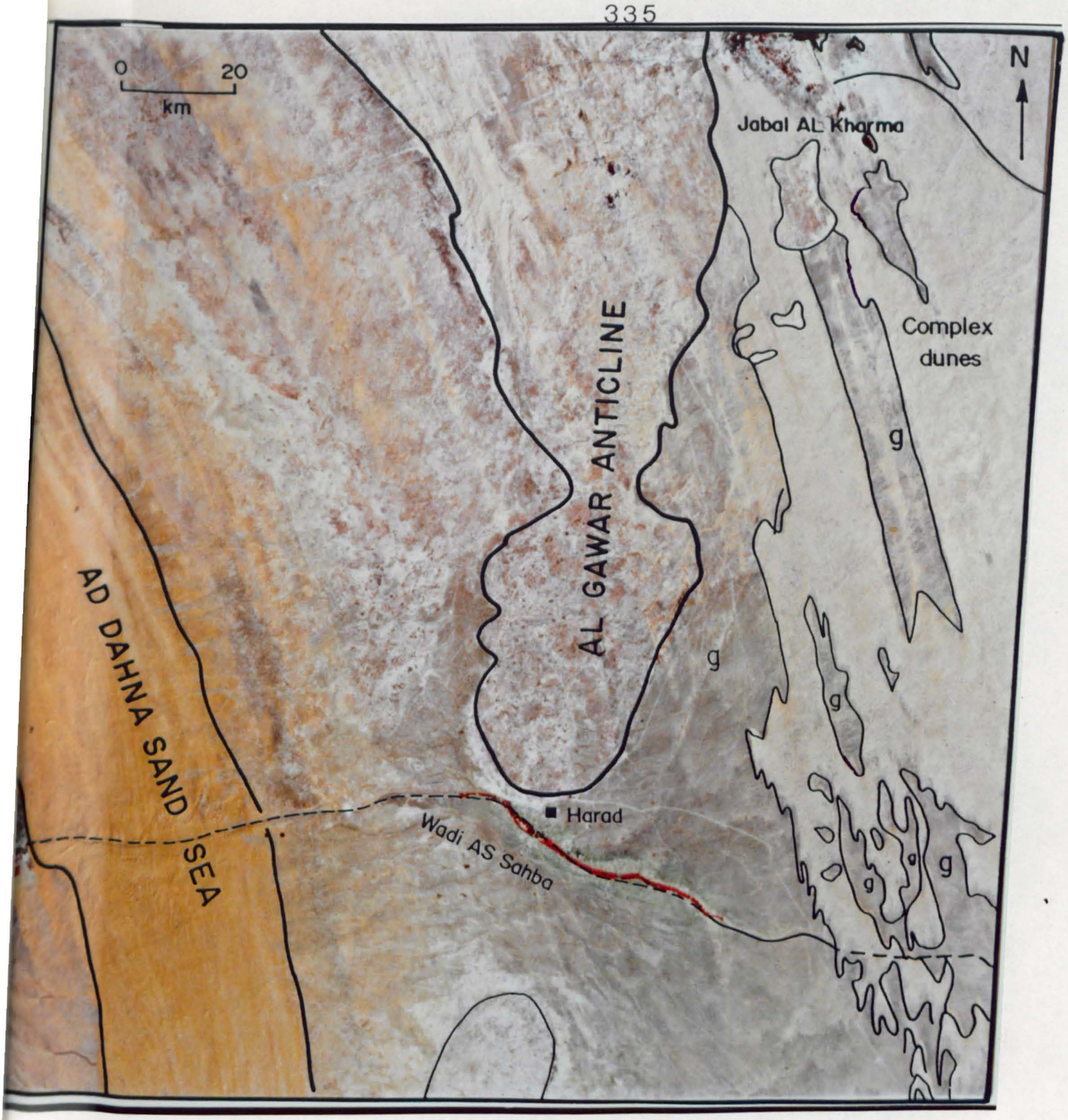

0
20
km
N
Jabal AL Kharma
Complex
dunes
AL GAWAR ANTICLINE
AD DAHNA SAND
SEA
Harad
Wadi AS Sahba
g

Figure 7.10



Figure 7.10

1973 and 1984 (Fig. 7.11). Other observations following image interpretation can be summarized as follows:

(i) The orientation of the sand bodies (northeast) controlled by the north-northwesterly winds remained the same.

(ii) The sand free corridors (annotated g in Fig. 7.9 & 7.10) between the dune bodies had not shifted significantly nor had they changed from the original dimensions. The largest corridor caused mainly by the mountain (Jabal Al Kharma), located upwind, had not shifted nor had it changed from the original dimensions (2.4 km (Width) x 17 km (length). The mountain rise about 150 meters from the surface.

(iii) There was no western shift of the dune field. This is illustrated by the fact that the sand-free area separating the western boundary of the dune field from the foothill of the Al Gawar anticline had not changed.

(iv) The widths and lengths of the chain barchans (see Chapter 6 for more discussion on this dune type) did not vary between 1973 and 1984 (average width is 3.6 km and average length is 8.4 km).

(V) The general shape of the chain barchans did not change indicating a consistent wind direction (NNW).

7.11 DISCUSSION

Repeated coverage by Landsat MSS imagery is a good tool for

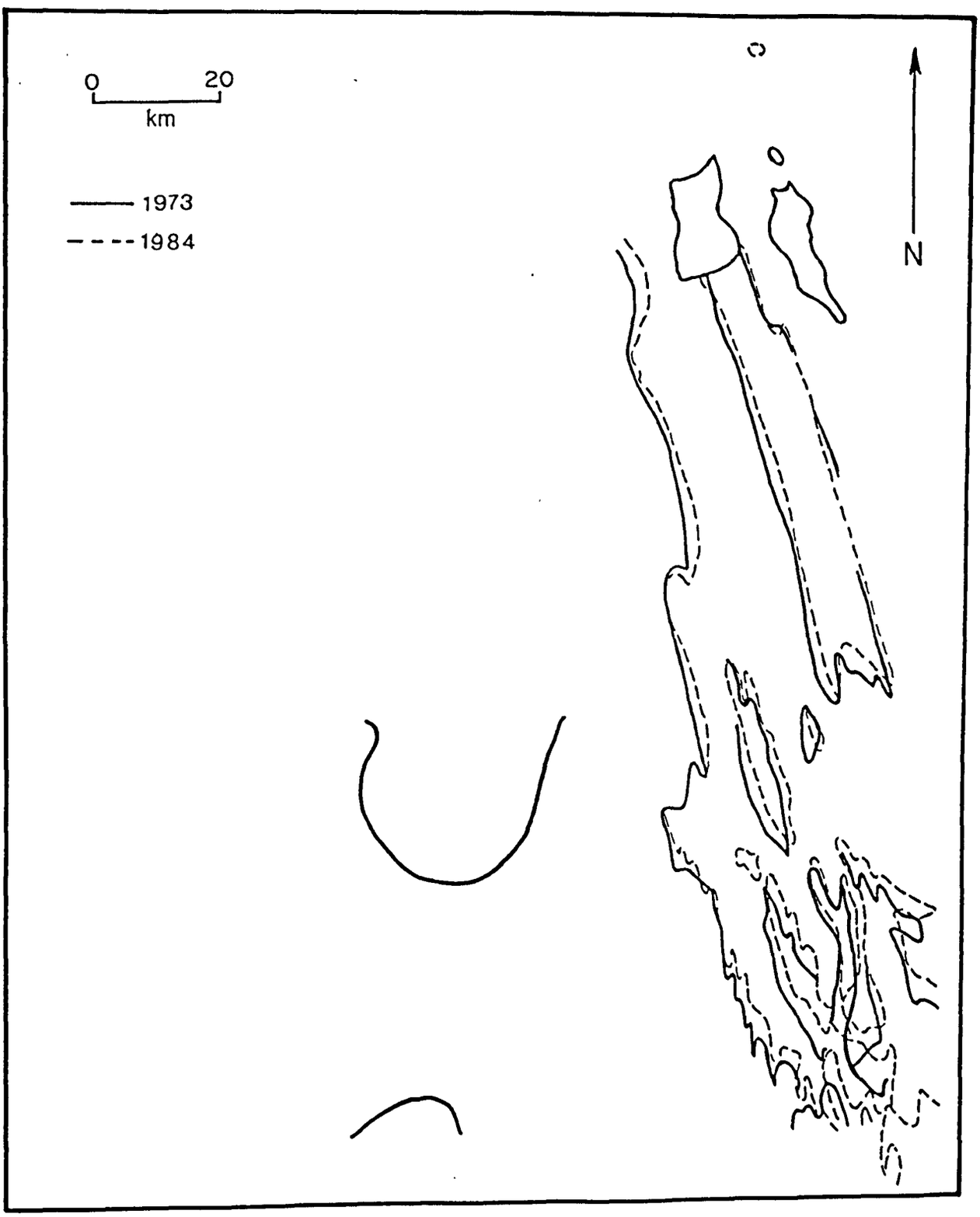


Figure 7.11 Dune pattern boundaries drawn from the 1973 and 1984 images. Dune field and sand free corridor positions did not change significantly.

monitoring regional sand distribution patterns. In study area (2) temporal changes of sand bodies between 1973 and 1984 were easily compared and mapped using unsophisticated methods. However, when multi-temporal Landsat MSS images was used for sand dune movement measurement (Case History 1) several problems were encountered. These problems include:

(i) Lack, in desert terrains, of sufficient ground control points necessary to achieve high registration accuracy using multi-temporal imagery.

(ii) Spatial resolution of Landsat MSS imagery (80 meters) falls short of detecting the relative slow movement of the investigated dunes (less than 8 metres/year) over the 12 year period for which images are available. The identification of individual dunes for this study was only possible because of their wide spacing and the high albedo contrast between sand and the substratum (sabkha). In areas where dunes are closely spaced, identification of individual dunes is more difficult.

(iii) The time span of 12 years used in this study was not enough to detect the relative slow movement of the dunes.

When compared with field data, aerial photographic interpretation gave more reliable results than those achieved from MSS imagery.

Aerial photographic and field investigation results confirm Bagnold's (1941) conclusion that under ideal conditions of uniform aeolian activity, leveled land surface, and comparable sand supply, small dunes would move faster than large ones. Such ideal conditions exist in the area selected for this study. However, these ideal conditions do not persist when dealing with an entire sand sea consisting of different dune types, land surfaces, and wind regimes. Faster movement of barchan dunes has been observed in the Jafurah with no significant correlation between the height and the rate of movement of these dunes (Fryberger et al., 1984 and Watson 1985). Fryberger et al (1984) reported an annual displacement of barchan dunes ranging between 6 and 28 metres with an average movement of 14.8 metres. Watson (1985) measured 68 barchan dunes using aerial photographs and reported an annual displacement ranging between 0.2 and 44.5 metres with an average movement of 14.68 metres. Table 7.7 summarises dune movement rates recorded in the Jafurah Sand Sea (including the author's measurement) and other parts of the world. Variations in results recorded in this investigation and those recorded by Fryberger et al, (1984) and Watson (1985) are attributed to the following factors:

(i) Dunes investigated in this study are located in a sabkha. Sabkhas are important trapping effect on moving sand because of their damp surfaces which tend to trap sand through cohesion thus reducing the amount of sand reaching the dunes. Another reason, is that usually the sabkha

Location	Reference	Number of Dunes	Mean Height	Range in Height	Travel Distance	Range in Travel Distance
PERU	Finkel (1959)	75	3.67	1.0 - 7.0	15.4	9.2 - 32.3
	Hastenrath (1967)	42	4.38	1.2 - 6.0	14.2	9.0 - 23.0
		50	4.12	0.4 - 6.0	30.7	17.0 - 56.0
	Lettau & Lettau (1969)	114	3.0	-	30.0	-
MEXICO	Inman et al (1966)	-	6.0	-	18.0	-
USA (California)	Long & Sharp (1964)	34	-	-	15.2	7.1 - 24.4
		47	5.89	2.7 - 12.2	25.0	14.2 - 39.2

Continued on next page ...

Table 7.7: Dune movement rates in some sand seas of the World.

Table 7.7 (Cont'd): Dune movement rates in some sand seas of the World.

MAURETANIA	Sarnthein & Walger (1974)	44	8.8	3.0 - 17.0	30.0	18.0 - 63.0
SAUDI ARABIA (Jafurah Sand Sea)	Fryberger et al (1984)	16	-	-	14.8	6.0 - 28.0
	Watson (1985)	68	8.5	3.2 - 34.0	14.68 (50 weeks)	0.2 - 44.5 (50 weeks)
(Jafurah Sand Sea)	Al Hinai (1988)	30	10.1	7.6 - 20.12	6.16 (12 months)	3.00 - 10.40 (12 months)

surfaces are covered completely by small 1-5 cm high salt ridges (Fryberger et al., 1984). Sand crossing the sabkhas become trapped in the lee of the these salt ridges-thus reducing sand drift rates.

(ii) Dune movements are affected directly and indirectly by the topography and vegetation density of the area. The Jafurah is characterized by the irregular topography and variations in vegetation density.

(iii) Dunes are themselves obstacles which reduce wind velocity in the downwind direction. As dune density (local crowding of the dunes) increases, their effect in reducing wind spead increases, and thus reducing the rate of dune movement.

Results obtained from this study should be used with caution if used to develop a predictive model of dune migration rates for the entire Jafurah Sand Sea.

CHAPTER 8

LANDSAT MSS INVESTIGATION OF POSSIBLE SUBMERGED SAND DUNES IN THE ARABIAN GULF.

8.1 INTRODUCTION

The study area shown as inset in Figure 8.1, is located approximately nine Kilometers off the eastern coast of Saudi Arabia, between Bahrain island and the Qatar peninsula. In this area the water is shallow and free of suspended sediments which is ideal for studying sea floor morphology using remote sensing data because of its translucency.

Landsat MSS and TM images representing the wave length range 0.45-0.6 μm were used to display the submarine form of shoals and sandbanks in coastal waters 8-10 metres deep. This occurs because of the partial penetration and transmission of blue-green, compared with longer wave length light, by clear water (Polcyn et al, 1970).

The digital image processing techniques used to optimise the display of the submarine features are discussed in Chapter 3.

This chapter is a discussion of the submerged features revealed on the the Landsat image data and their possible origin.

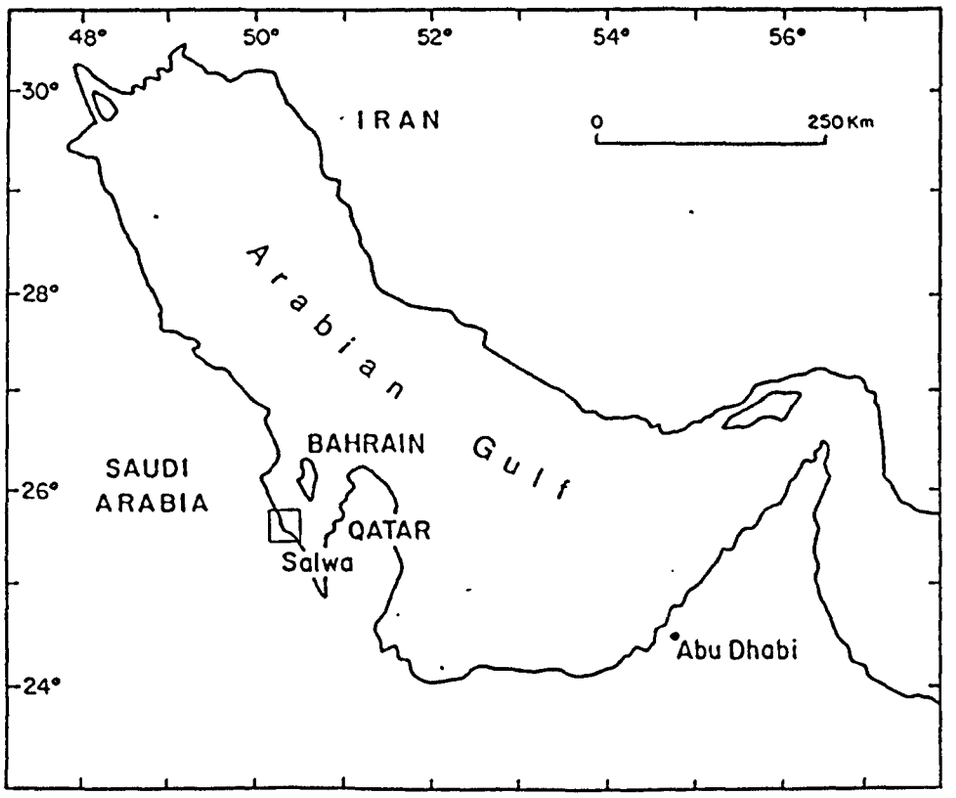


Figure 8.1 Location map of study area.

8.2 Physiography of the Arabian Gulf

The floor of the Arabian Gulf is an extension of the Arabian interior platform. The gently sloping basin floor is interrupted by geologic structures (such as salt domes), coral reefs, mud mounds, and shallow terraces before reaching a maximum depth of 75 m in the centre of the Gulf (Fryberger et al, 1984). Along the Saudi side the depth is around 8 to 10 m (Fig. 8.2).

Water salinities are about 36.5% in the centre of the Gulf, and more than 40% in some bays and lagoons (Fryberger et al., 1983). Sediments offshore along the Arabian coast are mainly calcareous sands and muds (Fig. 8.3). The highest percentage of calcium carbonate in the sediments corresponds to highest salinities (Emery, 1956). Sources of carbonate material offshore include shell debris including molluscs, corals, and algae, inorganically precipitated material, and airborne dust, which is highly calcareous (Emery, 1956). The proximity of the nearby prograding dune system is indicated by the presence of the quartz sediments in the western side of the Gulf (Doornkamp et al, 1980) and by the well rounded shape and reddish colour of some grains found by Emery (1956).

Water temperatures at the surface range from 15 to 32 degrees centigrade in winter and summer respectively. Regional tidal currents are oriented approximately parallel

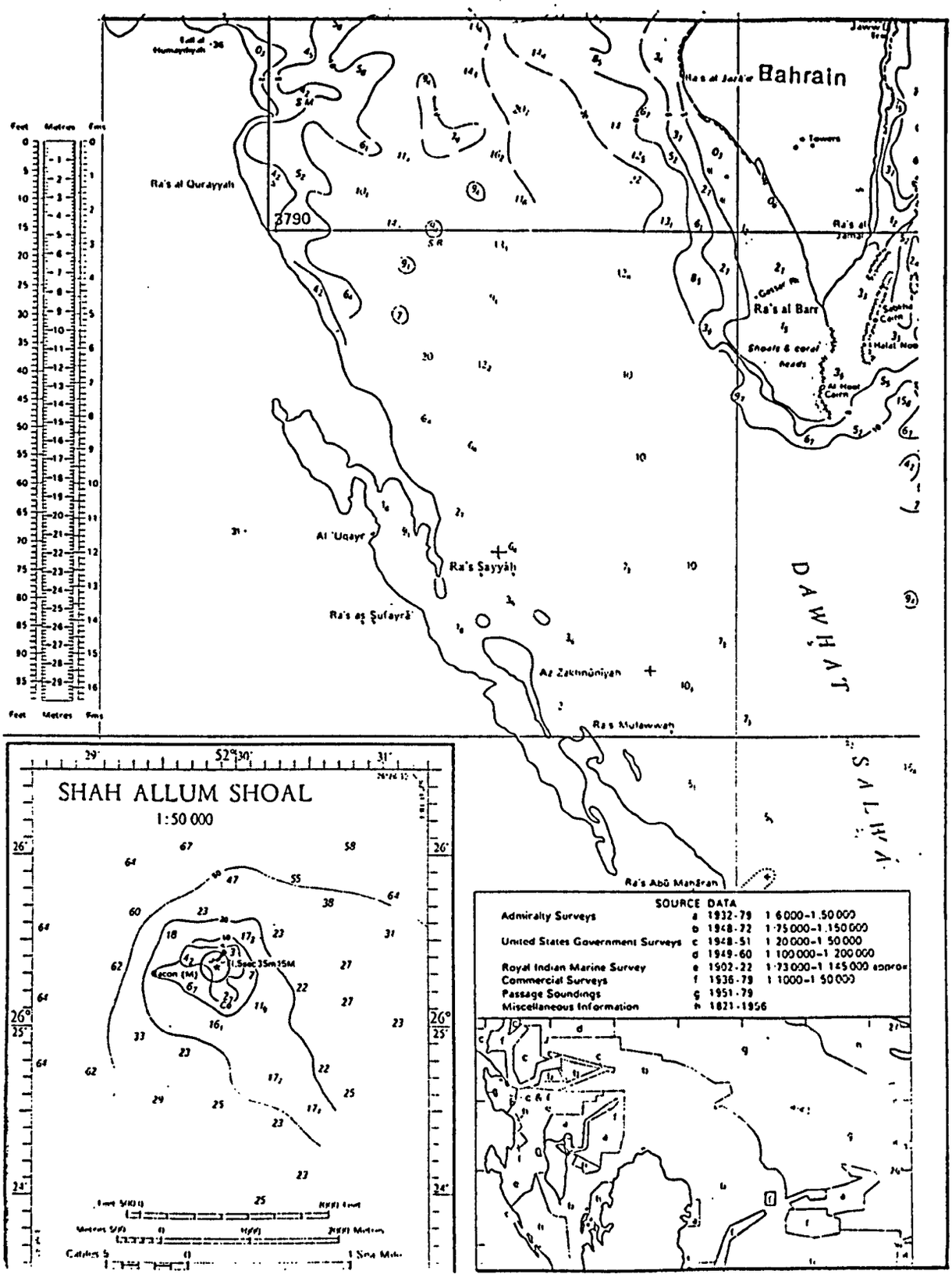


Figure 8.2 Bathymetric map showing water depth along The Saudi Coast.

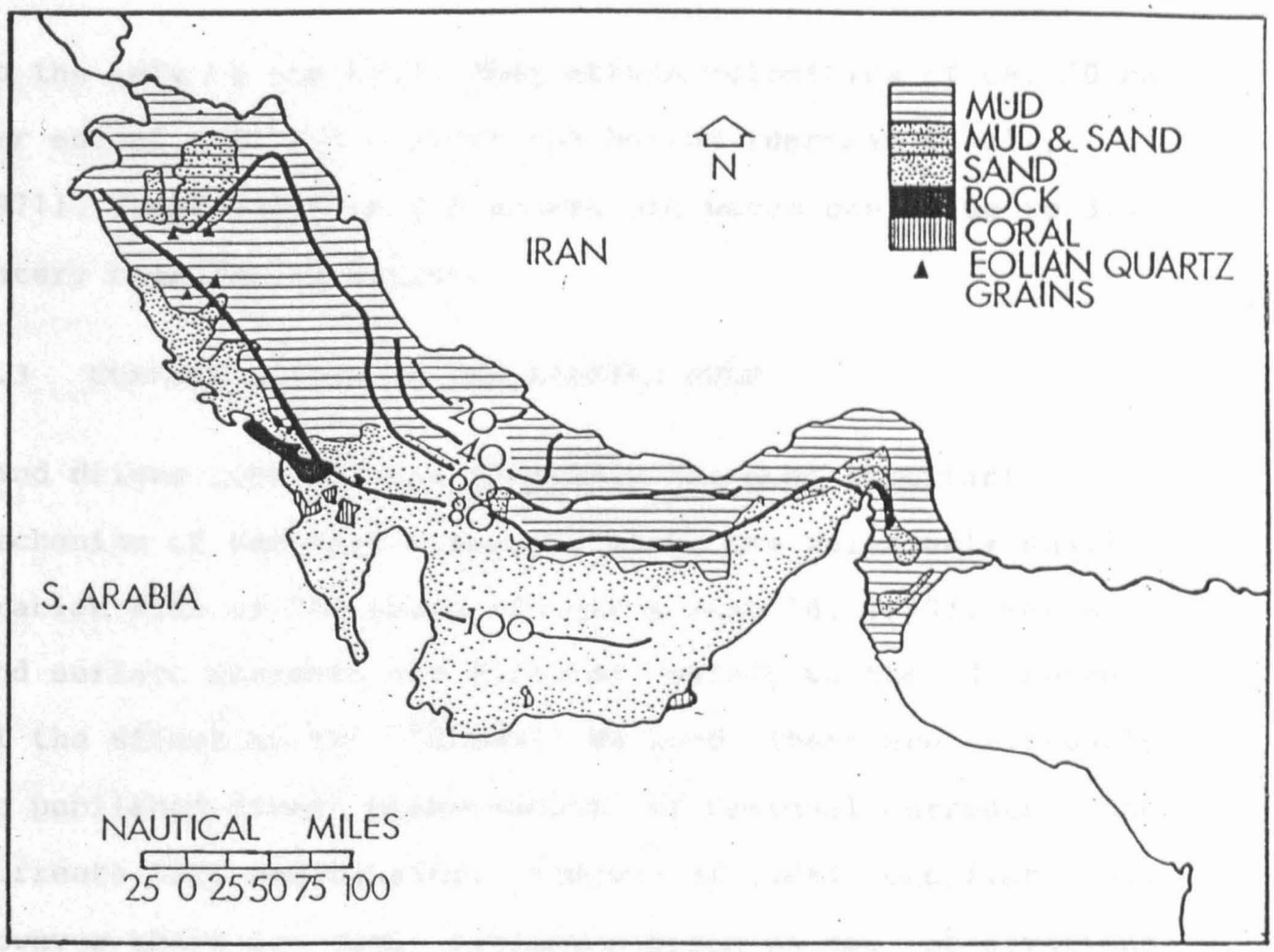


Figure 8.3 Sediments on floor of the Arabian Gulf. Contour lines show percentage of CaCo3 in sediments. After Emery (1956).

to the axis of the Gulf. They attain velocities of ca. 50 cm per second some 0-4 m above the bottom (Hartman et al., 1971). Tidal range is 2.5 metres and waves can be up to 3.5 meters high during storms.

8.3 CURRENT ACTION IN THE ARABIAN GULF

Wind driven currents are certainly the most important mechanism of sediment transport along the relatively shallow Arabian side of the basin (Purser & Seibold, 1973). Waves and surface currents are directed mainly to the SE because of the effect of the "Shamal" NW wind. There are virtually no published direct measurements of residual currents (the currents left behind after removal of tidal oscillations). However there are some estimates based on the observations of ships' drifts and of the distribution of salinity, and on the modelling of the dynamics of the water movement. Ship drift observations report a current strength of 0.1 and 0.2 m/sec (strongest in summer) along the western side of the Gulf (HMSO, 1977). Hunter (1983) produced a model of the overall residual currents in the Gulf. Hunter's predictions indicate an ouflow of water of strength around 0.05 and 0.1 m/sec along the bottom from the coastal areas off Saudi Arabia, Qatar and the United Arab Emirates.

8.4 QUATERNARY HISTORY

The present geomorphological situation of the region has not always been similar in the past. The effects of both

climatic and sea level changes have had a great influence on the geomorphological development of the area.

Details of the base level changes in the Gulf are imperfectly known. Doornkamp et al., (1980) gave a summary of the available evidence as follows:

(i) Evidence of a high sea level in the early Pleistocene of + 150 m was found in Oman Mountains, Saudi Arabian coast and Qatar.

(ii) Sea level has then fallen in stages resulting in the formation of terraces and inland sabkhas on the Arabian shore.

(iii) During this period more pluvial (wet) climate conditions dominated the region leading to increased stream erosion and wadi development. A deposit of coarse alluvial gravel was laid down in what is now called the Gulf of Salwa (Between Bahrain and Qatar). This deposit has been graded to a sea level of +90 m.

(iv) Subsequent to this deposition, Gulf of Salwa then suffered a tectonic subsidence (Kassler, 1973).

(v) Sea level then fell during the later Pleistocene to depths between -110 and -120 m (Sarnthein, 1972; Kassler, 1973). Thus continental conditions existed over much of the Arabian Gulf between 70,000 and 17,000 B.P. The Tigris-

Euphrates river system extended east as far as the straits of Hormuz. It was during this period of aridity that aeolian activity dominanted the region.

(vi) The exact timing of of the late Pleistocene and post-glacial rise in sea level are imperfectly known. However there is some agreement that sea level began to rise between 20,000 and 17,000 B.P, reaching its present level at about 5,000 B.P. The transgresive sea reached the -18 m level near Bahrain about 8,000 B.P and entered the Gulf of Salwa at about -7.2 m about 6,000 years ago.

Lakes in the Rub'al Khali and in An Nafud showed high levels in at least two different times, from 30,000 to 21,000 B.P, and from 9,000 to 6,000 B.P (McClure, 1978 & Whitney, et al, 1983). According to this evidence, it appears that a pronounced humid period developed during the first part of the Late-Pleistocene, in most or all of the Peninsula. During this episode, the present active dune fields were covered with vegetation and pluvial lakes existed in many areas of the Peninsula (McClure, 1978; Whitney, et al, 1983; Anton, 1984; Hotzl, et al, 1984).

In the Late Pleistocene-Early Holocene, there is much evidence showing that a marked increase in aridity occured in the Arabian and Saharan deserts (Hotzl, et al., 1978, 1984; Alayne and Grove, 1979; Butzer, 1980; Whitney, et al., 1983; Anton, 1983 & 1984). Dune systems started to form in the Rub'al Khali and An Nafud, and to a lesser extent in the Jafurah (Anton, 1983). According to existing age

determinations, the beginning of this episode can be estimated at about 21,000 years B.P. During this arid period, large dunes were formed in An Nafud (presently stabilized in most of the region; Whitney, et al. 1983) and in the Rub'al Khali (presently activated during the recent arid phase; Anton, 1983). In the Jafurah Sand Sea considerable aeolian activity is recorded in a large number of outcrops of aeolinites (Anton, 1983). According to age determinations of Lacustrine sediments in different areas of the Peninsula, this arid episode ended approximately 9,000 years B.P (Anton, 1983).

Shallow lakes started to form in the Rub'al Khali giving evidence for an increase in humidity coinciding with the beginning of the Holocene (dates 9,000-6,000 years B.P; McClure, 1978). These lakes started to dry up about 6,000 years B.P (McClure, 1978). Evidence from Nafud Alurayq shows a similar age for the last sub-aquatic deposits (about 5,600 years B.P; Whitney, et al, 1983). The present aridity in the Peninsula is believed to be a continuation of this arid period.

8.5 LANDSAT MSS AND TM INVESTIGATION

Landsat MSS band 1 digital image (0.5-0.6 μm) acquired on January 26th 1973 (path 176, row 42), and Landsat TM band 2 image (0.45 μm- 0.56 μm) acquired on Sept.26. 1984 (path 164 row 42) were used for this investigation.

Water, when free of suspended sediments transmits most of the light incident upon it and, under favourable conditions, the sea bed can be seen at depths of 20 m using Landsat data (Polcyn et al., 1970). Such favourable conditions exist in the Arabian Gulf.

The purpose of this investigation is to assess Landsat data for displaying submerged features in the shallow waters of the study area. Different water depths along the coast of the Gulf were also mapped using Landsat TM data and ground truth data (bathymetric maps). The image processing techniques used for this study are discussed in Chapter 3.

Figure 8.4 shows water depths displayed in different colours (image density slice classification) in the study area. It is clear, from the figure, that along the coast water depths ranges between 8 to 10 metres. Table 8.1 gives the DN (digital number) of the different classes (water depths) shown in Figure 8.4.

The enhanced Landsat MSS imagery, clearly shows the form of shoals and submarine sandbanks in the coastal sea between Saudi Arabia, Bahrain island and Qatar (Fig. 8.5). These features are detected on the Landsat imagery because of the difference in tone between them and the substratum.
Figure 8.6 is a Landsat MSS full resolution false colour subscene (MSS bands 4, 2, 1 shown as red, green, and blue respectively) showing both the offshore and onshore area. The offshore sandbanks appear as light green while the rest

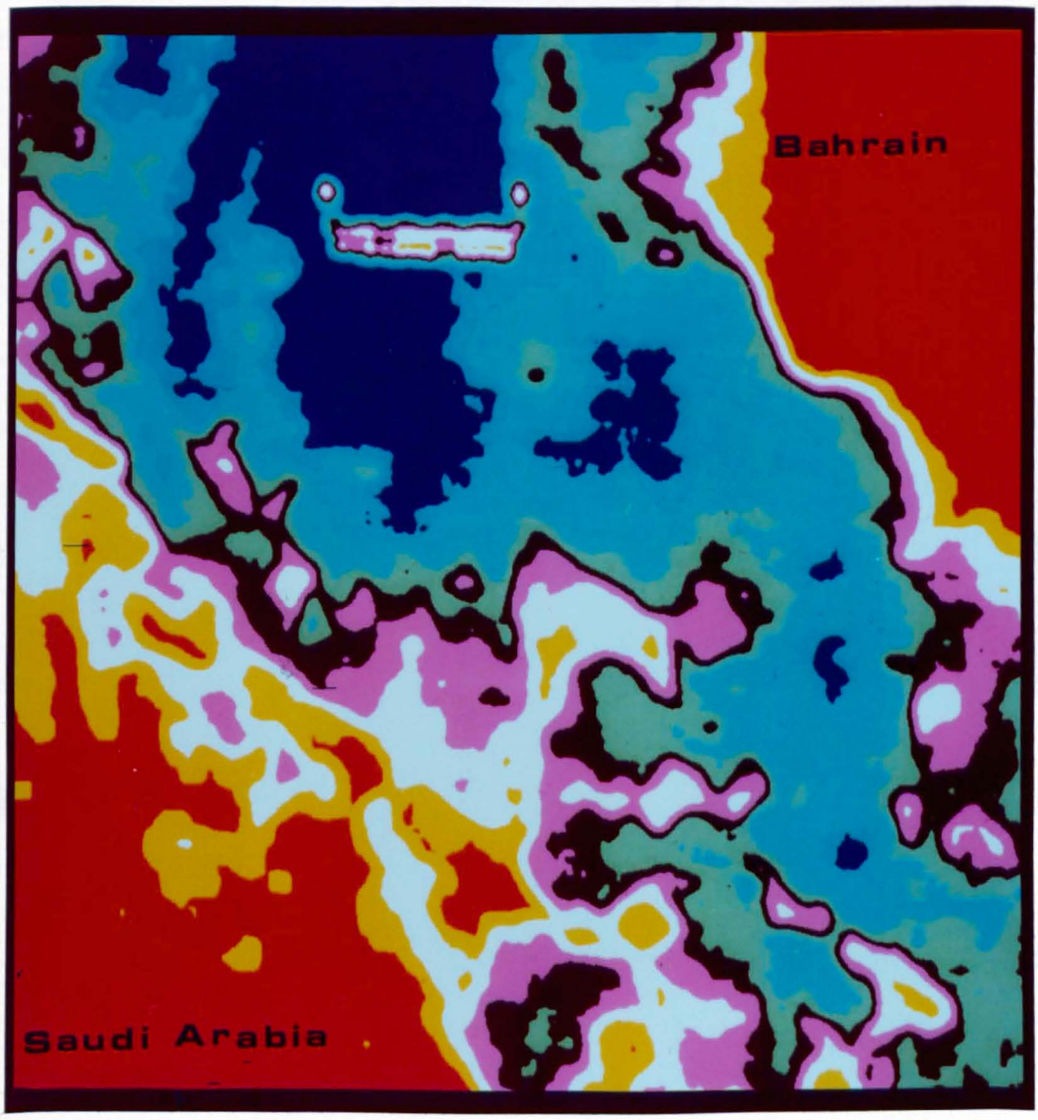


Figure 8.4 Landsat TM density sliced imagery. Water depths are displayed in different colours (see Table 8.1 for explanation of corresponding depths).

DN Range	Bathymetry Colour Image	Corresponding Water Depth in Metres
62 - 159	Dark blue	> 20
160 - 175	Light greyish blue	10 - 20
176 - 184	Cyan	--
190 - 202	Light green	8-10
203 - 214	Dark green	--
215 - 229	Magenta	--
230 - 245	Light pink	2-4
246 - 254	Yellow	0-2
255	Red	land

Table 8.1: The digital number (DN) values of the water depths observed on the Landsat TM band 2 imagery in the study area. The bathymetry colour image is shown in Fig. 8.4. Corresponding water depths are extracted from local bathymetric maps.

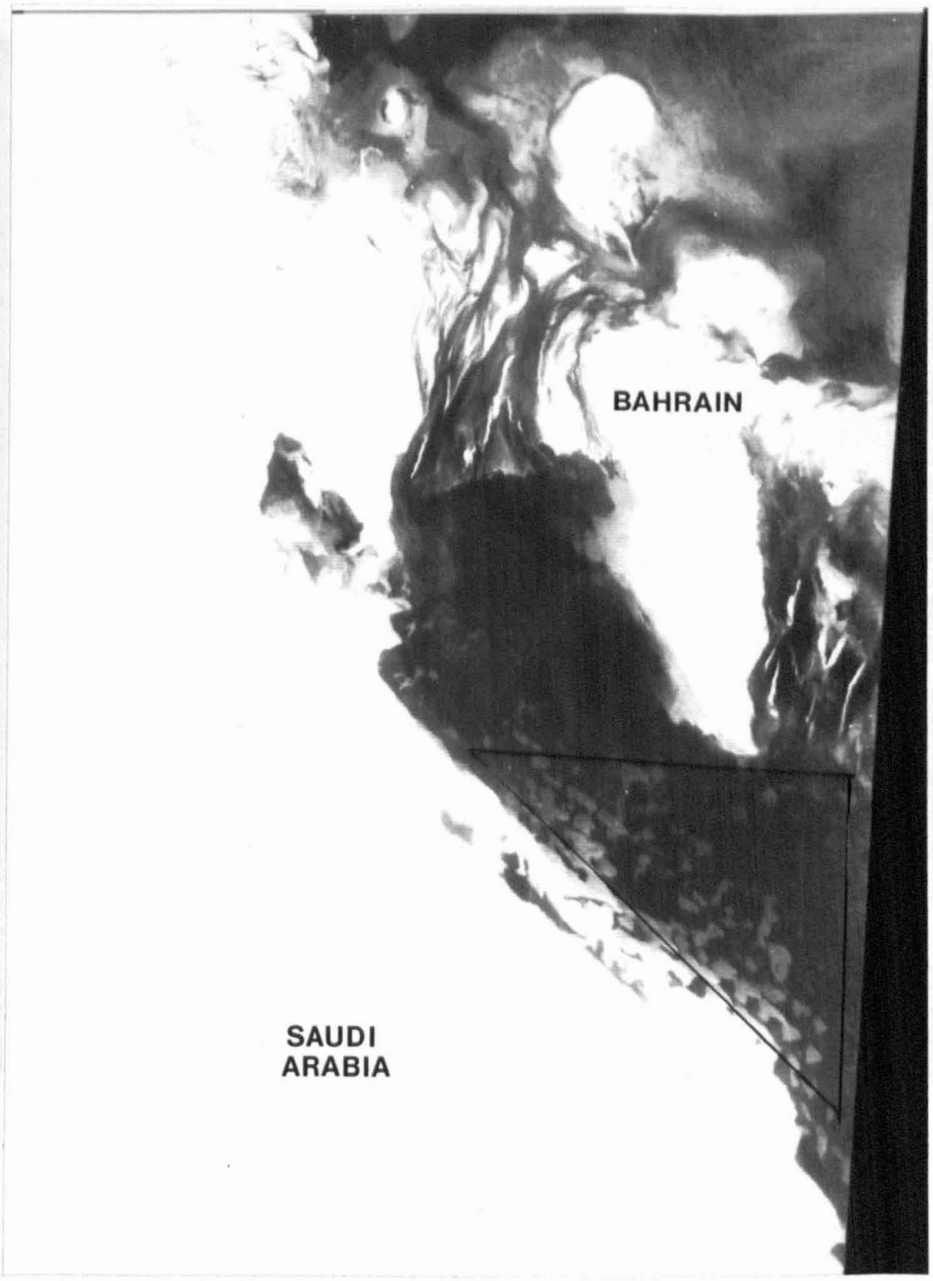
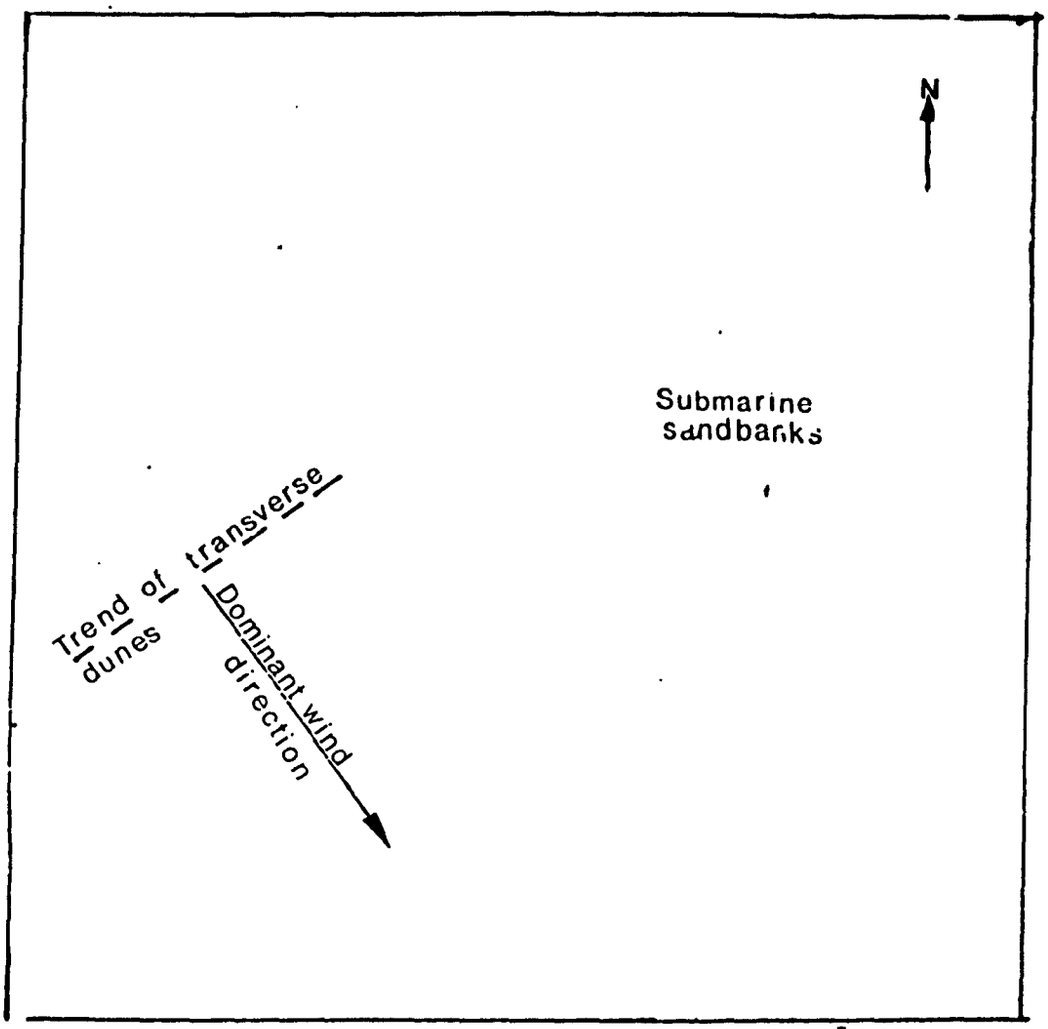


Figure 8.5 Landsat MSS band 1 imagery (176/42; 26 January 1973) interactively stretched to show offshore features. The submerged banks are cleary visible along the Saudi Coast.


N
Submarine sandbanks
Trend of transverse dunes
Dominant wind direction

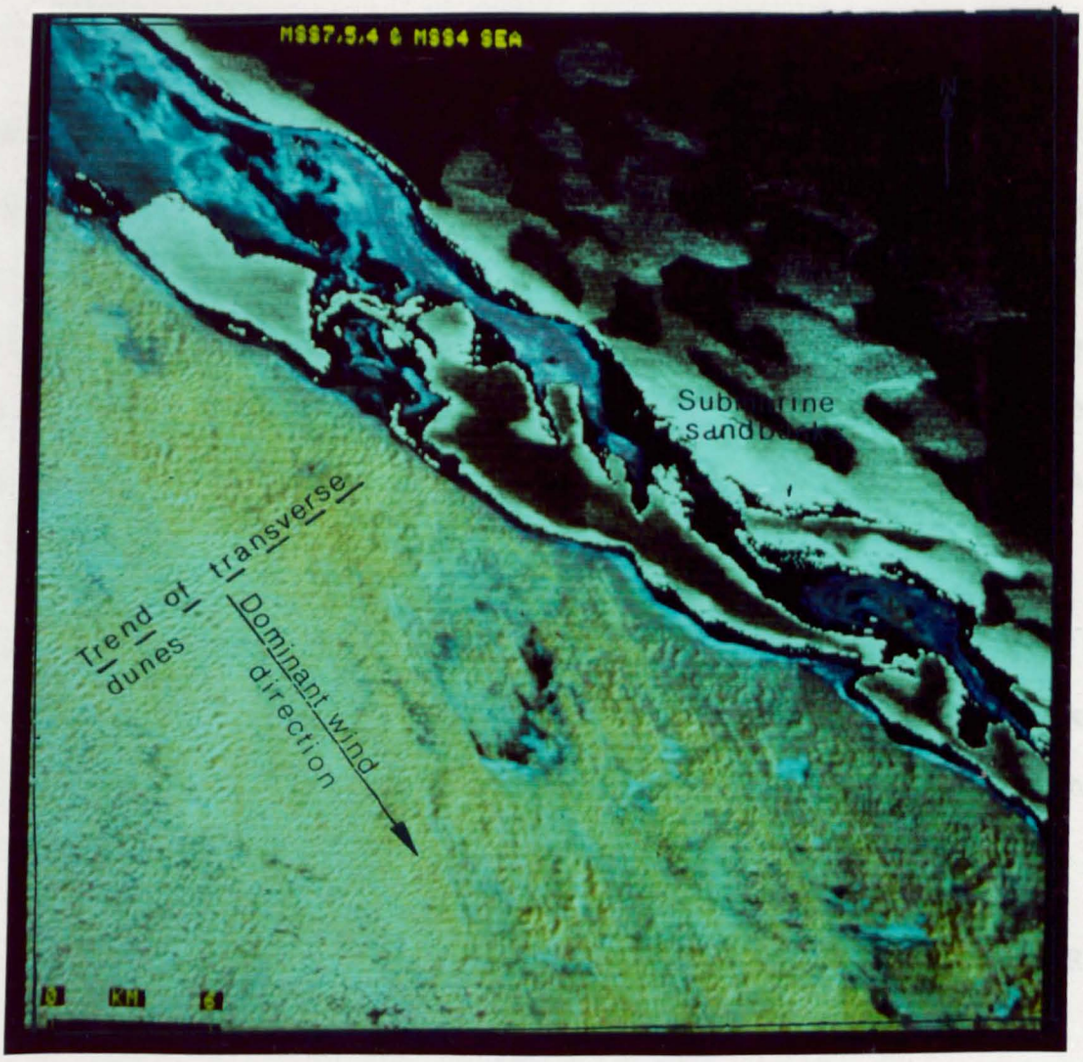


Figure 8.6 Combined image (false colour composite MSS bands 4 2 1) showing both offshore features and onshore areas.

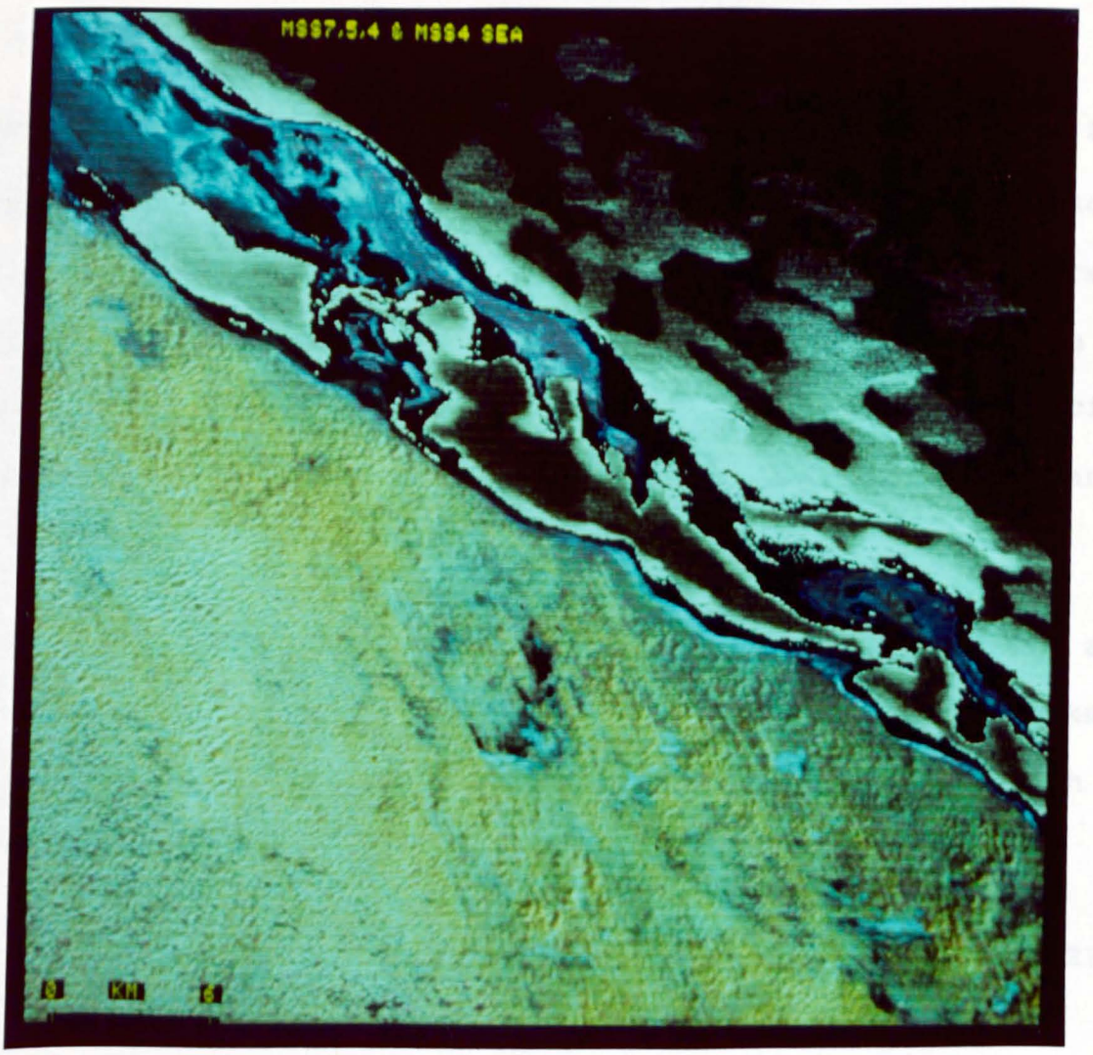


Figure 8.6 Combined image (false colour composite MSS bands 4 2 1) showing both offshore features and onshore areas.

of the area is dark.

Figure 8.7 is a Landsat TM imagery produced from TM band 1 (shown in red) and TM band 2 (shown in green) covering the same area as in Figure 8.6. The offshore sandbanks appears yellow in this imagery because of the high return of both blue and green light. The position of the sandbanks coincide with the the water depth of 8 to 10 metres or the DN range of 190-202 (Fig. 8.4; Table 8.1).

Table 8.2 gives the morphometry of these features (width and the spacing between them). The width ranges between 1.5 km to 3.2 km with an average of 2.5 km and an average length of 4.5 km.

8.6 COMPARISON BETWEEN ON-SHORE DUNES AND THE OFF-SHORE FEATURES.

The comparison between the on-shore dunes and the off-shore features is based mainly on shape, form, scale, and previous investigations. Landsat MSS and TM imagery, aerial photographs and echo-sounding monographs were used to investigate the morphology of both on-shore dunes and off-shore features. No under water investigation of the off-shore features was carried out during this research because of logistic and cost limitations. Hence, the evidence presented here comes mainly from the remote sensing data investigation.

ECHO SOUNDING INVESTIGATION: Two echo sounding traces were

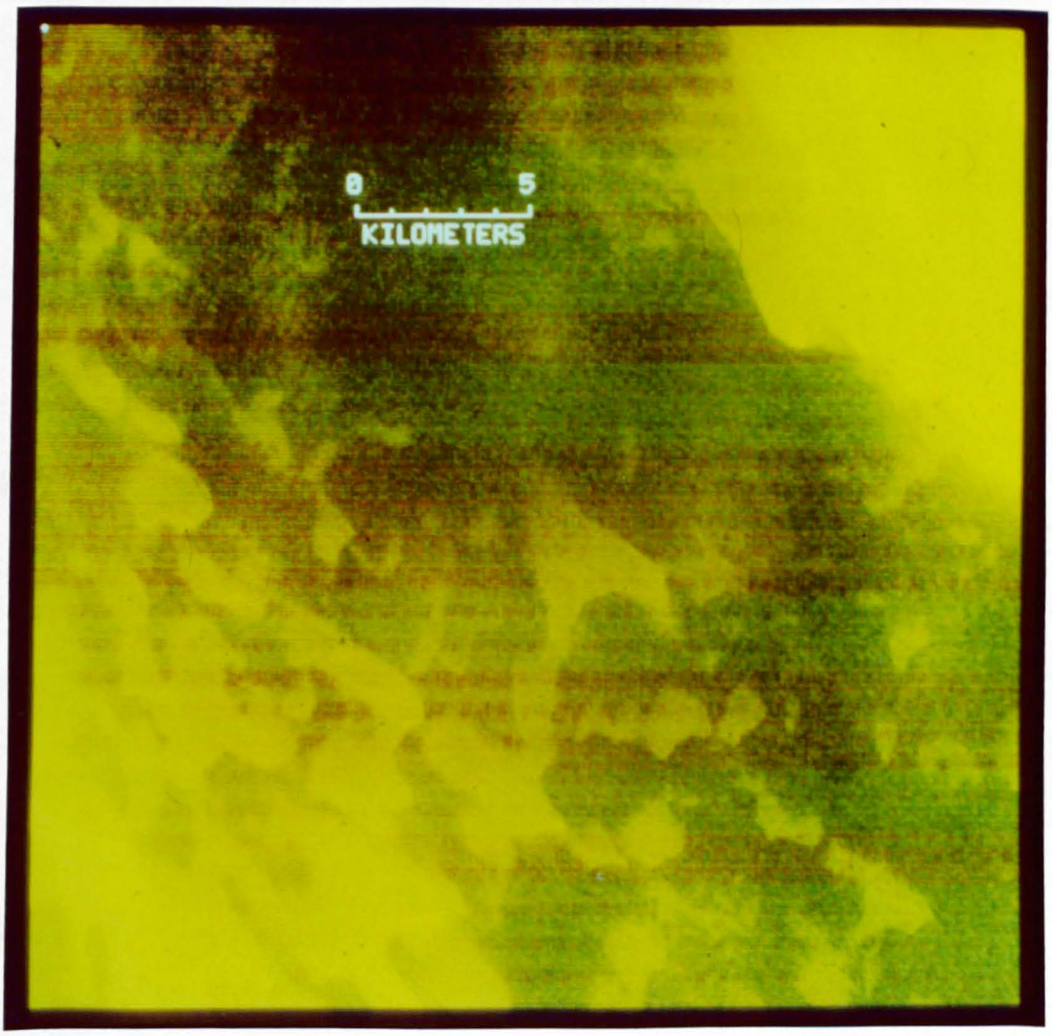


Figure 8.7 A combined Landsat TM band 1 (displayed in red) and TM band 2 (displayed in green) imagery (164/42; 16 January 1985) displaying the same submarine sand banks shown in Figure 8.6.

Submerged Features*	$\overline{W}$ (m)	$\overline{L}$ (m)
	2,500	4,500

Table 8.2: Morphometry of the submerged features based on Landsat TM (band 1) imagery (see Fig.8.6).

$\overline{W}$, means feature width, $\overline{L}$, means feature length.

* Measurement based on 20 samples.

run in the vicinity of the submerged sandbanks (north south direction) to investigate any variations in the submarine topography (Fig. 8.8). Figure 8.9 is a sediment echogram showing mounds (maximum height of 8 metres) which coincide with the position of some submarine features shown in the Landsat MSS and TM images (Fig.8.6 & Fig. 8.7). The gentle rise in the northern end and the sudden depression in the southern end of these features (as shown in the echograms) suggests a slipface pointing in the southern direction. The tops of the mounds according to Atkinson (1986, personal communication) consist of coarse, often lithified sand upon hard-bottomed biotopes develop, based mostly on algal and bivalve assemblages. On the sides and around the bases of the mounds, fine grained sands accumulate and here seagrass may grow. Unfortunately, these ecograms lacked the precise height measurement of these features.

SHAPE AND SIZE: The general shape and approximate barchanoid outlines of the submarine sandbanks, together with their orientation, shows a similarity with the onshore dunes. Figure 8.10 shows dunes prograding off-shore at Doha Dhalum north of the study area. The on-shore dunes (mostly domes and barchans) and the off-shore features are oriented at about N 55 E indicating a similar prevailing paleo-wind direction (NNE). However, the sizes of the two features are different. Measurement of widths of the nearby on-shore dunes range between 80 and 400 m and those of the off-shore features range between 1.5 to 3 km (Table 8.2 & 8.3). This

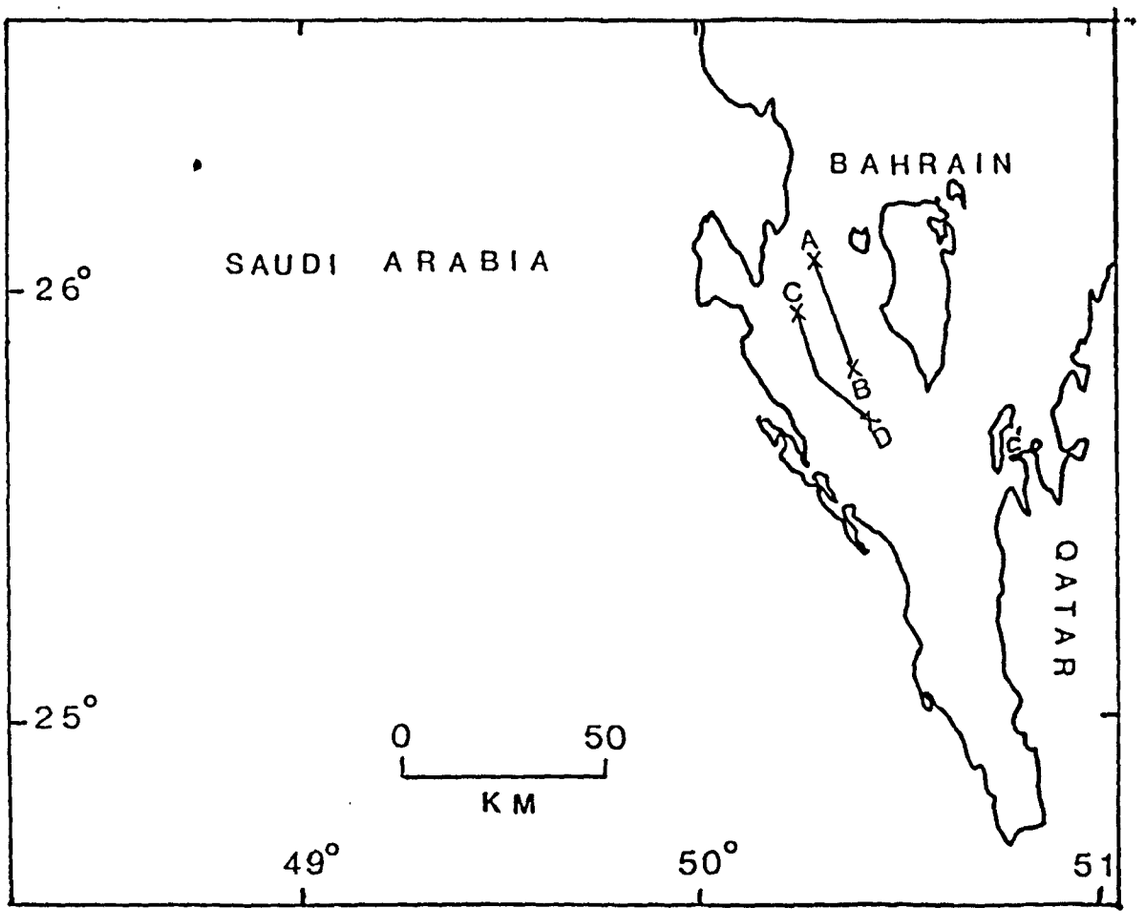


Figure 8.8 Location map of echo sounding profiles.

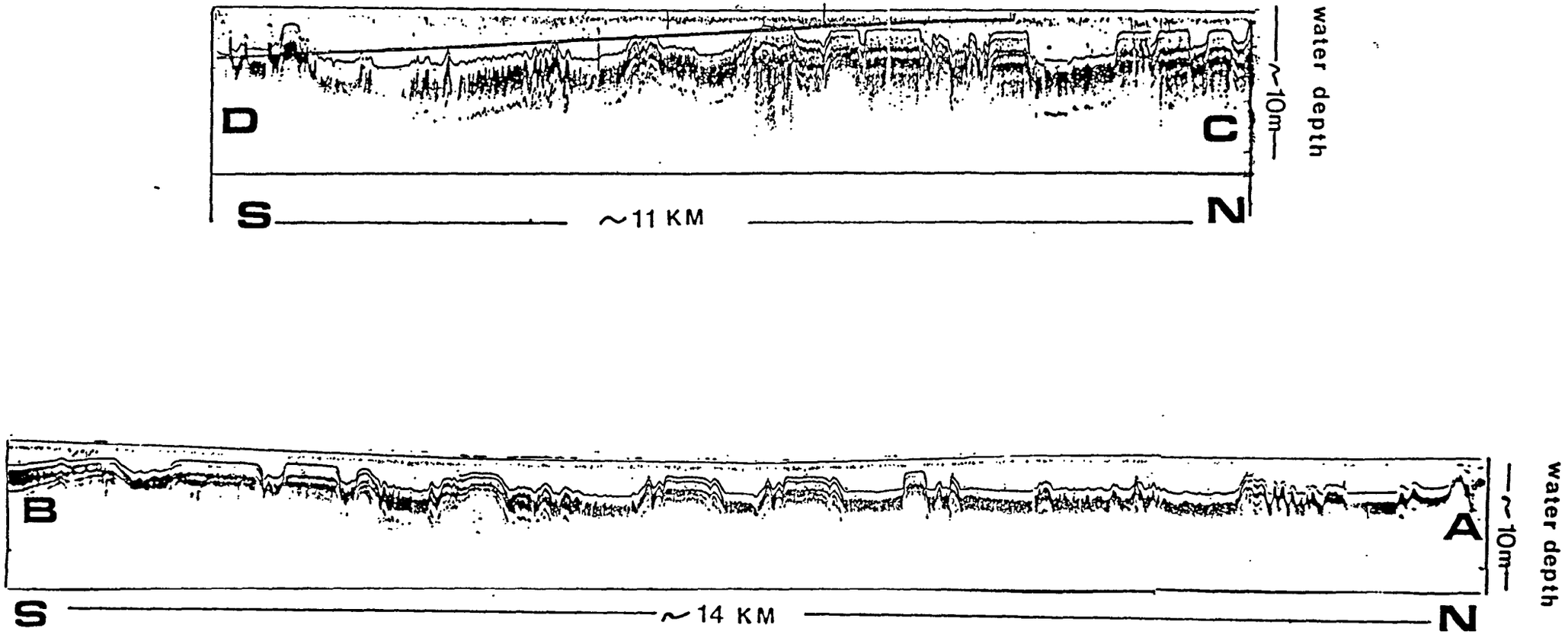


Figure 8.9 Sediment echograms of transect A-B & C-D (shown in Figure 8.8) showing mounds interpreted as possible submerged sand dunes. Dark areas represent soft sediments.

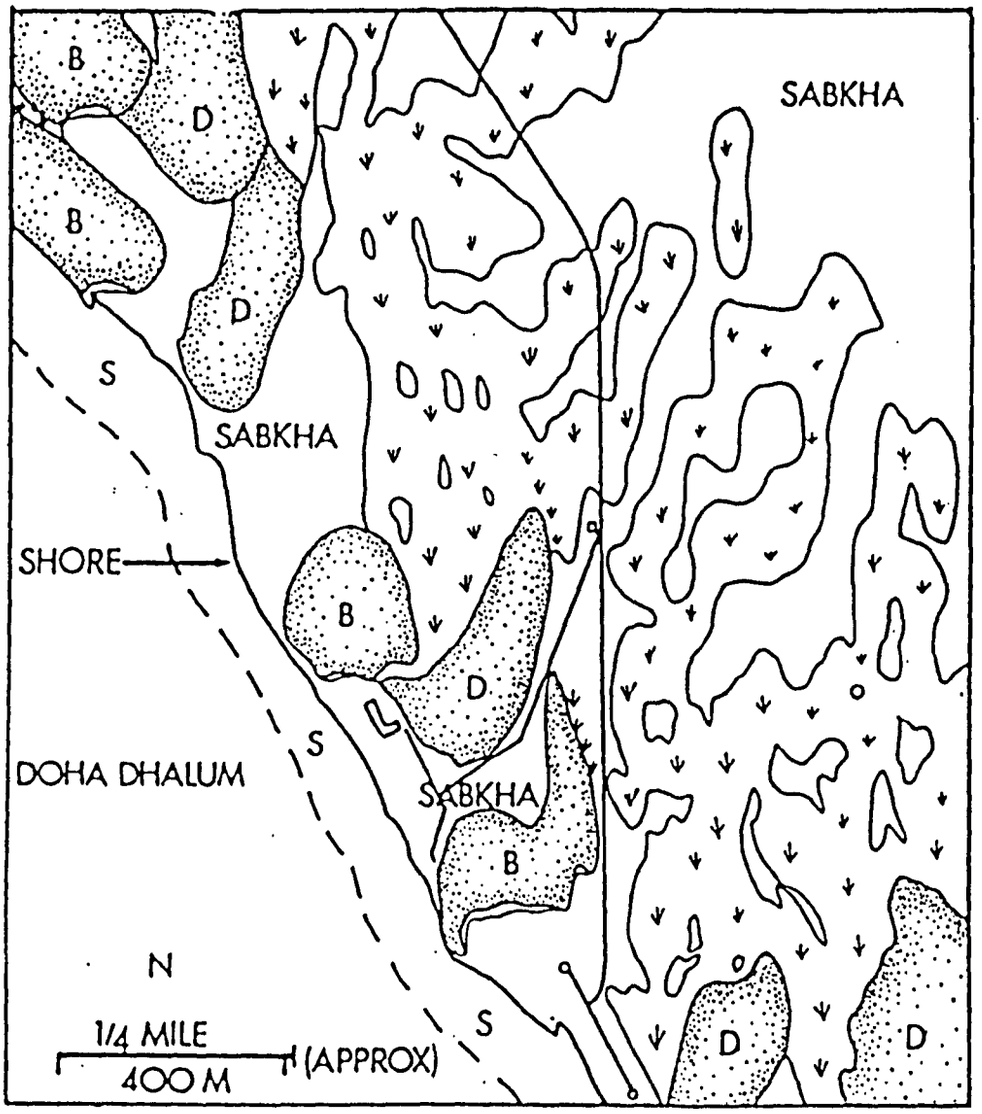


Figure 8.10 Onshore dunes prograding into water (Dohat Dhalum) north of the study area. Dome dunes (D) and barchans (B) are present. (S) indicates nearshore zone. Notice the similarity in morphology and distribution of these dunes and the offshore features shown in Figures 8.6 & 8.7.

Dune Type	$\overline{W}$ (m)	$\overline{L}$ (m)	$\overline{H}$ (m)
Barchan*	150	300	8
Barchanoid ridges*	400	350	8
Dome*	80	400	6

Table 8.3: Morphometry of the on-shore dunes measured in the field.

$\overline{W}$, means dune width; $\overline{L}$, means dune length;

$\overline{H}$, means dune height.

* Measurement based on 100 dune samples.

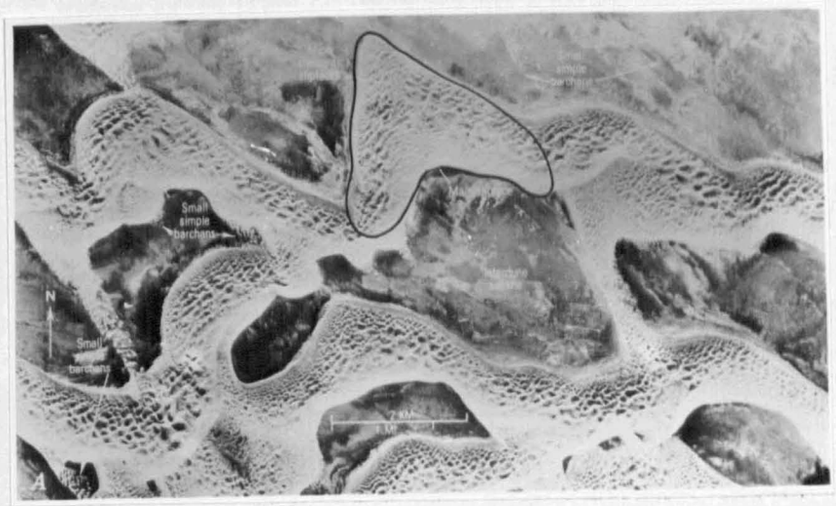
difference in size could be attributed to a stronger wind velocity in the past or possibly to remoulding by marine currents.

The form and scale of the submarine sandbanks is also similar to that of large aeolian dune complexes in the north eastern part of the Rub Al Khali area (Empty Quarter) of Saudi Arabia (Fig. 8.11a,b,c,d). In the Empty Quarter, individual compound crescentic dunes or "mega-barchans" as defined by Norris (1966) are generally larger than individual crescentic dunes. The mega-barchans are complicated in shape by the presence of smaller crescentic dunes on their gently-sloping windward flanks. Mega barchans in the Empty Quarter are about 3 Kilometers across. This is comparable with the scale of the submarine sandbanks (Fig. 8.11c). The outline form of both onshore dunes and submarine features are functions of the tonal contrast between sand and substrate which, in the Rub'al Khali, is a salt flat (Sabkha).

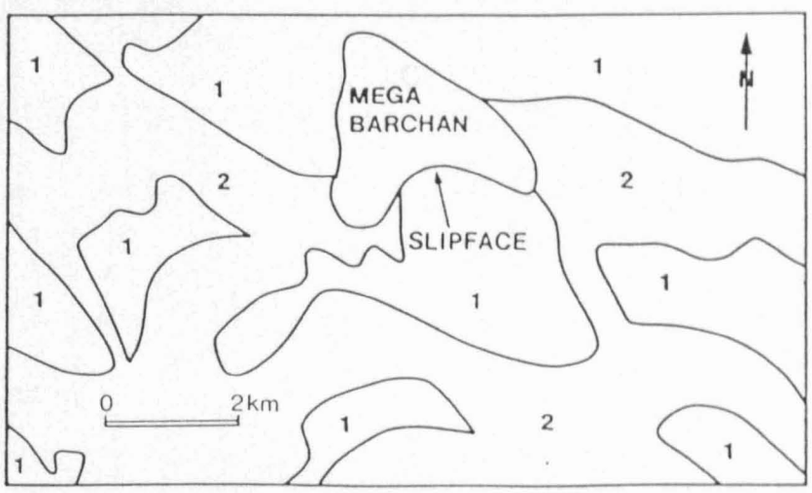
8.7 DISCUSSION

The scale, shape and orientation of the sandbanks revealed on the Landsat imagery suggest that they may be submerged aeolian dunes. Both shape (barcahnoid form) and orientation (N55 E) of the submerged features are similar to the on-shore dunes located in the Jafurah and the Rub'al Khali sand seas. The sizes of these features are comparable with

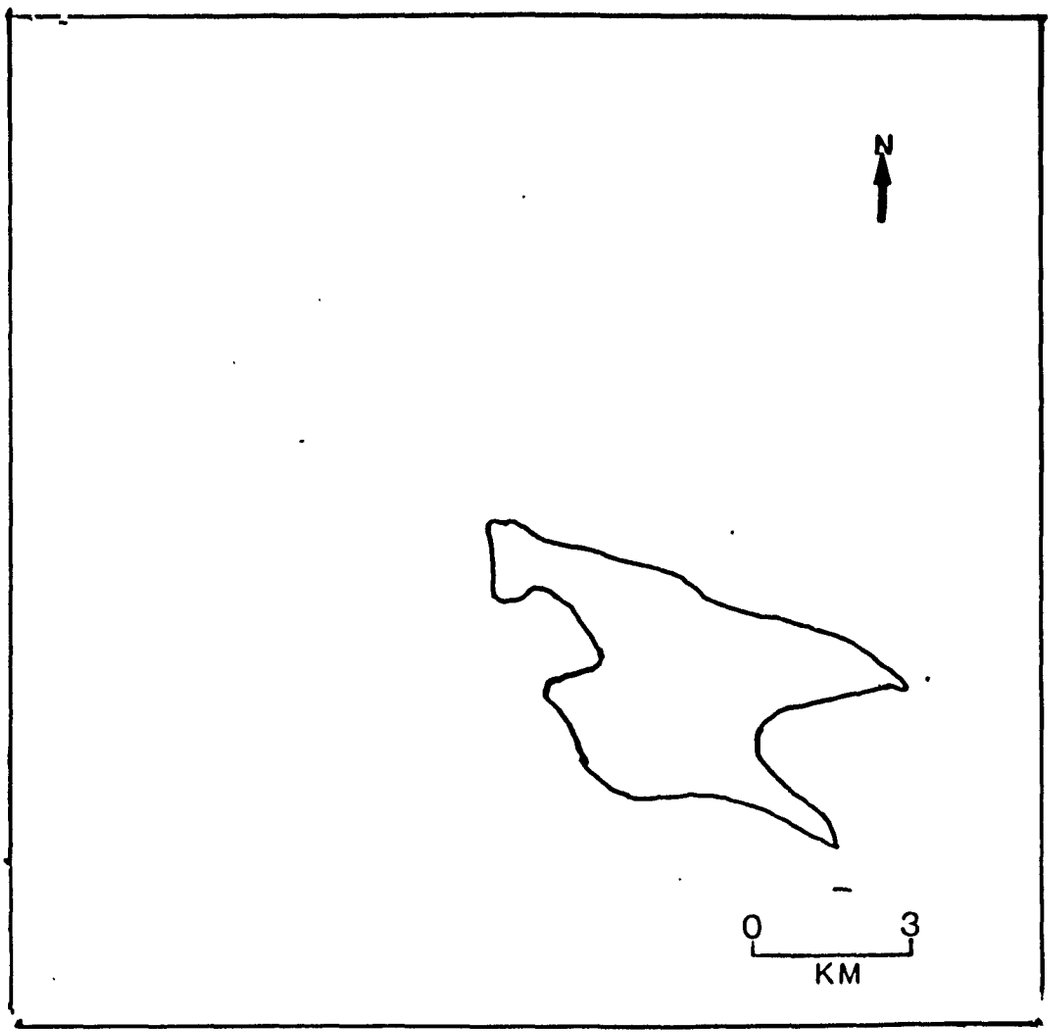
Figure 8.11 (a) Compound crescentic ridges in the eastern part of the Rub'al Khali sand Sea, approximately 23 N, 54 E. A giant crescentic dune is outlind for scale comparison with the submarine banks in the study area. The width of this mega dune is about 3 km and about 3.2 km long. Photograph by U.S Department of Defence (reproduced from McKee 1979a). (b) Interpretation map based on aerial photograph is shown in (a). Annotations (1) and (2) represent inter-dune sabkha and crescentic ridges respectively. Notice the similarity in shape and scale of these aeolian features and (c). (c) An enlargement of part of Figure 8.6 showing submerged sandbanks. A possible giant crescentic (mega-barchan) is outlined for comparison with the mega-barchan shown in (a). The width of this feature is about 3.2 km. (d) Interpretation map derived from (c). Annotations (1) and (2) are interpreted as possible inter-dune areas and crescentic ridges respectively.

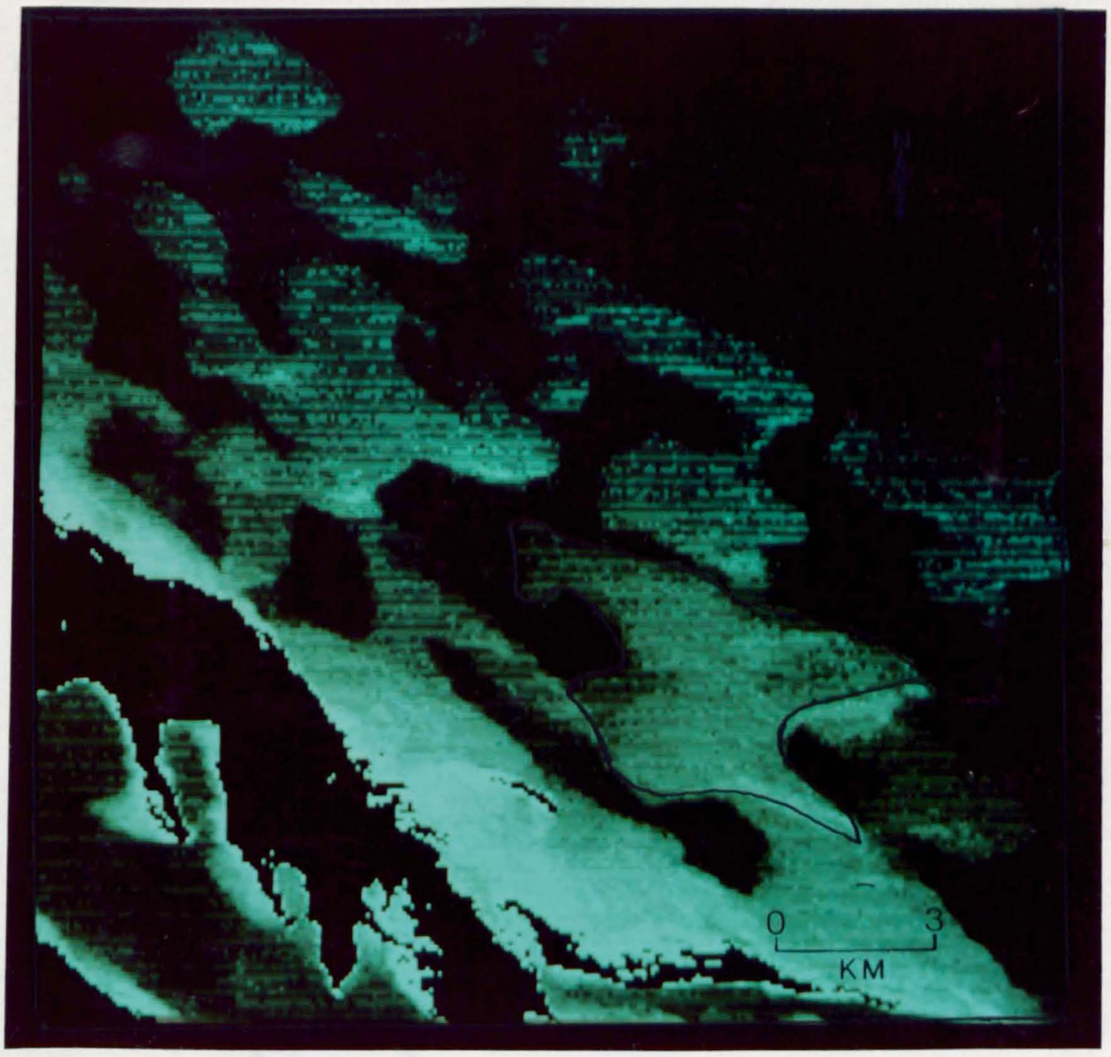

Small simple barchans
N

a

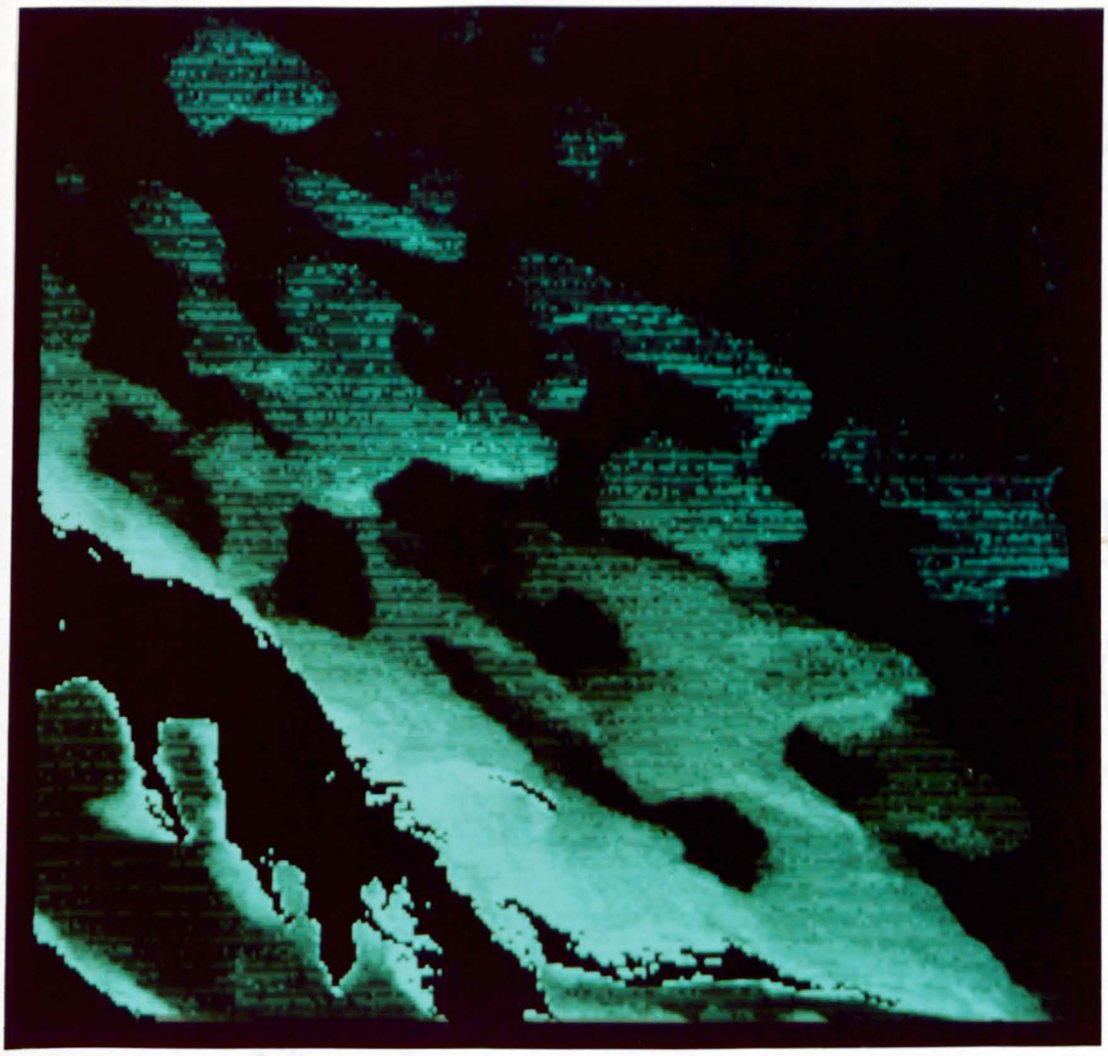

1
1
MEGA
BARCHAN
1
N
2
2
1
SLIPFACE
1
1
0
2km
1
2
1
1

(*b*)

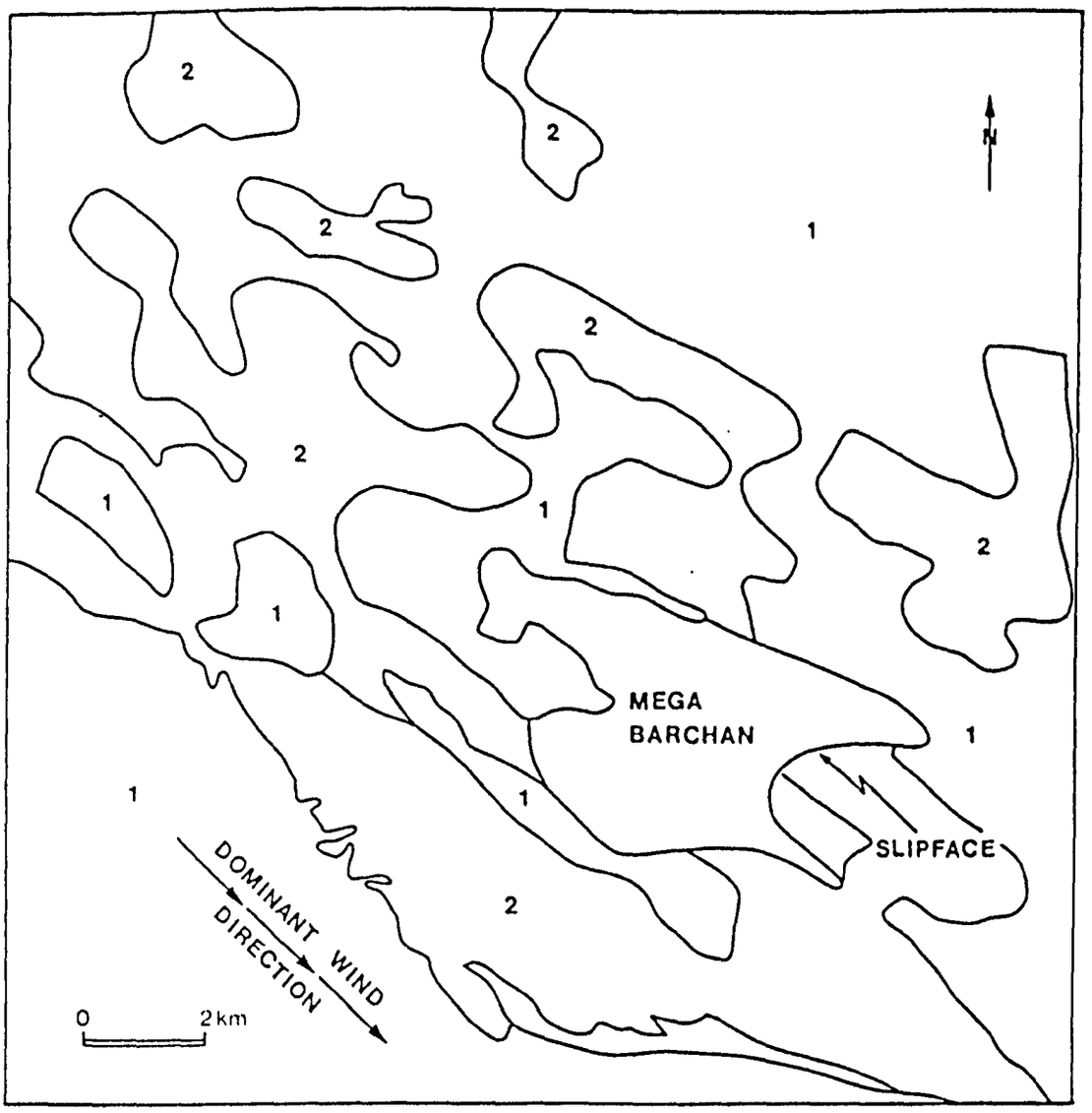

N
0
3
KM



C



C


2
2
2
2
2
1
1
1
1
1
1
1
2
2
2
N
MEGA
BARCHAN
SLIPFACE
DOMINANT WIND
DIRECTION
0
2km

d

the mega barchan dunes of the Rub'al Khali but not with the nearby dunes of the Jafurah. The difference in scale between the on-shore dunes of the Jafurah and the off-shore features on the floor of the Gulf of Salwa could be attributed to a change in the strength of the wind regime (stronger paleo-wind regime to a less vigorous present wind system). Whitney et al ., (1983) argued that there is a decrease in aeolian activity from late Pleistocene to the present. This decrease appears to be a worldwide climatic event because decreases in the rate of aeolian deposition are also recorded in marine sediments of the eastern Atlantic (Sarnthein et al., 1981). Other evidence supporting this argument is the existence of small active dunes on top of larger older stabilized dunes as is the case in the An Nafud (Figure 3 page 13 in: Whitney et al., 1983)and the Rub'al Khali sand seas (Fig. 8.11a). The formation of these small active dunes at the present indicates that modern wind environments are not capable of producing large size dunes. The present dune fields of the Jafurah were only formed recently. The evidence for the age of the Jafurah dunes can only be speculated from recent dune movement measurement in the area. Present day migrating barchans on sabkhas in the Jafurah are generally a few kilometers downwind of the identifiable sand source areas. Measurement of dune movement on a sabkha floor shows a maximum movement of 8 m/year (see Chapter 6 for dune movement measurement results). Hence, the oldest dunes should not be more than 1,000 years old.

However, if migration rates were slower during the first stages of dune migration, and if it is accepted that a wetter period happened between 2,500 and 1,000 years B.P (as suggested by Gasse et al., 1980) it is possible that dune migration in the Jafurah restarted between 3,000 to 4,000 years ago. This estimated age of the Jafurah dunes and the evidence of a less vigorous wind velocity during recent times could explain the difference in sizes between the documented on-shore dunes and the proposed submerged dunes.

The approximate barchanoid form of the submarine sandbanks suggests the intriguing possibility that they are the drowned dunes proposed by Doornkamp.et al., (1980) forming part of the aeolinites which include those of Qatar and Abu Dhabi (Shinn,1973). In 1980 Doornkamp et al produced many lines of argument to support the presence of drowned dunes in the Gulf of Salwa between Bahrain and the Saudi Arabian coast. Kassler (1973) suggested that the sands for Abu Dhabi dunes may have arrived there by migrating across the Gulf of Salwa and the Qatar peninsula prior to 7-800 years BP. Dune studies by Seltrust Engineering Ltd (1980) showing movement rates of about 8 meters per year in Qatar indicate that all Qatar's major dunes, which are in the southeastern part of the peninsula, could have migrated the 60 kilometers from the west coast in the 8-10000 years since sand supply was cut off by sea level rise. Figure 8.12 is a Landsat MSS false colour composite (bands 4, 2, 1) of Qatar showing the concentration of the dunes in the southeastern part.

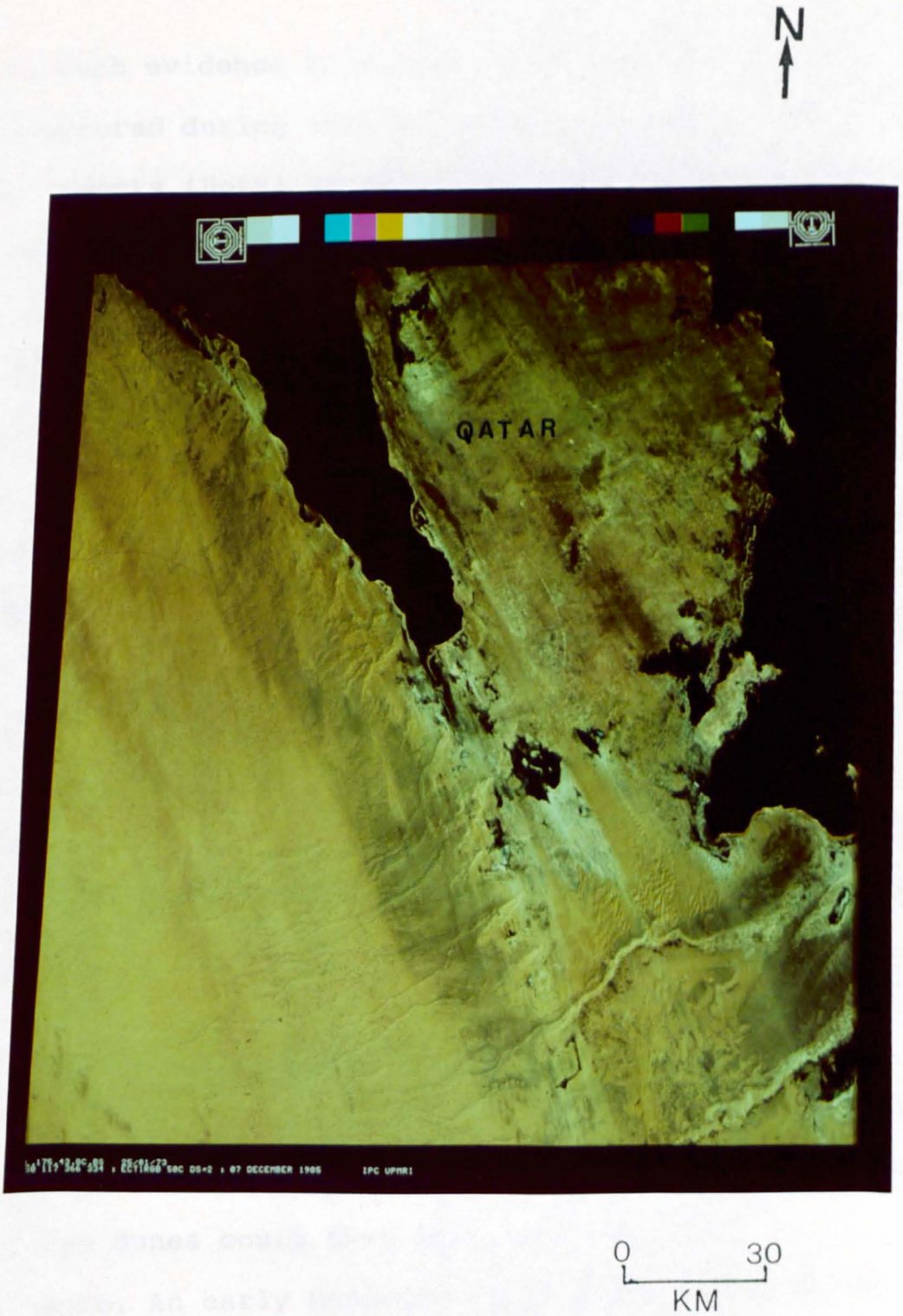


Figure 8.12 Landsat MSS false colour composite (4 2 1) acquired over Qatar (176/43; January 25 1973). Dunes are located mainly in the southeastern part of Qatar (right hand side of the imagery).

There is much evidence to suggest that a marked increase in aridity occured during late-Pleistocene in the Arabian and Saharan deserts (Hotzl et al., 1978, 1984; Alayne and Grove, 1979; Butzer, 1980; Whitney et al., 1983; Anton, 1983). During this arid period (estimated at about 21,000 B.P) large dunes were formed in the Rub'al Khali (today re-activiated during the recent arid phase) and An Nafud (still stabilized in most of the region). In the Jafurah sand sea, aeolian activity is recorded in a large number of aeolinites in Al Qurayah north of the study area (Anton, 1986). Aeolinites, composed of quartz sand and marine shells are also found in several locations in Bahrain (Doornkamp et al., 1980). If the detected submarine feature are indeed submerged sand dunes then there is a possibility that they were formed during this arid phase when the sea level was at a minimum of approximately -120 m.

The suggestive evidence that the detected features are drowned dunes raises the question of how could such dunes survive the erosive processes of submergence?. The answer is that these dunes could have been cemented prior to submergence. An early Holocene humid phase dated (9,000 - 6,000 years B.P; McClure, 1976) following the arid period could be the cause of the cementation of these dunes and the aeolinites found in Bahrain and Saudi Arabia. During this period shallow lakes started to form in the Rub'al Khali (McClure, 1976) and soils developed on the Dahna sand sea of Saudi Arabia (Anton, 1985) suggesting a strong humid phase.

An alternative interpretation of these submerged features is that they are barchanoid sand waves formed wholy by marine currents rather than by aeolian processes. The formation of such mega-sand waves of the size detected on the Landsat imagery requires a strong current. The strength of surface currents on the western side of the Gulf ranges between 0.1 and 0.2 m/sec (see section 8.3). This relatively weak current could only produce sand waves of amplitude ranging between 0.30 cm and 1.66 m as observed off northern Bahrain by Cloet (1954). The Landsat MSS imagery (acquired Jan, 1973; Fig. 8.6) and the Landsat TM imagery (acquired Jan, 1984; Fig. 8.7) reveals no modification in the morphology nor in the position of these sandbanks in the 12 years period indicating a possible nil current effect. However, a combination of an aeolian origin of these sandbanks followed by some modification by marine currents in the past is not ruled out.

8.8 SUMMARY

Digital image enhancement of Landsat MSS and TM images for the coastal area of eastern Saudi Arabia revealed large sandbanks in relatively clear water (8 to 10 m deep). In the area investigated, there is an interesting possibility that the sandbanks revealed may be fossil aeolian dunes, which could have migrated to their present submerged positions prior to their drowning during the last eustatic sea level rise (8,000-10,000 years BP). Several lines of evidence

support the submerged dune hypothesis were presented in this chapter. This evidence is however not conclusive and the submarine sandbanks need considerable on site investigation before this hypothesis can be confirmed.

Field work is obviously necessary to confirm the mechanism of formation of the sand bodies.

CHAPTER 9

CONCLUSIONS AND RECOMMENDATIONS

The investigation conducted for this research supports the following conclusions:

Production of false colour composites is essential in the identification of sand bodies (yellow) since these can be confused with cloud formations or salt deposits which appear similarly bright on black and white images. The best colour composite combination obtained for enhancing sand colour is the combination of bands 4 or 3 (7,6), 2 (5), and 1 (4) for MSS imagery and bands 4, 3 and 2 for TM imagery displayed as red, green, and blue respectively.

Colour transformation helped in showing sand colour variations between and within sand seas. Sand Colour variations are particularly useful in the interpretation of the dune morphology and the origin of sand sources.

Edge enhancement using different directional filters proved to be useful in sharpening dune edges making boundaries much easier to map. In addition, the power spectra are of considerable assistance in determining dune parameters (wavelength and orientation). The non-directional filters (textural) highlighted the need for the design of special filter masks with consideration to the sizes of the investigated dunes. Difference Gaussian (DoG) filters with

dune size prameters used in the design of the mask elements, gave excellent results. The use of these filters becomes very important when mapping dune sizes that are close to the spatial resolution of the imagery.

Comparisons between Landsat MSS bands showed that band 1 (green band) is very effective in the detection of iron coating in sand grains. Dune sands appear dark in MSS band 1 imagery. This finding can be used in tracing the origin of the sand source. MSS band 1 and TM band 2 proved to be very effective in penetrating shallow waters which helped in the mapping of the submarine sand banks found along parts of the Saudi Coast of the Arabian Gulf.

Digital image enhancement of Landsat MSS and TM images for the coastal area of eastern Saudi Arabia revealed large sandbanks in relatively clear water (8 to 10 m deep). In the area investigated, there is an interesting possibility that the sand banks revealed may be fossil aeolian dunes, which could have migrated to their present submerged positions prior to their drowning during the last eustatic sea level rise (8,000-10,000 years BP). The submarine sand banks need considerable on site investigation before this hypothesis can be confirmed.

Spatial resolution of Landsat MSS and TM images was assessed for sand dune mapping. In Landsat MSS imagery dunes (located in high contrast areas) which are 100 metres and more across were identified; in low contrast areas, dunes only larger

than 200 metres across were detected. In Landsat TM imagery dunes larger than 40 metres across (located in high contrast areas) were identified; in low contrast areas, dunes only larger than 70 metres were detected.

The LFC photographs provided an improvement in resolution and in the extent of the area covered in one photograph (356 x 175 km). Additional advantage of the LFC photographs is the stereo capability which permits measurement of dune heights to an accuracy of about 15 metres. The high spatial resolution of the LFC photographs helped in mapping small size dunes (widths 10 m and more) which are beyond the resolution offered by Landsat MSS and TM imagery.

Radar imagery provided a good basis for mapping dune types. Shuttle Imaging Radar (SIR-A) imagery showed no advantages over other forms of remote sensing data. In fact, Landsat MSS imagery with lower spatial resolution than the SIR-A imagery shows more definition of dune shapes. The limitations of the SIR-A imagery in sand dune mapping arises from restrictions in the radar look direction (one look direction).

Aerial photographs were examined to complement or substantiate interpretations drawn from other forms of remote sensing data. Infrared aerial photographs of 1:10,000 scale were found to be extremely helpful in detecting small size dunes (width 10 m and more), and to differentiate between vegetated sand sheets and parabolic dunes. At scales

of 1:60,000 and 1:80,000 panchromatic aerial photographs were useful in identifying narrowly spaced medium size barchanoid ridges and barchan dunes which were not recognizable in Landsat MSS or TM imagery. A scale of 1:25,000 is extremly useful in sand dune mapping and in morphometric measurements such as dune height, width, length, and the spacing between different dunes. At this scale, aerial photographs can be used as a ground truth for other remote sensing data. Moreover the stereo coverage of the aerial photographs helps in identifying orientation of slip faces for different dune types and thus mapping the direction of dune migration.

Repeated coverage by Landsat MSS imagery proved to be a good tool for depicting regional sand distribution patterns. In study area (2) temporal changes of sand bodies between 1973 and 1984 were easily compared and mapped. However, when multi-temporal Landsat MSS images were used for sand dune movement measurement in study area 1, several problems were encountered. These problems include:

(a) Lack of sufficient ground control points necessary to achieve high registration accuracy between multi-temporal images.

(b) Spatial resolution of Landsat MSS imagery (80 metres) is too coarse to detect the relatively slow movement of the investigated dunes (< 8 metres/year), over the 12 year period for which images are available. The identification of

individual dunes for this study was only possible because of their wide spacing and the high albedo contrast between sand and the substratum (sabkha). In areas where dunes are closely spaced, delineation of individual dunes is more difficult.

(c) The time span of 12 years used in this study was not enough to detect the relative slow movement of the dunes.

When compared with field data, aerial photographic interpretation gave more reliable results than those achieved from MSS imagery.

IMPLICATIONS TO A SAND CONTROL PROGRAM: This investigation has demonstrated the value of an integrated study of dune movement based on Landsat MSS imagery, aerial photography, and actual field measurement. In planning for a sand control program, deployment of such approach is considered to be vital for the following reasons:

(i) Acquisition of field data in deserts is difficult and expensive. Using space imagery and aerial photography reduces costs and hazards.

(ii) Landsat imagery with its uniform scale, repeatability, and large scale coverage is an effective tool in continuous monitoring of sand dune patterns. The example shows that the perspective gained from Landsat MSS images of study area (2) allows the relatively rapid identification of areas of dune accumulation and sand-free zones. These can then be mapped

with a good degree of accuracy at 1:250,000 scale. This information is important to the planning of agricultural expansion in the region, and to the selection of new village or city sites. This is particularily useful for urban planners, agricultural authorities, and military engineers.

(iii) With knowledge of the average rate of motion of the dunes and the direction of wind, it is possible to forecast dune positions in the future and to determine the places most likely to remain dune free for extended periods of time. For example, the number of years before the dunes will encroach upon a highway can be calculated (after allowing for errors) using multi-temporal imagery.

Future implementation of space imagery as a tool for monitoring dune movement is dependent upon acquiring higher spatial resolution imagery, establishing sufficient ground control points, and allowing a reasonable period of time for multi-temporal analysis. According to the results obtained from this study, spatial resolution should be between 5-10 meters, and a minimum of 30 ground control points should be identified on a Landsat MSS scene (185 x 185 km). The spatial resolution of SPOT imagery (see Appendix 1) on the panchromatic monochrome mode (10 metres), and the Large Format Camera photographs (10-12 metres) will provide a good basis for future monitoring systems. To take full advantage of SPOT and Large Format Camera imagery, it will be necessary to find more accurate means of generating ground

control points. This should be achievable in the near future using the U.S Navastar Global Positioning System, which will provide instantaneous position fixes to within 15 metres. A different method of generating ground control points is to plant the area of interest with artificial objects. An object of sufficient contrast with respect to its background, either brighter or darker, can change the overall radiance of a given pixel so that the object becomes detectable on the imagery. This can be achieved by installing mirrors, 24 inches in diameter (one mirror per pixel), on the ground and orienting them to the Landsat's view angle. Theoretically, these mirrors will be detected on the Landsat imagery because of sufficient reflection to saturate the associated pixels. The detected mirrors can then be used as control points in the multi-temporal image registration. The 24 inch diameter of the mirrors arranged in the pattern of an eye was used in a study of spatial resolution aspects in California desert (Colvocresses, 1974). In Colvocresses's study, the eye pattern was clearly detected on the Landsat MSS imagery. Different mirror diameters and shapes, however, can be tested to select the best combination for detection on the imagery.

Space platform imaging systems have a potential as data sources for ten-year-plus period studies of movement among medium-sized dunes (10-14 m high). In order to obtain the best results for sand movement and encroachment patterns over a ten-year period, test sites should be designated

immediately, and SPOT, TM and space photographic imagery should be archieved for later use. There is also a need for imaging systems to produce data which can be "degraded" in terms of spectral and spatial resolution for comparison with current or older imagery.

For future implementation of aerial photographs as tools for dune movement measurements and in order to achieve better accuracies the following should be taken into consideration:

(1) Multi-temporal photographs should have the same scale. A scale of 1:25,000 or more is recommended.

(2) Adequate ground control should be provided on all sets of the investigated photographs. If this is not available then artificial ground control points which can be detected on the aerial photographs should be planted on the ground prior to any planned flight.

(3) Points of known height on a locally flat area should be provided. This helps in reducing errors of dune height measurements especially in the absence of reliable topographic maps.

(4) Both plan and height control should be around the perimeter of the area under consideration.

(5) To achieve reliable results at least a one year span should be allowed between successive photographs. This allows minimum monitoring time of dune movement. It is also

recommended to study the wind velocity, direction and seasonal distributions prior to deciding on the flying date. In the Jafurah sand sea, for example, maximum wind velocity and hence maximum dune movement occurs during the "Shamal" season (July to September). Therefore, the period between July and September should be included to allow for maximum monitoring time of dune movement. Other sand seas of the world may experience different monitoring times of dune movement.

RECOMMENDATIONS FOR FURTHER RESEARCH:

The following list for further research ideas to be implemented in the future:

(i) Comparison between the current spaceborne imagery with the more recently developed high resolution sensors such as the satellite 'SPOT" in sand dune mapping.

(ii) Selection of new test site areas covering different sand sea of Arabia for continuous monitoring of sand movement using available and future remote sensing sensors.

(iii) Developing an artificial device detectable by all remote sensing sensors to be installed in selected areas of the desert and used as a ground control point reference for digital image to image registration.

(iv) Field investigation of the suspected submerged sand dunes detected in this study.

(v) Installing meteorological stations in selected desert sites which can send digital data to receiving stations through communication satellites for continous measurement of wind data, humidity, temperature and precipitation. This information will be vital in understanding the mechanics of dune movement.

REFERENCES

Abolkhair, Y.M., 1981, Sand encroachment by wind in Al-Hasa of Saudi Arabia, Indiana University, Bloomington. PhD. Thesis, 214 p.

Ahlbrandt, T.S., 1975, Comparisons of textures and structures to distinguish eolian environments. Killpecker Dune Field, Wyoming. The Mountain Geologist, 12, pp. 61-73.

Alayne, S.F., and Grove, A.I., 1979, Global maps of the late level fluctuation since 30,000 BP, Quaternary Research, 12, pp 83-118.

Al-Hinai, K.G., J.M. Moore, and P.R. Bush, 1987, Landsat image enhancement study of possible submerged sand dunes in the Arabian Gulf, International Journal of Remote Sensing, Vol. 2, pp. 251-258.

Al-Hinai, K.G., and J.M. Moore, 1987, Monitoring of sand migration in eastern Arabia by remote sensing. In: Proceedings, Twentieth International Symposium on Remote Sensing of Environment, Environmental Research Institute of Michigan, Ann Arbor, in press.

Al-Sayari, S., and Zotel, J., 1978, Quaternary period in Saudi Arabia, Springer, Verlag, Wien, New York, p. 355.

Andrew, H. c, and Hunt, B. R, 1977., Digital Image Restoration, Prentic Hall.

Anon., 1957, Glossary of Geology and Related Sciences. Washington: American Geological Institute, 545 p.

Anton, D., 1983, Modern aeolian deposits of the Eastern Province of Saudi Arabia. In: Brookfield & Ahlbrandt (eds.): Eolian Sediments and processes, Elsevier Sci. Publ., Amsterdam, 365-378.

Anton, D., 1984, Aspects of geomorphological evolution : paleosols and dunes in Saudi Arabia. In: Quaternary Period in Saudi Arabia, Vol. 2. Springer-Verlag,Wien, pp. 275-297.

Anton, D. and Ince, F., 1986, A study of sand colour and maturity in Saudi Arabia, Z. Geomotph. N.F., 30, 3, Berlin. Stuttgart, 339-356.

Anton, D and Vincent, P., 1986, Parabolic dunes of the Jafurah Desert, Eastern Province, Saudi Arabia, Journal of Arid Enivronments, 11, 187-198.

Anuta, P.E., 1977, Computer-assisted analysis techniques for remote sensing data interpretation. Geophysics, vol. 42, 468-481.

Atkinson, M., 1986 (Personal communication). The University of Western Australia, Dept. of Zoology, Nedlands, Western Australia.

Bagnold, R.A., 1941, 1971, The Physics of Blown Sand and Desert Dunes, Methuen and co. Ltd., London, 265 p.

Bagnold, R.A., 1951, Sand formation in Southern Arabia, Geog. Jour., 117. pp 78-86.

Bagnold, R.A., 1953, The surface movement of blown sand in relation to to meteorology. In: Desert Research, Proc. Int. Symp. held in Jerusalem, May 7-14, 1952, sponsored by the Res. Counc. of Israel and UNESCO, Research Council of Israel Pub., 2, 89-96.

Berlin, G. L., 1984, Application of SIR-B data for ground water exploration in the Arabian Shield and sand-drift monitoring in the An Nafud and Al Jafurah fringe areas, Kingdom of Saudi Arabia. In: The SIR-B Sience Investigation Plan, National Aeronautics and Space Adminstration - Jet Propulsion Laboratory, Pasadene, California, JPL Pub. No. 84-3, pp. 56-66.

Berlin, G. L, M. A. Tarabzouni, K. M. Sheikho, and A. Al-Naser, 1985, SIR-A and Landsat MSS observations on eolian sand deposits on the Al Labbah Plateau, Saudi Arabia. In: Proceedings, Nineteenth International Symposium on Remote Sensing of Environment, Environmental Research Institute of Michigan, Ann Arbor, Vol. 1, pp. 311-321.

Berlin, G. L, M. A. Tarabzouni, A. Al-Naser, K. M. Sheikho, and R. W. Larson, 1986, SIR-B subsurface imaging of a sand-buried landscape: Al Labbah Plateau, Saudi Arabia, IEEE

Transactions on Geoscience and Remote Sensing, Vol. G2-24, pp. 595-602.

Bernstein, R.C (editor), C. Colby, S.W. Murphey and J.P. Snyder., 1983, Image geometry and rectification. In: Manual of Remote Sensing (Chapter 21), American Society of Photogrammetry, Falls Church, Virginia, Vol. 1, pp. 873-922.

Billingsley, F.C., 1975, Noise consideration in digital image processing hardware; Topics in applied physics, Vol. 6, Picture Processing and Digital Filtering, edited by T.S Huang, Springer Verlag, Berlin-New York.

Blom, R. and C. Elachi, 1981, Spaceborne and airborne imaging radar observations of sand dunes, Journal of Geophysical Research, Vol. 86, pp. 3061-3073.

Blom, R., and M. Daily, 1981, Radar image processing for rock type discrimination. Digest 1981 Int. Geoscience and Remote Sensing Symp. (IGARSS '81), Washington, D.C., June 1-3, Vol. 2, pp. 574-581.

Blom, R., C. Elachi and D. Evans, 1982a, SIR-A images of sand dunes and volcanic fields. Digest 1982 Int. Geoscience Remote Sensing Symp. (IGARSS '82), Munich, FA-6, pp. 9.1-9.6.

Blom, R., C. Elachi. and A. Sheehan, 1982b, Radar scatterometry of sand dunes and lava flows, Digest 1981 Int.

Geoscience and Remote Sensing Symp. (IGARSS '81), Washington, D.C, June 1-3, Vol. 2, pp. 597-602.

Bloom, A.L., 1978 Geomorphology: A Systematic Analysis of Late Cenozoic Landforms. Prentice-Hall, Englewood Cliffs, New Jersey, 510 pp.

Bofah, K.K. and Al-Hinai, K.G., 1985, Field tests of porous fences in the regime of sand-laden wind. In: Proceedings, 6th Colloquim on Industrial Aerodynamics (June 19-21, 1985) Aachen, Fluid Mechanics Laboratory, 21 p.

Breed, C.S. and Grow, T., 1979, Morphology and distribution of dunes in sand seas observed by remote sensing in: A Study of Global Sand Seas. U.S Geol. Surv. Prof. Paper 1052, Chapter J, pp. 253-303.

Breed, C.S., Fryberger S.C., Andrews S., McCauley, C., Lennartz, F., Gebel, D., and Horstman, K., 1979, Regional studies of sand seas using Landsat (ERTS) imagery in: A Study of Global Sand Seas. US Geol.Surv.Prof.Paper 1052, Chapter K, PP 305-399.

Breed, C.S., and Breed, W.J., 1979, Dunes and other windforms of central Australia, and a comparison with linear dunes on the Moenhopi Plateau, Arizona. In : Apollo-Soyuz Test Project, Vol. 2 : Earth Observations and Photography, NASA, SP-412-Vol 2, pp 319-358.

Breed, C.S., J.F. McCauley, G.G. Schaber, A.S Walker, and G.L. Berlin, 1982, Data analysis-dunes on SIR-A images. In: Shuttle Imaging Radar-A (SIR-A) Experiment, JPL pub. 82-87, Jet Propulsion Laboratory, Pasadena, Ca, pp. 52-87.

Brera, A.M., 1979, Application of Landsat imagery to monitor sand dune movement, University of Tennessee Unpubl. PhD. Dissertation, 247 P.

Brown, R.J., 1960, Geomorphology of Western and Central Saudi Arabia , International Geological Congress, 21st Copenhagen, Report 21. pp 150-159.

Brunsden, D. and R. Cook, 1986, The Wahiba Sands, a description of the Wahiba Sands of Oman, prepared by members of the Royal Geographical Society, Oman Wahiba Sands Project 1986, 75 p.

Canas, A.A., 1988, "Personal communication", Physics Dept. Imperial College of Science and Technology, University of London.

Chapman, R.W., 1971, Climatic changes and the evolution of land forms in the Eastern Province of Saudi Arabia, Geol. Soc. Am. Bull, 82. pp 2713-2728.

Chapman, R.W., Geology and geomorphology of Saudi Arabia. In Al-Sayari, s., and Zotl, J., 1978, Quaternary Period in Saudi Arabia, Vol. 1, Springer-Verlag, Wien, New York. pp. 4-31.

Cloet, R.L., 1955, Sandwaves in the southern North Sea and in the Persian Gulf, Geogr. Jour., Vol. 7, No. 3, pp. 272-279.

Colvcoresses, A.P. (Editor), 1975, Platforms for remote sensors. In: Manual of Remote Sensing (Reeves, R.G, Anson, Abraham, and Landen, D, editors), American Society of Photogrammetry, Falls Church, Virginia, Vol. 1, pp. 538-588.

Condit, H.R., 1970, The spectra reflectance of American soils, Photogrammetric Engineering, 36, pp. 955-966.

Condit, C.D and Chavez, P.S., 1979, Basic concepts of computerized digital image processing for geologists, U.S Geol. Surv. Bull. 1462.

Cook, R.U. and A. Warren, 1973, Geomorphology in Deserts, B.T. Batsford Ltd, London, 349 p.

Cooper, W.S., 1967, Coastal dunes of California, Geological Society of America, Memoir, 104, pp. 139-151.

Davison, G.J., 1986, Ground control pointing and geometric transformation of satellite imagery, International Journal of Remote Sensing, vol 7, No.1, 65-74.

Doornkamp, J.C., Brunsden, D, and Jones, D.K.C (editors), 1980, Quaternary history. In: Geology, Geomorphology and Pedology of Bahrain (Norwich, U.K.: Geo Abstract. Ltd), p.411.

Elachi, C.C., 1980, Spaceborne imaging radar, geologic and oceanographic applications, Science, Vol. 209, pp 1073-1082.

Elachi, C.C., R. Blom, M. Daily, T. Farr and R.S Saunders, 1980, Radar imaging of volcanic fields and sand dune fields, implications for VOIR, in Proceedings of the Radar Geology Workshops, Snowmass, Colorado, JPL Publ., 80-61, pp. 114-150.

Elachi, C.C., W.E. Brown, J.B. Camino, T. Dixon, D.L. Evans, J.P. Ford, R.S. Saunders, C. Breed, H. Masurski, G. Schaber, L. Dellwig, A. England, H. MacDonald, P. Martin-Kaye and F. Sabins, 1982a, Shuttle imaging radar experiment, Science, Vol. 218, pp. 996-1003.

Elachi, C.C., D. Evans and P. Rebillard 1982b, Comparative analysis of co-registered SIR-A, Seasat and Landsat images, Digest 1982 Int. Geoscience and Remote Sensing Symp. (IGARSS '82) Munich, June, Vol. 2, FA-6, pp. 8.1-8.6.

El-Baz, F., 1976, Terrestrial sand patterns photographed by the Apollo-Soyuz Mission and similar features on Mars (abs). Lunar Science, 7: 236.

El-Baz, F., 1978, The meaning of desert colour in earth orbital photographs, Photogrammetric Engineering and Remote Sensing, Vol 44, pp. 69-73.

El-Baz, F., et al., 1979a, Preliminary analysis of coluor variations of sand deposits in the western desert of Egypt,

In: Apollo-Soyuz Test Project, Earth observations and photography, NASA SP-412-Vol 2, pp. 237-262.

El-Baz, F., 1979b, Coluor of desert surfaces in the Arabian Peninsula, In: Apollo-Soyuz Test Project, Earth observations and photography, NASA, SP-412-Vol 2, pp. 285-299.

El-Baz, F., Breed, C.S, Grolier, M.J. and McCauley, J.F., 1979, Eolian features in the Western Desert of Egypt and some applications on Mars, Journal of Geophysical Research, Vol. 84 B14), pp. 8205-8222.

El-Baz, F. (ed)., 1984, Deserts and Arid Lands. The Hague: Martinus Nijhoff Publishers, 222 p.

Emery, K.O., 1956, Sediments and water of the Persian Gulf. Bulletin of the American Association of Petroleum Geologists, 40: 2354-2383.

Evans, G, Murray, J.W, Biggs, H.E, Bater, R, and Bush, P.R., 1973, The oceanography, ecology, sedimentology and geomorphology of parts of the Trucial Coast Barrier Island Complex, Persian Gulf. In: The Persian Gulf, edited by B.H Purser, Berlin: Springer-Verlag, p. 233.

Finkel, H.J., 1961, Movement of Barchan dunes measured by aerial photogrammetry, Photogrammetric Engineering, 27. pp. 439- 444.

Folk, R.L., 1974, Petrology of Sedimentary Rocks, Hemphill Publishing Co., p. 182.

Fryberger, S.G., 1974, Techniques for the evaluation of surface wind data in terms of aeolian sand drift, U.S Geological Survey, Open File Report, 78-405. pp 1-25.

Fryberger, S.G., 1979, Dune forms and wind regime. In: McKee, E.D. (ed). A Study of Global Sand Seas. United States Geological Survey, Professional Paper 1052.

Fryberger, S.G. and Ahlbrandt, T.S., 1979, Mechanism for the formation of eolian sand seas. Zeitschrift fur Geomorphologie, 23, pp. 440-460.

Fryberger, S.G., Ahlbrandt, T.S., and Andrews, S., 1979, Origin, sedimentary features, and signification of low-angle aeolian sand sheet deposits, Great Sand Dunes National Monuement and Vicinity, Colorado, Journal of Sedimentary Petrology, V.49, No.3, pp. 733-746.

Fryberger, S.G., A.M, Al-Sari., T.S, Clisham., 1983, Aeolian dune, interdune, sand sheet, and siliciclastic sabkha sediments of an offshore prograding sand sea, Dhahran Area, Saudi Arabia, A.A.P.G. Bulletin, v.67, no.2, pp. 280-312.

Fryberger, S.G., A.M, Al-Sari., T.S, Clisham., S.R, Rizvi., and K.G, Al-Hinai., 1984, Wind sedimentation in the Jafurah Sand Sea, Saudi Arabia. Sedimentology, 31: pp. 413-431.

Gardner, R.A.M., 1981a, Reddening of dune sands - evidence from southeast India, Earth Surface Processes and Landforms, 6, pp. 459-468.

Gardner, R.A.M., 1981b, Reddening of tropical coastal dune sands, in: Residual Deposits ed. Wilson, R.C.L., Geological Society of London, Special Publication, 11, pp. 103-115.

Gardner, R.A.M., and Pye, K., 1981, Nature, origin and palaeoenviromental significance of red coastal and desert sand dunes, Progress in Physical Geography, 5, pp. 514-534.

Gary, M., R. McAfee, Jr and C.L Wolf, editors, 1972, Glossary of Geology. American Geological Institute, Washington, D.C, 805 p.

Gasse, F., 1980, Quaternary history of the Afar and Ethiopian rift lakes. In: The Sahara and the Nile, Williams, M.A.J and Faure, H. (editors), A.A. Balkema, Rotterdam. pp. 361-400.

Gillespie, A.R., 1980, Digital techniques of image enhancement. Chapter 6 in: Remote Sensing in Geology, Siegal, B.S & A.R Gillespie (eds.), New York: Wiley, 139-226.

Glennie, K. W., 1970, Desert Sedimentary Environment, Development in Sedimentology 14, New York, Elsevier Publ. Co., 222 p.

Gonzalez, R.C and Wintz, P., 1977, Digital Image Processing, Reading, Massachusetts: Addison-Wesley.

Hartman, M., Lange, H, Seibold, E. and Walger, E., 1971, Oberflachensediments im Persischen Golf und Golf Von Oman,

1. Geologisch-hydrologischer Rahmen und erste Sedimentolgische Ergebnisse, "Meteor" Forschungsergebnisse, Reihe C, 4, 76 p.

Hastenrath, S.L., 1967, The barchans of the Arequipa region, southern Peru, Zietschrift fur Geomorphologie, 11, pp. 300-311.

HMSO, 1977., The Marine Observers' Handbook, Her Majesty's Stationary Office, Meteorological Office report MO522.

Holm, D.A., 1953, Dome shaped dunes of Central Najd, Saudi Arabia, International Geological Congress, 19th, Algiers, Comptes Rendus 7, pp. 107-112.

Holm, D.A., 1957, Sigmoidal dunes, a transitional form, Geol. Soc. Am. Bull. 68: 1746 (Abstract).

Holm, D.A., 1960, Desert geomorphology in the Arabian Peninsula, Science, 132, pp. 1369-1379.

Holm, D.A., 1968, Sand dunes. In: Fairbridge, R.W. (ed). The Encyclopedia of Geomorphology. New York: Reinhold Book Corporatian, pp. 973-979.

Holm, D.A., 1974, Arabian desert, Encycl. Britanica, 15th ed., pp. 1051-1058.

Hotzl, H.A.R. Jado, A. Moser, W. Rauert, J.G. Zotl., 1984, Climatic fluctuations in the Holocene. In: The Quaternary

Period in Saudi Arabia, Vol. 2, Springer-Verlag. Wien. pp. 301-314.

Hunter, J.R., 1983, Aspects of the dynamics of the residual circulation of the Arabian Gulf. In : Coastal Oceanography, edited by M. G. Gade, A. Edwards and H. Svendsen, Plenum Press, New York and London, pp. 31-42.

Hunting Surveys Limited, 1977, Sand dune movement study south of Umm Said 1963-1976, Technical report submitted to the Government of Qatar, Ministry of Public Works, Hunting Surveys Ltd, England, 7 p.

Idso, S.B., 1976, Dust storms. Scientific American, 235 (4): 108-111, 113-114.

Inman, D.L., Ewing, G.C., and Corless, J.B., 1966, Coastal sand dunes of Guerrero Negro, Baja California, Mexico, Geological Society of America, Bulletin, 96, pp. 787-802.

Johnson, D., Kamal, R., Pierson, G., and Ransay, J., 1978, Sabkhas of Eastern Saudi Arabia, in: al-Sayari, S., and Zotl, J., 1978, Quaternary Period in Saudi Arabia, Springer-verlag-wien, New York.

Johnson, D., 1978, Gulf coastal region and its hinterland, general geology, in: al-Sayari, S., and Zotl, J., 1978, Quaternary Period in Saudi Arabia, Springer-Verlag-Wien, New York, pp. 45-56.

Jones, D.K.C, R.U. Cook and A. Warren., 1986, Geomorphological investigation, for engineering purposes, of blowing sand and dust hazard, Quaternary Jour. of Engineering Geol, Vol. 19, pp. 251- 270.

JPL, 1980, Radar Geology an Assessement. JPL Publ. 82-78.

JPL, 1982, The SIR-B Science Plan. JPL Publ. 82-78.

Justice, C.O, and Townshend , J.R.G., (1981), The use of Landsat data for land cover inventories of Mediterranean lands. In: (Chapter 6), Terrain Analysis and Remote Sensing, Townshend, J.R.G., (ed.). Allen and Unwin London, Boston.

Kassler, P., 1973, The structural and geomorphic evolution of the Persian Gulf. In: The Persian Gulf, edited by B.H Purser, Berlin: Springer-Verlag, p. 11.

Kemp, R.A., 1985, The causes of redness in some buried and non-buried soils in eastern England, Journal of Soil Science, 36, pp. 329-334.

Kerr, R.C., and Nigra, J.O., 1952, An analysis of aeolian sand control, Bull, Am. Assc. Pet. Geol., 36: 1541-1573.

Khalaf,F. and Al-Hashah, M.Z., 1983, Aeolian sedimentation in the north-western part of the Arabian Gulf. Journal of Arid Environments, 6: 319-332.

Kolla, V. and Biscaye, P.E., 1977, Distribution and origin of qyartz in the sediments of the Indian Ocean. Journal of Sedimentary Petrology, 47: 642-649.

Kolm, K.E, 1974, ERTS MSS imagery applied to mapping of sand dunes in Wyoming, In: Applied Geology and Archeology, the Holocene History of Wyoming, Wyoming Geological Survey Report Investigation No 10, pp 34-39.

Lancaster, N., 1981, Aspects of the morphometry of linear dunes of the Namib Desert. South African Journal of Science, 77, pp. 366-368.

Lancaster, N., 1982, Linear dunes, Progress in Physical Geography, 6, pp. 476-504.

Lancaster, N., 1983, Controls on dune morphology in the Namib Sand Sea, in: Eolian Processes and Landforms, Brookfield, M.E., and Ahlbrandt, T.S., Developments in Sedimentology, 38, Elsevier, Amsterdam, pp. 261-290.

Lancaster, N., 1984a, Characteristics and occurence of wind erosion features in the Namib Desert, Earth surface Processes and Landforms, 9, pp. 469-478.

Lancaster, N., 1984b, Aeolian sediments, processes and landforms, Journal of Arid Environments, 7, pp. 249-254.

Lancaster, N., 1985, Variations in wind velocity and sand transport on the windward flanks of desert sand dunes, Sedimentology, 32, pp. 581-593.

Lancaster, N., and Hallward, J.R., (not dated). A Bibliography of Desert Dunes, Dept. of Environmental and Geographical Sciences University of Cape Town.

Lettau, K., and Lettau, H., 1969, Bulk transport of sand by the barchans of the Pampa La Joya in Soythern Peru, Zeit. Fur. Geom., N.F., 13: 182-195.

Lillesand, T.M and Kiefer, A.R., 1979, Remote Sensing and Image Interpretation, Wiley, New York, 612 p.

Long, J.T., and Sharp, R.P., 1964, Barchan-dune movement in the Imperial Valley, California, Geological Society of America, Bulletin, 75, pp. 149-156.

MacDonald, H.C and W.P Waite, 1971, Optimum radar depression angles for geological analysis, Mod. Geol., Vol. 2, pp. 179-193.

Manual of Remote Sensing, 1983, American Society of Photogrammetry, Falls Church, Virginia, Vol 1 & 2.

Marrs, R.W. and Kolm, K.E. (eds), 1982, Interpretation of windflow characteristics from eolian landforms, Geological Society of America, Special Paper 192.

McCauley, J. F., G.G Schaber., C.S, Breed., M.J Grolier., C.V Haynes., B. Issawi., C. Elachi and R. Blom., 1982, Subsurface valleys and geoarcheology of the Eastern Sahara revealed by Shuttle radar. Science 218, pp. 1004-1020.

McClure, H.A., 1976, Radiocarbon chronology of late Quaternary lakes in the Arabian desert. Nature, 263, pp. 755-756.

McClure, H.A., 1978, At Rub'al Khali. In: Quaternary Period in Saudi Arabia, Vol. 1, Springer-Verlag, Wien, pp. 252-263.

McKee, E.D., 1966, Structures of dunes at White Sands National Monument, New Mexico (and comparison with structure of dunes from other selected areas), Sedimentology, Vol. 7, pp. 1-69.

McKee, E.D, Breed, C.S.and Lawrence, F.H., 1973, A study of morphology, provenance, and movement of desert sand seas in Africa, and Australia, Proceedings of the International Symposium on Remote Sensing of Environement, Environmental Research Institute of Michigan, Ann Arbor, Michigan, Paper G8, pp 291- 303.

McKee, E.D. and Breed, C.S., 1974a, A Synthesis of Sand Seas Throughout the World, U.S Geological Survey, Denver, Colorado, 95 p.

McKee, E.D. and Breed, C.S., 1974b, An investigation of major sand seas in desert areas throughout the world. Proceedings, Symposium on ERTS-1, Vol. 1, Sec. A. NASA Goddard Space Flight Center, pp. 665-679.

McKee, E.D. and Breed, C.S., 1974c, Preliminary report on dunes. In: Skylab 4, Visual Observations Project Report. NASA Technical Memorandum, TMS-58142: 9.1-9.9.

Mckee, E.D. and Breed, C.S., 1976, Sand seas of the world, USGS Prof. Paper 929, pp. 81-88.

McKee, E.D. and Breed, C.S., 1977, Sand seas of the world, in: ERTS-1 " A New Window on Our Planet" Geological Survey Professional Paper, 929: 81-88.

McKee, E.D., Breed, C.S. and Fryberger, S., 1977, Desert Sand Seas. In: Carr, G.P. et al. Skylab Explores the Earth. NASA Special Publication , SP-380: 5-48.

McKee, E.D., 1979a, A Study of Global Sand Seas (Edited by), US. Geol. Surv. Professional Paper 1052, USGPO, Washington.

McKee, E.D., 1979b, Introduction to a Study of Global Sand Seas. In: E. D. McKee (editor), A Study of Global Sand Seas. U.S Geological Survey Professional Paper 1052, pp. 3-19.

Middleton, N.J., 1986, Dust storms in the Middle East, Journal of Arid Enivronments, 10: 83-96.

Munsell, A.H., 1963, A color Notation. Munsell Book of Colors. Munsell Color Company, Baltimore/Maryland.

NASA, 1982 a, Landsat Data Users Notes, US Geological Survey, EROS Data Cetre, Sioux Falls, Issue No 23.

NASA, 1982 b, STS 2 OSTA 1 SIR-A Information Packet (81-111A-01 A). Greenbelt, Maryland: NASA Goddard Space Flight Centre.

Newton, L. and Dereny, E., 1986, Control extension utilizing Large Format Camera imagery, Proceedings 1980 ACSM-ASPRS Annual Convention, Washington D. C, ACSM-ASPRS, Falls Church, Va, U.S.A, Vol. 4, pp. 456-465.

Norris, R.M., 1966, Barchan dunes of Imperial Valley, California, J. Geol., 74, p. 292.

Oakes, G.D., 1987, Automatic Lineament Analysis Techniques for Remotely Sensed Imagery, Imperial College, University of London unpublished Ph.D Thesis.

Patterson, R.J. and D.J.J. Kinsman, 1981, Hydrologic framework of sabkha along Arabian Gulf. AAPG Bull., Vol. 65, pp. 1457-1475.

Philby, H. St.J.B., 1933, The Empty Quarter, New York, H. Holt and Co., 433 p.

Polcyn, F.C., Brown, W. L and Sattinger, I. J., 1970, The measurement of water depth by remote sensing techniques. Report No. 8973-26-F, Infrared and Optics Laboratory, Willow Run University of Michigan, Ann Arbor.

Powers, R.W., Ramirez, L.F, Redmond, C.D and Elberg, E.L., 1966, Geology of the Arabian Peninsula, sedimentary geology

of Saudi Arabia, U.S. Geological Survey. Professional Paper, 560 D: 1-147.

Pratt, W.K., 1978, Digital Image Processing , New York: Wiley.

Prospero, J.M., 1981, Arid regions as sources of mineral aersols in the marine atmosphere. In: pewe, T.L (ed.) Desert Dust: Origin, Characteristics and effect on Man. Geological Society of America Special Paper, 186: 71-86.

Purser, B.H and Evans, G., 1973, Regional sedimentation along the Trucial Coast, SE Persian Gulf. In: The Persian Gulf, edited by B. H. Purser, Berlin: Springer-Verlag, p. 211.

Purser, B. H. and Seibold, E., 1973, The principal environmental factors influencing Holocene sedimentation and diagensis in the Persian Gulf. In: The Persian Gulf, Holocene Carbonate Sedimentation and Diagensis in a Shallow Epicontinental Sea, edited by B. H. Purser, Berlin: Springer-Verlag, pp.1-9.

Pye, K., 1982, Negatively skewed aeolian sands from a humid tropical coastal dunefield, northern Australia. Sedimentary Geology , 31, pp. 249-266.

RAE., 1983 Users Guide: The United Kingdom National Remote Sensing Centre. Remote Sensing Unit, Royal Aircraft Establishment, Farnborough.

Rubin, D.M., 1984, Factors determining desert dune type. Nature, 309, pp. 91-92.

Sabins, F., 1978 , Remote Sensing Principles and Interpretation, W.H Freeman and Company, San Fransisco, California.

Sabins, F., 1986, Remote Sensing Principles and Interpretation. (2nd edition) W.H Freeman and Company, San Fransisco, California

Sarnthein, M., 1972, Sediments and history of the postglacial transgression in the Persian Gulf and Northwest Gulf of Oman. Marine Geolgy , Elsevier Publishing Company, Amsterdam, Vol. 12, pp. 245-266.

Sarnthein, M., and Walger, K., 1974, Der Aolische sandstorm aus der w-Sahara zur Atlantikkuste. Geologische Rundschau, 63, pp. 1065-1087.

Schowengerdt, R. A., 1983, Techniques For Image Processing and Classification in Remote Sensing. Orlando, Florida: Academic Press.

Seltrust Engineering Ltd., 1980, Qatar Geological Map and Explanatary Booklet, Doha, Qatar: International Development Technical Centre.

Selzak, M. H and Elbaz, F., 1979, Temporal changes as depicted on orbital photographs of arid regions in North

Africa. In Apollo-Soyuz Test Project, earth observations and photography, NASA, SP-412-Vol 2, pp 263-272.

Shinn, E. A., 1973, Sedimentary accretion along the leeward SE coast of Qatar Peninsula, Persian Gulf. In: The Persian Gulf, edited by B. H. Purser, Berlin: Springer-Verlag, P. 199.

Siegal, B.S. and A.R Gillespie, 1980, Remote Sensing in Geology. John Wiley & Sons, New York, Chiechester, Brisbane, Toronto, 702 p.

Slater, P. N., 1980, Remote Sensing: Optics and Optical Systems. Addison-Wesly, Reading, Mass.

Slater, P.N (ed), 1983, Photographic systems for remote sensing, 2nd edn, Colwell, R.N (ed), 231-91. Falls Church, Virginia: American Society of Photogrammetry.

Stewart, R.A, O.H Pilkey and B.W Nelson, 1965, Sediments of the northern Arabian Sea. Marine Geology, 3: 411-427.

Stone, R.O., 1967, A desert glossary. Earth Science Review, 3, pp. 211-268.

Sugden, W., 1963, Some aspects of sedimentation in the Persian Gulf. Journal of Sedimentary Petrology, 33: 355-364.

Taranik, J. W., 1978, Characteristics of the Landsat multispectral data system, U.S Geological Survey Open File Report, 78-187, Sioux Falls, S.D.

Thesiger, W., 1946, A new journey in Southern Arabia, Geog.Jou., 111: 1-21.

Thesiger, W., 1948, Across the Empty Quarter, Geog. Jou., 108: 129-145.

Thesiger, W., 1949, A further Journey across the Empty Quarter, Geog. Jou., 113: 21-46.

Tsoar, H., 1978, The dynamics of longitudinal dunes, Final Technical Report, DA-ERO 76-G-072, European Research Office, United States Army, London.

Tsoar, H., 1982, Internal stucture and surface geometry of longitudinal (seif) dunes, Journal of Sedimentary Petrology, 52, pp. 823-831.

Tsoar, H., 1983, Wind tunnel modelling of eco and climbing dunes, in: Eolian Sediments and Processes, ed. Brookfield, M.E., and Ahlbrandt, T.S., Developments in Sedimentology, 38, Elsevier, Amsterdam, pp. 247-260.

Tsoar, H., 1985, Profile analysis of sand dunes and their steady state signification, Geografiska annaler, 67A, pp. 47-59.

Tsoar, H., Rasmussen, K.R., Sorensen, M., and Willetts, B.B., 1985, Laboratory studies of flow over dunes, in: Proceedings of International Workshop on the Physics of Blown Sand, Memoirs, No. 8, Department of Theoretical Physics, Institute of Mathematics, University of Aarhus, ed.

Barndor f-Nielson, O.E., Moller, J.T., Rasmussen, K.R., Willets, B.B., pp. 327-350.

Tsoar, H., and Yaalon, D.H., 1983, Deflection of sand movement ona sinuous longitudinal (seif) dune: use of fluourescent dye as a tracer, Sedimentary Geology, 36, pp. 25-40.

US Geological Survey, 1979, Landsat Data Users Handbook Revised, Us Geol. Surv.

Walker, Y. and Theodore, R., 1979, Red Colour in dune sand. In: McKee, E.D (ed.): A Study of Global Sand Seas. U.S Geological Survey Professional Paper, 1052, pp. 62-81.

Warren, A., 1970, Dune trends and their implications in Central Sudan. Z. Geomorph. N.F. Suppl. 10: 154-180.

Warren, A., 1983, Arid geomorphology, Progress in Physical Geography, 9, pp. 397-401.

Warren, A., 1985, Arid geomorphology, Progress in Physical Geography, 9, pp. 434-441.

Warren, A., and Kay, S.A.W., 1987, Dune networks, in: Desert Sediments: Ancient and Modern, Geological Society Special Publication, edited by L.E. Frostick and I. Reid., No. 35, pp. 205-212.

Warren, A., and Knott, P., 1983, Desert dunes: a short review of needs in desert dune research and a recent study

of micrometeorological dune-initiation mechanisms in: Eolian Sediments and Processes, edited by Brookfield, M.E., and Ahlbrandt, T.S., Elsevier Developments in Sedimentology, 38, pp. 343-352.

Wasson, R.J., 1983, Dune sediment type, sand colour, sediment provenence and hydrology in the Strzelecki-Simpson Dunefield, Australia. In: Brookfield, M.E., and Ahlbrandt, T.S. (eds). Eolian Sediments and Processes. Developments in Sedimentology 38. Amsterdam: Elsvier, pp. 165-196.

Wasson, R.J., and Hyde, R., 1982, A test for the granulometric control of desert dune geometry, Earth Surface Processes and Landforms , 8, pp. 301-312.

Wasson, R.J., and Hyde, R., 1983, Factors determining desert dune type, Nature, 304, pp. 337-312.

Watson, A., 1985, The control of wind blown sand and moving dunes: a review of the methods of sand control in deserts, with observations from Saudi Arabia, Quaternary Journal of Engineering Geology , vol. 18 part 3, 237-252.

Whitney, J. W., Faulkender, D. J. and Rubin, M. 1983, The environmental history and present condition of the northern sand seas of Saudi Arabia. United States Geological Survey Open File Report. OF-03-95, 39 p.

Williams, R. O., 1979, ARAMCO meteorological and oceanic data book for the Eastern Province of Saudi Arabia, Dhahran,

Environmental Unit, Technical Services Department, Arabian American Oil Company, 135 p.

Wilson, I.G, 1971, Desert sand flow basins and a model for the development of Ergs, Geog. J., 137: 180-197.

Wilson, I.G., 1973, Ergs, Sedimentary Geology, 10: 77-106.

Wong, K. W., 1975, Geometric and cartographic accuracy of ERTS-1 imagery, Photogrammetric Engineering and Remote Sensing, Vol 41, pp 621-635.

GLOSSARY

SAND RELATED TERMS

Aeolian: Pertaining to wind; especially said of rocks, soils and deposits (such as loess, dune sand, and some volcanic tuffs) whose constituents were transported (blown) and laid down by atmospheric currents, or of landforms produced or eroded by the wind, or of sedimentary structures (such as ripple marks) made by the wind, or of geologic processes (such as erosion and deposition) accomplished by the wind.

Albedo: That fraction of total incident light reflected in all directions.

Angle of repose: Maximum angle at which loose material, such as talus or sand, is stable (Stone, 1967).

Barchan (or Barcan, Barchane, Barkan, Barkhan): Crescent-shaped sand dune formed, generally, by moderate winds and with a moderate sand supply. Windward slope is gentle and lee slope or slipface is at the angle of repose of dry sand (Stone, 1967).

Blowout dune: Sand accumulation derived from troughs or depressions, especially where the accumulation is of large size and rises to considerable height above the source area (Stone, 1967).

Chain barchan: Small barchans and barchanoid ridges linked

togther to form a large barchanoid shaped dune (width exceeding 3 km in the Jafurah Sand Sea; Al-Hinai, 1988).

Complex dune: Sand accumulation formed by the intersection of two or more dune types.

Compound dune: Sand accumulation formed by the intersection of two or more of the same dune type.

Crescentic dune: A barchan dune.

Crest (of dune): Highest part of dune.

Deflation: Removal of loose, granular particles by the wind, caused by less material coming upwind than leaving downwind.

Desertification: Process of conversion of land to desert.

Dune: Any accumulation of sand-size, windblown material (Stone, 1967).

Dust storm: Strong wind carrying large clouds of dust or silt and larger than a dust devil (Stone, 1967).

Longitudinal dune: Any linear dune ridge, usually more or less symmetrical in cross-profile, which extends parallel to the direction of the dominant wind (Stone, 1967).

Megabarchan: Giant barchan dunes that may be 100 m high or more (Stone, 1967).

Monsoon: Large-scale wind system which strongly influences

climate of large regions, and in which flow direction reverses from winter to summer.

Parabolic dunes: Long scoop-shaped hollow of sand with points tapering to the windward and whose groundplan approximates the form of a parabola (Stone, 1967).

Ripple: Small-scale aeolian or acqueous bedform of regularly repeated pattern.

Sabkha: An Arabic term for salt flat or salt-encrusted dry lake.

Sand drift: General term for all windblown sand. Also sand accumulation on steep slopes or in valleys; sand deposit formed to the lee of a gap between two obstructions (Stone, 1967).

Sand dune: Ridge or pile of sand resulting from aeolian action (Stone, 1967).

Sand sea: Extensive sand deposits consisting of several composite dune types.

Sand shadow: Wherever wind velocity is checked by a fixed obstruction, sand may strike the obstruction and then fall at its base or be swept into the lee of the obstruction and accumulate as a streamlined mound (Bloom, 1978).

Sand sheet: Sand area marked by an extremly flat surface broken only by small sand ripples (Stone, 1967).

Sand streak: Patches of sand lacking slipfaces and having sharply defined edges; often associated with topographical obstacles.

Seif (or Sif): An Arabic term (meaning sword) given for a variety of longitudinal dune or long dune chain oriented in the direction of wind movement.

Slipface: Steep face on the lee side of a dune which stands at the angle of repose of sand (Stone, 1967).

Star dune: Stationary dune, with arms extending in different directions as a result of wind blowing from multiple directions.

Transverse dune: Asymmetrical dune ridge transverse to the dominant direction of sand transporting winds, in which the leeward slope is at the angle of repose of sand (about 32 degrees) and the windward slope is compartively gentle. Barchans and barchanoid ridges are sometimes referd to as transvers dunes.

REMOTE SENSING AND IMAGE PROCESSING TERMS

Absorption: The process by which radiant energy is absorbed and converted into other forms of energy.

Angle of depression: In SLAR (Side Looking Airborne Radar) usage, the angle between the horizontal plane and passing

through the antenna and the line connecting the antenna and the target.

Angle of incidence: (1) The angle between the direction of incoming EMR (Electromagnetic Radiation) and the normal to the intercepting surface; (2) In SLAR systems this is the angle between the vertical and a line connecting antenna and target.

Atmospheric windows: Those wavelength ranges in which radiation can pass through the atmosphere with relatively little attenuation: in the optical portion of the spectrum, approximately 0.3-2.5, 3.0-4.0, 4.2-5.0, and 7.0-15.0 μm.

Attitude: The angular orientation of a remote sensing system with respect to a geographical refrence system.

Azimuth: (1,general) The geographical orientation of a line given as an angle measured clockwise from north. (2, radar) Direction at right angles to the antenna beam. In SLAR, the direction is parallel to ground track.

Backscatter: In radar usage, backscatter generally refers to that radiation reflected back toward the source.

Base-height ratio: Air base (ground distance between centres of successive overlapping photos) divided by aircraft height. This ratio determines vertical exaggeration on stereo models.

Bit: A digit (0 or 1) in binary notation.

Byte: A group of eight bits of digital data.

CRT: Cathod Ray Tube. A Vaccum tube that generates a focused and movable electron beam directed onto a sensitized screen. A television image tube is a CRT.

CCT: Computer Compatible Tape.

Colour Composite (multiband photography): A colour picture produced by assigning a colour to a particular spectral band. In Landsat, blue is ordinarily assigned to MSS band 1 (0.5-0.6 μm), green to band 2 (0.6-0.7 μm), and red to band 4 (0.8-1.1 μm), to form a picture closely approximating a colour infrared photograph.

Colour infrared film: Photographic film sensitive to energy in the visible and near infrared wavelengths, generally from 0.4-0.9 μm; usually used with a minus-blue (yellow) filter, which results in effective film sensitivity of 0.5-0.9 μm.

Contrast stretching: Modification of contrast in an image; usually used in reference to digital processing and usually implies an improvemnet in the contrast of the image.

DN: Digital Number: An integer used to represent a variable (usually brightness) in a digital image.

False Colour Composite: A colour image in which the dye colour is not the same as scene colour. Infrared Ektachrome film produces false colour images since the infrared exposure is represented as red, the red as green, and the green as blue.

Filter: Any physical device or mathematical function that is used to modify a spectrum.

Hue: One parameter used to describe a colour. Blue, green, yellow, and red are different hues.

Image rectification: The correction of an image for defects introduced by a camera or a sensor. Also referred to as image restoration.

Incidence Angle: the angle measured at the point of observation, between the illumination source and the normal to the surface.

Infrared: That portion of of the electromagnetic spectrum lying between the red end of the visible spectrum and microwave radiation.

Line Scanner: A device that produces a continuous strip image by means of scanning. When mounted in a moving platform, scanning is achieved by the forward motion of the platform and lateral movement of the imaging field by rotating or oscillating mirrors.

Microwave: A very short electromagnatic wave between 1 m

and 1mm in wavelength or 300 GHZ to 0.3 GHZ in frequency.

MSS: Used to denote the Multi-Spectral Scanner of Landsat.

MTF: Modulation Transfer Function: A measure of the sensitivity of a sensing system to data as a function of spatial frequency.

PDF: Probability Density Function: The frequency of occurrence of different DN in an image.

Pixel: A single sample of data or "picture element" in a digital image.

RBV: Return Beam Vidicon. A type of television image tube.

Saturation: The relative purity of of colour measured by the absence of white light.

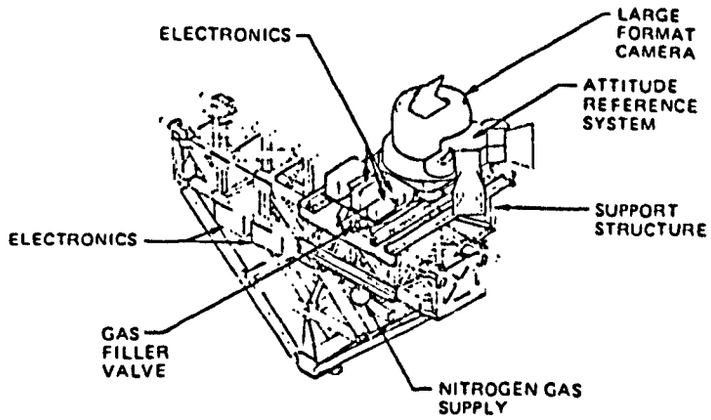
Spectral signature: The spectral characteristics by which a material may be recognized.

A P P E N D I X (1)

Satellites and Sensors
(RAE, 1983)

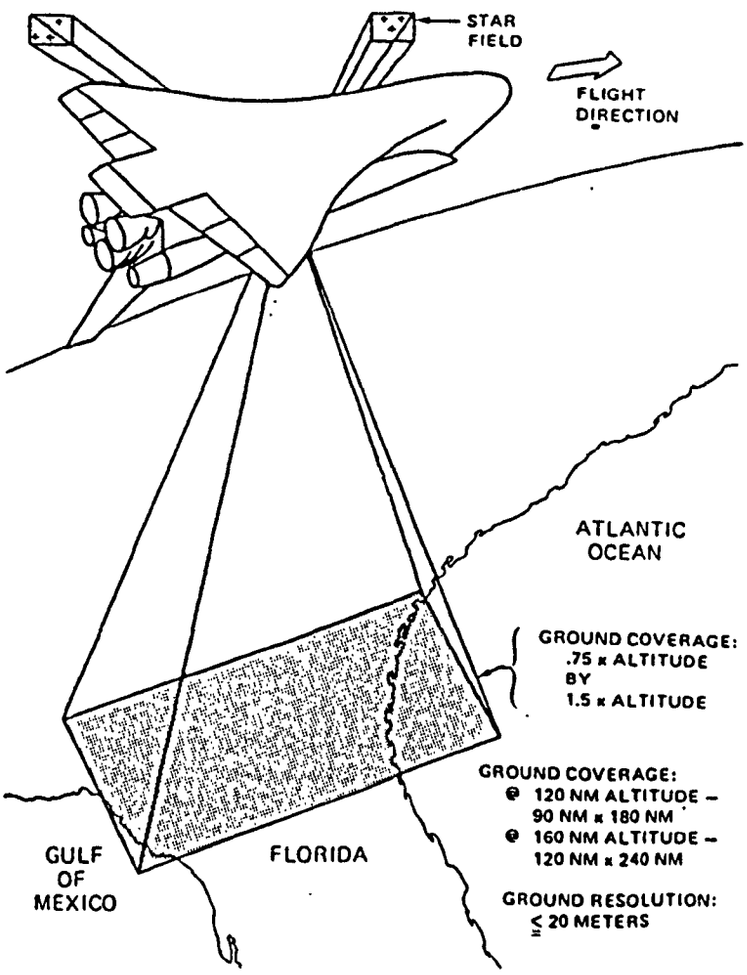
LARGE FORMAT CAMERA

The Large Format Camera (LFC) payload consists of a camera system (lens cone and film magazine, electronics assembly and nitrogen gas supply) attached to an Altitude Reference System (ARS) (stellar camera array with its support structure, environment enclosure and electronics system).



Parameters:–

Focal length:	305mm
Film format:	23 x 46cm
Forward overlap:	primary operating modes of 10%, 60%, 70% and 80%
Base height ratio:	60% OL = 0.6
	70% OL = 0.45
	80% OL = 0.3, 0.6, 0.9 & 1.2
Film capacity:	single magazine – 2400 frames



LFC payload ground coverage.

Performance:–

Flight altitude:	355-366km (one day/228 frames)
	258-266km (one day/335 frames)
	222-238km (six days/1684 frames)
Photo scale:	1:1,183,000 avg. (228 frames)
	1:860,000 avg. (335 frames)
	1:755,000 avg. (1684 frames)
Coverage per frame:	270 x 540km avg. (228 frames)
	197 x 394km avg. (335 frames)
	173 x 346km avg. (1684 frames)

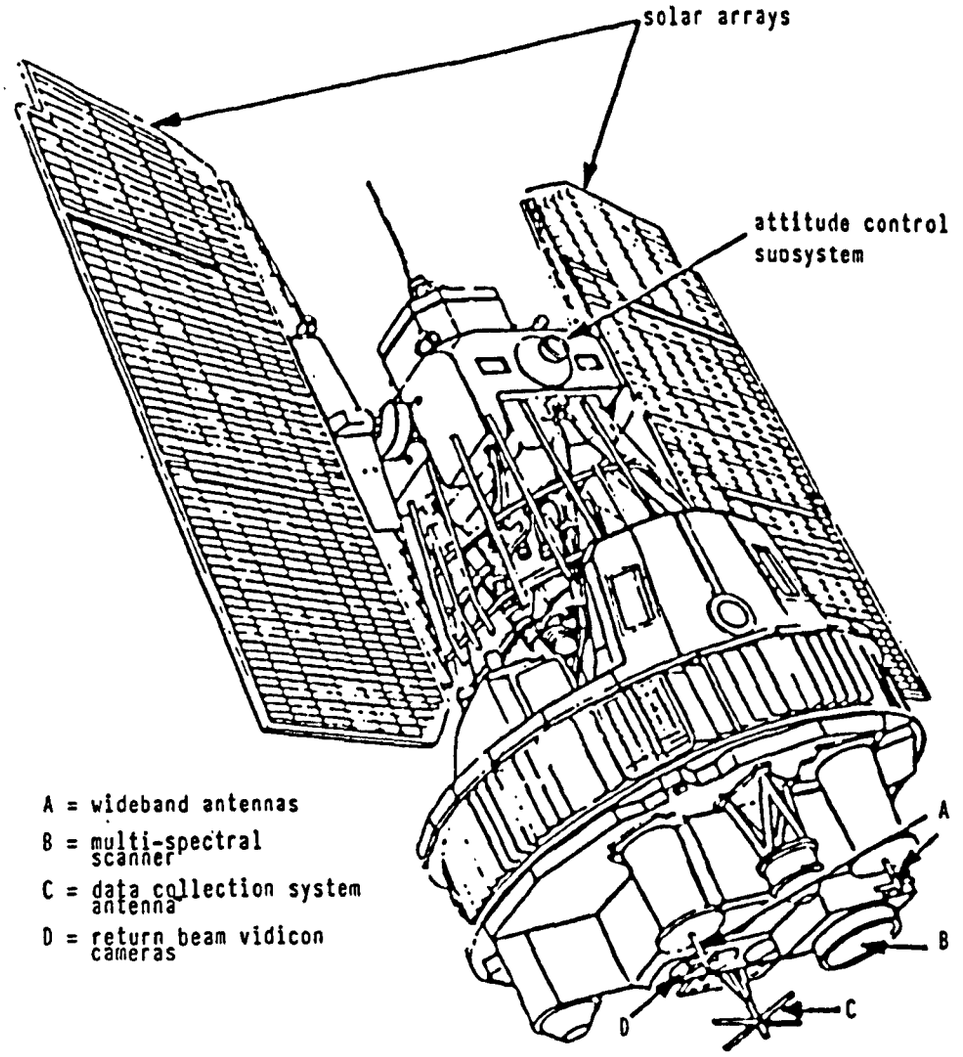
The LFC maiden voyage took place between 5 and 13 October 1984, aboard the Space Shuttle (Challenger) Mission 41-G (at the same time as the SIR-B experiment) and was an engineering flight to de-bug the system and provide imagery on four film types (colour, colour infra-red and two black and white negative films) for detailed performance analysis.

Although designed for map mapping purposes, the individual photographs are useful for qualitative studies in the earth resources disciplines – geology, geography, forestry, range management, agriculture, etc. Several investigators have worked with the imagery preparing 1:25,000 scale topographic maps with much smaller contours than previously considered possible.

LANDSATS 1, 2 and 3

Launch:
Landsat 1: 23 July 1972
operation ended: 6 January 1978
Landsat 2: 22 January 1975
operation ended:
25 February 1982
Landsat 3: 5 March 1978
standby mode: 31 March 1983

Orbital parameters:
Orbit: near polar
sun synchronous
Altitude: 919 km
Inclination: 99.09°.
Coverage: 82°N to 82°S.
Period: 103 minutes, crossing the equator at 9.30hrs local time.
Repeat cycle: 18 days.



Satellites and sensors

Landsat-1 was the first satellite designed to collect data about the Earth's surface and resources. Three satellites, initially called Earth Resources Technology Satellites (ERTS), launched by NASA between 1972 and 1978 comprised the first generation of the Landsat series.

The satellites' payload consisted of two sensors:

- return beam vidicon (RBV) cameras
- a four band multi-spectral scanner system (MSS)

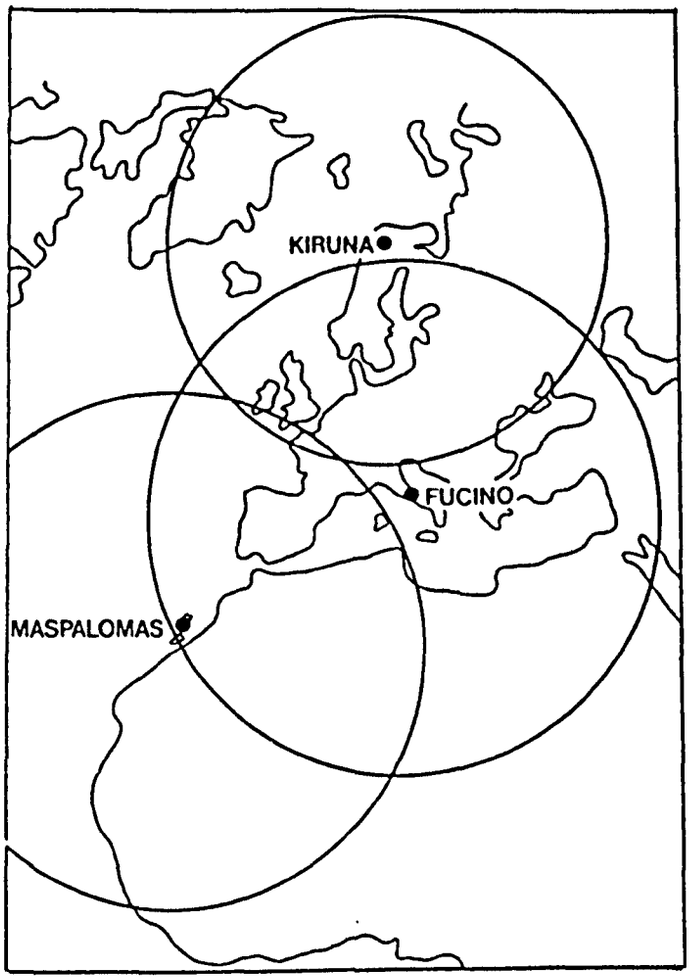
The data were either transmitted directly to specially equipped ground stations or stored on tape recorders for later transmission to data centres in the U.S.A. The Landsat receiving stations covering the U.K. and Europe are at Fucino in Italy and Kiruna in Sweden, both are part of the Earthnet programme.

Return Beam Vidicon Camera (RBV)

	Wavelength (μm)	Resolution	Image format and comments
Landsats 1 and 2 – three RBVs:			Simultaneous view from three cameras of a scene
Band 1	0.475-0.575 (blue-green)	80m	
Band 2	0.580-0.680 (yellow-red)	80m	185 x 185km with 14% side
Band 3	0.690-0.830 (red-near IR)	80m	overlap at the equator and 10% forward overlap.
Landsat 3 – two RBVs, single band:			Two side-by-side images,
	0.505-0.750 (visible to near IR – panchromatic)	40m	98 x 98km, four RBV images approximately coinciding with scene.

Multi-spectral Scanner (MSS)

	Wavelength (μm)	Resolution	Image format and comments
Landsats 1, 2 and 3:			
Band 4	0.50-0.60 (green)	80m	185 x 185km images with 10%
Band 5	0.60-0.70 (red)	80m	forward overlap and 14% side
Band 6	0.70-0.80 (red-near IR)	80m	overlap at the equator,
Band 7	0.80-1.10 (near IR)	80m	increasing towards the poles.
Landsat 3 only:			Range of thermal sensitivity:
Band 8	10.40-12.50 (thermal IR)	120m	Only a few scenes available of limited area.



Applications

The main application fields of the individual MSS bands were identified as:-

Band 4: mapping of sediment ladened water and delineation of shoals and reefs in shallow water.

Band 5: identification of cultural features – urban areas, roads, etc.

Band 6: vegetation studies and delineating boundaries between landforms, land and water.

Band 7: vegetation mapping and water/land separation. This band provides the best penetration of atmospheric haze.

Applications of Landsat data have been widespread in many fields, including:

- geology
- mineral and petroleum exploration
- forestry and agriculture
- hydrology
- coastal processes
- land use and land cover
- mapping environmental changes
- resources inventories
- pollution monitoring

The best use of satellite data such as that from the Landsat missions, has been made when the imagery is interpreted in conjunction with existing information and good ground knowledge of the area under investigation.

Data acquisition

The National Remote Sensing Centre is able to acquire Landsat data from the Earthnet coverage area outside the U.K., from the U.S. data centres and also from individual ground stations and centres around the world. Accounts are held at certain data centres to permit the acquisition of imagery in the shortest possible time.

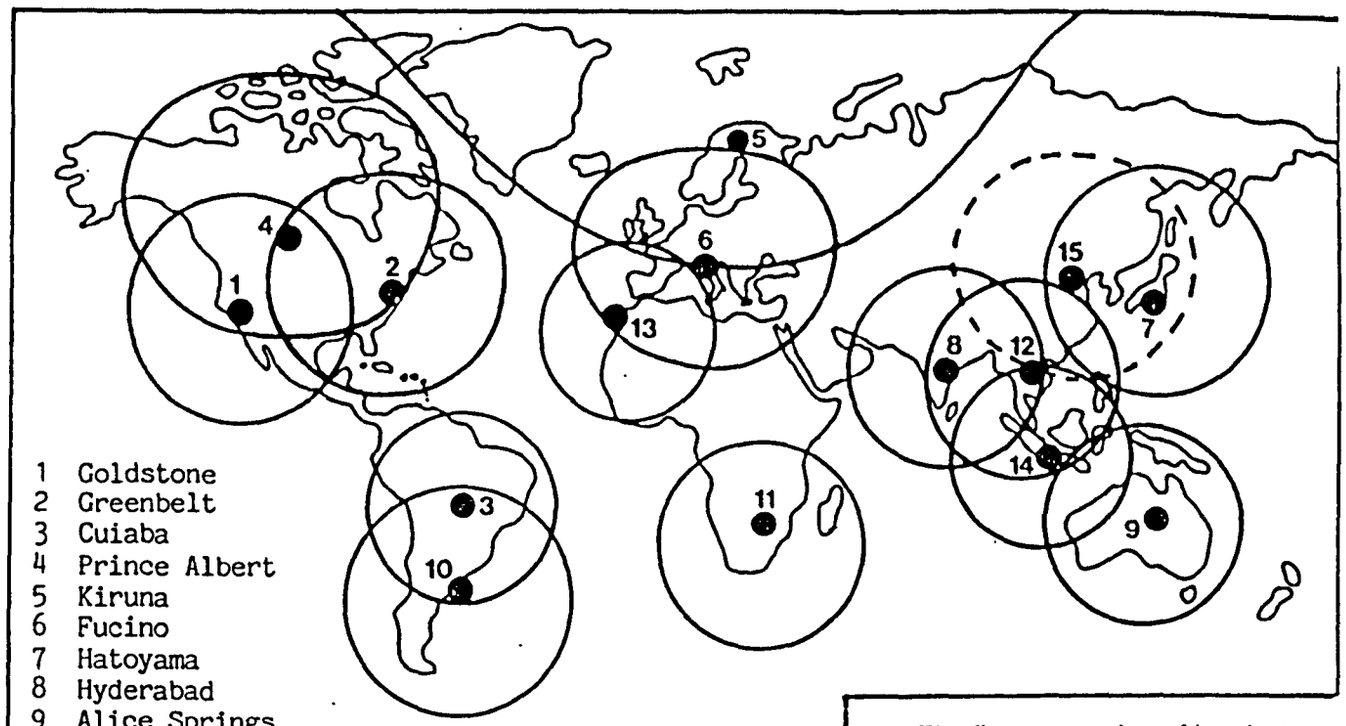
Data coverage

Coverage maps for both Landsats 1, 2 and 3 and Landsats 4 and 5 are included in Appendix 1, superimposed on these maps are the scenes held within the NRSC archive. A full listing of these scenes is provided in Appendix 2 with details of path/row, sensor, acquisition date, cloud cover, scene centre and country location.

NRSC archive

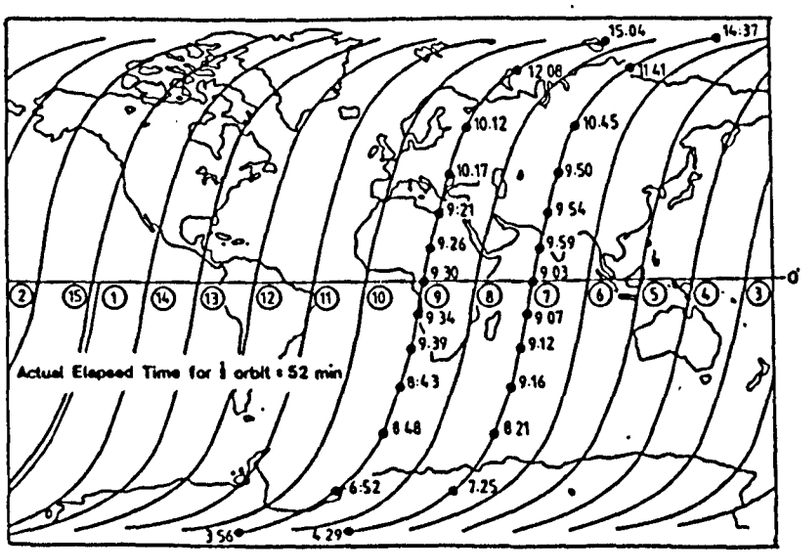
The Landsat archive at the National Remote Sensing Centre is one of the largest digital data archives outside of the U.S.A. It mainly comprises data from the Earthnet ground stations, as it is NRSC policy to acquire all cloud-free or low cloud cover scenes of the U.K. However, over recent years the worldwide archive has also been expanded.

Both digital data and photographic products can be supplied from the NRSC. The various products and services available are described elsewhere in the Data Users Guide, but for further information and price lists contact the NRSC.



Landsat receiving stations.

The first generation of Landsat satellites were launched into a sun synchronous, near-polar orbit, at an altitude of approximately 900km. The angle between the Sun, the centre of the Earth and the satellite was maintained at 37.5° as the Earth orbits the Sun, and the orbital plane is inclined at 99° to the equator. This type of orbital configuration ensures repeatable sun illumination conditions, aiding the comparison of yearly changes in vegetation and mosaicing of adjacent tracks.



Landsat orbital tracks for one day of coverage indicating variations in local time of data acquisition.

The satellite crosses the equator every 103 minutes. During this time, the Earth rotates a distance of 2760km under the satellite at the equator. When the satellite has completed 14 orbits, 24 hours has elapsed and the next westward track of data is acquired. In 18 days one satellite obtained coverage of nearly the entire Earth's surface, weather conditions permitting. The coverage pattern and overhead crossing time of one Landsat satellite during the period 1972 to 1983 are shown on the adjacent map. When two satellites were operational they were positioned nine days apart to allow a regular and more frequent data acquisition capability.

LANDSATS 4 and 5

Launch:
Landsat 4: 16 July 1982
Landsat 5: 1 March 1984

Orbital parameters:
Orbit: near polar
sun synchronous
Altitude: 705 km
Inclination: 98.2°.
Coverage: 81°N to 81°S.
Period: 99 minutes, crossing the equator at 9.45hrs local time.
Repeat cycle: 16 days.

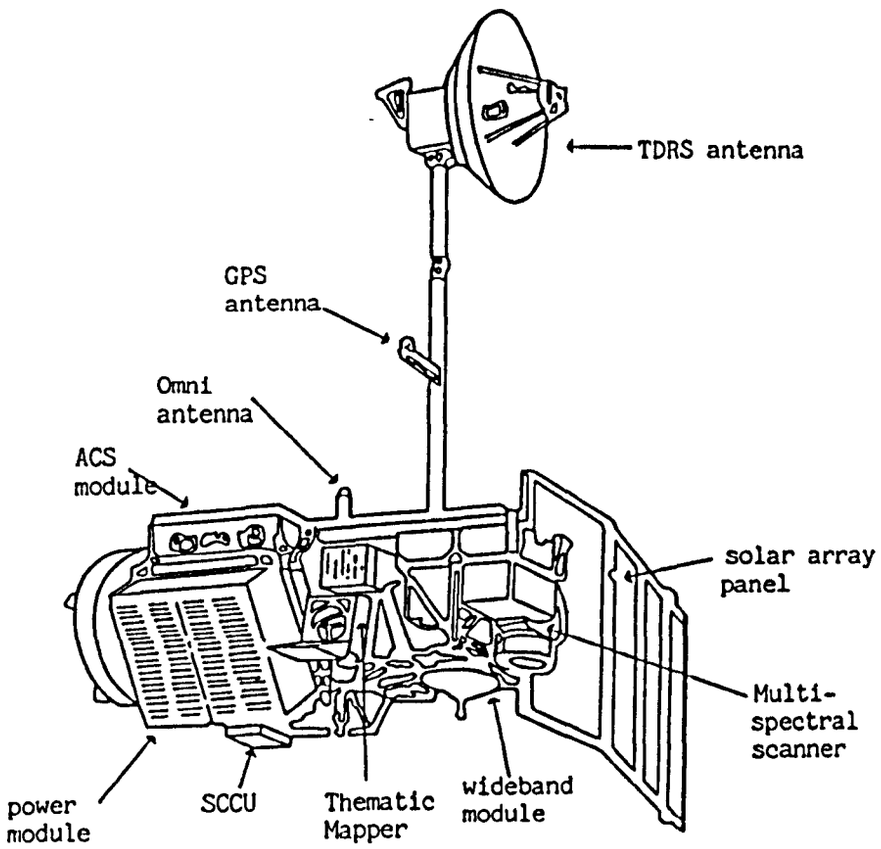
Satellites and sensors

The second generation of NASA's Landsat series was initiated in July 1982 with the launch of Landsat 4. In addition to the conventional multi-spectral scanner system (MSS – four wavebands and 80m ground resolution) familiar to all users of the earlier Landsats, the payload included the Thematic Mapper (TM), which recorded data in seven wavebands with a resolution of 30m in the visible, near and middle infra-red wavebands and 120m in thermal infra-red. Unfortunately power supply problems terminated the reception of TM data in February 1983, although MSS acquisition continues. However, Landsat 5 was launched on 1 March 1984 and both MSS and TM sensors, are operational.

Multi-Spectral Scanner

The MSS on Landsats 4 and 5 are similar to those flown on earlier Landsat missions. The ground pixel resolution is 80 by 80m. However, the four spectral bands are identified by a new numbering system – although the spectral coverage remains unchanged.

Landsats 1, 2 and 3	Landsats 4 and 5
Band 4	→ Band 1
Band 5	→ Band 2
Band 6	→ Band 3
Band 7	→ Band 4



Multi-Spectral Scanner (MSS)

	Wavelength (μm)	Resolution
Band 1	0.50-0.60 (green)	80m
Band 2	0.60-0.70 (red)	80m
Band 3	0.70-0.80 (red-near IR)	80m
Band 4	0.80-1.10 (near IR)	80m

Thematic Mapper

	Wavelength (μm)	Resolution
Band 1	0.45 - 0.52	30m
Band 2	0.52 - 0.60	30m
Band 3	0.63 - 0.69	30m
Band 4	0.76 - 0.90	30m
Band 5	1.55 - 1.75	30m
Band 6	10.40 - 12.50	120m
Band 7	2.08 - 2.35	30m

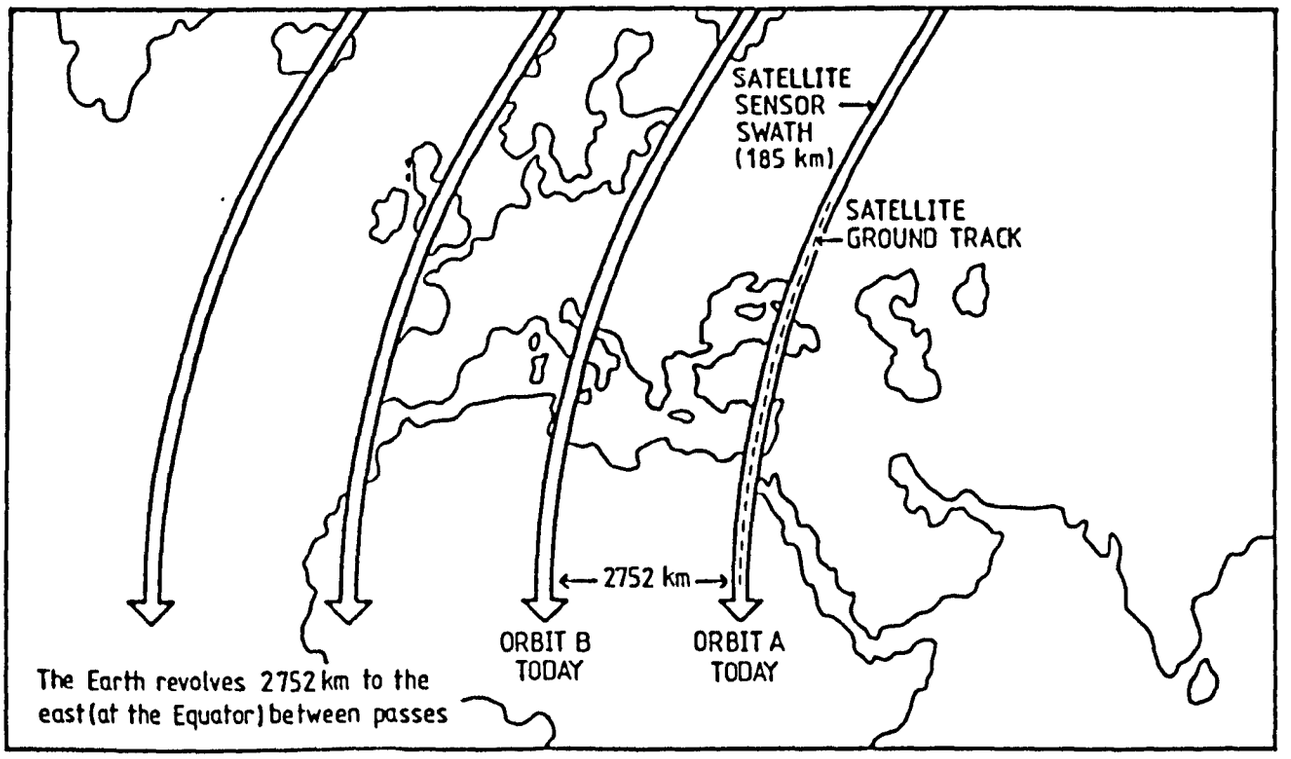
Both sensors provide image data with 185 x 185km coverage, with 5.4% forward overlap and 7.3% side overlap at the equator increasing at higher latitudes.

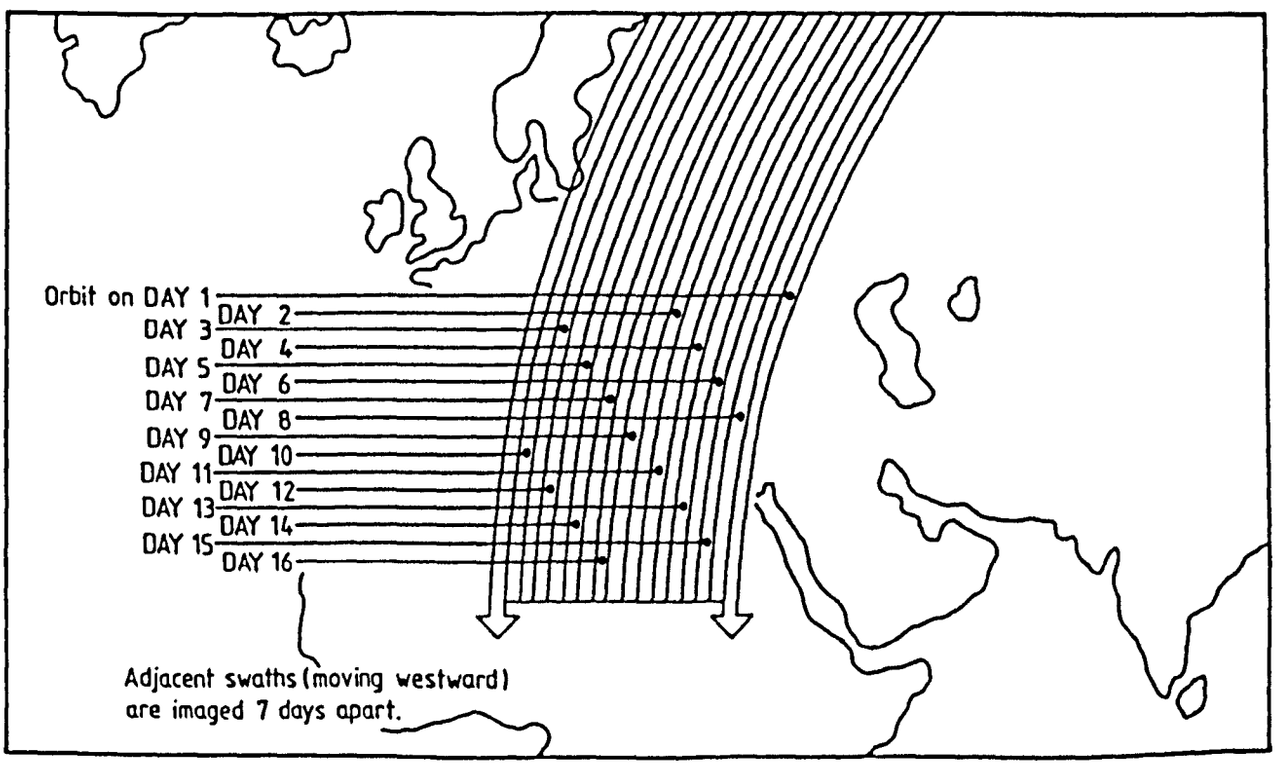
Orbit

The orbital configuration of the satellites creates a 16-day repeat cycle for each satellite. In other words, a specific satellite will travel along a particular ground track once every 16 days. The orbits of the two satellites are eight days out of phase. For either one of these satellites, the time interval between adjacent tracks is seven days. This arrangement contrasts with the 18-day orbital cycles of the first three Landsat satellites which resulted in a one day interval between orbits over adjacent tracks.

The MSS and TM sensors are aligned to scan the same geographical area of 185km wide directly below the oribtal path of the satellite.

There is a minimum side lap of 7.3% between adjacent orbits at the equator, increasing to a maximum of 84% at 80°N/S.



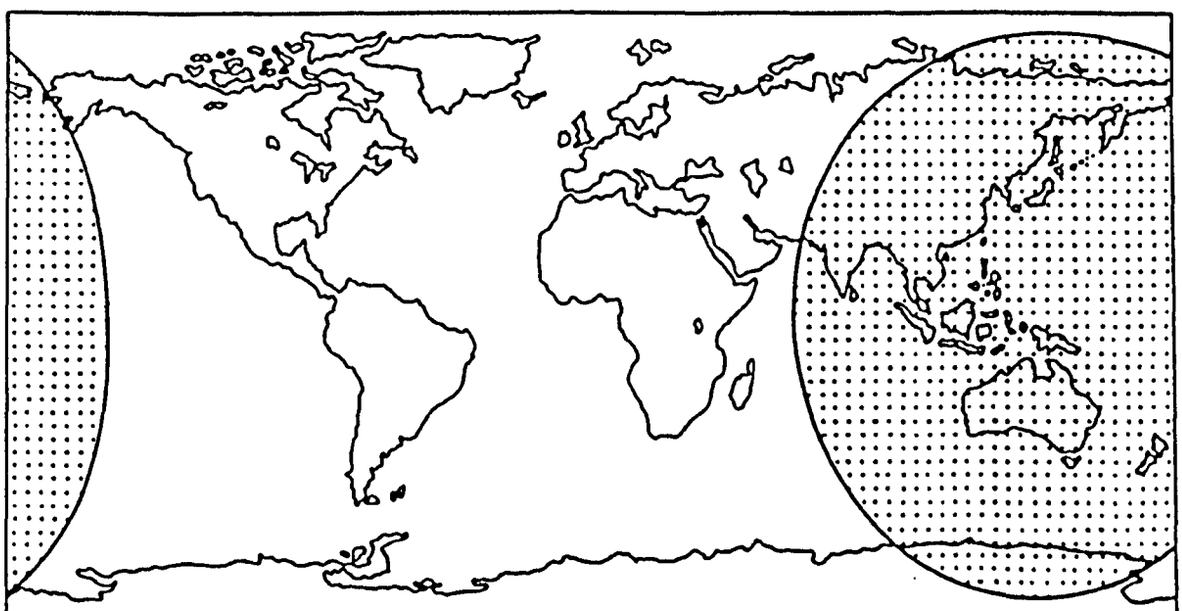


Coverage

Landsat 4 and 5 pass over the same ground track after completing 233 orbits of the Earth. This orbital repeat cycle is incompatible with the 251-orbit Worldwide Reference System (WRS) used to index MSS data from the previous Landsat satellites. A new system of path and row indices has been designed for both MSS and TM data from Landsat 4 and 5. A path index number is assigned to the ground track of each orbit. The new system consists of 233 orbital paths numbered east-to-west with the centre point of path 001 crossing the equator at 64.95 degrees west longitude. The data for each scene consist of the data acquired during a 25.87-second increment of the orbital motion of the satellite. This increment corresponds to approximately 5700 scan lines of image data. Both the MSS data and the TM data for each scene cover a surface area approximately 170km along-track by 185km across-track. A row index is assigned to each scene centre. Row one of each path starts at 80°51′ north latitude and the numbering increases southward through the equator (row 60) to 81°51′ south latitude (row 122). The satellites then travel northward for the ascending (night time) portion of each orbit, and row numbers increase from south-to-north through the equator (row 184) to 81°51′ north latitude (row 246). Thus, row indices 123 through 246 refer to scenes of night time TM thermal data which are not acquired on a routine basis.

The first three Landsat satellites relied upon onboard tape recorders to store data until the satellite passed within range of a ground station. These recorders were often the first component to fail. Landsat 4 and 5 use a new communications system, called the Tracking and Data Relay Satellite System (TDRSS), which eliminates the need for onboard recorders. TDRSS will eventually consist of two satellites (plus an in-orbit spare satellite) in geosynchronous orbits and a centralised ground receiving station located at White Sands, New Mexico. The first TDRSS satellite (TDRS-East) was launched on April 4, 1983 aboard NASA's space shuttle Challenger (mission STS-6). After overcoming problems caused by a malfunction of its booster rocket, the satellite reached its permanent station on October 17, 1983. TDRS-East is currently in geosynchronous orbit over the equator at 41° west longitude at an altitude of 35,890km.
for launch

The second TDRSS satellite was lost on board the Challenger disaster in January 1986 – further setting back an urgent programme that was already delayed by a year.



Shaded area indicates regions where data acquisition via TDRS-East is not possible

Thematic Mapper

Several major differences exist between the basic design of the MSS and the design of the TM. First, the TM acquires data during both the forward (west-to-east) and reverse (east-to-west) sweeps of its scan mirror. This bidirectional approach was adopted to reduce the rate of oscillation of the scan mirror and increase the dwell time of individual detectors upon the Earth's surface.

The TM does not rely on fibre optics, as does the MSS, to direct incoming electromagnetic energy onto photosensitive detectors. Fibre optics are incapable of transmitting 100 per cent of the incident energy from the focal plane to the sensor's detectors. Instead the TM focuses incident radiation directly onto detectors within a prime focal plane assembly. This assembly contains four sets of 16 detectors for four spectral bands in the visible and near infra-red portions of the spectrum. A cooled focal plane assembly contains two arrays of 16 indium antimonide (InSb) photodiodes for two middle infra-red spectral bands and four mercury cadmium telluride (HgCdTe) detectors for a thermal band.

The use of multiple detectors for each spectral band results in the generation of 16 scan lines of data for the six reflective bands and four lines of data for the thermal band during each sweep of the scan mirror. At any one instant, surface radiance is sensed by a total of 100 TM detectors.

The TM also offers improved radiometric sensitivity over the MSS, even though the spectral bandwidth and the IFOV of the TM detectors is significantly less than that of the MSS. In conjunction with the improved sensitivity, TM data are quantised to eight bits (256 digital counts) while MSS data are quantised to six bits (64 digital counts). This effectively corresponds to a four-fold increase in the grey scale being used to measure the intensity of Earth radiation in each discrete spectral band.

Applications

Band	
1	Sensitive to chlorophyll and cartonoid concentrations for soil/vegetation differentiation, deciduous/coniferous differentiation. Coastal water mapping.
2	Sensitive to green reflectance by healthy vegetation.
3	Sensitive to chlorophyll absorption for plant species differentiation.
4	Sensitive to near infra-red reflectance of healthy vegetation for biomass surveys.
5	Sensitive to vegetation moisture and snow/ cloud reflectance differences.
6	Thermal mapping.
7	Sensitive to vegetation moisture and to hydroxyl ions in minerals for geological mapping.

The TM acquires data in seven spectral bands. Four of these bands are located in portions of the spectrum not sensed by the MSS. The location and width of the seven bands were carefully chosen for sensitivity to certain natural phenomena and to minimise the attenuation of surface energy by atmospheric water. The table lists the spectral bands along with the rationale for selecting each band.

Another advanced feature of the TM is its spatial resolution. The TM instantaneous-field-of-view (IFOV) is 30m x 30m for the six reflective spectral bands (bands TM1 to TM5 and TM7) and 120m x 120m for the thermal band (band TM6). The MSS provides a resolution of approximately 80m x 80m in all bands.

SPOT

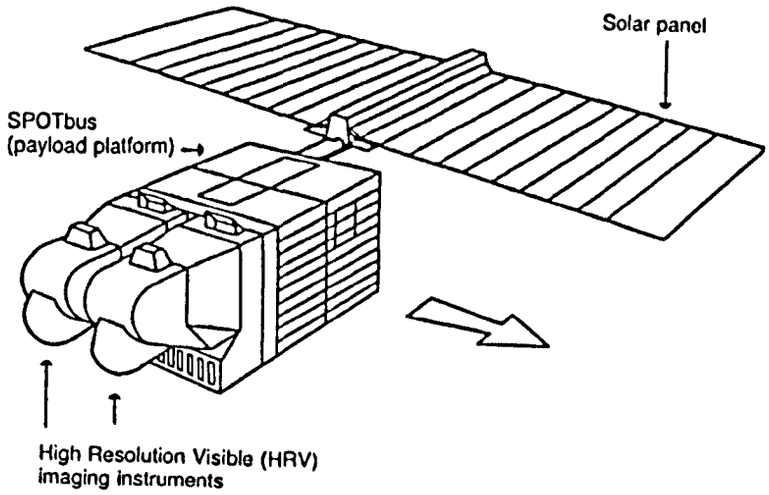
Launch: 22 February 1986

Orbital parameters:

orbit: near polar, sun-synchronous
altitude: 832km
inclination: 98.7°
timing: crossing equator at 10.30 local sun time (from N to S)
repeat cycle: 26 days

Sensors: High Resolution Visible (HRV)

	wavelength (μm)	resolution (m)
multi-spectral mode:		
Band 1	0.50-0.59	20
Band 2	0.61-0.68	20
Band 3	0.79-0.89	20
pancromatic mode:	0.51-0.73	10



Satellite and sensors

The SPOT (Systeme Probatoire d'Observation de la Terre) satellite has been designed by the French Centre National d'Etudes Spatiales (CNES) and built by French, Belgian and Swedish partners.

The payload of SPOT-1 consists of two identical high resolution visible (HRV) imaging instruments and a package comprising two magnetic tape data recorders and a telemetry transmitter.

The HRV sensors are designed to operate in either of two modes – panchromatic (black and white) or multi-spectral (colour) – in the visible and near infra-red portions of the spectrum.

The capabilities include:

- nadir viewing (vertical) providing a swath width of 117km
- off-nadir viewing (oblique) up to 27° from the vertical
- revisit possibilities to increase the frequency of imaging individual sites
- stereoscopic imaging

SPOT is the first satellite to use pushbroom sensors. These consist essentially of CCD (charged-coupled device) linear arrays. This approach avoids the problems associated with mechanical means of moving a scanning mirror. With the pushbroom device, the scanning of an individual line of a scene is performed electronically by successively measuring the current generated by each detector within the linear array. Each spectral band uses four linear arrays, each array consisting of 1728 elementary detectors (CCD devices).

Sun-synchronous orbit

The sun-synchronous orbit ensures the satellite always passes overhead at the same (solar) time. In its normal orbit, SPOT crosses the equator, going south, at about 10.30 a.m. and at that time precisely on 15 June of each year.

Nadir and off nadir viewing

Each HRV instrument can be pointed so that two adjacent strips of the Earth's surface are covered, giving a total swath width of 117km (nadir) and an overlap of 3km. Since the distance between adjacent ground tracks at the equator is about 108km, complete Earth coverage can be obtained with this fixed setting of instrument fields.

It will be possible to steer the mirrors of the HRV instruments to view obliquely (off nadir) up to 27° either side of vertical to cover an area of interest within a 950km wide strip centred on the satellite ground track.

The width of the observed swath varies between 60km for nadir viewing and 80km for extreme off nadir-viewing.

The programme of planned observations is controlled by the satellite's onboard computer. A sequence of recorded images may include both modes of operation (panchromatic and multi-spectral) and changes in each instrument's viewing directions.

SPOT scenes and data processing

Each SPOT scene is recorded in one of two possible modes: panchromatic (PA) or multi-spectral (XS). For instrument viewing directions close to the vertical, each scene covers an area of 60 x 60km. In contrast, scenes recorded at the extreme oblique viewing angles (27°) cover an area of 60 x 80km.

The Centre de Rectification des Images Spatiales (CRIS) is responsible for archiving SPOT raw data received by the Toulouse station and for carrying out additional standard image data processing operations. SPOT panchromatic and multi-spectral scenes can be pre-processed to any of four levels:

Level 1a

Essentially raw data apart from the normalisation of the CCD detector responses in each spectral band. Inter-band coefficients are also given. There is no geometric correction. Data are intended specifically for users requiring imagery that has undergone a minimum of processing – e.g. for stereoplotting and basic radiometric studies.

Level 1b

Includes full radiometric and geometric corrections (removal of systematic distortions due to effects of rotation and curvature of Earth, viewing angle and desmearing). Absolute location accuracy is 1500m (rms error), for vertical viewing and internal distortion is less than 10^{-2}. This is the basic level for interpretation and thematic mapping.

Level 2

A precision preprocessing level with bi-directional corrections on the basis of ground control points and rectification to a given cartographic projection – conformal Lambert, transverse Mercator, etc. (This level does not take into account distortions due to terrain relief.) Location accuracy is 50m (rms error) for vertical viewing, provided the elevation range within the scene area does not exceed 1250m. With maximum oblique viewing this accuracy specification can be met if the elevation range does not exceed 170m.

Level 2 scenes are oriented according to geographic North. Such processing can be performed only if sufficiently accurate maps are available to assist image correction.

Level S

Rectified using control points for registration with a SPOT reference scene. Registration accuracy is 0.5 pixels when two scenes are recorded at the same viewing angle. This product is intended primarily for multi-date studies.

Products

Computer Compatible Tapes

CCTs can be recorded at 6250 or 1600 bpi density. Given the total volume of a SPOT scene, a single 6250 bpi tape can accommodate an entire scene, however two or three 1600 bpi tapes will be required, depending on scene data volume.

CCTs will be available with the following specifications:

- band interleaved or band sequential.
- ASCII or EBCDIC character coding.

CCTs ordered from the NRSC are available in RAE format.

Photographic products

- Film. SPOT scenes recorded on photographic film will be available with the following standard characteristics:

  PA mode scenes:
  - 1 positive or negative b&w film per scene,

  XS mode scenes:
  - 3 positive or negative b&w films per scene,
  - 1 false colour type positive transparency.

Scale	Format	
	Level 1B	Level 2
1:400,000	240mm x 240mm	300mm x 350mm
1:250,000	480mm x 480mm	
1:200,000	480mm x 480mm	

Level 1A scenes will also be available on film, at the one scale of 1:266,000, to adapt the overall image dimensions to stereo plotter and other photogrammetric instruments.

- Paper print. Paper prints of all SPOT scenes will be offered at the standard scales indicated below, either as b&w or false colour prints.

Scale	Format	
	Level 1B	Level 2
1:250,000	480mm x 480mm	600mm x 700mm
1:200,000	480mm x 480mm	600mm x 700mm
1:125,000	960mm x 960mm	1,200mm x 1,400mm
1:100,000	960mm x 960mm	1,200mm x 1,400mm

Special products

SPOT Image and distributors plan to offer a range of special products including:

- digital and photographic mosaics.
- "twin pairs" (pairs of scenes recorded in the twin vertical viewing configuration).
- PA + XS combination.
- special colour composite products.
- linear combinations of spectral bands

Revisit capabilities

If the satellite's instruments were only capable of nadir viewing the revisit frequency for any given point would be 26 days. This interval is unacceptable for the observation of phenomena evolving on timescales ranging from several days to a few weeks, especially where cloud cover hinders the acquisition of usable data. However, with SPOT, the capability for off-nadir viewing during satellite passes in the vicinity of the area of interest considerably increases the revisit possibilities.

During the 26-day period separating two successive nadir satellite passes over a specific point on the Earth's surface, the programmable steering capability of the instruments allows the area to be observed on seven different passes if it were on the equator and on eleven occasions if at a latitude of 45°.

Stereoscopic viewing

Another important capability offered by off-nadir viewing is that of recording stereoscopic pairs of images of a given scene, i.e. images acquired at different viewing angles during successive satellite passes.

Theoretical studies and simulations imply the accuracy of altimetric restitution (elevation) can be expected to be:

- 10m across an entire scene after registration of several reference points.
- 5m relative accuracy for points separated by a few kilometres.
- sensitivity and threshold of relief perceptibility of 3 to 5m or better.

The main applications for stereoscopic imagery are in photogrammetry for cartographic purposes and photo-interpretation for geological, geomorphological and hydrological studies. The following will be possible:

- compiling topographic maps with uniform vertical contour interval of 20 to 50m.
- perception of large man-made structures and gross vegetation features.
- direct compilation of digital terrain models.

Data reception

In Europe, data will be received at ground stations near Toulouse (France) and Kiruna (Sweden), other stations exist or are planned around the world. Data can be transmitted, as it is recorded, when the satellite is within range of a image receiving station – an area of approximately 2600km in radius. On-board recording of image data is also possible of areas beyond the range of ground stations. In such cases the recorded data is transmitted to the SPOT Mission Centre at Toulouse.

SPOT Image

User information, promotional activities and access to data distribution are essential elements of a remote sensing programme. For SPOT these tasks are handled by the commercial company SPOT Image, which was established in 1982.

The objectives of SPOT Image are to:

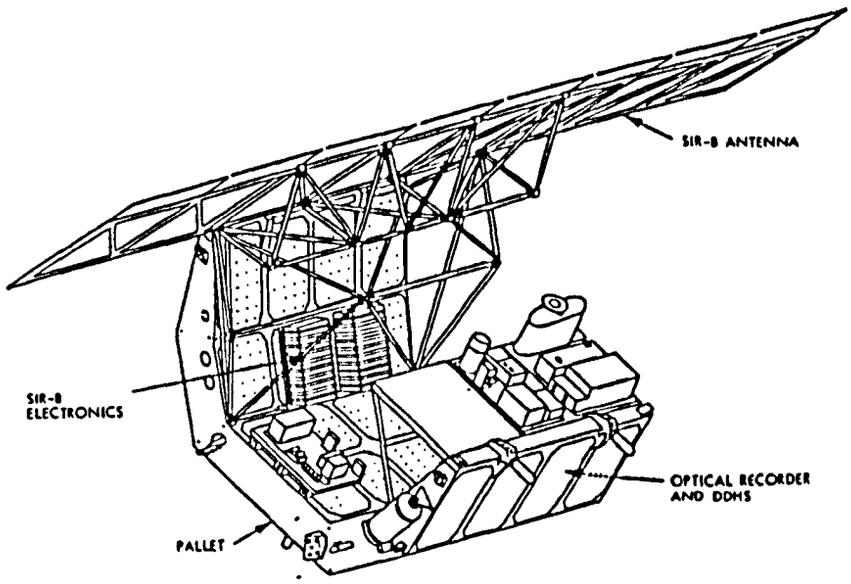
- promote the SPOT system.
- generate and process data.
- distribute data and images on a world-wide basis.

In order to facilitate acquisition of data, SPOT Image will develop an overall catalogue of SPOT data available globally, which will be accessible through an extensive network of remote terminals.

SHUTTLE IMAGING RADAR

The Shuttle Imaging Radar-B (SIR-B), which formed part of the scientific payload of the Shuttle Mission launched in October 1984, was the third in a series of spaceborne radar experiments conducted by NASA that began in 1978 with the launch of Seasat and continued in 1981 with SIR-A.

Imaging radar is a relatively new tool for acquiring synoptic coverage of the Earth's surface, and much research is required to understand its capabilities. However, the potential is great. Radar "sees" through cloud cover and can operate both night and day. It has also been demonstrated that radar has the capability of penetrating certain surface materials.



SIR-A mission objectives

In eight hours SIR-A collected data of 10 million km^2 of the Earth's surface – including many inaccessible areas, covered almost continuously by cloud, which were imaged for the first time. The objectives of the mission were:

- to carry out geoscientific investigations, which required a radar system alone or in combination with other sensors.
- to explore areas that are difficult to study using visible and thermal sensors, e.g. cloudy areas, dense forests.

	SIR-A	SIR-B
Launch:	12 November 1981	5 October 1984
Duration:	2.5 days	8.3 days
Orbital parameters:		
Altitude:	245km	352, 274, 255km
Inclination:	38°-40°	57°
Wavelength:	23cm L-band	23cm L-band
Frequency:	1.28GHz	1.28GHz
Polarisation:	HH	HH
Resolution:	40m at 7-look directions	30m at 4-look directions
Swath width:	50km	20-50km
Data Collection:	optical	digital and optical

Applications

- penetration of dry sand to discover fossil drainage patterns to assist studies of climatic change and provide information for the resource management of desert areas.
- geological studies
  – delineation of previously unmapped rock types and structures identified by microwave remote sensing.
  – mapping of rock units and structures, for the first time, in heavily forested areas.
- geomorphological mapping in desert and glacial environments.
- topographic and land use mapping in cloudy tropical areas.
- irrigation, soil moisture and salinity studies.

SIR-B mission objectives

Like Seasat and SIR-A, SIR-B operated in the L-band (23cm) and was horizontally polarised. However, SIR-B was designed to acquire digitally processed imagery at selectable incidence angles between 15° and 60°. Topography is revealed best at low incidence angles, with higher angles providing more information on surface roughness. The ability to image a specific area at a variety of incidence angles would provide an excellent means of characterising the terrain. Thus, one central objective of the SIR-B experiment was to study the effect of different illumination geometries on the data to allow decisions about the design of future imaging radar systems.

A P P E N D I X (2)

Fryberger, et al (1984, published paper)

Sedimentology (1984) 31, 413–431

Wind sedimentation in the Jafurah sand sea, Saudi Arabia

STEVEN G. FRYBERGER*, ABDULKADER M. AL-SARI, THOMAS J. CLISHAM†, SYED A. R. RIZVI *and* KHATTAB G. AL-HINAI

Research Institute, University of Petroleum and Minerals, Dhahran, Saudi Arabia

ABSTRACT

The Jafurah sand sea of the Eastern Province of Saudi Arabia extends along the Arabian Gulf coastline from Kuwait in the north to the Rub Al Khali in the south, a distance of about 800 km. Sand drifts southward to south-eastward from regions of high wind energy in the north to low wind energy in the south.

The aeolian landscape is zoned, with areas of deflation, transport and deposition from north to south. Drift rates in the zone of transport, near Abqaiq, range from 2 m^3 $m\text{-}w^{-1}yr^{-1}$ on sabkhas, to 29 m^3 $m\text{-}w^{-1}yr^{-1}$ on the crests of dunes. Average drift rates of approximately 18 m^3 $m\text{-}w^{-1}$ yr^{-1} observed during the study can cause about 1 m of accumulation per 5500 yr in a 100 km zone of deposition downwind, not including the bulk transport represented by the forward advance of dunes. Dune advance ranged from 23 m (2·9 m high dune) to 3 m (23 m high dune) during April–October 1980.

The study area consists of dune, interdune, sand sheet and siliciclastic sabkha terrains, each of which is characterized by differing drift rates, and differing rates of erosion or deposition. Sedimentation occurs by lateral movement of dunes and interdunes, and vertical accretion by sand sheets and sabkhas.

INTRODUCTION

In the past, workers such as Wilson (1971), Dubief (1952), and Bagnold (1954) have theorized extensively regarding the degree of mobility of wind-blown sand in the world's great deserts. Based on transport equations such as those of Bagnold (1954), and Lettau & Lettau (1969); other workers including Wilson (1971), and Fryberger & Ahlbrandt (1979) have proposed theories regarding the origin and development of aeolian sand seas. In general, these theories ascribe the origin of sand seas to wind shifting sand around vast areas in desert sedimentary basins—however, the movement of sand has never been measured directly on a regional basis. The purpose of this study was to ascertain directly the degree of activity of the Jafurah sand sea using sand trapping devices. Such information is vital to test theories of sand sea formation, and thus develop realistic geological models for use in studies of ancient rocks. The present degree of activity of modern deserts is also of importance in providing baseline data for comparison with possible glacial and interglacial wind systems to which the development of many modern sand seas seems inextricably linked, perhaps through alternation of fluvial and aeolian cycles of activity.

The Jafurah sand sea of Saudi Arabia is an excellent place to make such initial studies. The Jafurah is an elongate, 30–250 km wide sand sea extending down the western side of the Arabian Gulf, past Qatar and southward, finally merging into the sands of the Rub Al Khali (Fig. 1). The Jafurah extends from an area of high wind energy in the north to an area of low wind energy in the south near Al Ubaylah (Fig. 1).

Our studies were conducted in a narrow, 30 km wide choke point of the Jafurah near Abqaiq, through which most of the sand supplied by northern sources passes southward (Figs 2 & 3). South of the study area the Jafurah widens gradually to about 250 km maximum width near Al Ubaylah.

Present addresses: *McAdams, Roux and Associates, 730 Seventeenth Street, Suite 530, Denver, Colorado 80202 and †3731 East Fourth Street, Tucson, Arizona 85716, U.S.A.

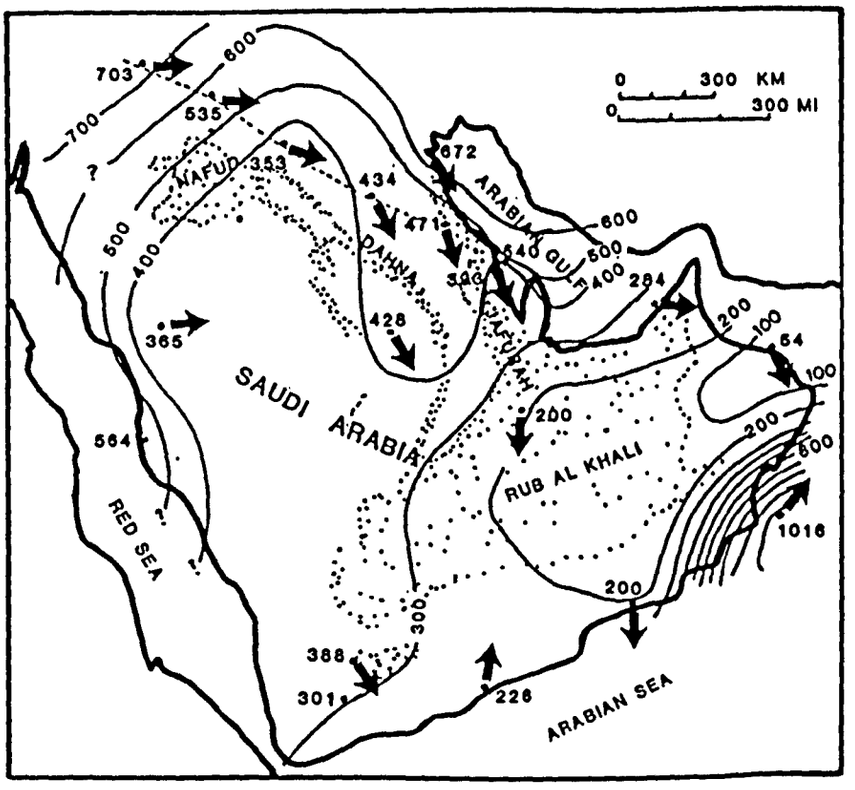


Fig. 1. Contour map of drift potentials (in vector units, v.u.'s) in Saudi Arabia, based on wind records from the National Climatic Center, Asheville, North Carolina. Contours along the Arabian Gulf coastline reveal the zonation of the Jafurah from high wind energy in the north to low wind energy in the south. Drift potentials are proportional to potential sand moving power of the wind, using the methods of Fryberger (1979). 1 v.u. equals about 0·07 m^3 $m\text{-}w^{-1}$. Arrows show resultant drift directions.

The Jafurah may be broadly divided into several zones. In the northern part of the sand sea, near Jubayl, much of the terrain consists of mature sand sheets (some with soil horizons), blowouts, and parabolic dunes, and sabkhas (Fig. 4C). This is a high energy zone of deflation (Fig. 5). The principal study area, in which we made most of our measurements, is near Abqaiq. This zone consists of immature sand sheets (Few soils), isolated dunes and dune complexes, and sabkhas. This is the zone of transport (Fig. 5). The southern zone, whose boundaries are poorly defined, extends from Hofuf southward. This is partly a zone of transport, but much deposition is occurring, and extensive belts of continuous dunes have developed (Fig. 2). Presumably some of the terrain zonation we observed in the Jafurah is related to the loss of wind energy southward, which is shown in Fig. 1.

CLIMATE

The climate is typically arid and hot, as reviewed by Williams (1979) and Breed *et al.* (1979). Wind energy release is highly seasonal, with a maximum occurring between May and July, the 'Shamal' season (Table 1). During this time, strong north to north-west winds blow southward toward the Rub Al Khali. The strength of these winds seems dependent to some degree upon the development of the Indian monsoon (Breed *et al.*, 1979).

This pattern of wind energy release differs from that in North Africa, in which maximum wind energy is related to strong frontal passages associated with movement of low pressure cells across the Mediterranean Sea. The winds of the Jafurah are much less violent, but may continue for extended periods (from

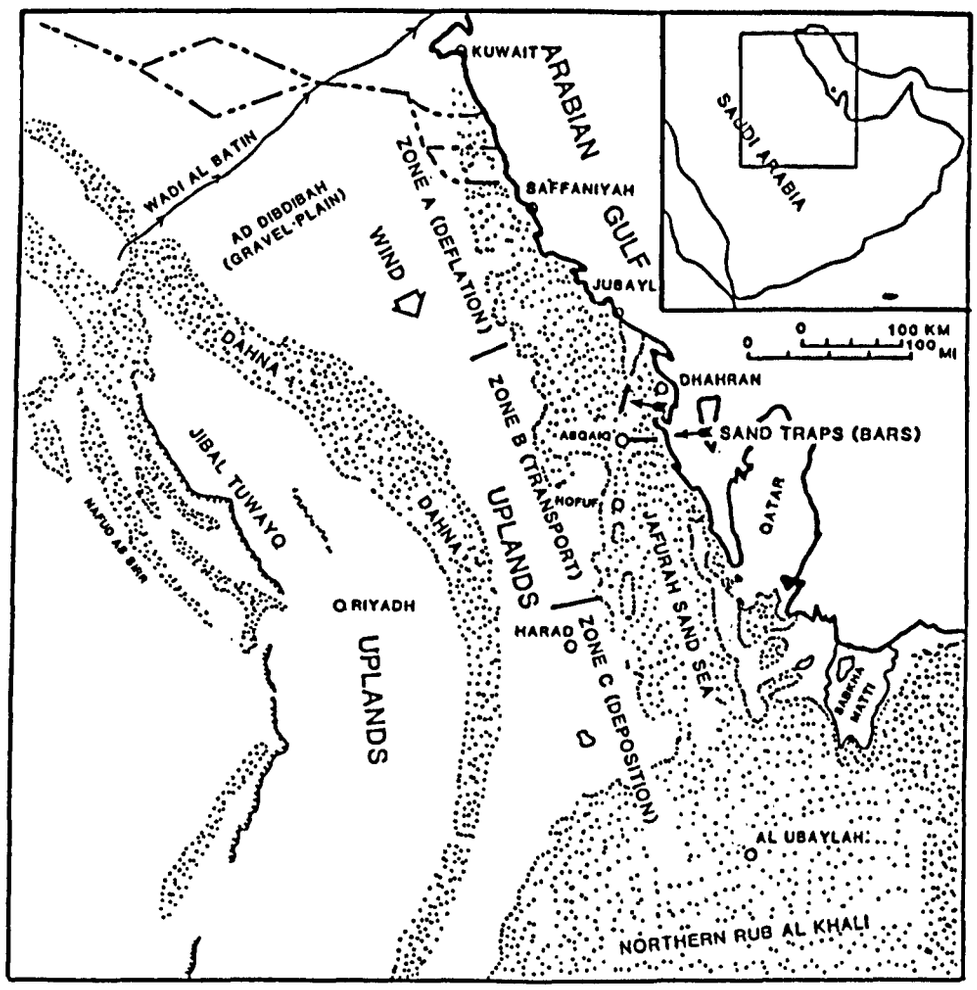


Fig. 2. Index map of the sand seas (dotted areas) of central and eastern Saudi Arabia. Zones of deflation, transport and deposition do not have precise boundaries, but reflect the authors' general observations based on surface travels and overflights. Short solid bars (marked by arrows) near Abqaiq show positions of the lines of sand traps.

2 to 3 weeks), with velocities of 11–16·5 m s^{-1}. Wind energy varies greatly from year to year (Table 1). In addition, even during Shamal season, a sharp diurnal pattern is imposed upon wind flow at the surface, with quiet spells at night and strongest winds during daytime (Fig. 6). Presumably this results from the development of a strong, low level inversion above the desert at night, and subsequent breakdown due to convective activity during daytime.

AEOLIAN TERRAINS OF THE STUDY AREA

The majority of our study area within the Jafurah sand sea consisted of wind-laid sands. Tertiary gravels, sandstones and lime marls are exposed at spots within the sand sea, and in addition form the western boundary of the Jafurah (Fig. 2). Wind deposits of the study area consist of dunes, interdunes, sand sheets, and aeolian siliciclastic sabkhas (see Fig. 4). The sedimentary features of these deposits are described elsewhere (Fryberger Al-Sari & Clisham, 1983), while the geomorphic features and depositional processes are reviewed below. The type of aeolian terrain was early recognized as an important factor influencing sand drift rates. Thus, our sand traps were placed to observe activity on these four basic terrain types. In addition, as described below, different terrain types responded differently to changes in wind regime during the study. Typical areal relationships of the aeolian terrain of the study area are summarized in Fig. 7.

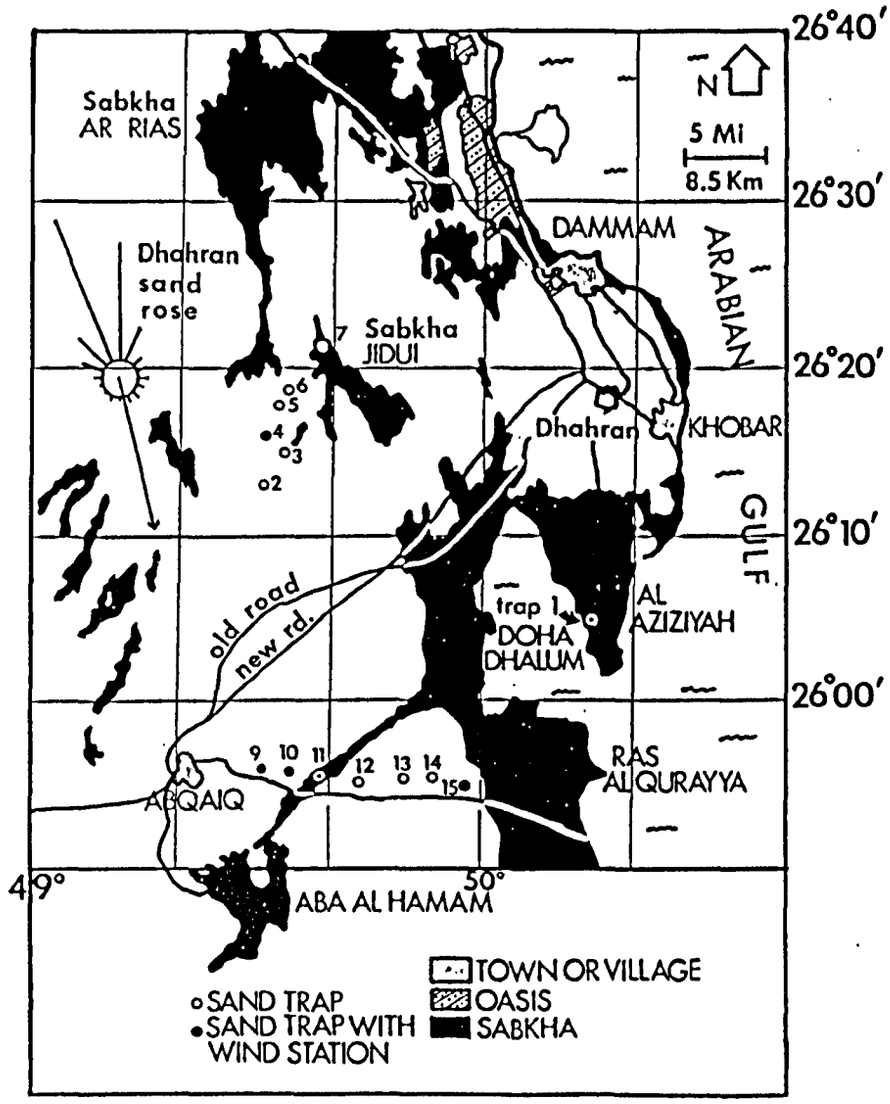


Fig. 3. Detail map of Dhahran – Abqaiq area showing positions of sand traps and wind stations. Note that sand trap 1 is on a sand sheet on Al Aziziyah Sabkha, near the coast. Trap site 8 was abandoned early in the study and is not shown. Dhahran sand rose shows potential sand transport based on wind records for Dhahran, obtained from the National Climatic Center, Asheville, N.C. (about 10 yr of observations). Compare with drift roses based on sand trap contents, Fig. 15.

Dunes

Within the study area most of the dunes are of the barchanoid type (after McKee, 1979) including barchans, barchanoid ridge, transverse ridge and dome dunes. These dunes are typically developed in unimodal wind regimes such as that of the Eastern Province of Saudi Arabia (see Sand Rose, Fig. 3). We were surprised at the abundance of dome dunes of all sizes in the study area, and at the constant evolution of dome dunes to barchans and vice versa at unpredictable places and times during the study. Two common types of vegetationally controlled dunes in the study area are the parabolic dune and the obstacle or 'coppice' dune (Fig. 4C).

Dunes in the study area exist in isolation, or in dune complexes 1 km wide and 1–5 km long, oriented with long axes transverse to the wind. Dune complexes are efficient subregional traps for sand, and thus tend to 'starve' areas of sand downwind.

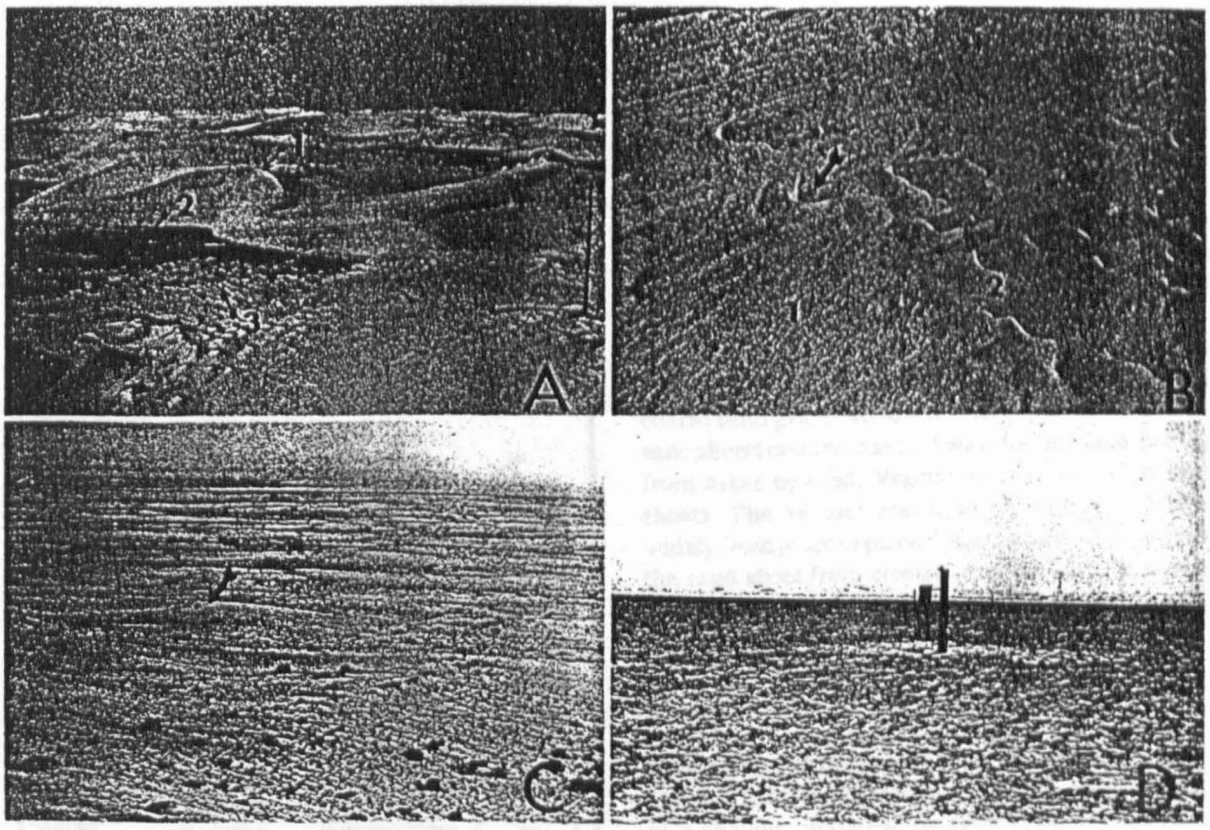


Fig. 4. Aeolian terrains of the study area: (A) View to NW near trap 5, showing barchanoid ridge dune (arrow 1), evaporitic interdune (arrow 2) and vegetated sand sheet (arrow 3). (B) View toward the east in the Abqaiq area (zone of transport), showing lightly vegetated sand sheet (1); and barchanoid dunes of dune complex (2). Note dry interdunes (arrow). (C) View toward the NE, north of Dammam (zone of deflation) with Arabian Gulf Coast in background, showing vegetated sand sheet with blowouts (arrow). (D) Sabkha at sand trap site 11. Dark surface is salt encrusted sand. Light material is fresh sand blown across the sabkha and trapped between salt ridges and other depressions.

Interdunes

Interdunes are flat to gently sloping areas between dunes, which are commonly topographically enclosed by them (see Fig. 4A and B). Interdune areas may be sites of erosion or deposition, and may be classified according to moisture content as dry, damp, wet, or evaporitic (Ahlbrandt & Fryberger, 1981). Interdunes which are topographically low usually have the greatest moisture content, by virtue of proximity to the groundwater table. If the groundwater is not overly brackish, abundant vegetation will develop in the interdune, provided dune movement is slow enough to allow time for plant growth. If groundwater is very saline, unvegetated salt-encrusted surfaces develop which are commonly characterized by salt ridges. High water tables result in the formation of interdune ponds.

Interdune terrains are the most complex in the study area (although the least extensive) due to the wide range in amount and salinity of moisture present. Vegetated, topographically low interdunes are commonly the most stable with respect to wind erosion or deposition. Topographically higher interdunes are least stable, and may be subject to extreme wind scour.

Sand sheets

Sand sheets in the study area are flat, or gently rolling tabular bodies of sand up to several metres thick which may extend many metres or even kilometres horizontally (Fig. 4B, C). Usually the direction of elongation of a sand sheet is parallel to the long-term effective wind direction, which is from the NW. Sand sheets are commonly vegetated and consist of more

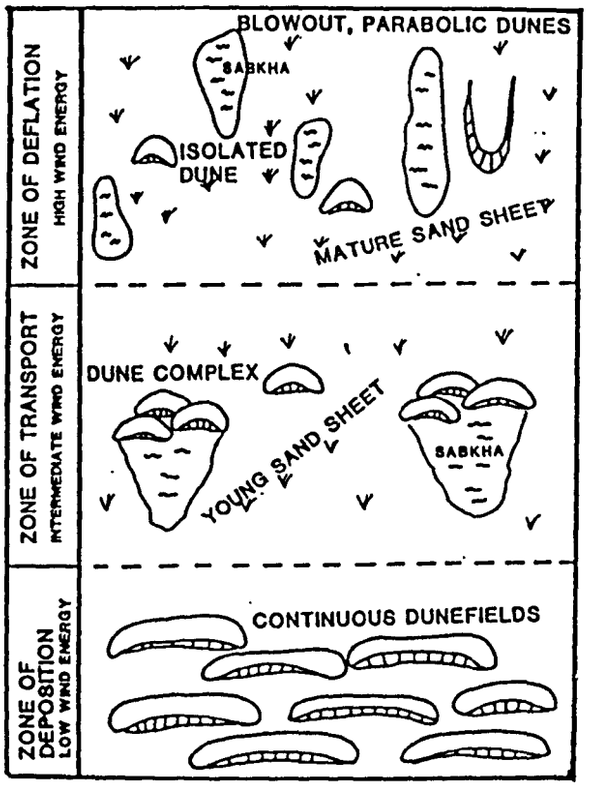


Fig. 5. Schematic diagram showing aeolian landscape associations characteristic of zones of deflation (high wind energy), transport (intermediate wind energy) and deposition (low wind energy). These zones, although poorly defined, seem to exist from north to south in the Jafurah sand sea at the present time (see Fig. 2).

poorly sorted sand than surrounding dunes. Some sand sheets are remnants of lower parts of previously existing dunes and contain dune avalanche cross-bedding dipping as much as 34°. Other sand sheets have developed from an initial sand patch which continued to accrete sand in horizontal layers of ripple-produced strata.

Sand sheets resist wind erosion because of the widespread occurrence of a protective surface layer of coarse sand grains up to 4 mm in diameter. However, sand sheets can serve as pathways for fine sand drifting from areas upwind. Vegetation is common on sand sheets. The amount and kind of vegetation ranges widely from place to place. Vegetation further protects the sand sheet from erosion, and inhibits the flow of sand across the sand sheet from areas upwind, thereby promoting deposition.

Sabkhas

Sabkhas in the study area are flat, salt-encrusted sandy plains. Their existence is dependent upon the presence of a shallow ground-water table (Fig. 4D). Sabkhas can be surfaces of deflation or deposition, depending on whether the water table is falling or rising, and on the availability of sand.

Small interdune erosional sabkhas result from wind scour in the lee of a dune to the top of the capillary fringe of the water table. Resulting deposits are only a few centimetres thick, due to the erosional interdunal setting and rapid movement of dunes. Large deposi-

Table 1. Dhahran average monthly drift potentials 1970–81 (in vector units, v.u.)

Year	Jan.	Feb.	Mar.	Apr.	May	June	July	Aug.	Sep.	Oct.	Nov.	Dec.	Annual
1970	25	23	43	51	187	157	138	88	74	56	17	88	945
1971	64	75	84	116	69	175	112	101	20	42	10	25	894
1972	16	17	27	17	55	66	75	10	26	1	21	29	359
1973	20	16	40	29	50	174	69	5	12	8	25	8	457
1974	20	8	14	29	27	27	33	32	8	1	5	18	222
1975	14	12	22	5	26	56	17	28	5	15	9	11	220
1976							No data						
1977	14	7	16	16	14	46	43	9	6	9	12	4	195
1978	12	4	15	19	12	58	23	35	9	2	17	2	208
1979	13	12	16	37	33	105	80	47	3	4	1	16	367
1980	16	15	23	46	28	50	26	25	8	6	3	15	261
1981	10	15	13	Not available									
Average monthly drift potential	20	19	28	37	50	91	62	38	17	14	12	22	

Average annual drift potential during 1970–80 = 413.
Calibration: v.u. represents about 0·07 m^3 $m\text{-}w^{-1}$
14 v.u. represents 1 m^3 $m\text{-}w^{-1}$.
Underlined values occurred during course of study.

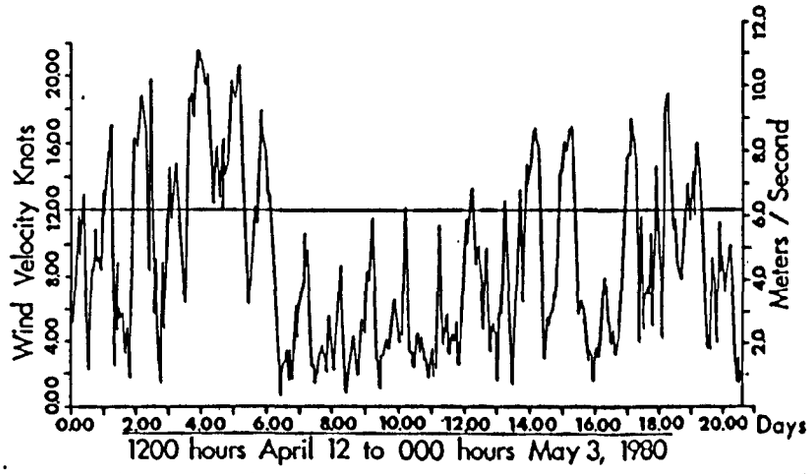


Fig. 6. Record of three weeks of sandstorms from April 12 to May 3 1980, at trap site 4. Horizontal line in centre of figure marks approximate threshold velocity of sand movement of about 6·2 m s^{-1} for 0·25 mm diameter sand grains. Thus, portions of the graph above this line record sandstorms.

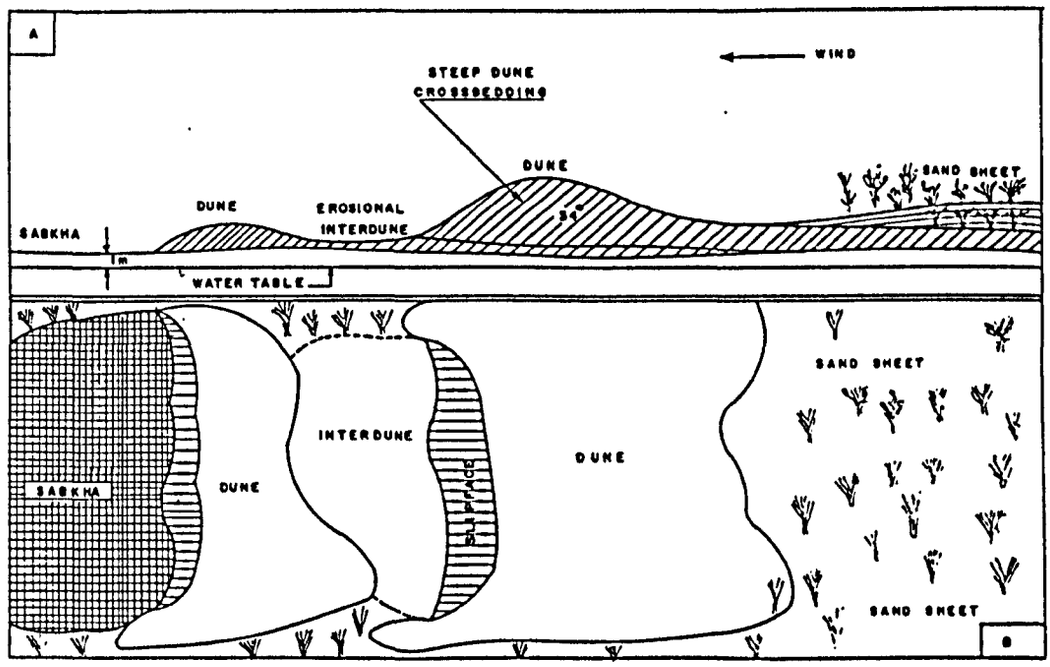


Fig. 7. Schematic drawing showing typical relationships of four types of aeolian terrain in the study area. The sabkha/dune/sand sheet superposition is typical of the area.

tional sabkhas, with 1 m or more of sediment vertically, and of wide areal extent are the result of subregional rise of groundwater table. Additionally some areally extensive sabkhas seem to consist of only a few centimetres of typical sabkha sediments overlying other sediments such as cross-bedded dune sands. Thus, it was necessary in all field work to make trenches in sabkhas to determine whether the geomorphic sabkha was underlain by an appreciable thickness of sabkha sediments. The sabkhas on which our sand traps were placed were each large, and in addition consisted of more than 1 m of typical sabkha sediment, indicating a history of sustained deposition.

Sabkhas are very stable geomorphically, usually experiencing less erosion or deposition than other terrains during the course of a year. Sabkhas are relatively exposed, because of their flat topography and lack of vegetation, thus high drift rates may occur.

However, salt ridges (Fig. 8) and occasionally the dampness of the sabkha surface tend to trap drifting sand. Resulting deposits have highly irregular bedding (Fig. 9). Drift rates are usually highest near the margins of sabkhas and lowest in the centres.

METHODS OF STUDY

Dune advance

Dune advance was measured during twelve months from October 1979 to October 1980 for 20 dunes near

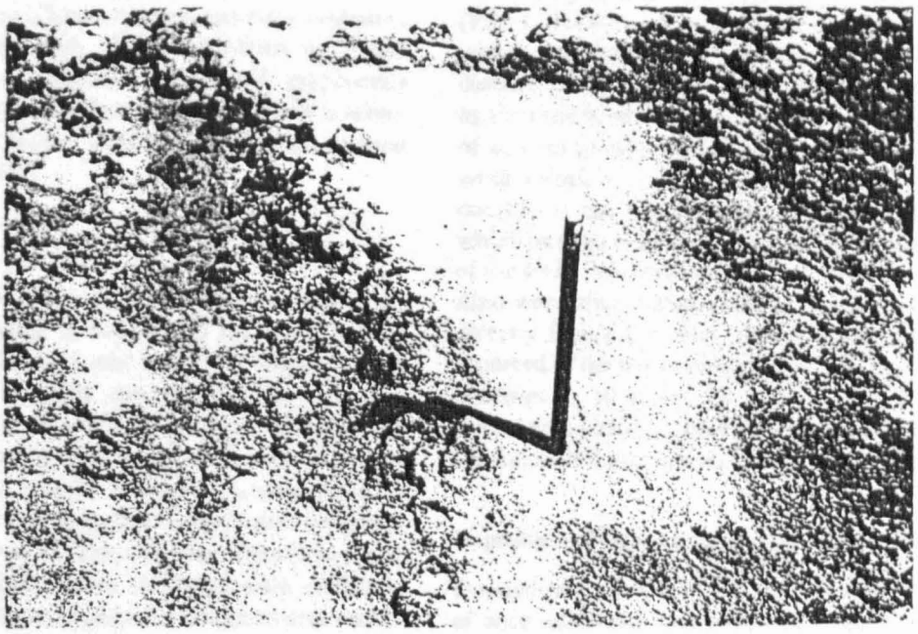


Fig. 8. Salt ridge and shallow layer of freshly deposited sand (white material) near trap 11. Pencil gives scale.

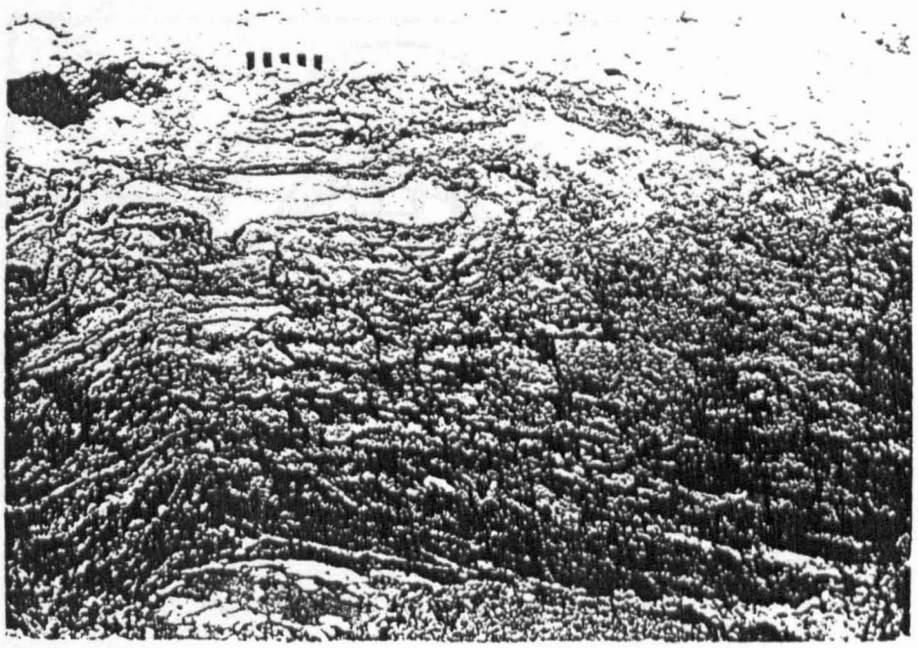


Fig. 9. Trench in sabkha at site 7, showing irregular layers resulting from slow upward growth of sabkha by episodic deposition of sand, followed by salt ridge formation. Water table is at base of trench. Bars on scale at upper left are 1 cm in width.

traps 4, 6, 9, 13 and 15. To obtain our data we first used a single stake, placed very near the slipface, with a single measurement to the nearest point at the base of the slipface. This method failed to record the differing degrees of activity of various parts of the slipface from month to month, as effective winds shifted direction 45° or more. A better method of measuring dune advance was to tape the distance to a number of places along the base of the slipface from a stake hammered into the ground about 15 m downwind of the dune. Dune advance was then evaluated by plotting successive slipface positions on graph paper at the appropriate scale, and graphically measuring average slipface displacement in a direction parallel to annual drift direction at the nearest sand trap (Fig. 10).

Drift rate

Drift rate (of wind-driven sand) was evaluated at all 14 study sites using a mechanical sand trap which swung to face the wind, and stored the trapped sand below ground in eight canisters labelled for the primary compass directions (Fig. 11a). These traps were checked at approximately 1 month intervals during the study. Usually several days were required to check all 14 traps; thus data on drift rates for given months (as shown in Table 2), are closely but not strictly comparable. When the traps were checked, the procedure was to remove the canisters and weigh the sand (whether wet, damp or dry), and to determine volume by using a graduated cylinder. Volumes routinely were 'compacted' volumes measured after tapping the graduated cylinder gently on the palm of the hand or the sand surface. Thus, values for volume reported here are slightly conservative.

Erosion and deposition

Erosion and deposition were measured using ten stakes emplaced in a fixed pattern near each sand trap (Fig. 11B). We used wooden stakes about 1·5 m long, which were hammered into the sand. Changes in the distance from the top of the stake to the sand surface against the base of the stake were then used as indices of erosion or deposition. With the first sand-moving wind a shallow scour pocket about 1 cm deep formed quickly at the base of each stake (Fig. 11C), after which no further scour occurred related to the presence of the stake. Distances from the top of the stake to the sand were always measured on the side of each stake directly facing the sand trap. Erosion or deposition reported at the test sites thus represents the average of readings at 10 stakes for each month. Stakes atop dunes were evenly spaced on both sides of the crest of the dune, and the trap was placed at the crest.

Depositional history of the sediments

Depositional history of the sediments in the vicinity of each study site was evaluated using trenches 0·5–1·5 m deep, usually with the trench face parallel to

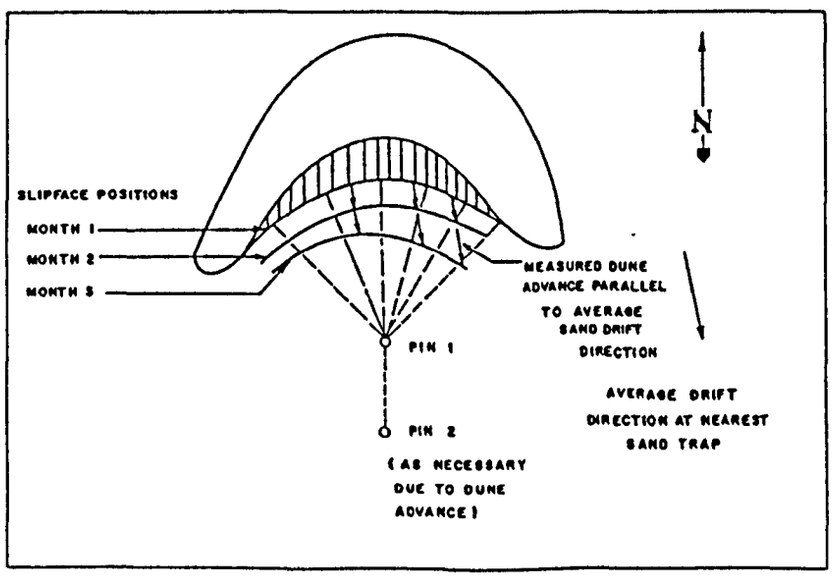


Fig. 10. Method of measuring dune advance.

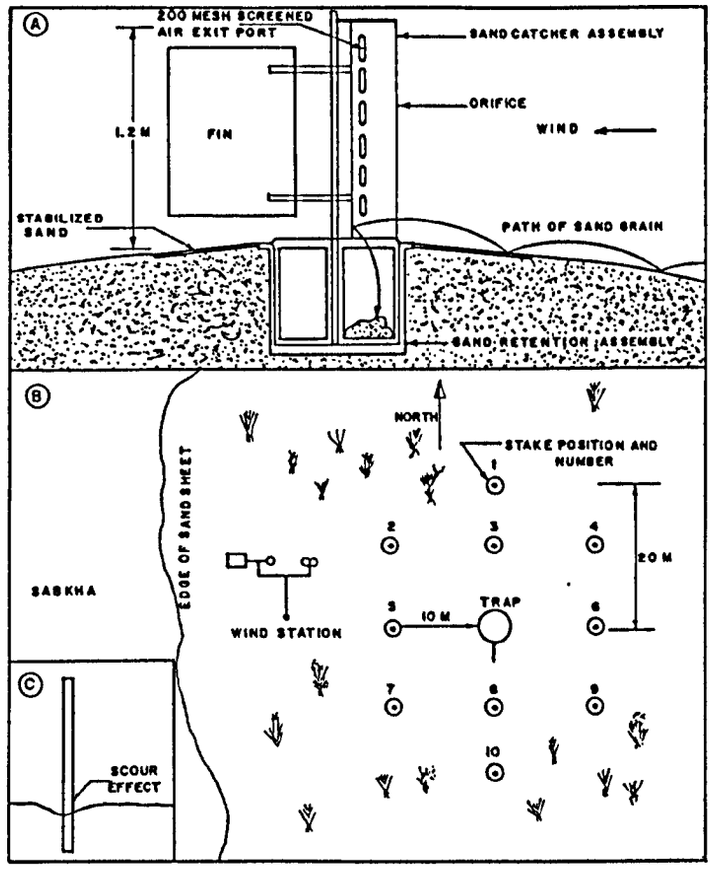


Fig. 11. Schematic diagram illustrating: (A) Sand trap principles of operation and design; (B) Trap, stake, and wind station layout; (C) Scour effect around base of a stake.

presumed wind direction (NW–SE). Results of these studies are described in Fryberger *et al.* (1983). Some interpretations of this report are supported by observations of sedimentary features in the trenches, of which about 200 were dug in the study area.

Wind regimes

Wind regimes were evaluated using data from conventional weather stations in the Arabian Peninsula (see Fig. 1). In addition, small data loggers and sensors were installed at sites 4, 9, 10 and 15. These stations recorded wind speed in metres per second (to nearest 0·1 m s^{-1}) and direction in degrees (at 1° intervals) in digital, computer-compatible form. Observations were taken by the battery-driven stations at 15 or 30-min intervals for about the last 9 months of the study. Data were recorded on small tape cassettes, which were changed monthly. The data were then transferred to the IBM 370 computer at the University of Petroleum and Minerals.

RESULTS OF THE STUDY

Dune advance

Dune advance during March 1980 to early October 1980 (7 months) was as much as 23 m for the smallest dune, which was only 2·9 m high (Fig. 12). Figure 12 incorporates data only during March 1980 to early October 1980, because we felt these data to be more accurate than those from October 1979 to February 1980, which were gathered using a single point of measurement on the slipface. For annual movement, values of dune advance shown in Fig. 12 can be increased by about 10–15%. The wide scatter in the diagram probably results from the use of different dune types (barchans, barchanoid ridges and domes) as well as from the different exposures of the studied dunes.

We deliberately sampled the widest possible range of dune sizes present in the area. The size distribution of measured dunes in Fig. 12 may slightly favour

Table 2. Drift rates observed during the study

Trap number	Terrain	Vegetation/400 m² No. indiv.	Vegetation/400 m² No. species	Adjusted average 30-day drift rate m³ m-w⁻¹* Oct. 1979	Nov.	Dec.	Jan. 1980	Feb.	Mar.	Apr.	May	June	July	Aug.	Sep.	Sums of esti-mates	Total drift for study period m³ m-w⁻¹
15	Barchan[1] dune	70	2	3·0	0·5	2·4	1·6	1·3	2·8	4·8	3·7	4·9	1·4	1·5	0·5	28·4	29·2
5	Dome[2] dune	175	2	0·8	0·8	1·2	2·6	1·0	2·8	3·9	2·4	5·9	2·0	3·0	0·4	26·8	27·5
2	Dome[3] dune	30	2	1·4	0·5	2·1	2·0	1·3	2·1	3·7	2·0	4·3	1·6	2·6	0·5	24·1	25·0
13	Interdune	66	4	1·8	0·3	1·1	0·6	0·8	0·8	1·4	1·6	2·6	1·4	0·5	0·1	13	12·8
9	Interdune	50	2	0·4	0·2	0·9	0·5	1·1	1·8	1·6	1·4	2·5	0·4	0·7	0·1	11·6	12·5
6	Interdune	28	2	0	0	0·2	0·5	0·9	1·0	0·7	0·3	0·2	0	0	0	3·8	3·7
12	Sand sheet	150	2	1·4	0·6	1·7	1·1	1·3	1·6	2·8	2·9	4·4	1·2	1·2	0·3	20·5	21·5
4	Sand sheet	420	4	0·9	0·5	1·7	1·9	1·1	1·5	1·7	1·6	5·4	0·6	1·3	0·2	18·4	19·7
10	Sand sheet	113	6	0·4	0·1	0·5	0·4	0·6	0·8	1·5	0·8	3·0	0·1	1·0	0·2	9·4	10·6
1	Sand sheet	280	2	0	0·1	0	0·1	0·3	0·4	1·4	0·8	3·5	0·4	0·5	0·1	7·6	8·9
14	Sand sheet	422	4	0·1	0	0·2	0·1	0·3	0·5	0·4	0·2	0·9	0·2	0·2	0·1	3·2	3·3
3	Sand sheet	462	4	0	0·1	0	0·1	0·1	0·3	0·4	0·1	0·7	0·1	0·1	0	2·0	2·3
11	Sabkha	0	0	0·1	0·1	0·2	0·2	0·5	0·4	0·7	0·2	2·6	0·2	0·6	0·1	5·9	6·5
7	Sabkha	0	0	0	0	0	0·6	0·3	0·1	0	0	2·1	1·4	0·9	0·1	5·5	5·5

[1] Dune height 6·7 m, slipface height 1·8 m.
[2] Dune height approx. 10 m.
[3] Dune height approx. 8 m.
* Times of measurement seldom coincided with the first day of the month. Thus, to compare months with one another average daily drift rate during the month was estimated from data spanning time intervals which approximated the desired 28–31 day months in question. Sums of estimates are shown next to measured drift as a rough gauge of error involved in this method. Additional information on plant communities in the Appendix.

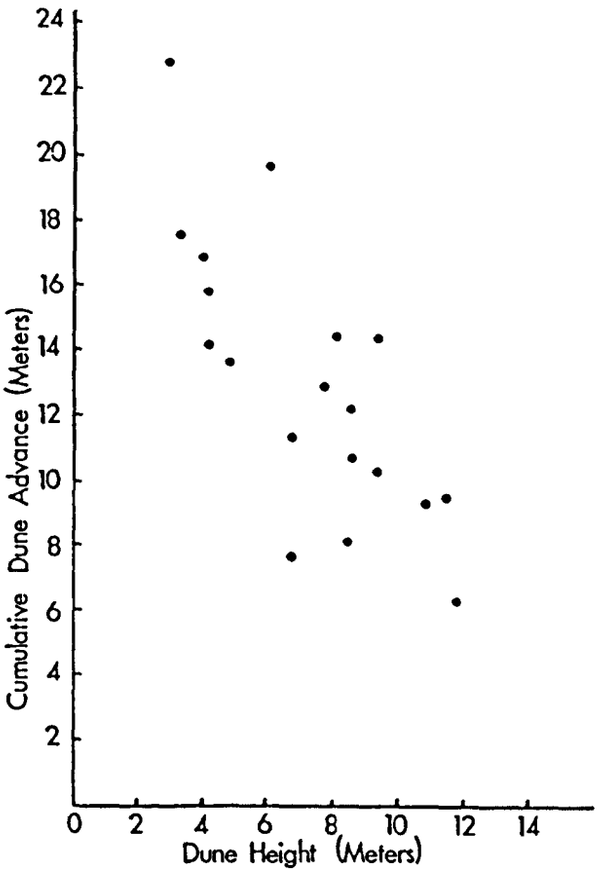


Fig. 12. Dune advance versus dune height from March 1979 to October 1980 (seven months).

larger dune types. Of the studied dunes, the average dune height was 7·6 m, the average slipface height was 5·7 m, and the average advance was 14·8 m.

One interesting phenomenon we observed was the continual changing of dome dunes to barchans, and vice versa. It seems that completely gradational forms exist between barchan and dome dunes, for any size of dune. Our ground and air observations revealed some extensive areas of dome and 'dome ridge' dunes in the Jafurah. Thus, it seems possible that dome dunes and dome ridges can exist as stable bedforms and migrate for considerable distances, and need not always be a part of an evolutionary sequence from dome to barchan as observed in more restricted desert settings by some workers (McKee, 1966; Ahlbrandt, 1973). The implication of this observation is that the dome dune is not mechanistically compelled to evolve into a barchan or other (slipface-bearing) type, but exists as do other types in equilibrium with ambient wind regime and sand supply.

The direction of dune advance in the study area was S to SE, generally parallel to the resultant drift direction indicated by the long-term wind records for Dhahran (see sand rose, Fig. 1) and locally parallel to measured drift directions indicated by the sand traps. In the coastal zone this results in an oblique offshore progradation of the sand sea into the Arabian Gulf, as described in Fryberger *et al.* (1983).

Changes in wind direction during our study were sufficient to shift activity from one part of a dune slipface to another, but not to displace an entire dune laterally. Reversals of wind direction, primarily during winter months, caused small northward-facing slipfaces atop larger dunes or caused cone-shaped vortex scars atop the dunes (Fig. 13). It seems plausible that infill of vortex scars (and blowouts) may account for the commonly observed trough crossbedding in the upper portions of dunes (McKee, 1966).

Sand drift

Drift rates varied widely from site to site during any given period (Table 2). In general they were dependent upon wind energy, but from site to site terrain type was the greatest control (Table 2). Drift rates were highest on the exposed tops of the dome and barchan dunes (Table 2), ranging from 25 to 29 m^3 m-w^{-1} during the study. Those high values undoubtedly resulted from the excellent exposure of the sites, and the acceleration of air over the dune. For comparison, drift potentials at the Dhahran airport during the study were equivalent to about 18 m^3 m-w^{-1} (see Table 1).

Drift rates in interdunes were lower, due to the sheltering effect of the upwind dune—both by reduction of wind energy and removal of oncoming sand by storage in the slipface or leeward slope. The interdune site at trap 6 was probably the most sheltered. Trap 6 was within the arms of a barchan dune with a 20 m long slipface, which approached to within 30 m of the trap (Table 2). The fall in drift rates at trap 6 from April onwards (despite the occurrence of the Shamal season in June) reflects this sheltering effect, and the gradual armouring of the floor of the interdune by coarse grains.

Traps 9 and 13 were in less sheltered positions, since the leeward slopes of dunes immediately upwind were smaller (trap 9, dome dune 5 m high; trap 13, barchan dune 8 m high, slipface 1·5 m high).

Annual drift rates on sand sheets ranged from 2·3 m^3 m-w^{-1} to 21·5 m^3 m-w^{-1}, an almost 10-fold difference. Differences in drift rates seemed in most

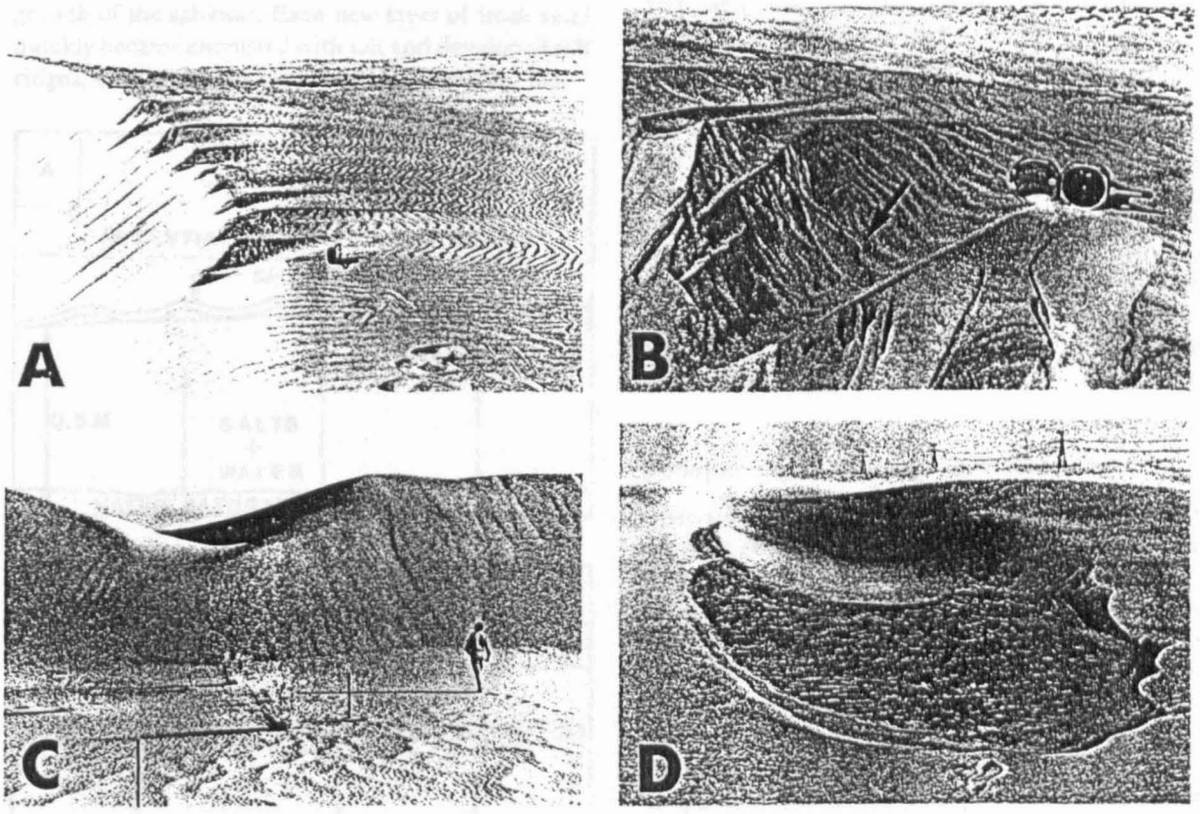


Fig. 13. Vortex scars and probable blowout on barchan dunes. Vortex scars form due to reversal of wind direction, which produces strong compression of airflow across the crest of a dune. Horizontal vortices commonly attach at a point on the brinkline of the dune, just below the highest part. Swirling air currents scour out a smooth, gently curving trough which is elongate across the upper part of the dune crestal area. (A) Series of closely spaced V-shaped vortex scars atop barchan dune near trap 4. (B) Close up of vortex scar at same site as (A) showing avalanche tongues extending down side of vortex scar (arrow). (C) Large blowout or possible vortex scar at barchan dune upwind of trap 6. Feature has typical trough shape, and curvature of a vortex scar. Winds from prevailing northerly direction have occurred since the feature formed, causing avalanching on the slipface. However, this feature is probably a blowout because trap 6 indicated that most sand movement was from the north during the period in which it must have formed. However, there was also substantial sand movement from the SE (reversal) during this period. Feature filled in to the normal dune profile within a month. (D) Vortex scar with flat, irregular bottom surface where wind has scoured to damp sand. Near trap 13, brunton compass (arrow) for scale.

instances to depend upon the numbers and species of plants. Well-vegetated sites with larger or more abundant vegetation experienced lowest drift rates (Table 2). Low drift rates at trap 1 (on a sand sheet on Al Aziziyah sabkha) resulted from the very coarse sand size and from the presence of the large sabkha (poor source) immediately upwind. The high drift rates at site 12 resulted from the excellent exposure of the site and from lack of vegetation (Table 2). Site 12 is a terrain transitional between unvegetated dome dunes and lightly vegetated sand sheet.

The low drift rates across the sabkhas at traps 11 and 7 were surprising, as we expected that such open areas would be easy pathways for sand (Table 2). Even during strong sandstorms, sand blowing on to the sabkha from areas upwind seldom reached the traps (which were in the centres of the sabkhas) in large quantities. This phenomenon occurred for two reasons. A minor reason must have been that damp areas on the sabkha trapped sand through cohesion. The most significant reason was that the sabkha surfaces were covered completely by small (1–5 cm high) salt ridges (see Fig. 8). Salt ridges formed at the sand–air interface, at the top of the groundwater capillary fringe, through evaporation and displacive crystal growth at the surface. Sand blown on to the sabkhas became trapped in the lee of these salt ridges, thus reducing measured drift rates in the centre of the

sabkha. This mechanism, along with rise of ground water table was the principal mechanism of upward growth of the sabkhas. Each new layer of fresh sand quickly became encrusted with salt and developed salt ridges, after which the cycle was repeated (Fig. 14).

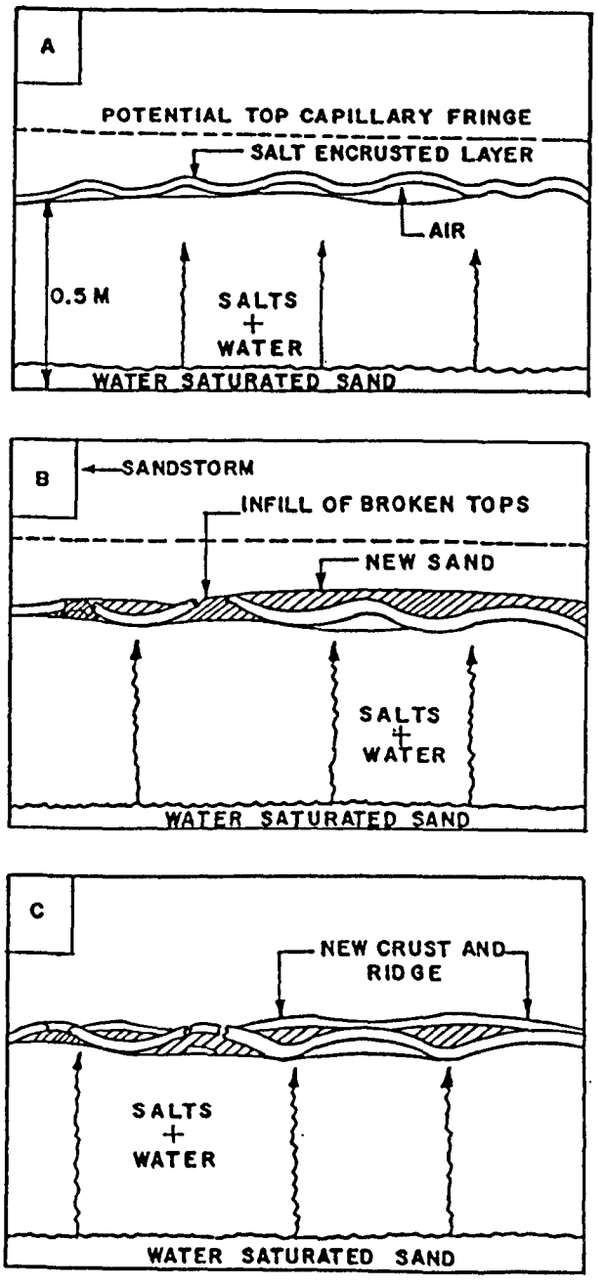


Fig. 14. Mechanism of upward growth of sabkhas by infill of salt ridges. (A) Layer of salt ridges forms atop sabkha followjng a storm. (B) New storm fills in hollows between salt ridges, or enters broken tops of hollow ridges. (C) Capillary fringe rises through new sand layer, evaporation and displacive crystal growth produces a new set of salt ridges.

Comparison with Dhahran data

The predicted drift rate during our study of about 18 m^3 m-w^{-1} from the Dhahran weather station lies at about the mid-range of our observations using sand traps in the field (from 2·3 to 29 m^3 m-w^{-1}). The best comparability is at trap 4, where drift rate was about 19·7 m^3 m-w^{-1}. It is apparent that data from conventional weather stations such as Dhahran may be used to estimate drift rates in the field, at least in this instance. However, it is equally apparent that type of terrain will have an important effect, with the most comparable measurements probably being those made on well exposed, lightly vegetated sand sheets, such as that at trap 4.

Geological significance of the drift rates

If the average drift rate during the study is assumed to be about 18 m^3 m-w^{-1} yr^{-1}, then the amount of sand crossing the 30 km wide strip of desert between Abqaiq and the coast (traps 9–15, Fig. 3) is about 540,000 m^3 yr^{-1}. Assuming for purposes of discussion that this material is deposited in a zone extending 100 km downwind of Abqaiq, rate of deposition would amount to $1{\cdot}8 \times 10^{-4}$ m yr^{-1}, or 5555 yr to deposit 1 m of sediment. This rate certainly seems rapid on the geological scale, especially when it is recalled that the period of the study was relatively calm (see Table 1). Seasons during which the average drift potential at Dhahran is attained (about 400 v.u. or 28 m^3 m-w^{-1}) would increase estimates proportionately.

Direction of sand drift

Annual sand drift directions were uniformly from the NW to the NE throughout the study area (Fig. 15). Effective wind regimes were more variable in inter-dune areas, due to eddying around upwind dunes (traps 6 and 9, Fig. 15).

Erosion and deposition

As might be expected, the differing aeolian terrains behaved in various ways during the study, experiencing widely varying rates of erosion and deposition, and responding in differing ways to the onset of the high energy Shamal season.

Sand sheets were generally stable terrain, although we observed some exceptions. Study sites 10, 14, 1 and 3 were all on moderately to well vegetated sand sheets which were in low areas, had few dunes in the

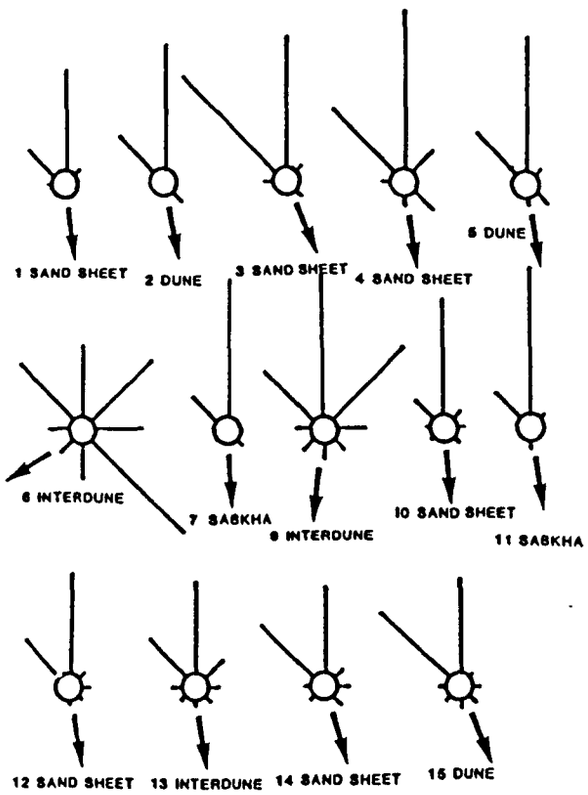


Fig. 15. Annual drift roses depicting sand transport from eight directions at the 14 test sites, during the year. Based on sand caught by the sand traps. Resultant arrows show average annual sand movement direction (resultant drift direction).

immediate vicinity and seemed stable (Table 2, Fig. 16). In contrast, sand traps 4 and 12 were in slightly more exposed positions, and experienced greater deposition and erosion, respectively. Some of the test sites seemed to change trend with the onset of the shamal season in May. Note the rapid increase in rate of deposition at site 4 from May to July, and the change from erosion to deposition at trap 1 during the same period (Fig. 16).

Sabkhas were the most stable terrain we observed. Both sabkha sites 7 and 11 seemed to experience slight erosion during the winter season, then slight deposition during the shamal season (Fig. 17). This may reflect the fact that each trap site was in the centre of the sabkha, and significant new sand did not reach the test sites until the strong sandstorms of May and June.

Interdunes were highly unstable. All three interdune sites (near traps 13, 9 and 6) experienced rapid erosion, with a maximum of over 40 cm at site 13 (Fig. 17). This caused considerable nuisance to us in field work, because it necessitated removal and re-burial of the sand trap so its rim would remain flush with the sand surface.

Drift rates in interdunes at sites 9, 13 and 6 were not high (note the 3·7 m^3 total for trap 6), despite the rapid rates of erosion (Fig. 17). Presumably the removal of sand by the dune upwind left the wind relatively free of sand. Thus winds moving past the interdune trap sites were undersaturated, picking up sand rapidly as they accelerated.

Dune sites were relatively stable despite their exposed position on the dune crest (Fig. 17). It is probable that the gradual erosion at sites 5, 2 and 15 reflects the movement of the bedform downwind. It is of interest to compare the stability of the dune sites to that of the interdune sites. If the movement of the bedform is neglected, it can be seen that the ratio of sand transported to sand eroded or deposited is much higher for the dunes than the interdunes. The 'dynamic stability index', the ratio of sand moved across a site to maximum erosion plus deposition vertically, is perhaps a more accurate assessment of the true stability of an aeolian terrain with respect to sand transport (Table 3). These data are of interest because they suggest possible explanations for changes in terrain behaviour during the shamal season. Terrains which have the least dynamic stability can experience extreme erosion or deposition when conditions change. By contrast, aerodynamically stable forms such as dunes can tolerate extreme changes in drift rates with only minor vertical adjustment.

Our study was reconnaissance in nature, and thus it is not possible at the present time to explain what factors in the environment are responsible for the wide range of dynamic stabilities observed for various terrains. Clearly, exposure of the site is important, and future studies would benefit from detailed appraisal of exposure—through quantitative description of surrounding terrain—which was not possible in this study.

Lateral and vertical sedimentation

A concept that derives from data in all the sections above is that in this study area sedimentation proceeds both laterally and vertically. Lateral sedimentation is accomplished mainly by the rapidly moving dunes. The interdunes we studied with sand traps were all erosional, however all were above water table (a necessity for placement of the traps). In interdunes close to the water table permanent deposition is more likely to occur, albeit as thin deposits (as described in

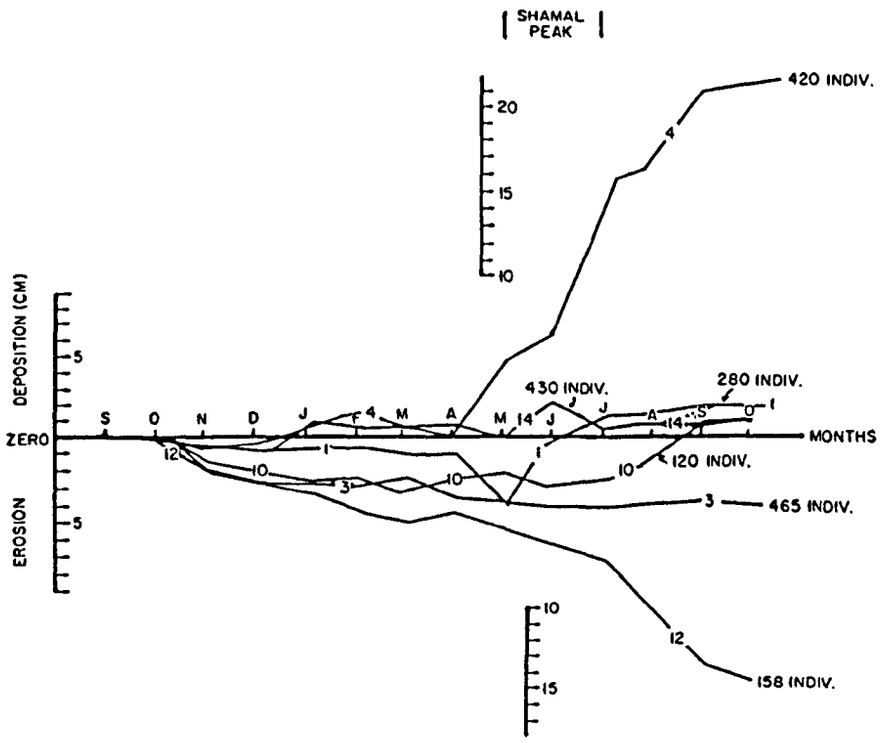


Fig. 16. Graph showing wind erosion and deposition at the trap sites located on sand sheets. Slight drop at all sites at beginning of experiment represents initial scouring at the base of the stakes. Number of individual plants at each site indicated at right end of each line.

Fryberger *et al.*, 1983). These deposits would represent a form of lateral accretion, however, since interdunes move with the dunes. By contrast, the observed dynamic instability of sand sheets, and growth of sabkhas by entrapment of sand between salt ridges, illustrates their potential as vertically accreting sedimentary units. Thus, in ancient rock systems, sequences of dune and interdune materials may be considered in the light of lateral passage of bedforms, but sand sheets and sabkhas perhaps more in the light of residual deposits which grow vertically through layer by layer of accretion.

CONCLUSIONS

This study has demonstrated the practicality of direct, regional study of sand drift rates, using sand traps, in modern sand seas. In the Jafurah Sand Sea, sand drifted southward to south-eastward at rates ranging from several m^3 m-w^{-1} yr^{-1} to over 29 m^3 m-w^{-1} yr^{-1}, depending upon terrain type, during the year of the study. When extrapolated through time, and across the width of the Jafurah in the study area, the observed rates of transport are geologically significant, and could lead to rapid sedimentation in areas of deposition downwind. The Jafurah sand sea seems to be zoned with respect to wind energy, with high wind energy in the north, and low wind energy to the south, where the Jafurah merges with the Rub Al Khali. Likewise, the desert geomorphology is similarly zoned; with areas of erosion, transport and deposition from north to south. Sedimentation in the Jafurah proceeds both by lateral migration (of dunes and interdunes) and vertical accretion (by sabkhas and sand sheets). The observed high degree of mobility of the dunes and wind-blown sand adds some support to theories of sand sea origin which require long distance drift of wind-blown sand.

ACKNOWLEDGMENTS

The authors gratefully acknowledge the assistance of McAdams, Roux and Associates, Cities Service Company, Amoco Production Company, and Arabian American Oil Company in making this work possible. The authors were also greatly assisted by helpful comments from Ralph Hunter, Andrew Warren, Sarah Andrews and Bud Rudesill.

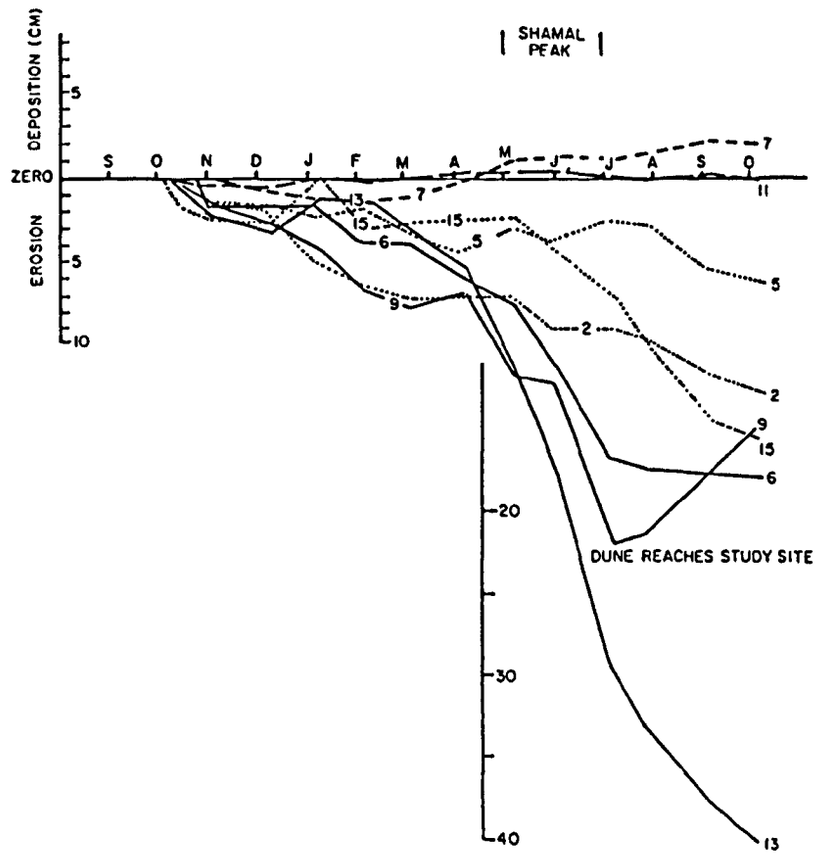


Fig. 17. Graph showing wind erosion and deposition at the trap sites on sabkhas (dashed lines), dunes (dotted) and interdunes (solid). Slight drop at all sites at beginning of experiment represents initial scouring at the base of the stakes.

Table 3. Dynamic stability of aeolian terrains

Site	Type of terrain	Annual drift rate (A) (m^3 m-w^{-1})	Sum of erosion and deposition (B) (m)	Dynamic stability index $(A)/(B)$	Average
7	Sabkha	5·5	0·04	138	394
11	Sabkha	6·5	0·01	650	
5	Dome dune	27·5	0·06	458	277
2	Dome dune	25·0	0·13	192	
15	Dome dune	29·2	0·16	182	
1	Sand sheet	8·9	0·06	148	145
10	Sand sheet	10·6·	0·4	265	
14	Sand sheet	3·3	0·02	165	
12	Sand sheet	21·5	0·15	143	
4	Sand sheet	19·7	0·22	90	
3	Sand sheet	2·3	0·04	58	
9	Interdune	12·5	0·22	57	37
13	Interdune	12·8	0·40	32	
6	Interdune	3·7	0·18	21	

REFERENCES

AHLBRANDT, T.S. (1973) *Sand dunes, geomorphology and geology, Killpecker Creek area, Northern Sweetwater County, Wyoming.* Ph.D. Thesis, Wyoming University, 174 pp.

AHLBRANDT, T.S. & FRYBERGER, S.G. (1981) Sedimentary features and significance of interdune deposits. In: *Recent and Ancient Nonmarine Depositional Environments: models for exploration* (Ed. by F. G. Ethridge and R. M. Flores), *Spec. Publ. Soc. econ. Paleont. Miner., Tulsa*, 293–314.

BAGNOLD, R.A. (1954) *The Physics of Blown Sand and Desert Dunes*, Methuen, London, 254 pp.

BREED, C.S., FRYBERGER, S.G., ANDREWS, S., MCCAULEY, C., LENNARTZ, F., GEBEL, D. & HORSTMAN, K. (1979) Regional studies of sand seas using landsat (ERTS) imagery. In: *A Study of Global Sand Seas* (Ed. by E. D. McKee). *Prof. Pap. U.S. geol. Surv.* 1052, 305–397.

DUBIEF, J. (1952) Le vent et le Deplacement du sable au Sahara, *Algiers Univ. Inst. Rech. Sahariennes Travaux*, 8, 123–164.

FRYBERGER, S.G. (1979) Dune forms and wind regime. In: *A Study of Global Sand Seas* (Ed. by E. D. McKee). *Prof. Pap. U.S. geol. Surv.* 1052, 137–169.

FRYBERGER, S.G. & AHLBRANDT, T.S. (1979) Mechanisms for the formation of eolian sand seas, *Z. geomorph.* 23, 440–460.

FRYBERGER, S.G., AL-SARI, A.M. & CLISHAM, T.J. (1983) Eolian dune, interdune, sand sheet and siliciclastic sabkha sediments of an offshore prograding sand sea, Dhahran Area, Saudi Arabia, *Bull. Am. Ass. Petrol. Geol.* 63, 280–312.

LETTAU, K. & LETTAU, H. (1969) Bulk transport of sand by the barchans of the Pampa de la Joya in southern Peru. *Z. Geomorph.* 13, 182–195.

MCKEE, E.D. (1966) Structures of dunes at White Sands National Monument, New Mexico (and a comparison with structures of dunes from other selected areas). *Sedimentology*, 7, 3–69.

McKee, E.D. (1979) Introduction to a study of global sand seas. In: *A Study of Global Sand Seas* (Ed. by E. D. McKee). *Prof. Pap. U.S. geol. Surv.* 1052, 1–17.

WILLIAMS, R.O. (1979) *ARAMCO meteorologic and oceanographic data book for the Eastern Province of Saudi Arabia*, Environmental Unit, Technical Services Department, Arabian American Oil Company, Dhahran, 133 pp.

WILSON, L.G. (1971) Desert sand flow basins and a model for the development of ergs. *Georgl J*, 137, pt 2, 180–199.

(*Manuscript received 12 August 1982; revision received 18 July 1983*)

APPENDIX

List of plant specimens collected from a 400 m^2 sampling area around sand traps. This appendix includes only pressed and catalogued specimens stored at the Research Institute. It is included to give the reader an appreciation for the typical plant communities we encountered at the study sites. Further data are available from S. A. R. Rizvi.

Scientific name	Family	Habit
Sand trap 1: coastal sand sheet		
Seidlitzia rosmarinus	Chenopodiaceae	Halophytic undershrub
Cyperus conglumeratus (tall ecotype)	Cyperaceae	Perennial sedge
Sand trap 2: Dome dune		
Cyperus conglumeratus (dwarf ecotype)	Cyperaceae	Perennial sedge
Cyperus conglumeratus (tall, stout ecotype)	Cyperaceae	Tall, stout, tufted perennial
Calligonum comosum	Polygonaceae	Tall, branched shrub
Sand trap 3: sand sheet		
Zygophyllum decumbeno	Zygophyllaceae	Succulent shrublet
Zygophyllum coccineum	Zygophyllaceae	Low succulent shrub
Tamarix passerinoides	Tamaricaceae	Tall shrub or small tree
Agriophyllum sp.	Chenopodiaceae	Branched, spring herb

A P P E N D I X (3)

Al-Hinai and Moore (1986, published paper)

MONITORING OF SAND MIGRATION IN EASTERN ARABIA BY REMOTE SENSING*

Khattab G. Al-Hinai

Research Institute,
University of Petroleum & Minerals,
Dhahran-Saudi Arabia.

and

John McMahon Moore

Department of Geology,
(Centre for Remote Sensing & Geophysics Section),
Imperial College of Science & Technology,
London, SW7 2BP,
England.

Abstract

Encroachment by wind-blown sand is a major economic problem for industrial installations, road and airport maintenance, urban development and agriculture in eastern Arabia. Acquiring basic information on sand dune migration in desert areas is difficult and expensive.

This study is an assessment of the usefulness of Landsat MSS imagery and aerial photographs as aids to field data for measuring sand dune movement in the Jafurah Sand Sea, eastern Arabia.

Estimates of dune movement have been made for a thirty-four year period (1949 - 1983), by registration and comparison of individual barchan and barchanoid ridge positions on several sets of aerial photographs at 1:60,000 and 1:80,000 scales. Digital registration of Landsat MSS imagery dated 1972 and 1984 has also been investigated as an aid to measurement of dune movement rates. Field measurement of dune movement during a one-year period was used as a ground check for the aerial photographic and Landsat MSS imagery investigation.

Individual dunes, larger than 100 metres across, can be identified in MSS imagery, but slow movement rates of large dunes (average 8 metres per year) over a 12-year period and the spatial resolution of Landsat MSS imagery (80 metres), together with the lack of precise ground control points, mean that Landsat MSS imagery is of limited value. Multi-temporal air photography gave more reliable results.

The need for long term multi-temporal high resolution imagery representing long periods of time and precise image registration techniques will be of vital importance in future remote sensing and monitoring schemes.

---

* presented at the Twentieth International Symposium on Remote Sensing of Environment, Nairobi, Kenya, 4 - 10 December 1986

1. INTRODUCTION

The continuing expansion of towns, agriculture, industry and transport infra structure within arid lands has increased the awareness of the problems caused by blowing sand. In the eastern province of Saudi Arabia, the oil fields have spurred economic development, especially during the last fifteen years. Petroleum installations, industrial complexes, residential developments, transport and communication facilities, and agricultural projects require protection and maintenance.

The action of wind upon unconsolidated surficial sediments can cause severe engineering problems in areas of scarce vegetation. Dune movement can cause burial of roads and agricultural areas, and abrasion of natural and man-made structures. One such area, where such problems were encountered on a large scale, is the Jafurah sand sea located in the eastern province of Saudi Arabia (Fig.1). The Jafurah Sand Sea is a region of strong unidirectional winds, and abundant sand dunes.

The difficulties of direct ground measurement and the cost of conducting full scale and monitoring experiments in remote areas is a major handicap in producing reliable and applicable data. In this study, Multi-spectral Scanner (MSS) imagery, and aerial photographs taken at different times are assessed as aids in measuring sand dune movement. The results were then compared with actual field measurements.

2. SAND MOVEMENT STUDIES

Bagnold (1941), Dubief (1952) and Wilson (1971) promulgated theories on the mobility of wind-blown sand in deserts. Lettau & Lettau (1969) and Fryberger & Albrandt (1979) developed equations representing sand drift rates. The movement of sand has never been measured directly on a regional basis, except for a study by Fryberger et al (1984), who monitored sand drift rates and Jafurah dune movement directly in the field. The main author of this paper participated in that study.

Aerial photographs and Landsat MSS imagery have been used by many scientists in the study of arid and semi-arid areas. Finkel (1966) studied the movement of barchan dunes using aerial photogrammetry on the southern coast of Peru. Berera (1979) utilised multi-temporal Landsat MSS imagery to investigate dune movement in the Sahara desert of Libya. He concluded that Landsat MSS imagery can be used to measure sand dune movement of greater than 1 km if proper image analysis and registration techniques are used. Ker & Nigra (1952) measured dune movement from aerial photographs between 1934 and 1949 in Al-Hofuf area of Saudi Arabia.

The movement of sand dunes has never been measured using co-ordinated Landsat MSS imagery, aerial photographs and actual field measurement. This paper reports an integrated study of dune movement in the Jafurah Sand Sea, based on field measurement, multi-temporal MSS images and aerial photographic investigation.

3. JAFURAH SAND SEA

The study area is in the Jafurah Sand Sea (Fig.1), an elongate, 30-250 km wide sand sea, extending down the western side of the Arabian Gulf, merging southward into the sands of the Rub al khali. Tertiary gravels, sandstones and lime marls form the sub-stratum and exposed locally within the sand sea and on the western boundary of the Jafurah. Wind deposits consist of dunes, interdunes, sandsheets and aeolian siliciclastic sabkhas. Most of the dunes are of the barchanoid type which includes barchans (crescent shaped), barchanoid ridges, transverse ridges and dome dunes. Two other common types

of vegetationally controlled dunes found in the study area are the parabolic dunes and the obstacle of "coppice" dunes.

The study area is typical desert with average annual rainfall of 65 mm. The wind direction is primarily from the north or northwest blowing southward towards the Rub al khali (Empty Quarter). Wind reversals occur mainly during winter, causing reversed slipfaces on the crests of dunes, but having little effect on overall sediment transport (Fryberger, et al, 1984). The magnitude of wind velocity is highly seasonal with maximum occurring between May and July (locally termed the "Shamal".

4. METHODOLOGY

This study is based on Multi-spectral Scanner (MSS) data in digital format from Landsats 1 and 5, together with aerial photographs and field measurements.

4.1 Landsat MSS Imagery

Two Landsat MSS images, representing cloud-free scenes 176/42 (Landsat 1), acquired September 4, 1972 and 164/42 (Landsat 5), acquired January 15, 1984 were used to represent a reasonable period of time (12 years) for dune movement measurement. Digital processing was carried out at Imperial College, using an International Imaging Systems (IIS) Model 70F/4 interactive processor (System 500) linked to a PDP 11/24 computer.

Landsat MSS data, although corrected for earth curvature and rotation, satellite attitude variations and sensor non-linearities, still contain geometric distortions with the centre of the scene located only to an accuracy of 1 km (Davison, 1986). These errors become important when images are to be registered. Hence, geometrically transformed imagery is required in order to locate common ground control points in different scenes of the same area and to perform multi-temporal analysis by registering images acquired at different times as "overlays" of the same area.

Processing was carried out in four stages:

(i) Pre-processing, including rectification and noise suppression;

(ii) Selection of ground control points; (iii) Image to image

registration; (iv) Measurement of dune displacement.

Pre-processing image restoration was carried out to remove "noise" and to replace data missing from "dropped" pixels and lines. A one-dimensional Tukey median filter was used, followed by standard de-striping procedures (Pratt, 1978). Geometric distortions caused by the earth's rotation and sensor sampling bias were then removed by using Nearest Neighbour re-assignment (Siegel and Gillespie, 1980).

Ground control points (GCPs) were selected using Landsat MSS band 4 (Landsat 4/5 nomenclature) data, as infra-red imagery is least affected by atmospheric haze. Ten to twelve GCPs were selected using coastline features, road intersections and sabkha-bedrock boundaries. Identification of GCPs proved to be difficult because of the lack of sufficient number of fixed points in active dune terrains. For this reason, the points selected were not distributed evenly throughout the image with slightly more along the coastlines and sabkha-bedrock boundary,, but less in active dune areas.

Image to image registration involves correlation of geographical control points and change in image geometry to compensate for variations in satellite attitude and altitude. In this study, Landsat MSS imagery of 1972 was taken as a reference frame, and the 1984 imagery was warped to register using GCPs identified in each image. A computer generated best-fit correlation estimated the average registration error for each GCP file. Average errors of between 0.7 and 0.8 pixels were achieved. A spatial transformation using Nearest Neighbour re-sampling was then performed to register the 1984 scene to the 1972 scene.

After transformation, two full resolution 512 x 512 pixels sub-scenes were displayed for dune displacement measurement (Fig. 2). Thirty major dunes were defined in each sub-scene. Displacement of these dunes between 1972 and 1984 was recorded by measuring the distance between crests of each dune, using sample and line pixel value subtractions. The difference between sample and line pixel values is the movement of the dune expressed in number of pixels (pixel size = 79 m).

4.2 Aerial Photographic Measurement

The entire area of eastern Arabia was flown in 1949 by Hunting Ltd. The scale of the photographs is approximately 1:60,000 (Fig.3). Because of the clear desert atmosphere, the pictures were very clear and each dune sharply outlined. Part of the area was re-photographed in 1983 to a scale of 1:80,000 (Fig.4). The selected area for this study was also covered by Landsat MSS imagery.

The purpose of this investigation is to measure the planimetric movement and the change in height of identified sand dunes over the thirty-four years period. The dune outline in each picture was reduced to a common scale of 1:25,000 using the CP1 plotting instrument at the University College London. Ground control points were established and marked from the bedrock-sabkha boundary located south of the mobile dunes. The sand dunes within the specified area were plotted with their heights recorded beside them. The measured height of the dune is the difference between the base and the crest of the dune.

The positions of the dunes were then drawn on a sheet of transparent paper using different colours to distinguish between the 1949 and the 1983 positions (Fig.5). The horizontal displacement of 30 barchans and barchanoid ridges were measured to an accuracy representing a distance of 2 metres on the ground. Dune height measurement was done to an accuracy of 2 metres.

4.3 Field Measurement

Dune advance was measured during twelve months from October 1979 to October 1980 for twenty dunes in selected areas of the Jafurah Sand Sea (Fryberger, et al, 1984). The method used for measuring dune advance was to tape the distance to a number of places along the base of the slipface from a stake hammered into the ground about 15 metres downwind of the dune. Dune advance was then evaluated by plotting successive slipface positions on graph paper at the appropriate scale and graphically measuring average slipface displacement in a direction parallel to the dominant wind direction (NNW). The same approach was applied to this study with emphasis on the area covered by both Landsat MSS imagery and aerial photographs.

Movement of thirty dunes were measured during a 12-month period from August 1984 to August 1985.

5. RESULTS OF THE STUDY

5.1 Landsat MSS Investigation

Dune advance between 1972 and 1984 ranged between 0 and 1 pixel (80 metres) depending on the height of the dune. Field data in this area suggests a maximum dune movement of 8 metres per year. Hence, during the period between 1972 and 1984 (12 years), the dunes would have migrated about 96 metres or approximately 1.2 of a pixel. Given the registration accuracy of 0.7 to 0.8 pixels, no reliable measurement could be achieved over this time period. However, comparison of the results from Landsat investigation and field data suggests that dune movements of 8-10 metres per year have occurred over the last twelve years.

5.2 Aerial Photographic Measurement

Dune position changes, plotted from the 1949 and 1983 photographs, are readily apparent on Fig.5. These changes indicate variation in the migration rates of individual dunes due to differences in dune heights. Table 1 gives a summary of annual displacement of thirty barchan and barchanoid ridges according to height of the crest of these dunes.

Planimetric measurement of dune displacement on 1:25,000 scale photo enlargements using a limited number of control points gave a planimetric accuracy of 2 metres.

Results obtained from aerial photographic interpretation show the following:

(i) Photogrammetric dune movement measurement results confirm those obtained from field investigation (Table 1).

(ii) Small dunes travel faster than large dunes with few exceptions.

(iii) Individual barchans move faster than barchanoid ridges.

(iv) Dunes with restricted sand supply upwind lost height (about 8.8 cm/year). Dunes with constant sand supply grew in height (5.8cm/yr).

(v) The direction of dune advance in the Jafurah area is S to SE. This is generally parallel to the long-term wind direction for the Dhahran area (Williams, 1979). The general north-east orientation of long axes of dunes studied did not vary during the thirty-four years period.

5.3 Field Measurement

Table 1 gives a summary of data obtained during August 1984 to August 1985 (12 months period). Dune advance varied between 8 metres for small dunes (10 metres high) and 4 metres for larger dunes (18 metres high). These results correlate with aerial photographic measurements (Table 1) and are consistent with the crude measurements obtained from Landsat MSS investigation.

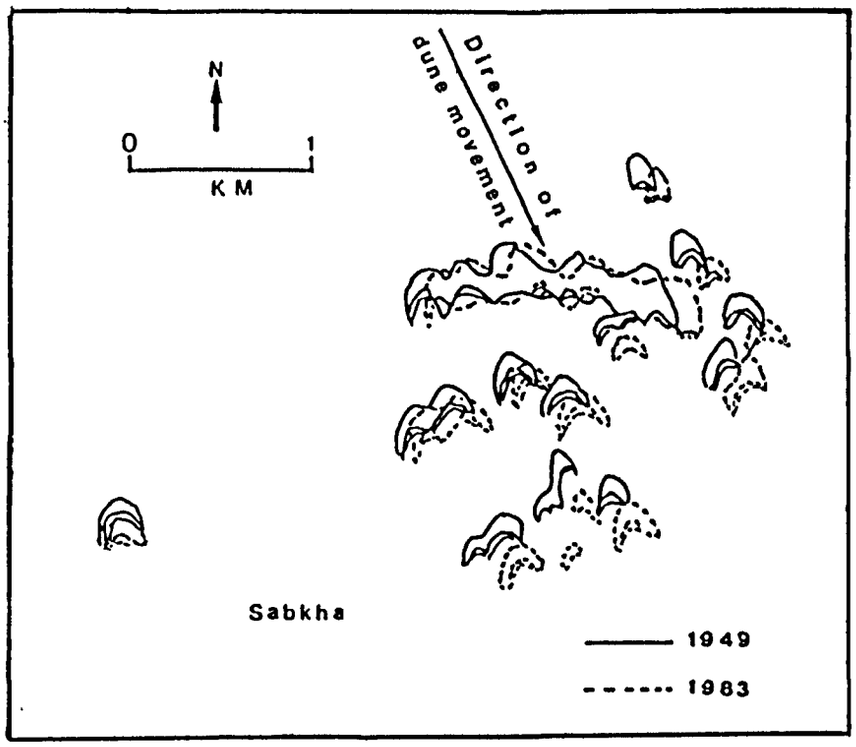


Figure 5. Displacement of dunes between 1949 and 1983 (measured from aerial photographs).

Dune Height (Metres)	10	12-13	14	16	17-18	18-20
Annual Displacement(m)						
Field measurement	8	7	6	5	4	3
Air photo measurement	8	6	5.8	2.9	2.2	2.9

Table 1. Average annual displacement of 30 barchans and barchanoid ridges according to dune height (aerial photographic measurement and field measurement).

6. DISCUSSION AND CONCLUSION

Repeated coverage by Landsat MSS imagery provides a good basis for monitoring regional and cover mapping. Several problems complicate establishment of accurate dune movement measurement. These problems include:

(a) Lack of sufficient ground control points necessary to achieve high registration accuracy using multi-temporal imagery in desert terrains.

(b) Spatial resolution of Landsat MSS imagery (80 metres) falls short of detecting the relative slow movement of the investigated dunes (8 metres/year) over the twelve-year period, for which images are available. The identification of individual dunes for this study was only possible because of their wide spacing and the high albedo contrast between sand and the substratum (sabkha). In areas where dunes are closely spaced, identification of individual dunes is more difficult.

(c) The time span of twelve years used in this study was not enough to detect the relative slow movement of the dunes.

Future use of space imagery as a tool for dune movement monitoring is dependent upon higher spatial resolution images, good ground control and a reasonable period of time for multi-temporal analysis. According to the results obtained from this study, spatial resolution should be between 5-10 metres. A minimum of thirty ground control points should be identified on a Landsat MSS scene (185 x 185 km). The spatial resolution of SPOT imagery on the panchromatic monochrome mode (10 metres), and the Large Format Camera photographs (10-12 metres) will provide a good basis for future monitoring systems. To take full advantage of SPOT and Large Format Camera imagery, it will be necessary to find more accurate means of generating ground control points. This should be achievable in the near future using the U.S. Navastar Global Positioning System, which will provide instantaneous position fixes to within 15 metres.

Aerial photographic interpretation gave more reliable results than that achieved from MSS imagery. This study also confirms Bagnold's (1941) theory that, under ideal conditions of uniform aeolian activity, levelled land surface and comparable sand supply, small dunes would move faster than large ones. Such ideal conditions exist in the area selected for this study. These ideal conditions do not persist when dealing with an entire sand sea consisting of different dune types, land surfaces and wind regimes. Faster movement of barchan dunes has been observed in other superficial deposits of the sand sea, and there is no significant correlation between the height and the rate of movement of these dunes (Fryberger, et al, 1984 & Watson, 1985). Hence, results obtained from this study should be used with caution when attempting to develop a predictive model of dune migration rates for the entire sand sea.

Space platform imaging systems have a potential as data sources for ten-year-plus time period studies of movement among medium-sized sand dunes (10-14 m high). In order to obtain the best results for sand movement and encroachment patterns over a ten-year period, test sites should be designated immediately, and SPOT, TM and space photographic imagery should be archived for later use. There is also a need for imaging systems to produce data which can be "degraded" in terms of spectral and spatial resolution for comparison with current or older imagery.

With thoughtful advance planning, multi-temporal space imagery has great potential for use in developing desertification and aeolian sediment movement studies over long periods into the future.

7. ACKNOWLEDGMENTS

This study was carried out as part of a PhD research project at the Imperial College of Science and Technology and sponsored by the University of Petroleum and Minerals-Dhahran, Saudi Arabia. Landsat MSS images and aerial photographs, used in this study, were supplied by the Research Institute - University of Petroleum and Minerals. Special thanks to Dr. Abdullah Dabbagh, Director of the Institute, for his assistance during the fieldwork and for his valuable comments.

8. REFERENCES

Bagnold R. A., 1941. The Physics of Blown Sand and Desert Dunes. Methuen, London.

Berera A. M., 1979. Application of Landsat Imagery to Monitor Sand Dune Movement in the Sahara Desert: University of Tennessee unpublished PhD dissertation, p 247.

Davison G. J., 1986. Ground Control Pointing and Geometric Transformation of Satellite Imagery. Int. J. Remote Sensing, Vol. 7, No. 1, pp 65 -74.

Dubief J., 1952. Le vent et le deplacement du sable au Sahara, Algiers Univ. Inst. Rech. Sahariennes Travaux, 8, pp 123 - 164.

Finkel H. J., 1966. The movement of barchan dunes measured by aerial photogrammetry. Photogrammetric Engineering. pp 439 - 444.

Fryberger S. G., Al-Sari A. M., Clisham T. J., Rizvi S. A. and Al-Hinai K. G., 1984. Wind sedimentation in the Jafurah Sand Sea, Saudi Arabia. Sedimentology V.31, pp 413 - 430.

Fryberger S. G. and Ahlbrandt T. S., 1979. Mechanisms for the formation of eolian sand seas, Z. geomorph. V.23, pp 440 - 460.

Ker R. C. and Nigra J. O., 1952. Eolian Sand Control. Bull. Am. Ass. Petrol. Geol. V. 36, No. 8, pp 1541 - 1573.

Lettau K. and Lettau H., 1969. Bulk transport of sands by the barchans of the Pampa de la Joya in Southern Peru. Z. Geomorph. 13, pp 182 - 195.

Pratt W. K., 1978. Digital Image Processing. Wiley & Sons, New York, pp. 330.

Siegal B. S. and Gillespie A. R., 1980. Remote Sensing in Geology. Wiley & Sons, New York. pp 153.

Watson A., 1985. The control of wind-blown sand and moving dunes: a review of the methods of sand control in deserts, with observations from Saudi Arabia. Quarterly Journal of Engineering Geology. V. 18, Part 3, pp. 237 - 252.

Williams R. O., 1979. ARAMCO meteorologic and oceangraphic data book for the Eastern Province of Saudi Arabia, Environmental Unit, Technical Services Department, Arabian American Oil Company, Dhahran, pp 133.

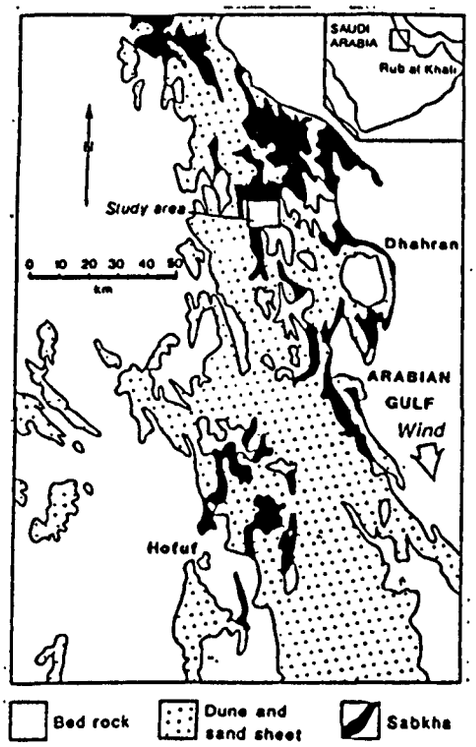


Figure 1. Map of study area and northern Jafurah sand sea showing distribution of dunes, sand sheets, sabkhas and exposed bedrock.

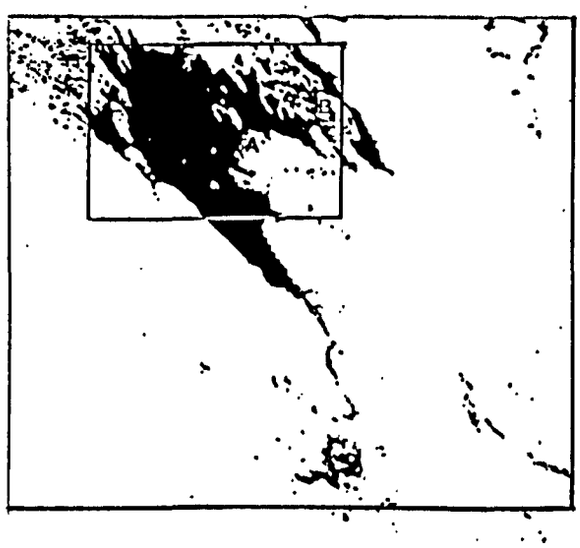


Figure 2. MSS sub-scene (35 x 35 km, approx.) extracted from Landsat scene 176/42 showing the study area. Annotation A & B on fixed bedrock outcrops. The area is the same as in Fig. 3 and 4.

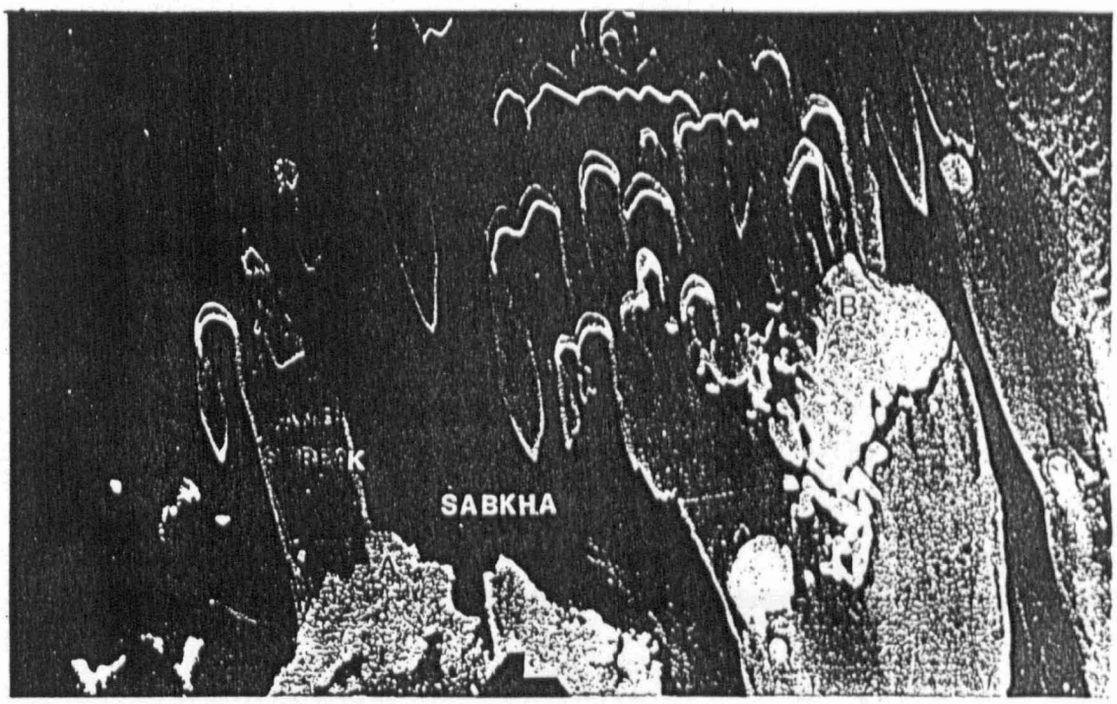


Figure 3. Aerial photograph (1949) showing dunes in the study area. Annotations A and B are fixed bedrock outcrops (approx. scale 1:60,000).

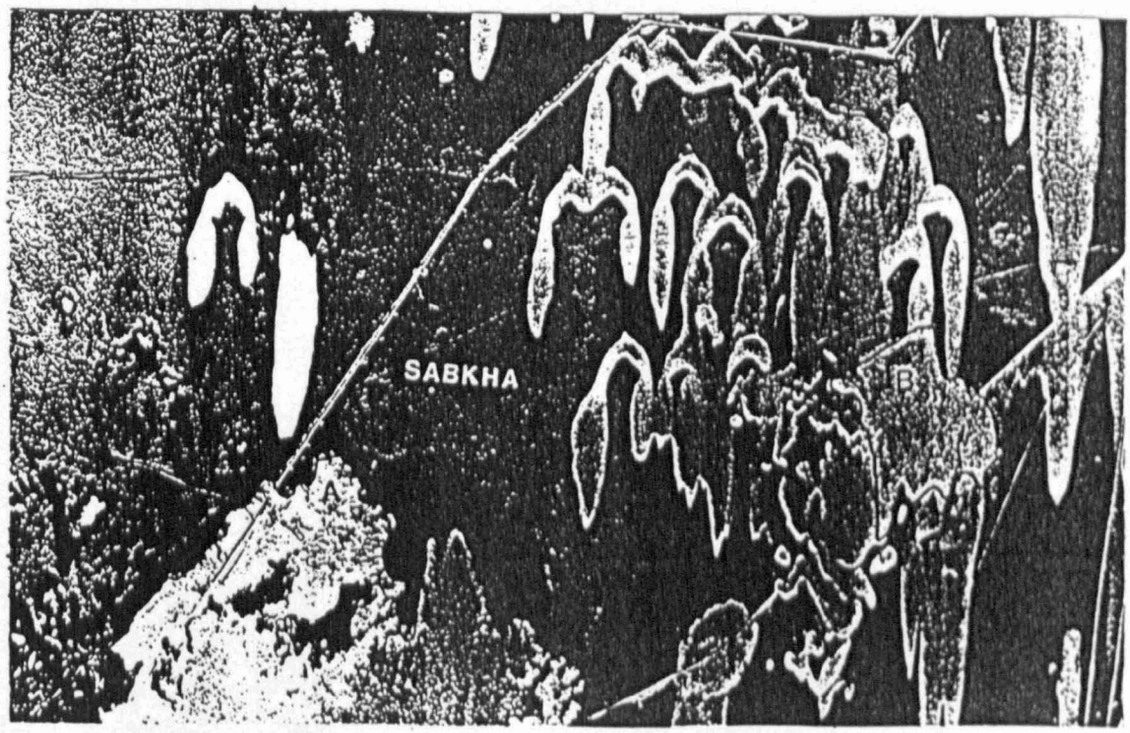


Figure 4. Aerial photograph (1983) of the same area shown on Fig.3. Annotations A and B are fixed bedrock outcrops (approx. scale 1:80,000.).

A P P E N D I X (4)

Al-Hinai, et al (1987, published paper)

INT. J. REMOTE SENSING, 1987, VOL. 8, NO. 2, 251–258

LANDSAT image enhancement study of possible submerged sand-dunes in the Arabian Gulf

KHATTAB G. AL-HINAI, JOHN McMAHON MOORE
and PETER R. BUSH

Geology Department and Centre for Remote Sensing,
Imperial College of Science and Technology, London SW7 2BP, England

(Received 1 August 1986; in final form 18 September 1986)

Abstract. Digital image enhancement of selected LANDSAT Multispectral Scanner (MSS) image data for the coastal area of eastern Saudi Arabia reveals large sandbanks in relatively clear water, 8–10 m deep. LANDSAT MSS imagery of wave length range 0·5–0·6 μm was masked digitally to remove onshore spectral data and the contrast range of sea areas enhanced to display tonal variations which correspond in form to major barchanoid-shaped shoals on the sea floor. The shape, scale and orientation of the sandbanks suggest that they may be submerged aeolian dunes. If these sandbanks are submerged dunes, they predate the last eustatic sea level rise (8000–10 000 years BP) and must have been stabilized by cementation prior to submergence in order to survive palaeo-wind and current erosive action.

1. Introduction

The study area, indicated by the box in figure 1, is located approximately 9 km off the eastern coast of Saudi Arabia, between Bahrain island and the Qatar peninsula. A LANDSAT MSS image representing the wavelength range 0·5–0·6 μm was used to show the submarine form of shoals and sandbanks in coastal waters 8–10 m deep. The

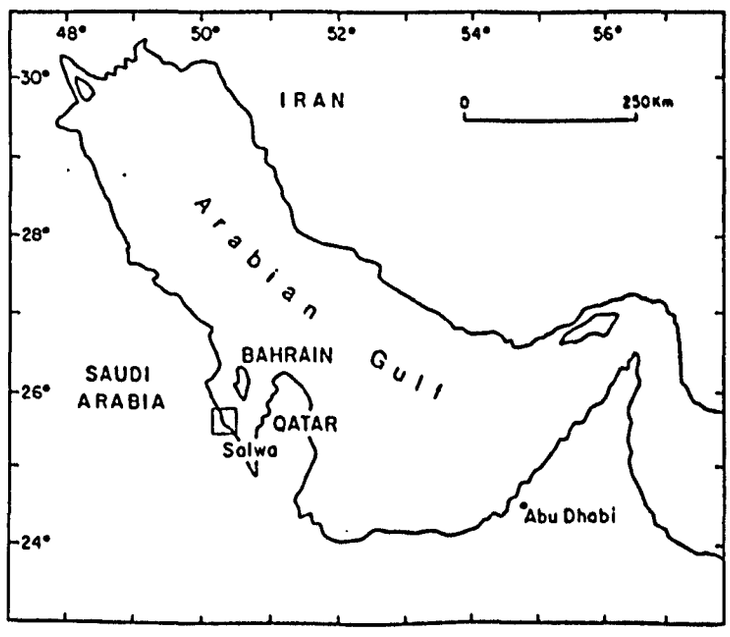


Figure 1. Location of study area.

submarine features are visible in such images because of the partial penetration and transmission of blue-green light by clear water (Polcyn *et al.* 1970).

This letter describes the enhancement procedures used to optimize the display of these submarine features and includes a preliminary hypothesis on the origin of the submerged sandbanks, a topic which will be reported more fully at a later date (Al-Hinai 1987).

2. Enhancement techniques

A LANDSAT MSS band 1 (LANDSAT 4/5 nomenclature) digital image (0·5–0·6 μm wavelength range), acquired on 26 January 1973 (path 176, row 42), was digitally pre-processed for noise removal (sixth-line dropouts, and sixth-line banding).

In order to display tonal features to the best advantage, land and sea areas were each separately masked in turn, and contrast enhanced independently. This was achieved by application of an interactive contrast stretch to MSS band 1 which saturated land areas as white leaving a full range of tone (digital numbers, or DN) for areas of sea (figure 2).

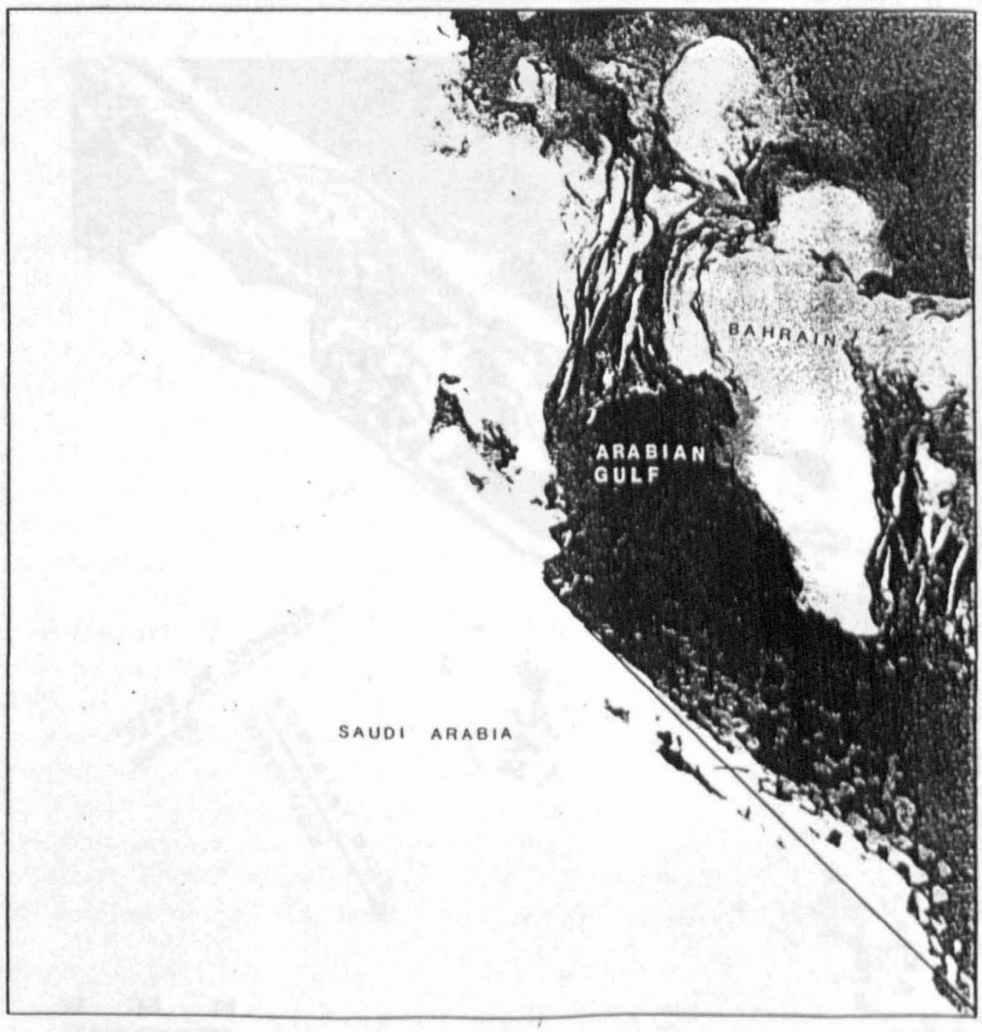


Figure 2. Band 1 MSS imagery (176/42: 26 January 1973) interactively stretched to show offshore features. The submerged sandbanks discussed in this Letter occur in the area outlined.

Data for MSS band 2 (0·6–0·7 μm) and MSS band 4 (0·8–1·1 μm) were then contrast enhanced separately, using a piecewise linear function which clips the histogram tails at the 0·25 and 99·75 percentiles and sets the mean at 128 DN. Using the offshore image (MSS 1) as a digital mask, the stretch parameters were exclusively drawn from the land, thus optimizing the onshore contrast in the band 2 and band 4 images. Each stretched image was then merged with the offshore image to produce a colour composite image representing the land and sea areas. This colour composite image is reproduced in monochrome as figure 3.

3. Image interpretation

The enhanced image (figure 3) clearly shows the form of shoals and submarine sandbanks in the coastal sea between Saudi Arabia, Bahrain island and Qatar.

The general shape and approximate barchanoid outlines of the submarine sandbanks, together with their orientation, indicate that these banks could be submerged aeolian dunes related to a palaeo-wind system blowing north-north-westward. This is a similar orientation to that in certain nearby onshore dunes.

The form and scale of the submarine sandbanks is similar to those of large aeolian

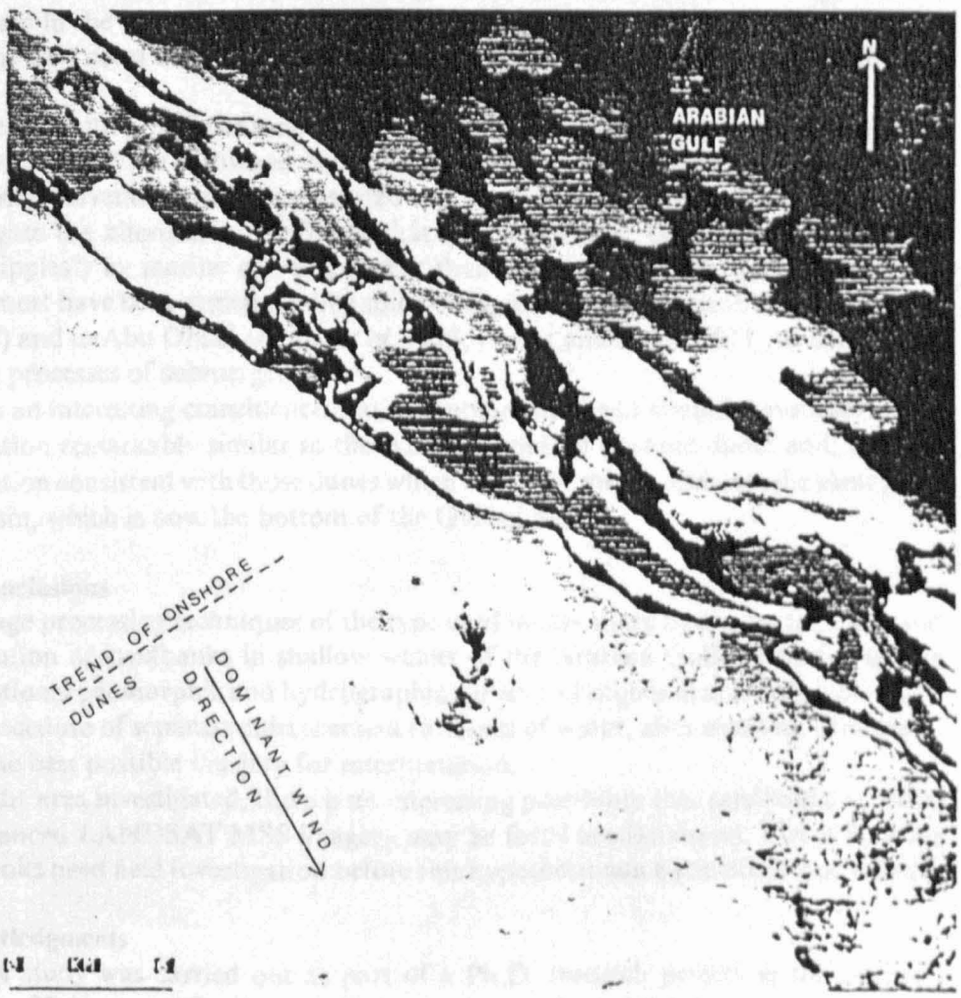


Figure 3. Combined image (false colour composite MSS bands 4 2 1 reproduced in black and white) showing both offshore and onshore areas.

dune complexes in the north-eastern part of the Rub Al Khali area (Empty Quarter) of Saudi Arabia (figure 4). In the Empty Quarter, individual compound crescentic dunes or 'mega-barchans' as defined by Norris (1966) are generally larger than individual crescentic dunes. The mega-barchans are complicated in shape by the presence of smaller crescentic dunes on their gently-sloping windward flanks. Mega-barchans in the Empty Quarter are about 3 km across. This is a comparable scale with that of the submarine sandbanks (figure 4(*c*). The outline form of both onshore dunes and submarine features are functions of the tonal contrast between sand and substrate which, in the Empty Quarter, is a mud plain (*sabkha*).

4. Discussion

The approximate barchanoid form of the submarine sandbanks suggests the intriguing possibility that they are the drowned dunes proposed by Doornkamp *et al.* (1980), forming part of the fossil dune systems which include those of Qatar and Abu Dhabi (Shinn 1973). Doornkamp *et al.* (1980) produced many lines of argument to support the presence of drowned dunes in the Gulf of Salwa between Bahrain and the Saudi Arabian coast. Kassler (1973) suggested that the sands for Abu Dhabi dunes may have arrived there by migrating across the Gulf of Salwa and the Qatar peninsula prior to 7000–8000 years BP. Dunes studies by Seltrust Engineering Ltd (1980) showing movement rates of about 8 m per year in Qatar indicate that all Quatar's major dunes, which are in the south-eastern part of the peninsula, could have migrated the 60 km from the west coast in the 8000–10 000 years since sand supply was cut off by sea level rise.

The suggestion that the sandbanks identified and defined by this image enhancement study may be drowned dunes is tentative. Clearly some modification by submarine currents must have occurred and further work is obviously necessary to investigate the alternative possibility that the banks have been wholly created (as mega-ripples?) by marine currents rather than aeolian processes. Submerged fossil dunes must have been cemented, like some of those on Bahrain island (Doornkamp *et al* 1980) and in Abu Dhabi (Evans *et al.* 1973, Purser and Evans 1973), to survive the erosive processes of submergence.

It is an interesting coincidence that the submarine banks should; have a form and orientation remarkably similar to those of documented onshore dunes and; have an orientation consistent with those dunes which may have migrated across the same piece of terrain, which is now the bottom of the Gulf of Salwa.

5. Conclusions

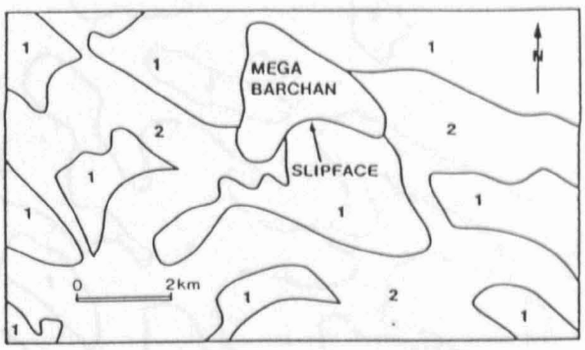
Image processing techniques of the type used in this study to display the form and distribution of sandbanks in shallow waters of the Arabian Gulf are useful aids to conventional geomorphic and hydrographic survey techniques in areas of clear water. The procedure of separate enhancement for areas of water, after masking land areas, gives the best possible imagery for interpretation.

In the area investigated, there is an interesting possibility that sandbanks revealed by enhanced LANDSAT MSS imagery may be fossil aeolian dunes. The submarine sandbanks need field investigation before this hypothesis can be confirmed or refuted.

Acknowledgments

This study was carried out as part of a Ph.D. research project at the Imperial College of Science and Technology and was sponsored by the University of Petroleum

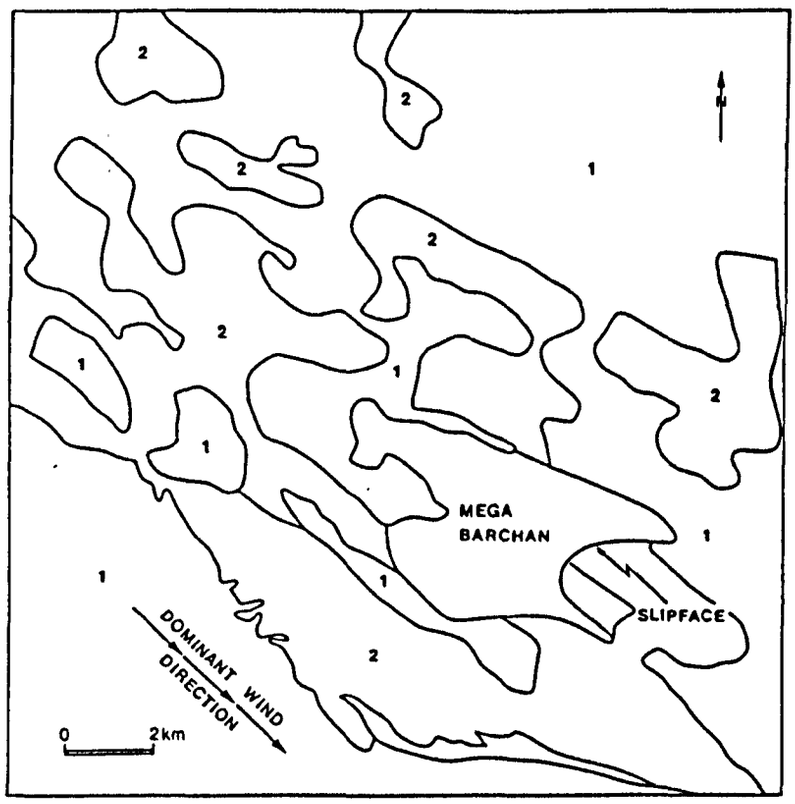

Small simple barchanoid
Small simple barchanoid
Small simple barchanoid
Small simple barchanoid
N
(a)



(*b*)



(*c*)



(*d*)

Figure 4. (*a*) Compound crescentic ridges in the eastern part of the Empty Quarter (Rub Al Khali) sand sea. Approximately 23 N, 54 E. A giant crescentic dune is outlined for scale comparison with the submarine banks in the Arabian Gulf. The width of this mega-dune is about 3 km and it is about 3·2 km long. Photograph by U.S. Department of Defence (reproduced from McKee 1979). (*b*) Interpretation map based on aerial photograph shown in (*a*). Annotations (1) and (2) represent inter-dune *sabkha* areas and crescentic ridges respectively. Notice the similarity in shape and scale of these aeolian features and (*c*). (*c*) An enlargement of part of figure 3 showing submerged sandbanks. A possible giant crescentic dune (mega-barchan) is outlined for comparison with the mega-barchan shown in (*a*). The width of this dune is about 3·2 km. (*d*) Interpretation map derived from (*c*). Annotations (1) and (2) are interpreted as possible inter-dune areas and crescentic ridges respectively.

and Minerals, Dharan, Saudi Arabia. The authors would like to thank Dr. Abdullah Dabbagh, director of the Research Institute at the University of Petroleum and Minerals for his assistance in using the image processing facility there for this study and for his valuable comments. Special thanks to Dr. Andrew Watson for his discussion on dune submergence and to Mr. Jake Brunner for his assistance in the image processing.

References

Al-Hinai, K. G., 1987, Application of remote sensing to desert superficial deposits in Saudi Arabia. Ph.D. thesis, London University (in preparation).

Doornkamp, J. C., Brunsden, D., and Jones, D. K. C. (editors), 1980. Quaternary history. In *Geology, Geomorphology and Pedology of Bahrain* (Norwich, U.K.: Geo Abstract. Ltd), p. 411.

EVANS, G. MURRAY, J. W., BIGGS, H. E., BATER, R., and BUSH, P. R., 1973, The oceanography, ecology, sedimentology and geomorphology of parts of the Trucial Coast Barrier Island Complex, Persian Gulf. In *The Persian Gulf*, edited by B. H. Puurser (Berlin: Springer-Verlag), p. 233.

HUNTING SURVEYS LTD., 1977, Sand dune movement study, south of Umm Said. Technical report, Ministry of Public Works, Qatar.

KASSLER, P., 1973, The structural and geomorphic evolution of the Persian Gulf. In *The Persian Gulf*, edited by B. H. Purser (Berlin: Springer-Verlag), p. 11.

MCKEE, E. D. (editor), 1979, A study of global sand seas. Geological Survey Professional Paper 1052, Washington.

NORRIS, R. M., 1966, Barchan dunes of Imperial Valley, California. *J. Geol.*, 74, p. 292.

POLCYN, F. C., BROWN, W. L., and SATTINGER, I. J., 1970, The measurement of water depth by remote sensing techniques. Report No. 8973-26-F, Infrared and Optics Laboratory, Willow Run University of Michigan, Ann Arbor.

PURSER, B. H., and EVANS, G., 1973, Regional sedimentation along the Trucial Coast, SE Persian Gulf. In *The Persian Gulf*, edited by B. H. Purser (Berlin: Springer-Verlag), p. 211.

SELTRUST ENGINEERING LTD, 1980, *Qatar Geological Map and Explanatory Booklet* (Doha, Qatar: International Development Technical Centre).

SHINN, E. A., 1973, Sedimentary accretion along the leeward SE coast of Qatar Peninsula, Persian Gulf. In *The Persian Gulf*, edited by B. H. Purser (Berlin: Springer-Verlag), p. 199.

A P P E N D I X (5)

Dune height measurements using LFC photographs

in South-eastern Rub' al Khali

Profile A-B shown in Figure 6.14

X,Y	Point coordinates
Z	Ground point heights
H	Dune heights
P	Distance along profile
m	Metres

B

	Xm	Ym	Zm	Hm	Pm
AB	33023.0	51751.8	86.3		13.8
AB	32999.2	51748.6	86.3	68	-11.6
AB	33318.6	51556.2	18.4		361.9
AB	34712.4	50616.1	21.7		2042.9
AB	35022.2	50165.0	226.1	175	2558.6
AB	35504.2	49832.2	50.7		3143.4
AB	36474.6	49325.0	50.7	200	4226.2
AB	36724.9	49118.6	250.3		4549.8
AB	37554.7	48610.3	250.3		5521.1
AB	38075.0	48237.3	47.5		6161.2
AB	38818.7	47661.4	47.5	213	7100.6
AB	39983.7	46470.8	260.8		8743.8
AB	40768.9	45998.6	65.3		9655.3
AB	41180.9	46097.3	65.3	179	9932.9
AB	41770.2	45593.8	244.6		10704.4
AB	42575.9	45096.9	201.0	77	11649.4
AB	42884.5	44847.1	124.3		12045.4
AB	43831.9	44134.8	103.3		13230.1
AB	43975.0	44065.1	176.8	166	13387.2
AB	44419.9	43868.3	70.9		13864.8
AB	45638.8	43085.9	70.9		15312.4
AB	46386.6	42535.8	180.8	128	16240.3
AB	46836.3	42221.7	52.4		16788.8
AB	47592.9	41635.4	52.4	144	17744.7
AB	47939.2	41338.5	197.0		18198.4
AB	48560.9	40656.5	112.1		19099.6
AB	48863.7	40322.0	87.9	157	19540.6
AB	49321.2	39872.1	245.4		20175.0
AB	49980.0	39113.0	80.6		21155.5
AB	51136.0	38712.6	302.0		22325.0
AB	51474.9	38291.5	302.0	228	22846.4
AB	52163.1	38530.3	74.2		23269.7
AB	52673.9	38300.9	74.2	224	23820.6
AB	53051.3	37819.0	298.0		24404.8
AB	53795.4	37411.6	67.7		25248.5
AB	54848.2	36789.1	67.7	155	26468.8
AB	55650.9	36493.4	222.8		27298.9
AB	55930.9	36034.0	72.6		27788.7
AB	56729.4	35251.3	72.6	201	28890.5
AB	57190.6	34064.7	273.7		29955.1
AB	57933.1	33733.8	25.7		30750.2
AB	59736.2	32776.0	81.4		32773.9
AB	61837.0	31131.8	81.4	209	35438.9
AB	62414.0	30857.1	289.1		36068.2
AB	62859.0	30373.0	289.1	185	36711.6
AB	63298.0	30209.3	103.3		37164.0
AB	63416.9	30109.0	103.3		37319.1
AB	63686.6	29867.6	293.9	108	37678.8
AB	64414.6	29326.8	185.7		38585.5
AB	64676.8	29109.4	71.7		38925.2
AB	66790.7	27672.3	71.7	45	41480.7
AB	73301.7	22606.4	117.0		49724.2
AB	73666.8	22402.1	287.5		50104.7
AB	74084.1	22155.1	92.8		50622.8
AB	75791.5	20644.4	92.8	220	52891.7
AB	75542.2	20093.0	312.5		53017.5
AB	76235.0	20021.8	91.9		53617.0
AB	77738.6	19285.4	127.5	141	55265.7
AB	78125.1	19124.0	288.3		55673.4
AB	78571.7	18578.5	308.5	191	56355.2
AB	78946.1	18339.8	117.0		56798.4

AB	80753.2	17325.6	373.9	58856.8
AB	81358.9	16535.2	116.2 (258)	59811.1
AB	81944.6	16033.4	116.2	60580.1
AB	82275.5	15869.4	303.6	60944.0
AB	83053.0	15415.2	220.4 (83)	61840.0
AB	83430.2	14969.1	108.9	62407.5
AB	85565.2	13554.2	117.8	64966.3
AB	85704.5	13394.4	228.5 (111)	65172.9
AB	86071.9	13201.8	109.7	65583.3
AB	86862.8	12690.4	109.7	66523.6
AB	87083.8	12444.1	343.2 (233)	66847.3
AB	87629.1	12166.4	155.0	67451.7
AB	90087.9	10174.4	155.0	70611.8
AB	90518.7	9962.8	311.7 (157)	71004.7
AB	91475.3	9357.7	311.7	72214.3
AB	91935.5	9001.2	158.2	72796.2
AB	96381.8	5654.4	159.8	78360.4
AB	96461.7	5581.3	248.7 (89)	78468.1
AB	97032.2	5180.3	140.4	79165.3
AB	97459.0	4714.5	138.0	79784.6
AB	97825.5	4165.5	296.3 (158)	80404.5
AB	98283.2	3948.4	150.1	80902.0
AB	100950.6	2192.3	150.1	84091.8
AB	101508.2	2378.9	348.0 (198)	84433.7
AB	101901.4	1997.6	121.0	84975.7
AB	106038.1	-1002.5	121.0	90085.8
AB	106361.3	-1232.4	284.2 (163)	90482.4
AB	106882.1	-1583.4	165.5	91110.1
AB	107520.5	-2012.7	165.5	91879.0
AB	108109.7	-2394.8	386.0 (220)	92580.3
AB	108395.9	-2718.9	89.5	93002.1
AB	110504.4	-4552.3	134.0	95785.2
AB	110997.0	-4622.4	319.0 (155)	96225.2
AB	111388.6	-5096.7	178.4	96820.6
AB	113354.2	-6387.6	177.6	99169.7
AB	113601.1	-6502.3	292.3 (115)	99437.0
AB	113998.3	-6854.3	181.6	99965.1
AB	114484.2	-7129.2	296.3	100519.9
AB	114742.3	-7427.6	184.9 (111)	100904.0
AB	115186.2	-7697.1	305.2	101421.5
AB	115398.5	-7857.2	159.0 (146)	101687.4
AB	117689.8	-9591.5	188.1	104560.4
AB	117882.6	-9753.2	327.0	104811.4
AB	118555.0	-10153.8	188.1 (139)	105591.0
AB	120905.5	-11584.8	185.7	108334.3
AB	121493.5	-11839.7	302.8 (117)	108960.5
AB	121583.1	-11780.0	302.8	108998.4

A

REPEAT OBSERVATIONS

AB	33026.0	51691.5	141.2	56.7
AB	33008.3	51716.7	141.2	-29.4
AB	33297.5	51503.6	28.9	375.7
AB	35138.6	50303.2	30.5	2571.2
AB	35250.5	50138.3	174.3	2757.3
AB	35582.5	49879.4	55.6	3178.0
AB	36587.6	49328.3	55.6	4317.5
AB	37143.3	49206.3	204.2	4850.9
AB	37578.3	48860.7	205.1	5402.8
AB	38122.2	48408.7	62.1	6104.7
AB	38024.1	47726.7	62.1	7238.2
AB	40046.4	46321.4	255.9	8041.7
AB	40623.1	45930.2	99.2	9543.6
AB	41350.9	45732.9	99.2	9924.2
AB	41241.9	45393.4	208.4	10397.7
AB	41619.2	45170.3	79.0	10832.8
AB	43586.2	43935.8	79.0	13147.0

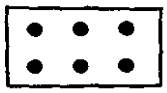
AB	44236.1	43609.1	98.4	13864.5
AB	45472.7	42910.4	98.4	15276.6
AB	46201.4	42454.8	193.7	16134.6
AB	46927.0	42078.4	61.2	16945.0
AB	47616.6	41657.3	62.1	17751.6
AB	47686.1	41483.8	197.0	17907.7
AB	48382.2	40960.6	89.5	18778.1
AB	48819.5	40707.6	78.2	19281.4
AB	49069.2	40511.2	78.2	19598.6
AB	49506.9	40144.7	247.9	20167.3
AB	50172.8	39558.9	104.9	21048.2
AB	50356.8	39443.3	222.8	21266.2
AB	50817.1	39168.8	128.3	21800.5
AB	51315.4	39004.1	128.3	22303.0
AB	51569.5	38859.2	188.1	22594.4
AB	52130.6	38598.2	65.3	23204.4
AB	52595.8	38372.3	66.1	23715.9
AB	53066.2	37982.4	281.0	24324.3
AB	53745.5	37198.5	43.5	25329.3
AB	56271.9	35082.0	83.9	28614.3
AB	56360.5	34572.2	271.3	28985.5
AB	56983.5	34163.5	292.3	29729.7
AB	57872.9	33755.8	85.5	30688.6
AB	59187.4	32897.5	77.4	32256.7
AB	59180.9	32205.5	230.9	32660.7
AB	59750.8	31841.4	83.1	33335.2
AB	62214.2	31194.3	83.1	35710.4
AB	62338.5	30855.9	298.0	36007.3
AB	62815.8	30069.4	182.4	36854.2
AB	63277.4	29559.7	306.0	37527.6
AB	64306.5	28977.7	171.1	38701.8
AB	64562.5	28817.7	78.2	39008.0
AB	66129.2	27677.0	70.9	40941.0
AB	66279.7	27346.9	233.3	41257.1
AB	66518.3	27062.1	305.2	41618.1
AB	67409.8	26375.1	93.6	42743.3
AB	70398.8	24480.8	81.4	46273.9
AB	70214.9	24055.8	328.7	46378.0
AB	70737.3	23794.1	272.1	46953.4
AB	71277.5	23518.8	99.2	47551.4
AB	73301.4	22716.2	99.2	49653.7
AB	73641.0	22525.1	270.5	50047.0
AB	74148.3	22233.0	103.3	50629.4
AB	78027.5	19349.9	111.3	55462.1
AB	78215.0	19228.2	304.4	55685.3
AB	78561.5	19048.1	289.9	56071.8
AB	79121.6	18699.2	123.5	56730.3
AB	80369.6	17963.9	122.6	58173.2
AB	80356.9	17584.4	281.8	58384.1
AB	80891.7	17267.0	335.9	59003.4
AB	81459.8	16901.0	110.5	59678.4
AB	82160.8	16258.6	110.5	60622.6
AB	82461.1	15905.6	279.4	61072.9
AB	82937.0	15641.7	300.4	61613.1
AB	83497.2	15233.9	149.3	62306.0
AB	84936.5	14326.0	106.5	64004.4
AB	85210.6	13995.1	247.1	64420.4
AB	85575.0	13805.6	209.0	64826.7
AB	86040.7	13531.3	134.9	65364.9
AB	87121.3	12874.6	117.0	66742.4
AB	87209.7	12410.1	272.9	66969.2
AB	87659.0	12197.9	136.4	67457.5
AB	90217.1	10238.7	155.8	70678.5
AB	90683.0	10109.7	260.8	71131.6
AB	91330.8	9593.9	321.4	71958.8

AB	93981.4	7479.9	113.8	75345.5
AB	96114.5	6127.5	114.6	77866.3
AB	96453.8	5764.3	243.8	78354.1
AB	96912.2	5533.5	158.2	78860.8
AB	97682.0	4600.2	137.2	80032.1
AB	97837.5	4473.0	268.1	80232.6
AB	98537.8	4137.8	142.8	80996.1
AB	100837.9	2424.1	144.5	83904.7
AB	101262.8	2491.2	325.4	84169.0
AB	101643.4	2292.4	325.4	84594.0
AB	102102.9	1964.8	138.8	85158.2
AB	106171.1	-1071.1	138.0	90233.7
AB	106327.5	-1169.3	263.2	90418.1
AB	107012.8	-1565.2	152.5	91205.5
AB	107543.2	-2050.1	239.8	91919.2
AB	108165.6	-2433.5	348.0	92648.3
AB	108380.5	-2949.9	149.3	93125.1
AB	110721.2	-4436.1	134.0	95892.5
AB	111157.8	-4648.6	278.6	96370.9
AB	111483.8	-4887.9	169.5	96775.3
AB	113390.0	-6473.0	185.7	99248.8
AB	113694.1	-6633.3	295.5	99589.1
AB	113900.3	-6766.5	182.4	99834.2
AB	114330.6	-7028.7	182.4	100336.5
AB	114427.8	-7183.0	343.2	100505.8
AB	114792.7	-7346.8	202.6	100897.4
AB	115213.5	-7648.3	298.8	101415.1
AB	115480.0	-7865.9	153.3	101758.6
AB	117883.5	-9560.9	219.6	104699.4
AB	118102.5	-9744.7	297.2	104984.6
AB	118407.3	-10071.2	196.2	105422.8
AB	118587.6	-10703.4	195.4	106749.8
AB	119678.1	-10750.3	262.4	106850.6
AB	120162.1	-10981.5	177.6	107378.5
AB	120837.1	-11300.3	177.6	108112.7
AB	121239.2	-11348.6	328.7	108467.6
AB	121552.4	-11527.4	156.6	108826.4
AB	121596.1	-11820.8	214.7	109032.8

LIFE SCIENCES & MEDICINE COLLECTION
IMPERIAL COLLEGE, LONDON SW7 2AZ

MORPHOLOGY AND DISTRIBUTION OF SAND DUNES IN THE JAFURAH SAND SEA.

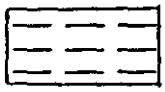
EXPLANATION:



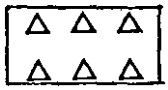
Quaternary Sabkha: with barchans & barchanoid ridges.



Transverse Dunes: Barchans & barchanoid ridges.



Sand Sheets: with parabolic and dome dunes.



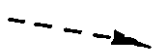
Complex dunes: Transverse dunes & sand sheets.



Chain barchans.



Substratum (gravel and/ or bedrock).

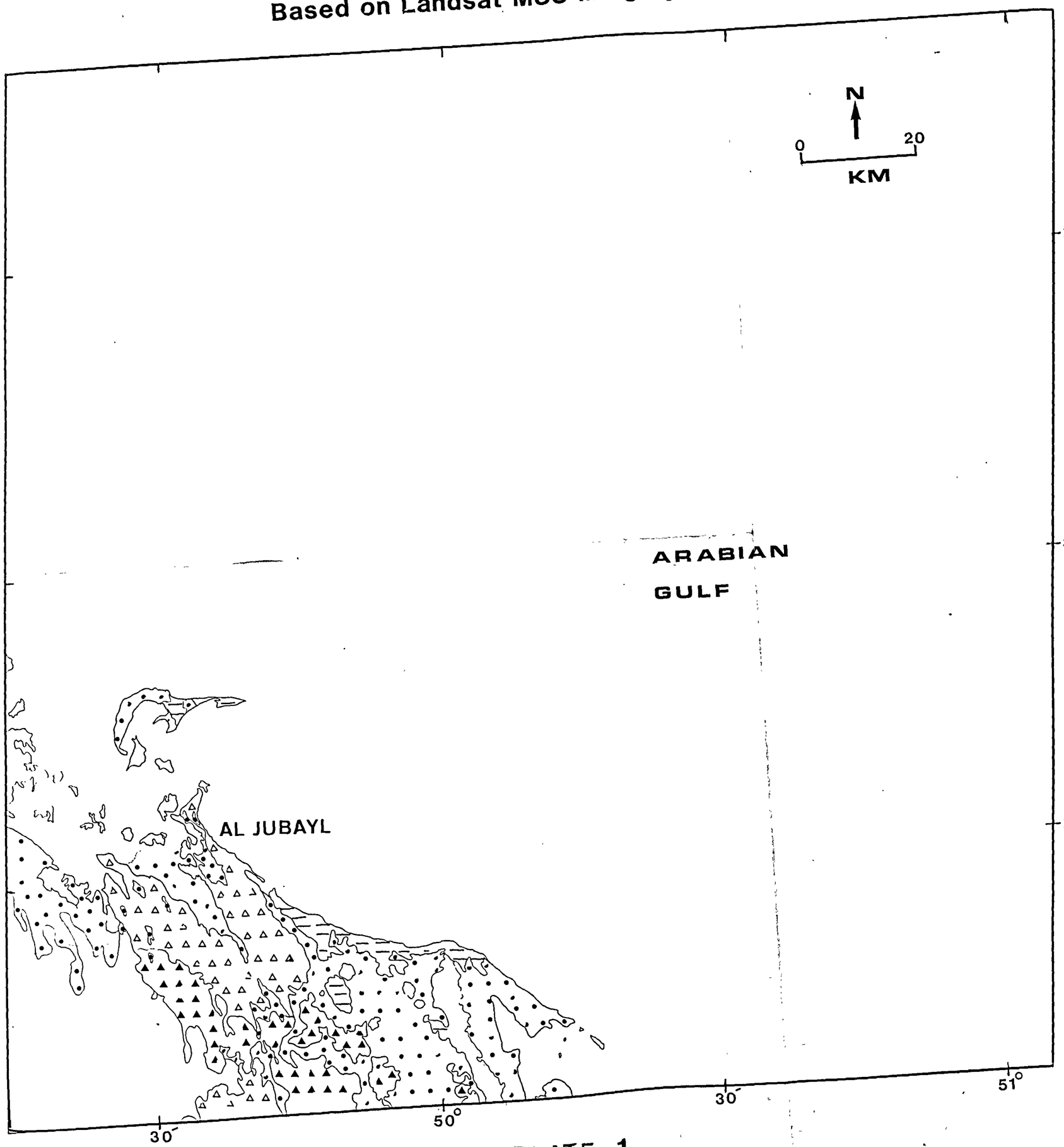


Old wadi channels.

WATTS LIBRARY

MORPHOLOGY AND DISTRIBUTION OF SAND DUNES IN THE JAFURAH SAND SEA

Based on Landsat MSS imagery



KEY ON
PAGE 171

PLATE 1

WATTS LIBRARY

MORPHOLOGY AND DISTRIBUTION OF SAND DUNES IN THE JAFURAH SAND SEA

Based on Landsat MSS imagery

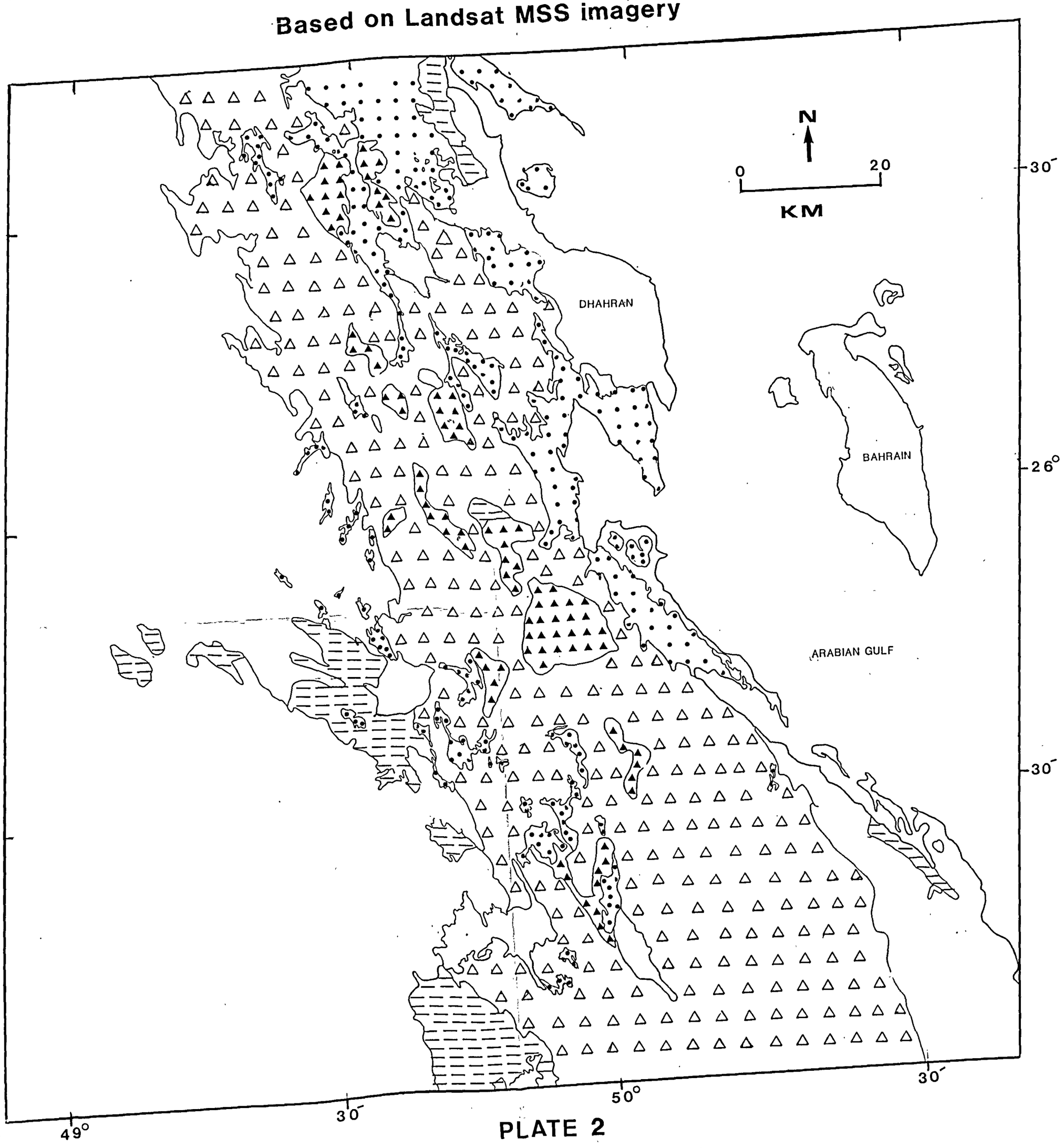


PLATE 2

WATTS LIBRARY

MORPHOLOGY AND DISTRIBUTION OF SAND DUNES IN THE JAFURAH SAND SEA

Based on Landsat MSS imagery

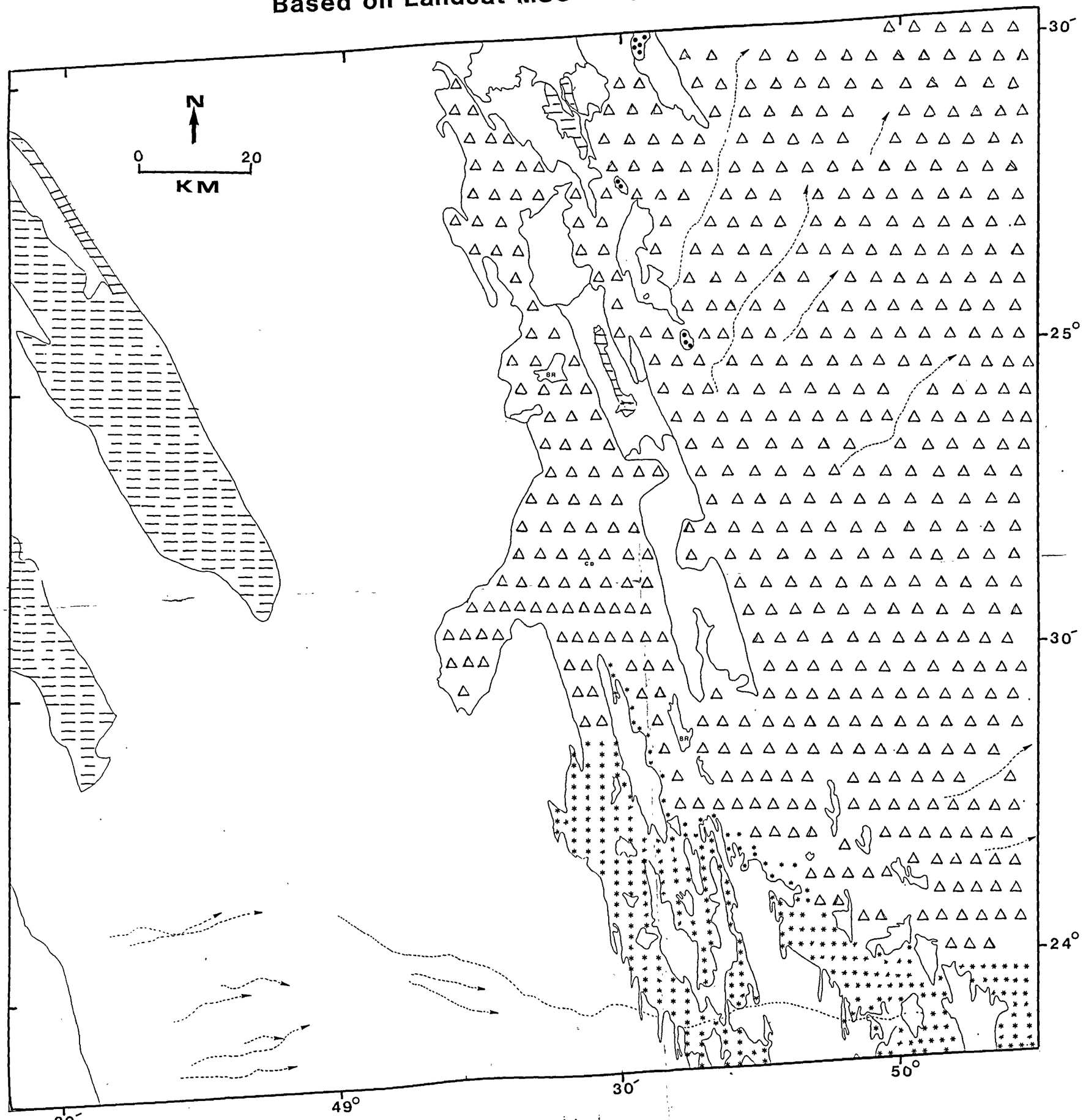


PLATE 3

WATTS LIBRARY

MORPHOLOGY AND DISTRIBUTION OF SAND DUNES IN THE JAFURAH SAND SEA

Based on Landsat MSS imagery

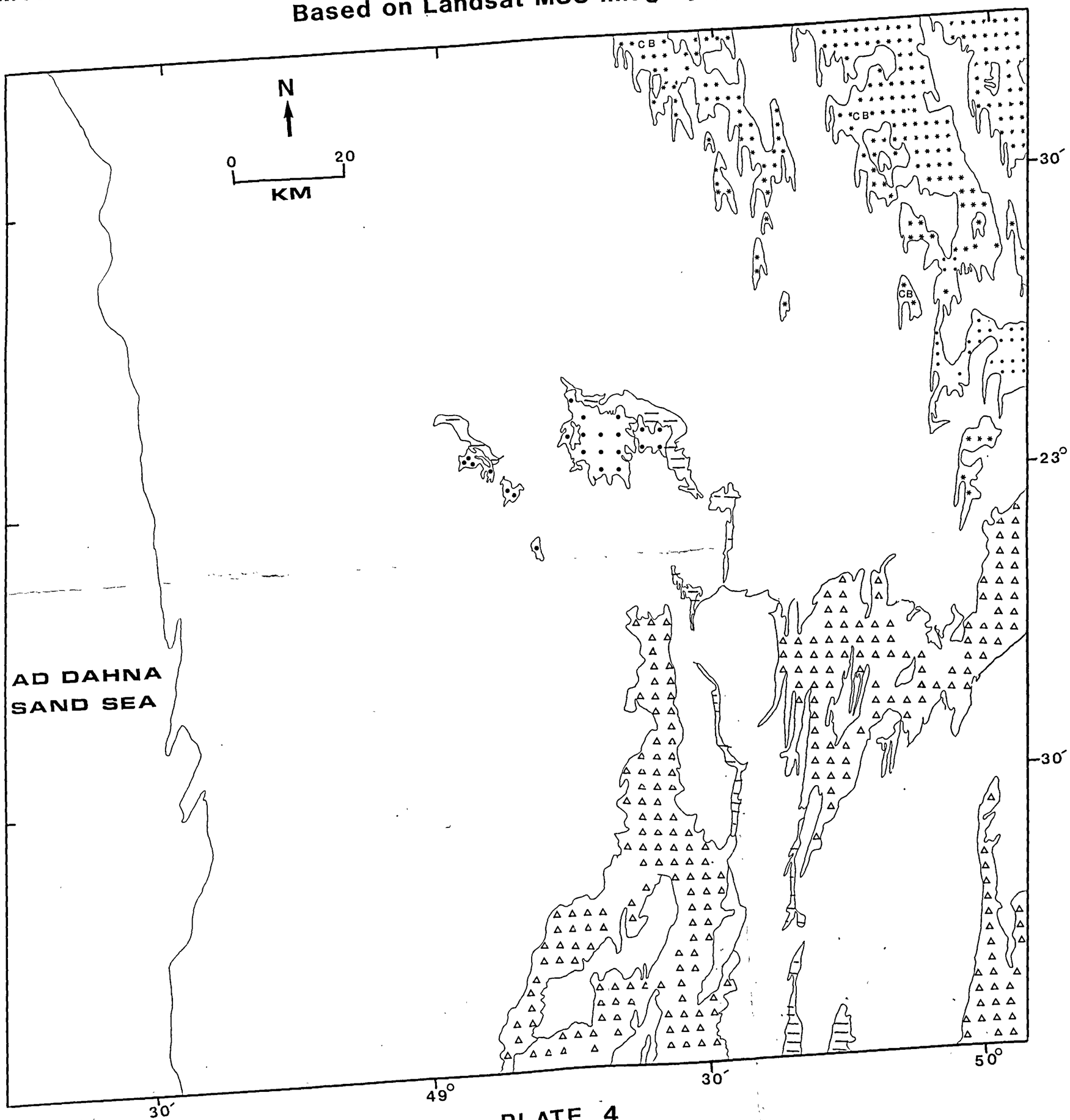


PLATE 4

WATTS LIBRARY

MORPHOLOGY AND DISTRIBUTION OF SAND DUNES IN THE JAFURAH SAND SEA

Based on Landsat MSS imagery

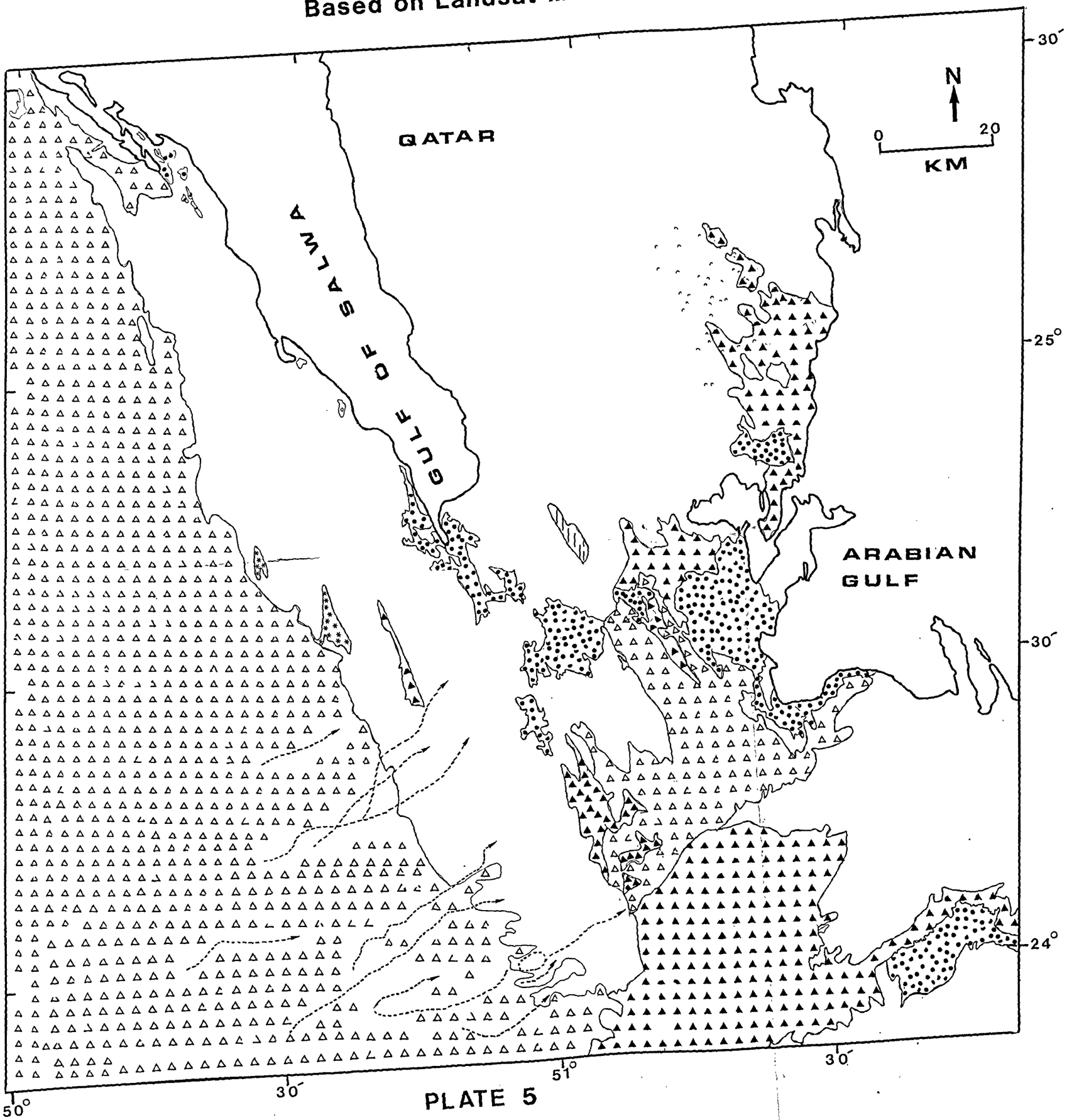


PLATE 5

WATTS LIBRARY

MORPHOLOGY AND DISTRIBUTION OF SAND DUNES IN THE JAFURAH SAND SEA

Based on Landsat MSS imagery

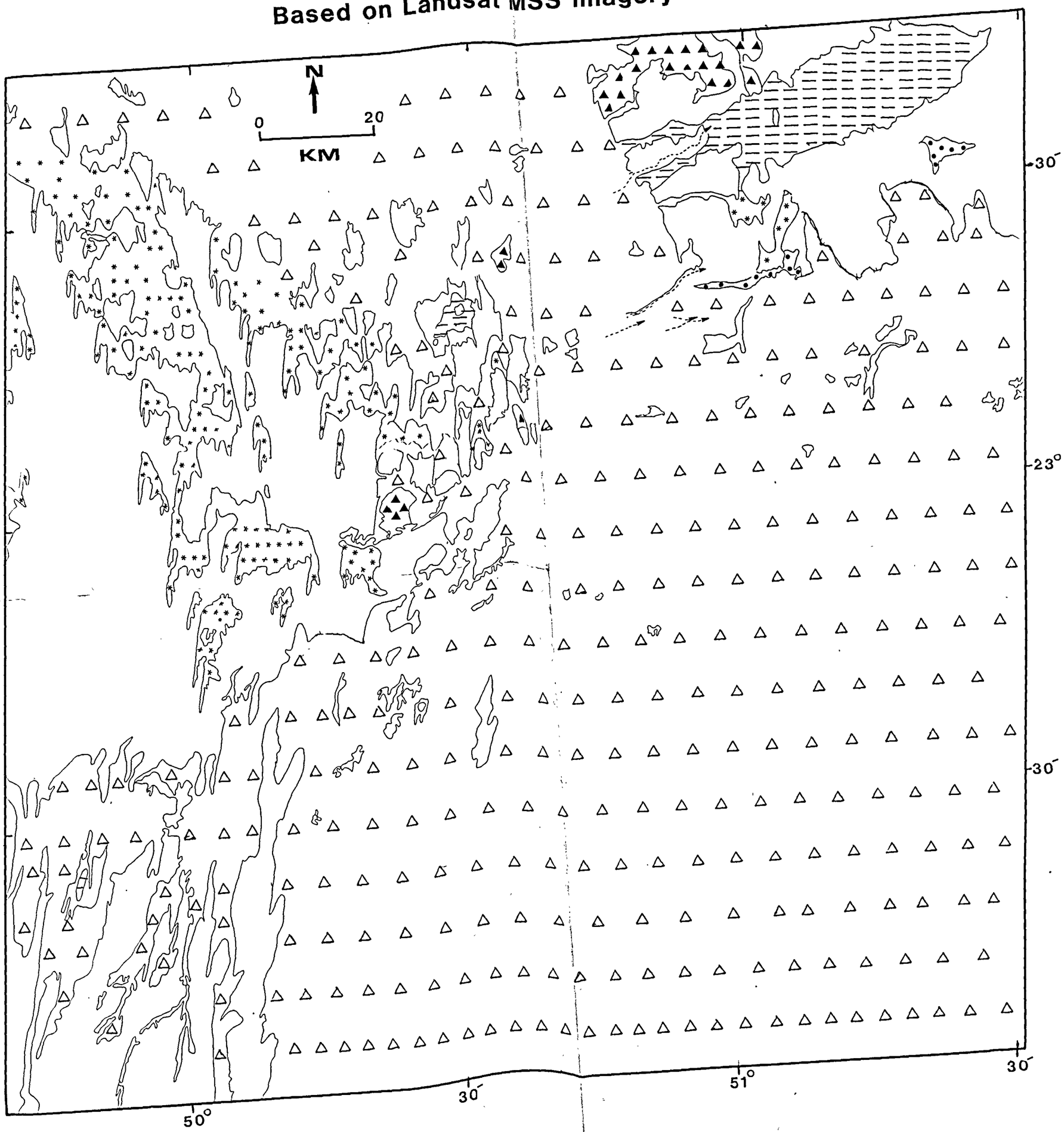


PLATE 6